

Ancestral cattle return to
Europe's wild spots *p. 1144*

Books to inspire budding
scientists *pp. 1152 & 1160*

High harmonics born
of ultraviolet *p. 1225*

Science

\$10
4 DECEMBER 2015
sciencemag.org

AAAS

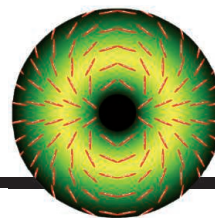
SPECIAL ISSUE

WHY WE
AGE



CONTENTS

4 DECEMBER 2015 • VOLUME 350 • ISSUE 6265



1172

Untangling classical entanglement

SPECIAL SECTION

Aging

INTRODUCTION

1180 Toward healthy aging

NEWS

1182 Why we outlive our pets
By D. Grimm

1186 Death-defying experiments
By J. Cohen

1188 The final countdown
By E. Underwood

REVIEWS

1191 Healthy aging: The ultimate preventative medicine
M. Kaeberlein et al.

1193 Human telomere biology: A contributory and interactive factor in aging, disease risks, and protection
E. H. Blackburn et al.

1199 Stem cells and healthy aging
M. A. Goodell and T. A. Rando



1204 Mitochondrial dysfunction and longevity in animals: Untangling the knot
Y. Wang and S. Hekimi

1208 NAD⁺ in aging, metabolism, and neurodegeneration
E. Verdin

PERSPECTIVE

1214 Gut microbiota and aging
P. W. O'Toole and I. B. Jeffery

ON THE COVER



Hands of a 78-year-old man and a 9-month-old baby reveal signs of aging. This special issue focuses on the biology of aging and the goal

of increasing healthy life span. See page 1180. Photo: Erin Scott

SEE ALSO ► EDITORIAL P. 1135
► PODCAST ► VIDEO

NEWS

IN BRIEF

1136 News at a glance

IN DEPTH

1138 MUD TSUNAMI WREAKS ECOLOGICAL HAVOC IN BRAZIL

Researchers analyze sludge for heavy metals and assess potential for recovery
By H. Escobar

1139 DNA HELPS BUILD MOLECULAR LIBRARIES FOR DRUG TESTING

Pharmaceutical firms and biotech companies embrace DNA-encoded chemical libraries
By T. Gura

1140 U.K. RESEARCH WINS HOLLOW VICTORY

Budget is protected for 5 years, but lags because of past inflation
By E. Stokstad

1142 JAPANESE PROBE PRIMED FOR SECOND RUN AT VENUS

Akatsuki spacecraft aims to plumb planet's weird atmosphere
By D. Normile

1143 DATA CHECK: NSF'S NOVEL SOLUTION TO A WORKLOAD CRUNCH

Hiring more rotators and clamping down on submissions helped avert a labor crisis
By J. Mervis



Cave paintings of aurochs in Lascaux, France.

FEATURES

1144 BRINGING BACK THE AUROCHS

By conjuring the extinct ancestor of modern cattle, breeders are making Europe just a little bit wilder
By E. Stokstad

1148 BORN TO REWILD

A father and son's quixotic quest to bring back a lost ecosystem—and save the world
By E. Kintisch

► VIDEO

INSIGHTS

BOOKS ET AL.

1152 SB&F PRIZES FOR EXCELLENCE IN SCIENCE BOOKS

1160 ROYAL SOCIETY YOUNG PEOPLE'S BOOK PRIZE

PERSPECTIVES

1162 MITOCHONDRIA SHAPE CARDIAC METABOLISM

Quality control of mitochondria in cardiac muscle affects heart function
By R. A. Gottlieb and D. Bernstein

► RESEARCH ARTICLES PP. 1220 & 1221

1163 PHAGE THERAPY REDUX—WHAT IS TO BE DONE?

Bacteriophage biology should move beyond a model system to support human health
By R. Young and J. J. Gill

1165 A SPEEDY MARRIAGE IN SUPRAMOLECULAR CATALYSIS

Cross-coupling reactions can be accelerated by trapping the metal catalyst in a confined space
By K. Yan and M. Fujita

► REPORT P. 1235

1166 CORRIDORS FOR PEOPLE, CORRIDORS FOR NATURE

How can the environmental impacts of roads be reduced?
By N. M. Haddad

1168 CAN PARIS PLEDGES AVERT SEVERE CLIMATE CHANGE?

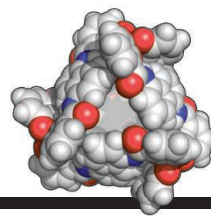
Reducing risks of severe outcomes and improving chances of limiting warming to 2°C
By A. A. Fawcett et al.

1170 POLITICAL AGENCY: THE KEY TO TACKLING CLIMATE CHANGE

Individuals play a central role in the transformations required to avoid dangerous climate change
By K. O'Brien

Science Staff	1132
New Products	1270
Science Careers	1271

CONTENTS



1165 & 1235

Prompting platinum
in a capsule

4 DECEMBER 2015 • VOLUME 350 • ISSUE 6265

1176



1171 SILICA-SUPPORTED CATALYSTS GET A NEW BREATH OF LIFE

Methods emerge for dispersing metals
as stable nanoparticles on silica surfaces
By S. Soled

1172 CLASSICAL ENTANGLEMENT?

Entanglement is a property of the
quantum world; classical systems need
not apply *By E. Karimi and R. W. Boyd*

SCIENCE PRIZE ESSAY

1174 TEAMWORK: THE TUMOR CELL EDITION

Subclone cooperation maintains tumor
growth *By A. S. Cleary*

LETTERS

1176 EXOSKELETON PROGRESS YIELDS SLIPPERY SLOPE

By D. Greenbaum

1176 TORTURE'S INEFFICIENCY LONG ESTABLISHED

By D. R. Witzling

1176 POLLUTION THREATENS MIGRATORY SHOREBIRDS

By Z. Tang et al.

1177 TECHNICAL COMMENT ABSTRACTS

RESEARCH

IN BRIEF

1217 From *Science* and other journals

RESEARCH ARTICLES

HEART MITOCHONDRIA

1220 Parkin-mediated mitophagy
directs perinatal cardiac metabolic
maturation in mice *G. Gong et al.*

RESEARCH ARTICLE SUMMARY; FOR FULL
TEXT: dx.doi.org/10.1126/science.aad2459

1221 Imbalanced OPA1 processing and
mitochondrial fragmentation cause
heart failure in mice *T. Wai et al.*

RESEARCH ARTICLE SUMMARY; FOR FULL
TEXT: dx.doi.org/10.1126/science.aad0116

► PERSPECTIVE P. 1162

REPORTS

1222 PEROVSKITE LEDS

Overcoming the electroluminescence
efficiency limitations of perovskite light-
emitting diodes *H. Cho et al.*

1225 LASER PHYSICS

Ultraviolet surprise: Efficient soft x-ray
high-harmonic generation in multiply
ionized plasmas *D. Popmintchev et al.*

1231 QUANTUM HALL EFFECT

Evidence for a fractional fractal
quantum Hall effect in graphene
superlattices *L. Wang et al.*

1235 CATALYSIS

A supramolecular microenvironment
strategy for transition metal catalysis
D. M. Kaphan et al.

► PERSPECTIVE P. 1165

1238 SOLAR PHYSICS

Particle acceleration by a solar flare
termination shock *B. Chen et al.*

1242 BLACK HOLES

Resolved magnetic-field structure and
variability near the event horizon of
Sagittarius A* *M. D. Johnson et al.*

1245 EDUCATION

Democratizing education? Examining
access and usage patterns in massive
open online courses *J. D. Hansen and
J. Reich*

1248 WATER RESOURCES

Local flow regulation and irrigation
raise global human water consumption
and footprint *F. Jaramillo and G. Destouni*

1251 NEURODEVELOPMENT

Single-cell transcriptomics reveals
receptor transformations during olfactory
neurogenesis *N. K. Hanchate et al.*

1255 PROTECTED AREAS

Protected areas and global conservation
of migratory birds *C. A. Runge et al.*

1258 GENE REGULATION

Single-base pair differences in a shared
motif determine differential *Rhodopsin*
expression *J. Rister et al.*

1262 HUMAN GENETICS

De novo mutations in congenital heart
disease with neurodevelopmental and
other congenital anomalies *J. Homsy et al.*

DEPARTMENTS

1135 EDITORIAL

Japan's longevity challenge
By Hiroko Akiyama

► AGING SECTION P. 1180

1286 WORKING LIFE

Science made me a better parent
By Ignacio Amigo



SCIENCE (ISSN 0036-8075) is published weekly on Friday, except the last week in December, by the American Association for the Advancement of Science, 1200 New York Avenue, NW, Washington, DC 20005. Periodicals mail postage (publication No. 484460) paid at Washington, DC, and additional mailing offices. Copyright © 2015 by the American Association for the Advancement of Science. The title SCIENCE is a registered trademark of the AAAS. Domestic individual membership and subscription (51 issues): \$153 (\$74 allocated to subscription). Foreign postage extra: Mexico, Caribbean (surface mail) \$55; other countries (air assist delivery) \$85. First class, airmail, student, and emeritus rates on request. Canadian rates with GST available upon request. GST #R1254 88122. Publications Mail Agreement Number 1069624. Printed in the U.S.A. Change of address: Allow 4 weeks, giving old and new addresses and 8-digit account number. Postmaster: Send change of address to AAAS, P.O. Box 96178, Washington, DC 20090-6178. Single-copy sales: \$10.00 current issue, \$15.00 back issue prepaid includes surface postage; bulk rates on request. Authorization to photocopy material for internal or personal use under circumstances not falling within the fair use provisions of the Copyright Act is granted by AAAS to libraries and other users registered with the Copyright Clearance Center (CCC) Transactional Reporting Service, provided that \$30.00 per article is paid directly to CCC, 222 Rosewood Drive, Danvers, MA 01923. The identification code for Science is 0036-8075. Science is indexed in the Reader's Guide to Periodical Literature and in several specialized indexes.

Editor-in-Chief Marcia McNutt

Executive Editor Monica M. Bradford **News Editor** Tim Appenzeller

Managing Editor, Research Journals Katrina L. Kelner

Deputy Editors Barbara R. Jasny, Andrew M. Sugden(UK), Valda J. Vinson, Jake S. Yeston

Research and Insights

SR. EDITORS Caroline Ash(UK), Gilbert J. Chin, Lisa D. Chong, Julia Fahrenkamp-Uppenbrink(UK), Pamela J. Hines, Stella M. Hurlty(UK), Paula A. Kiberstis, Marc S. Lavine(Canada), Kristen L. Mueller, Ian S. Osborne(UK), Beverly A. Purnell, L. Bryan Ray, Guy Riddihough, H. Jesse Smith, Jelena Stajic, Peter Stern(UK), Phillip D. Szurmi, Brad Wible, Nicholas S. Wigginton, Laura M. Zahn **ASSOCIATE EDITORS** Brent Grocholski, Keith T. Smith, Sacha Vignieri **ASSOCIATE BOOK REVIEW EDITOR** Valerie B. Thompson **ASSOCIATE LETTERS EDITOR** Jennifer Sills **CHIEF CONTENT PRODUCTION EDITOR** Cara Tate **SR. CONTENT PRODUCTION EDITOR** Harry Jack, Lauren Kmec **CONTENT PRODUCTION EDITORS** Jeffrey E. Cook, Chris Filiatreau, Cynthia Howe, Barbara P. Ordway, Catherine Wolner **SR. EDITORIAL COORDINATORS** Carolyn Kyle, Beverly Shields **EDITORIAL COORDINATORS** Ramatoulaye Diop, Joi S. Granger, Lisa Johnson, Anita Wynn **PUBLICATIONS ASSISTANTS** Aneera Dobbins, Jeffrey Hearn, Dona Mathieu, Le-Toya Mayne Flood, Shannon McMahon, Scott Miller, Jerry Richardson, Rachel Roberts(UK), Alice Whaley(UK), Brian White **EXECUTIVE ASSISTANT** Anna Bashkurova **ADMINISTRATIVE SUPPORT** Janet Clements(UK), Lizanne Newton(UK), Maryrose Madrid, Laura-Nadine Schuhmacher (UK, Intern), Alix Welch (Intern), John Wood(UK)

News

NEWS MANAGING EDITOR John Travis **INTERNATIONAL EDITOR** Richard Stone **DEPUTY NEWS EDITORS** Daniel Clery(UK), Robert Coontz, Elizabeth Culotta, David Grimm, David Malakoff, Leslie Roberts **CONTRIBUTING EDITOR** Martin Enserink(Europe) **SR. CORRESPONDENTS** Jeffrey Mervis, Elizabeth Pennisi **NEWS WRITERS** Adrian Cho, Jon Cohen, Jennifer Couzin-Frankel, Carolyn Gramling, Eric Hand, Jocelyn Kaiser, Catherine Maticic, Kelly Servick, Robert F. Service, Erik Stokstad(Cambridge, UK), Emily Underwood **INTERNS** Hanae Armitage, Emily DeMarco, Annick Laurent, Laura Olivieri, Juan David Romero **CONTRIBUTING CORRESPONDENTS** Michael Balter(Paris), John Bohannon, Ann Gibbons, Mara Hvistendahl, Sam Kean, Eli Kintisch, Kai Kupferschmidt(Berlin), Andrew Lawler, Christina Larson(Beijing), Mitch Leslie, Charles C. Mann, Eliot Marshall, Virginia Morell, Dennis Normile(Tokyo), Heather Pringle, Tania Rabesandratana(London), Gretchen Vogel(Berlin), Lizzie Wade(Mexico City) **CAREERS** Donisha Adams, Rachel Bernstein **COPY EDITORS** Julia Cole, Jennifer Levin (Chief) **ADMINISTRATIVE SUPPORT** Jessica Williams

Executive Publisher Rush D. Holt

Publisher Kent R. Anderson **Chief Digital Media Officer** Rob Covey

BUSINESS OPERATIONS AND PORTFOLIO MANAGEMENT DIRECTOR Sarah Whalen **BUSINESS SYSTEMS AND FINANCIAL ANALYSIS DIRECTOR** Randy Yi **MANAGER OF FULFILLMENT SYSTEMS** Neal Hawkins **SYSTEMS ANALYST** Nicole Mehmedovic **ASSISTANT DIRECTOR, BUSINESS OPERATIONS** Eric Knott **MANAGER, BUSINESS OPERATIONS** Jessica Tierney **BUSINESS ANALYSTS** Cory Lipman, Cooper Tilton, Celeste Troxler **FINANCIAL ANALYST** Robert Clark **RIGHTS AND PERMISSIONS ASSISTANT DIRECTOR** Emilie David **PERMISSIONS ASSOCIATE** Elizabeth Sandler **RIGHTS, CONTRACTS, AND LICENSING ASSOCIATE** Lili Kiser

MARKETING DIRECTOR Elise Swinehart **ASSOCIATE DIRECTOR OF ACQUISITION AND RETENTION** Julianne Wielga **MARKETING ASSOCIATE** Elizabeth Sattler **SR. MARKETING EXECUTIVE** Jennifer Reeves **ASSOCIATE DIRECTOR, CREATIVE SERVICES** Tzeitel Sorrosa **ART ASSOCIATE** Seil Lee **JR. ART ASSOCIATE** Kim Huynh **ASSISTANT COMMERCIAL EDITOR** Selby Frame **MARKETING PROJECT MANAGER** Angelissa McArthur **PROGRAM DIRECTOR, AAAS MEMBER CENTRAL** Peggy Mihelich **FULFILLMENT SYSTEMS AND OPERATIONS** membership@aaas.org **MANAGER, MEMBER SERVICES** Pat Butler **SPECIALISTS** LaToya Casteel, Terrance Morrison, Latasha Russell **MANAGER, DATA ENTRY** Mickie Napoleoni **DATA ENTRY SPECIALISTS** JJ Regan, Brenden Aquilino, Fiona Giblin

DIRECTOR, SITE LICENSING Tom Ryan **DIRECTOR, CORPORATE RELATIONS** Eileen Bernadette Moran **SR. PUBLISHER RELATIONS SPECIALIST** Kiki Forsythe **PUBLISHER RELATIONS MANAGER** Catherine Holland **PUBLISHER RELATIONS, EASTERN REGION** Keith Layson **PUBLISHER RELATIONS, WESTERN REGION** Ryan Rexroth **SALES RESEARCH COORDINATOR** Aiesha Marshall **MANAGER, SITE LICENSE OPERATIONS** Iqo Edim **SENIOR PRODUCTION SPECIALIST** Robert Koeppke **SENIOR OPERATIONS ANALYST** Lana Guz **FULFILLMENT ANALYST** Judy Lillibridge **ASSOCIATE DIRECTOR, MARKETING** Christina Schlecht **MARKETING ASSOCIATES** Thomas Landreth, Isa Sesay-Bah

WEB TECHNOLOGIES SR. DEVELOPER Chris Coleman **DEVELOPERS** Dan Berger, Jimmy Marks, Ryan Jensen **SR. PROJECT MANAGER** Trista Smith

MULTIMEDIA DIRECTOR OF ANALYTICS Enrique Gonzales **SR. WEB PRODUCER** Sarah Crespi **WEB PRODUCER** Alison Crawford **VIDEO PRODUCER** Nguyen Nguyen **SENIOR MEDIA PRODUCER** Meghna Sachdev

DIRECTOR OF OPERATIONS PRINT AND ONLINE Lizabeth Harman **DESIGN/PRINT STRATEGY MANAGER** Jason Hillman **QUALITY TECHNICAL MANAGER** Marcus Spiegel **PROJECT ACCOUNT MANAGER** Tara Kelly **DIGITAL PRODUCTION MANAGER** Lisa Stanford **ASSISTANT MANAGER DIGITAL/PRINT** Rebecca Doshi **SENIOR CONTENT SPECIALISTS** Steve Forrester, Antoinette Hodal, Lori Murphy, Anthony Rosen **CONTENT SPECIALISTS** Jacob Hedrick, Kimberley Oster

DESIGN DIRECTOR Beth Rakouskas **DESIGN EDITOR** Marcy Atarod **SENIOR DESIGNER** Garvin Grullón **DESIGNER** Chrystal Smith **GRAPHICS MANAGING EDITOR** Alberto Cuadra **SENIOR SCIENTIFIC ILLUSTRATORS** Chris Bickel, Katharine Sutliff **SCIENTIFIC ILLUSTRATOR** Valerie Altounian **SENIOR ART ASSOCIATES** Holly Bishop, Nathalie Cary, Preston Huey **SENIOR PHOTO EDITOR** William Douthitt **PHOTO EDITORS** Leslie Blizard, Christy Steele

DIRECTOR, GLOBAL COLLABORATION, CUSTOM PUBLICATIONS, ADVERTISING Bill Moran **EDITOR, CUSTOM PUBLISHING** Sean Sanders: 202-326-6430 **ASSISTANT EDITOR, CUSTOM PUBLISHING** Tianna Hicklin: 202-326-6463 **ADVERTISING MARKETING MANAGER** Justin Sawyers: 202-326-7061 **science_advertising@aaas.org** **ADVERTISING MARKETING ASSOCIATE** Javia Flemmings **ADVERTISING SUPPORT MANAGER** Karen Foote: 202-326-6740 **ADVERTISING PRODUCTION OPERATIONS MANAGER** Deborah Tompkins **SR. PRODUCTION SPECIALIST/GRAPHIC DESIGNER** Amy Hardcastle **PRODUCTION SPECIALIST** Yuse Lajimimuhip **SR. TRAFFIC ASSOCIATE** Christine Hall **SALES COORDINATOR** Shirley Young **ASSOCIATE DIRECTOR, COLLABORATION, CUSTOM PUBLICATIONS/CHINA/TAIWAN/KOREA/SINGAPORE** Ruolei Wu: +86-186 0082 9345, rwu@aaas.org **COLLABORATION/CUSTOM PUBLICATIONS/JAPAN** Adarsh Sandhu + 81532-81-5142 asandhu@aaas.org **EAST COAST/E. CANADA** Laurie Faraday: 508-747-9395, FAX 617-507-8189 **WEST COAST/W. CANADA** Lynne Stickrod: 415-931-9782, FAX 415-520-6940 **MIDWEST** Jeffrey Dembski: 847-498-4520 x3005, Steven Loerch: 847-498-4520 x3006 **UK EUROPE/ASIA** Roger Gonçalves: TEL/FAX +41 43 243 1358 **JAPAN** Katsuyoshi Fukamizu(Tokyo): +81-3-3219-5777 kfukamizu@aaas.org **CHINA/TAIWAN** Ruolei Wu: +86-186 0082 9345, rwu@aaas.org

WORLDWIDE ASSOCIATE DIRECTOR OF SCIENCE CAREERS Tracy Holmes: +44 (0) 1223 326525, FAX +44 (0) 1223 326532 tholmes@science-int.co.uk **CLASSIFIED advertise@sciencecareers.org** **U.S. SALES** Tina Burks: 202-326-6577 **Nancy Toema:** 202-326-6578 **SALES ADMINISTRATOR** Marci Gallun **EUROPE/ROW SALES** Axel Gesatzki, Sarah Lelange **ASSISTANT Kelly Grace** **JAPAN** Hiroyuki Mashiki(Kyoto): +81-75-823-1109 hmashiki@aaas.org **CHINA/TAIWAN** Ruolei Wu: +86-186 0082 9345 rwu@aaas.org **MARKETING MANAGER** Allison Pritchard **MARKETING ASSOCIATE** Aimee Aponte

AAAS BOARD OF DIRECTORS **RETIRING PRESIDENT, CHAIR** Gerald R. Fink **PRESIDENT** Geraldine (Geri) Richmond **PRESIDENT-ELECT** Barbara A. Schaaf **TREASURER** David Evans **SHAW CHIEF EXECUTIVE OFFICER** Rush D. Holt **BOARD** Bonnie L. Bassler, May R. Berenbaum, Carlos J. Bustamante, Stephen P. A. Fodor, Claire M. Fraser, Michael S. Gazzaniga, Laura H. Greene, Elizabeth Loftus, Mercedes Pascual

SUBSCRIPTION SERVICES For change of address, missing issues, new orders and renewals, and payment questions: 866-434-AAAS (2227) or 202-326-6417, FAX 202-842-1065. Mailing addresses: AAAS, P.O. Box 96178, Washington, DC 20090-6178 or AAAS Member Services, 1200 New York Avenue, NW, Washington, DC 20005

INSTITUTIONAL SITE LICENSES 202-326-6730 **REPRINTS:** Author Inquiries 800-635-7181 **COMMERCIAL INQUIRIES** 803-359-4578 **PERMISSIONS** 202-326-6765, permissions@aaas.org **AAAS Member Services** 202-326-6417 or http://membercentral.aaas.org/discounts

Science serves as a forum for discussion of important issues related to the advancement of science by publishing material on which a consensus has been reached as well as including the presentation of minority of conflicting points of view. Accordingly, all articles published in Science—including editorials, news and comment, and books reviews—are signed and reflect the individual views of the authors and not official points of view adopted by AAAS or the institutions with which the authors are affiliated.

INFORMATION FOR AUTHORS See pages 678 and 679 of the 6 February 2015 issue or access www.sciencemag.org/about/authors

SENIOR EDITORIAL BOARD

Robert H. Grubbs, *California Institute of Technology*, Gary King, *Harvard University*
Susan M. Rosenberg, *Baylor College of Medicine*, Ali Shalithard, *Northwestern University*
Feinberg School of Medicine, Michael S. Turner, *U. of Chicago*

BOARD OF REVIEWING EDITORS (Statistics board members indicated with \$)

Adriano Aguzzi, *U. Hospital Zürich*
Takuzo Aida, *U. of Tokyo*
Leslie Aiello, *Wenner-Gren Foundation*
Judith Allen, *U. of Edinburgh*
Sonia Altizer, *U. of Georgia*
Sebastian Amigorena, *Institut Curie*
Kathryn Anderson, *Memorial Sloan-Kettering Cancer Center*
Meinrat O. Andreae, *Max-Planck Inst. Mainz*
Paola Arlotta, *Harvard U.*
Johan Auwerx, *EPFL*
David Awechselom, *U. of Chicago*
Clare Baker, *University of Cambridge*
Jordi Bascompte, *University of Zurich*
Jacundo Batista, *London Research Inst.*
Ray H. Baughman, *U. of Texas, Dallas*
David Baum, *U. of Wisconsin*
Carlo Beenakker, *Leiden U.*
Kamran Behnia, *ESPCI-ParisTech*
Yasmine Belkaid, *NIH, NIH*
Philip Benfey, *Duke U.*
Stephen J. Benkovic, *Penn State U.*
May Berenbaum, *U. of Illinois*
Gabriele Bergers, *U. of California, San Francisco*
Bradley Bernstein, *Massachusetts General Hospital*
Peer Bork, *EMBL*
Bernard Bourdon, *École Normale Supérieure de Lyon*
Chris Bowler, *École Normale Supérieure*
Ian Boyd, *U. of St. Andrews*
Emily Brodsky, *U. of California, Santa Cruz*
Ron Brookmeyer, *U. of California Los Angeles (\$)*
Christian Büchel, *U. Hamburg-Eppendorf*
Joseph A. Burns, *Cornell U.*
Carter Tribble Butts, *U. of California, Irvine*
Gyorgy Buzsaki, *New York U. School of Medicine*
Blanche Capel, *Duke U.*
Mats Carlsson, *U. of Oslo*
Ib Chorkendorff, *U. of Denmark*
David Clapham, *Children's Hospital Boston*
David Clary, *U. of Oxford*
Joel Cohen, *Rockefeller U., Columbia U.*
James J. Collins, *MIT*
Robert Cook-Deegan, *Duke U.*
Alan Cowman, *Walter & Eliza Hall Inst.*
Robert H. Crabtree, *Yale U.*
Roberta Croce, *Vrije Universiteit*
Janet Currie, *Princeton U.*
Jeff L. Dangi, *U. of North Carolina*
Tom Daniel, *U. of Washington*
Frans de Waal, *Emory U.*
Stanislas Dehaene, *Collège de France*
Robert Desimone, *MIT*
Claude Desplan, *New York U.*
Ap Dijksterhuis, *Radboud U. of Nijmegen*
Dennis Discher, *U. of Pennsylvania*
Gerald W. Dorn II, *Washington U. School of Medicine*
Jennifer A. Doudna, *U. of California, Berkeley*
Bruce Dunn, *U. of California, Los Angeles*
William Dunphy, *Caltch*
Christopher Dye, *WHO*
Todd Ehlers, *U. of Tübingen*
David Ehrhardt, *Carnegie Inst. of Washington*
Tim Elston, *U. of North Carolina at Chapel Hill*
Gerhard Ertl, *Fritz-Haber-Institut, Berlin*
Barry Everitt, *U. of Cambridge*
Ernst Fehr, *U. of Zurich*
Anne C. Ferguson-Smith, *U. of Cambridge*
Michael Feuer, *The George Washington U.*
Toren Finkel, *NHLBI, NIH*
Kate Fitzgerald, *U. of Massachusetts*
Peter Fratzl, *Max-Planck Inst.*
Elaine Fuchs, *Rockefeller U.*
Daniel Geschwind, *UCLA*
Karl-Heinz Glassmeier, *TU Braunschweig*
Ramon Gonzalez, *Rice U.*
Julia R. Greer, *Caltch*
Elizabeth Grove, *U. of Chicago*
Nicolas Gruber, *ETH Zurich*
Kip Guy, *St. Jude's Children's Research Hospital*
Taekjip Ha, *U. of Illinois at Urbana-Champaign*
Christian Hassel, *Ludwig Maximilians U.*
Michael Hasselmo, *Boston U.*
Martin Heimann, *Max-Planck Inst. Jena*
Yka Helariutta, *U. of Cambridge*
James A. Hendler, *Rensselaer Polytechnic Inst.*
Janet G. Hering, *Swiss Fed. Inst. of Aquatic Science & Technology*
Kai-Uwe Hinrichs, *U. of Bremen*
Kei Hirose, *Tokyo Inst. of Technology*
David Hodell, *U. of Cambridge*
David Holden, *Imperial College*
Lora Hooper, *UT Southwestern Medical Ctr. at Dallas*
Raymond Huey, *U. of Washington*
Auke Ijspeert, *EPFL Lausanne*
Steven Jacobsen, *U. of California, Los Angeles*
Kai Jonsson, *EPFL Lausanne*
Peter Jonas, *Inst. of Science & Technology (IST) Austria*
Matt Kaeberlein, *U. of Washington*
William Kaelin Jr., *Dana-Farber Cancer Inst.*
Daniel Kahne, *Harvard U.*
Daniel Kammen, *U. of California, Berkeley*
Masashi Kawasaki, *U. of Tokyo*
Y. Narry Kim, *Seoul National U.*
Joel Kingsolver, *U. of North Carolina at Chapel Hill*
Robert Kingston, *Harvard Medical School*
Etienne Kochlin, *École Normale Supérieure*
Alexander Koldkin, *Johns Hopkins U.*
Leonid Kruglyak, *UCLA*
Thomas Langer, *U. of Cologne*
Mitchell A. Lazar, *U. of Pennsylvania*
David Lazer, *Harvard U.*
Thomas Lecuit, *IBDM*
Virginia Lee, *U. of Pennsylvania*
Stanley Lemon, *U. of North Carolina at Chapel Hill*
Ottoline Leyser, *Cambridge U.*
Wendell Lim, *U.C. San Francisco*
Marcia C. Linn, *U. of California, Berkeley*
Jianguo Liu, *Michigan State U.*
Luis Liz-Marzan, *CIC biomaGUNE*
Jonathan Losos, *Harvard U.*
Kai Lu, *Chinese Acad. of Sciences*
Christian Lüscher, *U. of Geneva*
Laura Machesky, *CRUK Beatson Inst. for Cancer Research*
Anne Magurran, *U. of St. Andrews*
Oscar Marin, *CSIC & U. Miguel Hernández*
Charles Marshall, *U. of California, Berkeley*
C. Robertson McClung, *Dartmouth College*
Graham Medley, *U. of Warwick*
Tom Misteli, *NCI*
Yasushi Miyashita, *U. of Tokyo*
Mary Ann Moran, *U. of Georgia*
Richard Morris, *U. of Edinburgh*
Alison Moutser-Reif, *NC State U. (\$)*
Thomas Murray, *The Hastings Center*
James Neuman, *Stanford U. School of Med.*
Daniel Neukam, *U. of California, Berkeley*
Kitty Niemeijer, *U. of Twente*
Pär Nordlund, *Karolinska Inst.*
Helga Nowotny, *European Research Advisory Board*
Ben Olken, *MIT*
Joe Orenstein, *U. of California Berkeley & Lawrence Berkeley National Lab*
Harry Orr, *U. of Minnesota*
Andrew Oswald, *U. of Warwick*
Steve Palumbi, *Stanford U.*
Jane Parker, *Max-Planck Inst. of Plant Breeding Research*
Giovanni Parmigiani, *Dana-Farber Cancer Inst. (\$)*
Donald R. Paul, *U. of Texas, Austin*
John H. J. Petrini, *Memorial Sloan-Kettering Cancer Center*
Samuel Pfaff, *Salk Institute for Biological Studies*
Joshua Plotkin, *U. of Pennsylvania*
Albert Polman, *FOM Institute AMOLF*
Philippe Pouchin, *CNRS*
Jonathan Pritchard, *Stanford U.*
David Randall, *Colorado State U.*
Colin Renfrew, *U. of Cambridge*
Felix Rey, *Institut Pasteur*
Trevor Robbins, *U. of Cambridge*
Jim Roberts, *Fred Hutchinson Cancer Research Ctr.*
Barbara A. Romanowicz, *U. of California, Berkeley*
Amy Rosenzweig, *Northwestern University*
Jens Rostrup-Nielsen, *Haldor Topsøe*
Mike Ryan, *U. of Texas, Austin*
Mitsunori Saitou, *Kyoto U.*
Shimon Sakaguchi, *Kyoto U.*
Miguel Salmeron, *Lawrence Berkeley National Lab*
Jürgen Sandkühler, *Medical U. of Vienna*
Alexander Schier, *Harvard U.*
Randy Seeley, *U. of Cincinnati*
Vladimir Shalaev, *Purdue U.*
Robert Siliciano, *Johns Hopkins School of Medicine*
Denis Simon, *Arizona State U.*
Uri Simonsohn, *U. of Pennsylvania*
Alison Smith, *John Innes Centre*
Richard Smith, *U. of North Carolina (\$)*
John Speakman, *U. of Aberdeen*
Allan C. Spradling, *Carnegie Institution of Washington*
Jonathan Sprent, *Garvan Inst. of Medical Research*
Eric Steig, *U. of Washington*
Paula Stephan, *George State U. and National Bureau of Economic Research*
Molly Stevens, *Imperial College London*
V. S. Subrahmanian, *U. of Maryland*
Ira Tabas, *Columbia U.*
Sarah Teichmann, *Cambridge U.*
John Thomas, *North Carolina State U.*
Shubha Tole, *Tata Institute of Fundamental Research*
Christopher Tyler-Smith, *The Wellcome Trust Sanger Inst.*
Herbert Virgin, *Washington U.*
Beth Vogelstein, *Johns Hopkins U.*
Cynthia Volkert, *U. of Göttingen*
Douglas Wallace, *Dalhousie U.*
David Wallace, *Weizmann Inst. of Science*
Ian Walmsey, *U. of Oxford*
Jane-Ling Wang, *U. of California, Davis*
David A. Wardle, *Swedish U. of Agric. Sciences*
David Waxman, *Fudan U.*
Jonathan Weissman, *U. of California, San Francisco*
Chris Wikle, *U. of Missouri (\$)*
Ian A. Wilson, *The Scripps Res. Inst. (\$)*
Timothy D. Wilson, *U. of Virginia*
Rosemary Wyse, *Johns Hopkins U.*
Jan Zaenen, *Leiden U.*
Kenneth Zaret, *U. of Pennsylvania School of Medicine*
Jonathan Zehr, *U. of California, Santa Cruz*
Len Zon, *Children's Hospital Boston*
Maria Zuber, *MIT*

BOOK REVIEW BOARD

David Bloom, *Harvard U.*, Samuel Bowring, *MIT*, Angela Creager, *Princeton U.*, Richard Sweder, *U. of Chicago*, Ed Wasserman, *DuPont*

Japan's longevity challenge

Japan is the frontrunner of aging societies in terms of longevity and the proportion of the elderly in the population. In 2030, one-third of the population will be older than age 65, and 20% will be older than 75 years. Moreover, 75-year-old seniors in Japan are as physically healthy as those a decade younger, according to a recent government survey. If Japan is to deal effectively with the highly aged society of the future, and benefit from this growing sector of its society, it must come up with a new socially inclusive system for people living into their nineties or more.

Currently, Japan treats the period after retirement at age 65 as the “sunset years” of one’s life, effectively discouraging even healthy retirees from working. This situation challenges Japan’s social security system and the national economy. In 1965, 9.1 persons could support one senior citizen in the social security system. This dependency ratio is now 2.4 persons to one senior, and should decrease to 1.3 to one in 2050. Social security benefits will exceed 100 trillion yen in 2030. With 15% of the work force expected to be lost by then, meeting this need will be a problem. The good news is that according to a government survey, over 80% of seniors would like to work after retirement and contribute to the economy rather than be a recipient of government assistance.

Putting these considerations together, an expansion of job opportunities for seniors is essential if Japanese society is to enhance the labor force, social security finance, and economic development. There are workable strategies to address these challenges. Currently, 80% of Japanese are expected to be healthy until their mid-70s and want to contribute to society. Thus, maintaining a healthy life span for this population is essential not only for supplementing the shrinking labor force, but for containing health care costs and bolstering the consumer market with active seniors.

To achieve this healthy life span, maintaining senior quality of life is crucial. New living environments are needed that will allow seniors to “age in place” while nurturing good physical, mental, and social habits that could delay, or even avert, the onset of declining conditions such as frailty and dementia. Lifelong learning will allow seniors not only to maintain their overall well-being, but to integrate into a working society. Here,

universities should expand programs that help seniors to improve skills, gain new knowledge, and nurture new interests. Japan also must accommodate a diversity of health and lifestyle issues of the senior community by providing a variety of workplaces and work styles. Employers can capitalize on an individual’s strengths while compensating for weaknesses. Innovative approaches can be devised for the work-sharing of abilities as well as of time. Advances in information technology and robotic technology can address an employer’s concerns about safety and productivity that hamper employment of older workers. For example, telecommuting and biomechanical assistive technology (such as a “smart suit” for manual labor) would not

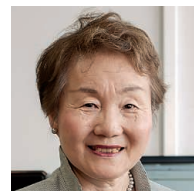
only improve the work environment for senior workers, but lead to healthy and enjoyable work places for workers of all ages. A new government project in Kashiwa City, in cooperation with Tokyo University, is an experimental community designed to support a long-lived society in these ways, and its social infrastructure could serve as a model for other community projects.

The current employment system and senior life environment in Japan are built on an obsolete model of life span. Today, someone celebrating a 65th birthday can expect about 20 years of a “second life” ahead. The next generation of elderly will be healthier and better educated. Given the right platform, they can continue to be active contributors to society well into their golden age.

– Hiroko Akiyama



“The next generation of elderly will be healthier and better educated.”

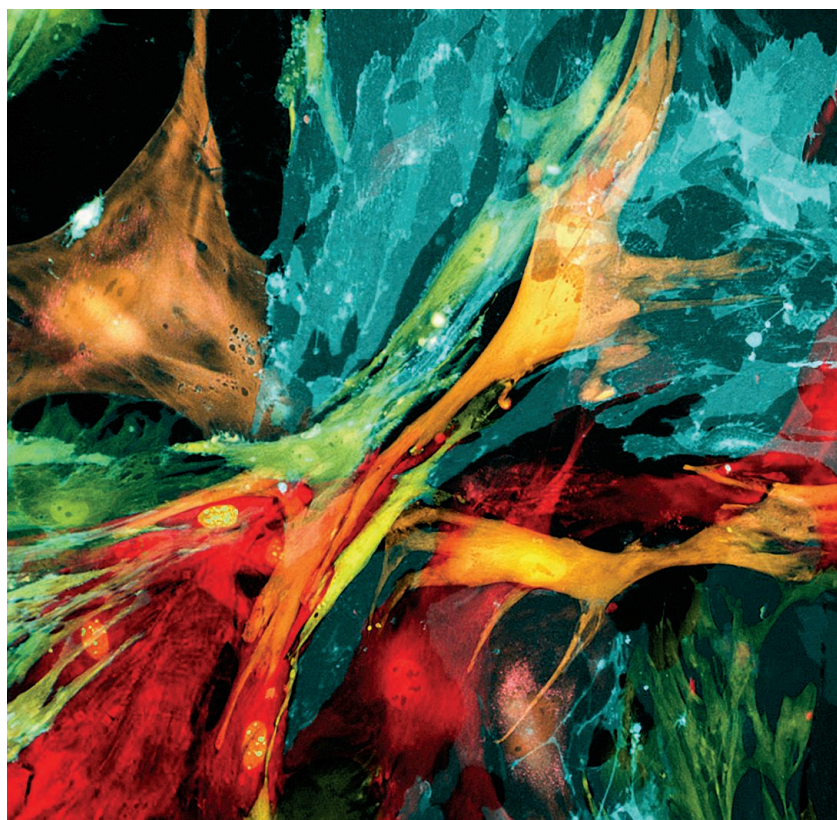


Hiroko Akiyama is a professor at the Institute of Gerontology at the University of Tokyo, 7-3-1 Hongo, Bunkyo-ku, Tokyo, Japan. E-mail: akiyama@iog.u-tokyo.ac.jp

Global investment in Ebola research in 2014 in response to the West African epidemic, according to G-FINDER, an annual report on R&D on neglected diseases. Before 2014, G-FINDER didn't keep track because of Ebola's very low disease burden.

IN BRIEF

BioArt finds beauty in spreading cells, Ebola, roundworms



The above image isn't of a glass coffee table sculpture; it shows how fluorescent labeling can be used to track the spread of cells from different tumors in mice with pancreatic cancer. From these multicolored cells to roundworms congregating to feed on bacteria to structural proteins of the Ebola virus, the 2015 winners of the Federation of American Societies for Experimental Biology's (FASEB) BioArt competition reveal the artistic—even disconcertingly attractive—side of some of the less attractive subjects in the biomedical and life sciences. In all, the winners of the fourth annual competition, unveiled last week on FASEB's website (www.faseb.org), include 11 images and two videos.

AROUND THE WORLD

U.N. notes AIDS progress, gaps

GENEVA, SWITZERLAND | Of the estimated 36.9 million people in the world infected with HIV, 70% of them live in sub-Saharan Africa. Of these, 49% do not know their HIV status, according to a report released last week by the Joint United Nations Programme on HIV/AIDS, and about 57% are not receiving antiretroviral drugs. The document, published on the eve of World AIDS Day, 1 December, celebrates the progress that has been made in reversing the spread of HIV/AIDS by getting antiretrovirals to 15.8 million people by June of 2015. But it also notes that many countries are still far from meeting World Health Organization guidelines issued in September, which recommend early antiretroviral treatment for every infected person. Recent evidence shows that fully suppressing infection by initiating treatment early benefits an individual's health and sharply decreases transmission rate. But in sub-Saharan Africa, the report notes, an estimated 68% of infected people remain untreated.

French call for terror studies

PARIS | Many French researchers have welcomed a call by the National Center for Scientific Research (CNRS) for study proposals to help understand and prevent terrorism in the wake of the 13 November attacks that killed 130 and profoundly shocked the country. The call came in a 18 November letter from CNRS president Alain Fuchs, who described it as "a rare



Memorials commemorate victims of the Paris attacks.

PHOTOS: (LEFT TO RIGHT) HEINZ BAUMANN, SEAN T. GLENN, MARY KAY ELLSWORTH, AND KENNETH W. GROSS / ROSWELL PARK CANCER INSTITUTE / FASEB BIOART COMPETITION; © PACIFIC PRESS / CORBIS

Downloaded from www.sciencemag.org on December 6, 2015



A study of zebrafish upends a key argument against awareness in fish.

Fish show signs of sentience in 'emotional fever' test

Scientists have long believed that fish aren't capable of the same awareness as humans because they fail the "emotional fever" test. Birds, mammals (including humans), and at least one species of lizard experience a slight rise in body temperature—about 1°C to 2°C—when exposed to new environments; the fever is linked to emotions because it's triggered by an outside stimulus, yet produces behavioral and physiological changes. Previous tests suggested that toads and fish don't react this way, but a new experiment reported last week in the *Proceedings of the Royal Society B* suggests fish

can indeed get stressed. Researchers confined some zebrafish to a chamber in a tank containing water at about 27°C (zebrafish prefer water of about 28°C), and allowed others to swim freely around five other chambers in the tank, each heated to a temperature between 17.92°C and 35°C. After about 15 minutes, the team set the confined fish free to roam through the chambers. The stressed fish spent more time in warmer waters than did the control fish, thus raising their body temperatures by about 2°C to 4°C—the fish equivalent of an emotional fever, the scientists say.

opportunity for researchers to express a form of solidarity with all those who, directly or indirectly, have been affected" by the attacks. The letter doesn't specify topics of interest or a budget, but CNRS promises "a rigorous, simple and rapid procedure" for applicants that will allow the first research results to emerge next year. <http://scim.ag/Attackstudies>

Spain to create funding agency

MADRID | The Spanish government finally made good on its promise to create a national science funding agency on 27 November when it announced the launch of the State Research Agency. The government says the new body, which was promised in a science law passed in 2011, will create a more stable funding stream and "more agile, flexible, and autonomous" management procedures. Although Spain's scientific community had long pleaded for a granting agency, some have doubts about the plan. Few operational details have been revealed, and there are questions about the scientific independence of the agency's

management. Some researchers also wonder about the agency's future if the ruling People's Party loses Spain's parliamentary elections, slated for 20 December. <http://scim.ag/SpainFunding>

FINDINGS

New signs of dinosaur proteins

In a series of papers since 2007, researchers led by Mary Schweitzer, a paleontologist at North Carolina State University in Raleigh, have reported that they've isolated fragments of intact collagen—a protein found in connective tissue and bones—from dinosaurs as old as 80 million years. Critics have raised concerns that the protein fragments were contaminants from bacteria or other organisms, as proteins normally decay within a few hundred thousand years after an animal dies. Now, Schweitzer and a new set of colleagues report in the *Journal of Proteome Research* that they have extracted samples from what appear, under a microscope, to be blood vessels in bone. After analyzing these samples, the team

says, they found signatures of vertebrate collagen and blood proteins.

Gender overlaps in human brains

Human brains do not fit neatly into "male" and "female" categories, scientists reported this week in the *Proceedings of the National Academy of Sciences*. The researchers used existing sets of MRI brain images to measure the volume of gray matter (the knobby tissue that contains the core of nerve cells) and white matter (the bundles of nerve fibers that transmit signals) in the brains of more than 1400 individuals. Based on a few structural differences found more often in men or women—for example, men generally had a larger left hippocampus, associated with memory—the team created a continuum of "femaleness" to "maleness" for the entire brain. But the majority of the studied brains, they found, were a mosaic of male and female structures; only 0% to 8% of the brains contained all-male or all-female structures. <http://scim.ag/genderbrains>



NATURAL DISASTERS

Mud tsunami wreaks ecological havoc in Brazil

Researchers analyze sludge for heavy metals and assess potential for recovery

By **Herton Escobar**, in *Espírito Santo, Brazil*

When Dante Pavan first heard the news of last month's mining dam collapse in southeastern Brazil, he never imagined that the wave of sludge would travel all the way to his family's old farmstead, hundreds of kilometers downstream. But as the scale of the disaster became clearer, the zoologist threw sampling gear in his truck and sped north from São Paulo for a rendezvous with the killer mud. When he saw the Doce River stained a dark orange by the iron-laced mine tailings, his first reaction was that the river "is going to turn into a fossil bed."

Now, he and other researchers are trying to forecast the river's prospects for recovery from the disaster, unleashed on 5 November when a dam holding approximately 50 million cubic meters of waste from iron mines burst without warning near the city of Mariana in Minas Gerais state. Pavan is part of a network of scientists, backed by crowdfunding, that is analyzing river samples to assess the environmental impacts independently of the government and the mining companies that managed the dam. One controversy they hope to settle is whether the sludge was laced with two dozen heavy metals, including arsenic, cop-

per, and mercury, and whether such toxic contamination will persist and spread through the food chain, delaying recovery.

The immediate impacts of the tsunami were tragic. It buried villages downstream, killing at least 13 people, mostly in Bento Gonçalves, the district nearest the dam. Within a day, the wave reached the Doce, one of Brazil's largest rivers outside the Amazon basin, and traversed 600 kilometers before spilling into the Atlantic Ocean on 21 November. Before the mud reached the

sea on the north coast of Espírito Santo state, environmentalists raced to dig up hundreds of nests of endangered loggerhead and leatherback sea turtles and move them to a safe haven. Brazil dispatched its new oceanographic research vessel, the *Vital de Oliveira*, to monitor the mud plume's effects on marine life. Speaking at the climate summit in Paris earlier this week, Brazil President Dilma Rousseff called the dam collapse "the worst environmental disaster in the history of Brazil."

In the Doce and two small rivers near the dam, the sludge destroyed the base of the food chain—plankton, algae, freshwater shrimp, and other life forms—says Pavan, an independent consultant who specializes in environmental impact assessments for infrastructure projects in the Amazon. "From what we can see on the surface, the impacts are tremendous," adds Alexandre Martensen, a Brazilian ecologist at the University of Toronto in Canada who helped organize the network of researchers responding to the disaster.

Pavan was one of the first scientists to sample the spill, and his quick response could shed light on how long those impacts might last. Downstream from where he first encountered the mud, he collected water and sediment samples before and after its

Trail of destruction

After a mining dam burst on 5 November, a mud tsunami killed at least 13 people in Bento Gonçalves district and devastated aquatic life in the Doce River.



A Brazilian Navy ship on 22 November skirts a plume of killer mud spilling from the Doce River into the Atlantic Ocean.

passage. Dozens of scientists in several labs will study these and other samples still being collected; the University of Brasília will take the lead on the heavy metal analyses. They hope to sort out conflicting claims about the nature of the pollution.

The mine's owner, Samarco—jointly held by two of the world's largest mining companies, Vale and BHP Billiton—insists that the tailings deposited behind the dam were simply clay and silt. Analyses carried out by the federal government corroborate that claim; state and municipal agencies, however, say they have found elevated levels of heavy metals at downstream sites. Vale and BHP Billiton argue that the river's sediments were polluted before the mud arrived. The federal and state governments have sued the companies for 20 billion reais (about \$5 billion) in damages.

Long stretches of the Doce are still stained orange, and authorities have declared the water unfit for swimming, drinking, or fishing. River conditions should be back to normal in a few months, after summer rains flush out most of the sediments, predicts Paulo Rosman, a coastal and oceanographic engineer at the Federal University of Rio de Janeiro. "The worst has passed," he says. But regardless of whether the sludge carried toxic metals, aquatic life will be slow to recover, in no small measure because the river was in a fragile state at the outset. Its ecosystems were already under assault from pollution and excessive runoff. And because of an extreme, ongoing drought, the Doce had little water to dilute the sludge and few sanctuaries where aquatic life could escape the orange tide.

In the river's lower reaches, researchers teamed up with local fishers to rescue native fish, mollusks, and crustaceans before the onslaught and transfer them to breeding tanks. The goal was to create a "genetic reservoir" of biodiversity, so that species could be reintroduced if necessary. In the meantime, scientists will have a rare opportunity to observe a major river reboot its ecosystems. Most of the Doce River's fish biomass was resilient exotic species like tilapia and dorado, which are likely to have an upper hand over native species during recolonization, says Adriano Paglia, an ecologist at the Federal University of Minas Gerais in Belo Horizonte.

"It's possible some local species will disappear," Paglia says. "Whatever comes back will be just a sample of the diversity that existed before." ■

Herton Escobar writes for *O Estado de S. Paulo newspaper*.

BIOCHEMISTRY

DNA helps build molecular libraries for drug testing

Pharmaceutical firms and biotech companies embrace DNA-encoded chemical libraries

By Trisha Gura

In the painstaking work of synthesizing vast numbers of compounds and identifying those that are the best candidate drugs, researchers have cultivated a capable new lab assistant: DNA. At a meeting last month just outside Boston, chemists and biologists discussed the promise of DNA-encoded chemical libraries (DELs), which rely on DNA's unique talents to track, select, and even synthesize compounds that bind to enzymes, receptors, and other biological targets. Faster, cheaper, and more versatile than traditional screening methods, the technology is a potential game-changer for academics who want to probe the workings of biological molecules, and it has already yielded drug candidates entering clinical trials.

DEL "is no longer a technology in development," says Christopher Davie, manager of Discovery Chemistry at GlaxoSmithKline (GSK) and co-organizer of the First Boston Symposium of Encoded Library Platforms, held in Waltham, Massachusetts. "It's really an established platform now." And it is allowing basic scientists and small companies to generate impressive libraries of molecules, on a scale once reserved for big pharma, and select from them the most useful compounds.

DELs are built in multiple ways, but the basic idea is to label chemical building blocks or newly made compounds with

short DNA fragments that serve as "bar codes" for identification. In some cases, chemists record the steps of building a compound by tacking on another snippet of DNA after each chemical reaction (see diagram, below). The resulting compounds are then tested for their ability to bind a target. To identify those that bound so that they can be resynthesized, researchers

simply read the combined DNA sequence. In other cases, chemists tag molecular subunits with complementary single strands of DNA. When these strands come together to hybridize, they pull the building blocks close together so that they are more likely to react to form a compound. Repeated cycles with various reactant combinations allows the generation of many, diverse compounds.

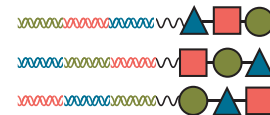
In traditional high throughput screens, potential compounds are added individually to wells containing the target to see if any inhibit or otherwise affect target activity. While that approach can be automated with robotics, it still makes testing large numbers of compounds relatively slow and expensive. Harnessing DNA to fashion molecular libraries, in contrast, allows immense numbers of compounds to be tested at the same time, in a single vessel, reducing the cost of screening by up to six orders of magnitude, according to some estimates.

In 1992, Sydney Brenner and Richard Lerner at the Scripps Institute in San Diego, California, were the first to propose the full

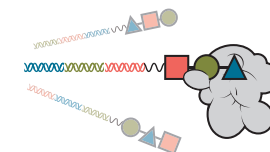
The DNA advantage

DNA can aid the search for drug candidates by recording how each compound is built and identifying any that bind to a target.

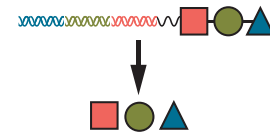
1 After each new chemical building block is added, a DNA tag for that block is appended.



2 The library of compounds is applied to a drug target to find those that bind.



3 Reading the DNA tags of any "hits" reveals assembly order.



4 Compounds can be resynthesized and developed into drug leads.



DEL approach. They realized that the recently invented polymerase chain reaction (PCR) made it possible to quickly and easily amplify—and thereby detect—the DNA tag on a compound bound to a target. That compound could then be resynthesized without the DNA attached for further testing. Brenner and Lerner “had it nailed,” says meeting co-organizer Robert Goodnow, Jr., executive director of the Chemistry Innovation Center at AstraZeneca in Waltham, Massachusetts. They proffered “all the critical pieces necessary to start this technology.”

But Brenner and Lerner only offered “a thought experiment,” Goodnow notes. It took the next two decades for chemists to prove out the method, generating DNA-tethered compounds that could bind biological targets—and alter their activity. In 2006, big pharma signaled that it was warming to the concept: GSK acquired Praecis Pharmaceuticals, a startup in Waltham, Massachusetts, that was using DEL technology to generate potential drug candidates. Now “there isn’t a big pharma company without a deal” with a group specializing in DELs, says chemist Nils Jakob Vest Hansen, a former scientist at Praecis who spun off his own unique variant of the technology to found Vipergen ApS in Copenhagen.

“We have proven that we can make libraries with this sort of chemical diversity and actually find ligands” [for drug targets], adds Christine Donahue, GSK’s head of NCE Molecular Discovery. “We are now asking, ‘Can we find a medicine?’”

The answer appears to be a cautious yes. GSK’s most-advanced, DEL-derived candidate, a former-Praecis “hit,” targets an enzyme called soluble epoxide hydrolase and is now entering phase II clinical trials for chronic obstructive pulmonary disease. Other potential drugs discovered via DELs are in the pipeline for pulmonary fibrosis, psoriasis, and other inflammatory diseases.

DELs can also illuminate basic biology, chemical biologist David Liu at Harvard University told the meeting. Liu has created a library of 14,000 so-called DNA-templated macrocycles: sturdy, ringed compounds, usually built of carbon, that have been assembled using the pairing of single-stranded DNAs to orchestrate their chemical synthesis. He applied the library to a potential target for diabetes, a zinc-binding enzyme that breaks down insulin.

Scientists had speculated for 6 decades that inhibiting this metalloprotease, called insulin-degrading enzyme (IDE), could help diabetics by raising insulin levels in the blood. Traditional high throughput screens had yielded inhibitors, but animal tests showed that they lacked the specificity or stability necessary to target only the insulin-destroying function of the enzyme. Trying a new way, Liu mixed his whole library of DNA-templated macrocycles with the IDE target and fished out a macrocycle dubbed 6bK. It locked onto the enzyme in an unexpected place, binding to a pocket not found in other metallo-proteases, located away from the site where the insulin-cutting takes place.

In follow-up in vitro experiments, Liu and collaborators showed that 6bK blocked IDE activity, and in standard, oral tests of glucose tolerance in obese mice it consistently lowered blood sugar. But when the test was conducted with injected rather than ingested glucose, 6bK had a paradoxical effect: making the animals more diabetic. Liu’s team ultimately found that IDE destroys not just insulin but also two hormones that can alter blood sugar: glucagon and amylin. Preserving them—more than insulin—by globally blocking IDE pushes the animals into diabetes.

Liu now hopes to parlay that discovery into druglike compounds that can selectively block IDE’s ability to degrade insulin. Using 6bK, his team did a traditional screening of 20,000 compounds from the Broad Institute in Cambridge, Massachusetts, to see if any could displace 6bK from its binding pocket on the enzyme. The team identified several compounds that protected insulin from breakdown, while allowing IDE to continue destroying glucagon and amylin. After chemically optimizing these compounds to boost potency, Liu is currently discussing prospects for further development with several pharmaceutical companies and venture capital groups. Whether or not a medicine results, he says the work shows the power of DELs for both basic research and drug development.

The speed and low cost of DELs is “liberating,” says chemist Dario Neri at ETH in Zürich, Switzerland, who gave the keynote address at the symposium. “Years ago, I could not dream of competing with a large pharmaceutical company for a high throughput facility. But with this technology we can.” ■

Trisha Gura is a writer in Boston.

FUNDING

U.K. research wins hollow victory

Budget is protected for 5 years, but lags because of past inflation

By Erik Stokstad

At first, the reaction was relief. U.K. research was braced for a swing of the budget at last week, when the Conservative government announced its blueprint for spending over the next 5 years. Science, however, was spared the painful cuts inflicted on other areas of government spending. But now, “as the dust settles, more people are thinking this is not such a good deal,” says cell biologist Jenny Rohn of University College London, head of the lobby group Science is Vital.

One reason for the second thoughts: After 5 years of eroding budgets, researchers fear that the flat, “ring-fenced” budgets promised by finance minister George Osborne will not repair the damage. Scientists are also concerned that the government’s penchant for lobbying money at special initiatives is undermining researchers’ ability to decide on priorities. “It’s not a strategic way of doing things, and that has caused unease,” says physicist Athene Donald of the University of Cambridge.

The build-up to the 5-year spending review had been tense. The government wants to balance the United Kingdom’s £742 billion annual budget and pay down the debt. After the Conservatives won a surprise majority in the general election in May, Osborne asked departments, including the Department for Business, Innovation & Skills (BIS) which handles most of the public science spending, to draw up plans for cuts of up to 40%. “That set alarm bells ringing,” says Paul Crowther, an astrophysicist at the University of Sheffield.

In the event, research got off lightly when Osborne revealed his spending plan: The science budget will be held constant in real terms, with adjustments for inflation. “It could have been a hell of a lot worse,” says Philip Moriarty, a physicist at the University of Nottingham.

Osborne was lucky with a surprise

£27 billion from lower interest on the national debt and predicted rising tax revenue. Annual BIS funding will still fall 17% to £11.5 billion for 2020, but the science portion of its portfolio—£4.7 billion a year—will be protected. This includes the money that the U.K.'s Medical Research Council (MRC) and six other research councils distribute as grants and general funding awarded to universities based on overall research quality. In addition, BIS will spend £6.9 billion over 5 years for science facilities and infrastructure such as Britain's share of the Square Kilometre Array radio telescope and a new polar research ship.

Osborne also announced a doubling of energy research funding to £100 million per year, with half to be spent on small modular nuclear reactors. "It's a strong signal that we need more energy innovation," says Richard Jones, vice chancellor of the University of Sheffield. But that strong signal doesn't extend as far as the Department of Energy & Climate Change, which faces a 22% budget cut including £1 billion meant to support carbon capture and storage demonstration plants.

Much of the funding for health research is channeled through the United Kingdom's National Health Service, which was awarded £1 billion a year for the National Institute for Health Research (NIHR), a slight bump up from previous budgets. NIHR supports biomedical research centers and, like the MRC, funds investigator-initiated grants. In addition, the state-owned company Genomics England will receive £250 million over 5 years, a 12.6% boost, according to *Science's*

analysis, to help it finish sequencing the genomes of 100,000 people. Another £150 million from the capital budget will go toward an institute for research on dementia. And a fund using £1 billion of U.K. overseas development aid and run in collaboration with the Bill & Melinda Gates Foundation will support research and development of vaccines, drugs, and tests for malaria and other infectious diseases.

In spite of the good news, U.K. researchers remain worse off than they were in 2010, because for the past 5 years the science budget was not protected against inflation and eroded in real terms. The Campaign for Science & Engineering, a lobbying group, estimates that the erosion has deprived the research councils and other recipients of £1 billion over 5 years. The impact has been felt by facilities such as the £400-million ISIS neutron source in Oxfordshire, which has run for two-thirds its usual number of days as it couldn't pay electricity costs, according to a recent report from the House of Commons' Science and Technology Committee.

Research leaders point out that this has caused the United Kingdom to slip further down the international funding table. The U.K. government, they say, spends a smaller fraction—0.49% in 2013—of gross domestic product on public funding of science and technology than do other industrialized countries—about 40% less

than Germany and the United States. "You simply can't survive in a competitive environment like that," says neuroscientist Colin Blakemore of University of London's School of Advanced Study, a former director of the MRC.

Meanwhile, the government is launching research initiatives in a way that some scientists question. As part of the ring-fenced science budget, Osborne touted a new £1.5 billion fund for infectious disease that will, in effect, reduce the sums remaining for researchers to devote to scientific priorities they choose. "The government is more and more deciding what areas of science should be funded," Blakemore worries.

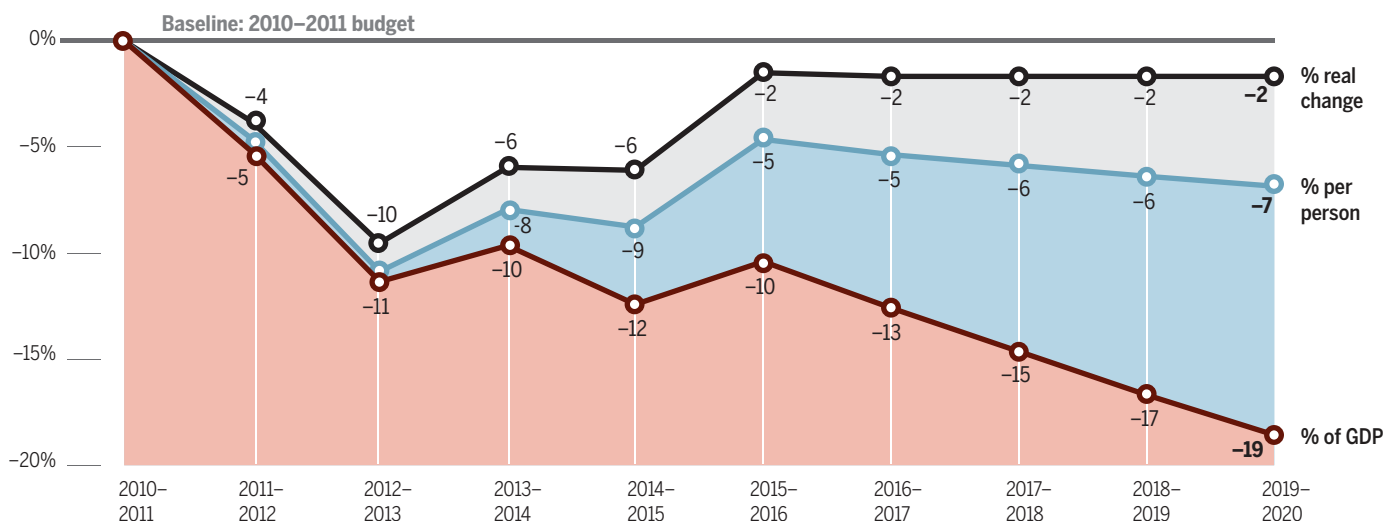
A recent review of the research councils by Paul Nurse, president of the Royal Society, calls for a new top-level fund for interdisciplinary research, grand challenges, and rapid-response grants. Although Osborne said the government would follow Nurse's recommendations, it's not clear how big that fund will be and whether it will also sap the budgets of the research councils. Some of these questions may be answered when the detailed funding allocations for the councils are announced early next year. Nurse hopes that his recommendations—including the creation of an overarching council called Research UK, to be headed by a distinguished scientist—will help raise the stature of science. ■

"As the dust settles, more people are thinking this is not such a good deal."

Jenny Rohn, Science is Vital

Mending a broken ring fence

The science budget for the United Kingdom was protected from cuts between 2010 and 2015, but its real value was eroded by inflation. Going forward, the budget will be adjusted for inflation. That may not stop a decline in investment relative to GDP.



SPACE SCIENCE

Japanese probe primed for second run at Venus

Akatsuki spacecraft aims to plumb planet's weird atmosphere

By Dennis Normile, in Sagami-hara, Japan

Believers in second chances will be rooting next week for a space probe as it tries again to orbit Venus. Japan's Akatsuki spacecraft, designed to study the planet's curious atmosphere, shot past its target in December 2010 when its main engine malfunctioned. After whipping around the sun 10 times since then, the star-crossed probe will get its shot at redemption on 7 December, when mission control plans to use four small attitude-control thrusters to slow it on its latest approach to Venus.

Planetary scientists are crossing their fingers that the improvised retrorockets do the job. "It's risky," says Colin Wilson, a Venus specialist at the University of Oxford in the United Kingdom. However, he says, "I've great trust in the expertise of Akatsuki controllers and the team behind them."

Akatsuki's 2-year mission aims to peel away some of the mystery of Venus's dense, cloudy atmosphere. Mostly carbon dioxide, it includes a 20-kilometer-thick layer of sulfuric acid clouds, and it sweeps over the planet at speeds exceeding 300 kilometers per hour, or 60 times faster than Venus itself rotates. What drives the superrotation "is a fundamental physics question," says Sanjay Limaye, a planetary scientist at the University of Wisconsin, Madison, and member of the Akatsuki scientific team. To try to answer it, the probe will use a suite of cameras to observe cloud formation and movement as well as heat flux from the planet's surface to the upper atmosphere. It will also record lightning flashes and send radio signals through the atmosphere to receivers on Earth to probe its temperature and composition.

Akatsuki is the second spacecraft in a decade to peer into the venusian atmosphere. The European Space Agency's (ESA's) Venus Express mission, which ran from 2006 to 2014, "filled in quite a bit of the knowledge gap about [Venus'] clouds and atmosphere," Limaye says. Venus Express revealed that the atmosphere seems to be suffused with water vapor, that there is an unexpectedly large temperature gradient from surface to upper atmosphere, and that the superrotation is, perplexingly, speeding up. But it did not solve the superrotation mystery. Combining data from Venus Express and Akatsuki "certainly will lead to an improvement

of the understanding of the dynamics of the atmosphere of Venus," says Håkan Svedhem, Venus Express project scientist at ESA in Noordwijk, the Netherlands.

Launched on 20 May 2010, Akatsuki experienced smooth sailing until the orbital insertion attempt that December. After losing contact with the craft, controllers with the Japan Aerospace Exploration Agency's Institute of Space and Astronautical Science (ISAS) here determined that Akatsuki's main thruster, which should have slowed the craft enough for Venus's gravity to grab it, had fired for less than 3 minutes of an intended 12-minute burn. Analyses and lab-

oratory tests suggested that leaking vapor from the fuel-burning oxidizer had reacted with fuel vapor, forming salt deposits that clogged a valve.

When the thruster fired, the supply of fuel was restricted, resulting in an oxygen-rich, fuel-poor mixture that burned so hot it destroyed the engine. "It was quite disappointing, but that's space development," says Akatsuki principal investigator Masato Nakamura. The craft was stranded in a solar orbit that has now brought it close enough to Venus for a second try.

The Akatsuki saga is not the first time ISAS scientists have had to improvise to save a spacecraft. Hayabusa, an asteroid sample return mission, improbably made it back to Earth in 2010 with specks of asteroid dust after overcoming engine failures, fuel loss, and communications blackouts during its 6-billion-kilometer, 7-year odyssey (*Science*, 23 December 2011, p. 1629).

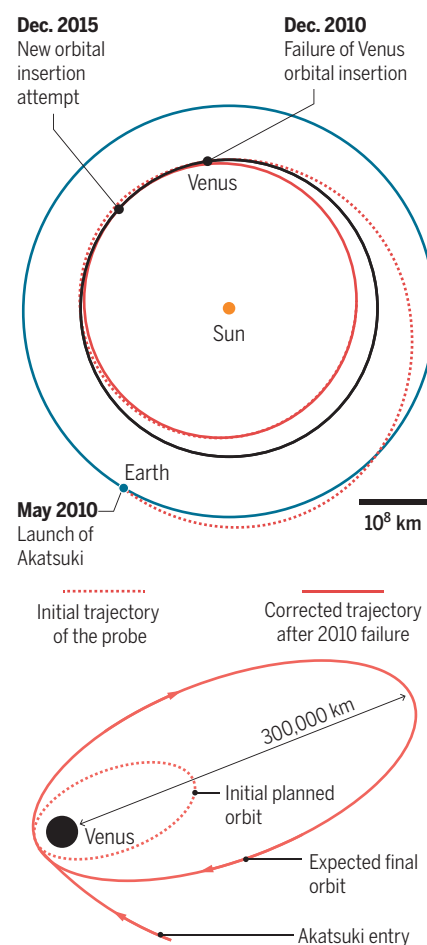
Akatsuki should be an easier ship to right. With the main engine disabled, ISAS scientists knew they would have to rely on the small attitude control thrusters to steer the craft into orbit. On 7 December, 5 years to the day after their first attempt at achieving orbit, controllers will fire the four thrusters on the bottom of the craft for 20 minutes. If that burn does not slow Akatsuki enough for Venus's gravity to grab it, the team will flip the craft and fire the four top thrusters.

If all goes according to plan, Akatsuki will enter an elliptical orbit that will take the spacecraft 300,000 kilometers away from Venus at the farthest point—much farther than the 80,000 kilometers originally intended. The new orbit will call for a new observational strategy. To track cloud movements, scientists had planned to capture images at 2-hour intervals and stitch them into movies. With the cameras now so far away during most of the orbit, the images will be smaller and lower resolution. The team will snap pictures every 30 minutes to compensate.

One lingering worry is Akatsuki's main antenna. The spacecraft strayed close to the sun on its odyssey. The ISAS team has confirmed that the cameras survived temperatures that ran much hotter than anticipated. But the solder anchoring the high-gain antenna may have melted, compromising the craft's ability to transmit data. Nakamura's team won't be able to test the antenna until after the craft is in orbit. ■

Second time a charm?

A failed engine burn sent Akatsuki whizzing past Venus in 2010. After 10 loops around the sun, controllers next week will use attitude control thrusters to slow the probe enough, they hope, to lock into a venusian orbit.



BEHIND THE NUMBERS

NSF's novel solution to a workload crunch

By Jeffrey Mervis

The National Science Foundation (NSF) frequently cites its low overhead costs when asking Congress for more money for research. But there's a downside to that efficiency—the risk of overloading the program officers who manage research grants.

The workload problem became acute in 2004, after the number of proposals submitted to NSF had soared by 37% in the previous 3 years to almost 44,000. That surge had sent success rates plummeting from 31% to 24%, a level that alarmed researchers. And there was no matching increase in NSF's cadre of roughly 400 program officers.

Fearing that program officers would be drowned by the flood of applications, then-NSF Director Arden Bement attacked the two factors that determine their workload: the number of proposals NSF receives and the size of the staff that manages them. He succeeded: The average number of proposals handled annually by a program officer has declined by 11% in the past decade, from 109 in 2004 to 97 last year.

On the demand side, NSF clamped down on new solicitations, a mechanism that tends to generate more proposals than would arrive over the transom without special prompting. Some NSF programs also reduced submission windows from twice a year to annually in hopes that researchers would send in fewer proposals.

The changes had their intended effect. Over the past decade, the annual number of proposals has grown by less than 1%, reaching 48,051 in 2014. (There was a 2-year spike as researchers competed for a \$3-billion windfall in federal stimulus spending during the Great Recession, with applications topping 55,000 in 2010. But the numbers dropped quickly, and for the past 3 years applications have been flat.)

At the same time, NSF's scientific staff grew. NSF employed roughly 25% more program officers in 2014 than it had in 2004, a rise from 402 to 496 with a peak of 503 in 2012. The increase far exceeds the

9% boost over the decade in NSF's overall workforce, to just above 1300.

To add program officers without boosting NSF's overhead costs, Bement took advantage of the unusual nature of the agency's scientific workforce and the way its budget is structured. The key was an increased reliance on "rotators"—scientists who come to the agency for a few years under a 1970s law that allows such temporary absences from their home institution, typically a university, to work for the federal government. The number of rotators jumped 50%, to 190, between 2004 and 2012, according to NSF's Office of Inspector General. That is double the growth rate of the overall pool of program officers. Today, nearly one-third of NSF's program officers are rotators, a much higher percentage than at any other federal agency.

NSF says rotators bring with them fresh ideas gained through their recent experiences in the lab. As an inducement, rotators can remain faculty members and receive their university salary, which is usually higher than an equivalent federal employee would earn. In fact, some members of Congress think it's too sweet a deal. At a recent hearing, legislators pressed NSF officials

to justify the additional cost, estimated at \$36,000 per rotator.

But NSF likes rotators for another reason that doesn't get discussed openly: They are paid out of the agency's research account. That's a winning political strategy because lawmakers would much rather give any additional dollars to NSF's research budget than to its management account, which funds the rest of NSF's workforce.

Such savvy maneuvering hasn't blunted NSF's annual call for additional staffing. NSF Director France Córdova asked for 15 new positions in her 2016 budget request—a boost that is "vital for managing increasing numbers of proposals and the subsequent increase in workload," she told a Senate spending panel earlier this year. Congress has yet to act on that request. ■

50
percent

Increase between 2004
and 2012 in the number
of rotators, visiting scientists
who do stints at NSF.

Bringing back the aurochs

By conjuring the extinct ancestor of modern cattle, breeders are making Europe just a little wilder

By **Erik Stokstad**, in *Sfântu Gheorghe, Romania*

Ronald Goderie glances skeptically at a rickety wooden fence in the Danube delta. After a marathon journey from the Netherlands, some of the most unusual cattle in the world are about to arrive in this lonely corner of eastern Romania. “Don’t underestimate their strength,” the Dutch ecologist warns the son of a local farmer who will help take care of the herd. The dozen brawny creatures must remain quarantined in the pen for 24 days to satisfy veterinarians that they are disease-free. Goderie’s

worry is that the cattle may leap the fence, or smash through it.

For 7 years, Goderie has been breeding this line of animals with a remarkable vision in mind. The *Taurus* cattle are his latest creations in a long quest to resurrect the aurochs, the fearsome ancestor of today’s cattle. The last of their kind died in the 17th century. But the genes that endowed aurochs with traits such as massive horns and a grand stature persist, diluted and dispersed across dozens of cattle breeds.

Several efforts are underway to collect these genes by cross-breeding heritage cat-

tle, which predate the rise of industrial agriculture. Creating a facsimile of primeval cattle is not the only goal. Goderie and others intend to set the tough, self-sufficient animals free as part of an ambitious long-term aim to “rewild” millions of hectares of abandoned farmland. They are counting on the heavyweights’ grazing and trampling to prevent forests from encroaching on diverse grasslands. Rewilding Europe, a nonprofit conservation group, has provided about €200,000 over the past few years to help establish herds of cattle that resemble aurochs in Croatia, Portugal,



Spain, and now Romania.

Here in the Danube delta, Goderie hopes the Taurus cattle will not only graze former farmland, but also trample new paths through the reeds, creating habitat that will benefit birds and other wildlife. “Large herbivores grazing along the water’s edge, thousands of birds, wolves chasing the Taurus—this is our dream landscape,” says Deli Saavedra, a regional manager with Rewilding Europe, which paid €15,000 to transport the cattle some 3000 kilometers by road and river.

Now, the breeders hope that genetics can get them closer to their dream. The nuclear genome of a 6750-year-old fossilized aurochs from the United Kingdom, published in October in *Genome Biology*, has helped confirm that the heritage breeds are most genetically similar to the original aurochs. Sequencing could also assist in pinpointing genetic markers that will accelerate and refine the work. “Back-breeding is a fairly crude way of developing an aurochsl-like animal,” says David MacHugh, a geneticist at University College Dublin. Cloning an aurochs remains a distant prospect, as that would require finding an intact set of original chromosomes in a fossilized cell or stitching together new ones from the existing cattle genome.

In any case, a genuine aurochs might be too dangerous, so breeders are content to approximate the beast. As Henrique Pereira

of the German Centre for Integrative Biodiversity Research in Leipzig puts it, “Having the closest breed to the aurochs has emotional value.”

IN HIS CHRONICLES of Rome’s battles against the Gallic tribes, Julius Caesar described the aurochs of southwest Europe. “These are a little below the elephant in size,” he wrote with a touch of exaggeration. “Their strength and speed are extraordinary; they spare neither man nor wild beast which they have espied.” Fossils suggest that aurochs bulls stood as tall as 1.8 meters at the shoulder—roughly a quarter taller than a Holstein cow—and may have weighed a metric ton. They had menacing horns, with those of bulls up to an estimated 20 centimeters thick and nearly 130 centimeters long.

Cave painters depicted aurochs on the walls of Lascaux, France, more than 17,000 years ago, and after the woolly mammoth went extinct several thousand years ago, the aurochs lived on as the tallest and heaviest mammal on the continent. Ecologists believe the animals helped maintain grassland ecosystems by roaming and consuming plants that smaller herbivores couldn’t digest.

Aurochs were put on the path to extinction about 10,000 years ago, when farmers in the Near East began domesticating them. (Oxen, despite their similar-sounding name, are domesticated and castrated bulls.) Those not tamed were hunted for meat. By the 13th century C.E., aurochs hung on only in Eastern Europe. As their

numbers dwindled, royalty reserved the exclusive right to kill them. The last known survivor died in a game reserve in 1627 in what is now Poland.

First to propose resurrecting the aurochs was Feliks Paweł Jarocki, a zoologist at the University of Warsaw. In the early 19th century, he sketched out an idea to bring back the aurochs by back-breeding existing kinds of cattle. Animal husbandry had always been a forward-looking enterprise, aimed at creating breeds with enhanced features, such as more meat or milk. Jarocki’s radical suggestion was to head backward in time by collecting relict traits.

No one tried that until the 1920s. Working in Berlin and Munich, Lutz and Heinz Heck—both zoo directors—crossed rare cattle from Germany, France, Spain, and other countries. By the early 1930s, the Hecks had fashioned a muscular breed with long horns. Touted as an example of Aryan-style eugenics, herds of Hecks were released onto the private hunting grounds of Hermann Göring, second-in-command of the Nazi party.

Heck cattle survived the war, and their offspring can still be found in zoos, nature reserves, and a few farms. In 1991, the nature conservation organization Arbeitsgemeinschaft Biologischer Umweltschutz (ABU), in Bad Sassendorf, Germany, introduced five Heck cattle to a nature reserve to help restore meadows and floodplains by grazing saplings. The Heck cattle got the job done, but even blue-ribbon specimens lack distinctive aurochs features such as lean limbs and a long head. ABU zoologist

Taurus cattle bearing primitive traits emerge from the mist at Kempen-Broek nature reserve in the Netherlands.



Margret Bunzel-Drücke wanted animals that look more like aurochs. “I just like the idea,” she says. “Maybe it’s romantic.”

In 1997, Bunzel-Drücke and colleagues began crossing Heck cattle with Italian Chianina, the world’s tallest cattle, and with Sayaguesa of Spain, which have long heads and white muzzles. Progress has been slow, she says. The generation time for cattle is 2 to 3 years, and some characteristics—such as the direction that curving horns point—only become permanent later in life, so breeders must wait to decide which individuals should be mated. Even if the first generation of offspring looks good, some of the next will lose desired traits or express unwanted ones, due to Mendelian inheritance. Breeders striving for a purebred animal must keep selecting and crossing the best offspring until the progeny have two copies of all the relevant gene variants. It’s a numbers game: Larger herds have higher odds of desired genetic combinations while preventing too much inbreeding. Because of limited pasture area, the ABU herd only has about 100 animals.

Hoping to make faster progress, a program at Hortobágy National Park in eastern Hungary has about 600 Taurus cattle in fenced pastures totaling 2400 hectares. Biologists with the Cologne Zoological Garden in Germany launched the effort after introducing wild horses to Hortobágy,

Prime traits

The aurochs went extinct 400 years ago, but its genes persist in living breeds. By crossing heritage cattle, breeders are combining key traits.

Forelocks

Long, curly hair.

Coat color

Deep brown to black, with a white stripe running down the back. Light-colored muzzle.

Horns

Light-colored with dark tips. Up to 130 cm long and 20 cm wide at base.



Size

Larger aurochs stood 155–180 cm tall at the shoulder.

Shape

Long and slender legs, elongated and large head, strong neck and shoulder muscles.



a montane grassland that once was prime habitat for aurochs. “We wanted to have at least the illusion of a wild animal,” says Waltraut Zimmermann, a zoologist who recently retired from the zoo. She and colleagues have bred the Heck cattle with African Watusi, which have some of the largest horns among cattle, and various hybrids. Zimmerman says the program is close to having a pure-bred animal.

THE LATEST WRANGLERS to try their hand at reviving the aurochs are two startups in the Netherlands. One was founded by Goderie, a self-employed ecologist who attributes his fascination with cattle to childhood visits to a farm, where he was impressed by their size and range of behaviors. “I got infected with the cow virus quite early,” he says.

Goderie created the nonprofit Taurus Foundation a quarter-century ago to promote “natural grazing” by cattle in Dutch nature reserves. He started stirring the primordial gene pool in 2008, when he launched his effort to breed aurochslke cattle that would be better adapted to Europe’s wild places. Working with scientific advisers, Goderie narrowed a list of about 30 primitive breeds to six with obvious hallmarks, including long-legged Maremmiana; imposing Sayaguesa and Limia; and thick-horned Maronesa. Bulls and cows were brought to two nature reserves in the Netherlands, now

totaling about 300 animals.

The third generation, including those sent to the Danube delta, bears a good resemblance to aurochs, says Johan van Arendonk, a cattle geneticist at Wageningen University in the Netherlands, who advises the program. “I’m very pleased with what they have managed so far.”

In 2013, collaborator Henri Kerkdijk-Otten quit the Taurus Foundation and started the Uruz Project, named after the old Germanic word for aurochs. Kerkdijk-Otten is crossing only two heritage breeds at a time, which he says should lead more quickly to true-breeding lineages—ones in which matings always produce offspring with the same traits. The breeds, such as Watusi, are relatively common and should have higher genetic diversity. “We can have aurochslke animals in just two generations with a minimum number of setbacks,” he says.

Genetic findings suggest that both programs have a solid basis. Richard Crooijmans, an animal geneticist at Wageningen University, and doctoral student Maulik Upadhyay compared 770,000 genetic markers, known as single nucleotide polymorphisms, from a range of heritage cattle with data from the aurochs genome. The results, which they submitted for publication last month, show that



On the last leg of a journey from the Netherlands, Taurus cattle arrive in the Danube delta of Romania, where they will help maintain habitat for birds and other creatures.

the Italian Maremmana and the Spanish breeds are genetically among the closest to the aurochs, and that they preserve different chunks of the ancient animal's genome.

Geneticists might someday be able to provide specific guidance to breeders. Now, they have to wait until animals are well into adulthood to know whether they have inherited DNA for some aurochs traits. To speed up the process, Crooijmans plans to sequence the genomes of 16 individuals from seven breeds in Goderie's program. This should reveal genetic markers linked to the desired physical features. Such markers would reveal animals with the right genes, so they could be selected for mating as soon as they are sexually mature.

Within a decade, Goderie hopes, Taurus herds will be roaming free in biomes as diverse as deltas and arid scrublands. Working with Rewilding Europe, he has already established small herds in Portugal and in Croatia's Velebit Mountains. In October, six Taurus joined wild horses on a former military base in the Czech Republic, where they were introduced by the nonprofit European Wildlife. "Nearly all our cattle can survive quite extreme environments," Goderie says. He hopes they will be aided not only by strength and hardiness but also by wiles.

A reason for optimism is that defensive behaviors have emerged in other primitive cattle breeds that have gone feral. In the mountains of southern Bulgaria, for example, Rhodope shorthorns defend themselves from wolves by forming a ring at night with their calves inside. Goderie hopes that natural selection will further hone his Taurus's survival instincts as they fend for themselves. (Legally, however, they are not wild animals. E.U. regulations require, among other things, that cattle be given ear tags, generally within 3 days after birth, and some nations require vaccination and annual blood tests.)

The arrivals have gotten a mixed reception. Some forestry officials fear that the large herbivores will harm young trees if they wander out of the grasslands, says Rewilding Europe's Saavedra. But local farmers welcome the newcomers, he says. They sign multiyear contracts to watch over the cattle, in exchange for half of the offspring. Farmers hope the new genes will reduce inbreeding in their own herds.

ON A GRAY OCTOBER MORNING, Goderie adds Romania to the list of Taurus stomping grounds. The destination is a narrow field in the Danube delta near the small fishing town of Sfântu Gheorghe, accessible only by boat.

After driving from the Netherlands, a gleaming red truck floats down the last

Europe goes wild

In addition to back-bred Taurus cattle, researchers and land managers have released a variety of other herbivores, including heritage breeds, into nature reserves and abandoned farmland. Wolves and bears are naturally returning, raising hopes that wilder ecosystems will result.

1. Faia Brava reserve, Portugal

Rugged, dry woodlands where wolves are returning. Cattle live in a fenced 1000 ha reserve.

2. Oostvaardersplassen, the Netherlands

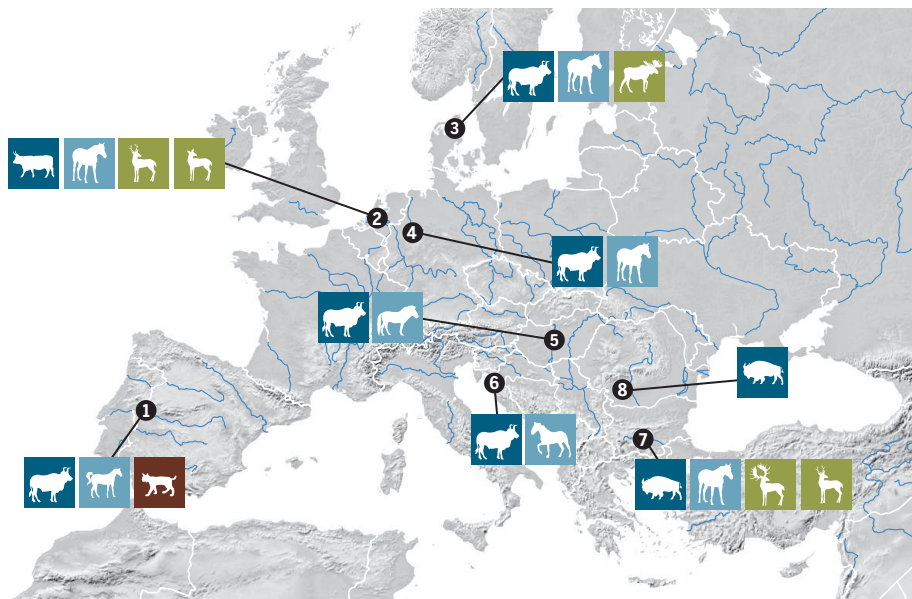
A reclaimed wetland and early experiment in rewilding, this 56 km² reserve attracted controversy when cattle starved during severe winters.

3. Lille Vildmose, Denmark

A rare raised peat bog, which the Aalborg tourist bureau calls "Denmark's answer to the savannah of East Africa." Red deer and boar live in fenced forests.

4. Lippeaue Naturschutzgebiet, Germany

Inside a 1.2 km² nature reserve, grazers help control saplings in the floodplain of the Lippe river, which flows through farmland.



5. Hortobágy National Park, Hungary

At 800 km², the largest seminatural grassland in Europe. Electric fences limit cattle and horses to a 2.4 km² reserve.

6. Velebit Mountains, Croatia

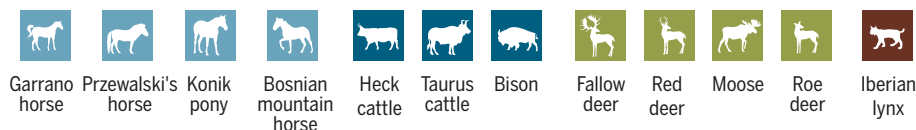
Forested limestone canyons with wolves, brown bears, and Eurasian lynx. Cattle and horses reintroduced to graze abandoned grasslands.

7. Rhodope Mountains, Bulgaria

A wildlife hot spot, these grasslands and forests are home to wolves, bears, raptors, and vultures. Rewilding aims to bring back large herbivores.

8. Southern Carpathians, Romania

Forests and grasslands with wolves and other predators. Bison brought from Sweden, Germany, and other countries now roam a 150 ha reserve.



reach of the Danube on a rusty, 30-meter-long barge. The nervous cattle are stamping their hooves and rocking the truck. "Ooomma," murmur the Dutch handlers to soothe them. As a tugboat nudges the barge against the riverbank, Goderie must solve a problem. The truck is too heavy to drive on the sandy ground. He and several assistants carefully coax the cattle in groups of four onto a jerry-rigged hay cart, which a tractor pulls the last few hundred meters to the pen.

Goderie readily admits that a dozen Tau-

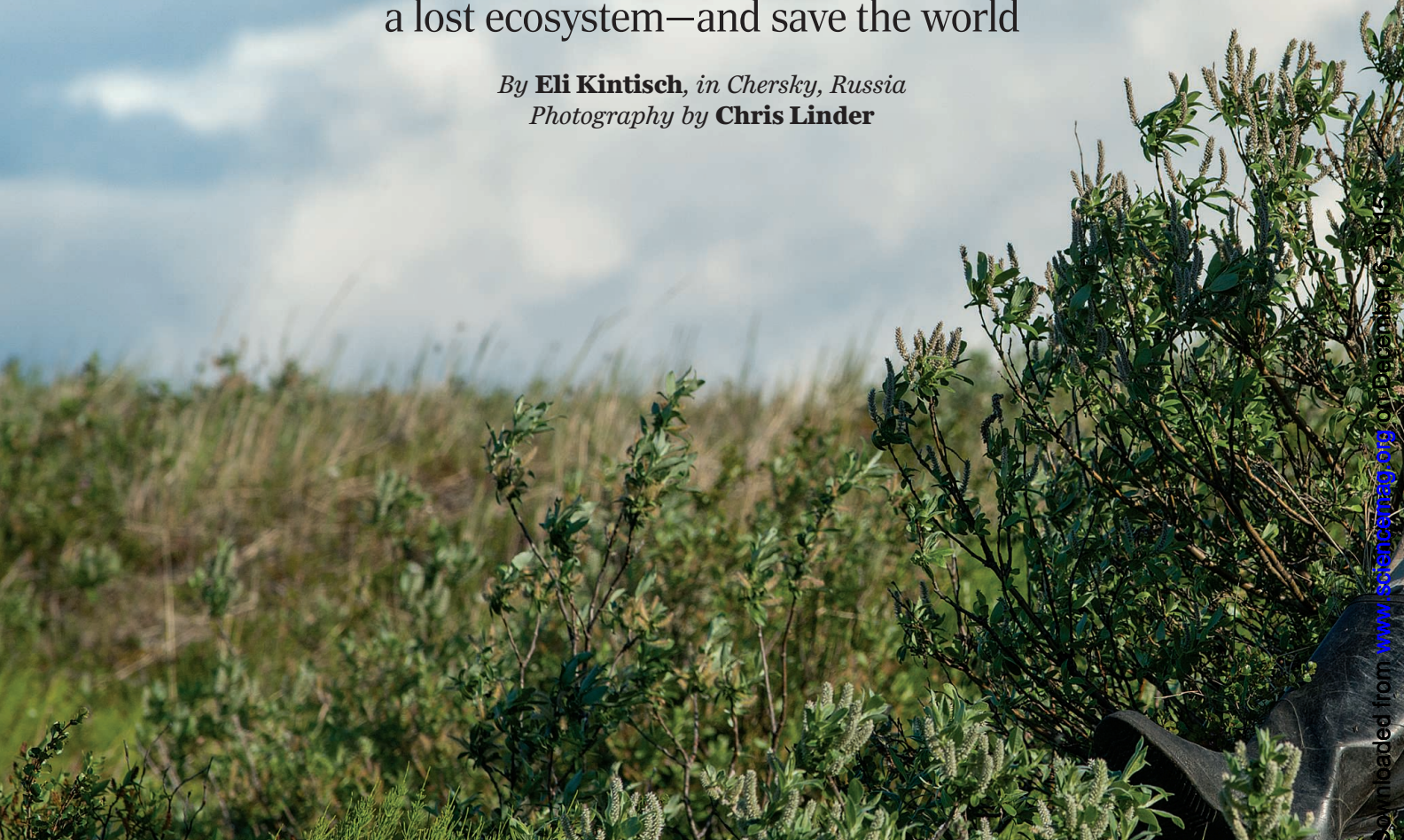
rus cattle by themselves won't greatly enhance habitat in the delta, where countless farms with sheep and other livestock were abandoned over the last century. Alexandra Panait of Rewilding Europe agrees. "There is so much left to be done in the delta," she says. "Step by step. Hoof by hoof."

But as the last cows and bulls rush into the pen, Goderie exults in the moment. "Mission accomplished," he exclaims. With Taurus as standard bearers, the aurochs's genetic legacy has reclaimed a little more of its ancient realm. ■

Born to rewild

A father and son's quixotic quest to bring back
a lost ecosystem—and save the world

By **Eli Kintisch**, in Chersky, Russia
Photography by **Chris Linder**



In April 2011, Nikita Zimov climbed into a heavy duty truck with six elk in the back and set out from Novosibirsk, a major city in southern Siberia, on a 4000-kilometer trek to the edge of the world. Time was not on his side. He had to reach the Arctic town of Chersky, where he and his father, Sergey, run a hardscrabble research outpost called the Northeast Science Station (NESS), before the spring thaw melted the frozen rivers that serve as winter roads in northern Siberia. White wooden crosses marked spots along the winding road where unlucky drivers had perished. Two weeks into his journey, just 40 kilometers from home, Zimov hit a snowbank—his brakes were shot—and the truck tipped over. Unscathed, he phoned his father and spent the next 4 hours, cold and exhausted, leaning against a flimsy tarp

that covered the truck's roof to keep the elk, also uninjured, from bolting. "I was miserable," he says. "Almost literally insane."

Sergey swooped in to rescue Nikita and the elk, and the animals finally reached their destination: Pleistocene Park, a 14,000-hectare reserve near Chersky founded by the elder Zimov 19 years ago. It's a grand experiment to test whether large herbivores—elk, moose, reindeer, horses, and bison—can, simply by grazing, bring back a grass-dominated ecosystem called the mammoth steppe. That biome dominated the northern reaches of Eurasia and North America for 2 million years, until the end of the last glacial period some 13,000 years ago, when the landscape turned to mossy tundra and sparsely forested taiga.

If the Zimovs are right, a brighter future for the entire globe may hinge on the experi-

ment's success. A decade ago, Sergey and colleagues estimated that permafrost encircling the upper Northern Hemisphere contains a whopping 1 trillion tons of carbon—twice earlier estimates—and that this vast pool may be on the brink of leaking into the atmosphere. The finding was a clarion call to climate scientists to take the arctic carbon threat seriously. "This is the most dangerous territory in the world in terms of climate change," Zimov declares.

Zimov's calculations and field measurements soon persuaded his colleagues. "Sergey comes up with these wild ideas. They seem implausible, but they turn out to be right," says longtime collaborator Terry Chapin, an ecologist at the University of Alaska, Fairbanks. Now, Zimov is straining credibility again with his proposal for containing the threat. He has called for rewild-



Ecologist Sergey Zimov believes restoring the Pleistocene mammoth steppe will protect permafrost and provide habitat for millions of herbivores.

vostok. Instead they capitalized on the Soviet collapse, gathering up speedboats and trucks at steep discounts and stockpiling food and fuel in shipping containers. “We were feasting off the dead carcass of the Soviet Union,” says Nikita, who as a teenager spent a summer cleaning a 33-meter-long shipping barge that his dad would convert into a floating research station.

The son of a Soviet naval officer, Sergey Zimov had a maverick’s temperament from the start, and it flourished in Chersky’s post-Soviet isolation. He questioned the prevailing theory for why mammoths, bison, and other arctic megafauna died out at the end of the Pleistocene. Most scientists believed the warming climate disrupted northern ecosystems, changing the steppe grassland to tundra and starving the beasts. Zimov thought proponents of that idea had cause and effect reversed. He knew that in northern Siberia, taiga and tundra turned grassy wherever it was disturbed, whether by wild horses or by one of Stalin’s gulags. In 1988, Zimov penned up 25 Yakutian horses, a breed adapted to the cold, and watched how they quickly transformed mossy wet tundra into grassy pasture by gnawing on shrubs and fertilizing the soil. He theorized that herbivores had maintained the expansive mammoth steppe, and the land only turned to taiga and tundra after their numbers fell for another reason—presumably human hunting.

Intrigued by Zimov’s ideas, Chapin and James Reynolds, an ecologist at Duke University in Durham, North Carolina, visited NESS in the summer of 1993. “Zimov is like a spinning tornado of chaos, confusion, and creativity,” Reynolds penned in his diary. They weren’t immediately sold on his big idea. Zimov “takes a few data points and if his hypothesis works, he’s convinced,” Chapin says. But the discussions were invigorating, he says, and Reynolds came up with a model that reproduced Zimov’s conclusion. In 1995, the trio and Russian colleagues published a paper in *American Naturalist* declaring that “human hunting could have played as great a role as climate” in extirpating Arctic megafauna.

Zimov saw implications for the future as well. Pleistocene grasslands in northern Russia and northwest Alaska accumulated organic material over hundreds of thousands of years. The yedoma soil distilled from all that plant material is some of the most carbon-rich on the planet, and the soil runs deep, with an average thickness of 25 meters. It is now preserved under the tundra, deep-frozen in permafrost.

ing the Arctic: repopulating vast swaths of the permafrost zone of Eurasia and North America with large herbivores. By restoring the mammoth steppe, he says, those megafauna would help to keep the permafrost intact even as the atmosphere warms.

“Sergey is a visionary, a challenger of paradigms,” says ecologist Heather Alexander of University of Texas, Brownville. But this particular vision may be a fantasy. Recreating the mammoth steppe’s estimated herbivore density—20 large animals per square kilometer—would mean sustaining millions of beasts in Siberia. Yet the Zimovs have struggled to keep a handful of herbivores alive in Pleistocene Park—a speck in the vastness of Siberia. As a testament to the challenge, the elk that Nikita risked his life to bring to Chersky had all died or hopped a fence and escaped within a year of their arrival. Sergey

Zimov, however, appears unfazed by the gulf between the reality so far and his monumental vision. “It’s probably the biggest project ever,” he says, nonchalantly.

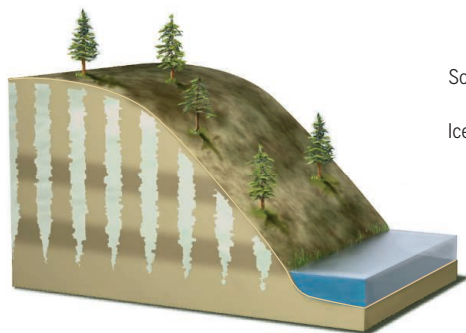
SERGEY, with three colleagues, in 1980 established NESS in a wooden hut along a small river near Chersky as an Arctic research redoubt of the Pacific Institute of Geography in Vladivostok. Soviet-era Chersky was a bustling hub for gold miners and for scientists in transit to research bases near the North Pole. When the Soviet Union unraveled in 1991, “people were fleeing [Chersky], but Sergey said we should stay,” says ornithologist Eugene Potapov, a long-time visiting scientist at NESS who works at Bryn Athyn College in Pennsylvania.

As Chersky emptied, NESS scientists ignored an official request to return to Vladi-

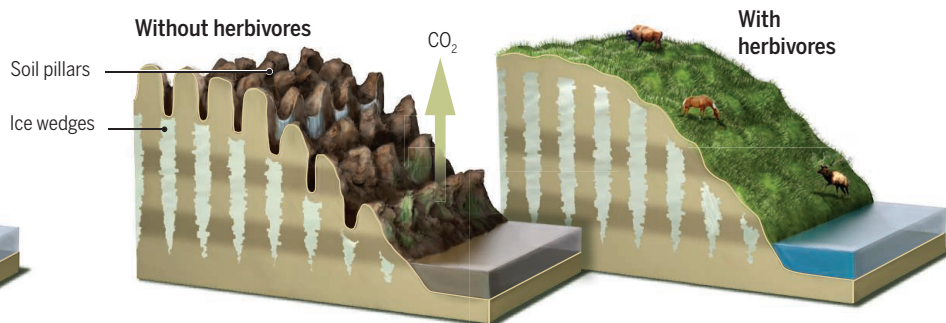
Averting an Arctic apocalypse

Zimov and colleagues have warned that thawing Arctic permafrost will release prodigious quantities of greenhouse gases. Introducing horses, deer, bison, and other large herbivores, they argue, would restore arctic grasslands. By insulating the permafrost, pastures would keep the soil and ice wedges from melting into a swampy morass—and keep much of the carbon safely bottled up.

Current landscape



15 years after 3°C climate warming



Zimov and Chapin saw yedoma as a time bomb. A decade ago in *Science*, they concluded that estimates of carbon content in Arctic soils were grossly underestimated, and that under “extreme” but plausible conditions some 500 billion tons of carbon would be liberated from yedoma within a century (16 June 2006, p. 1612). (Since then, the consensus Arctic carbon estimate has risen by another 50%; one recent study estimated that at the current atmospheric warming rate, carbon dioxide (CO₂) and methane released from permafrost would warm the planet by an additional 0.3°C by 2100.) Zimov had “basically discovered and explored a pool of vulnerable carbon approximately equal to the entire pool in plants and unfrozen soils,” says ecologist Chris Field of the Carnegie Institution for Science in Palo Alto, California.

By then, Zimov was seeing, on a small scale, the devastating effects of warming temperatures in the Arctic. At a 3-hectare plot near Chersky, Zimov 11 years ago used a bulldozer to strip away the moss and soil that insulate yedoma in the summer. Ice wedges in the exposed permafrost rapidly melted, laying bare the pitted, thawing soil. Soil bacteria set to work freeing CO₂ and methane. Today, the site is pocked with 3-meter-deep melt pools and bizarre pillars of gray dirt. “This is the future we are facing if we cannot stabilize the permafrost,” Zimov says.

TO AVERT THAT FATE, Zimov has proposed geoengineering permafrost on a global scale. He started small, with Pleistocene Park, a 45-kilometer boat ride up the Kolyma River from Chersky. Its modest entrance features a disgruntled cat and a metal fence in a patch of mud. Inside, 50 hectares of grasses have replaced scraggly larch and moss. Idling by a lakeshore are

Yakutian horses whose grazing helped the grasses gain ground. The park, Sergey says, is “a war zone between two ecosystems.”

It’s also a war between Zimov’s vision and some mundane challenges. Key among them, he says, is raising an army of herbivores without government support. The Zimovs have ranged hundreds of kilometers to stalk moose, driving them into rivers where they can haul the calves into boats and make off with them. In 2010, the Zimovs ventured 1000 kilometers north across the Arctic Ocean, steering clear of polar bears, to purchase six musk oxen from a wildlife reserve on Wrangel Island. Maintaining the menagerie has proven as difficult as acquir-

ing it: Dozens of Yakutian horses have fallen prey to bears and other predators or died after eating cowbane, a poisonous member of the hemlock family. Four bison from relatively balmy Moscow died of exposure during the harsh Chersky winter. These days about 70 animals roam the park, a fraction of the 1000 Sergey hoped to have amassed by now.

Even so, the browsers are helping to spare the permafrost from climate warming. Grasses are better than mosses, shrubs, and trees at reflecting sunshine, so they are more effective insulators in the summer, when for weeks the Arctic sun doesn’t set. During the rest of the year, when northern Siberia is blanketed in snow, herbivores keep the permafrost frozen by ensuring it is exposed to the frigid Arctic air. By trampling down the snow, they compact it and make it a poorer insulator; in some cases they sweep away the snow altogether to graze. In Pleistocene Park, two temperature loggers in boreholes show average permafrost temperatures 2°C colder in the grazed area. That temperature difference is “enough to protect the permafrost,” Nikita says.

Others aren’t so sure. If winters become warm enough, says Michelle Mack, a soil ecologist at Northern Arizona University in Flagstaff, trampling or sweeping away snow could have the opposite effect, allowing warmth to penetrate the soil more quickly. “It may well be that Sergey is right,” she says, but the Zimovs haven’t made their case rigorously with models or data.

Chapin points out that other than cutting global greenhouse gas emissions, no solutions, apart from Zimov’s, have emerged to address the “dire” prospect of permafrost carbon release. Zimov himself says it’s too early to draw firm conclusions. “Pleistocene Park is an experiment that must be contin-



Nastya Zimova cares for a moose calf purchased from a hunter for Pleistocene Park.



In a fenced-in section of Pleistocene Park, bison and other herbivores have transformed taiga into pasture. Scaling up is a daunting challenge.

ued for tens of years,” he says over moose stew one evening in NESS’s dining room, a soaring round room crowned with a massive Soviet-era satellite dish.

But on his 60th birthday last summer, Sergey and a few dozen friends and colleagues celebrated his semiofficial retirement with salmon caviar and vodka toasts at NESS. Now, the fate of Sergey’s living experiment rests with his son.

IN THE EARLY 2000s, Nikita attended one of Russia’s top science high schools, in Novosibirsk, and then stayed there at the state university for undergraduate and master’s degrees in math and computer modeling. Life in Novosibirsk offered more opportunities than moribund Chersky, where many buildings are abandoned and sinking into the thawing permafrost. “I didn’t think I would want to return,” he says.

“Getting Nikita to come [back] was the hardest scientific problem of my life,” Sergey says. Nikita worried whether he could build on his father’s legacy. “I know I can’t compete with my dad as a scientist. [But] I’m interested in managing the station, growing the park.”

Over the years, NESS has grown into a sprawling compound that serves dozens of visiting scientists with soil and biological labs, state-of-the-art instruments, and tow-

ers that collect atmospheric data. “There’s nowhere comparable to Sergey’s station in the Russian Arctic,” says marine ecologist Robert Max Holmes of the Woods Hole Research Center in Falmouth, Massachusetts. Nikita wants to maintain that infrastructure in a remote hot spot for Arctic field studies. With tensions high between Russia and the West, that’s a daunting challenge. Two major U.S. research grants—one supporting NESS as a teaching lab for undergraduate and graduate students and the other paying for the remote sensing—ended this year, with no promises for renewal. The Russian government, meanwhile, provides only measly salaries.

Yet fully testing Zimov’s ideas will take more money, land, and animals. To lay the groundwork, Nikita plans to expand Pleistocene Park’s fenced area. And to raise awareness inside Russia, the station recently created a 300-hectare preserve eight time zones to the west, near Moscow. Called Wild Field, the pasture filled with horses, sheep, deer, antelope, and cows is meant to simulate the mammoth steppe, minus mammoths and other lost megafauna.

On the prowl for major funding, Nikita showed his father’s touch for schmoozing at the American Geophysical Union meeting in San Francisco, California, last December, treating colleagues to a party in his hotel

room featuring Siberian vodka and beer chilling in an ice-filled bathtub. The many Arctic scientists who flock to Chersky bring dollars and euros that could help sustain the station and Pleistocene Park.

But running NESS is more rollercoaster ride than party. One day in early July, Nikita took a dozen visiting graduate students waterskiing on the Kolyma River in a dilapidated motorboat, with techno music blasting from a portable stereo. The next day came a cluster bomb of lows. The person who maintains an atmospheric sensing tower told Nikita he intended to quit; plant samples that visiting German botanists wanted to bring home were 160 kilograms too heavy, and sure to create a hassle at the airport; and a moose calf for which Nikita had paid \$500 escaped after jumping a makeshift pen that Sergey had built. “I told him that he should hire a carpenter, but no, he insisted he would do it himself,” Nikita says. He watches his father, wearing a mosquito head net with a hole at mouth level for an ever-present cigarette, head off on an all-terrain vehicle in search of the stray calf.

“He is stubborn,” Nikita says with a shrug. “And I am stubborn.” ■

Reporting for this article was supported by a grant from the Pulitzer Center on Crisis Reporting.

ROYAL SOCIETY YOUNG PEOPLE'S BOOK PRIZE

Destination: Imagination

This year's finalists for the Royal Society Young People's Book Prize cover topics as diverse as antimatter and the microbiome, but they share at least one thing in common. Whether encouraging readers to track the constellations in the night sky, begin their own bone collections, or master some simple sign language, each book invites kids to take a hands-on approach to learning. The competition, which began in 1988, celebrates well-written, accessible books that inspire "under-14s" to learn more about science. The shortlist below was compiled by a jury of adult judges, but the winning title, *Utterly Amazing Science*, was chosen by young people on judging panels throughout the United Kingdom. Which one would have secured your young reader's vote?

Jake's Bones

Reviewed by **Julia Fahrenkamp-Uppenbrink**

In this richly illustrated book, 13-year-old Jake McGowan-Lowe explains to young readers what they can learn about animals from their bones. The book is based largely on Jake's collection of animal bones, most of which he has collected in his native Scotland since he was 6 years old. Combining scientific fact with personal experience, the book provides a wealth of detail while remaining accessible throughout. Young readers are likely to be drawn to Vulpy the fox, Oscar the hedgehog, George the roe deer, and many of the other animal skeletons that Jake presents. The enthusiasm of the author for his subject is tangible, and the practical tips about how to collect bones and how to look after your collection were enough to send my children to their wellington boots, notebook and other tools in hand. Readers who feel that they have not yet seen enough bones after reading the book should turn to Jake's blog, www.jakes-bones.com, which has attracted more than 500,000 visitors to date.

365 Science Activities

Reviewed by **Rich Stone**

For my 11th birthday, my parents gave me something I'd long desired: a chemistry set. The countless hours of experimentation instilled an appreciation for science, and the scientific method, that continue to this day. I learned about distinguishing acids from bases and how, say, mixing hydrogen perox-

ide and potassium iodide could freak out my mother. But in hindsight, my horizon was limited. The worlds of biology and physics were largely terra incognita. I wish I had had a book like *365 Science Activities* in elementary school. The authors have compiled a wide range of activities illustrated with cartoons and diagrams. Whether it's building an echo box out of a shoebox to learn about sound vibrations, making cardboard bugs that stand on water to learn about surface tension, or coaxing yeast to produce carbon dioxide to learn how bread rises, each activity makes use of stuff lying around the house or materials that can be bought cheaply in a department store. Most of the activities do not require adult supervision. A few struck me as filler—for example, making shadow puppets—but the vast majority yield nuggets of insights into scientific processes that should enable a lifelong appreciation for science to take root at a young age.

Tiny

The Invisible World of Microbes

Reviewed by **Caroline Ash**

This is a lovely book that even young children who cannot yet read for themselves would relish. The ambition is high: to explain the significance of the world of microorganisms that cannot be seen by the naked eye. The text by Nicola Davies and the delicate and charming illustrations by Emily Sutton combine highly effectively to show how the tiniest living organisms intervene in vast processes such as mountain erosion, climate, and epidemics. A boy and a girl accompany the reader through depictions of microbial scale: A teaspoon of dirt is compared to the



Find out whether darker crayons melt faster than lighter ones with the help of *365 Science Activities*.

population of India; a poliovirus particle is compared with Paramecium. Descriptions of form and function and ideas of the sheer ubiquity of microbes are shared with these characters across a dinner-table scene (even the cat has a bowl to sit in) and in the compost heap and garden. In terms of imagery, Sutton has succeeded in encapsulating concepts that many scientists struggle with. The mind boggles at her highly detailed depiction of bacterial replication.

Utterly Amazing Science

Reviewed by **Jennifer Sills**

Prepare to immerse yourself in the exciting worlds of chemistry and physics as you peruse this collection of fundamental facts and eye-catching visuals. Each page features interactive elements—an atom pops off the page, flaps lift to provide more information about the chemical structure of each material on a bicycle, and a crank turns to show how a piston moves in an engine. The text moves logically from atoms and molecules to states of matter, mixtures and solutions, basic chemical reactions, and materials. It progresses to force, gravity, and magnetism and then moves on to machines and friction. The final pages explore energy, light, and heat. The book does not shy away from precise vocabulary. For example, a discussion of chemical mixtures defines colloids and then gives three examples: emulsions, aerosols, and foams. Yet each word is clearly described with examples ("When you use hairspray, you create a cloud of tiny liquid droplets floating in air. This kind of mixture is called an aerosol") and illustrated with simple diagrams. The book offers answers to many common questions: What makes sticky notes stick? Why don't planes fall? How do bike brakes work? It even provides instructions for 13 "Do this at home" experiments

(and, inexplicably, one similarly formatted “Don’t try this at home” experiment). After reading, get ready to join your child as he or she creates a non-Newtonian fluid out of cornstarch, floats a paper clip on water’s skin, and saves a falling egg from crash landing by outfitting it with a parachute.

Night Sky Watcher

Reviewed by **Keith Smith**

This beginner’s guide to the night sky provides an engaging introduction to stargazing. There’s no need for a telescope because most of the observations can be done with the naked eye and the rest with a decent pair of binoculars. Each double-page spread is covered by a large color illustration, surrounded by informative labels, interesting fact boxes, and suggestions for practical activities. The book will be most useful for those ages 8 to 13, but younger children will still enjoy the pictures and colorful presentation, and even adults may learn something new (I certainly did!). After starting with some basic facts about the night sky and practical tips on how to observe it, the book runs through the different objects that can be seen. Recognizable constellations such as Orion and The Plough are introduced first and then used to guide the reader to less obvious sights via “star-hopping,” which is clearly described. Both Northern and Southern Hemisphere sights are included, although there are a few confusing references to “summer” or “winter” without specifying which hemisphere. A section on planets leads on to the Moon, both richly illustrated. The book ends with an eclectic selection of “unusual sights,” such as com-

ets, meteor showers, and eclipses, which should keep any budding young stargazer going back to the night sky.

Frank Einstein and the Antimatter Motor

Reviewed by **Hadassah Nusinovich Ucko, Solomon Nusinovich Ucko, and Yevgeniya Nusinovich**

This book tells a fictional story about Frank Einstein, a boy genius who is trying to win his town’s science prize. He plans to use the prize money to save his grandfather’s workshop. His arch rival is T. Edison, a brilliant bully who tries to steal his inventions. The story follows Frank; his best friend, Watson; and their two friendly self-assembled robots, Klink and Klank, as they try to invent an antimatter-powered motor and outwit Edison and his chimpanzee assistant. This book is geared toward late elementary school-age children, and it contains plenty of child-friendly humor and clever plot twists. It also includes numerous scientific facts and explanations of the concepts behind Frank’s inventions, cleverly illustrated with easy-to-understand diagrams labeled as “figures” to mimic the style of a scientific work. By using a chimpanzee character that is clever but cannot talk, the author also weaves in lessons in sign language, with the chimpanzee’s words fully illustrated with the matching signs and an American Sign Language alphabet provided for reference at the end of the book. The book is so entertaining that children may not even notice how much they are learning as they read it.

10.1126/science.aad8618



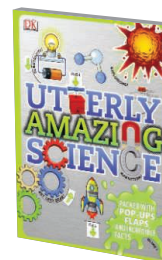
Jake's Bones
Jake McGowan-Lowe
Ticktock, 2014.
64 pp.



365 Science Activities
Minna Lacey, Lisa Gillespie, Lucy Bowman
Usborne, 2014.
128 pp.



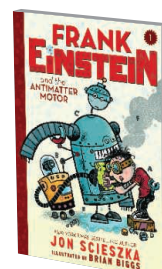
Tiny
The Invisible World of Microbes
Nicola Davies, illustrated by Emily Sutton
Walker, 2014. 34 pp.



Utterly Amazing Science
Robert Winston
DK Children, 2014. 32 pp.



Night Sky Watcher
Raman Prinja
QED, 2014. 120 pp.



Frank Einstein and the Antimatter Motor
Jon Scieszka, illustrated by Brian Biggs
Amulet, 2014. 192 pp.



Composite image of the Crab nebula, a supernova remnant in the Milky Way galaxy.

PHOTO: ESA/Herschel/PACS/MESSENGER/PROGRAMME SUPERNOVA REMNANT

PERSPECTIVES

METABOLISM

Mitochondria shape cardiac metabolism

Quality control of mitochondria in cardiac muscle affects heart function

By **Roberta A. Gottlieb¹** and **Daniel Bernstein²**

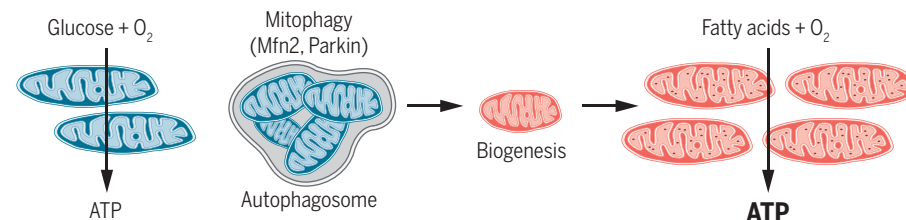
The adult human heart is an intensely metabolically active organ, with a content of mitochondria that primarily use fatty acids for adenosine triphosphate (ATP) production. Two papers in this issue, by Gong *et al.* (1) on page 1220 and by Wai *et al.* (2) on page 1221, illustrate the importance of mitochondrial quality control in cardiac function during fetal life and in the adult heart.

During fetal life—a relatively hypoxic environment, and one in which cardiac workload is considerably lower—glucose is the major source for energy production. At birth, the heart undergoes dramatic metabolic remodeling. Gong *et al.* examined whether this remodeling is accomplished by metabolic switching of fetal mitochondria to fatty acid metabolism or whether fetal mitochondria are replaced by adult organelles. The authors used mutant mice that lack the ability to translocate the cytosolic protein Parkin to the mitochondria. Parkin is a component of a multiprotein E3 ubiquitin ligase complex that targets proteins for degradation. Gong *et al.* demonstrate the requirement for mitochondrial autophagy to eliminate fetal mitochondria. Thus, these mitochondria become isolated from the rest of the cell within a double-membraned vesicle known as an autophagosome, where they are destroyed (see the figure). This “mitophagy” is followed by the expansion of mitochondrial membranes with oxidative phosphorylation complexes optimized for fatty acid oxidation and maximal ATP production. Loss of Parkin-dependent mitophagy during postnatal remodeling results in persistence of fetal mitochondria adapted to glucose utilization but unable to meet the contractile demands of the heart, leading to failure. These results support the growing recognition of the role of mitophagy in mitochondrial plasticity and metabolic reprogramming.

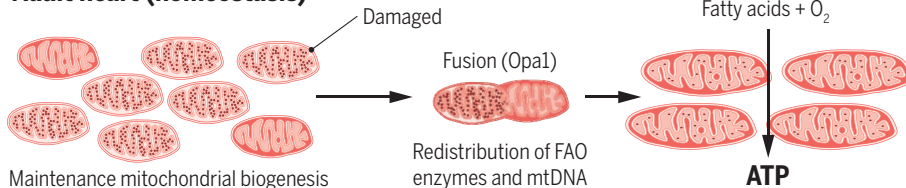
Maintaining mitochondrial quality in long-lived cells, such as cardiomyocytes, depends on a delicate balance of mitochondrial fusion, fission, mitophagy, and biogenesis. When cells experience metabolic or environmental stresses, mitochondrial fusion and fission maintain functional organelles. An increase in fusion leads to mitochondrial elongation, whereas an increase in fission fragments mitochondria. Wai *et al.* generated mice with cardiac-specific deletion of the peptidase YME1L (yeast mitochondrial

ous disruption of Opa1 processing in heart and skeletal muscle largely abrogated heart failure without affecting mitochondrial fragmentation. The authors show that glucose intolerance arising from the skeletal muscle disruption of Opa1 processing resulted in normalization of glucose uptake in the heart, revealing a fascinating instance of metabolic communication between heart and skeletal muscle. This finding led Wai *et al.* to a detailed investigation of metabolic remodeling and ultimately the discovery that a high-fat

Perinatal heart (during transition)



Adult heart (homeostasis)



Mitochondrial remodeling in the heart. During the perinatal transition, mitochondria adapted to glucose oxidation are eliminated via Mfn2-Parkin-dependent mitophagy. Mitochondrial biogenesis then gives rise to organelles adapted to fatty acid oxidation to support contractility. In the adult heart, damaged mitochondrial components must be replaced; their redistribution requires Opa1. FAO, fatty acid oxidation; mtDNA, mitochondrial DNA.

escape 1-like). Lack of this enzyme affects processing of the dynamin-like guanosine triphosphatase Opa1 (optic atrophy 1), which is required for the morphogenesis of inner membrane folds (cristae) in mitochondria, inner membrane fusion, and mitochondrial quality control. Using this elegant approach, the authors dissected the opposing roles of full-length Opa1, believed to regulate fusion, versus short-length Opa1, thought to regulate fission. When this intervention was targeted to cardiomyocytes in the adult mouse, it resulted in mitochondrial fragmentation and a shift to glucose utilization, which are morphologic and functional changes typical of the failing heart. Surprisingly, simultane-

diet could drive the glucose-utilizing heart mitochondria to revert to fatty acid oxidation, despite the defect in Opa1 processing.

The studies of Gong *et al.* and Wai *et al.* made use of complex genetic models supplemented by detailed proteomic and metabolomic analyses to dissect the role of mitochondrial dynamics in heart function. Gong *et al.* used mutant mice in which the mitochondrial protein mitofusin 2 (Mfn2), which is essential for fusion, is either not phosphorylated (AA mutant) or constitutively phosphomimetic (EE mutant); the former impeded Parkin translocation to mitochondria, whereas the latter facilitated translocation. Although the AA mutant

¹Heart Institute, Cedars-Sinai Medical Center, Los Angeles, CA 90048, USA. ²Department of Pediatrics, Stanford University, Palo Alto, CA 94304, USA. E-mail: roberta.gottlieb@cshs.org

had little impact on mitophagy induced by fasting, it revealed an important role for Mfn2-Parkin-dependent mitophagy in the critical perinatal window, when mitochondrial metabolic remodeling is maximal. Parkin-dependent mitochondrial remodeling occurs in other settings, including ischemic preconditioning (3), ischemia (4), statin cardioprotection (5), and sepsis (6), some of which involve metabolic remodeling (7, 8). Mitophagy is used to accomplish functional remodeling of mitochondria in a mouse myoblast cell line during differentiation to myotubes (9). Thus, it is likely that the Mfn2-Parkin pathway described by Gong *et al.* is not unique to the perinatal period but may also be invoked in other instances of large-scale metabolic remodeling.

Gong *et al.* and Wai *et al.* illuminate the critical relationships among mitochondrial morphology, quality control, fuel utilization, and cardiac function. For example, whereas it has been suggested (10) that morphologic mitochondrial fragmentation is infrequent in the adult heart, the study by Wai *et al.* demonstrates substantial fragmentation despite the structural rigidity of the cardiomyocyte. This expands the controversy over the importance of mitochondrial fusion and fission in the mature heart. One limitation of both studies is their reliance on genetically altered mice to perturb mitochondrial dynamics. Although powerful, such models offer fewer insights into mitochondrial physiology in the healthy heart. The field will be advanced by the development of better tools to monitor mitochondrial turnover in vivo (11). A critical next step is to determine the roles of mitochondrial fission and fusion in normal cardiovascular physiology and adaptation to nonpathologic stressors. A more complete understanding of how mitochondrial quality control contributes to cardiac homeostasis is needed to fully appreciate the link between impaired mitophagy and inflammation, revealed by recent studies (12, 13). This enhanced understanding of the role of mitochondrial dynamics in the heart should open possibilities for harnessing these processes for therapeutic potential. ■

REFERENCES

1. G. Gong *et al.*, *Science* **350**, 1220 (2015).
2. T. Wai *et al.*, *Science* **350**, 1221 (2015).
3. C. Huang *et al.*, *J. Cardiovasc. Transl. Res.* **3**, 365 (2010).
4. C. Huang *et al.*, *PLOS ONE* **6**, e20975 (2011).
5. A. M. Andres *et al.*, *Antioxid. Redox. Signal.* **21**, 1960 (2013).
6. J. Piquereau *et al.*, *Autophagy* **9**, 1837 (2013).
7. S. M. Nadtochiy *et al.*, *J. Mol. Cell. Cardiol.* **88**, 64 (2015).
8. K. Kamisoglu *et al.*, *Crit. Care* **19**, 71 (2015).
9. J. Sin *et al.*, *Autophagy* **10**, 1080/15548627.2015.1115172 (2015).
10. Y. Chen, Y. Liu, G. W. Dorn 2nd, *Circ. Res.* **109**, 1327 (2011).
11. G. Hernandez *et al.*, *Autophagy* **9**, 1852 (2013).
12. K. Shimada *et al.*, *Immunity* **36**, 401 (2012).
13. T. Oka *et al.*, *Nature* **485**, 251 (2012).

10.1126/science.aad8222

MICROBIOLOGY

Phage therapy redux – What is to be done?

Bacteriophage biology should move beyond a model system to support human health

By Ry Young^{1,2} and Jason J. Gill^{1,3}

Phage therapy is the use of bacteriophages—viruses that infect and replicate within a bacterium—to treat pathogenic bacteria. This approach had a short history in the premolecular era of Western medicine, but it died out before the mid-20th century mainly as a result of justly critical reports from the American Medical Association and the development of chemical antibiotics (1). Now, the global antibiotic resistance crisis and a new appreciation for the importance of the human microbiota have led to a resurgence of interest in phage therapy, not only in the classic sense of treating bacterial infections (2) but also for its potential role in modulating microbiota (3). A landmark 2015 meeting (4) on phage-based therapeutics hosted by the U.S. National Institute of Allergy and Infectious Diseases (NIAID)

included not only phage biologists but also participants from private companies, public and governmental research organizations, clinicians, and the federal regulatory community. Opinions on the practicality of phage applications replacing traditional antibiotic regimens ranged from full-speed ahead, mostly from the biotechnology industry, to overt skepticism on the part of some physicians. In any case, participants left the meeting convinced that a “Phage Therapy 2.0” is on its way.

The primary focus in this new impetus is on the tailed phages, or *Caudovirales*, the most numerous and diverse biological entities in the biosphere (5). These have a head, containing a linear double-stranded DNA molecule of 15 to 500 kilo-base pairs; a tail; and, in most cases, tail fibers (see the figure). The phage makes specific contacts with surface features (receptors) on its bacterial prey, using the tail itself or the tail fibers, or both. Once the DNA is injected into the cell through the tail, the phage pursues a replicative cycle that culminates in host lysis, liberating typically hundreds of progeny virions. Some *Caudovirales* phages, designated as temperate or lysogenic, have the additional

ability to become stable components of the host genome by forming dormant prophages.

Classic phage therapy relied on the isolation and use of naturally occurring phages found in the environment, and this trend dominates the recent literature. Phages are isolated, screened for their host ranges among pathogenic bacterial strains, and then evaluated in vitro or in vivo in animal models, sometimes formulated as mixtures of individual phages to cover the broadest host range. Besides phages themselves, two other phage-related therapeutics are emerging: lysins (6) and tailocins (7). Muralytic enzymes, or lysins, are used by phages both in the penetration of the DNA through the cell

envelope and in the host lysis process that releases the progeny virions (6). These enzymes kill Gram-positive bacteria very rapidly, exhibit genus-level specificity, and, to date, do not generate resistant organisms.

Tailocins, or phage tail-like bacteriocins, are essentially “headless” phages. Upon adsorption to a receptor, a tailocin particle effects lethal damage to the host cell envelope and thus exhibits single-hit lethality (7, 8). Engineered tailocins can be retargeted to heterologous hosts and have several inherent advantages, in that they can be deployed without the prospect of the environmental release of recombinant DNA and can be administered as a defined dose (8).

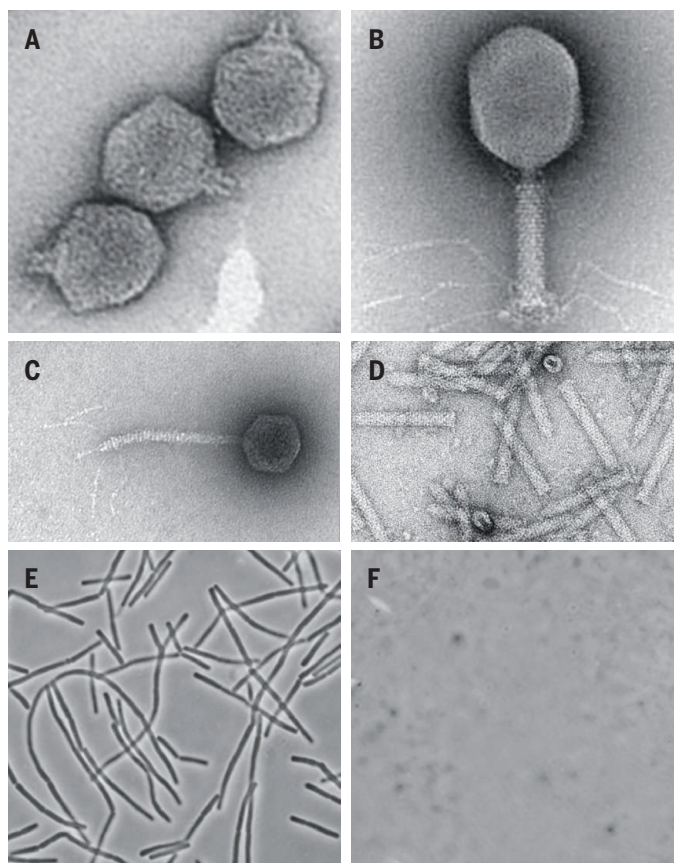
In the clinical and commercial sphere, recent consolidation of several phage therapy companies has brought more focused pipelines for clinical product development. As would be expected, bacterial pathogens that are already difficult to treat with conventional antibiotic therapy are receiving most of this early attention, including *Pseudomonas aeruginosa*, *Staphylococcus aureus*, and *Clostridium difficile*. All three of the phage-based strategies described above (phage therapy, tailocins, and lysins) are being pursued commercially, with products now in varying stages of preclinical development. A handful of phase 1 and 2 clinical trials have been conducted or are in progress. Perhaps the largest of these is the ambitious Phagoburn study, evaluating phages as a treatment for

“...‘Phage Therapy 2.0’ is on its way.”

infections associated with burn wounds (9). Several companies have already developed and marketed phage products for controlling food-borne pathogens such as *Escherichia coli* O157:H7 and *Listeria monocytogenes* (10). These developments were attractive early applications for phages, owing to the genetic homogeneity of the target bacteria and the lower regulatory barriers for registration of phages as food-processing aids.

Among the next steps that will be required for continued momentum is a prudent reassessment of the regulatory environment. The positive engagement of members of the regulatory community at the NIAID meeting was reassuring in this regard. Phages are inherently harmless to eukaryotic cells, so the health risks associated with phage therapeutics stem primarily from the debris in the source bacterial lysates and the immunological sequelae attendant to the introduction of virions into human tissues. Nevertheless, some phage-specific rules should be established (2). For example, the use of lysogenic phages should be prohibited, mainly because they usually carry genes that alter the pathogenic potential of their hosts. In addition, the identity of the host receptor should be established for any phage proposed for therapeutic use, in part because this would seem a minimal hurdle for any therapeutic but also so that combinations of phages can be assembled that are less likely to generate resistant hosts that are defective for a single receptor.

Some effort toward standardization of phage collections and consistent use of phages across studies would also help the development of the field. To date, almost all of the published preclinical phage therapy studies have used their own phages for each study. Major hospitals should establish validated phage collections for in extremis, compassionate use applications, where, in many instances, the bacterial pathogen has been identified and could be tested for sensitivity to a library of phages (2). As with many other narrow-spectrum



Phage therapy reboot. (A to C) Three paradigm Caudovirales. (A) podophage T7, stubby tail; (B) myophage T4, contractile tail; (C) siphophage lambda, flexible tail; (D) tailocin (contractile type) (14); (E and F) a field of *Bacillus anthracis* before and 3 s after addition of 1 µg/ml lysin.

antibacterials, the specificity of phages requires the availability of rapid methods for identifying bacterial pathogens as a necessary development in any scenario involving phage-based therapeutics.

The early abandonment of phage therapy by the 1940s was largely due to the poor understanding of what phages were or how they functioned (1). Several newer phage therapy initiatives are attempting to leverage modern synthetic biology techniques such as in vitro genome assembly or yeast-based engineering platforms, based on the idea that virulence and specificity features of effective phages can be identified and reassorted combinatorially to produce “ideal” killer phages optimized for various pathogens (11, 12). On this point, phage biology is still a “mile deep and an inch wide,” much of it derived from studies of classic phages like T4, T7, and lambda, chosen for their facile genetics in domesticated laboratory strains. Despite its depth and rigor, this record is too narrow and elderly to be a stable underpinning for the coming tsunami of phage genomics, or for the application or engineering of phages as antibacterials in systems far removed from *E. coli* K-12.

Aside from receptor recognition, many phages require intimate interactions with other host components, such as chaperones and transcription factors, to complete their life cycles, and these interactions must be understood in greater detail if routine engineering of phages is to become a reality. Moreover, plaque formation on agar plates or lysis of bacteria in shaker flasks is not likely to be a good predictor for efficacy in a therapeutic scenario. How phages are transported into the niches inhabited by their bacterial targets in vivo, and how they interact with bacteria in their normal physiological state in the body, need serious attention. In addition, there are new reports that phages have evolved features to exploit the surface architecture of human tissues for enhancing bacterial predation (13). This discovery points to enhanced prospects for the application of phage engineering but also is indicative of how many surprises may be in store for us now that phage biology is moving beyond its historic role as a model system. Unlike chemical antibiotics, phages are biological entities of incredible diversity and adapt-

ability. That’s the good news and the bad news, especially since the majority of phage genes are of unknown function. In sum, caution, diligence, rigor, and patience are necessary if phage biology is to realize its full potential in support of human health. ■

REFERENCES

1. W.C. Summers, *Annu. Rev. Microbiol.* **55**, 437 (2001).
2. J. J. Gill, R. Young, in *Emerging Trends in Antibacterial Discovery: Answering the Call to Arms*, A. A. Miller, P. F. Miller, Eds. (Horizon Scientific, Norwich, UK, 2011), pp. 367–410.
3. A. Reyes, M. Wu, N. P. McNulty, F. L. Rohwer, J. I. Gordon, *Proc. Natl. Acad. Sci. U.S.A.* **110**, 20236 (2013).
4. NIAID Conference: Bacteriophage Therapy: An Alternative Strategy to Combat Drug Resistance; <https://respond.niaid.nih.gov/conferences/bacteriophage/>.
5. H. Brüssow, R.W. Hendrix, *Cell* **108**, 13 (2002).
6. V.A. Fischetti, *Curr. Opin. Microbiol.* **11**, 393 (2008).
7. M. G. Ghequire, R. De Mot, *Trends Microbiol.* **23**, 587 (2015).
8. S.R. Williams, D. Gebhart, D.W. Martin, D. Scholl, *Appl. Environ. Microbiol.* **74**, 3868 (2008).
9. www.phagoburn.eu/about-phagoburn.html
10. R. Nannapaneni, K. A. Soni, in *Biofilms in the Food Environment*, A. L. Pomotto III, A. Demirci, Eds. (Wiley Blackwell, Chichester, UK, 2015), pp. 131–144.
11. F. L. Nobrega, A.R. Costa, L. D. Kluskens, J. Azeredo, *Trends Microbiol.* **23**, 185 (2015).
12. H. Ando et al., *Cell Systems* **1**, 187 (2015).
13. J. J. Barr et al., *Proc. Natl. Acad. Sci. U.S.A.* **112**, 13675 (2015).
14. P. Geet et al., *Nat. Struct. Mol. Biol.* **22**, 377 (2015).

¹Center for Phage Technology, Texas A&M University, College Station, TX 77843, USA. ²Department of Biochemistry and Biophysics, Texas A&M University, College Station, TX 77843, USA. ³Department of Animal Science, Texas A&M University, College Station, TX 77843, USA. Email: ryland@tamu.edu; jason.gill@tamu.edu

A speedy marriage in supramolecular catalysis

Cross-coupling reactions can be accelerated by trapping the metal catalyst in a confined space

By KaKing Yan and Makoto Fujita

Enzymes catalyze a wide range of slow biological reactions by crafting their local environments to accommodate and interact with reactants (1). Chemists aiming to design synthetic systems with enzyme-like activity have previously introduced conventional catalysts directly into an enzyme pocket to facilitate reactions of interest (2). On page 1235 of this issue, Kaphan *et al.* (3) use a related strategy to speed up an alkyl-alkyl cross-coupling reaction that is prohibitively slow on its own (4). However, instead of a natural enzyme, the authors use a synthetic cocatalyst that forms a cage around

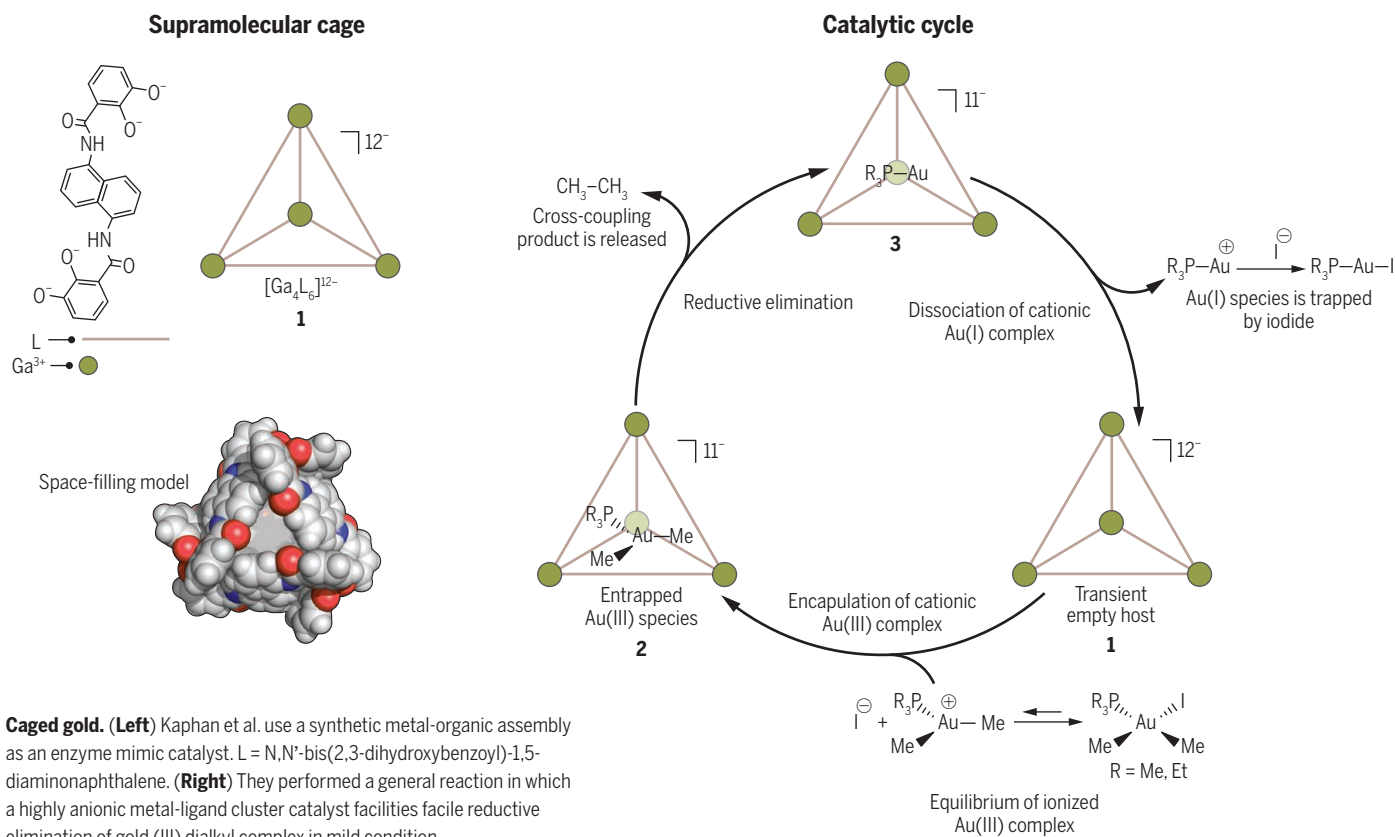
their organometallic catalysts. The synthetic enhances the rate of a key step of the reaction, reductive elimination, by at least a factor of seven.

The authors use a supramolecular cage that is self-assembled from organic ligand molecules (linkers) and metal ions (nodes) (see the figure, left). The host molecule is highly anionic and contains a hydrophobic cavity that favors entrapment of cationic compounds, including different organic and organometallic molecules. In such host-guest systems, noncovalent interactions—such as aromatic interactions, electrostatics and, hydrophobic effects—govern the interaction between the host and guest molecules. These comparatively weak forces can stabilize reactive intermediates (5–7), accelerate chemical reactions (8), and direct chemical processes to produce nonthermodynamic products (9–11).

A key property of enzyme catalysis is substrate size exclusion. The host's recognition of appropriately shaped and sized guests is often used in nature but rarely incorporated into standard homogeneous or heterogeneous catalysis. Kaphan *et al.* found that, in their system, the size of the phosphine ligand on the guest complexes is crucial. If this ligand is too big, the substrate is neither entrapped nor catalyzed. If the ligand is too small, catalyst deactivation is observed.

The vast majority of chemical reactions are catalyzed by transition metal compounds. In many of these processes, reductive elimination is a key product-forming step. In the case of gold-catalyzed reactions, previous studies have suggested that reductive elimination from the Au(III) center proceeds through ligand dissociation before the release of the carbon-carbon bond coupling product (4, 12, 13). Based on their data, Kaphan *et al.* argue for a different process, in which halide dissociates from the gold complex before it is encapsulated by the host. This generates a transient cationic Au(III) dialkyl complex within the anionic cage cavity. Due to the steric congestion imposed by the cage, the entrapped Au(III) complex spontaneously undergoes alkyl-alkyl cross-coupling to give an alkane product (see the figure, right). This reaction would be very sluggish without the supramolecular cage.

Department of Applied Chemistry, University of Tokyo, Tokyo, Japan. E-mail: yan.kaking@appchem.t.u-tokyo.ac.jp; mfujita@appchem.t.u-tokyo.ac.jp



Studies that integrate transition metal catalysis with a supramolecular assembly often use one of two general strategies. In the first, the metal catalyst is covalently linked to the ligand framework. This method is widely applied in metal-organic framework (MOF) catalysis through postsynthetic modification (14). The second strategy is that used by Kaphan *et al.*, in which catalysts are trapped in the cavity of a framework using noncovalent interactions. For both strategies, previous studies reported modest rate acceleration or product inhibition, limiting the value of these systems for practical applications. Kaphan *et al.* observed neither limitation. Instead they found enzyme-like behavior: Elemental steps of a catalytic cycle can be accelerated to a practical level; reaction mechanisms differ in the presence and absence of the supramolecular host; and size selectivity of substrates is imposed by the host molecule. These are all appealing features not only to organic chemists but also to biochemists and material scientists.

Despite the impressive work by Kaphan *et al.*, use of supramolecular catalysts in practical industrial applications is still a long way off. The major road block is the limited range of substrates that can be catalyzed compared with well-known homogeneous or heterogeneous catalysts. Small changes in substrate can lead to dramatic drops in reactivity or selectivity (15). Nevertheless, it is remarkable that the performance of Kaphan *et al.*'s meticulously designed system is on a par with that of natural enzymes. More important, the work may stimulate other chemists to integrate synthetic supramolecular systems with existing transition metal catalysts to achieve reactivity that neither alone can reach. ■

REFERENCES

1. R. Wolfenden, M. J. Snider, *Acc. Chem. Res.* **34**, 938 (2001).
2. T. K. Hyster, L. Knörr, T. R. Ward, T. Rovis, *Science* **338**, 500 (2012).
3. D. M. Kaphan, M. D. Levin, R. G. Bergman, K. N. Raymond, F. D. Toste, *Science* **350**, 1235 (2015).
4. W. J. Wolf, M. S. Winston, F. D. Toste, *Nat. Chem.* **6**, 159 (2014).
5. P. Mal, B. Breiner, K. Rissanen, J. K. Nitschke, *Science* **324**, 1697 (2009).
6. D. J. Cram, M. E. Tanner, R. Thomas, *Angew. Chem. Int. Ed. Engl.* **30**, 1024 (1991).
7. T. Iwasawa, R. J. Hooley, J. Rebek Jr., *Science* **317**, 493 (2007).
8. J. Hastings, D. Fiedler, R. G. Bergman, K. N. Raymond, *J. Am. Chem. Soc.* **130**, 10977 (2008).
9. M. Yoshizawa, M. Tamura, M. Fujita, *Science* **312**, 251 (2006).
10. D. M. Kaphan, F. D. Toste, R. G. Bergman, K. N. Raymond, *J. Am. Chem. Soc.* **137**, 9202 (2015).
11. D. M. Dalton *et al.*, *J. Am. Chem. Soc.* **137**, 10128 (2015).
12. A. Tamaki *et al.*, *J. Am. Chem. Soc.* **96**, 6140 (1974).
13. S. Komiya, J. K. Kochi, *J. Am. Chem. Soc.* **98**, 7599 (1976).
14. Z. Q. Wang, S. M. Cohen, *Chem. Soc. Rev.* **38**, 1315 (2009).
15. D. H. Leung *et al.*, *J. Am. Chem. Soc.* **129**, 2746 (2007).

10.1126/science.aad7245

ECOLOGY

Corridors for people, corridors for nature

How can the environmental impacts of roads be reduced?

By Nick M. Haddad

Transportation corridors have long helped to spread people into more remote places (1). In the past century, a burgeoning road network has grown in concert with the human population, connecting people across entire continents. The immense benefits of roads connecting people to agriculture, natural resources, mines, and each other must be reconciled with their severe environmental degradation.

Roads directly replace nature on the road's path. Low-intensity paths of soil or stone clear natural habitats, and asphalt and concrete erase nature entirely. At least 64 million lane-km of paved and unpaved roads cover 19 million hectares of Earth's surface (see the graph) (2). The road network is expected to grow in concert with the growing human population and rising consumption (3).

Roads also initiate effects that radiate outward. Natural systems near roads and their rights of way (the areas reserved and cleared adjacent to them) are degraded by exposure to changes in wind, temperature,

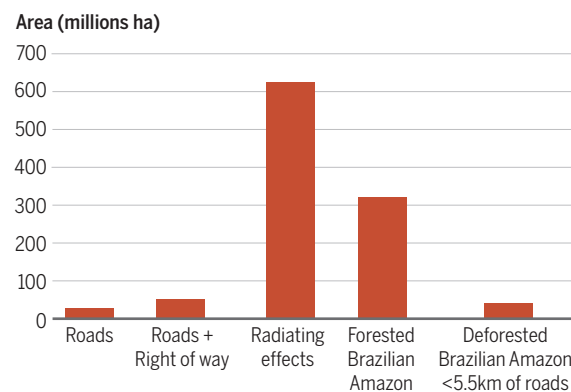
and nutrients and by increased abundances of destructive invasive species (see the graph) (4). Nearly 70% of U.S. forest lies within 1 km of a road (5). Effects of road disturbances can be extensive; for example, carbon sequestration is lowered within 1.5 km of tropical forest borders, thus degrading ecosystems and reducing the benefits of these forests to people (6).

Even more devastating, roads have spill-over effects, with people clearing newly accessible forests, plowing prairies, and draining wetlands (see the graph). Be it urban build-out in the southeastern United States (7) or deforestation in the Brazilian Amazon (8), roads spawn clearing of natural areas.

Finally, although roads create corridors for people, they sever corridors for wild nature. Just as people require corridors for transportation, wildlife requires natural corridors for their dispersal and migration. Roads isolate plant and animal populations, thus degrading diversity and ecosystems. A single road reduces gene flow by bighorn sheep to levels expected for populations separated by more than 15 km (9). The conflict between connections for people and those for wildlife

becomes most apparent when vehicles and wildlife collide, estimated at 1 to 2 million collisions with large animals annually that cost \$8 billion in the United States alone (10).

The effects of roads can be reduced through judicious routing, design, and reduction. Both in developed and developing regions, such careful road planning can benefit people while minimizing harm to the environment (4, 10, 11). Proper road siting, design, and management not only helps to protect valuable ecosystem services and biodiversity but also allows natural ecosystems to aid in control of erosion, flooding, and landslides. Collaboration between national governments and international development agencies can prevent the worst environmental outcomes (12). For example, spatial planning for a highway connecting



Radiating effects of roads. The global areas affected by roads are compared to the area of the forested Amazon and to deforested land area in the Brazilian Amazon that lies within 5.5 km of roads (8). The road area is calculated as their length (2) times a standard road width of 3 m. The right of way (the maintained area immediately adjacent to the road) was assumed to be 10 m wide, a minimum width to account for variation across nations. The radiating area of degrading effects caused by roads in habitats unmaintained for roads was taken as 100 m wide (50 m on each side of the road) for each lane. These distances are well within common effects propagating from habitat borders to their interiors. [Data for area of forested Amazon comes from PRODES, 2012 data, which is publicly available at <http://www.dpi.inpe.br/prodesdigital/prodes.php>]



Road impacts. Roads often have detrimental effects on the surrounding environment, as seen for this logging road through a deforested area of Borneo.

the capitals of Acre and Rondônia in Brazil included measures to reduce deforestation in an adjacent land area of 250,000 km². In Costa Rica, Braulio Carrillo National Park was created in conjunction with a highway connecting San José and Puerto Limón (4).

Roads can be sited to benefit people while minimizing their environmental and social costs. Laurance *et al.* (11) have identified regions around the globe where road creation would have high agricultural benefit and low environmental cost, and other regions where road creation should be avoided because of low agricultural benefit and high environmental cost. Scientific efforts like these to systematically account for costs and benefits of roads, especially where agricultural use is expanding, will now have to be adopted by the national, regional, and local governments that plan and create roads.

It is possible to connect landscapes for nature along or across roads. Along roads, restoration of natural vegetation in public land maintained adjacent to roads offers support for the plants and animals whose habitats have been cleared. Such efforts are increasingly adopted in the developed world. One model is the U.S. state of Iowa, which maintains these areas for prairie and other habitats. Given that much of the land adjacent to roads is already in the public domain, resto-

ration of native habitats will connect landscapes, especially along low-traffic roads with lower rates of animal mortality. To reduce the likelihood of further land-use change adjacent to roads, protected areas can be created that also include sensitive areas nearby (4).

Once roads are sited, the potential conflict between people and nature can be avoided through construction of compatible corridors across roads for wildlife. Road overpasses and underpasses can be created to mimic natural corridors. These are endowed with environmental conditions needed for plants and animals to pass. Such corridors are created in increasing numbers in North America, Europe, Asia, and Australia. Where done well, these corridors for nature are wide (50 to 100 m to accommodate all wildlife), unobstructed, and well-spaced (2 km), with fencing along roadsides that guides animals away from cars and toward safe passage (10, 13, 14).

Targeted siting of new roads will be most immediate in reducing environmental harm, and corridors and roadside conservation can help to protect wildlife. But an even stronger future vision would reduce the rate and extent of road construction. This is at odds with the growing number and affluence of people. Yet, alternative systems of transportation are possible. For example, less branched and more connected roads can minimize loss and fragmentation of habitat (7, 15), and shifts from road to rail for transport between major

hubs reduce incentives to transform land use between them (3). ■

REFERENCES

1. R. Grollemund *et al.*, *Proc. Natl. Acad. Sci. U.S.A.* **112**, 13296 (2015).
2. *The World Factbook 2013-14* (Central Intelligence Agency, Washington, D.C., USA, 2013).
3. J. Dulac, *Global Land Transport Infrastructure Requirements: Estimating Road and Railway Infrastructure Capacity and Costs to 2050* (International Energy Agency, Paris, France, 2013).
4. L. Mandle, R. M. Griffin, J. H. Goldstein, *Natural Capital and Roads: Managing Dependencies and Impacts on Ecosystem Services for Sustainable Road Investments* (Natural Capital Project, Stanford, CA, 2014).
5. K. H. Riitters, J. D. Wickham, *Frontiers in Ecology and the Environment* **1**, 125 (2003).
6. R. Chaplin-Kramer *et al.*, *Nature Communications* **10**, 1038/ncomms10158 (2015).
7. A. J. Terando *et al.*, *PLOS ONE* **9**, DOI: 10.1371/journal.pone.0102261 (2014).
8. C. P. Barber, M. A. Cochrane, C. M. Souza, W. F. Laurance, *Biological Conservation* **177**, 203 (2014).
9. C. W. Epps *et al.*, *Ecology Letters* **8**, 1029 (2005).
10. N. M. Lister, M. Brocki, R. Ament, *Frontiers in Ecology and the Environment* **13**, 493 (2015).
11. W. F. Laurance *et al.*, *Nature* **513**, 229 (2014).
12. L. Mandle *et al.*, *Conservation Letters*, DOI:10.1111/conl.12201.
13. J. P. Beckmann, A. P. Clevenger, M. Huijser, J. A. Hilty, *Safe Passages: Highways, Wildlife, and Habitat Connectivity* (Island Press, 2012).
14. A. P. Clevenger, M. P. Huijser, *Wildlife Crossing Structure Handbook: Design and Evaluation in North America* (Western Transportation Institute, 2011).
15. C. Barrington-Leigh, A. Millard-Ball, *Proc. Natl. Acad. Sci. USA* **112**, 8244 (2015).

ACKNOWLEDGMENTS

I thank R. Dunn, L. Mandle, and A. Terando for comments, and C. Jenkins and N. McCoy for assistance.

10.1126/science.aad5072

CLIMATE POLICY

Can Paris pledges avert severe climate change?

Reducing risks of severe outcomes and improving chances of limiting warming to 2°C

By Allen A. Fawcett,¹ Gokul C. Iyer,^{2†} Leon E. Clarke,² James A. Edmonds,² Nathan E. Hultman,^{3*} Haewon C. McJeon,² Joeri Rogelj,⁴ Reed Schuler,⁵ Jameel Alsalam,¹ Ghassem R. Asrar,² Jared Creason,¹ Minji Jeong,² James McFarland,¹ Anupriya Mundra,² Wenjing Shi²

Current international climate negotiations seek to catalyze global emissions reductions through a system of nationally determined country-level emissions reduction targets that would be regularly updated. These “Intended Nationally Determined Contributions” (INDCs) would constitute the core of mitigation commitments under any agreement struck at the upcoming Paris Conference of the Parties to the United Nations Framework Convention on Climate Change (UNFCCC) (1). With INDCs now reported

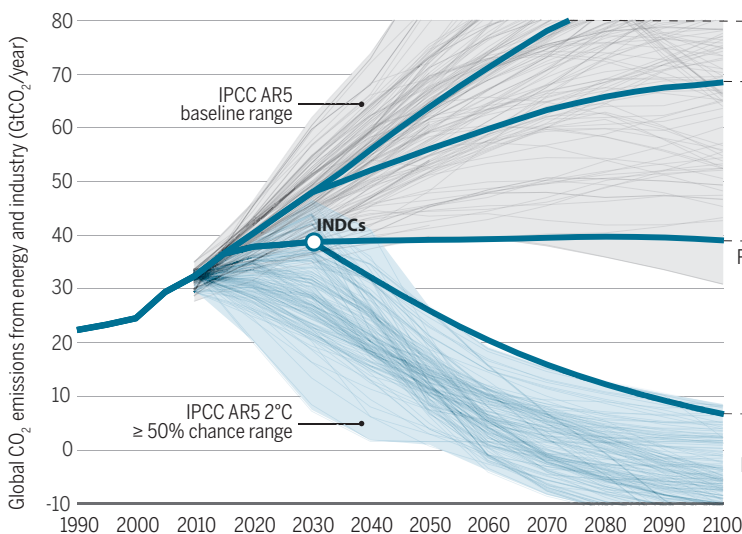
from more than 150 countries and covering around 90% of global emissions, we can begin to assess the role of this round of INDCs in facilitating or frustrating achievement of longer-term climate goals. In this context, it is important to understand what these INDCs collectively deliver in terms of two objectives. First, how much do they reduce the probability of the highest levels of global mean surface temperature change? Second, how much do they improve the odds of achieving the international goal of limiting temperature change to under 2°C relative to preindustrial levels (2)? Although much discussion has focused on the latter objective (3–5), the former is equally important when viewing climate mitigation from a risk-management perspective.

POLICY A comprehensive assessment of these questions depends on two important consid-

erations. First, although the current negotiations seek to create a durable framework for mitigation action, the current round of INDCs extend only through 2025 or 2030 (1). Because temperature change depends on cumulative emissions over the entire century and beyond (6, 7), the INDCs must be viewed as a first step in a longer process, with an important part of their contribution being the subsequent paths that they, and the Paris framework, enable. Assessing the implications of Paris therefore requires consideration of multiple possible emissions pathways beyond 2030. Second, because of uncertainties in the global carbon-cycle and climate-system response (7), the contribution of the INDCs to global temperature change needs to be assessed from a probabilistic perspective rather than a deterministic one (8).

Accordingly, we calculate probabilistic temperature outcomes over the 21st century for four global emissions scenarios meant to represent different possible future developments with and without INDCs. Our analysis indicates that the INDCs deliver improvements for both objectives—both reducing the probability of the worst levels of temperature change to 2100 and increasing the probability of limiting global warming to 2°C (see the figure). However, the degree to which either objective is achieved will depend on the level of ambition beyond 2030.

A Emissions pathways



B Temperature probabilities

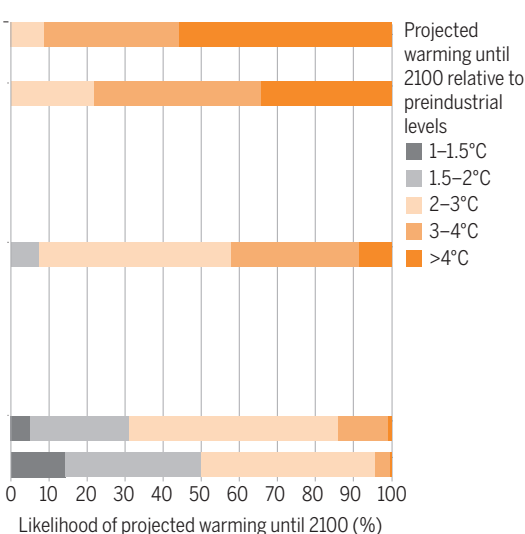


Fig. 1: Global CO₂ emissions and probabilistic temperature outcomes of Paris. (A) Global CO₂ emissions from energy and industry (includes CO₂ emissions from all fossil fuel production and use and industrial processes such as cement manufacture that also produce CO₂ as a byproduct) for the four emissions scenarios explored in this study. The IPCC AR5 emissions ranges are from (12). The IPCC AR5 baseline range comprises scenarios that do not include new explicit GHG mitigation policies throughout the century. The IPCC AR5 2°C ≥ 50% range comprises scenarios that limit global warming until 2100 to less than 2°C with at least a 50% chance. The faint lines within the IPCC ranges represent the actual emissions trajectories that determine the range (12). (B) Likelihoods of different levels of increase in global mean surface temperature change during the 21st century relative to preindustrial levels for the four scenarios. Although (A) shows only CO₂ emissions from energy and industry, temperature outcomes are based on the full suite of GHG, aerosol, and short-lived species emissions generated by the GCAM (9) simulations (see SM). The Illustrative 50% scenario in (B) corresponds to an emissions pathway that achieves a 50% chance of maintaining temperature change below 2°C until 2100 (see SM). Other 50% pathways could lead to a range of temperature distributions depending on cumulative CO₂ emissions and representations of other GHGs.

EMISSIONS PATHWAYS. To develop the emissions pathways (see the figure, part A), we use a global integrated assessment model [GCAM (9)], although our core findings do not hinge on the particular character of this model [see the supplementary materials (SM)]. Probabilistic temperature outcomes over the 21st century are then calculated using a global climate model [MAGICC (10)] in a setup representing the latest climate-sensitivity assessment of the Intergovernmental Panel on Climate Change (IPCC) (11).

Our analysis begins with two reference scenarios. The Reference–No policy scenario assumes no new greenhouse gas (GHG) mitigation actions throughout the 21st century and serves as a counterfactual against which to compare the other scenarios. The Reference–Low policy scenario illustrates a world in which there are no new GHG mitigation actions through 2030, and countries “muddle through” with weak policies beyond 2030 that achieve a 2% annual rate of improvement in CO₂ emissions per unit of Gross Domestic Product (GDP) (“decarbonization rate”) (see SM and table S1).

The Paris–Continued ambition and Paris–Increased ambition scenarios illustrate potential implications of the INDCs. Both assume that parties meet their INDC goals through 2030 (see SM and table S4), but then assume different decarbonization rates beyond 2030. We do not take up the question of how likely individual countries are to achieve their INDCs, but rather assume that these goals are met and pursue the question of how that successful implementation shapes potential future options.

The Paris–Continued ambition scenario assumes that countries continue to decarbonize their economies beyond 2030 with the same annual decarbonization rate that was required to achieve their INDCs between 2020 and 2030. If their decarbonization rate is below a specified minimum (2% per year), they instead follow a path defined by that 2% minimum rate (table S1). In contrast, the Paris–Increased ambition scenario assumes a higher minimum decarbonization rate (5% per year) beyond 2030. This minimum rate is consistent with the average decarbonization rate required by the European Union and the United States to achieve their INDCs from 2020 to 2030 (SM).

TEMPERATURE PROBABILITIES. Using the above scenarios, we estimate probabilistic temperature outcomes over the 21st century (see the figure, part B). The Paris–Continued ambition scenario reduces the probability of temperature change exceeding 4°C in 2100 by 75% compared with the Reference–Low policy scenario and by 80% compared with the Reference–No policy scenario. If mitigation efforts are increased beyond 2030, as in the Paris–Increased ambition scenario, the chance of exceeding 4°C is almost eliminated.

The INDCs hold open the possibility of maintaining temperature changes below 2°C, although none of our scenarios eliminates the possibility that temperature change could exceed 2°C. In the Paris–Continued ambition scenario, the probability of limiting warming to 2°C increases to 8% as

“the contribution of the INDCs to global temperature change needs to be assessed from a probabilistic perspective rather than a deterministic one....”

opposed to virtually no chance in the two Reference scenarios. If ambition is scaled up after 2030—as in the Paris–Increased ambition scenario—the probability of limiting warming to 2°C increases to about 30%. If we assume even greater post-2030 emissions reductions, the probability of limiting warming to less than 2°C could be 50% or more. Indeed, many scenarios in the literature assume emissions through 2030 that are comparable to or higher than our Paris scenarios, yet limit warming to 2°C in 2100 with at least 50% probability, with many exceeding 66% (see the figure, part A) (12). These scenarios include rapid emissions reductions beyond 2030. Many also include negative global emissions in the second half of the century, based on large-scale deployment of bioenergy in conjunction with carbon capture and storage (13–15).

Two key factors should be considered when interpreting results of this analysis. First, to limit warming to any level, CO₂ emissions at the global level must ultimately be brought to zero (6). Although the two Paris scenarios provide meaningful benefits relative to the two Reference scenarios, if emissions are not brought swiftly to zero beyond 2100, the chances of extreme temperature change after 2100 could be much

higher and the chance of limiting warming to 2°C much lower.

Second, the above analysis is based on one set of assumptions about key drivers of emissions such as technologies, regional population, and GDP. Although it is beyond the scope of this study to assess probabilities of achieving future emissions pathways, alternative assumptions are certainly possible (14), and the choice of assumptions might influence emissions pathways as well as precise probabilities associated with scenarios in this study. [Implications of alternative drivers are explored in figs. S5 to S8 and the (SM).] Nevertheless, key qualitative insights will remain the same: The Paris scenarios reduce probabilities of extreme warming and increase the probability of limiting global warming to 2°C this century, but depend on a robust process that allows pledges to be progressively tightened over time. ■

REFERENCES AND NOTES

- UNFCCC, INDCs as communicated by Parties (UNFCCC, Bonn, Germany, 2015); <http://bit.ly/INDC-UNFCCC>.
- UNFCCC, in *Report of the Conference of the Parties on its 18th session, Addendum, Part Two: Action taken by the Conference of the Parties at its 18th session*, Doha, Qatar, from 26 November to 8 December 2012 (FCCC/CP/2012/8/Add.1, UNFCCC, Bonn, Germany, 2012), pp. 1–37.
- UNFCCC, *Synthesis Report on the Aggregate Effect of the Intended Nationally Determined Contributions* (UNFCCC, Bonn, Germany, 2015); <http://unfccc.int/resource/docs/2015/cop21/eng/07.pdf>.
- Climate Action Tracker, *How close are INDCs to 2° and 1.5°C pathways?* (CAT, 2015); <http://bit.ly/EmissionsGap>.
- Climate Interactive, <https://www.climateinteractive.org/>.
- M. Collins et al., in *Climate Change 2013: The Physical Science Basis. Contribution of Working Group I to the Fifth Assessment Report of the IPCC* (Cambridge Univ. Press, Cambridge, 2013), pp. 1029–1136.
- IPCC, *Climate Change 2014: Synthesis Report. Contribution of Working Groups I, II and III to the Fifth Assessment Report of the IPCC* (IPCC, Geneva, 2014).
- S. T. Waldhoff, A. A. Fawcett, *Clim. Change* **107**, 635 (2011).
- GCAM Wiki documentation (2015); https://wiki.umd.edu/gcam/index.php/Main_Page.
- M. Meinshausen, S. C. B. Raper, T. M. L. Wigley, *Atmos. Chem. Phys.* **11**, 1417 (2011).
- J. Rogelj et al., *Environ. Res. Lett.* **9**, 031003 (2014).
- IPCC, AR5 Scenario Database (IPCC, Geneva, 2015); <http://bit.ly/Ar5Scenario>.
- G. Iyer et al., *Technol. For. Soc. Change* **90** (PA), 103 (2015).
- L. Clarke et al., in *Climate Change 2014: Mitigation of Climate Change. Contribution of Working Group III to the Fifth Assessment Report of the IPCC*, O. Edenhofer et al., Eds. (Cambridge Univ. Press, Cambridge, 2014), pp. 413–510.
- K. Riahi et al., *Technol. For. Soc. Change* **90** (PA), 8 (2015).

ACKNOWLEDGMENTS

G.C.I., L.E.C., J.A.E., H.C.M., M.J., and A.M. and were partially supported by the Global Technology Strategy Program, a research program at JGCRI. N.E.H. was supported by the William and Flora Hewlett Foundation. Analysis of mitigation potential and levels of national mitigation action related to the conclusions of this paper was supported by the U.S. Department of State (IAA 19318814Y0012) and the U.S. Environmental Protection Agency (EPA) (IAA DW–8992406301). The views and opinions expressed in this paper are those of the authors alone and do not necessarily state or reflect those of the U.S. Government, the Department of State, the EPA, or CEQ, and no official endorsement should be inferred.

SUPPLEMENTARY MATERIALS

www.sciencemag.org/content/350/6265/1168/suppl/DC1

10.1126/science.aad5761

Published online 26 November 2015

¹U.S. Environmental Protection Agency, Washington, DC 20460, USA. ²Joint Global Change Research Institute, Pacific Northwest National Laboratory and University of Maryland, College Park, MD 20740, USA. ³School of Public Policy, University of Maryland, College Park, MD 20742, USA. ⁴Energy Program, International Institute for Applied Systems Analysis (IIASA), A-2361 Laxenburg, Austria. ⁵U.S. Department of State, Washington, DC 20520, USA. *On temporary assignment at the Council on Environmental Quality (CEQ), Washington, DC 20506, USA. †Corresponding author. E-mail: gokul.iyer@prnl.gov

CLIMATE CHANGE

Political agency: The key to tackling climate change

Individuals play a central role in the transformations required to avoid dangerous climate change

By Karen O'Brien

This month, representatives from more than 190 nations are gathering in Paris to participate in the 21st Conference of the Parties (COP21). There is widespread demand for a universal and binding political agreement that will limit the global average temperature increase to less than 2°C above its preindustrial value. But an agreement by itself does not guarantee action and desirable outcomes, and current pledges are far from sufficient to limit warming to 2°C. Nor are new technologies and energy infrastructure a panacea. Meeting this ambitious target and adapting to the impacts and risks associated with a warmer world will require transformations of a scope, magnitude, speed, and penetration that are unprecedented in human history. Without an instruction manual, where do we begin?

A good place to start is to look at political agency, which in the context of climate change refers to the capacity to positively influence the collective future through transformative change. Research on transformation identifies various pathways through which to address climate change, including technological innovations, market mechanisms, government regulations, new economic models, and the promotion of lifestyle and behavioral changes. The relative importance of each is widely contested (1). Should we call upon individuals to ride a bicycle, eat less meat, and avoid flying, or instead try to create support for such behaviors by constructing bicycle lanes, increasing vegetarian options, and ending fossil fuel subsidies?

Climate solutions are likely to emerge from interactions among all of the above. But can individuals really make a difference? Their perceived influence has generally been limited to behavioral change, consumption choices, voter participation, and the setting of examples. Such actions are important

but do not address structural factors—the norms, rules, regulations, and institutions that influence individual and collective preferences and actions that are key to social transformations.

Increased consumption, long-distance vacations, and individualized transportation are material and cultural manifestations of a larger social context (2). Some argue that changing this context calls for radical approaches, such as transforming the capitalist economic system with its assumption and goal of continuous growth (3). The current emphasis on “green growth” is considered to be a reformist approach, rather than one that will effectively reconfigure systems and practices (4).



Rising waters. Floodwaters in Malabon City north of Manila, Philippines on 15 March 2012. Climate change is expected to increase the flood risk in many parts of the world unless greenhouse gas emissions are reduced drastically.

Because of the scope and scale of transformations needed to reduce climate change risks and vulnerability, a more expansive view of political agency is required—a view that captures an individual's ability to contribute to transformations both by changing behavior and by influencing structures and systems. Political agency has traditionally been reserved for political parties, unions, bureaucracies, states, and international actors, as well as individual leaders who are entrusted with the power to act on behalf of others (5). A broader and deeper understanding of political agency recognizes that individual change and collective change are, in fact, connected.

In recent years, committed individuals have been working with cities, schools, businesses, communities, nations, and government institutions and networks, with the intent to challenge energy policies, change investment practices, rethink disaster risk management strategies, and transform aspects of everyday life that were previously considered non-negotiable (6). A broader notion of political agency recognizes that such seemingly small actions of individuals can have widespread global effects (7). Cooperative behavior can cascade through social networks, and each person in a network influences more people than they might think (8). The prevailing opinion in a population can be reversed rapidly when only 10% of the committed agents propose and argue for an alternative opinion (9). Rapid large-scale transformations thus can and often do emerge from changes at the individual and local levels. By expressing political agency, individuals play an important, yet often overlooked, role in transformations toward sustainability.

The political agency of individuals is evidenced through a proliferation of climate change initiatives. These include grassroots movements such as 350.org, the World Mayors Council on Climate Change, the Youth Climate Movement, the Women's Earth and Climate Action Network, and other organizations made up of individuals who are confronting entrenched interests, challenging old practices, and engaging directly with alternatives that emphasize sustainability and social justice. The political agency of individuals can also be expressed through decisions made within traditional organizations, such as companies involved in the Oil and Gas Climate Initiative, the Norwegian government's withdrawal of pension fund investments in coal-burning utilities, and the Guardian newspaper's expanded focus on climate change.

Nonetheless, the speed of transformations necessary to mitigate and adapt to climate change in an equitable and sustainable manner is likely to require not only a broader notion of political agency, but also a deeper one. A deeper notion of political agency draws attention to the beliefs, values, and world views that maintain habits and the status quo (10). Beliefs may include the ideas that change has to come from the top, that economic legacies are separate or more important than ecological legacies, or that reducing CO₂ levels alone will address the challenges of climate justice and global sustainability. Political agency involves questioning assumptions and challenging what is taken by many as given, recognizing that

worldview transformations can play an explicit role in the development of prosocial, life-affirming behavior (11). It also involves engaging with alternatives and pursuing solutions that may be invisible to the mainstream view, such as permaculture.

A wider and deeper sense of political agency is a potent but so far mostly latent force for transformation. Changing one's diet, mode of transport, or political vote can be important. But transformations to sustainability will depend on individuals expressing political agency in many different ways, which can include participating in grassroots community initiatives such as the transition town movement, starting conversations with family and friends about alternative vacation ideas, or engaging with sustainability solutions through art and literature. What is important here is the recognition that individuals can effect change by engaging with ideas, activities, and conversations that trigger reflection and collaborative action.

COP21 is expected to attract as many as 50,000 participants, reflecting a growing recognition that business-as-usual approaches are insufficient for avoiding dangerous climate change (12). A recent survey conducted in 20 countries by the Pew Research Center shows that most of the public believes that policy changes will not be enough, and that lifestyle changes will be necessary to address climate change (13). In the aftermath of the Paris climate conference, one lifestyle change will stand out as key: cultivating political agency to lead transformative change. The delegates who gather at COP21 will define the boundaries for climate change that are considered acceptable and achievable, but it is individuals who will ultimately decide the future. ■

REFERENCES

1. K. Ehrhardt-Martinez et al., in *Climate and Society: Sociological Perspectives*, R. E. Dunlap, R. J. Brulle, Eds. (Routledge, London, 2015), pp. 93–106.
2. E. Shove, *Contemp. Soc. Sci.* **6**, 2158 (2012).
3. M. Pelling, D. Manuel-Navarrete, M. Redcliff, in *Climate Change and the Crisis of Capitalism: A Chance to Reclaim Self, Society and Nature*, M. Pelling, D. Manuel-Navarrete, M. Redcliff, Eds. (Routledge, London, 2012), pp. 1–17.
4. F. W. Geels et al., *Glob. Environ. Change* **34**, 1 (2015).
5. R. Marchetti, in *Contemporary Political Agency: Theory and Practice*, B. Maiguashca, R. Marchetti, Eds. (Routledge, London, 2013), pp. 1–13.
6. F. R. Westley et al., *Ecol. Society* **18** (3), 27 (2013).
7. A. El Khoury, *Globalization Development and Social Justice: A Propositional Political Approach* (Routledge, London, 2015).
8. J. H. Fowler, N. A. Christakis, *Proc. Natl. Acad. Sci. U.S.A.* **107**, 5334 (2010).
9. J. Xie et al., *Phys. Rev. E* **84**, 011130 (2011).
10. K. O'Brien, E. Selboe, in *The Adaptive Challenge of Climate Change*, K. O'Brien, E. Selboe, Eds. (Cambridge Univ. Press, Cambridge, 2015), pp. 1–23.
11. M. M. Schlitz, C. Vieten, E. M. Miller, *J. Consciousness Studies* **17** (7–8), 18 (2010).
12. T. Neef, *Environ. Sci. Policy* **31**, 157 (2013).
13. Pew Research Center, *Global Concern about Climate Change: Broad Support for Limiting Emissions* (5 November 2015); www.pewglobal.org/2015/11/05/global-concern-about-climate-change-broad-support-for-limiting-emissions.

10.1126/science.aad0267

CATALYSIS

Silica-supported catalysts get a new breath of life

Methods emerge for dispersing metals as stable nanoparticles on silica surfaces

By Stuart Soled

In heterogeneous catalysis, metals, metal oxides, and metal sulfides are traditionally dispersed as nanoscale particles on a support with a large surface area, so as to maximize the number of exposed active sites. Historically, alumina supports have been used for the majority of refining applications, but where acid sites catalyze unwanted isomerization or oligomerization reactions, silica would be a better choice. Despite this advantage, silica has often been considered a problematic support—an “ice skating rink”—because of the difficulty of forming strongly interact-

“The present state of knowledge also allows a reassessment of processes where alumina has been used but may not be optimal.”

ing precursors that wet the surface to yield well-dispersed particles. However, the past two decades have witnessed slow but steady progress in advancing several science-based approaches that will allow industrial-scale preparation of silica-supported catalysts.

Noble metals used as industrial catalysts play key roles in hydroisomerization, dehydrocyclization, hydrogenation, and ring-opening reactions, which are important in catalytic reforming, aromatic saturation, and lubricant dewaxing. Because noble metals often cost thousands of dollars per kilogram, low loadings of the metal (generally 0.1 to 1 weight percent) are necessary, and forming nanoscale particles is necessary to expose a large fraction of surface atoms. Worldwide, the refining market for catalysts is a >\$5 billion enterprise in which the two largest process areas for supported catalysts, catalytic reforming and hydroprocessing, constitute >50% of that total (1). Reported data indicate

that silica-supported catalysts represent <1% of the total in these two areas.

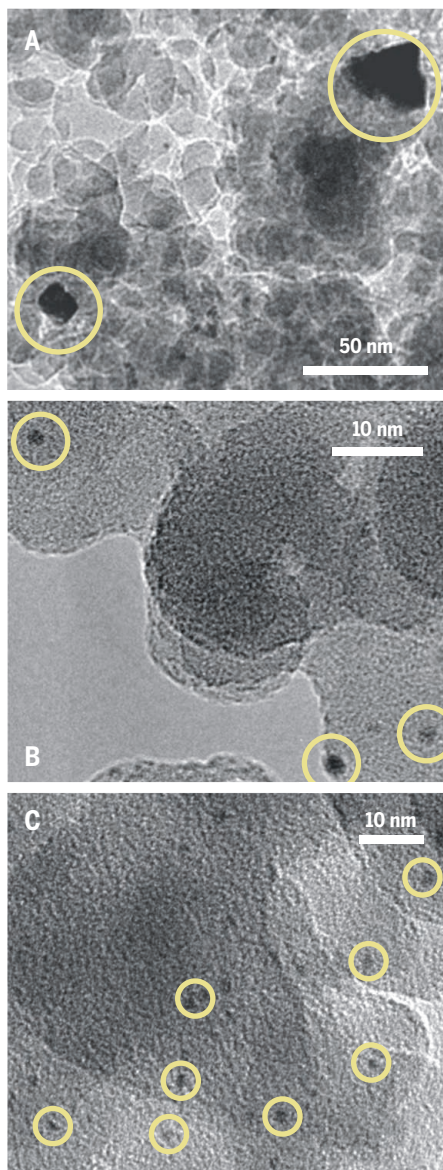
An early design strategy for supported metal catalysts was reported in an intriguing 1979 paper that applied colloidal chemistry methodology to supported catalysts (2). Specifically, the surface of a metal-oxide support particle suspended in water will assume a charge depending on the pH of the suspension and the nature of the metal oxide surface. Small, highly charged cations attached to surface OH groups keep the surface negatively charged through a wide pH range. An electrostatic attraction between the oxide support and the impregnate can be created by matching the impregnate charge (by using either an anionic or cationic species) with the pH of the suspension. When the pH of the suspension containing the small support particles is at a pH lower than the support isoelectric point, the support surface is positively charged and an anionic precursor is chosen; the opposite is done if the pH is above the isoelectric point of the support. For example, platinum tetraamine hydroxide cationic complexes adsorb on a negatively charged alumina support at pH above 9. This approach is widely applicable as long as an appropriate precursor complex is available in the correct pH range. This technique also scales fairly easily to the complex surfaces of industrial catalyst supports. In newer embodiments, core-shell metal structures on bimetallics are created by sequential addition of appropriate precursors (3). This approach has been applied to multiple systems by Regalbuto and co-workers (4).

Another approach controls the environment used during precursor decomposition by creating discrete intermediates that can interact more strongly with the support. For example, with supported copper or cobalt catalysts, introduction of nitric oxide (NO) during the thermal decomposition (calcination) of the cobalt nitrate precursor on silica produces evenly spaced metal-oxide nanoparticles that are then easy to reduce to uniformly distributed metal crystallites (5, 6).

The introduction of NO appears to create hydroxy-nitrate intermediates that wet the silica well, whereas metal oxides formed by calcining the noninteracting nitrate precursor

Corporate Strategic Research, ExxonMobil Research and Engineering Co., 1545 Route 22, East Annandale, NJ 08801, USA. E-mail: stu.soled@exxonmobil.com

sors form large oxide particles and large, clustered metal particles after reduction. Different temperatures, gas exposures, and modes of drying can make a large difference in particle formation, as evidenced by the preparation of uniform cobalt on silica particles by using fluid bed drying at 100°C in a nitrogen rather than air flow (7). These approaches, which have been led by de Jong, de Jongh, and their co-workers are also scalable. However, for each system, the particular technique (NO addition, drying variations, etc.) must be empirically determined.



Size selection on silica. (A and B) Transmission electron micrographs (TEMs) show a sample prepared with an aqueous tetraamine platinum hydroxide solution and calcined at 350°C followed by reduction. The result is a distribution of metal particle sizes. (C) The TEM shows a platinum-arginine preparation with air calcination at 425°C. Small, uniformly distributed metal crystals form upon reduction.

A third approach involves using simple water-soluble bifunctional organics—amino alcohols or amino acids—to form impregnates that interact strongly with silica. These bifunctional organics (such as triethanolamine and arginine) provide major advantages compared to using simple organic acids, which have served as more commonly used dispersion aids. With supported ruthenium and iridium, the preparation of optimal catalysts requires partial decomposition of the impregnate to form an anchored complex, which is then reduced and cleaned by hydrogenolysis to remove the organic fragment (8). In this way, ruthenium or iridium oxides, which are mobile on the silica surface, never form.

Other noble metals that do not have mobile oxide phases, such as platinum, palladium, and rhodium, can have their organic complex oxidized and reduced (see the figure). This technique has the advantage of keeping the two metals mixed and is well suited for making bimetallic alloy particles. It is widely applicable to most transition metals, but at high metal loadings and for large-scale preparations, the oxidation of organics must be controlled to avoid runaway exothermic reactions. In that regard, it is probably more suitable for noble metals that are generally kept at low loading levels.

These new approaches and our increased understanding of the scientific basis of controlling impregnations, metal nanostructures, and site homogeneity on silica-supported catalysts portend a wider use of these catalysts in the future. The present state of knowledge also allows a reassessment of processes where alumina has been used but may not be optimal. Increasing efforts to learn to control textural properties (surface areas, pore sizes, and pore volumes) on physically strong extrudates will also help propel this area forward, as most applications require this type of support particle. ■

REFERENCES

1. "World Catalysts," *Industry Study #2989* (The Fredonia Group, Cleveland, OH, 2013); www.freedoniagroup.com/brochure/29xx/2989smwe.pdf.
2. J. P. Brunelle, in *2nd International Symposium on Scientific Basis of Heterogeneous Catalysts* (Elsevier, Amsterdam, 1979), pp. 211–232.
3. H.-R. Cho, J. R. Regalbuto, *Catal. Today* **246**, 143 (2015).
4. J. R. Regalbuto, in *Silica and Silicates in Modern Catalysis*, I. Halasz, Ed. (Transworld Research Network, Kerala, India, 2010), pp. 345–374.
5. M. Wolters, P. Munnik, J. H. Bitter, P. E. de Jongh, K. P. de Jong, *J. Phys. Chem. C* **115**, 3332 (2011).
6. P. Munnik, N. A. Krans, P. E. de Jongh, K. P. de Jong, *ACS Catal.* **4**, 3219 (2014).
7. P. Munnik et al., *J. Phys. Chem. C* **115**, 14698 (2011).
8. S. Soled, in *Synthesis of Solid Catalysts*, K. P. de Jong, Ed. (Wiley, 2009), pp. 353–366.

10.1126/science.aad2204

PHYSICS

Classical entanglement?

Entanglement is a property of the quantum world; classical systems need not apply

By Ebrahim Karimi¹ and Robert W. Boyd^{1,2}

Since the inception of quantum theory, scientists and philosophers have been puzzled by the apparent indeterminacy of physical properties prior to the measurement process. These problems suggest that quantum mechanics might ultimately be incompatible with basic notions of “realism”—that is, the view that a physical system possesses inherent properties that are independent of procedures used to measure them. This issue lies at the core of the famous gedanken experiment of Einstein, Podolsky, and Rosen (EPR) (1) and of attempts to develop a conceptual understanding (2–4) of EPR correlations.

The concept of entanglement was initially introduced by Schrödinger (2) in his response to EPR. Entanglement refers to the strong, nonclassical correlations that can exist between two spatially separated quantum systems. Over the past 40 years or so, numerous studies have confirmed that nature does behave in the manner described by Schrödinger (5). In particular, the laws of physics have been found to be inherently nonlocal: The results of a measurement at one position in space can dictate the possible outcome of a measurement performed at a different position.

In recent years, the term entanglement has come to be used in a more general context, including single-particle entanglement (6, 7) and classical entanglement (8–11). We do not endorse this new nomenclature. Ascribing a new meaning to a term that has been in wide use in quantum physics for more than 80 years can only lead to confusion. But more deeply, these new situations lack the key feature—nonlocality—that led to the concept of entanglement in the first place. For example, single-particle

¹Department of Physics and Max Planck Centre for Extreme and Quantum Photonics, University of Ottawa, Ottawa, Ontario K1N 6N5, Canada. ²Institute of Optics, University of Rochester, Rochester, NY 14627, USA. E-mail: ekarimi@uottawa.ca; boydrw@mac.com

entanglement refers to correlations of two different degrees of freedom of an individual particle; this situation cannot lead to nonlocal correlations. Moreover, a classical system cannot possess any quantum correlations (classical correlations are incapable of describing quantum correlations).

For the situations just described, we prefer to use the term “nonseparable states.” To see why, we must examine the relation between entanglement and nonseparability. A basic tenet of quantum mechanics is that the wave function of any entangled state is necessarily nonseparable. For example, consider the quantum state $|\psi\rangle = (|a\rangle_1|b\rangle_2 + |b\rangle_1|a\rangle_2)/\sqrt{2}$, where $|a\rangle_1$ means that particle 1 is in quantum state a , the other (spatially separated) particle 2 is in state b , and similarly for the other quantities. The state ψ has the property that if a measurement of particle 1 shows it to be in state a , then a measurement of particle 2 will certainly show it to be in state b , and vice versa. Nonetheless, before any measurement is performed, there is an equal probability for each particle to be in either state a or b . Although all entangled states are nonseparable, it is not true, in our view, that all nonseparable states are entangled (see the figure). We prefer not to describe nonseparable states in terms of entanglement, because there is no sense of nonlocality for this situation. In fact, no classical system can produce true quantum entanglement, of the sort that Einstein called “spooky action at a distance.”

Let us next recall the work of John Bell (3), who examined whether correlations in the EPR form could be explained in terms of “local hidden variables.” The idea here is that these correlations could be the consequence of some classical random process involving a degree of freedom that is unknown to (hidden from) the experimenters. These variables are local, in the sense that they are carried separately by each of the particles. Bell was able to show that if a certain inequality involving directly measurable quantities were violated, then this violation would rule out the possibility of interpretation in terms of local hidden variables. To date, experimental studies (5) have produced evidence in favor of conventional quantum mechanics and have ruled out alternative local and crypto-nonlocal statistical interpretations (3, 4).

Turning now to some deeper issues involving single-particle and classical entanglement: In the single-particle case, nonseparability among different degrees of freedom of a single particle can be used to test other statistical models, such as noncontextual realistic models (7). However, several studies have recently reported

“...the term entanglement has come to be used in a more general context, including single-particle entanglement and classical entanglement. We do not endorse this new nomenclature.”

(9–11) the violation of a Bell inequality for nonseparable classical systems, and some have even suggested this violation would shift the quantum-classical boundary (10). If such a paradoxical interpretation were to be valid, it would indicate basic flaws with the current understanding of quantum mechanics.

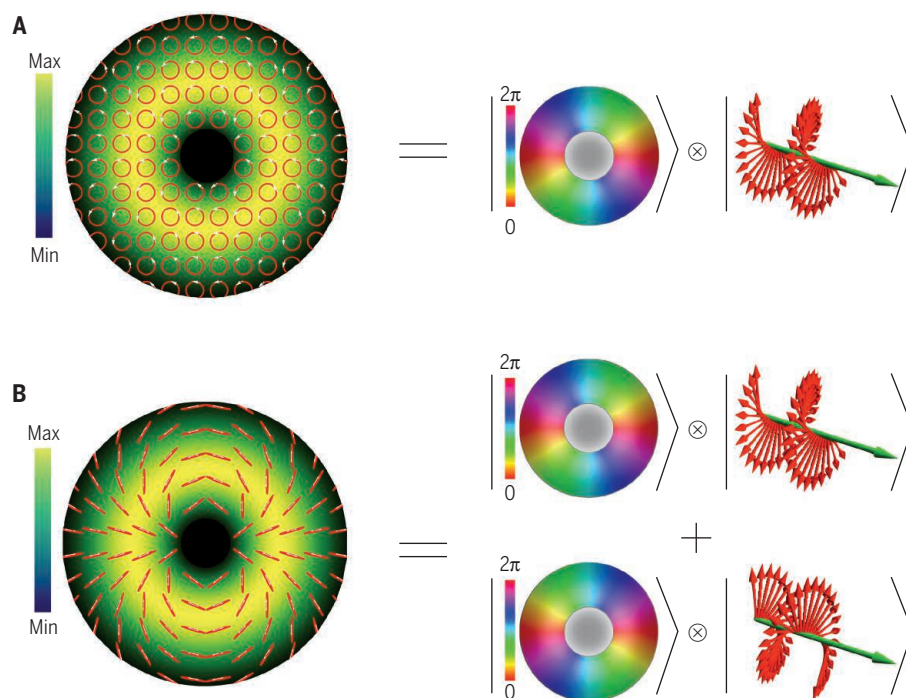
However, in our view such an interpretation is not correct. These violations do not indicate quantum behavior, as they occur only at a purely formal level. Expressions derived to describe nonlocal, two-particle entanglement (that is, Bell inequalities) have been evaluated with laboratory results

obtained from an entirely different physical system, which involve various degrees of freedom of a classical (9–11) system. It is not surprising that these expressions can take on meaningless values, as argued already in (8). It should also be clear that these tests cannot provide information on the nature of quantum theory, because there is no need to invoke quantum mechanics to describe classical physics. We point out, however, that even though these nonseparable classical states cannot be used to address any fundamental questions in quantum mechanics, they are proving to be useful in applications such as quantum metrology (12) and quantum information.■

REFERENCES

1. A. Einstein, B. Podolsky, N. Rosen, *Phys. Rev.* **47**, 777 (1935).
2. E. Schrödinger, *Math. Proceed. Camb. Philos. Soc.* **31**, 555 (1935).
3. J. S. Bell, *Physics* **1**, 195 (1964).
4. A. J. Leggett, *Found. Phys.* **33**, 1469 (2003).
5. S. Gröblacher et al., *Nature* **446**, 871 (2007).
6. Y. Hasegawa et al., *Nature* **425**, 45 (2003).
7. E. Karimi et al., *Phys. Rev. A* **82**, 022115 (2010).
8. R. J. C. Spreeuw, *Found. Phys.* **28**, 361 (1998).
9. M. A. Goldin et al., *J. Opt. Soc. Am. B* **27**, 779 (2010).
10. X. F. Qian et al., *Optica* **2**, 611 (2015).
11. X. Song et al., *Sci. Rep.* **5**, 14113 (2015).
12. F. Töppel et al., *New J. Phys.* **16**, 073019 (2014).

10.1126/science.aad7174



Separable and nonseparable states of a classical light field. (A) A circularly polarized light beam with an azimuthally varying phase distribution. Such a state is said to be separable, as it can be represented as the product of a spatially varying phase distribution and a polarization state vector. (B) A linear superposition of the state of (A) with another state with the opposite phase variation and the opposite circular polarization (7). In this case, the state of polarization varies as a function of position across the light beam, and the state cannot be described as the separable product of a function of position and a state of polarization.

ESSAY

SCIENCE & SCILIFELAB PRIZE ESSAY

Teamwork: The tumor cell edition

Subclone cooperation maintains tumor growth

By Allison S. Cleary

A remarkable degree of heterogeneity exists within individual breast cancers. Indeed, intratumoral heterogeneity has been appreciated since the 19th century, when Rudolf Virchow and other early pathologists noted the morphologic heterogeneity among individual tumor cells. More recently, cancer genome-sequencing studies have revealed the presence of multiple genetically distinct tumor cell populations, termed subclones, coexisting within individual breast cancers (1–5). This intratumoral heterogeneity poses significant challenges in treatment efforts, but it also raises interesting questions about the nature of tumor progression.

The leading theory that attempts to explain genetic subclonal diversity within tumors is the clonal evolution theory that applies the principles of Darwinian evolution to expanding tumor cell populations (6). As such, individual subclones are often depicted as self-interested competitors in a battle for the position as the dominant, or “fittest,” tumor cell clone. However, in nature, the “fitness” of a given species often depends upon its ability to interact and cooperate with others in its environment. If we consider genetically distinct tumor cell subclones as discrete species within the tumor microecosystem (7), would those same ecological principles apply? In fact, could the genetic heterogeneity within individual breast cancers be a cause, rather than a consequence, of clonal evolution and tumor progression?

As a graduate student in Edward Gunther's laboratory at the Pennsylvania State University College of Medicine, I became fasci-

nated with the idea that this commonly observed subclonal diversity might have a functional role in breast tumor development and progression. For my graduate dissertation project, I chose to investigate this idea further using the classic MMTV-Wnt1 mouse mammary tumor model (8). In this model, mammary-specific expression of the Wnt1 oncogene is known to produce tumors with

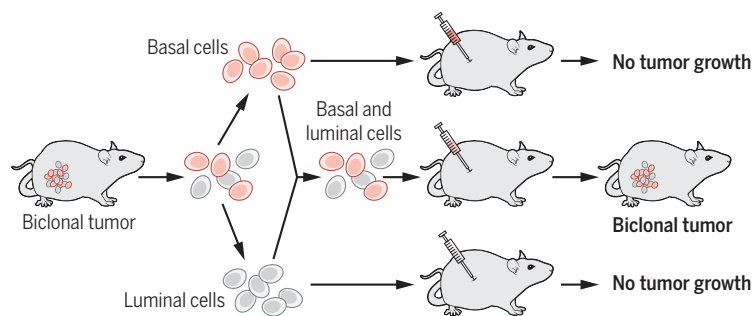
a mixed-lineage histology: that is, the tumors consist of both luminal and basal epithelial cell populations. Secreted Wnt1 protein is produced exclusively by the luminal epithelial population and interacts with the basal cell population through short-range paracrine signals (9). The mixed-lineage character of these tumors was generally thought to derive from a hierarchical organization, in which tumors originated from a common progenitor cell whose progeny were capable of differentiating into both of the component epithelial lineages (9–12). Thus, although exhibiting apparent cellular heterogeneity, all of the tumor cells were thought to represent a single clone.

Using somatic mutations in the *HRas* oncogene as a marker for clonality, we found that some tumors did indeed conform to a hierarchical organization and displayed identical *HRas* mutations in both the luminal and basal tumor cell subsets. Yet, for other

tumors, mutations in *HRas* were detectable only within the basal epithelial compartment. Conversely, *Wnt1* expression, as determined by quantitative reverse transcription polymerase chain reaction (qRT-PCR) and set (as high or low) relative to an unsorted sample, was markedly enriched within the luminal subset. Consequently, these tumors contained at least two genetically distinct subclones: one composed of *Wnt1*^{high} *HRas*^{wild-type} luminal cells and another composed of *Wnt1*^{low} *HRas*^{mutant} basal cells (13). What's more, this apparent biclonality proved to be a stable property within the tumors. Notably, after isolating each of the subclones, we found that neither was capable of propagating tumor growth alone. An admixture of the two populations, however, was found to be extremely tumorigenic, which suggested a cooperative relationship existed between the two subclonal groups (see the figure).

Next, we wondered what would happen if that cooperative interaction was interrupted. We knew that tumor growth for this model strictly depended upon continued Wnt1 signaling. But, if the cells were deprived of that signal, could tumor growth be rescued by providing access to an alternate source of Wnt1? We hypothesized that, if these tumors were truly biclonal and dependent upon a cooperative interaction between the two subclones, then the cells might be able to reestablish a similarly interdependent relationship with an unrelated population of cells—for instance, one derived from a completely separate animal. To address this question, we utilized an inducible version of the MMTV-Wnt1 model in which Wnt1 production is contingent upon administration of the small molecule, doxycycline. Biclonal tumors generated in this inducible model were then transplanted into the mammary fat pads of either wild-type host mice or mice in which Wnt1 is continuously expressed. Upon withdrawal of doxycycline, tumors on the wild-

type host animals regressed completely. However, after doxycycline withdrawal, the tumors transplanted onto the Wnt1 host animals regressed only partially before exhibiting rapid tumor regrowth. Further molecular analysis revealed that the relapsed tumors were not only biclonal, but chimeric: composed of donor-derived *Wnt1*^{low} *HRas*^{mutant} basal cells and host-derived *Wnt1*^{high} *HRas*^{wild-type} luminal cells (13). Indeed, these chimeric tumors had recruited Wnt1-producing luminal cells from the surrounding epithelium



Wnt1 tumors with a biclonal organization require both subclones for tumor propagation.

Tumors identified as containing genetically distinct luminal *Wnt1*^{high} *HRas*^{wild-type} and basal *Wnt1*^{low} *HRas*^{mutant} subclones were separated by fluorescence-activated cell sorting (FACS) into their component cell populations and then transplanted, either separately or as a 1:1 admixture, into mammary fat pads of wild-type host animals. Animals receiving either subclone alone failed to develop tumors, whereas the cell mixture containing both subclones was highly tumorigenic.

*Pennsylvania State University College of Medicine, Hershey PA 17078, USA. E-mail: acleary@hmc.psu.edu

and had incorporated those new cells into the growing tumors, which restored the bclonal cooperative interaction. In fact, many of the chimeric tumor relapses had completely replaced the original luminal cell clone with a new one. Together, these results demonstrated a functional codependence between the distinct tumor cell subclones within these tumors. It also reinforced the idea that there may be a selective advantage for the active preservation of subclonal heterogeneity, in some cases.

Indeed, our study (13) was among the first to definitively establish a functional requirement for interclonal cooperation within a spontaneous mammalian tumor model. Since then, several additional studies have described cooperative interactions between various tumor cell subpopulations (14–17), which suggests that this may be a relatively common mechanism for the maintenance of subclonal diversity. Recent studies have also reported a role for interclonal cooperation in the process of tumor metastasis as well (18, 19).

Ultimately, it has yet to be determined what role interclonal cooperativity plays in human breast cancers. Although normal mammary gland physiology depends heavily upon various paracrine interactions among the diverse populations of cells that make up the mammary ductal epithelium, the degree to which human breast tumor cells maintain comparable paracrine relationships remains unknown. Should interclonal cooperation prove to be an important driver of human breast cancers, it may proffer opportunities for intervention via pharmacologic uncoupling of key interclonal interactions. ■

REFERENCES

1. S. P. Shah *et al.*, *Nature* **461**, 809 (2009).
2. L. Ding *et al.*, *Nature* **464**, 999 (2010).
3. S. Nik-Zainal *et al.*, *Cell* **149**, 994 (2012).
4. S. P. Shah *et al.*, *Nature* **486**, 395 (2012).
5. N. Navin *et al.*, *Nature* **472**, 90 (2011).
6. P. C. Nowell, *Science* **194**, 23 (1976).
7. G. H. Heppner, *Stem Cells* **11**, 199 (1993).
8. A. S. Tsukamoto, R. Grosschedl, R. C. Guzman, T. Parslow, H. E. Varmus, *Cell* **55**, 619 (1988).
9. S. Kim, S. Goel, C. M. Alexander, *PLOS ONE* **6**, e19310 (2011).
10. Y. Li *et al.*, *Proc. Natl. Acad. Sci. U.S.A.* **100**, 15853 (2003).
11. B. Y. Liu, S. P. McDermott, S. S. Khwaja, C. M. Alexander, *Proc. Natl. Acad. Sci. U.S.A.* **101**, 4158 (2004).
12. R. W. Cho *et al.*, *Stem Cells* **26**, 364 (2008).
13. A. S. Cleary, T. L. Leonard, S. A. Gestl, E. J. Gunther, *Nature* **508**, 113 (2014).
14. M. Zhang *et al.*, *Cancer Discov.* **5**, 520 (2015).
15. M. Archetti, D. A. Ferraro, G. Christofori, *Proc. Natl. Acad. Sci. U.S.A.* **112**, 1833 (2015).
16. A. Marusyk *et al.*, *Nature* **514**, 54 (2014).
17. F. Mateo *et al.*, *Mol. Cancer* **13**, 237 (2014).
18. G. Gundem *et al.*, *Nature* **520**, 353 (2015).
19. J. Calbo *et al.*, *Cancer Cell* **19**, 244 (2011).

ACKNOWLEDGMENTS

I am extremely grateful to my Ph.D. adviser, E. J. Gunther, for his mentorship. I also thank all of the members of the Gunther lab, both past and present, especially T. L. Leonard and S. A. Gestl.



GRAND PRIZE WINNER: CELL AND MOLECULAR BIOLOGY

Allison Cleary

Allison Cleary for her essay “Teamwork: The tumor cell edition.” She is originally from Denver, Colorado, and completed her undergraduate degree in Molecular, Cellular, and Developmental Biology at the University of Colorado where she was first introduced to basic science research. From there, she continued her studies at the Pennsylvania State University College of Medicine in their combined M.D., Ph.D. program. While at Penn State, she was fortunate to complete her

Ph.D. thesis research in the laboratory of Dr. Edward Gunther, studying mammary gland physiology and breast cancer. Cleary is currently finishing up her M.D. degree and is in the process of applying to Pathology Residency Programs on the Physician-Investigator Track. She hopes to be able to continue her work in breast cancer and tumor heterogeneity during this next phase in her training.



CATEGORY WINNERS: GENOMICS AND PROTEOMICS

Ludmil Alexandrov

Ludmil Alexandrov for his essay “Understanding the origins of human cancer.” Dr. Alexandrov is an Oppenheimer Fellow in the Theoretical Biology and Biophysics Group at Los Alamos National Laboratory. He earned his Bachelor of Science degree in Computer Science from Neumont University and received his Master’s of Philosophy in Computational Biology as well as his Ph.D. in Cancer Genetics from the University of Cambridge. He is a recipient of the 2015 Weintraub

Award for Graduate Research and, in 2013, he was listed by Forbes magazine as one of the “30 brightest stars under the age of 30” in the field of Science and Healthcare. His work is focused on understanding the mutational processes responsible for human cancer and human ageing. In 2015, his research was highlighted by the American Society of Clinical Oncology as an important step forward in the fight against cancer.



ECOLOGY AND ENVIRONMENT

Adam T. Ford

Adam T. Ford for his essay “The mechanistic pathways of trophic interactions in human-occupied landscapes.” Dr. Ford is a wildlife ecologist interested in how predator-prey interactions are shaped by human-modified landscapes. He received a B.Sc. from the University of Victoria (British Columbia), a M.Sc. from Carleton University (Ontario), and his Ph.D. from the University of British Columbia with Assistant Professor Jacob Goheen. Ford is currently a Liber

Ero Postdoctoral Fellow in Conservation Science, based at the Department of Integrative Biology at the University of Guelph (Ontario). The research described in his essay sheds new light on the relationships of people, large carnivores, their herbivore prey, and plants in an East African savanna.



TRANSLATIONAL MEDICINE

Johannes F. Scheid

Johannes F. Scheid for his essay “HIV-specific B cell response in patients with broadly neutralizing serum activity.” Growing up in New York and Germany in a family of scientists, Dr. Scheid was fascinated early in life by the career of a physician scientist. During medical school at the Charité University, Berlin, he decided to pursue a Ph.D. at The Rockefeller University. His Ph.D. was based on the observation that some HIV patients develop potent antibodies against HIV. The

Ph.D. was awarded the 2012 Harold Weintraub award. After completing medical school and his Ph.D., he worked for 1 year at The Rockefeller University and now continues his clinical training at the Massachusetts General Hospital in Boston.

For the full text of all winning essays and further information, see <http://scim.ag/SciLifeLab>.

ESSAY

SCIENCE & SCILIFELAB PRIZE

Understanding the origins of human cancer

Analyzing the DNA sequences of more than 12,000 cancer patients revealed signatures of mutational processes

By Ludmil B. Alexandrov

All cancers originate from a single cell that starts to behave abnormally, to divide uncontrollably, and, eventually, to invade adjacent tissues (1). The aberrant behavior of this single cell is due to somatic mutations—changes in the genomic DNA produced by the activity of different mutational processes (1). These mutational processes include exposure to exogenous or endogenous mutagens, abnormal DNA editing, the incomplete fidelity of DNA polymerases, and failure of DNA repair mechanisms (2). Early studies that sequenced *TP53*, the most commonly mutated gene in human cancer, provided evidence that mutational processes leave distinct imprints of somatic mutations on the genome of a cancer cell (3). For example, C:G>A:T transversions predominate in smoking-associated lung cancer, whereas C:G>T:A transitions occurring mainly at dipyrimidines and CC:GG>TT:AA double-nucleotide substitutions are common in ultraviolet light-associated skin cancers. These patterns of mutations matched the ones induced experimentally by tobacco mutagens and ultraviolet light, respectively, the major, known, exogenous carcinogenic influences in these cancer types, and demonstrated that examining patterns of mutations in cancer genomes can yield information about the mutational processes that cause human cancer (4).

When I started my Ph.D. at Mike Stratton's lab at the Wellcome Trust Sanger Institute, large-scale global initiatives, such as the International Cancer Genome Consortium, had started performing molecular characterization of thousands of cancer patients around the world (5). However, at that time, there had only been limited characterization of patterns of mutations

imprinted by mutational processes. During my Ph.D. studies, I explored the possibility of leveraging the available cancer genomics data to elucidate the mutational processes operative in human cancer. I started by conceptualizing the problem and developing a mathematical model that describes the interconnection between the activity of mutational processes in cancer cells and the mutational catalogs generated by next-generation sequencing of cancer genomes (6).

The mathematical model was subsequently used to develop a computational approach (6), which I later applied to thousands of sequenced human cancers (7).

Biologically, the somatic mutations in a cancer genome are the cumulative result of the mutational processes that have been active since the very first division of the fertilized egg from which the cancer cell was derived (2). Different mutational processes often generate unique combinations of mutation types, and we termed these patterns “mutational signatures.” Multiple distinct mutational signatures may be recorded on the genome of a single cancer cell and, as such, an individual cancer genome is insufficient for identifying all imprinted mutational signatures. However, the availability of thousands of samples in which mutational signatures are present with different

frequencies makes it possible to decipher their patterns. Mathematically, a set of mutational catalogs of cancer genomes could be examined as a linear mixture of unknown numbers of mutational signatures. The mutational catalogs of these cancer genomes are known from DNA sequencing, and the aim is to identify the patterns of the mutational signatures as well as the number of mutations attributed to each signature in each sample. This problem belongs to a well-known class of blind source separation (BSS) problems, in which mixtures of recordings need to be separated with very little information about the underlying mixing process. To solve this cancer-specific BSS problem in a practical way, I developed a computational framework that uses the previously established multiplicative update algorithm for non-negative matrix factorization (8). The framework was extensively evaluated with simulated and real data, demonstrating that it allows one to accurately identify mutational signatures both from whole-genome and whole-exome sequenced samples (6).

Initially, I applied the developed computational framework to the somatic mutations found in 21 whole-genome sequenced breast cancers (9, 10). Analysis revealed the existence of multiple distinct mutational signatures (9), and we were able to explore the activity of these signatures over time (10). This initial application of the developed computational framework was followed by a comprehensive global analysis of mutational signatures across the spectrum of human neoplasia (7). I curated the majority of publicly available data and compiled a data set encompassing ~5 million somatic mutations from the mutational catalogs of 7042 primary cancers of 30 different classes. These data revealed the existence of 21 distinct mutational signatures in human cancer. Some were present in many cancer types, notably a signature attributed to the APOBEC family of cytidine deaminases (7,



CATEGORY WINNER: GENOMICS AND PROTEOMICS

Ludmil Alexandrov

Ludmil Alexandrov is an Oppenheimer Fellow in the Theoretical Biology and Biophysics Group at Los Alamos National Laboratory. He earned his Bachelor of Science degree in Computer Science from Neumont University and received his Master's of Philosophy in Computational Biology as well as his Ph.D. in Cancer Genetics from the University of Cambridge. He is a recipient of the 2015 Weintraub Award for Graduate Research and, in 2013, he was listed

by Forbes magazine as one of the “30 brightest stars under the age of 30” in the field of Science and Healthcare. His work is focused on understanding the mutational processes responsible for human cancer and human aging. In 2015, his research was highlighted by the American Society of Clinical Oncology as an important step forward in the fight against cancer.

Theoretical Biology and Biophysics (T-6), Los Alamos National Laboratory, Los Alamos, NM 87545, USA. *E-mail: lba@lanl.gov

17); others were confined to a single cancer class. For some of these processes, the underlying biological mechanism is still unknown. However, some of the identified mutational signatures were associated with age of cancer diagnosis, tobacco smoking, exposure to ultraviolet light, treatment with anticancer drugs, presence of *BRCA1* or *BRCA2* mutations, activity of polymerase η , activity of polymerase ϵ , and inactivation of

mismatch repair genes.

The performed comprehensive pan-cancer analysis was complemented by a plethora of studies focusing on individual cancer types. In the last year of my Ph.D. studies, I contributed to further elaborating the understanding of mutational signatures in breast cancer (12), prostate cancer (13–15), liver cancer (16), renal cancer (17), B cell lymphoma (18), a diverse set of child-

hood cancers (19), multiple myeloma (20), and acute lymphoblastic leukemia (21). Additionally, I participated in mapping the signatures of the somatic mutational processes in human mitochondria (22) as well as in understanding the mutational processes operative in normal somatic cells (23, 24). Overall, the pan-cancer analysis and the hitherto mentioned research resulted in identifying 30 distinct signatures of somatic

Signatures of mutational processes in human cancer				
Detailed patterns of the mutational signatures as well as most up-to-date information could be found at our website (25).				
SIGNATURE NUMBER	CHARACTERISTIC MUTATIONAL PATTERN	MOST COMMON CANCER TYPES	PROPOSED ETIOLOGY	ETIOLOGY PROPOSED BASED ON:
Signature 1	C>T at CpG	All cancer types	Deamination of 5-methylcytosine	Similarity of the mutational pattern
Signature 2	C>T at TpC	Twenty-two different cancer types	<i>APOBEC1</i> , <i>APOBEC3A</i> , or <i>APOBEC3B</i>	Similarity of the mutational pattern
Signature 3	Uniform mutational signature	Breast, ovarian, and pancreatic cancer	Defective repair of DNA double-strand breaks based on homologous recombination	Statistical association with mutations in <i>BRCA1</i> or <i>BRCA2</i>
Signature 4	C>A mutations with strand bias	Lung, head and neck, and liver cancer	Tobacco smoking	Similarity of the mutational pattern and statistical association
Signature 5	Mostly uniform mutational signature with some peaks of T>C mutations at ApT	All cancer types	Unknown etiology	N/A
Signature 6	C>A mutations and C>T at GpC mutations	Seventeen different cancer types but most prevalent in colorectal and uterine cancers	Defective DNA mismatch repair	Similarity of the mutational pattern and statistical association
Signature 7	C>T at dipyrimidines	Malignant melanoma and lip cancers	Ultraviolet light	Similarity of the mutational pattern
Signature 8	C>A mutations with a moderate strand bias	Breast cancer and medulloblastoma	Unknown etiology	N/A
Signature 9	T>G transversions at ApT and TpT	Chronic lymphocytic leukemias and B-cell lymphomas	Polymerase η	Similarity of the mutational pattern and statistical association
Signature 10	C>A at TpCpT and C>T at TpCpG	Colorectal and uterine cancers	Polymerase ϵ	Statistical association
Signature 11	C>T substitutions	Malignant melanoma and glioblastoma multiforme	Treatment with temozolomide	Similarity of the mutational pattern and statistical association
Signature 12	T>C substitutions with strand bias	Liver and uterine cancer	Unknown	N/A
Signature 13	C>A and C>G at TpC	Twenty-two different cancer types	<i>APOBEC1</i> , <i>APOBEC3A</i> , or <i>APOBEC3B</i> and <i>REV1</i>	Similarity of the mutational pattern
Signature 14	C>A mutations and C>T at GpC mutations	Low grade glioma and uterine cancer	Unknown etiology	N/A
Signature 15	C>T at GpC mutations	Stomach and lung cancer	Defective DNA mismatch repair	Similarity of the mutational pattern
Signature 16	T>C mutations at ApT with extremely strong strand-bias	Liver cancer	Unknown etiology	N/A
Signature 17	T>G at TpT and T>C at CpT	Esophagus cancer, liver cancer, stomach cancer, and B-cell lymphoma	Unknown etiology	N/A
Signature 18	C>A mutations	Neuroblastoma	Unknown etiology	N/A
Signature 19	C>T mutations	Pilocytic astrocytoma	Unknown etiology	N/A
Signature 20	C>A and C>T mutations	Stomach cancer	Defective DNA mismatch repair	Similarity of the mutational pattern

Signatures of mutational processes in human cancer (continued)				
Detailed patterns of the mutational signatures as well as most up-to-date information could be found at our website (25).				
SIGNATURE NUMBER	CHARACTERISTIC MUTATIONAL PATTERN	MOST COMMON CANCER TYPES	PROPOSED ETIOLOGY	ETIOLOGY PROPOSED BASED ON:
Signature 21	T>C mutations	Stomach cancer	Unknown etiology	N/A
Signature 22	T>A mutations	Urothelial (renal pelvis) carcinoma and liver cancers	Exposure to aristolochic acid	Similarity of the mutational pattern and statistical association
Signature 23	C>T mutations	Liver cancer	Unknown etiology	N/A
Signature 24	C>A mutations with strand bias	Liver cancers	Exposures to aflatoxin	Similarity of the mutational pattern and statistical association
Signature 25	T>A mutations with strand bias	Hodgkin lymphomas	Unknown etiology	N/A
Signature 26	T>C mutations	Breast, cervical, stomach and uterine cancer	Defective DNA mismatch repair	Statistical association
Signature 27	T>A mutations with strand bias	Kidney cancer	Unknown etiology	N/A
Signature 28	T>G mutations	Stomach cancer	Unknown etiology	N/A
Signature 29	C>A mutations with strand bias	Gingivo-buccal oral squamous cell carcinoma	Tobacco chewing	Statistical association
Signature 30	C>T mutations	Breast cancers	Unknown etiology	N/A

mutational processes, most of which were previously unknown.

These 30 mutational signatures are briefly summarized in the table.

In summary, my Ph.D. thesis provided a basis for deciphering mutational signatures from cancer genomics data and developed the first comprehensive census of mutational signatures in human cancer. The results reveal the diversity of mutational processes underlying the development of cancer and have far-reaching implications for understanding cancer etiology, as well as for developing cancer prevention strategies and novel targeted cancer therapies. ■

REFERENCES AND NOTES

1. M.R. Stratton, *Science* **331**, 1553 (2011).

2. L.B. Alexandrov, M.R. Stratton, *Curr. Opin. Genet. Dev.* **24**, 52 (2014).

3. M. Hollstein *et al.*, *Mutat. Res.* **431**, 199 (1999).

4. B. Vogelstein, K.W. Kinzler, *Nature* **355**, 209 (1992).

5. T.J. Hudson *et al.*; International Cancer Genome Consortium, *Nature* **464**, 993 (2010).

6. L.B. Alexandrov, S. Nik-Zainal, D. C. Wedge, P.J. Campbell, M. R. Stratton, *Cell Reports* **3**, 246 (2013).

7. L.B. Alexandrov *et al.*; Australian Pancreatic Cancer Genome Initiative; ICGC Breast Cancer Consortium; ICGC MMML-Seq Consortium; ICGC PedBrain, *Nature* **500**, 415 (2013).

8. D.D. Lee, H.S. Seung, *Nature* **401**, 788 (1999).

9. S. Nik-Zainal *et al.*; Breast Cancer Working Group of the International Cancer Genome Consortium, *Cell* **149**, 979 (2012).

10. S. Nik-Zainal *et al.*; Breast Cancer Working Group of the International Cancer Genome Consortium, *Cell* **149**, 994 (2012).

11. S. Nik-Zainal *et al.*, *Nat. Genet.* **46**, 487 (2014).

12. L.R. Yates *et al.*, *Nat. Med.* **21**, 751 (2015).

13. G. Gundem *et al.*; ICGC Prostate UK Group, *Nature* **520**, 353 (2015).

14. M. K. Hong *et al.*, *Nat. Commun.* **6**, 6605 (2015).

15. C. S. Cooper *et al.*; ICGC Prostate Group, *Nat. Genet.* **47**, 367 (2015).

16. K. Schulze *et al.*, *Nat. Genet.* **47**, 505 (2015).

17. N. Kanu *et al.*, *Oncogene* **34**, 5699 (2015).

18. R. Wagener *et al.*, *Leukemia* **29**, 1612 (2015).

19. A. Shlien *et al.*; Biallelic Mismatch Repair Deficiency Consortium, *Nat. Genet.* **47**, 257 (2015).

20. N. Bolli *et al.*, *Nat. Commun.* **5**, 2997 (2014).

21. E. Papaemmanuil *et al.*, *Nat. Genet.* **46**, 116 (2014).

22. Y.S. Ju *et al.*, *eLife* **3**, (2014).

23. I. Martincorena *et al.*, *Science* **348**, 880 (2015).

24. S. Behjati *et al.*, *Nature* **513**, 422 (2014).

25. Mutational Signatures, The Cancer Genome Project; <http://cancer.sanger.ac.uk/cosmic/signatures>.

10.1126/science.aad7363

ESSAY

SCIENCE & SCILIFELAB PRIZE

The mechanistic pathways of trophic interactions in human-occupied landscapes

Field studies reveal more complicated relationships between African wild dogs, their prey, and the plants eaten by the prey than predicted by theory

By Adam T. Ford*

From children's stories to the logos of professional sports teams, images on commercial products, and the icons of conservation, few organisms capture our imagination like large carnivores.

From a scientific perspective, understanding the context in which predators shape ecosystem processes is one of the most pressing endeavors in modern ecology (1). In central Kenya, large carnivores—such as leopards and globally endangered African wild dogs—prey upon antelope, which themselves limit the abundance of plants. These wildlife species vie with commercial ranchers, as well as traditional pastoralists and their livestock for limited resources (2). Together, these actors interact against a backdrop of pronounced environmental variation and the unique patchwork of trees on grassland that characterizes tropical savannas. Through my dissertation research, I combined long-term monitoring of wildlife populations, high-resolution satellite imagery, fine-scale tracking of animal movements, and a series of field experiments to quantify these interactions and their consequences for ecosystem structure.

Specifically, I discovered that impala—an abundant, deer-sized antelope—are caught between “the devil and the deep blue sea”: they must avoid the claws and teeth of their predators and the thorny and chemical defenses of their food (3, 4). Global Positioning System (GPS) tracking reveals that impala avoid areas characterized by dense tree cover (see the figure). In such areas, leopards and wild dogs more effectively attack and kill their prey, which makes tree cover “risky” when viewed through the eyes of an impala (3). However, trees are also an important food source for impala, and feeding trials showed that impala prefer trees with fewer thorns, even if these less-thorny trees are better

defended with noxious chemicals (3). This combination of habitat and food preferences means that impala deplete the abundance of their preferred (and less thorny) forage in safe habitats, yet forgo access to this preferred forage in risky habitats. Consequently, an impala's fear of being eaten increases the

prevalence of thorny trees in safe areas, and safeguards less-thorny trees in risky areas.

There are three critical implications of this study (3). First, and from the perspective of a plant, there are two pathways to success—either defend yourself from herbivores by growing large thorns or thrive in areas that are risky to your enemies. Second, fear of predation and diet preference interact to shape the spatial patterning of tree species across entire landscapes (about 200 km²). Third, because the open areas in which impala aggregate for safety arise from old (>10-year) cattle corrals, traditional pastoralism plays a key role in shaping the interactions among carnivores, their prey, and plants. The implications of this last point are profound, because it demonstrates that people are inextricably embedded within this food web. Indeed, the preferred plants that impala relinquish in risky areas could be used for livestock forage, a critical ecosystem service that may help mitigate the impact of episodic droughts that plague East Africa.

Whereas fear of predation can powerfully shape ecosystems and animal behavior (3, 5), so too can the direct consumption of prey. After a 20-year absence, African wild dogs naturally recolonized areas of central Kenya and now prey upon the region's most abundant antelope, the dik-dik. Theory predicts that this strong, top-down pressure in the food chain should trigger a trophic cascade; in other words, after wild dog recovery, herbivory by dik-dik will relent and plant abundance will increase. To test this prediction, I linked the movement and diet composition of wild dog packs with changes in the size of the dik-dik population over a 14-year period. I then identified which plants are vulnerable to browsing by dik-dik. Finally, I quantified herbivory by means of a series of replicated and controlled dik-dik exclosures, separately established before and after wild dog recovery.

There were strong, top-down effects in this food chain, but no evidence that wild dog recovery caused a trophic cascade. The population of dik-dik declined by 33% because of predation by wild dogs, and dik-dik reduced the abundance of some tree species by up to 84% (6). However, the effect of herbivory did not diminish in the presence of wild dogs (6). This finding was surprising because overall plant growth (both inside and outside dik-dik exclosures) was greater following wild dog recovery. Had experiments not been used, as often is

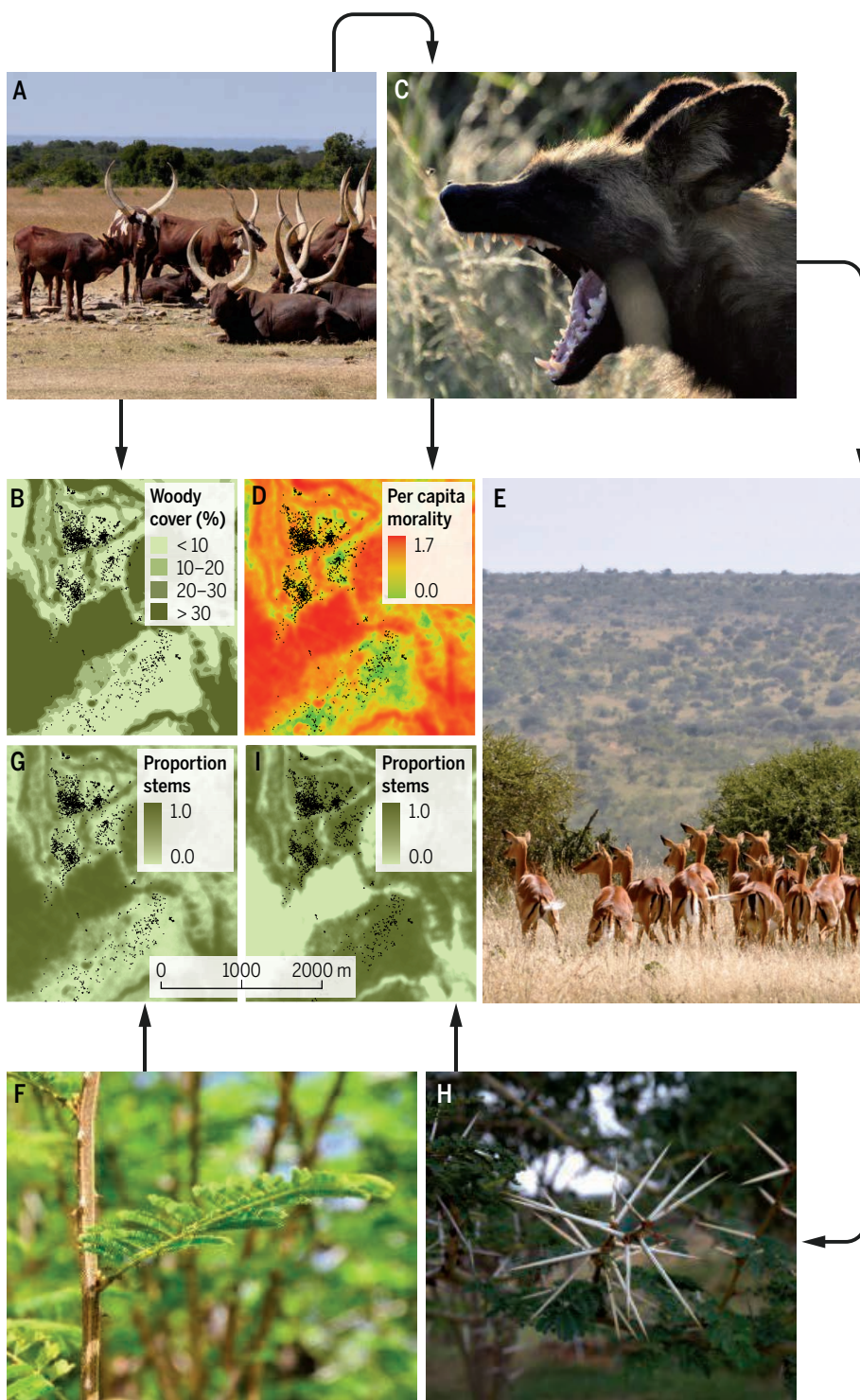


CATEGORY WINNER: ECOLOGY AND ENVIRONMENT

Adam T. Ford

Adam T. Ford is a wildlife ecologist interested in how predator-prey interactions are shaped by human-modified landscapes. He received a B.Sc. from the University of Victoria (British Columbia), a M.Sc. from Carleton University (Ontario), and his Ph.D. from the University of British Columbia with Assistant Professor Jacob Goheen. Ford is currently a Liber Ero Postdoctoral Fellow in Conservation Science, based at the Department of Integrative Biology at the University of Guelph (Ontario). The research described in his essay sheds new light on the relationships of people, large carnivores, their herbivore prey, and plants in an East African savanna.

Department of Integrative Biology at the University of Guelph, Guelph, Ontario, Canada. *E-mail: adamford@uoguelph.ca



How trophic cascades emerge. Some key interactions between people, large carnivores, antelope, and plants in a savanna landscape. The creation and abandonment of (A) cattle corrals creates openings in (B) woody cover. Areas of high woody cover are used by predators, like (C) African wild dogs, for hunting, which coincides with (D) the distribution of predation risk [shown here as the per-capita risk of mortality] across the landscape. As a result, prey, like (E) the impala, avoid areas of high woody cover and find safety in the open areas created by abandoned cattle corrals. The GPS-recorded movements of (E) an adult female impala, are shown by the black dots in panels (B) and (D). This animal was tracked every 20 min over the course of a year. Impala prefer and suppress the abundance of less-thorny acacia plants, like (F) *Acacia brevispica*, compared with thorny species like (H) *Acacia etbaica*. As result of impala's risk-avoidance behavior and diet preference, (G) the proportion of stems in the tree community containing the less-thorny species is highest in the risky areas that impala avoid (see black dots tracking impala movement); whereas (I) thorny plants are more abundant in the open areas where impala aggregate (as shown by the black dots in GPS). Details of this study are described in (3).

the case in large-carnivore studies, I would have incorrectly concluded the existence of a trophic cascade. My results highlight the very important finding that a positive correlation between plant and large carnivore biomass is insufficient evidence to validate a trophic cascade.

The potential for large carnivores to trigger trophic cascades has been used to justify the conservation of these iconic species and to restore landscapes (1, 7). Until now, there have been significant gaps in the empirical support for this interaction, particularly when applied to savannas (8). Specifically, widespread reliance on correlative methods has made it challenging to attribute changes in plant and herbivore biomass to trophic cascades (8). These natural experiments often lack control and replication and, therefore, suffer from confounding variation (8). Moreover, previous work in this field has been conducted primarily in the temperate biomes of Europe and North America. In the absence of a more rigorous assessment of the trophic cascade hypothesis, and one that involves a greater diversity of species and biomes, there is a void in our knowledge of how some of the world's most recognizable and charismatic carnivores interact with their environment. Given the loss of large carnivores from many parts of the world (1, 7, 9), their recovery in other areas (6, 10), and efforts being made to conserve these species in human-occupied landscapes (11–13), it is critical that we develop a clearer understanding of when and where trophic cascades will emerge. Through the pairing of experiments with landscape-level analyses, my research has unraveled the ecological contexts that determine when large carnivores generate trophic cascades in an African savanna.

REFERENCES AND NOTES

1. J. A. Estes *et al.*, *Science* **333**, 301 (2011).
2. A. T. Ford, J. M. Fryxell, A. R. Sinclair, in *Antelope Conservation in the 21st Century: From Diagnosis to Action*, J. Bro-Jorgensen, Ed., from a symposium of the same name, London, 17 and 18 November 2011 (Wiley-Blackwell, Hoboken, NJ, in press), chap. 2.
3. A. T. Ford *et al.*, *Science* **346**, 346 (2014).
4. R. M. Pringle *et al.*, *Proc. R. Soc. London Ser. B* **281**, 20140390 (2014).
5. A. T. Ford, J. R. Goheen, *J. Mammal.* **96**, 918 (2015).
6. A. T. Ford *et al.*, *Ecology* **96**, 2705 (2015).
7. W. J. Ripple *et al.*, *Science* **343**, 1241484 (2014).
8. A. T. Ford, J. R. Goheen, *Trends Ecol. Evol.* 10.1016/j.tree.2015.09.012 (2015).
9. R. Dirzo *et al.*, *Science* **345**, 401 (2014).
10. G. Chapron *et al.*, *Science* **346**, 1517 (2014).
11. A. T. Ford, A. P. Clevenger, *Conserv. Biol.* **24**, 1679 (2010).
12. A. T. Ford, A. P. Clevenger, M. P. Huijser, A. Dibb, *Wildl. Biol.* **17**, 253 (2011).
13. M. Barrueto, A. T. Ford, A. P. Clevenger, *Ecosphere* **5**, art27 (2014).

ACKNOWLEDGMENTS

I extend my heartfelt gratitude to Jacob Goheen—my Ph.D. adviser—who provided creativity, humor, guidance, and unwavering support to help me achieve my dreams.

10.1126/science.aad7134

ESSAY

SCIENCE & SCILIFELAB PRIZE

HIV-specific B cell response in patients with broadly neutralizing serum activity

Antibody characterization from single B cells led to identification of monoclonal antibodies with broad and potent activity against HIV

By Johannes F. Scheid*

Since its discovery in 1981, HIV has killed over 25 million people; more than 33 million humans are now infected worldwide. Despite extensive efforts, a vaccine against HIV remains elusive. The reason for this lies in HIV's remarkable mutability.

Soon after HIV infection, the immune system attacks the virus, which then escapes immune recognition by mutating its surface envelope protein, gp140. The escaped viral variants are targeted again by the immune system, and what follows is a race between virus and the immune system in which the virus continually diversifies and remains one step ahead in most patients. It is surprising, that 5 to 10% of HIV patients eventually develop high titers of "broadly neutralizing" serum antibodies that neutralize a diverse panel of HIV isolates (see the figure, part A). Until recently, very little

was known about the composition of these broadly neutralizing serum responses, which is why I set out to characterize them during my Ph.D. thesis.

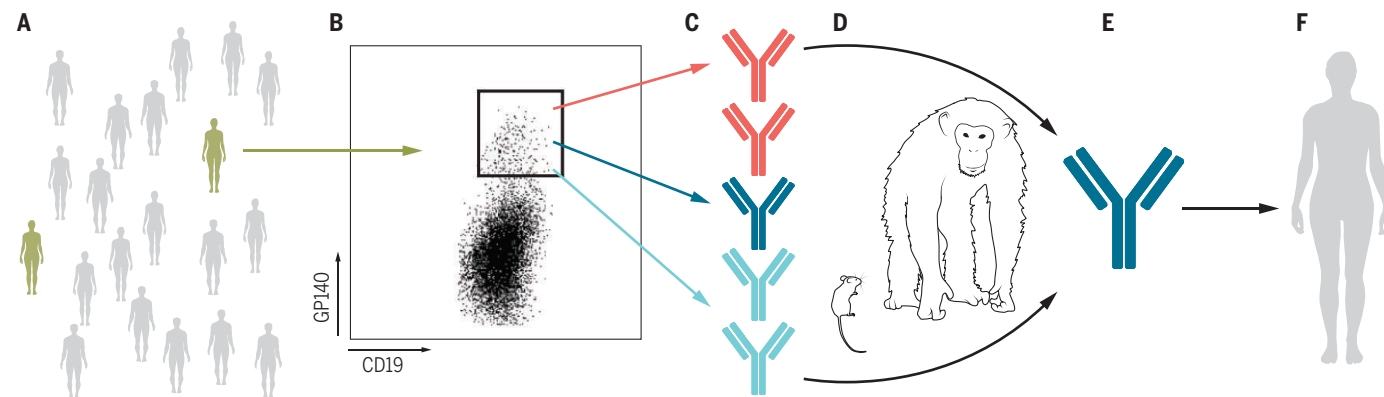
For this, I developed a technique that allowed me to isolate single HIV-specific memory B cells (1). Memory B cells originate from germinal center reactions and carry their affinity matured antibodies on the cell surface (2). I exploited this feature using a fluorescently labeled version of gp140 and flow cytometry in order to identify a population of gp140-binding B cells (see the figure, part B). Once we identified this population, we used single-cell sorting and polymerase chain reaction (PCR) to amplify the immunoglobulin genes of single gp140-specific B cells (see the figure, part C) (3, 4).

We applied this technique to six different HIV-infected patients with broadly neutralizing sera. From these patients, we cloned 432 monoclonal antibodies specific for gp140; this allowed us to gain insight into the molecular nature of these individuals' HIV antibody responses (3). We found that each response comprised 22 to 50 differently expanded B cell clones. The majority

of these families of antibodies displayed extraordinary levels of somatic hypermutation. Cloning each antibody's matching heavy- and light-chain gene into expression vectors allowed us to reproduce the antibodies and to characterize their epitopes, affinity, and neutralizing activity. We found that 70% of the antibodies bound to the gp120 portion of the gp140 trimer and 30% bound to gp41 (3, 5). The gp120-specific antibodies bound with nanomolar affinities to sub-epitopes, including the CD4-binding site (CD4bs), gp120 core, the variable loops, or the CD4-induced site on gp140 (3, 6). The proportion of clones targeting these epitopes varied among different patients, in contrast to previous results, which reflected immunodominance of certain epitopes. When we tested them for neutralizing activity, we were able to reconstitute the breadth of serum neutralizing activity in two out of the four patients in this study but only with high concentrations of pooled antibodies. This indicated to us that we were missing an important part of the activity in the patients' sera.

To address this, I turned to a characteristic feature of the HIV antibodies we had found; their high levels of mutation. I knew the mutations were central to antibody function

Massachusetts General Hospital, Boston, MA 02114, USA.
The Rockefeller University, New York, NY 10021, USA.
*E-mail: fscheid@partners.org



Isolation and testing of broadly neutralizing antibodies against HIV. (A) Five to 10% of HIV-positive individuals eventually develop broad and potent serum neutralizing activity. (B) Fluorescence-activated cell sorting plot of a single-cell sort of gp140-specific B cells. (C) Single-cell antibody cloning of differently expanded B cell clones shown in red, dark blue, and light blue, respectively. (D) In vivo testing of the therapeutic and protective effect of antibodies in humanized mice and nonhuman primates. (E) Selection of highly potent and broad monoclonal antibodies. (F) Clinical testing in phase-I human trials.



CATEGORY WINNER: TRANSLATIONAL MEDICINE

Johannes F. Scheid

Growing up in New York and Germany in a family of scientists, Johannes Scheid was fascinated early in life by the career of a physician scientist. During medical school at the Charité—University, Berlin, he decided to pursue a Ph.D. at The Rockefeller University. His Ph.D. was based on the observation that some HIV patients develop very potent antibodies against HIV. The Ph.D. was awarded the 2012 Harold Weintraub award. After completing medical school

and his Ph.D., he worked for 1 year as an instructor in clinical investigation at The Rockefeller University and now is continuing his clinical training at the Massachusetts General Hospital in Boston.

because they lost their binding and neutralizing activity when reverted to their germline sequences (3, 7). This high frequency of mutations could, however, impede our antibody identification if mutations occurred in PCR primer-binding sites. I therefore opted to move the 5' primer further upstream and away from potentially mutated regions. In side-by-side comparisons, we found that the redesigned PCR primer set recovered highly mutated clones not identified with the original primers. We then decided to combine this improved amplification strategy with single-cell sorting, in which a modified version of gp120 (2CC core) was used as a target antigen. The 2CC core was shown to preferentially bind to neutralizing antibodies directed at the CD4bs and CD4-induced site on gp140 (8). Similar to our previous findings, a majority of the 576 new antibodies we cloned from two new and two of the previously studied patients were members of differently expanded B cell clones (9). However, many of the clones now carried even more mutations than we had previously observed. Moreover, six highly mutated B cell clones showed potent and broad neutralizing activity directed to the CD4bs and a new epitope that bridges gp120 and gp41 (9–11). The best performing of the new antibodies, 3BNC117, showed an average 80% inhibitory concentration on 95 different HIV strains of 1.4 μ g/

ml; this was broader and more potent than any of the previously described antibodies against HIV (9).

The exceptional potency and breadth of 3BNC117 set off a number of collaborative studies to investigate its *in vivo* therapeutic effect (see the figure, parts D and E). These revealed that 3BNC117 alone or in combination with other neutralizing antibodies could suppress plasma viremia to levels below detection in mice and nonhuman primates (12, 13). Moreover, intravenous administration of 3BNC117 protected rhesus macaques from challenge with simian HIV (13). In a phase-I human clinical trial conducted at The Rockefeller University Hospital, eight out of eight viremic individuals off antiretroviral therapy who received one dose of 3BNC117 at 30 mg/kg body weight showed rapid decreases in their viral loads, from 0.8 to 2.5 \log_{10} depending on the individual (14). Further clinical trials with 3BNC117 are under way (see the figure, part F).

To determine whether broad and potent CD4bs antibodies share common sequence features, we aligned the 10 best CD4bs antibodies from our study (9). This revealed a conserved consensus sequence that covered 68 immunoglobulin heavy chain variable region (Igh-V) residues. In addition, all 10 of these antibodies arose from only two closely related germline *Igh-V* genes. Given

that these antibodies were isolated from different individuals infected with different HIV strains, this key observation suggests that the path to this class of antibodies is restricted—an important consideration for ongoing efforts to elicit this class of antibodies by vaccination (9, 15, 16).

This project has started an exciting journey from a bedside observation that certain individuals develop broad serum activity against HIV, to the bench, where we developed a technique to characterize this type of activity, and back to the bedside, where one of these antibodies is now being infused in clinical trials (see the figure). The single-B cell isolation approach has now been adapted and modified by other groups working on HIV (17, 18). By investigating some exceptional antibody responses against this constantly evading virus, our colleagues and we hope to broaden our therapeutic armament against HIV and design an efficient HIV vaccine. ■

REFERENCES AND NOTES

1. J. F. Scheid *et al.*, *J. Immunol. Methods* **343**, 65 (2009).
2. G. D. Vitoria, M. C. Nussenzweig, *Annu. Rev. Immunol.* **30**, 429 (2012).
3. J. F. Scheid *et al.*, *Nature* **458**, 636 (2009).
4. H. Wardemann *et al.*, *Science* **301**, 1374 (2003).
5. J. Pietzsch *et al.*, *J. Virol.* **84**, 5032 (2010).
6. J. Pietzsch *et al.*, *J. Exp. Med.* **207**, 1995 (2010).
7. H. Mouquet *et al.*, *Nature* **467**, 591 (2010).
8. B. Dey *et al.*, *PLOS Pathog.* **5**, e1000445 (2009).
9. J. F. Scheid *et al.*, *Science* **333**, 1633 (2011).
10. R. Diskin *et al.*, *Science* **334**, 1289 (2011).
11. L. Scharf *et al.*, *Cell Reports* **7**, 785 (2014).
12. F. Klein *et al.*, *Nature* **492**, 118 (2012).
13. M. Shingai *et al.*, *Nature* **503**, 277 (2013).
14. M. Caskey *et al.*, *Nature* **522**, 487 (2015).
15. P. Dosenovic *et al.*, *Cell* **161**, 1505 (2015).
16. T. Zhou *et al.*, *Cell* **161**, 1280 (2015).
17. D. R. Burton, J. R. Mascola, *Nat. Immunol.* **16**, 571 (2015).
18. P. D. Kwong, J. R. Mascola, *Immunity* **37**, 412 (2012).

ACKNOWLEDGMENTS

I would like to thank the HIV-positive individuals for their invaluable help. I thank Michel Nussenzweig and Svetlana Mojsos for the gift of their friendship and mentorship, as well as all Nussenzweig lab members and collaborators for their support, especially Hugo Mouquet, Hedda Wardemann, Marina Caskey, and Florian Klein. Without their help this work could not have been performed.

10.1126/science.aad7133

LETTERS

Edited by Jennifer Sills

Exoskeleton progress yields slippery slope

W. CORNWALL'S FASCINATING News Feature on the growing use of exoskeletons in the military—i.e., robotically augmented ambulatory systems—documented a number of technical hurdles yet to be overcome in this emerging technology (“In pursuit of the perfect power suit,” 16 October, p. 270). In addition to their military potential, exoskeletons will aid many civilians suffering from restricted mobility. However, despite their possibilities, exoskeletons pose substantial ethical, legal, and social concerns that will quickly become all the more relevant with the rapid growth of both the military and civilian industries.

The ability to augment otherwise healthy individuals with military-grade exoskeletons starts us down the slippery slope of human enhancement, a challenging area with broad repercussions in conventional society ranging in applications from medicine to sports. Additionally, in transforming soldiers into quasi-machines, we risk further dehumanizing warfare and its human actors, raising the potential for abuse not only by the enemy, but by commanding officers. This capacity for exploitation can also affect civilian workers who will use exoskeletons in heavy industries.

Even corrective uses associated with restoring abilities to the disabled raise social justice concerns relating to the availability of, and accessibility to, this life-altering technology. Therapeutic implementations may also compel us to redefine nontrivial concepts of disability and ableness in light of the growing capacity to technologically supplement human frailties; additionally, current legal and regulatory structures may be unable to appropriately fit newly abled individuals within current disability conventions.

Not only will exoskeletons likely raise novel legal issues relating to product liability, but the potential to implant brain machine interfaces (BMIs) within the posterior parietal cortex, resulting in preconscious control over the exoskeleton, may challenge longstanding near-universal tenets of criminal law. In most jurisdictions, an individual cannot be guilty of a crime if they lack the threshold *mens rea* and *actus reus* (i.e., a guilty mind resulting in a guilty action). BMIs, particularly those supplemented with artificial intelligence,



A soldier tests a system built to augment walking performance. The ethical, legal, and social implications of exoskeletons such as this one have yet to be explored.

could result in arguably involuntary actions that confound criminal culpability and conceivably put into question even more fundamental issues of free will. In anticipating, promptly acknowledging, and perhaps even tackling these and other concerns, we can preempt and preclude potentially hampering legislation and regulation that might inhibit innovation.

Dov Greenbaum

Zvi Meitar Institute for Legal Implications of Emerging Technologies, Interdisciplinary Center, Herzliya Israel and Department of Molecular Biophysics and Biochemistry, Yale University School of Medicine, New Haven, CT 10463, USA.
E-mail: dov.greenbaum@yale.edu

Torture's inefficiency long established

IN THE 16 October issue, R. J. McNally reviews a book by Shane O'Mara, *Why Torture Doesn't Work* (“Cruel and unuseful punishment,” Books *et al.*, p. 284). I applaud the efforts of the reviewer and the author to publicize this issue, and I would like to remind readers that the inefficiency of torture has long been established, in modern times first and foremost by the Central Intelligence Agency (CIA) itself—the organization at the heart of the current torture dilemma.

McNally claims that “few scholars have

scrutinized” the question of whether “abusive questioning reliably causes people to reveal truthful information that they would otherwise refuse to disclose,” but this is only true in a qualified sense. In the 1950s and 1960s, the CIA managed a series of front organizations, such as the Human Ecology Fund, to issue grants for empirical studies of human stress responses. The CIA enlisted numerous behavioral science researchers who did not know that their research was contributing to a torture manual (1, 2).

Although using neuroscience may be a new way to demonstrate that physical distress induces “neurocognitive deficits,” the CIA had well determined by 1963 that “psychologists and others who write about physical or psychological duress frequently object that under sufficient pressure subjects usually yield but that their ability to recall and communicate information accurately is as impaired as the will to resist” (3). The CIA's Counterintelligence Interrogation (KUBARK) manual also observed that “in general, direct physical brutality creates only resentment, hostility, and further defiance” rather than useful information (4).

The purpose of torture is not to produce useful information; rather, “all coercive techniques are designed to induce regression” (3)—that is, specifically, to erase the individual will by exploiting the psychological and physical dependence of captives on their captors. Ending the practice of torture would seem to involve more than a new, convincing demonstration of its inutility as a means of obtaining information. In this light, then, perhaps the more important assumption to reexamine relates to the disturbing notion that torture has any purpose beyond the exacting of pain, control, and domination.

David R. Witzling

University of Wisconsin-Milwaukee, Milwaukee, WI 53212, USA. E-mail: drw@frametheweb.com

REFERENCES

1. D.H. Price, *Anthropol. Today* **23**, 8 (2007).
2. D.H. Price, *Anthropol. Today* **23**, 17 (2007).
3. KUBARK Counterintelligence Interrogation, IX.B (1963); <http://nsarchive.gwu.edu/NSAEBB/NSAEBB122/CIA%20Kubark%201-60.pdf>.
4. KUBARK Counterintelligence Interrogation, IX.F, (1963).

Pollution threatens migratory shorebirds

IN ADDITION TO the destruction and loss of coastal wetlands along migration routes (“Hostile shores,” C. Larson, News Features, 9 October, p. 150), contamination in the Yellow Sea poses a critical threat to migratory shorebirds.

China's coastal wetlands have suffered from serious pollution, and Bohai Bay in the northwestern Yellow Sea has been particularly affected. Annual fluxes of mercury, cadmium, lead, and arsenic from 13 coastal cities in this area are estimated to be 30, 400, 1400, and 2000 tons per year, respectively, into Bohai Bay (1). The pollution of inorganic nitrogen and phosphorous, oil, and heavy metals has led to a sharp decline of fishery resources (2), greatly decreasing the food supply available to migratory shorebirds.

Pollutants in water, mud, and organisms from the area can cause substantial harm to bird health. For example, cadmium, arsenic, and lead in fish and shellfish from Yantai exceeded the limits in China's food safety standard (3), and the DDT levels in shellfish exceeded the wildlife quality criteria at most sampling sites in Bohai Bay (4). Some metals and persistent organic pollutants can accumulate in shorebirds, by means of biomagnifications along the food chains. Many chemicals can cause changes



Kentish plover

to the avian thyroid gland and/or disruptions in the reproductive system, although acute mortality has rarely been reported. For example, exposure of Kentish plovers to the Prestige oil spill adversely affected their reproductive performance by changing egg quality (5). Moreover, the Yellow Sea region has been contaminated heavily with plastic debris (6), which can result in health disorders and even death (7).

Some emerging anthropogenic pollutants may result in unexpected negative impacts on bird behaviors. Offshore wind energy applications are increasing in the region, including in Rudong and the Bohai Bay, the two most critical sites in the whole flyway. Electromagnetic radiation generated from wind farms is likely an emerging threat to bird orientation (8). In addition, artificial lights in the coastal zones could have negative and deadly effects, especially on fledglings (9).

Zhenwu Tang,¹ Qifei Huang,^{2*}
Zhiqiang Nie,² Yufei Yang²

¹Environmental Research Academy, North China Electric Power University, Beijing, 102206, China.

²State Key Laboratory of Environmental Criteria and Risk Assessment, Chinese Research Academy of Environmental Sciences, Beijing, 100012, China.

*Corresponding author.
E-mail: huangqf@craes.org.cn

REFERENCES

1. Z. G. Cui, thesis, Ocean University of China (2008) [in Chinese].
2. S. S. Xu, thesis, University of Chinese Academy of Sciences (2011) [in Chinese].
3. M. Wang *et al.*, *Chin. J. Food Hyg.* **24**, 67 (2012) [in Chinese].
4. Y. S. Fan *et al.*, *Mar. Environ. Sci.* **27**, 25 (2008) [in Chinese].
5. M. Vidal, J. Domínguez, *Biol. Conserv.* **191**, 178 (2015).
6. North China Sea Branch of State Oceanic Administration, *Marine Environment Bulletin of North China Sea* (2014) (North China Sea Branch of SOA, Qingdao, 2015) [in Chinese].
7. C. M. Rochman *et al.*, *Nature* **494**, 169 (2013).
8. A. Balmori, *Sci. Total Environ.* **496**, 314 (2014).
9. A. Rodríguez *et al.*, *J. Ornithol.* **156**, 893 (2015).

TECHNICAL COMMENT ABSTRACTS

Comment on "Worldwide evidence of a unimodal relationship between productivity and plant species richness"

Lauri Laanisto and Michael J. Hutchings

Fraser *et al.* (Reports, 17 July 2015, p. 302) report that a hump-backed model describes the worldwide relationship between productivity and plant species richness in grassland communities. We reanalyze their data from a larger-scale perspective, using a local species pool. This influences richness far more strongly than productivity, and, when this is taken into account, the hump-backed richness-productivity relationship disappears.

Full text at <http://dx.doi.org/10.1126/science.aad4836>

Response to Comment on "Worldwide evidence of a unimodal relationship between productivity and plant species richness"

Lauchlan H. Fraser, Meelis Pärtel, Jason Pither, Anke Jentsch, Marcelo Sternberg, Martin Zobel

Laanisto and Hutchings claim that the local species pool is a more important predictor of local plant species richness than biomass and that when the species pool is considered there is no hump-backed relationship between biomass and richness. However, we show that by calculating a more appropriate measure of species pool, community completeness, both regional and local processes shape local richness.

Full text at <http://dx.doi.org/10.1126/science.aad4874>

TECHNICAL COMMENT

PLANT ECOLOGY

Comment on “Worldwide evidence of a unimodal relationship between productivity and plant species richness”

Lauri Laanisto^{1*} and Michael J. Hutchings²

Fraser *et al.* (Reports, 17 July 2015, p. 302) report that a hump-backed model describes the worldwide relationship between productivity and plant species richness in grassland communities. We reanalyze their data from a larger-scale perspective, using local species pool. This influences richness far more strongly than productivity, and, when this is taken into account, the hump-backed richness-productivity relationship disappears.

Since it was first proposed more than 40 years ago, the unimodal relationship [hump-backed model (HBM)] between plant species richness and productivity has been one of the most persistent models in plant ecology (1). Although it has been confirmed many times at a local scale (2, 3), its applicability at a global scale is still debated (1–8). While the HBM certainly applies in some regions and habitats, such as high-latitude grasslands (3), richness-productivity relationships tend to be positive in tropical areas (2–4). It is known that ecosystem stability and regional dispersal patterns influence diversity at different productivities (2) and that species' habitat productivity preferences are often determined by phylogenetic niche conservatism (4). Consequently, the plant species richness-productivity relationship is strongly contingent upon large-scale historical and biogeographical differences between habitats and species (2, 3, 9). However, such factors have so far been poorly integrated into richness-productivity models (2, 7, 10, 11). Only after assessing their influence on richness should the influence of more localized ecological processes, such as competition, be taken into consideration.

The case for adopting a different approach to assessment of the relationship between plant species richness and productivity locally and globally follows from numerous metastudies that have shown a diversity of empirical relationships between species richness and environmental parameters, including productivity, in different geographical regions. These different relationships have been attributed to divergent species pool dynamics and differences in evolutionary history (2–4, 9, 10). Thus, the shape of local richness-productivity relationships appears to be primarily

dependent on large-scale processes, with local-scale interactions having less influence (3).

The HBM has been subjected to several regional and global meta-assessments, with contradictory outcomes. This has mainly been interpreted as a consequence of methodological inconsistencies between case studies included in the meta-data (1, 6, 12). A logical step to address this problem is to conduct meta-experiments using consistent methodology (1, 5, 12), but the results of two recent global-scale HBM meta-experiments, using very similar methods, have also been contradictory; one found no relationship between plant

species richness and productivity (5), whereas the other found a hump-backed relationship (1). The raw data of the latter study has been made available (13), and the results presented here are based on further analysis of these data.

The sampling design of Fraser *et al.*'s study (1) is based on 8-m-by-8-m grids, with each containing 64 1-m² plots. Altogether, there were 157 grids (13). Living and standing dead biomass and species richness data were collected from each plot from every grid (1). Collection of species pool data was optional for contributors to the meta-experiment (12), and species pool data were not used in Fraser *et al.*'s analysis, even though comparison of absolute values of species richness on a global scale for different habitats is considered problematic at best, and the use of species pool data has been recognized as preferable (9, 11). To estimate local species pool sizes, we extracted data on the total number of species recorded in each grid. There was a strong positive correlation between the size of the local species pool and the mean species richness of the plots within each of the grids (Fig. 1). Local species pool size had a much stronger effect on mean species richness ($r^2 = 0.74$) (Fig. 1) than productivity (r^2 values ranging from 0.071 to 0.127, depending on spatial scale of analysis) [see figure S2 in (1)].

We then calculated the mean living + dead biomass per plot in each grid (productivity, *sensu* Fraser *et al.*) and the mean percentage of the local species pool that was recorded in the plots in each grid. The relationship between mean percentage of the local species pool recorded in the plots and mean productivity was not significant, and there was no evidence of a hump-backed relationship between these variables (Fig. 2).

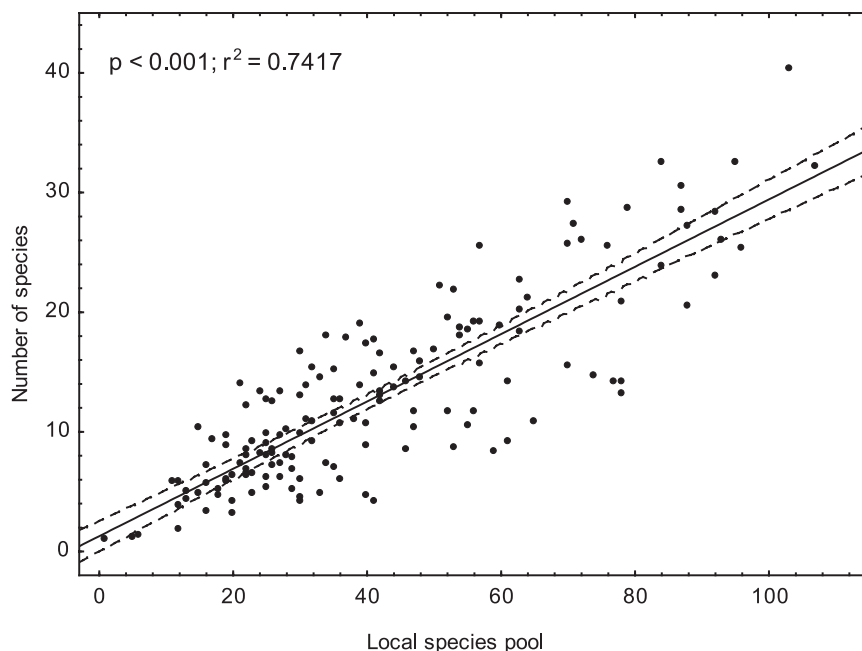


Fig. 1. Relationship between the mean number of species found in the plots of a single grid (number of species) and the total number of species found in that grid (local species pool). Each dot ($n = 157$) represents one 8- by 8-m grid containing 64 1-m² plots. [Data from (9)]

¹Institute of Agricultural and Environmental Sciences, Estonian University of Life Sciences, Kreutzwaldi 5, 51014 Tartu, Estonia.

²School of Life Sciences, University of Sussex, Falmer, Brighton, Sussex BN1 9QG, UK.

*Corresponding author. E-mail: laanisto@ut.ee

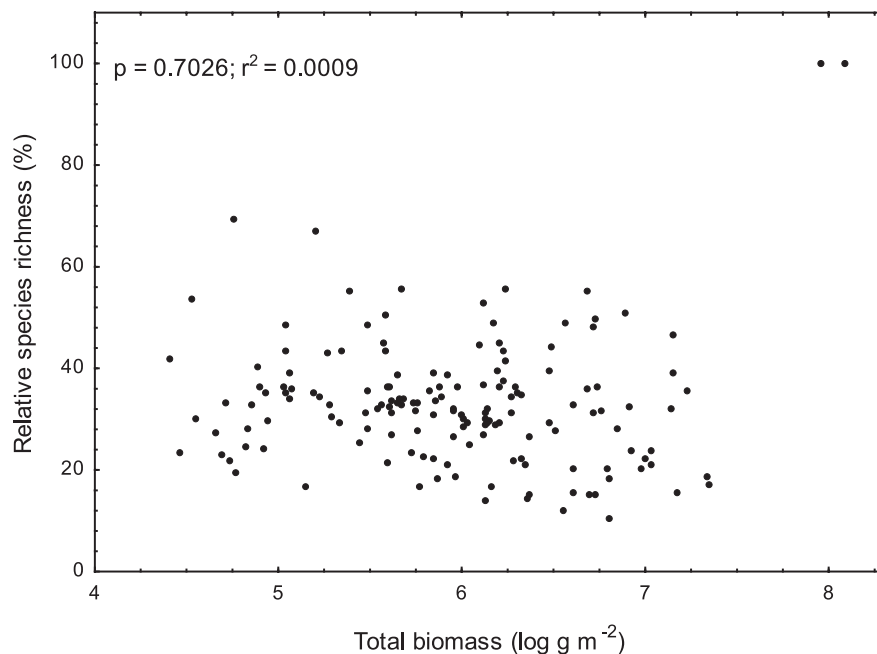


Fig. 2. Relationship between mean percentage of local species pool represented in the plots and mean productivity (living+standing dead biomass) in the plots ($n = 157$). When only live biomass is used as a measure of productivity, a slightly positive relationship between these variables is observed ($r^2 = 0.0339$, $P = 0.0236$), but there is no evidence of a hump-backed relationship. However, this positive relationship is strongly influenced by the data from the two most productive sites in the data set (i.e., the two data points at the top right of Fig. 2). These were both temperate wetland grasslands in Ohio [sites 90 and 92 in (9)] at which only a single species was recorded within the grids. This species was also found in all of the plots within each of the grids. Thus, a mean of 100% of the local species pool was present in the plots of both grids; excluding these data causes the relationship between percentage of local species pool represented in the plots and mean living biomass in the plots to become nonsignificant ($r^2 = 0.0082$, $P = 0.2717$). [Data from (9)]

This analysis shows the critical role of large-scale factors—in this case, the size of the local species pool—in determining plant species richness (9) and that the inclusion of pertinent (macro) ecological context in the analysis significantly improves the explanatory power of the data and changes the shape of the relationship between plant species diversity and productivity.

The question of whether there are general laws and principles in ecology has been long debated

and remains open. One point of view is that historical contingency, and the complexity of ecological phenomena, prevent the existence of generalizations that amount to laws in ecology (14). Another view is that ecological laws do exist, but with many exceptions (15), making it very difficult to find models that apply to all or even most ecological systems (2, 3, 14). A possible exception is the positive correlation between the size of the local species pool and local species

richness. This appears to be one of very few consistent patterns in ecology, despite all the contingent processes and interactions involved in the assembly of ecological communities (15), suggesting that studies of species richness conducted at large spatial scales and across many habitat types should consider species pool size as potentially the most influential determinant of local species richness (9). The analysis presented here demonstrates that it has far more power than productivity for explaining plant species richness at a global scale. This contribution shows a simple way of including local species pool size estimates in species richness-productivity studies when it is not possible to undertake complete species inventories.

REFERENCES AND NOTES

1. L. H. Fraser *et al.*, *Science* **349**, 302–305 (2015).
2. M. Zobel, M. Pärtel, *Glob. Ecol. Biogeogr.* **17**, 679–684 (2008).
3. M. Pärtel, L. Laanisto, M. Zobel, *Ecology* **88**, 1091–1097 (2007).
4. L. Laanisto, P. Urbas, M. Pärtel, *Glob. Ecol. Biogeogr.* **17**, 320–326 (2008).
5. P. B. Adler *et al.*, *Science* **333**, 1750–1753 (2011).
6. J. D. Fridley *et al.*, *Science* **335**, 1441–b (2012).
7. R. Waide *et al.*, *Annu. Rev. Ecol. Syst.* **30**, 257–300 (1999).
8. M. Huston, *Am. Nat.* **113**, 81–101 (1979).
9. M. Zobel, *J. Veg. Sci.* **2015**, 10.1111/jvs.12333 (2015).
10. H. V. Cornell, S. P. Harrison, *Annu. Rev. Ecol. Syst.* **45**, 45–67 (2014).
11. N. J. Gotelli, R. K. Colwell, *Ecol. Lett.* **4**, 379–391 (2001).
12. L. H. Fraser, A. Jentsch, M. Sternberg, *J. Veg. Sci.* **25**, 1160–1166 (2014).
13. Data from (1); Dryad Digital Repository; <http://dx.doi.org/10.5061/dryad.038q8> (2015).
14. A. Plutynski, in *The Oxford Handbook of Philosophy of Biology*, M. Ruse, Ed. (Oxford Univ. Press, New York, 2008), pp. 504–524.
15. J. H. Lawton, *Oikos* **84**, 177–192 (1999).

ACKNOWLEDGMENTS

This research was supported by Estonian Research Council's grants IUT 21-1, IUT 8-3, and PUT 607. Author contributions: L.L. designed the study and performed analysis, and L.L. and M.J.H. wrote the paper.

18 September 2015; accepted 4 November 2015
10.1126/science.aad4836

TECHNICAL RESPONSE

PLANT ECOLOGY

Response to Comment on “Worldwide evidence of a unimodal relationship between productivity and plant species richness”

Lauchlan H. Fraser,^{1*} Meelis Pärtel,² Jason Pither,³ Anke Jentsch,⁴ Marcelo Sternberg,⁵ Martin Zobel²

Laanisto and Hutchings claim that the local species pool is a more important predictor of local plant species richness than biomass and that when the species pool is considered, there is no hump-backed relationship between biomass and richness. However, we show that by calculating a more appropriate measure of species pool, community completeness, both regional and local processes shape local richness.

Species diversity varies from habitat to habitat. Because species diversity has been related to ecological processes and ecosystem functions, it is important to predict whether species diversity may be high or low in any given environment (1). Our recent Report (2) provides evidence from data collected from grasslands in 19 countries and six continents of a unimodal relationship between herbaceous species richness and aboveground plant biomass plus plant litter, such that the maximum potential species richness occurs at intermediate levels of biomass production. We tackled the question of the diversity-productivity relationship because of its foundational role in ecological research and its controversial history (2–7). The data were collected at the 1-m² scale, within 8-m-by-8-m grids, so that we could test linear and quadratic regressions at 1, 2, 4, 9, 16, 25, and 64 m² scales. At each scale, the best descriptor of the relationship was a concave quadratic regression, but explanatory power diminished with increasing scale (2).

We point to the relevance of our findings and the scaling approach in our analysis because it provides a comparative to Laanisto and Hutchings (8). Through a reanalysis of our data, Laanisto and Hutchings (8) argue that the local species pool has a stronger effect on species richness than primary productivity. We are in agreement that large-scale processes play a role in governing local-scale diversity, but it is challenging to account for large-scale processes in

an empirical study such as ours. Thus, instead of addressing whether it is more reasonable to seek for a relationship between species richness and primary productivity, or local species pool, we would rather ask what the relative role of local and regional factors is in shaping the em-

pirically observed relationship between diversity and productivity.

Laanisto and Hutchings emphasize geographic variation in the shape of the response curve (“While the HBM [hump-backed model] certainly applies in some regions and habitats, such as high-latitude grasslands ... richness-productivity relationships tend to be positive in tropical areas”). In fact, there are two confounding aspects in this statement: geographical region (with different biogeographic history) and ecosystem type (grassland versus forest). Positive relationships come predominantly from forests (9). We chose to avoid mixing different ecosystems because of the different processes that may be acting.

In their figure 1, Laanisto and Hutchings’s regression of local richness versus species pool is problematic because these two variables are inherently related, not independent, and local richness cannot exceed species pool size (10). Furthermore, all species recorded in an 8-m-by-8-m grid underestimates the local species pool. There are some techniques to overcome this problem—for example, estimating species pool size using Chao estimations (11). When applying this technique, we achieve a more complete estimate (Fig. 1A).

In figures 1 and 2 in (8), the analysis used by Laanisto and Hutchings could be more mathematically correct by calculating community completeness. When plotting richness against species pool, there is an upper limit where we do not have

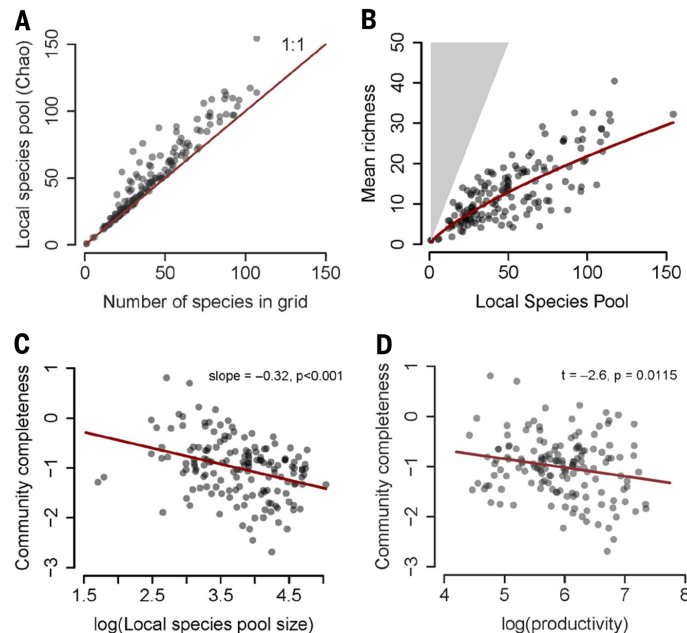


Fig. 1. Regional and local processes shape local species richness in globally distributed grasslands. The relationship between (A) the Chao estimation of local species pool found in the plots of a single grid [local species pool (Chao)] and the total number of species found in that grid; (B) the mean number of species found in the plots of a single grid (mean richness) and the local species pool (the shaded area represents impossible values where no data points can be found); (C) the log(richness/dark diversity) (community completeness) and the log(local species pool); and (D) the community completeness and the mean biomass found in the plots of a single grid [log(Productivity)]. Each dot ($n = 157$) represents one 8-m-by-8-m grid containing 64 1-m² plots [data from (14)]. Semitransparent dots are used to indicate overlapping revealed as a darker shade.

¹Department of Natural Resource Sciences, Thompson Rivers University, Kamloops, BC, Canada. ²Department of Botany, Institute of Ecology and Earth Sciences, University of Tartu, Tartu, Estonia. ³Department of Biology, University of British Columbia, Okanagan Campus, Kelowna, BC, Canada. ⁴Department of Disturbance Ecology, Bayreuth Center of Ecology and Environmental Research, University of Bayreuth, Bayreuth, Germany. ⁵Department of Molecular Biology and Ecology of Plants, Tel Aviv University, Tel-Aviv, Israel.

*Corresponding author. E-mail: lfraser@tru.ca

data points because richness cannot be larger than the pool. We can, however, apply a recently developed technique to model the overall trend between pool and richness using a log-ratio method of community completeness: $\log(\text{local richness}/\text{dark diversity})$, dark diversity includes species that belong to the species pool but are currently not present locally (10, 12, 13). We cannot calculate completeness for sites where there is no dark diversity—i.e., two monoculture sites were excluded, but these two points were outliers in any event. When we back-transform the trend line, we can see that the local richness is indeed positively related to local species pool size (Fig. 1B). The trend line, however, has a significant curvature. Curvature can be measured as the negative slope between community completeness and log species pool size (Fig. 1C). Thus, local richness is not a constant proportion of species pool, and when the size of the species pool increases, relatively fewer species are represented in 1-m² plots. This means that there are likely some local processes limiting richness.

Community completeness is a better way to express how the local species pool is realized in local plots than percentage (there are no upper and lower limits), and it works in log scale. Community completeness is negatively related to site productivity (log total biomass) (Fig. 1D). Here, the species pool effect has been taken into account, but we still see that, at high productivity, the species pool is realized less in local plots compared with low productivity. This can be due to competition. Thus, both regional and local processes shape local richness, but local processes are probably more important at high productivity.

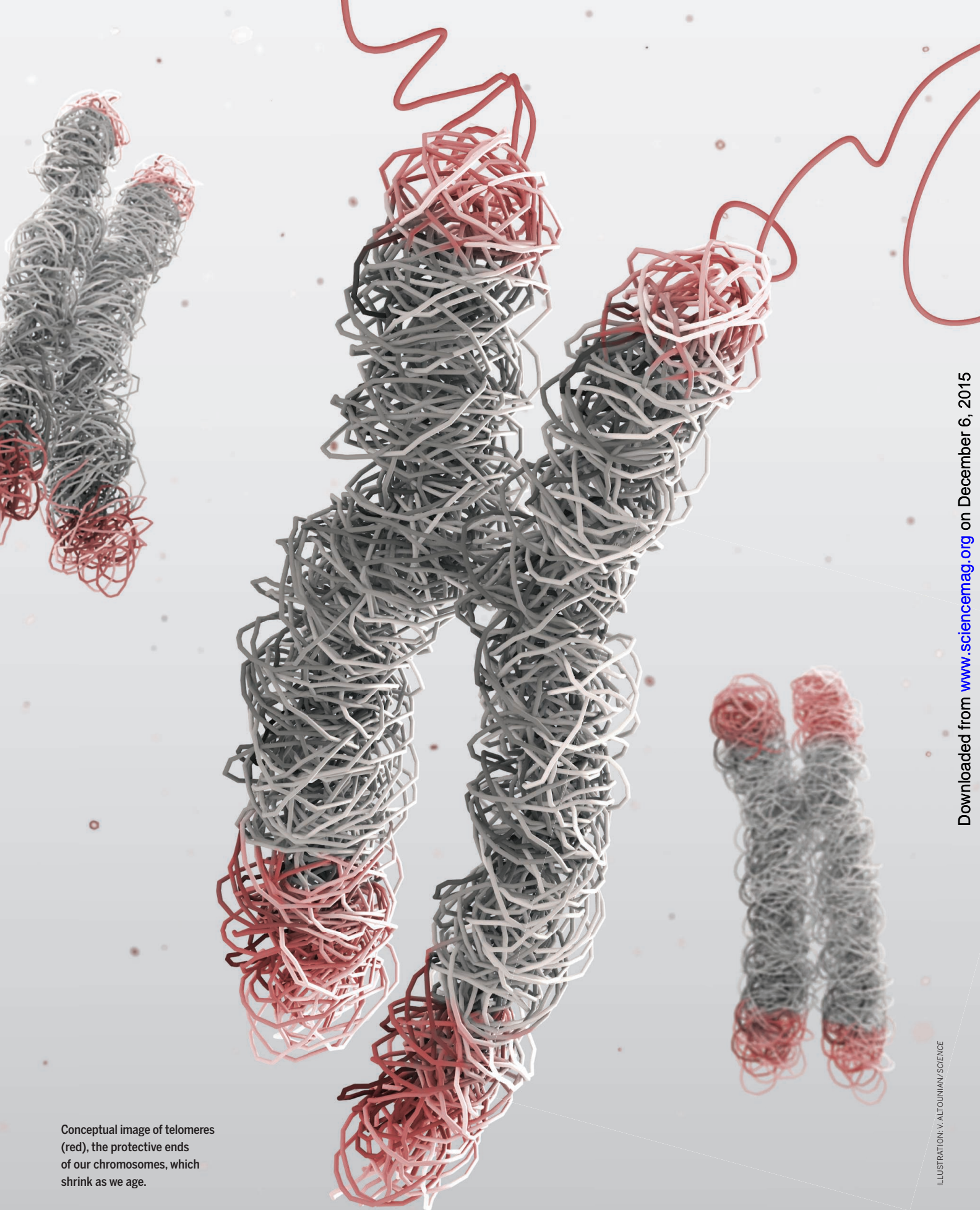
REFERENCES AND NOTES

1. K. J. Gaston, *Nature* **405**, 220–227 (2000).
2. L. H. Fraser *et al.*, *Science* **349**, 302–305 (2015).
3. J. P. Grime, *J. Environ. Manage.* **1**, 151–167 (1973).
4. P. B. Adler *et al.*, *Science* **333**, 1750–1753 (2011).
5. J. D. Fridley *et al.*, *Science* **335**, 1441-b (2012).
6. X. Pan, F. Liu, M. Zhang, *Science* **335**, 1441-a (2012).
7. J. B. Grace *et al.*, *Science* **335**, 1441-c (2012).
8. L. Laanisto, M. J. Hutchings, *Science* **350**, 1177 (2015).
9. W. K. Cornwell, P. J. Grubb, *Oikos* **100**, 417–428 (2003).
10. R. C. Szava-Kovats, M. Zobel, M. Pärtel, *Oikos* **121**, 321–326 (2012).
11. A. Chao *et al.*, Species estimation and applications, in *Encyclopedia of Statistical Sciences, Second Edition*, N. Balakrishnan, C. B. Read, B. Vidakovic, Eds. (Wiley, New York, 2005), pp. 7907–7916.
12. M. Pärtel, R. Szava-Kovats, M. Zobel, *Trends Ecol. Evol.* **26**, 124–128 (2011).
13. M. Pärtel, R. Szava-Kovats, M. Zobel, *Folia Geobot.* **48**, 307–317 (2013).
14. Data from (2); Dryad Digital Repository; <http://dx.doi.org/10.5061/dryad.038q8> (2015).

ACKNOWLEDGMENTS

We thank the Herbaceous Diversity Network (HerbDivNet) for the data set that has generated insights into plant diversity patterns and processes. This work was supported by a Natural Sciences and Engineering Research Council Discovery Grant Canada awarded to L.H.F. and J.P., the Estonian Research Council (20-28, 20-29), and a European Regional Development Fund Centre of Excellence Frontiers in Biodiversity Research awarded to M.P. and M.Z.

28 September 2015; accepted 4 November 2015
10.1126/science.aad4874



Conceptual image of telomeres (red), the protective ends of our chromosomes, which shrink as we age.

ILLUSTRATION: V. ALTOUNIAN/SCIENCE

Downloaded from www.sciencemag.org on December 6, 2015

TOWARD HEALTHY AGING

PUTTING OFF THE INEVITABLE

By **Stella Hurtley, Leslie Roberts,**
L. Bryan Ray, Beverly A. Purnell, and Caroline Ash

The dream of cheating death has evolved into a scientific quest to extend healthy life span. Scientists and doctors are looking for ways to maximize the number of years that we live free of chronic diseases, cancer, and cognitive decline.

But before we can intervene, we have to understand the cellular and molecular mechanisms that drive aging and senescence. Some clues reside in our telomeres, the tips of our chromosomes that shrink with age. Others lie in our stem cells, which can only go on for so long repairing our tissues. Our mitochondria, too, the so-called powerhouses of the cell, may hold some answers to prolonging youthfulness. Other research points to changes in the gut microbiota associated with frailty in the aged. At a mechanistic level, the modulation of coenzyme NAD⁺ usage or production can prolong both health span and life span. Current geroscience initiatives aim to harness basic insights in aging research to promote general advances in healthy aging.

Questions remain throughout the aging field. By tweaking everything from genes to diets to environmental temperature and mating, scientists have created Methuselah flies and other remarkably long-lived animals while garnering fundamental insights into the biology of aging. Still, researchers puzzle over the most basic questions, such as what determines the life spans of animals. Meanwhile, a handful of molecular biologists are searching for ways to measure a person's biological, as opposed to chronological, age, but that quest, too, has proved elusive.

An ever-growing literature addresses both theoretical and pragmatic approaches to the challenge of aging. In this special issue, we have focused mainly on the cellular aspects of mammalian aging, with the goal of spurring future developments in promoting health span, if not life span.



INSIDE

NEWS

Why we outlive our pets *p. 1182*

Death-defying experiments *p. 1186*

The final countdown *p. 1188*

REVIEWS

Healthy aging: The ultimate preventative medicine *p. 1191*

Human telomere biology: A contributory and interactive factor in aging, disease risks, and protection *p. 1193*

Stem cells and healthy aging *p. 1199*

Mitochondrial dysfunction and longevity in animals: Untangling the knot *p. 1204*

NAD⁺ in aging, metabolism, and neurodegeneration *p. 1208*

PERSPECTIVE

Gut microbiota and aging *p. 1214*

RELATED ITEMS

► EDITORIAL *p. 1135*

► PODCAST

► VIDEO

WHY WE OUTLIVE OUR PETS

Cats and dogs are revealing some surprising insights
into how animals age *By David Grimm*



Lily, a long-haired dachshund,
at 8 months, 2 years, 7 years,
and 15 years.

Downloaded from www.sciencemag.org on December 6, 2015

PHOTO: DOG YEARS: FAITHFUL FRIENDS, THEN & NOW BY AMANDA JONES, PUBLISHED BY CHRONICLE

Jeane Calment has nothing on Creme Puff, the cat. The oldest living human made it to the ripe age of 122—not bad for a species with an average life span of 71 years. But Creme Puff, a Texas feline that allegedly subsisted on bacon, broccoli, and heavy cream, more than doubled the longevity of her kind,

surviving a reported 38 years. Bluey, an Australian cattle dog, was no slouch either. At age 29, he became the oldest canine on record, living more than twice as long as the average pooch.

For centuries, scientists have tried to understand the human life span. What sets the limits? What can be done to slow down the clock? Now, they're beginning to ask the

same questions of our pets. As in humans, the answers have been hard to come by. But some intriguing hypotheses are emerging—ideas that may help explain everything from why small dogs live longer than big ones to why cats tend to outlast our canine pals.

Figuring out how animals age is a “fascinating problem,” says Daniel Promislow, an evolutionary geneticist at the University



of Washington, Seattle, and co-leader of the Dog Aging Project, which aims to extend the canine life span. “It integrates behavior, reproduction, ecology, and evolution. If we can understand how to improve the quality and length of life, it’s good for our pets and it’s good for us. It’s a win-win.”

SCIENTISTS HAVE BEEN PONDERING the mysteries of aging for more than 2000 years. “The reasons for some animals being long-lived and others short-lived, and, in a word, causes of the length and brevity of life call for investigation,” wrote Aristotle in 350 B.C.E. The Greek philosopher suspected the answer had something to do with moisture: Elephants outlast mice, he reasoned, because they contain more liquid and thus take longer to dry up. The idea hasn’t exactly held water, but Aristotle’s observation that bigger animals tend to live longer has. Indeed, it’s the only trend today’s scientists agree on.

“All of the other hypotheses have fallen apart,” says Steven Austad, a biogerontologist at the University of Alabama, Birming-

“I don’t think there’s a set max. longevity for any species. ... Maybe a thousand years from now you could have a dog that lives 300 years.”

João Pedro de Magalhães,
University of Liverpool

ham. One of the most popular ideas of the past 100 years has been that animals with higher metabolic rates live shorter lives because they run out their body clock faster. But “it hasn’t held up,” Austad says. Parrot hearts can beat up to 600 times per minute, for example, but they outlive by decades many creatures with slower tickers. Other assumptions, for example that short-lived animals generate more tissue-damaging free radicals or have cells that stop dividing sooner, also lack strong evidence. “A lot of simple stories have vanished,” he says.

Austad should know something about animals. He worked as a lion trainer in the early 1970s, until one of the big cats tore up his leg—an injury that persuaded him to study, rather than tame, the world’s creatures. By the mid-1980s, he was observing opossum behavior in Venezuela as a postdoc when he began to notice how quickly the marsupials aged. “They’d go from being in great shape to having cataracts and muscle wasting in 3 months,” he says. Austad also noticed something even more intriguing: Opossums on a nearby island free from predators seemed to age slower—and live longer—than their mainland counterparts.

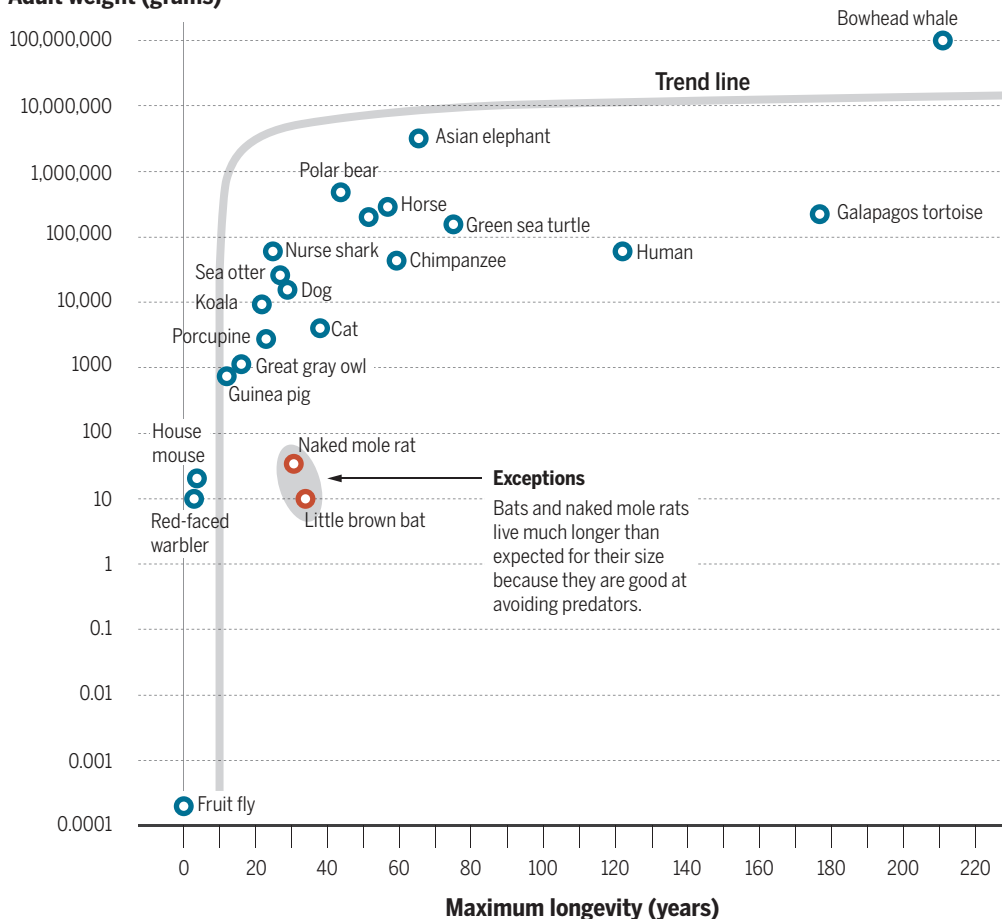
The observation helped explain why Aristotle’s key insight continues to hold true. Large animals tend to live longer, says Austad, because they face fewer dangers. It’s not a simple question of survival, he says, but rather the result of millions of years of evolutionary pressure. Whales and elephants can afford to take their time growing because no one is going to attack them, he explains. And that means they can invest

resources in robust bodies that will allow them to sire many rounds of offspring. Mice and other heavily preyed-on small animals, on the other hand, live life in fast-forward: They need to put their energy into growing and reproducing quickly, not into developing hardy immune systems, Austad says. “You wouldn’t put a \$1000 crystal on a \$5 watch.”

Longevity favors the big guys

As a general rule, larger animals live longer than smaller ones.

Adult weight (grams)



WHEN IT COMES TO OUR PETS, the bigger-is-better theory gets flipped on its ear. Cats live an average of 15 years, compared with about 12 years for dogs, despite generally being smaller. And small dogs can live twice as long as large ones.

Yet the lesson of Austad’s opossums may still apply. Gray wolves, the ancestors of dogs, live a maximum of 11 or 12 years in the wild, whereas wildcats can live up to 16 years. This suggests that the two species face different evolutionary pressures, Austad says. Wolves are more social than cats and thus more likely to spread infectious disease, he says; wildcats, on the other hand, keep to themselves, reducing the spread of disease, and are adept at defending against predators. “Cats are so incredibly well-armed, they’re like porcupines”—an animal that notably also has a long life span for its size, more than 20 years. Indeed, two other small animals that are good at avoiding danger, naked

Poppy, recognized as the world's oldest cat in 2014, lived to the ripe age of 24.



mole rats and bats, can live 30 and 40 years, respectively. (Mole rats spend most of their time underground, whereas bats can simply fly away.) Mice, meanwhile, live just a couple of years—unless they're eaten first.

When it comes to why small dogs tend to outlive big ones, the story gets a bit more complicated. Large dogs like the 70-kilogram Irish Wolfhound are lucky to make it to age 7, whereas tiny pooches like the 4-kilo Papillon can live 10 years longer. Most dog breeds are less than a couple of hundred years old, so evolutionary pressure clearly isn't at work. Instead, hormones like insulin-like growth factor 1, which swells dogs to big sizes, may play a role; researchers have linked the protein to shorter life spans in a variety of species, though the mechanism is unclear. Larger canines also tend to grow faster, notes the Dog Aging Project's Promislow, which could result in "jerry-built" bodies that are more susceptible to complications

and disease. Big dogs do tend to have more health problems than small ones—German Shepherds are prone to hip dysplasia, for example, and Siberian Huskies are plagued by autoimmune disorders—though these could also be the result of inbreeding.

Despite the differences between cats and dogs, both pets are living longer than ever before. Dog life expectancy has doubled in the past 4 decades, and housecats now live twice as long as their feral counterparts. The reasons can largely be chalked up to better health care and better diet. Americans will spend \$60 billion on their pets this year, with a large chunk of that going to human-like health care (think annual physicals and open-heart surgery) and premium food. "The same things that allow us to live longer also apply to our pets," says João Pedro de Magalhães, a biogerontologist at the University of Liverpool in the United Kingdom who maintains AnAge, the world's largest

database of animal life spans. The trend may not continue, though: More than half of U.S. pets are overweight or obese, and they are exposed to the same pollutants and carcinogens we are.

All of this uniquely positions dogs and cats to solve the riddle of how we ourselves grow old. After all, we have more medical records on them than on any other animal, save humans, and we learn more about their biology and genomes every day. Perhaps they hold the clues to slowing down the body clock for all of us—and maybe even stopping it. "I don't think there's a set max. longevity for any species," Magalhães says. "The real question is, 'How far can we go?' Maybe a thousand years from now you could have a dog that lives 300 years."

That's good news, especially if our life spans increase dramatically as well. After all, who wants to live forever if you can't live with your best friend? ■



This 1463-day-old mouse is part of a long-lived cohort at The Jackson Laboratory.

for a growth hormone receptor, GHR-KO 11C was a beneficiary of Bartke's effort to tease out the forces that drive aging. Other researchers have bred or engineered animals from mice down to flies, worms, and even yeast to vastly exceed their normal spans. The effort is yielding insights into aging, but researchers concede that there is also a *Guinness World Records*-ish fascination about it. "My animal lives longer than yours' is highly clickable," says Richard Miller, who studies the biology of aging at the University of Michigan, Ann Arbor.

Miller's own elderly mice have enjoyed a few brief moments in the limelight. The first came 2 years before GHR-KO 11C squeaked to fame when Miller claimed the title of having "the world's oldest normal lab mouse." Dubbed IdG1-030, the mouse lived 1449 days, and its death elicited an obituary in the ironically short-lived *Science of Aging Knowledge Environment*. "Born and raised in a small plastic cage in Ann Arbor, Michigan, IdG1-030 was one of a set of quintuplets born to a mated pair whose own parents had romped, poor but free, in the barnyards of Moscow, Idaho," read the heart-wrenching obit. The goal was to compare wild mice with their laboratory cousins, which have been bred for short life spans to make it easier to complete experiments.

As Miller stressed in IdG1-030's death notice, his lab had not restricted the caloric intake of the mouse, a tried-and-true way to extend the life span of many species, including mice. Miller wrote that his mouse "was clearly willing to accept an asterisk in the record books as the price for a life of ready access to all-you-can-eat meals." Today, several lab mice have passed their fourth birthdays, including one in Miller's lab named Yoda, a nod to the oldest Jedi master in *Star Wars*. "We now have at least five genes, two diets, and five drugs that extend mouse life spans," Miller says. "There's an enormous amount that's been learned."

Geneticist Gary Churchill at The Jackson Laboratory in Bar Harbor, Maine, currently has the oldest living mice, several of which are 4.5 years old. "They've been dropping off," Churchill laments. "I'm not holding my breath, but we could still make it to 5 years."

RESEARCHERS WHO STUDY *Drosophila melanogaster*, the fruit fly elevated to superstar status in genetic studies by Nobel laureate Thomas Hunt Morgan, have never reported a Yoda, GHR-KO 11C, or IdG1-030. "There is no oldest fly," says Marc Tatar, an

DEATH-DEFYING EXPERIMENTS

Pushing the limits of life span in animals could someday help lengthen our own

By Jon Cohen

On 8 January 2003, a mouse made news because it died.

Unlike other caged animals that gain notoriety, this dwarf mouse was not particularly cute or charismatic. He had not performed a silly pet trick or some astonishing intellectual feat. This laboratory mouse, a resident of Southern Illinois University in Carbondale, won notoriety because he lived 1819 days. "He missed his fifth birthday by a week, which is kind of unheard of in life span for a mouse," says Andrzej Bartke, the zoologist who ran the

lab that bred and studied the murine wonder unimaginatively dubbed GHR-KO 11C.

Bartke is too modest: It *was* unheard of. Lab mice typically live half as long, and GHR-KO 11C had, by Bartke's calculations, lived beyond 180 human years. "As pleasant as it was for us to get this notice and publicity, it's an n of 1," he stresses. "I didn't get too excited." (Some colleagues suspect there was a lab mix-up and GHR-KO 11C did not live as long as reported, but—reluctant to be seen as competing for a ridiculous title—keep their doubts quiet.)

Deliberately mutated to knock out a gene

evolutionary biologist at Brown University. “We don’t really pay that much attention. People who work on *Drosophila* look at cohorts and populations.”

Nobody even knows the average life span of *Drosophila*, Tatar says, because the flies are so sensitive to diet, temperature, access to mates, and other environmental forces. “In my lab, the average might be 40, 50 days, and long-lived ones might be 80 or 90.” That said, his lab and others have shown that they can produce long-lived fly populations by mutating genes—including the comically named *Indy* (I’m not dead yet)—that affect metabolic pathways.

Evolutionary biologist Michael Rose, whom Malcolm Gladwell profiled in *The New Yorker* in 1996 for his creation of “Methuselah” flies, pushed their life spans to 4 months and more by selectively breeding them for longevity. Rose, who works at the University of California (UC), Irvine, insists that he no longer is interested in setting records. Just the same, he says, “Our Methuselah flies wipe the floor with everyone else’s mutant *Drosophila*,” adding, “what most people work with in most labs is inbred garbage.” His lab now studies how aging can be stopped. “It renders the question of the longest-lived organism meaningless,” he says.

James Carey’s landmark fly studies also challenge the notion of an upper age limit. Carey, an entomologist at UC Davis, and colleagues studied 1.2 million medflies at a factory in Mexico that bred sterile versions of these fruit-destroying pests as part of a biological control strategy. The work, reported in *Science* in 1992, helped overturn the theory that mortality risks increase with age. The percentage of medflies that die at a certain day, it turns out, decreases as they age. So if you have a population of medflies that reaches 100 days, you might see 10% of them die by 110 days, but between 110 and 120 days the mortality rate could drop to 9%. “It was a big surprise that there’s a slowing of mortality,” Carey says. “You still have a high probability of dying, but it’s just not as high.”

The findings suggest that “there’s not a wall of death,” he says. He points to Jeanne Calment, the longest-lived human on record, who died in France at age 122. “It’s inconceivable to me that 122 will never ever be broken in the history of humankind,” he says.

LONGEVITY RESEARCHERS have had the most success increasing the life span of *Caenorhabditis elegans*, the soil roundworm that Nobel laureate Sydney Brenner brought into the lab in 1963 to study neural development. “We have single gene mutations with the greatest percentage increase in any animal life span by far,” says molecular geneticist Robert Shmookler Reis of the University of Arkansas for Medical Sciences in Little Rock.

In 2008, Reis and colleagues reported in *Aging Cell* that two strains of *C. elegans* with mutations in the same gene, *age-1*, had an average life span of 145 to 190 days—nearly 10 times longer than the wild-type worms living in the same environment. The oldest worm in their study lived 270 days. “We were astonished,” Reis says. “The first time we did it I said ‘No, no, they can’t still be

relative of the jellyfish made up of three lineages of self-renewing stem cells that—unlike in other species—do not lose their capacity to replace themselves as they age. Evolutionary biologist Daniel Martínez of Pomona College in Claremont, California, in 1998 published a study in *Experimental Gerontology* describing how 145 *Hydra* had lived in his lab for 4 years without any signs of aging, leading to his claim that they “may be potentially immortal.” His work purported to end a century-old scientific debate about whether these creatures age.

“After I published this initial paper I stopped,” Martínez says. “I couldn’t figure out what to do. You can’t study aging in something that doesn’t age.” The *Hydra* had to be fed three times a week with live brine shrimp and were fussy about salinity (hate it), their own waste, temperature, and overfeeding. “I was just sick of them,” he said. “I put them in alcohol and killed them.”

When researchers from a Max Planck institute in Germany convinced Martínez that there was more to learn from these apparently immortal animals, he restarted his experiments. Working together, the two groups now have *Hydra* that are 10 years old. “There’s no evidence of aging, no decay in reproduction, and no sign of mortality,” he says. The team also has shown that *FoxO*, a gene that increases tolerance to oxidative stress—and is linked to longevity in *Drosophila* and *C. elegans*—may play a central role in *Hydra*’s ability to maintain its stem cells.

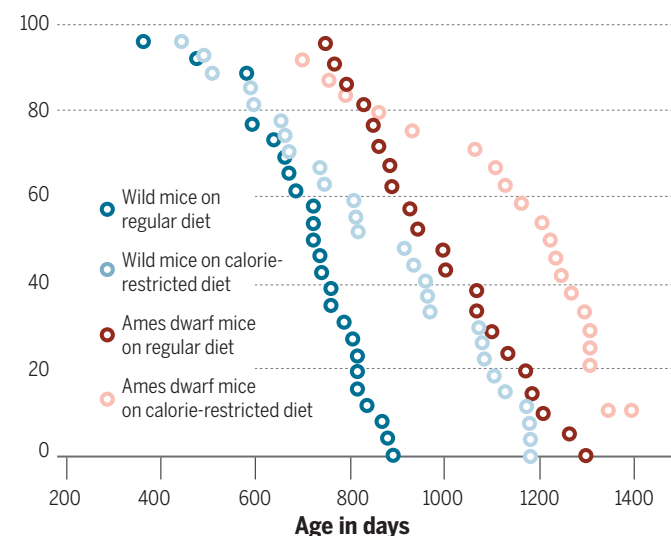
In contrast to *H. vulgaris*, its cousin, *H. oligactis*, will senesce if confronted by lowering water temperatures. Basically, the cooler water prompts the *Hydra* to switch from its usual, asexual mode of reproduction to sexual reproduction. “They switch from being stem cells into differentiated cells,” Martínez notes. Now, he’s comparing the two *Hydra* species to learn what controls the change.

Last year Martínez’s collaborators claimed in *Nature* that 5% of adults cared for in a lab would still be alive after 1400 years; the others would have died of accidents and disease, but not old age. “I’m reluctant to say that what we’re going to learn in *Hydra* will make us immortal,” Martínez says. “But you never know when you’re going to learn something that will apply to humans.” ■

Getting more mileage from mice

Dwarf genes and very low-calorie diets independently contribute to mouse survival.

Percent survival in group



alive, you must be looking at descendants of the starting worms.’ Except these worms were absolutely sterile!” The researchers are still working to explain the extraordinarily long life spans, but have evidence that their longevity is tied to silencing of insulinlike signaling pathways and stress responses.

The worms, bizarrely, had “near normal” motility and feeding rates—similar to wild-type worms at one-tenth their age—until they neared death. “The last few worms to die are always on their last legs,” says Reis, who quickly adds, “I know they don’t have legs, but they don’t look that great.”

THE SPECIES that still holds the lab longevity sweepstakes is *Hydra vulgaris*, a tiny



THE FINAL COUNTDOWN

In the race to find a biological clock, there are plenty of contenders

By **Emily Underwood**

A few years ago, molecular biologist John Sedivy took an online quiz billed as a test of his true, “biological” age. Among questions about how often he smoked and exercised was an odd one: what kind of car he drove. Sedivy first checked the box for a small sedan. Then, out of curiosity, he

switched his answer to a large SUV.

Opting for the bigger vehicle subtracted 3 years from his age. Later, at an aging conference in Europe, the Brown University researcher joked that Americans had figured out the secret to longevity: “Drive big honking cars.”

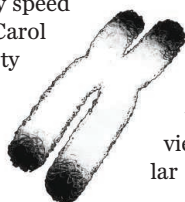
More-scientific efforts to determine biological age—how rapidly a person’s body

is aging, regardless of their chronological age—are equally fraught, Sedivy says. After decades of failed efforts to identify “biomarkers” in blood and different tissues that correspond to the aging process, scientists still don’t agree on whether “biological age” can be measured, or even what it means. Indeed, despite some companies’ claims, “there’s no way that you can take



a sample of someone's skin or blood and tell them what their true 'biological' age is," he says.

Yet the allure of an objective test for aging is powerful. Such a test could, for example, aid the search for antiaging drugs and help doctors plan treatments for older patients. Recent advances in the molecular biology of aging have yielded a host of candidates. All rely on molecular changes linked to aging, but all are confounded by individual variation or by other processes, such as disease, that may speed or slow aging. As aging pioneer Carol Greider of Johns Hopkins University in Baltimore, Maryland, puts it, "My guess is that there is going to be a huge amount of heterogeneity in any marker."



TELOMERE LENGTH. In the 1980s, a trio of biologists—Grieder; Elizabeth Blackburn, then at the University of California (UC), Berkeley; and Jack Szostak, then at Harvard Medical School in Boston—wowed the scientific world with the discovery that protective caps on the ends of chromosomes, called telomeres, must maintain a certain length for cells to continue dividing. They also found a mechanism for repairing and lengthening damaged telomeres: an enzyme called telomerase.

The work later won the Nobel Prize, in part because it promised profound insights into aging. Because telomeres get shorter every time a cell divides, many researchers viewed them as a clocklike molecular aging signature. Despite intriguing

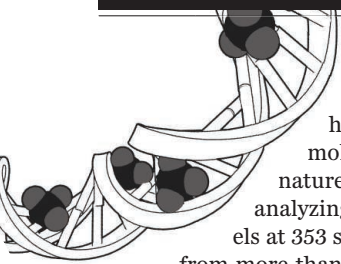
population-wide correlations between telomere length, disease, and mortality, however, subsequent efforts to use telomeres as the long-sought aging biomarker have sputtered, Greider says. Among the confounding variables is the diversity of telomere lengths among people of the same age, she notes. Recently, scientists have also discovered an apparent tradeoff between the age-buffering effects of long telomeres and a greater risk of some cancers, she adds.

Such caveats have not prevented a number of companies and researchers, including Greider's former mentor Blackburn, from developing commercial telomere-based tests. In 2010, Blackburn co-founded the Menlo Park, California-based company Telome Health, now Telomere Diagnostics, which provides analyses of telomere length in cells from a person's saliva to their doctors. Although the tests are not meant to predict how long an individual will live, Blackburn emphasizes, they may help physicians evaluate a patient's risk for a variety of age-related diseases and early mortality. Blackburn has recently distanced herself from the company—a year ago she donated all her shares to a non-profit organization.

Grieder served on the advisory board of a Menlo Park-based biotechnology company called Geron in the 1990s, but left because she felt the company was overstating the tests' clinical benefits. She still doubts that such tests hold much value for consumers at present. Only extremely short telomeres, resulting from genetic disorders known as telomere syndromes, are known to cause disease, she says.

Others share her skepticism. The value of such tests for individuals lies mostly in their "cocktail party" appeal, says Jerry Shay, a biologist at the Texas Southwestern Medical Center in Dallas. Still, Shay serves as consultant to the Madrid-based company Life Length, which claims to be able to calculate a person's biological age by the median length of their telomeres for roughly \$395 a pop. He's convinced that the tests do more good than harm—if one's telomere age were higher than expected, "that might be tap on the shoulder, letting you know that you're doing something wrong" in terms of lifestyle or diet, he says.

GENES AND DNA. In 2013, bioinformaticist and geneticist Steve Horvath at UC Los Angeles, proposed a new aging clock based on epigenetics, DNA alterations due to the addition and removal of chemical tags called methyl groups. Methylation can alter gene expression, and its pattern across the genome is known to evolve over the course of a lifetime.



Horvath has discovered what he believes to be a molecular aging signature in that pattern. By analyzing methylation levels at 353 sites on the genome from more than 13,000 human tissue samples, he developed an algorithm that can predict an individual's chronological age with more than 90% accuracy. Then he zeroed in on specific organs and tissues to measure his algorithm's performance. Would it show that tissues that are more prone to disease age faster than the body's average?

He found provocative patterns: cancer-prone breast tissue, for example, was several years older than the body as a whole, according to his epigenetic clock. Samples of cerebellum taken from deceased centenarians, in contrast, showed a comparatively youthful pattern of DNA methylation.

Horvath isn't yet sure what causes these differences, but he hopes they point to fundamental aging mechanisms that might be delayed or interrupted with drugs or other interventions. Although a number of independent labs have replicated his findings, scientists need a better understanding of what drives the epigenetic clock before the approach can be used in the clinic, says Horvath, who has no plans to commercialize his clock right now.

Other groups are attempting to use different genetic indicators to distinguish patterns of healthy aging from those of disease. This month, researchers described an approach based on certain mutations that accrue steadily over time in human tissue. Unlike the bursts of mutations triggered by exposure to environmental factors such as UV light or tobacco smoke, these mutational "signatures" show a strong, linear correlation with a person's chronological age, says Ludmil Alexandrov, a theoretical biologist at the Los Alamos National Laboratory in New Mexico and co-author of the new study, published in *Nature Genetics*. People who accumulate these mutations faster than others may age faster and be at higher risk of cancer, he adds.

All such markers need to be independently replicated and better understood before the community will embrace them, Sedivy says. Prospective, longitudinal studies testing whether people with specific patterns of methylation or gene expression are actually at higher risk of disease or death are also badly needed, Greider says.

LONG-LIVED PROTEINS. Although gene expression and methylation clearly change with time, neither is a direct measure of the damage that time inflicts on the body's cells as they age, says Martin Hetzer, a molecular biologist and co-director of the Glenn Center for Aging Research at the Salk Institute in San Diego, California. Hetzer recently introduced another, speculative aging clock, based on the changes that accumulate in the body's oldest proteins.

Unlike cells in the liver or intestines, which regularly regenerate, nerve cells in the brain and some cells in the heart never divide. "They are literally as old as you are," Hetzer says. Scientists have long assumed that even if the cells do not regenerate, the proteins within them must be replaced on a regular basis. Recently, however, Hetzer and colleagues made what he describes as a "shocking" discovery in mice: Rather than constantly being replaced, some proteins actually persist throughout an animal's entire life span.

Because long-lived proteins are more likely to accumulate damage and lose function, they might be a way to track the aging process, Hetzer and his team believe. In a September study in *Cell Systems*, they extracted tens of thousands of proteins from the livers and brains of 6-month-old mice—the equivalent of young human adults—and compared them with proteins from the same tissues in geriatric, 24-month-old mice. They found 468 changes in protein abundance between the young and old animals—some proteins increased with age, whereas others declined—as well as 130 proteins that changed location over time.

Most of the age-related changes in the rats occurred in the brain and involved proteins key to functions such as neuronal plasticity, cell organization, and memory formation. This is "super interesting," Hetzer says, because aging-related neurodegenerative diseases often involve damaged or misfolded proteins, such as the amyloid protein that builds up in the brains of patients with Alzheimer's disease. Amyloid doesn't normally last long in the brain, but might do so under diseased conditions, or when it gloms together in the telltale plaques of the disease, Hetzer speculates.

The team is now searching for a way to track chemical changes and damage in long-lived proteins, and explore their effect on

cellular function and aging, he says. Even if they do discover an aging clock based on proteins, he adds, it could be hard to turn into a practical aging test because invasive biopsies or postmortem samples are needed to extract the telltale proteins.

METABOLITES IN BLOOD. A practical aging biomarker should be cheap, and easy to detect in blood samples, says Eline Slagboom, a molecular epidemiologist at Leiden University Medical Center in the Netherlands. Her group is running a multi-generational study of 3500 people ages 40 to 110, looking at metabolites in blood serum and plasma that correspond to cardiovascular health, depression, dementia, diabetes, and mortality. One candidate is a substance called α 1-acid-glycoprotein, which has been

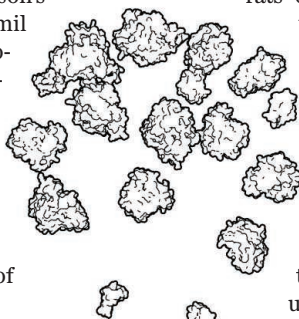
shown to increase with age and be associated with higher mortality risk. Slagboom's group is also exploring the relation between metabolic health and aging in a joint study with 20 other Dutch cohorts, including 25,000 people between the ages of 15 and 110.

In a smaller study, Slagboom and her colleagues are sizing up the entire field of aging clocks by pitting them head-to-head.

They are collecting data on telomere length, methylation, metabolites, and gene expression in 6000 people ages 20 to 90, to determine which, if any, marker best predicts mortality and disease.

The stakes are high, says Luigi Fontana, a systems biologist at Washington University in St. Louis in Missouri. Meaningful biomarkers are "really, really important" to move aging research forward, because they could enable short-term clinical trials of promising antiaging drugs such as rapamycin, he says. They could also help tease out which elderly people are healthy enough to benefit from a hip replacement or new medication, who needs extra support, training, or nutrition before such an intervention, or who shouldn't be treated at all, Slagboom says.

In the end, no single marker is likely to give a definitive reading of a person's true age, Sedivy says—it will take multiple markers to paint a true picture. Nor will tests focused on any single organ or tissue reveal how much of a person's allotted time remains. Aging researchers, he says, should take their cue from the way a mechanic would size up a used car: as a collection of parts, aging at different rates, some more critical than others. After all, "if you blow a tire, it's not so serious," Sedivy says. But, "blow a transmission, and you're dead." ■



Healthy aging: The ultimate preventative medicine

Matt Kaeberlein,^{1*} Peter S. Rabinovitch,¹ George M. Martin^{1,2}

Age is the greatest risk factor for nearly every major cause of mortality in developed nations. Despite this, most biomedical research focuses on individual disease processes without much consideration for the relationships between aging and disease. Recent discoveries in the field of geroscience, which aims to explain biological mechanisms of aging, have provided insights into molecular processes that underlie biological aging and, perhaps more importantly, potential interventions to delay aging and promote healthy longevity. Here we describe some of these advances, along with efforts to move geroscience from the bench to the clinic. We also propose that greater emphasis should be placed on research into basic aging processes, because interventions that slow aging will have a greater effect on quality of life compared with disease-specific approaches.

The major focus of biomedical research has traditionally been the pathogenesis and treatment of individual diseases, particularly those with substantial effects on morbidity and mortality. Within the U.S. National Institutes of Health (NIH) there are institutes dedicated to research toward treatments for cancer (National Cancer Institute); eye disease (National Eye Institute); heart, lung, and blood disease (National Heart, Lung, and Blood Institute); infectious disease (National Institute of Allergy and Infectious Diseases); arthritis, musculoskeletal, and skin diseases (National Institute of Arthritis and Musculoskeletal and Skin Diseases); neurological disease and stroke (National Institute of Neurological Disorders and Stroke); and diabetes, digestive disease, and kidney disease (National Institute of Diabetes and Digestive and Kidney Diseases). Even at the National Institute on Aging (NIA), more than one-third of the 2014 research budget was allocated for a single target—Alzheimer's disease—and this percentage has increased to more than 50% in 2015. This disease-specific focus has unquestionably had a profound effect on medical care and human health; many new treatments have been developed that are helping people live longer today than ever before. However, despite notable advances in management, we have been largely unsuccessful at postponing, ameliorating, or preventing the accumulation of morbidities during aging. As a consequence, people are living longer but often suffering from multiple diseases or disabilities of aging. This has important societal and economic implications. Many families struggle to care for elderly relatives who survive for years or even decades with reduced quality of life, while nations devote an increasing proportion of finite resources toward medical care for aging populations.

Introducing geroscience

These issues have, in part, spurred efforts to increase recognition of the importance of basic

research on the biology of aging. This has resulted in a series of major advances in a field once known as biogerontology but which has recently become known as geroscience. Such work has demonstrated that biological aging is modifiable and has provided tangible approaches to enhance healthy longevity. A promising new initiative, the NIH Geroscience Interest Group, has been created to expedite collaborative efforts to discover the mechanisms of aging that constitute the major risk factor for virtually all of their focused disease

"It is clear that directly targeting aging is theoretically superior to treating individual chronic diseases, but until recently, translational approaches to achieve this goal have been just that—purely theoretical."

interests (1). The underlying hypothesis is that delaying the rate of biological aging would simultaneously delay the onset and progression of each of these diseases, a prediction supported by experimental data in laboratory models (2). This has at least two major implications for translational biomedical research. First, it is critical to account for the biological effects of aging when developing therapies for chronic disease, something that is often not appropriately managed in preclinical studies that use young animal models. Consider, for example, the efficacy of vaccine therapies, which generally work potently in young animals but poorly in the context of an aged immune system. Most preclinical studies in this area involve young animals, yet the corresponding clinical applications are, in many instances, targeted toward the elderly. A specific case for which this

may have important implications is in the development of cancer immunotherapies (3).

The second and most profound implication from the link between aging and disease is that successful modifications of the intrinsic rates of aging will provide a much more effective approach for improving healthy longevity, relative to strategies aimed at treating or curing an individual disease. This will occur because therapies aimed at a single chronic disease, even when maximally successful, are generally unable to affect other diseases of aging. The added value from targeting the underlying processes of aging directly, and thereby delaying multiple age-related declines in function, has been referred to as the "longevity dividend" (4). Efforts to quantify this dividend, based on projections from preclinical experimental data, predict substantial benefits in individual quality of life (health span), as well as important society-wide economic and productivity gains (5).

It is clear that directly targeting aging is theoretically superior to treating individual chronic diseases, but until recently, translational approaches to achieve this goal have been just that—purely theoretical. This is now changing. Over the past decade, numerous studies have identified key mechanisms of aging (6), along with targeted interventions that modulate those mechanisms and extend healthy longevity in laboratory model systems. Within the past few years, we have begun to see the first steps toward translation of these laboratory discoveries into clinical applications.

Translational geroscience

Now we will focus on the initial forays into translational geroscience and the major challenges and opportunities they present. We have identified several interventional strategies for which there is evidence of attenuating or reversing the biological aging process in model systems; therefore, these strategies may have translational potential for improving human health span (Box 1). Our list is not exhaustive, nor does it predict precisely where the field will go; rather, it indicates those areas that currently appear most promising for the development of effective interventions to enhance a person's quality of life by delaying aging. To determine the broad utility of a particular intervention for improving healthy longevity in people, several questions must be addressed, including: (i) Is it relatively easy to implement? (ii) Can it be effective when started in mid-life (or later)? (iii) Do the benefits outweigh the risks?

However, there are at least two major hurdles to overcome before clinical interventions in aging can be rigorously validated in people. The first is the time scale over which human aging occurs. One way to assess the efficacy of an intervention for delaying biological aging is to demonstrate substantial improvements in the progression of aging-related conditions. Yet, unless there are intermediate outcomes, this method may require very long clinical trials, because many aging-related conditions progress over decades. Recent advances toward the development of true biomarkers of biological aging rate (i.e., epigenetic or metabolic signatures) may provide surrogate measures,

¹Department of Pathology, University of Washington, Seattle, WA 98195, USA. ²Molecular Biology Institute, University of California, Los Angeles, Los Angeles, CA 90095, USA.

*Corresponding author. E-mail: kaeber@uw.edu

Box 1. Geroscience interventions with translational potential.

Dietary restriction: Dietary restriction (DR) is the most studied intervention for delaying aging (16). Although not universally effective, a majority of studies have documented significant increases in both life span and health span when DR is applied in laboratory models, including nonhuman primates (17). Limited studies also indicate important health benefits, including reversal of disease risk factors (16), in people who practice DR. Although DR is not a viable translational approach at the population level, research in this area has incited the search for alternative dietary modifications (e.g., low-protein diets) or small-molecule DR mimetics (e.g., mTOR inhibitors, see below) that can provide the health benefits of DR without requiring reduced food consumption.

Exercise: A large body of literature provides evidence that the health benefits of exercise are consistent with the enhancement of health span (18, 19). However, poor compliance, especially in the elderly population, makes this intervention challenging to apply. Thus, there is high interest in developing pharmacologic interventions that would synergize with lower levels of exercise.

mTOR inhibitors: Rapamycin extends life span and promotes health span in mice, as well as in simpler organisms. Treatment beginning late in life is sufficient to extend life span, reverse cardiac decline, and improve immune function in mice (20). A recent study also reported that a rapamycin derivative significantly boosts immune function in elderly people (10).

Metformin and acarbose: Metformin and acarbose are widely used antidiabetes drugs. Metformin improves health span in mice and may slightly extend life span (21), whereas acarbose markedly extends life span in male mice and modestly extends life span in female mice (22). In a nonrandomized retrospective analysis, diabetic patients taking metformin have reduced mortality compared with diabetic patients not receiving metformin, and they may live longer than nondiabetics not receiving metformin (23).

NAD precursors and sirtuin activators: As discussed by Verdin in a companion Review (24), nicotinamide adenine dinucleotide (NAD) precursors such as nicotinamide riboside and nicotinamide mononucleotide have been reported to improve health span in mouse models of muscle aging and cognitive decline. The mechanism of action is not clear, but it may involve activation of sirtuin NAD-dependent protein deacetylases, along with enhanced mitochondrial function (25). Other, possibly more specific, sirtuin activators also improve health span and slightly extend life span in mice (26).

Modifiers of senescence and telomere dysfunction: Senescent cells accumulate during aging and secrete factors that promote inflammation and cancer (27). As discussed in the companion Review by Blackburn *et al.* (28), telomere dysfunction is a major cause of cell senescence, and strategies to enhance telomerase function offer promise for improving health span (29), although the possibility of increased cancer risk must be addressed. Likewise, genetic and pharmacological strategies to target and kill senescent cells enhance both life span and markers of health in short-lived mice with high levels of senescent cells (30, 31).

Hormonal and circulating factors: Age-related changes in important hormones (including sex-steroids, growth hormone, and insulin-like growth factor 1) are well documented; however, the risks and benefits of hormone supplementation in aging remain largely controversial (32). As discussed in the companion Review by Goodell and Rando (33), heterochronic parabiosis experiments in which the circulatory system of an aged mouse is shared with that of a young mouse suggest that additional, more subtle humoral factors affect age-associated declines in several tissues, including the brain, muscle, liver, and heart (34). Some progress has been made toward defining these factors (35), and an effort is under way to determine whether transfusion of young plasma can delay Alzheimer's disease (36).

Mitochondrial-targeted therapeutics: As discussed in the companion Review by Wang and Hekimi (37), mitochondrial dysfunction is a major contributor to aging and age-related diseases, although the mechanisms are more complex than initially suggested by the Harman's free radical theory of aging (38). Attention is now being directed to interventions that augment mitochondrial function, energetics, and biogenesis, including mitochondrial-targeted antioxidants and NAD precursors (39).

although these will also need to be validated, at least initially, in a similar manner. These strictures are greatly relaxed, however, if the inter-

vention can be shown to reverse physiological parameters of aging. Although this is a higher bar to reach, there is evidence that it may be achieved

by some interventions that target mechanisms of aging. For example, mTOR inhibitors such as rapamycin (Box 1) can partially rejuvenate immune stem cell (7) and cardiac (8, 9) function in mice and can perhaps also restore immune function in elderly people (10). The second major challenge for clinical assessment of interventions that modify biological aging is a regulatory one, at least in the United States. At present, efforts to target the basic processes of biological aging do not have a defined regulatory path at the U.S. Food and Drug Administration (FDA). Thus, it may not yet be possible to receive FDA approval for an intervention whose primary indication is to delay the onset, rates, or progression of aging. However, in consultation with the FDA, a strategy has recently been proposed that would enable researchers to partially bypass these hurdles and assess the efficacy of metformin against human aging in a randomized, double-blind clinical trial over 5 to 6 years. The Targeting Aging with Metformin (TAME) clinical trial seeks to enroll individuals who have already been diagnosed with any age-associated condition for the purpose of determining whether metformin is effective at delaying the diagnosis of other age-associated conditions (11). Because the time between diagnosis of the first and second age-associated conditions will be compressed, the study is expected to detect delays on the order of 15 to 30% (depending on the specific age-related condition). Should the results prove to substantially delay the onset of aging disorders, the TAME study may provide a possible regulatory path for clinical trials of agents designed to retard biological aging.

As an intermediate to human clinical studies, one option is to apply translational geroscience to companion (pet) dogs (12). Dogs suffer from many of the same age-associated diseases and functional declines that affect humans, albeit at an accelerated rate, and veterinary practitioners are adept at recognizing and diagnosing geriatric diseases in dogs. Dogs also have substantial genetic and phenotypic diversity. Moreover, companion dogs and cats share the human environment to an extent unmatched by any other nonhuman animal. Substantial increases in healthy longevity in companion dogs would not only provide important insights into similar efforts in people but would also directly improve the quality of life for pet dogs and their owners. A pilot study assessing the effects of short-term rapamycin treatment on cardiac aging in middle-aged companion dogs is under way (13), and a longer-term intervention study has been proposed that would also assess the effects of rapamycin treatment on cancer incidence, cognitive decline, immune function, mobility, and life expectancy in middle-aged dogs (12).

Future prospects

We have briefly outlined the case for concerted efforts to determine the mechanisms by which intrinsic processes of aging lead to many of the most devastating human health disorders, including heart disease, diabetes, cancer, and dementia. We have also pointed to promising advances in

translational research that have the potential to delay or conceivably prevent most such disorders. However, there is a caveat that requires more thorough investigation: the degree to which interventions that retard aging and delay the onset of age-related disorders will be accompanied by a compression of morbidity. In other words, will such interventions regularly lead to an increase in the ratio of health span to life span? Will our medicated centenarians lead fulfilling lives with eventual sudden collapse, or will they suffer from proportionally protracted durations of chronic disease? Although some research on centenarians suggests a compression of morbidity (14)—and rapamycin, in particular, appears to disproportionately enhance many measures of health span in mice (15)—future progress in geroscience interventions will need to be carefully monitored.

REFERENCES AND NOTES

1. J. B. Burch et al., *J. Gerontol. A Biol. Sci. Med. Sci.* **69** (suppl. 1), S1–S3 (2014).
2. M. Kaeberlein, *F1000Prime Rep.* **5**, 5 (2013).
3. C. Gravekamp, D. Chandra, *Crit. Rev. Oncol.* **18**, 585–595 (2013).
4. S. J. Olshansky, D. Perry, R. A. Miller, R. N. Butler, *Ann. N. Y. Acad. Sci.* **1114**, 11–13 (2007).
5. D. P. Goldman et al., *Health Aff.* **32**, 1698–1705 (2013).
6. L. Fontana, L. Partridge, V. D. Longo, *Science* **328**, 321–326 (2010).
7. C. Chen, Y. Liu, Y. Liu, P. Zheng, *Sci. Signal.* **2**, ra75 (2009).
8. J. M. Flynn et al., *Aging Cell* **12**, 851–862 (2013).
9. D. F. Dai et al., *Aging Cell* **13**, 529–539 (2014).
10. J. B. Mannick et al., *Sci. Transl. Med.* **6**, 268ra179 (2014).
11. E. Check Hayden, *Nature* **522**, 265–266 (2015).
12. M. Kaeberlein, *Vet. Pathol.* 10.1177/0300985815591082 (2015).
13. E. Check Hayden, *Nature* **514**, 546 (2014).
14. A. S. Ash et al., *J. Gerontol. A Biol. Sci. Med. Sci.* **70**, 971–976 (2015).
15. S. C. Johnson, G. M. Martin, P. S. Rabinovitch, M. Kaeberlein, *Sci. Transl. Med.* **5**, 211fs40 (2013).
16. D. Ormodei, L. Fontana, *FEBS Lett.* **585**, 1537–1542 (2011).
17. R. J. Colman et al., *Nat. Commun.* **5**, 3557 (2014).
18. E. M. Mercken, B. A. Carboneau, S. M. Krzysik-Walker, R. de Cabo, *Ageing Res. Rev.* **11**, 390–398 (2012).
19. B. Wang, D. R. Ramey, J. D. Schettler, H. B. Hubert, J. F. Fries, *Arch. Intern. Med.* **162**, 2285–2294 (2002).
20. S. C. Johnson, P. S. Rabinovitch, M. Kaeberlein, *Nature* **493**, 338–345 (2013).
21. W. De Haes et al., *Proc. Natl. Acad. Sci. U.S.A.* **111**, E2501–E2509 (2014).
22. D. E. Harrison et al., *Aging Cell* **13**, 273–282 (2014).
23. C. A. Bannister et al., *Diabetes Obes. Metab.* **16**, 1165–1173 (2014).
24. E. Verdin, *Science* **350**, 1208–1213 (2015).
25. S. Imai, L. Guarente, *Trends Cell Biol.* **24**, 464–471 (2014).
26. S. J. Mitchell et al., *Cell Reports* **6**, 836–843 (2014).
27. J. Campisi, L. Robert, *Interdiscip. Top. Gerontol.* **39**, 45–61 (2014).
28. E. H. Blackburn, E. S. Epel, J. Lin, *Science* **350**, 1193–1198 (2015).
29. B. Bernardes de Jesus, M. A. Blasco, *Curr. Opin. Cell Biol.* **24**, 739–743 (2012).
30. D. J. Baker et al., *Nature* **479**, 232–236 (2011).
31. Y. Zhu et al., *Aging Cell* **14**, 644–658 (2015).
32. C. C. Zoumboulis, E. Makrantonaki, *Rejuvenation Res.* **15**, 302–312 (2012).
33. M. A. Goodell, T. A. Rando, *Science* **350**, 1199–1203 (2015).
34. M. J. Conboy, I. M. Conboy, T. A. Rando, *Aging Cell* **12**, 525–530 (2013).
35. A. Bitto, M. Kaeberlein, *Cell Metab.* **20**, 2–4 (2014).
36. M. Scudellari, *Nature* **517**, 426–429 (2015).
37. Y. Wang, S. Hekimi, *Science* **350**, 1204–1207 (2015).
38. M. Gonzalez-Freire et al., *J. Gerontol. A Biol. Sci. Med. Sci.* **70**, 1334–1342 (2015).
39. D. F. Dai, Y. A. Chiao, D. J. Marcinek, H. H. Szteto, P. S. Rabinovitch, *Longev. Healthspan* **3**, 6 (2014).

ACKNOWLEDGMENTS

Geroscience in our laboratories and the labs of others at the University of Washington is supported by the Nathan Shock Center of Excellence in the Basic Biology of Aging, NIA grant P30AG013280.

10.1126/science.aad3267

REVIEW

Human telomere biology: A contributory and interactive factor in aging, disease risks, and protection

Elizabeth H. Blackburn,^{1,*} Elissa S. Epel,² Jue Lin¹

Telomeres are the protective end-complexes at the termini of eukaryotic chromosomes. Telomere attrition can lead to potentially maladaptive cellular changes, block cell division, and interfere with tissue replenishment. Recent advances in the understanding of human disease processes have clarified the roles of telomere biology, especially in diseases of human aging and in some aging-related processes. Greater overall telomere attrition predicts mortality and aging-related diseases in inherited telomere syndrome patients, and also in general human cohorts. However, genetically caused variations in telomere maintenance either raise or lower risks and progression of cancers, in a highly cancer type-specific fashion. Telomere maintenance is determined by genetic factors and is also cumulatively shaped by nongenetic influences throughout human life; both can interact. These and other recent findings highlight both causal and potentiating roles for telomere attrition in human diseases.

The telomere is a highly regulated and dynamic complex at chromosome ends, consisting of a tract of tandemly repeated short DNA repeats and associated protective proteins (Fig. 1) (1).

The telomere protects the genomic DNA through various mechanisms. One function is to prevent the end of the linear chromosomal DNA from being recognized as a broken end. This prevents processes—such as DNA end-joining, DNA recombination, or DNA repair—that would lead to unstable chromosomes. The general chromosomal DNA replication machinery cannot completely copy the DNA out to the extreme ends of the linear chromosomes. Over the course of cell divisions, this leads to attrition of chromosome ends. This deficiency can be resolved in eukaryotes by the cellular ribonucleoprotein enzyme telomerase, which can add telomeric repeat sequences to the ends of chromosomes, hence elongating them to compensate for their attrition (2).

Other damage-causing mechanisms can also contribute to telomere-shortening processes; these include nuclease action, chemical (such as oxidative) damage, and DNA replication stress. To offset these various processes, telomerase, as well as recombination between telomeric repeats, can act to replenish telomere length (3).

In many human cell types, the levels of telomerase (or of its action on telomeres) are limiting, and in humans, telomeres shorten throughout the life span. The degree of shortening is roughly proportionate to risks of common, often comorbid, diseases of aging as well as mortality risk. Inherited telomere syndromes (4, 5) have been

highly informative for dissecting the roles and interactions of telomere maintenance defects in the general population's human aging and age-related diseases. Declining telomere maintenance has pathophysiological effects on cells that can lie upstream of, as well as interact with, a number of the cellular hallmarks of aging (6). Because the effects of compromised telomere maintenance in humans play out in cell- and tissue-specific ways, they consequently differ between

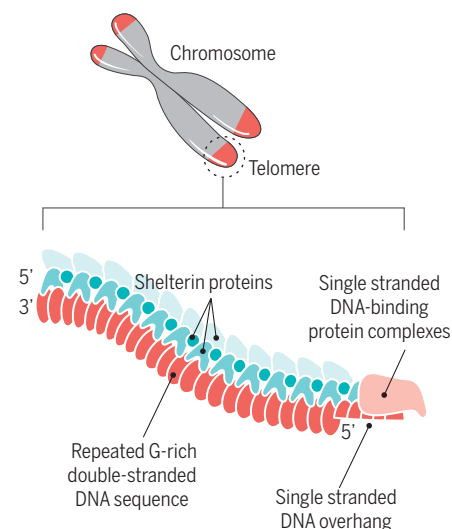


Fig. 1. Telomere structure. The human telomere complex consists of a chromosomal-terminal tract of a tandemly repeated DNA sequence bound by protective shelterin component proteins, with additional protective proteins on the overhanging single-stranded end region of the telomeric DNA repeat. This simplified schematic does not indicate details of the protein structures or of the architecture of the telomeric complex.

¹Department of Biochemistry and Biophysics, University of California, San Francisco, CA 94143, USA. ²Department of Psychiatry, University of California, San Francisco, CA 94143, USA.

*Corresponding author. E-mail: elizabeth.blackburn@ucsf.edu

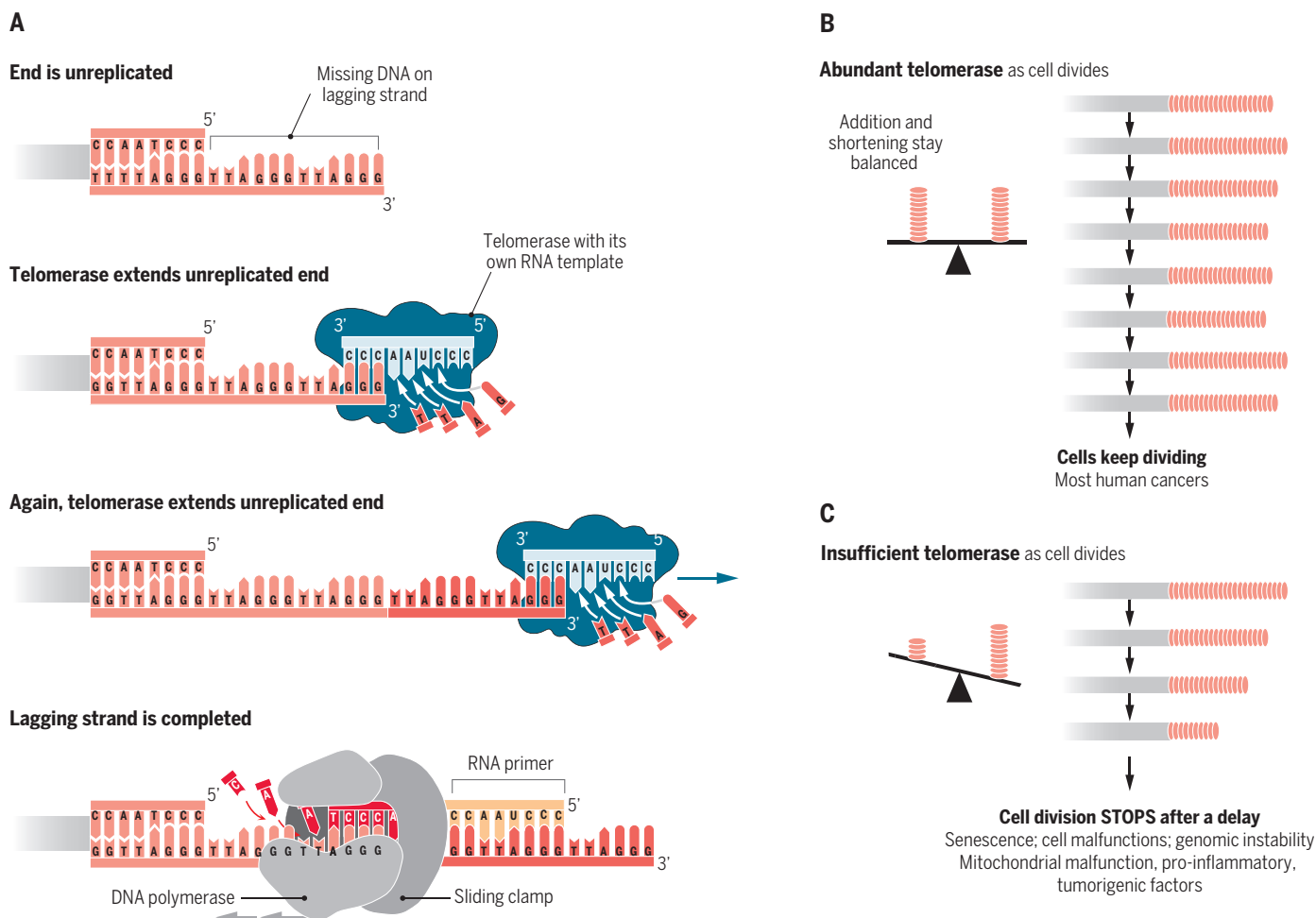


Fig. 2. Long-term maintenance of telomeric DNA length requires telomerase. (A) Replication of telomeric DNA. Elongation of one DNA strand, via the reverse transcriptase mechanism of telomeric DNA synthesis by telomerase, is followed by synthesis of the other telomere DNA strand by DNA polymerase. (B) As cells divide, shortening of telomeres through incomplete DNA replication and other processes causing attrition can be balanced by compensatory telomere-elongating action by telomerase. (C) Net telomere shortening when telomerase is insufficient leads to critically short telomeres. Telomere damage signaling leads to cessation of cell division and other cellular responses.

the various diseases of aging. Particularly among cancers, genetic determinants for longer telomeres raise risks in cancer type-specific ways. Recent advances in understanding the links of mortality and aging-related diseases to telomere maintenance, driven by genetic and nongenetic inputs, highlight the roles of telomere maintenance in diseases of aging, and their subtleties, in humans. Telomere biology in model systems has been extensively reviewed (1–4, 7–11).

Here, we will focus on human genetic and clinical findings as to whether telomere shortness in humans is a bystander or a cause of diseases and syndromes of aging. The best current understanding is that telomere shortening can both promote and be a result of disease etiology and progression and may in some situations set up a vicious cycle that interacts with other disease processes.

Telomere loss and replenishment

Many adult human cells, such as fibroblasts, have very low or no detectable telomerase. Such

cells, in tissue culture, undergo progressive telomere shortening. When the telomeres become critically short or sufficiently damaged, the deprotected telomeres set up a sustained form of DNA damage signaling. This causes altered transcriptional profiles, and cells to become senescent. Depending on cell type, the senescent cell characteristics have various consequences (Fig. 2) (11).

In humans and model organisms (including mammalian), telomeric DNA is often particularly susceptible to damage and abnormalities that occur genome-wide. First, the G-cluster-rich telomeric DNA is chemically more prone to oxidative damage reactions than is the general genome (12). Second, the telomere-bound protective proteins block or deflect DNA repair processes (10). Third, as a result, the sustained DNA signaling elicited by telomeric DNA damage is not resolved (7), and often cannot be unless by telomerase action, which, as described above, is often limiting in human cells.

It may seem paradoxical that telomeres, which are a part of the genome dedicated to genomic

protection, are so susceptible to damage. However, telomeres may be “first responders” to threats to genomic stability and problems with DNA maintenance, by which telomeric DNA acts as the “canary in the coal mine,” altering the cells’ responses before damage to informational genetic coding sequences occurs.

In general, although in cells of most human tissues telomeres shorten throughout human life, the idea of a constantly ticking mitotic clock is also over-simplistic. It is heavily confounded by, among other factors, the variable levels of telomerase activity—and hence variable capacities for telomere length replenishment—in stem cells. These can constantly renew somatic tissue cells. For example, telomerase is enriched in hemopoietic and intestinal villus stem cells and their transit amplifying cells in growth phase hair follicle cells, and in other stem cells including germline lineage cells and embryonic stem cells. Furthermore, it is not known how much of the normal senescence or death observed in many human cells in vivo can be attributed to causes other than

telomere-initiated DNA damage signaling resulting from loss of telomere protection (17).

Telomere regulation is highly interactive

Human telomeric DNA forms a scaffold for a hierarchy of proteins ranging from nucleosomal histones to shelterin components to conditionally associating DNA repair factors (Fig. 1) (1). Telomere replenishment and its regulation are part of extensive networks of cellular interactions. These include tight regulation of telomerase expression and action and of a complex of telomere-protective proteins called shelterin. In addition to protecting telomeres from deleterious DNA damage response processes (1), shelterin components have dual roles: They both recruit telomerase to telomeres and prevent it from acting on them in highly regulated fashions. Other factors, including DNA repair proteins, also pay transient visits to telomeres, some via shelterin component-specific interactions. Shelterin components have other functions besides telomere maintenance (Box 1). Thus, they have exquisitely balanced roles, and a dynamically regulated balance of shelterin component actions is important, rather than simply having larger amounts of them.

Aging in humans versus model organisms

Apart from overt signs of aging in humans—such as hair graying, skin wrinkling and spotting, muscle wasting, and altered adiposity—susceptibility to diseases dramatically increases as we enter the last decades of life. Such aging-related diseases prominently include, but are not restricted to, insufficient immune function, cardiovascular diseases, cancers, diabetes, depression, and cognitive decline. Some of these seemingly unrelated age-related diseases occur together in the same person more often than expected by chance (comorbid diseases).

Life spans vary by over 5 orders of magnitude across eukaryotes. Extrapolating findings from laboratory model systems may present problems because of the long, multidecades time frame of human aging, as well as differences such as body mass and other evolutionary differences. Telomeres shorten throughout the human life span, including during the aging portion of life. In marked contrast, critical telomere shortening appears to be negligible during the normal aging of the mostly much more short-lived animal models used for laboratory studies of aging. Thus (unless telomere maintenance is experimentally deleted genetically), laboratory mice and rats normally die of old age with intact and relatively long telomeres (13), as do other commonly studied short-lived nonmammalian models, such as the worm *Caenorhabditis elegans* (9), zebrafish (14), and the African turquoise killifish (8). During evolution, the telomerase-mediated system of telomere maintenance was completely lost from the fruit fly *Drosophila* (15). Determining which mechanistic underpinnings of aging are applicable to humans requires consideration of the steps or mechanism (or mechanisms) that are rate-limiting on the human aging time frame. These are not necessarily the same ones that are rate-limiting in a shorter-lived mammal.

Genetics: Telomere compromise can cause diseases

That inadequate telomere maintenance can cause several eukaryotic aging phenotypes in laboratory model organisms is demonstrated only by experimentally deleting telomere maintenance genes (4, 8, 9, 13, 16, 17). For example, in mice a complete null genotype for a telomerase component or a telomere protective protein causes, after telomeres have shortened sufficiently to become deprotected, characteristic accelerated aging phenotypes (4, 13). The challenge has been to deter-

mine the degree to which, in humans, telomere maintenance deficiency causes these same disease processes during normal aging.

Monogenetic inherited disorders of telomere maintenance clearly demonstrate, at the simplest conceptual level, that unprotected telomeres can play causal roles in aging and diseases of aging of humans. Such diseases are caused by Mendelian mutations that compromise telomere function. They usually (but not always) manifest as very short telomeres in vivo. This results from excessive telomere shortening, with consequent loss of telomere capping and protection. As described above, the resultant signaling from the damaged telomeres causes phenotypes that lead to diseases.

Such single-gene inactivating mutations are known in 11 human genes to date. Each mutated gene has a known, molecularly defined, direct function in telomere maintenance: It encodes either a telomerase component (TERC, TERT, DKC1, NOP10, NHP2, or WRAP53) or a telomere-binding protein, found on telomeres in vivo and shown experimentally to have an essential telomere protection function (TINF2, RTEL1, POT1, CTC1, and TPP1) (4, 5).

These inherited diseases comprise a seeming plethora of tissue- and organ-specific pathologies and disease classifications. All are united by one common causal molecular mechanism: the response to unprotected (usually drastically shortened) telomeres. They parallel many phenotypes of experimental mouse models that are null for a telomere maintenance gene (18–20). We refer to this clinically diverse collection of monogenetic mutation diseases as “inherited telomere syndromes.” These diseases are frequently autosomal-dominant. In humans, functional haploinsufficiency often underlies the pathology and gene dose, and hence the level of the relevant telomere maintenance pathway gene product is important for protection against an organism-wide range of diseases and syndromes.

In patients, clinical variability, incomplete penetrance, and variable expressivity of the mutation occur (5). Yet inherited telomere syndromes are increasingly understood to fall into characteristic patterns. They can include one or more of the following: loss of immune function through loss of bone marrow stem cell reserves, certain cancers (hematological such as leukemias and myelodysplastic syndrome, or squamous-cell skin and gastrointestinal cancers), pulmonary fibrosis (accounting for the most frequent single-gene mutational cause of this disease), gastrointestinal disorders, liver cirrhosis, and neuropsychiatric conditions. Patients often have additional phenotypes of accelerated aging, including diabetes, myocardial infarction, hair graying, and skin pigmentation (20).

Mouse models of telomerase deficiency usually require several generations before their progressive telomere shortness reaches the point when phenotypes manifest (4, 8, 9, 13, 16). Similarly, a hallmark of monogenetic human telomere syndromes is genetic anticipation, with succeeding generations of mutation carriers in a family pedigree having successively earlier disease onsets,

BOX 1. Recently emerged off-telomere functions of shelterin components.

Various shelterin components are found throughout the nucleus as well as on telomeres; some of these are transcription factors that act genome-wide. Multiple shelterin components, from budding yeast to mammals (and thus presumably in humans), show highly regulated binding to a plethora of genomic nontelomeric sites, where they control transcription of several cell and developmental stage-specific gene networks. For example, the evolutionarily conserved shelterin RAP1 has transcriptional roles. Genetic manipulations of RAP1 in mice cause gender-specific obesity even though the telomeres are not damaged. Hence, other gene networks, in addition to DNA damage and stress responses, are controlled by shelterin components acting as transcription factors and can be affected by their balance at telomeres versus other genomic locations (61).

Shelterin components, in turn, are themselves regulated by gene expression and modification pathways that are cell type- and developmental stage-specific. For example, a well-studied longevity-promoting transcription factor, FOXO3, increases the expression of the essential telomere-protective POT1a in mouse neuronal stem cells. Such regulation may be especially important for these recently recognized off-telomeric roles of shelterin components. Thus, the influence of telomere complexes extends from transcriptional responses caused by DNA damage responses to uncapped telomeres, to the multifunctional shelterin components that act as transcription factors to reprogram networks that include metabolic genes (61).

These multiple layers reveal nuanced, two-way conversations between telomere integrity and cellular and organism functions. How they interplay throughout multiple tissues and stages of human life is likely to be complex.

and the types of diseases are also characteristically different down the generations. Particularly in later generations of families, early death results. Together with the mouse models, these observations provided a crucial insight: proof that short telomeres themselves are the major mechanistic cause of the disease phenotypes. Strikingly, disease even manifests in noncarrier offspring when they inherit short telomeres from an affected carrier parent (4, 5, 21).

Telomeres also exert context-dependent impacts on diseases. As well as telomere syndrome symptoms, human carriers of monogenetic telomerase mutations develop emphysema and chronic obstructive pulmonary disease, specifically if they are smokers (22). The interactive nature of telomere compromise is elegantly demonstrated by combining telomerase deletion with a mutation for a disease gene. In diverse genetically defined mouse transgenic models of human monogenetic diseases, even at early generations after telomerase loss in the double-mutant mice, telomere shortness and dysfunction synergize with the genetic lesion to cause the full organism-wide range of human symptoms and pathology, which in the single-mutant animals is often incomplete (Box 2) (23–25). Thus, telomere dysfunction can interact with other disease etiologies and could contribute aspects to human diseases that originate from other primary causes. Furthermore, in addition to attrition from lack of telomerase-mediated replenishment, other forms of telomere damage, such as oxidative damage accumulating with age, could also underlie contributions of telomere dysfunction to diseases of aging.

Disease potentiator and mortality predictor

Although the inherited telomere syndromes often manifest earlier and with greater severity, their phenotypes are those of diseases that increase dramatically with aging in the general human population. Many of the common diseases of human aging—including poor immune function (26), cancers (27, 28), diabetes (29), and cardiovascular disease (30)—are predicted by and/or associated with shortness of telomeres in total leukocytes or peripheral blood mononuclear cells (PBMCs).

Mean leukocyte telomere length (LTL) or PBMC TL reflects systemic influences on telomere maintenance in other tissues and, importantly, the senescent status of circulating cells of the immune system. A role for inflammation has been extensively documented for the pathological progression of such diseases as cardiovascular disease, diabetes, and possibly dementias. Because of the pro-inflammatory processes engendered by immune cell senescence, telomere attrition in immune cells has relevance for the etiology of these conditions.

Most human diseases of aging are influenced by complex genetic as well as nongenetic inputs. The mouse model examples (Box 2) show that causality inferred for a disease could be incomplete if telomere shortness is not taken into account. Unbiased genome-wide association studies (GWASs) on loci that affect white blood cell

BOX 2. Additive/synergistic effects of telomere attrition and specific disease genes.

In mouse models with $Wrn^{-/-}$ $Terc^{-/-}$ double (62) or $Wrn^{-/-}$ $BlmM3/M3$ $Terc^{-/-}$ triple mutations (23), the telomerase deletion phenotypes appear in earlier generations after deletion of TERC, as opposed to the sixth generation in a $Terc^{-/-}$ but otherwise wild-type background (23, 62).

Additional phenotypes specific to human Werner and Blooms are also observed and are more severe than are $Wrn^{-/-}$ or $Wrn^{-/-}$ $BlmM3/M3$ mice with wild-type TERC. Recent in vitro work showed that added telomerase protects Werner syndrome lineage-specific human stem cells from premature aging (24), which reinforces a previous finding that indicated that telomere dysfunction contributes to premature aging phenotype in Werner syndrome (63).

In the diabetic Akita mouse that carries a mutation in the insulin gene, $Ins2C96Y/WT$, misfolded insulin causes endoplasmic reticulum stress and leads to β -islet cell apoptosis (25). TERC deletion in the Akita background leads to increased β -islet cell apoptosis and greater loss of glucose tolerance compared with that from the $Ins2C96Y/WT$ mutation alone, suggesting that the assault of telomere dysfunction and ER stress are additive.

Duchenne muscular dystrophy is a muscle-wasting disease caused by a mutation in dystrophin, which results in muscle degeneration and premature death. The mouse model with the same human mutation has surprisingly mild phenotypes. However, double-mutant mice that lack dystrophin and have shortened telomeres ($mdx/mTRKO$) develop phenotypes that mirror those seen in humans, including severe functional cardiac deficits such as ventricular dilation, contractile and conductance dysfunction, and accelerated mortality (64). These cardiac defects are accompanied by telomere erosion. Telomere length in cardiomyocytes of the $mdx/mTRKO$ G2 mouse is shorter than that of the G2 mouse in which mTR was knocked out, demonstrating that the dystrophin mutation exacerbates telomere attrition. Again, a synergistic effect is seen for both the telomere and Duchenne muscular dystrophy phenotypes.

These findings broaden the scope of possible consequences of shortened telomeres for aging and disease and highlight that often, “the action is in the interaction.”

(leukocyte) human telomere length have consistently uncovered loci containing known telomerase and telomere-protective protein genes. Mendelian randomization established a causal relationship for LTL shortness and increased coronary artery disease (CAD) risk in one such large European study (31). This identified seven top common-gene variant alleles that together explain ~1% of the total LTL variation. The top-scoring five (TERC, TERT, NAF1, OBFC1, and RTE1) of these seven genes encode components with molecularly defined, direct actions on telomeres. The allele scores for these same seven common genes linked to shorter telomeres were predictive in additive fashion of risk of CAD. The risk for CAD was ~20% higher than usual in those individuals with the highest allele score for six out of these seven top-scored shorter-telomere gene common variants (31). Common single-nucleotide polymorphisms (SNPs) of NAF1 and OBFC1 have also been shown to associate with coronary heart diseases (CHD) (32, 33). Cardiovascular and other diseases of general population aging are also seen in monogenetic inherited telomere syndromes. Hence, at least some common diseases, such as CAD and CHD, may be considered as partial “telomere syndromes.” A recent paper also reported that the short telomere length allele of two of the SNPs described in (31) (TERT and OBFC1) is associated with higher risks for Alzheimer’s disease (34), thus establishing a causal relationship between short TL and a higher risk for AD.

The minimum telomere length needed to ensure human telomere protective stability in white

blood cells is 3.81 kb (35). Thus, a small change in human white blood cell telomeres has a bigger functional impact than its absolute magnitude might suggest. For example, the GWAS LTL gene (31) with the largest effect, the telomerase RNA component TERC, causes a mean telomere length decrease of 117 base pairs (bp) per TERC telomere-shortening allele. In a typical middle-aged adult’s ~5-kb repeat leukocyte telomeric DNA tract length, this allele effect represents an ~10% drop in the effective 1.19 (that is, 5 – 3.81) kb functional telomere reserve. Mean LTL is usually the measure performed for feasibility and cost reasons, and it is unknown to what extent the more resource-intensive measurement of the shortest telomeres will add information useful for many clinical studies.

As humans age, average telomere length declines, and mortality increases. Chronological age accounts for less than 10% of human telomere length variation. Recent large cohort studies have clarified that independent of age and other previously known mortality risk factors, the degree of telomere shortness is also a clear statistical predictor of human all-cause mortality (36, 37). But telomere length maintenance is highly interactive, and as described below, telomere measures show much greater predictive power when combined with other factors.

A recent California 100,000-adult study, in which 75 years is the age of maximum mortality risk, showed that in humans aged above 75 years, the trend of telomere shortness with age is reversed (38). This V-shaped relationship and trend

to longer cross-sectional telomeres in the oldest subjects suggests that increased telomere length with increasing exceptional longevity is associated with selection for survival. This interpretation is reinforced by previous findings: LTL in the Nicoya Peninsula Exceptional Longevity population in Costa Rica was consistently longer for the Nicoya Peninsula population compared with the control Costa Rica population across ages, but only until the age defined as extreme longevity—95 years and above—at which age the two groups' telomere length curves converged (39). This selection bias can help explain some previous mixed findings on telomere length and mortality.

Most mortality in the large cohorts studied to date for LTL results from common diseases of aging, prominently cardiovascular diseases, cancers, and diabetes. Therefore, predictions of future incidences of such diseases and of future mortality are expected to be consistent. Indeed, in a graded fashion, white blood cell telomere shortness prospectively predicted higher future incidences (new diagnoses) of both cardiovascular diseases and all cancers combined, across the following 10 years (40). In a large cohort, it predicted both cardiovascular and all-cancers mortality in a 7-year average follow-up (36). Short telomeres predicting future disease onset is consistent with telomere attrition having a causal role but is not proof. The proof for a partial contributory role for telomere shortness came from the GWASs on CAD described above. It is biologically consistent with the disease and mortality phenotypes of inherited telomere syndrome patients and mice null for a telomere maintenance gene.

Cancers: Telomerase teetering on the brink

In tumor cells, which often behave as though effectively immortalized, telomere maintenance becomes ensured by various routes. In 80 to 90% of fully malignant human tumors, cancer cell telomerase activity is up-regulated compared with normal tissue counterparts. Yet the more than 200 types of cancers in humans result from a wide range of cancer etiologies and series of events. As expected from this diversity, cancers vary regarding how telomere maintenance up-regulation—or its compromise—promotes the complex processes of cancer etiology and progression. On the one hand, the inherited telomere syndromes show that organism-wide inadequate telomerase action causes high frequencies of hematological, squamous cell, and gastrointestinal tumors. These all involve tissues whose high demands for stem cell replenishment become compromised by the lack of telomere maintenance. Mutations in the gene encoding shelterin component POT1 cause a specific human glioma type (brain tumor), and the molecular nature of these mutations indi-

cates that they may cause improperly capped telomeres or possibly alter telomerase action (41). On the other hand, a germline activating mutation in the promoter of the telomerase component TERT, identified in a family pedigree, that increased TERT expression only ~1.4-fold was sufficient to cause fully penetrant melanoma (42). Also, in multiple population-based cohorts, common germline longer-LTL variants in known telomere maintenance genes, especially telomerase genes, raised risks of melanomas, nonsmokers' lung cancer, and many gliomas (43). Thus, even mildly over-activating telomere maintenance promotes risks of subsets of cancers. Telomere maintenance—promoting alleles potentially prolong survival of certain cancer-prone or precancerous cells, increasing their chances of undergoing the multiple steps that generate tumors.

Nongenetic factors: Life stressors and lifestyle

Heritability estimates of human telomere length range from 30 to 80%. Very short telomeres are inherited in telomere syndrome mutation families (21). Similarly, it has been suggested

Hence, the impacts of genetic versus nongenetic causes of longer telomeres differ on cancers (Fig. 3). Nongenetic, including epigenetic, influences on telomere maintenance therefore are of considerable interest for their roles in disease etiologies.

In humans, associations between stress and telomeres can be seen early in life. Newborn human telomere length was shorter in proportion to the stress levels experienced by the mother during her pregnancy (47). Degrees of exposure to violence or neglect in childhood and to various categories of adverse childhood events (ACEs) were associated with substantially shorter telomere lengths, as measured either in children or retrospectively in adults (48). “Dose-dependent” effects of exposure to stressors on telomere shortness have also been observed in adults. Examples include durations of exposures to domestic violence, unmedicated depression, or caregiving for a family member with chronic illness (49). Experimental studies exposing young birds to stress demonstrate that chronic psychological stress is a causal factor in telomere shortening (50).

Mechanisms of the stress-telomere relationship are starting to be examined and are likely multifold. The transmission of maternal stress to offspring may be mediated through direct effects, parental shorter gamete telomere length, epigenetics, or indirect effects, such as by alterations in the intrauterine environment due to elevated stress hormones or poor nutrition (50, 51). Several studies in birds have shown maternal transmission of stress is in part through glucocorticoid exposure in either mother or egg (50). In humans, shorter telomeres are associated with greater cortisol reactivity (52), and in vitro work suggests that high glucocorticoids may dampen down telomerase activity (53).

Such studies provide suggestive evidence that chronic psychological stress may be one causal factor in telomere shortness in humans. Adults with major depressive disease tend to have shorter telomere length (54), especially with greater severity and duration of depression (55). Telomere shortness is thus likely a result of the disease, although shortening may also precede onset of depression in children at high risk (52).

Other factors reported to be associated with telomere length range from social and environmental factors to lifestyle factors, such as smoking or exercise (49, 56). Although observed telomere length, or a telomere-related allele, may alone have a small effect on disease, the effect can be magnified by, for example, depression (57) or smoking (58, 59). Thus, interactive effects of nongenetic and genetic telomere determinants are potentially powerful and are relatively unexplored.

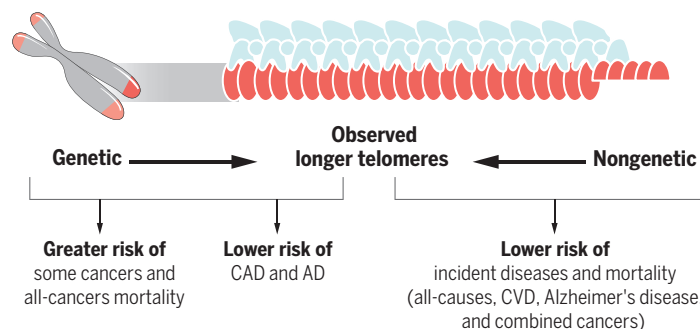


Fig. 3. Different inputs to telomere maintenance have disease-specific consequences. Observed telomere length results from combined genetic and nongenetic inputs. Longer observed telomeres are associated with lower overall risks for mortality and diseases. The variants of telomere maintenance genes that promote longer telomeres decrease CAD and Alzheimer's disease risks yet raise risks of specific cancer types and for combined all-cancers mortality. Nongenetic influences that lead to better telomere length maintenance are protective.

that in the general population, in addition to conventional heritable genetic factors, the direct inheritance of telomeres through the parental gametes could account for a considerable proportion of the estimated heritability of telomere length (44).

However, telomere length heritability declines with age (45), and substantial nongenetic influences, especially shared environmental influences, have been demonstrated (46). Epigenetic influences on telomere length may help mediate the large number of now-recognized nongenetic environmental and other factors that affect telomere maintenance. When just the telomere-lengthening alleles of three telomere maintenance genes were considered alone, they increased all-cancers mortality risk (36). Yet with longer observed telomeres, all-cancers mortality was lower.

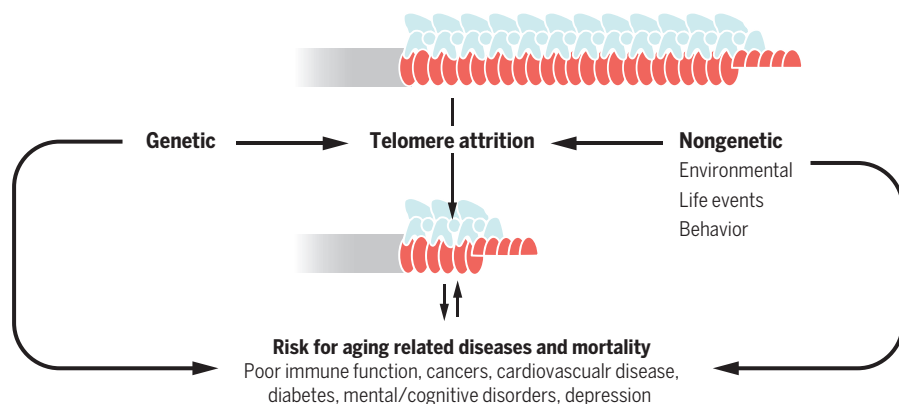


Fig. 4. Relationship of telomere attrition to human aging-related diseases. Telomere attrition is depicted as an underlying, shared, interactive contributor to the etiologies of aging and aging-related diseases. Because both nongenetic and genetic influences affect it, telomere maintenance is a malleable and integrative indicator of overall health.

Clinical ramifications and conclusions

A single mechanism—loss of telomere protective function—causes the inherited telomere syndromes that result in aging-like disease pathologies. Their organism-wide nature provides a strong hint that in the often comorbid diseases of aging (such as diabetes and cardiovascular disease), telomere shortness could similarly be a shared underlying contributing factor (Fig. 4).

Except for rare telomere syndromes, telomere measures only produce statistical estimates of probability and alone are not specifically diagnostic for an individual. Because telomere length is affected by so many nongenetic factors, measures of telomere length maintenance may be a proxy for assessing the “exposome”—that is, all of the exposures promoting disease. Research on interactions between independent and overlapping pathways influencing human telomere length is in its earliest stages. It will be important, in the new era of precision medicine studies, to determine whether combining other predictors—genomic associations, clinical, behavioral, and disease data—with telomere length measures can increase the precision of predicting disease progression and outcomes. A striking example of synergism comes from a study of a cohort of bladder cancer patients. Shorter mean LTL measured at the time of diagnosis in bladder cancer was not alone significantly associated with future mortality. However, when combined with a depression diagnosis, median survival time was reduced from 200 months (all other groups) to 31 months in multivariate analyses that adjusted for demographic and clinical variables (57).

Telomere maintenance in humans encompasses a surprisingly delicate trade-off between reducing risks of many aging-related diseases while raising risks of certain less common but often lethal cancers. Clinically unproven unregulated nostrums purporting to boost telomerase action thus could plausibly engender long-term cancer risks. Telomere biology is best viewed in

context: It shows promise as a powerful interactive factor that could be helpful in precision medicine for clinical health monitoring and assessing disease. How genetic and nongenetic determinants of telomere length maintenance may interact—with each other and with other disease etiologies—to become rate-limiting for disease risks requires future research. Early observational evidence from human studies indicates that health behaviors may buffer effects of stress or depression on telomere length (56) and that behavioral interventions may improve telomere maintenance in certain settings (60). Continued mechanistic research will increase understanding of the plasticity of telomere maintenance and identify when and how intervention can be effective for affecting disease and health.

REFERENCES AND NOTES

1. A. Sfeir, T. de Lange, *Science* **336**, 593–597 (2012).
2. E. H. Blackburn, C. W. Greider, J. W. Szostak, *Nat. Med.* **12**, 1133–1138 (2006).
3. Z. Xie et al., *Cell* **160**, 928–939 (2015).
4. M. Armanios, E. H. Blackburn, *Nat. Rev. Genet.* **13**, 693–704 (2012).
5. G. Glusker, F. Touzot, P. Revy, Y. Tzfati, S. A. Savage, *Br. J. Haematol.* **170**, 457–471 (2015).
6. E. Sahin et al., *Nature* **470**, 359–365 (2011).
7. A. J. Cesare, M. T. Hayashi, L. Crabbe, J. Karlseder, *Mol. Cell* **51**, 141–155 (2013).
8. I. Harel et al., *Cell* **160**, 1013–1026 (2015).
9. B. Meier et al., *PLoS Genet.* **2**, e18 (2006).
10. W. Palm, T. de Lange, *Annu. Rev. Genet.* **42**, 301–334 (2008).
11. A. Simm, J. Campisi, *Exp. Gerontol.* **59**, 1–2 (2014).
12. S. Petersen, G. Saretzki, T. von Zglinicki, *Exp. Cell Res.* **239**, 152–160 (1998).
13. M. A. Blasco et al., *Cell* **91**, 25–34 (1997).
14. M. Anclchin et al., *Dis. Model. Mech.* **6**, 1101–1112 (2013).
15. J. M. Mason, H. Biessmann, *Trends Genet.* **11**, 58–62 (1995).
16. P. Missios et al., *Nat. Commun.* **5**, 4924 (2014).
17. J. K. Alder et al., *Proc. Natl. Acad. Sci. U.S.A.* **112**, 5099–5104 (2015).
18. M. Armanios, *J. Clin. Invest.* **123**, 996–1002 (2013).
19. T. Vulliamy et al., *Nature* **413**, 432–435 (2001).
20. A. J. Walne, I. Dokal, *Br. J. Haematol.* **145**, 164–172 (2009).
21. L. C. Collopy et al., *Blood* **126**, 176–184 (2015).

22. S. E. Stanley et al., *J. Clin. Invest.* **125**, 563–570 (2015).
23. X. Du et al., *Mol. Cell. Biol.* **24**, 8437–8446 (2004).
24. H. H. Cheung et al., *Stem Cell Rev.* **2**, 534–546 (2014).
25. N. Guo et al., *PLOS ONE* **6**, e17858 (2011).
26. S. Cohen et al., *JAMA* **309**, 699–705 (2013).
27. I. M. Wentzensen, L. Mirabello, R. M. Pfeiffer, S. A. Savage, *Cancer Epidemiol. Biomarkers Prev.* **20**, 1238–1250 (2011).
28. H. Ma et al., *PLOS ONE* **6**, e20466 (2011).
29. J. Zhao, K. Miao, H. Wang, H. Ding, D. W. Wang, *PLOS ONE* **8**, e79993 (2013).
30. P. C. Haycock et al., *BMJ* **349**, g4227 (2014).
31. V. Codd et al., *Nat. Genet.* **45**, 422–427, e1–e2 (2013).
32. H. Ding et al., *Clin. Interv. Aging* **9**, 857–861 (2014).
33. C. G. Maubaret et al., *PLOS ONE* **8**, e83122 (2013).
34. Y. Zhan et al., *JAMA Neurol.* **72**, 1202–1203 (2015).
35. T. T. Lin et al., *Br. J. Haematol.* **167**, 214–223 (2014).
36. L. Rode, B. G. Nordestgaard, S. E. Bojesen, *J. Natl. Cancer Inst.* **107**, djv074 (2015).
37. B. L. Needham et al., *Epidemiology* **26**, 528–535 (2015).
38. K. Lapham et al., *Genetics* **200**, 1061–1072 (2015).
39. D. H. Rehkopf et al., *Exp. Gerontol.* **48**, 1266–1273 (2013).
40. P. Willeit, J. Willeit, A. Kloss-Brandstätter, F. Kronenberg, S. Kiechl, *JAMA* **306**, 42–44 (2011).
41. K. M. Walsh et al., *Neuro-oncol.* **15**, 1041–1047 (2013).
42. S. Horn et al., *Science* **339**, 959–961 (2013).
43. K. Nexerova, S. J. Elledge, *eLife* **4**, e09519 (2015).
44. T. De Meyer et al., *Eur. J. Hum. Genet.* **22**, 10–11 (2014).
45. S. L. Bakaysa et al., *Aging Cell* **6**, 769–774 (2007).
46. J. B. Hjelmberg et al., *J. Med. Genet.* **52**, 297–302 (2015).
47. S. Entringer et al., *Proc. Natl. Acad. Sci. U.S.A.* **108**, E513–E518 (2011).
48. L. H. Price, H. T. Kao, D. E. Burgers, L. L. Carpenter, A. R. Tyrka, *Biol. Psychiatry* **73**, 15–23 (2013).
49. J. Lin, E. Epel, E. Blackburn, *Mutat. Res.* **730**, 85–89 (2012).
50. M. F. Haussmann, B. J. Heidinger, *Biol. Lett.* **11**, 20150396 (2015).
51. J. L. Tarry-Adkins et al., *FASEB J.* **27**, 379–390 (2013).
52. I. H. Gotlib et al., *Mol. Psychiatry* **20**, 615–620 (2015).
53. J. Choi, S. R. Fauce, R. B. Effros, *Brain Behav. Immun.* **22**, 600–605 (2008).
54. N. S. Schutte, J. M. Malouff, *Depress. Anxiety* **32**, 229–238 (2015).
55. D. Lindqvist et al., *Neurosci. Biobehav. Rev.* **55**, 333–364 (2015).
56. E. Puterman, J. Lin, J. Krauss, E. H. Blackburn, E. S. Epel, *Mol. Psychiatry* **20**, 529–535 (2015).
57. J. Lin et al., *Cancer Epidemiol. Biomarkers Prev.* **24**, 336–343 (2015).
58. J. Gu et al., *Cancer Prev. Res. (Phila.)* **4**, 514–521 (2011).
59. J. Raschenberger et al., *Sci Rep* **5**, 11887 (2015).
60. C. A. Lengacher et al., *Biol. Res. Nurs.* **16**, 438–447 (2014).
61. J. Ye, V. M. Renault, K. Jamet, E. Gilson, *Nat. Rev. Genet.* **15**, 491–503 (2014).
62. S. Chang et al., *Nat. Genet.* **36**, 877–882 (2004).
63. L. Crabbe, A. Jauch, C. M. Naeger, H. Holtgreve-Grez, J. Karlseder, *Proc. Natl. Acad. Sci. U.S.A.* **104**, 2205–2210 (2007).
64. F. Mourikioti et al., *Nat. Cell Biol.* **15**, 895–904 (2013).

ACKNOWLEDGMENTS

We thank our many colleagues and apologize to those whose work we were unable to cite owing to article length constraints. E.H.B. acknowledges support from NIH (grants GM026259 and CA096840) and from the Barbro and Bernard Osher Foundation. E.H.B. and E.E. report no conflicts of interest; E.H.B. and E.E. were former cofounders of a company, Telomere Health (now Telomere Diagnostics), but donated all their shares to a nonprofit organization. J.L. owns stock in Telomere Diagnostics.

10.1126/science.aab3389

Stem cells and healthy aging

Margaret A. Goodell^{1*} and Thomas A. Rando^{2*}

Research into stem cells and aging aims to understand how stem cells maintain tissue health, what mechanisms ultimately lead to decline in stem cell function with age, and how the regenerative capacity of somatic stem cells can be enhanced to promote healthy aging. Here, we explore the effects of aging on stem cells in different tissues. Recent research has focused on the ways that genetic mutations, epigenetic changes, and the extrinsic environmental milieu influence stem cell functionality over time. We describe each of these three factors, the ways in which they interact, and how these interactions decrease stem cell health over time. We are optimistic that a better understanding of these changes will uncover potential strategies to enhance stem cell function and increase tissue resiliency into old age.

The aging process remains one of the central mysteries of biology, both from an evolutionary perspective (why we age) and from a mechanistic perspective (how we age).

Organismal aging is the failure of an integrated system that balances genetic programs for survival and reproduction. As reflected in the “disposable soma” theory (1), resources that are available to an organism are allocated either to survival or to reproduction, both of which are essential for the propagation of the species as evolved in the wild. However, additional factors come into play when species are protected from extrinsic causes of mortality (such as predation, starvation, and exposure), as is the case for modern *Homo sapiens* as well as animals on farms, in zoos, and in the laboratory. In those cases, individuals within the species are more likely to live far beyond the ages of their wild counterparts, allowing the emergence of phenotypes of aging and age-related diseases that would rarely if ever be manifest in the wild; we consider this “protected aging.”

One of the central features of protected aging is prolonged survival beyond the ages of peak reproductive fitness (Fig. 1). The fact that individual members of any species rarely live beyond this stage in the wild means that there would have been no evolutionary pressure to select for genetic mechanisms to assure maintenance of somatic tissues into old age. The homeostatic mechanisms that are necessary to preserve function throughout life are thus predicted to lose robustness over time. Furthermore, for most species, growth-suppressive mechanisms take over from growth-promoting mechanisms around the time of reproductive maturity. This critical transition, and the perpetuation of growth-suppressive

mechanisms beyond it, likely account for the progressive degradation of tissue function that characterizes protected aging. As such, what is generally called “aging” represents the intersection of a gradually failing system selected for early growth and reproductive fitness with the cumulative effects of growth-suppressive mechanisms and acquired somatic insults. Modulation of any aspect of this network could potentially accelerate or decelerate the process of aging.

The ability of an organism to ensure healthy function during adult life depends on homeostatic mechanisms. In many organs of mature vertebrates, resident stem cells participate in tissue maintenance and regeneration after injury, with variations in these roles across different tissues. For example, neural stem cells (NSCs) are important for ongoing generation of new neurons in specific regions of the brain but play a limited role in damage repair. In contrast, skel-

etal muscle stem cells (MuSCs, or satellite cells) play a minimal role in muscle maintenance but vigorously engage in regeneration after injury. Hematopoietic stem cells (HSCs) and intestinal stem cells (ISCs) do both, contributing to ongoing production of differentiated cells and also repairing tissue after injury.

During protected aging, the extent to which stem cells continue to maintain their cognate tissues depends on their own health. Although stem cells have characteristics (e.g., turnover rate, a specialized niche) that may protect them from insults associated with aging, data also indicate that stem cells deteriorate with age (2). Furthermore, any aberrations in stem cells may be carried forward into their differentiated progeny, contributing to tissue aging. As such, the question remains as to how effectively stem cell populations maintain tissue health, what the limitations of that capacity are, and what the mechanisms are that ultimately lead to decline in stem cell function. Research in stem cells and aging is geared toward these questions, with one long-term goal being the maintenance or restoration of youthful characteristics in aged somatic stem cells to promote healthy tissue aging. Here, we focus on three major areas of recent research in stem cell aging: genetic mutations, epigenetic changes, and extrinsic factors. We also consider how these influences are interrelated, and how in the future we might be able to enhance stem cell function and increase tissue resiliency into old age by modulating these factors.

Somatic mutations, stem cells, and age

For decades, we have understood that environmental insults such as irradiation and xenobiotic exposure can lead to accumulation of somatic mutations in a variety of tissues. Indeed, this

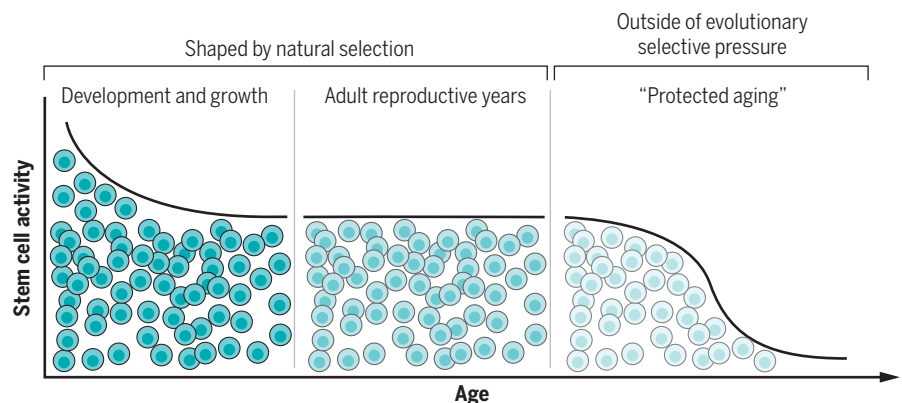


Fig. 1. Model of stem cell use over the life span. During embryogenesis and organismal growth, stem cells are highly active and contribute to tissue formation and growth. During the prime reproductive phase, growth is suppressed. Stem cells maintain and repair tissues. Properties of stem cells during these first two phases would be subject to forces of natural selection, because these phases of survival and reproduction would be critical to the propagation of the species. Beyond the period of reproductive maturity as fecundity declines, which is also the period of “protected aging,” cell and tissue functions are predicted to be under little or no evolutionary pressure, both because they are predicted to have negligible effect on species survival and also because, in the wild, survival beyond this point markedly diminishes. It is during this phase that stem cell functionality (although not necessarily stem cell number) declines in most tissues, in some cases precipitously.

¹Stem Cells and Regenerative Medicine Center, Center for Cell and Gene Therapy, and Department of Pediatrics, Baylor College of Medicine, Houston, TX 77030, USA. ²Glenn Center for the Biology of Aging and Department of Neurology and Neurological Sciences, Stanford University School of Medicine, Stanford, CA 94305, USA, and Center for Regenerative Rehabilitation, Veterans Administration Palo Alto Health Care System, Palo Alto, CA 94304, USA.

*Corresponding author. E-mail: goodell@bcm.edu (M.A.G.); rando@stanford.edu (T.A.R.)

concept underlies views of increased cancer incidence with age. However, it has remained unclear how the accumulation of somatic mutations affects either organismal aging or aging of stem cells. Recent work from the hematopoietic system has begun to shed some light on these issues.

If somatically acquired mutations are rare, most cells in the peripheral blood should be virtually identical in their genome sequence; hence, blood can be used to assess the “germline status” of an individual’s genetic complement. However, deep genome sequencing studies investigating mutations that contributed to leukemia development revealed that normal blood cells often harbor passenger mutations (unrelated to the leukemia) much more frequently than expected (3). These data indicate that blood progenitors acquire random mutations constantly, on the order of 10 mutations per HSC per year, many of which then appear in small fractions of differentiated blood progeny (3). When this deep sequencing approach was extended to blood samples from tens of thousands of individuals across many ages, a striking pattern arose: Specific somatically acquired genetic variants were often present in a large fraction of blood cells (Fig. 2), up to 70% in some cases (4–7). Although blood cells were thought to be generated from ~1000 active stem cells in young adults (8), the explanation for the high proportion of blood cells with particular somatic mutations was that a single stem cell clone was dominating the generation of the peripheral blood in some individuals. This collapse of highly polyclonal into quasi-monoclonal hematopoiesis increases with age; between 5 and 20% of 70-year-olds show clear evidence of this state, and almost all individuals above the age of 90 are estimated to have a single dominant stem cell clone generating a substantial proportion of their blood (9).

The notion of clonal collapse is revolutionizing our view of HSC dynamics with age, and there is intense interest in understanding the potential mechanisms of this phenomenon. One clue has come from examining the genes that are most commonly mutated in these large clones. Mutations in about 20 genes are recurrently associated with clonal hematopoiesis. The top two, *DNMT3A* and *TET2*, are epigenetic regulators that control DNA methylation status. Both are frequently mutated across many hematologic malignancies, and their loss leads to increased numbers of stem and progenitor cells (promoting self-renewal) while hindering their ability to differentiate in mouse models (10–13), although the precise mechanisms through which these mutations act is not well understood. The

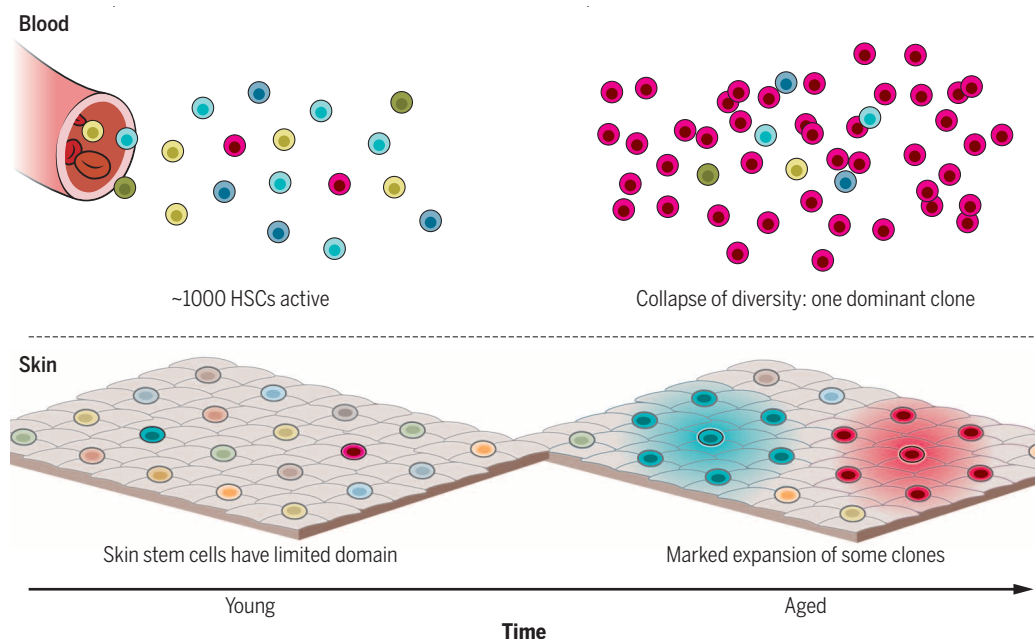


Fig. 2. Stem cell diversity and dynamics with age. Top: Peripheral blood from young individuals is generated from around 1000 active stem cells. By the age of 70, the clonal diversity collapses, resulting in dominance of one HSC clone, such that about 20% of individuals have one clone that dominates 20 to 80% of blood cell production. Bottom: Representation of the surface of skin. Young skin is continuously replenished from stem cells, each with a highly restricted domain (represented by circles). Random mutations generate small variations across the surface in terms of stem cells and their progeny (colored circles). With time, some clones expand markedly, resulting in clonally derived patches with a common set of genetic variants (18).

third recurrently mutated gene, *TP53*, is the most frequently mutated gene across all cancers (14) and its product, p53, is considered the “guardian of the genome” because of its central role in regulating cellular responses to stress and DNA damage. In mice, *TP53* has been shown to regulate HSC proliferation (15) and its deficiency leads to age-related stem cell expansion (16). With each HSC acquiring around 10 mutations per year, any individual stem cell will harbor 700 to 800 mutations in later decades of life (3). Most of these mutations will be neutral, although some will have a deleterious effect, potentially leading to the arrest or elimination of those cells. Thus, mutations seen in advanced age are those compatible with the cell’s long-term survival.

Together, data from humans and mice suggest that acquired somatic mutations can confer a growth or survival advantage to the target stem cell, enabling its expansion and leading to a preponderance of its progeny in the blood with age. What are the long-term health implications? The vast majority of individuals who exhibit clonal hematopoiesis will not develop hematologic malignancy during their remaining life span. Nonetheless, they are at significantly higher risk of developing age-associated blood diseases such as myelodysplastic syndrome, aplastic anemia, and leukemias (5) associated with the acquisition of additional mutations. Moreover, individuals with clonal hematopoiesis are at higher risk for earlier mortality when all causes are considered, with myocardial infarctions and strokes having

the strongest association (5). Furthermore, aging-associated diseases such as type 2 diabetes have also been correlated with blood-based genomic aberrations (17). The mechanisms behind these correlations are not understood, but mutations in stem cell regulators likely affect the function of their progeny; HSCs are continuously generating an array of immune cells, platelets, and red blood cells, all of which have an impact on disease resistance, inflammation, clotting, and tissue oxygenation. Because the blood system supports all tissues in the organism, any age-related impairment of stem cells manifest in their progeny could conceivably affect distant tissues and therefore healthy aging.

Is there evidence for aging-associated clonal expansion of stem cells in other tissues, and does this affect tissue health? This phenomenon, although not yet examined on a large scale, is known to occur in other tissues. For example, stem cells are generally responsible for generating the differentiated epithelial cells in a very restricted surface area of young skin. However, in normal aged Sun-exposed skin, marked expansion of clones associated with specific mutations—including *TP53* and the stem cell regulator *NOTCH1*—occurs well beyond those original boundaries (18). Remarkably, almost 20% of normal skin cells have these potent expansion-promoting *NOTCH1* mutations. The relatively low incidence of cancer acquisition despite the high frequency of clones bearing cancer-associated mutations is a testament to the mechanisms that restrain

malignancy development. The effect of these expanded mutant clones on age-related changes of tissue function (including the critical barrier function of the skin), and on organismal health generally, is unknown but warrants investigation, given the striking associations of clonal collapse in the hematopoietic system.

Together, these and other studies demonstrate that somatic mutations that arise in stem cells confer an advantage that leads to their expansion within a tissue over many years. Many of the somatic mutations repeatedly observed are associated with cancer, and this may underlie the correlation between tissue-specific cancer incidence and stem cell proliferation (19). More important, we expect that clonal dominance in the blood, and possibly in other tissues, can have broad effects on healthy aging of the cognate tissues.

Epigenetic erosion with age

Epigenetic regulation refers to the mechanisms, mainly DNA methylation and histone modifications, that license regions of the genome for expression while shutting down others. There has been great interest in understanding the extent to which erosion of these genome-scale regulatory mechanisms leads to dysregulated control of

gene expression, contributing to the decline of stem cell and tissue function with age. Genetic evidence in model organisms has supported the notion that aberrant epigenetic regulation affects organismal aging. For example, in *Caenorhabditis elegans*, a genetic screen revealed that loss of function of *Wdr5*—a gene encoding a histone methyltransferase that leads to trimethylation of lysine 4 on histone 3 (designated as H3K4me3 and generally considered to be a mark of expressed genes)—led to extended life span (20). Although H3K4me3 generally marks promoters, the histone mark covers the entire coding unit at a subset of genes controlling cellular identity; this pattern is associated with very high gene expression and transcriptional elongation (21). However, research is needed to understand why reduction of H3K4me3 should be correlated with longer life span. Similar efforts in yeast have shown that lower levels of another histone mark, H3K36me3, reduced replicative life span, whereas ablating genes that diminish the mark increased yeast life span (22). Reduction of the H3K36me3 mark was associated with transcriptional infidelity and cryptic transcripts.

How do these and other findings relate to aging in mammalian stem cells? Although not exten-

sively examined, current data support the concept that epigenetic regulation erodes in aging stem cells. In concordance with the *C. elegans* findings, H3K4me3 tends to increase in aging HSCs, particularly on the genes involved in maintaining HSC identity (23). In both HSCs and MuSCs, the repressive H3K27me3 mark increased with age (23, 24). In HSCs, this increase was associated with repression of some genes that direct specific differentiation programs such as the lymphoid fate, known to diminish with age. In MuSCs, the increase was associated with repression of genes encoding histone genes themselves (24); this finding is of interest because of the relationship between histone gene expression and yeast replicative life span (25). Interestingly, mesenchymal stem cells (MSCs) from aged individuals show a decline in H3K9me3, a mark associated with proper maintenance of heterochromatin. Loss of this mark is also found in MSCs harboring the Werner's progeria syndrome mutation (26), again linking epigenetic erosion with aging.

Finally, age-related changes in DNA methylation have been examined in HSCs. DNA methylation was decreased at genes associated with the promotion of self-renewal and was increased near genes associated with differentiation (23, 27). Polycomb proteins are factors generally involved in gene silencing. Regions with histones bearing Polycomb-associated marks (H3K27me3) tended to become hypermethylated, a phenomenon noted previously in other tissues in mouse and human (28). Changes in methylation may play a role in inhibiting the expression of tumor suppressor genes, thereby increasing the possibility of malignant transformation.

Overall, these epigenetic changes in aging stem cells are consistent with the functional deficits that have been repeatedly observed: With aging, HSCs appear to increase in numbers but simultaneously lose differentiation capacity (23, 27). Nonetheless, the extent to which these changes are correlative versus causal is not yet clear and merits further exploration. In HSCs and MuSCs, the precise epigenetic regulation observed at young ages appears to drift. This drift is aligned with the general aging process: The identity and general function of the stem cells remain the same, but they cannot regenerate their cognate tissues quite as well as they did before.

Extrinsic factors affect aging stem cells

The influence of the local and systemic environment on stem cell function during protected aging has been demonstrated by exposing young stem cells to an aged environment, and vice versa. These studies have used strategies such as heterochronic transplantation, in which cells derived from a donor of one age are transplanted into a recipient of a different age, or heterochronic parabiosis, in which two mice of different ages are adjoined to create a shared circulatory system, thus exposing cells in one animal to the systemic environment of the other (29) (Fig. 3). When young stem cells were sub-

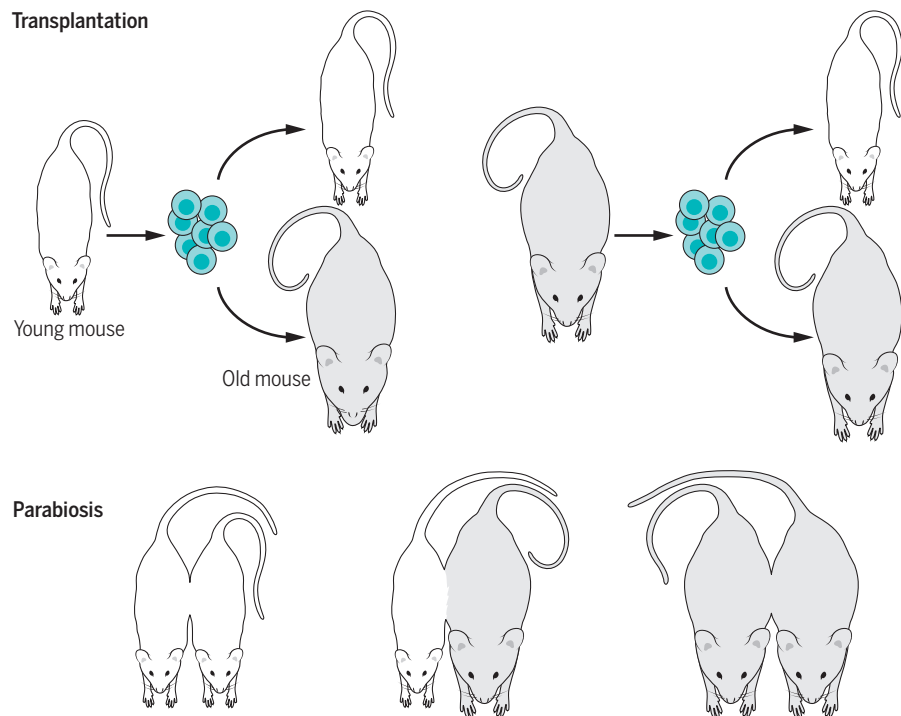


Fig. 3. Intrinsic and extrinsic factors influence age-related changes in stem cell function.

Distinguishing cell-intrinsic changes from cell-extrinsic changes (e.g., arising from the cellular environment) in cell function has been aided by heterochronic studies. In heterochronic transplantation, stem cells isolated from either young or old donors are transplanted into young or old hosts, and cellular function is then analyzed in these four-way comparisons (young into young, young into old, old into young, old into old). In parabiosis, animals are joined to promote the development of a single, shared circulatory system, thus exposing cells in one animal to the systemic environment of the other animal. In this case, the cellular functions in young or old partners in the heterochronic pairs (young-to-old) are compared to those in isochronic pairs (young-to-young and old-to-old).

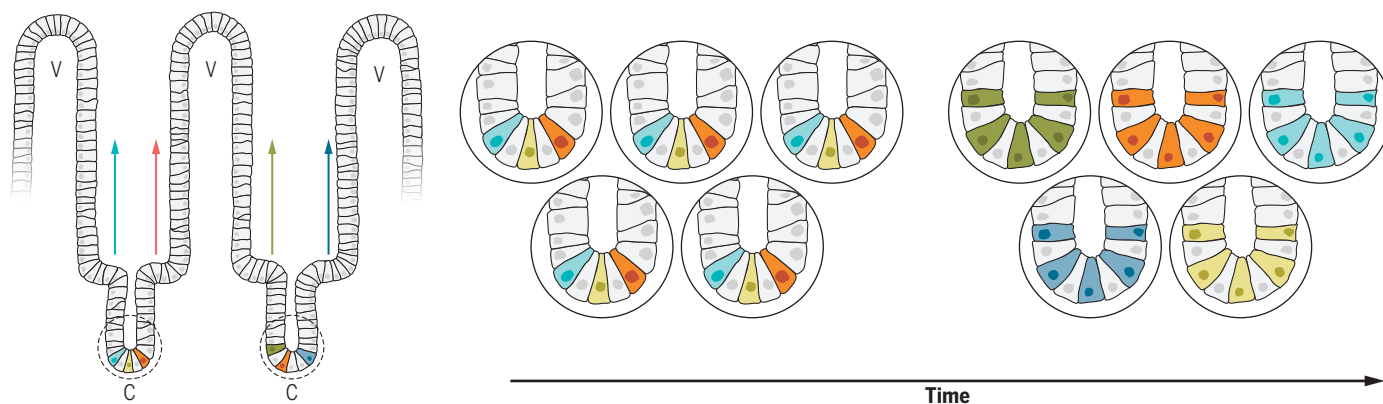


Fig. 4. Neutral drift of stem cell populations. Left: The small intestine comprises villi (v) containing differentiated cells that are replenished (arrows) from the progeny of stem cells residing in the crypts (c). Right: When crypts are viewed from above, en face (as if cut on the dashed line), several stem cell domains (each represented by a different color) are present. With age, the crypt stem cells continuously compete with each other, such that over time, all the stem cells in an individual crypt originate from one stem cell. These presumptions are based on mouse data (44). Certain genetic alterations and environmental conditions can accelerate this process.

parabiosis, they exhibited functional decline that resembled accelerated aging (30, 31). On the other hand, the converse was also true: Aged cells placed in a young environment or exposed to a youthful systemic milieu exhibited more youthful characteristics, suggesting that it may be possible to ameliorate certain aging features. These findings have led to the search for “age-promoting” factors in old blood (see below) and for “youth-promoting” factors in young blood (32–34) [but see also (35)]. Together, these studies demonstrate that stem cells are profoundly influenced by their environment and imply that blood-borne factors may be responsible for at least some of the age-associated declines in stem cell functionality.

Efforts to identify specific aging-associated circulating factors have repeatedly highlighted pro-inflammatory molecules, such as cytokines in the blood, as key drivers of cell and tissue aging (36). One of the first “aging factors” identified by heterochronic parabiotic studies was the cytokine CCL11 (37). The levels of this protein increase with age in the blood, and administration of this cytokine into the circulation of young animals led to a decline in NSC activity, as occurs during normal aging. Likewise, the related inflammatory cytokine Rantes was found to be elevated in the HSC niche with age and to contribute to the age-related myeloid skewing in the hematopoietic lineage (37).

In addition to cytokines, other immune system-associated molecules have been shown to change with age and promote aging phenotypes. Plasma levels of the complement protein C1q were shown to increase with age and to promote age-related MuSC decline by activation of the Wnt signaling pathway (38, 39). Similarly, β 2-microglobulin, a component of the major histocompatibility complex, was found to be elevated in the blood of aged mice and to contribute to an age-related decline in NSC function (40). The increase in proinflammatory factors, along with the concomitant

decrease in factors that promote tissue repair, likely contributes to aging phenotypes in many tissues.

Somatic natural selection of stem cells

From the studies discussed above, we can appreciate at least three key influences on somatic stem cells within an aging organism. Stem cells acquire many somatic mutations over time, they experience epigenetic drift, and they are bathed in a broader milieu that can negatively influence function. Among the cells in any given stem cell population, each cell brings its unique characteristics (e.g., mutations) and experiences (e.g., exposure to local cytokines) to the evolving adaptive landscape. We propose that these forces interact over time to result in selective pressure on individual stem cells: Stem cells that have acquired, through somatic mutation or epigenetic drift, the characteristics best adapted to the aged environmental milieu will become enriched in the population, as a result of Darwinian-like natural selection that occurs *in vivo* during aging (“somatic natural selection”). These stem cells have characteristics that confer optimal survival in the protected aging environment, regardless of other functional capabilities. Any detrimental characteristics they have assumed will be conveyed to the tissue via their progeny, in proportion to their relative abundance.

This view of clonal dynamics has both theoretical and experimental foundations. Mathematical modeling of stem cell populations predicts that constant competition in a closed environment will lead to domination by one stem cell, even in the absence of any selection (so-called “neutral drift”) (41), analogous to population drift of species leading to fixation of traits even without selection, particularly in small populations (42). Moreover, certain mutations or environmental pressures should accelerate this phenomenon, selecting for stem cells with particular adaptations [akin to a changed fitness landscape (43)].

Studies of the murine small intestine have borne out these ideas. Differentiated cells of the intestinal villi are continuously replenished by stem cells that reside at their bases in specialized crypts. Each crypt contains several stem cells that compete to populate the adjacent villi. Even in the absence of selection, individual stem cells overtake an entire crypt in a completely random fashion, as predicted by neutral drift theory (Fig. 4) (44, 45). Mutations that even marginally increase proliferation, such as in the *K-ras* oncogene, accelerate crypt donality (46). In specific environmental contexts, some mutations appear particularly adaptive. Stem cells with a *Tp53* mutation have no advantage in a normal crypt, but in an inflammatory environment that mimics colitis, the *Tp53*-mutant stem cells rapidly take over and their progeny dominate production of the entire crypt (47).

Although not established experimentally, we speculate that similar forces lead to the emergence of clonal dominance as a feature of the aging hematopoietic system (Fig. 2). This hypothesis would predict that few of the acquired mutations in HSCs would confer an advantage in the young environment, allowing hematopoiesis to remain highly polyclonal. By contrast, the same mutations, compounded by epigenetic drift, could confer a distinct survival and/or proliferative advantage in the changing milieu of age, allowing for the expansion of specific HSCs and clonal dominance. Indeed, in young mice, *Tp53* knockout HSCs have no particular advantage, but in old hosts they expand relative to their normal counterparts (16). We speculate that *DNMT3A* and *TET2* mutations may similarly confer an advantage in the aging environment. This view is supported by the observation that some mutations associated with clonal hematopoiesis (e.g., in splicing factors) only become prevalent after the seventh decade (5, 7, 9), which suggests that the aging environment is particularly important for the emergence of HSC clones with these mutations. This model of continuous Darwinian

selection acting on variants across a population in a changing landscape also applies to cancer development, an inherently aging-associated phenomenon (48).

Considered more broadly, highly dynamic tissues such as the gut and bone marrow have stem cells that, in effect, continuously compete with each other. Thus, any cell-intrinsic change, genetic or otherwise, that confers a growth or survival advantage may lead to predominance of particular stem cells (Fig. 5). This is important because the selective environment (adaptive landscape) changes with age. In aged organisms, factors such as systemic inflammation may offer an advantage to stem cells with particular characteristics. The stem cells that respond best in an aged or injured environment may not be the most effective at regenerating healthy tissue if their progeny also bear somatic mutations or exhibit epigenetic drift. These general principles are likely in effect throughout many tissues, albeit manifesting differently depending on factors such as tissue turnover rate, local interactions among stem cells, physical constraints on cell interchange, and the magnitude of alterations in the adaptive landscape. For example, in tissues such as skeletal muscle, in which there is thought to be lower stem cell interchange and tissue turn-

over, internal competition and selective forces may be less important. Even in the gut, stem cell competition occurs almost exclusively within, and not between, individual crypts. Thus, gaining a broader understanding of the role that somatic stem cell competition plays across many tissues will be important in the future.

Finally, how do the environment and somatic mutations interact together with epigenetic modulation? Epigenetic drift likely occurs even in the absence of particular somatic mutations, driven by, and promoting adaption to, the changing environmental milieu. The frequent selection for mutations in epigenetic regulators (e.g., *DNMT3A* and *TET2*) may suggest that these afford a degree of epigenetic plasticity that hastens adaption to the aged environment.

Conclusions

Taken together, recent studies on somatic mutations, epigenetic drift, and the environmental influences on stem cells usher in a new view of aging and the challenges to preserving healthy tissue function over time. After organismal growth ceases, stem cells effectively maintain tissues through the peak reproductive years. Subsequently, there are no effective mechanisms that have been evolutionarily selected to preclude the

gradual loss of cell and tissue health. Instead, a variety of genetic, epigenetic, and environmental factors allow drift until the aging environment acts strongly enough to select for particular (usually detrimental) characteristics (Fig. 5). The mutant stem cells that accumulate with age are not causes of aging per se; they simply exploit the aged environment to become dominant. In turn, the functional deficiencies they confer on their progeny contribute to the phenotypes associated with aging.

With these views, what strategies or interventions can be envisioned to extend healthspan by targeting stem cells? Two approaches emerge naturally from the studies discussed. First, it seems as if the phenotypes of aging stem cells may be at least partially reversible. As noted above, heterochronic parabiosis studies suggest that factors in young blood might partially ameliorate the functional deficits of aged stem cells (30, 31). Furthermore, the injection of plasma from young mice into the circulation of aged mice has recently been shown to induce a more youthful state of cells in the brain of the old animal (32). These findings indicate that at least some aspects of cellular aging may be reversible, perhaps through reprogramming of the epigenome (49). Indeed, interventions that clearly extend organismal life span even when applied late in life, such as rapamycin treatment (50), may enhance stem cell function in aged animals. As such, it may be that treatments that directly enhance the function of aged stem cells do so by acting on the epigenome to adopt a more youthful state.

Is it possible to reduce the acquisition of somatic mutations? Most are probably the inevitable consequence of cell division and deamination events that result in C→T transitions (51, 52).

Assuming we cannot eliminate mutations altogether, another approach would be to alter the adaptive landscape so as to select for more functional cells. By the time that the protected aging phase begins, stem cells will already have acquired a burden of somatic mutations (a largely inevitable consequence of cell division) and have drifted epigenetically. We suggest that monitoring changes and modulating the environment early—such as reducing inflammatory mediators and otherwise slowing the transition of the systemic environment that occurs with age—may limit the development of clonal dominance, allowing the polyclonal state to be sustained longer (Fig. 5). Alternatively, providing a new adaptive landscape in which different stem cell variants are better adapted to thrive could likewise contribute to the maintenance of tissue health. Along these lines, it is interesting that genetic manipulations early in life that preserve proliferative homeostasis of gut stem cells in *Drosophila* lead to life-span extension (53). It may be that early life treatments that extend life span, such as caloric restriction, do so in part by altering the adaptive landscape to prevent detrimental clonal dominance and preserve tissue function. We are optimistic that better understanding of

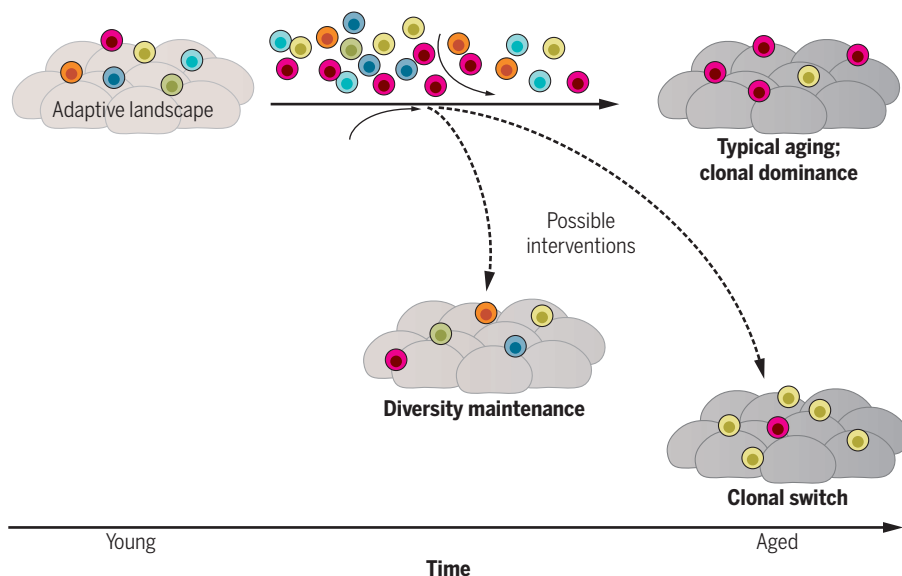


Fig. 5. Model of age-related selection for stem cells with new characteristics and potential outcomes. In young individuals, a polyclonal population of HSCs gives rise to a heterogeneous population of blood cells. With age, stem cells acquire somatic mutations and experience epigenetic drift. Concurrently, attrition (“collapse”) of some clones occurs and the adaptive landscape gradually shifts. This may be caused in part by changes in humoral factors (such as circulating cytokines or inflammatory factors) or changes in the cellular environment that regulates the stem cells, the so-called niche (change could occur in niche composition or behavior). The result of a changing landscape and clonal attrition may be a population bottleneck that provides an opportunity for clones with a selective advantage to expand. Ultimately, this leads to quasi-monoclonality and to the dominance of particular clones. In principle, it could be possible to intervene to alter the forces that drive toward deleterious quasi-monoclonality (dashed arrows). Any intervention that suppresses the change in the adaptive landscape would tend to preserve the healthy polyclonality (diversity maintenance) of youth. Likewise, understanding any growth or survival advantages conferred upon HSCs with “nondeleterious” somatic mutations or epigenetic changes could allow for a rational modulation (“clonal switch”) of the adaptive landscape to select for those clones rather than deleterious clones.

the mechanisms of stem cell dysregulation and selection with age will enable new rational interventions based on these principles.

REFERENCES AND NOTES

1. T. B. Kirkwood, *Cell* **120**, 437–447 (2005).
2. L. Liu, T. A. Rando, *J. Cell Biol.* **193**, 257–266 (2011).
3. J. S. Welch et al., *Cell* **150**, 264–278 (2012).
4. M. Xie et al., *Nat. Med.* **20**, 1472–1478 (2014).
5. S. Jaiswal et al., *N. Engl. J. Med.* **371**, 2488–2498 (2014).
6. G. Genovese et al., *N. Engl. J. Med.* **371**, 2477–2487 (2014).
7. T. McKerrell et al., *Cell Rep.* **10**, 1239–1245 (2015).
8. S. N. Catlin, L. Busque, R. E. Gale, P. Guttorp, J. L. Abkowitz, *Blood* **117**, 4460–4466 (2011).
9. T. McKerrell, G. S. Vassiliou, *Sci. Transl. Med.* **7**, 306fs38 (2015).
10. G. A. Challen et al., *Nat. Genet.* **44**, 23–31 (2012).
11. C. Quivoron et al., *Cancer Cell* **20**, 25–38 (2011).
12. K. Moran-Crusio et al., *Cancer Cell* **20**, 11–24 (2011).
13. M. Ko et al., *Proc. Natl. Acad. Sci. U.S.A.* **108**, 14566–14571 (2011).
14. C. Kandath et al., *Nature* **502**, 333–339 (2013).
15. Y. Liu et al., *Cell Stem Cell* **4**, 37–48 (2009).
16. M. Dumble et al., *Blood* **109**, 1736–1742 (2007).
17. A. Bonnefond et al., *Nat. Genet.* **45**, 1040–1043 (2013).
18. I. Martincorena et al., *Science* **348**, 880–886 (2015).
19. C. Tomasetti, B. Vogelstein, *Science* **347**, 78–81 (2015).
20. E. L. Greer et al., *Nature* **466**, 383–387 (2010).
21. K. Chen et al., *Nat. Genet.* **47**, 1149–1157 (2015).
22. P. Sen et al., *Genes Dev.* **29**, 1362–1376 (2015).
23. D. Sun et al., *Cell Stem Cell* **14**, 673–688 (2014).
24. L. Liu et al., *Cell Rep.* **4**, 189–204 (2013).
25. J. Feser et al., *Mol. Cell* **39**, 724–735 (2010).
26. W. Zhang et al., *Science* **348**, 1160–1163 (2015).
27. I. Beerman et al., *Cell Stem Cell* **12**, 413–425 (2013).
28. S. Maegawa et al., *Genome Res.* **20**, 332–340 (2010).
29. I. M. Conboy, T. A. Rando, *Cell Cycle* **11**, 2260–2267 (2012).
30. I. M. Conboy et al., *Nature* **433**, 760–764 (2005).
31. S. A. Villeda et al., *Nature* **477**, 90–94 (2011).
32. S. A. Villeda et al., *Nat. Med.* **20**, 659–663 (2014).
33. C. Elabd et al., *Nat. Commun.* **5**, 4082 (2014).
34. M. Sinha et al., *Science* **344**, 649–652 (2014).
35. M. A. Egerman et al., *Cell Metab.* **22**, 164–174 (2015).
36. C. Franceschi et al., *Mech. Ageing Dev.* **128**, 92–105 (2007).
37. A. V. Ergen, N. C. Boles, M. A. Goodell, *Blood* **119**, 2500–2509 (2012).
38. A. S. Brack et al., *Science* **317**, 807–810 (2007).
39. A. T. Naito et al., *Cell* **149**, 1298–1313 (2012).
40. L. K. Smith et al., *Nat. Med.* **21**, 932–937 (2015).
41. A. M. Klein, B. D. Simons, *Development* **138**, 3103–3111 (2011).
42. S. Wright, *Am. Nat.* **63**, 556–561 (1929).
43. S. Wright, *Proc. Sixth Int. Congr. Genet.* **1**, 356–366 (1932).
44. H. J. Snippet et al., *Cell* **143**, 134–144 (2010).
45. C. Lopez-Garcia, A. M. Klein, B. D. Simons, D. J. Winton, *Science* **330**, 822–825 (2010).
46. H. J. Snippet, A. G. Schepers, J. H. van Es, B. D. Simons, H. Clevers, *EMBO Rep.* **15**, 62–69 (2014).
47. L. Vermeulen et al., *Science* **342**, 995–998 (2013).
48. A. I. Rozhok, J. DeGregori, *Proc. Natl. Acad. Sci. U.S.A.* **112**, 8914–8921 (2015).
49. T. A. Rando, H. Y. Chang, *Cell* **148**, 46–57 (2012).
50. D. E. Harrison et al., *Nature* **460**, 392–395 (2009).
51. L. B. Alexandrov et al., *Nature* **500**, 415–421 (2013).
52. S. Behjati et al., *Nature* **513**, 422–425 (2014).
53. B. Biteau et al., *PLOS Genet.* **6**, e1001159 (2010).

10.1126/science.aab3388

REVIEW

Mitochondrial dysfunction and longevity in animals: Untangling the knot

Ying Wang and Siegfried Hekimi*

Mitochondria generate adenosine 5′-triphosphate (ATP) and are a source of potentially toxic reactive oxygen species (ROS). It has been suggested that the gradual mitochondrial dysfunction that is observed to accompany aging could in fact be causal to the aging process. Here we review findings that suggest that age-dependent mitochondrial dysfunction is not sufficient to limit life span. Furthermore, mitochondrial ROS are not always deleterious and can even stimulate pro-longevity pathways. Thus, mitochondrial dysfunction plays a complex role in regulating longevity.

The primary and most essential function of mitochondria is to produce energy for the cell. The oldest explanation for aging, the rate-of-living theory, postulates that aging and life span are regulated by the rate of energy metabolism, with lower rates leading to longer life spans. However, the appeal of the rate-of-living theory has been weakened by its failure to accurately predict the observed relationships between energy expenditure and life span. This is not to say that mitochondrial and energy metabolism don't play a crucial role in aging, but their relationship to aging might not be simple. Mitochondria do much more than produce energy. Particularly relevant to aging, the mitochondrial electron transport chain (ETC) leaks electrons and generates reactive oxygen species (ROS) during normal respiration. Thus, a potentially harmful elevation of ROS production occurs when the ETC function is perturbed. The mitochondrial free-radical theory of aging posits that biological aging results from the production of ROS and the ensuing damage. However, direct manipulation of cellular ROS levels within the biologically meaningful range does not accelerate aging or decrease life span. Here we review the relationships between normal mitochondrial function, mitochondrial dysfunction, ROS generation, and life span.

Deleterious mitochondrial dysfunction

Numerous studies have described damage to mitochondria in aged cells and organisms, including in human samples. This damage includes a gradual decline in respiratory chain capacity, decreased activities of individual ETC complexes, elevated oxidative damage, decreased mitochondrial content, morphological abnormalities in mitochondrial structure, and increased fragility of aged mitochondria during experimental isolation (Fig. 1) (1). In exploring

the implications of these observations for the aging process, a key question is whether the observed damage and dysfunction are severe enough to cause the other degenerative phenotypes of aging.

There is no doubt that mitochondrial dysfunction can severely damage the organism. Human patients with mutations in mitochondrial DNA (mtDNA) or in nuclear genes coding for proteins that function in the mitochondrial ETC are generally severely affected. They often show multisystem disorders that include myopathy, encephalopathy, stroke, and hearing loss (2). Most mitochondrial disorders present with neurological and muscular symptoms. It is thus generally postulated that cells with high energy demands, such as those in the central nervous system and muscles, are more susceptible to the reduced energy output of defective mitochondria and are consequently more strongly affected by mitochondrial impairment. There is, however, considerable clinical variability among mitochondrial disease patients, and some mutations only affect particular tissues, reflecting a diversity of distinct disease mechanisms that are still poorly understood. To understand these conditions, a variety of mouse knockout (KO) models have been developed for nuclear-encoded mitochondrial proteins (3). These include mutants carrying KO mutations in genes that are required for the assembly and function of ETC complexes, mutants with defects in the production of mobile electron carriers [cytochrome c and ubiquinone (UQ)], and mutants lacking necessary factors for the maintenance of mitochondrial dynamics or the integrity of mtDNA. In virtually every case, complete germline KO causes embryonic to perinatal lethality. Tissue-specific conditional KOs, mostly targeted to neurons or muscles, result in abnormal mitochondria with severe deficits in respiratory chain function, giving rise to a variety of disease phenotypes. Most show severe progressive loss of tissue function, such as progressive skeletal muscle weakening, movement impairment, and neurobehavioral abnormalities. All result in death within the first year of life,

Department of Biology, McGill University, Montreal, Quebec H3A 1B1, Canada.

*Corresponding author. E-mail: siegfried.hekimi@mcgill.ca

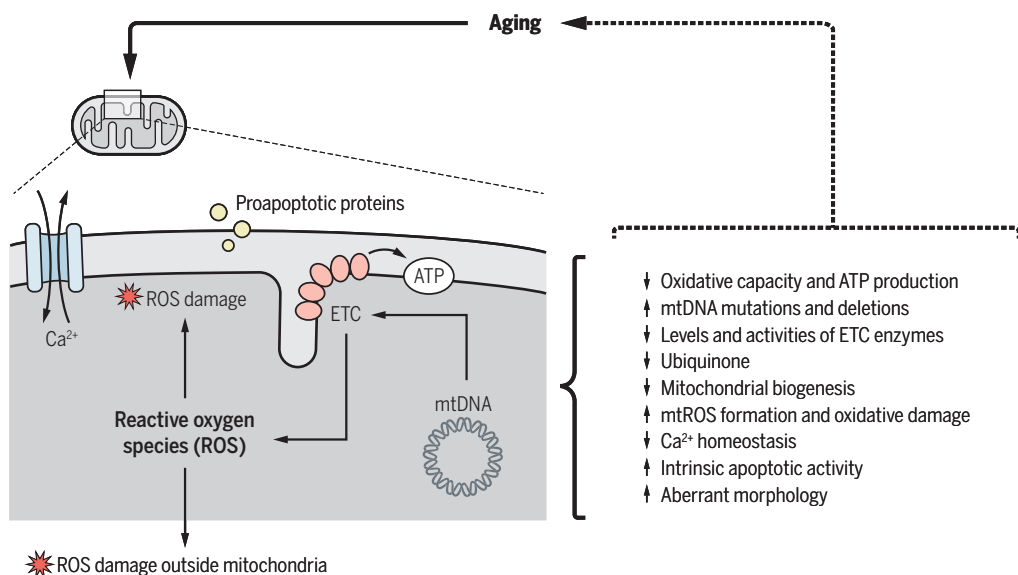


Fig. 1. Age-dependent gradual mitochondrial dysfunction. Various mitochondrial defects are found to accompany aging. However, their role in causing aging is unclear.

with life spans reduced to less than 40% of the normal (3).

Much research on why mitochondrial dysfunction gradually develops with time has focused on mtDNA. Mutations and deletions in mtDNA increase with age, and clonally expanded mtDNA damage is more abundant in those areas of aged tissue that also show mitochondrial ETC dysfunction (4). These findings and many earlier studies led to the notion that continuous accumulation of mtDNA damage may play a causal role in the aging process. One particular model that has been used to study this is the “mutator” mouse. In these mice, the proofreading function of the mtDNA polymerase gamma (*Polg*) is defective, which leads to the accumulation of random mutations and deletions in mtDNA (5, 6). Decreased life span and an array of phenotypes reminiscent of normal aging have been observed in homozygous mutator mice (*Polg*^{D257A/D257A}). The mice exhibit decreased content and activity of ETC complexes, lower respiratory chain capacity, and lower ATP (adenosine 5'-triphosphate) levels, as well as an activation of apoptotic pathways (5, 6). However, most studies of the mutator mice have reported negligible increases in oxidative stress, which often accompanies disruption of ETC function in the KO mouse models described above (6). This is of interest because oxidative stress, whether causative of aging or not, has been commonly regarded as a reliable biomarker of aging. In fact, it has often been suggested that ROS could be responsible for aging by acting as mutagens on mtDNA in somatic cells, inducing a vicious cycle in which the mtDNA mutations lead to defective ETC function, thereby producing even more mtDNA-damaging ROS. It is thus noteworthy that a recent study using a mitochondria-targeted mass spectrometry probe detected an increase in hydrogen peroxide in the mutator mice close to the end of their life span

(7). However, no increase was found in young mutator mice, despite their already elevated level of mtDNA mutations, nor was any increase found in old wild-type mice by this technique. Thus, although high mitochondrial ROS may contribute to the shorter life span of mutator mice, a hypothesis that is supported by the beneficial effects of some antioxidant interventions (8), its role in normal aging is probably not of great importance. In *Drosophila* and human brain tissue, age-related increases in mtDNA mutations are not caused by oxidative stress (9, 10), further weakening the vicious-cycle hypothesis of mitochondrial aging.

Beyond this, the quantitative findings with the mutator mouse argue against the notion that damage to mtDNA causes aging. In the homozygous mutator mice, life span is shortened, but the mtDNA mutation load is much higher than that detected in aged animals or elderly humans (11). Heterozygous mutator mice are born with a mutation burden 30 times higher than that of aged wild-type mice, yet they lack overt phenotypes and have a normal life span (11). This calls into question whether the naturally occurring slow

accumulation of age-related mtDNA mutations has a leading role in causing aging, rather than representing only one of the types of damage accumulation that accompany aging. A different mouse strain, the mtDNA deleter mouse, is also relevant in this context. These mice accumulate large-scale mtDNA deletions in postmitotic tissues but do not have a shortened life span, although they exhibit late-onset respiratory dysfunction in a subset of tissues (12). These findings further undermine the notion that damage to mtDNA or mitochondrial dysfunction is sufficient to accelerate aging.

Uncoupling mitochondrial dysfunction and aging

Not all partial losses of mitochondrial function result in shortened life span, and some can even result in increased life span (13). UQ is an obligate electron carrier in the ETC, and MCLK1 (also known as COQ7) is the penultimate enzyme in the mitochondrial UQ biosynthetic pathway. Mice missing one copy of *Mclck1* appear superficially normal and live longer than their wild-type littermates, despite markedly reduced mitochondrial respiration. Overall UQ concentrations in whole mitochondria extracts are normal in these heterozygous mice, but they are lower in the inner membrane fraction. This causes a decrease in respiratory chain capacity, which in turn results in low ATP generation. Production of mitochondrial ROS (mtROS) appears to be increased in the mutant, whereas overall ROS levels are not. The extended longevity of these mutants is also associated with slow development of the biomarkers of aging, high macrophage expression of HIF-1 α (hypoxia-inducible factor 1 α), and an enhanced immune response (13). However, it is not known whether these phenotypes are necessary or sufficient for the observed increase in longevity.

SURF1 is an inner mitochondrial membrane protein required for the assembly of complex IV (cytochrome c oxidase), a protein complex needed for oxidative phosphorylation. A knockout model of *Surf1*, in which a premature stop codon was inserted into exon 7, resulted in viable mice with

Box 1. Benefits of preserving or boosting mitochondrial function.

PGC-1 is a transcription coactivator of mitochondrial biogenesis, oxidative metabolism, and ROS-handling enzymes. Overexpression of PGC-1 α has been used to preserve or boost mitochondrial function. In mice, increased muscle PGC-1 α leads to preservation of muscle function during aging (40). In fruit flies, overexpression of PGC-1 α in intestinal stem and progenitor cells leads to a longer life span (41). The mechanisms underpinning these effects are uncertain.

NAD⁺ (nicotinamide adenine dinucleotide) is a coenzyme for many reactions in oxidative phosphorylation and the tricarboxylic acid cycle. NAD⁺ levels decline with age. Boosting NAD⁺ levels has been shown to increase life span in *C. elegans* and improve health indicators in old mice (17, 42). The effects are mediated by sirtuins and are associated with more and healthier mitochondria.

increased life span (14). These mice exhibited the anticipated decrease in complex IV activity, which was 30 to 50% of normal. Mitochondrial respiration was mildly affected in some tissues, but no change in mtROS production was detected. Other phenotypic features include lower fat mass, elevated protein expression of the mitochondrial biogenesis regulator PGC-1 α (peroxisome proliferator-activated receptor gamma coactivator 1 α) (Box 1), increased insulin sensitivity, resistance to calcium-induced neuronal death, and an increase in the expression of some of the proteins involved in the mitochondrial unfolded protein response (UPR^{mt}) (14–16). There are other indications that the UPR^{mt} could participate in life-span determination in mammals: Conserved longevity-promoting interventions, such as overexpression of SIRT1 and rapamycin and resveratrol treatments, induce the UPR^{mt} in mammalian cells (17, 18). However, it remains unclear how the loss of SURF1 extends life span. SOD2 is a mitochondrial matrix superoxide dismutase that serves as a first line of defense against oxidative stress by converting superoxide to hydrogen peroxide. *Sod2* heterozygous (*Sod2*^{+/-}) mice show increased oxidative stress, as indicated by inactivation of ROS-sensitive enzymes, higher sensitivity to oxidative stress, impaired mitochondrial respiration, and higher levels of DNA oxidative damage in both the nucleus and mitochondria (19). Despite this, *Sod2*^{+/-} mice appear normal and have a wild-type life span. Thus, mitochondrial damage induced by a decrease in antioxidant defenses is not sufficient to compromise longevity in mice.

It is conceivable that impaired mitochondrial function does not shorten life span until it reaches a critical threshold. This argument provides a potential rationale for why, despite the prime importance of mitochondria for many cellular functions, some mitochondrial defects, such as those mentioned above, are not associated with a shortened life span. However, even mice that have suffered severe and prolonged mitochondrial dysfunction are able to live as

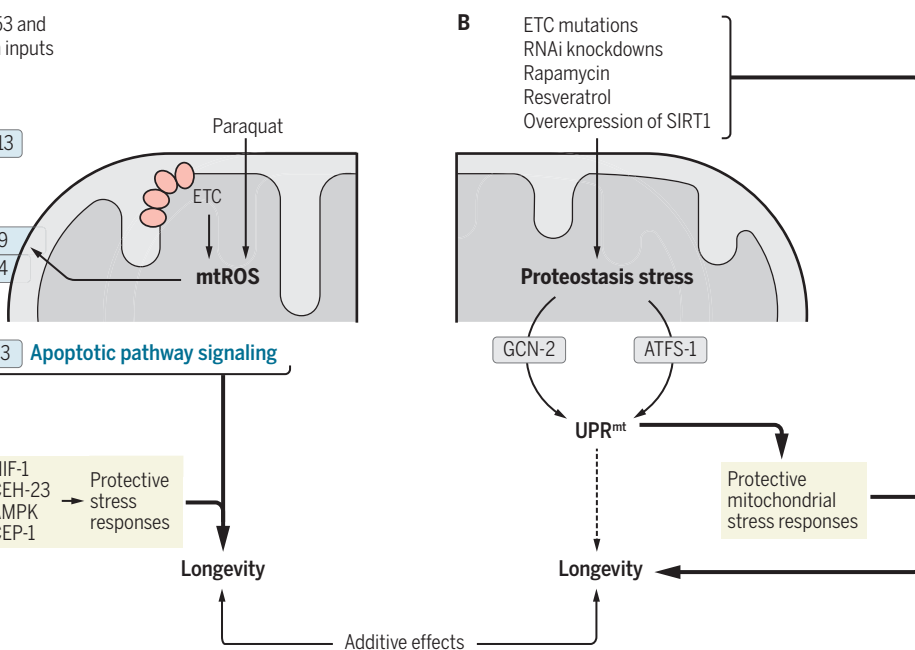


Fig. 2. Pro-longevity responses to mitochondrial stress. (A) In *C. elegans*, pro-longevity signaling by mtROS acts through the intrinsic apoptosis pathway. This is further modulated by key stress-response pathways. (B) The UPR^{mt} has been suggested to link mitochondrial stress to life-span extension, but it is still uncertain whether its activation alone is sufficient to extend life span.

long as control mice when mitochondrial function is partially restored at mid-life (20). Mutant mice in which the *Mcl1* gene was globally deleted in 2-month-old adults (*aogMcl1* KO) showed a severe loss of UQ and impaired mitochondrial respiration. Heart, kidney, and skeletal muscles had only 50% of the normal respiratory rate. The mutant mice died at around 9 months of age with severe phenotypes, including small size, absence of fat, hair loss, low blood glucose, elevated lactate, low triglycerides, intervals of catatonia, and severe neurological symptoms (20). UQ biosynthesis can be restored in the absence of the MCL1-catalyzed step by treatment with an appropriate unnatural biosynthetic precursor, 2,4-dihydroxybenzoate (2,4-DHB) (21). Treatment of KO mice with 2,4-DHB shortly before death led to virtually full phenotypic recovery, with animals looking essentially wild-type (except for a small deficit in weight), despite only partial normalization of mitochondrial function.

The treatment resulted in full restoration of a normal life span, even though the mice had lived almost their entire lives with mitochondrial dysfunction (20). Thus, neither chronic nor acutely severe mitochondrial dysfunction is sufficient to produce irreversible phenotypes that limit life span.

Insights from invertebrate studies

Several of the studies with vertebrates described above fail to support a causal role for mitochondrial dysfunction in the aging process. Moreover, recent work with invertebrate animal model systems suggests that mitochondrial dysfunction in fact can lead to the generation of intracellular signals that stimulate anti-aging processes. It is widely assumed that the mechanisms of aging are conserved and can be studied in model organisms, including the nematode *Caenorhabditis elegans* and the fruit fly *Drosophila melanogaster*. In *C. elegans*, *clk-1* is the ortholog of the mouse *Mcl1* gene discussed above. Twenty years ago, the *clk-1* mutant was the first long-lived mutant to be described in which increased longevity was associated with mitochondrial dysfunction (22). Several more long-lived *C. elegans* mutants were subsequently found to be associated with mitochondrial dysfunction (23, 24). In addition, it was found that using RNA interference (RNAi) to knock down *C. elegans* genes whose products function in mitochondria frequently resulted in increased life spans (25, 26), a phenomenon that also appears to be conserved in *Drosophila* (27) and possibly mice (18). At least some of the mutations appear to increase life span by mechanisms

Box 2. ROS in other mechanisms of life-span extension.

ROS acting as signals have been linked to the longevity resulting from disturbed insulin and insulin-like growth factor 1 signaling in *C. elegans* (43). Mitochondria also have frequently been implicated in the longevity associated with caloric restriction (CR). In *C. elegans*, a CR regime imposed by inhibition of glycolysis via 2-deoxy-D-glucose promotes ROS formation and subsequent longevity (44). However, mtROS generated by paraquat can further extend the life span of the eating-defective *eat-2* mutant, suggesting that the mechanism of CR is distinct from the life-span extension initiated by mtROS (28). The *C. elegans* transcription factor SKN-1 (homolog of vertebrate NRF1/2), which is crucial to the response to oxidative stress, also has recently been implicated in linking mitochondrial function to CR (45).

that are distinct from those that underlie the effects of RNAi (23). However, whether distinct mechanisms are at work, and even which mechanisms are engaged by RNAi knockdowns to induce longevity, remain controversial.

Long-lived electron transport chain mutants

A point mutation in the *C. elegans isp-1* gene, which encodes the iron sulfur protein of mitochondrial respiratory complex III, leads to mitochondrial dysfunction but also to a dramatically increased life span (24). The mitochondrial dysfunction in the *isp-1* and similar long-lived ETC mutants, such as the *nwo-6* mutant, elevates mitochondrial superoxide generation (28). This elevation appears to be necessary for extended longevity, which is suppressed by treatment with antioxidants. A pro-longevity role for superoxide generation is further supported by the observation that treatment with very low concentrations (0.1 mM) of the mitochondrial superoxide generator paraquat can dramatically increase the life span of wild-type animals without impairing their mitochondrial function, but

“There is no doubt that mitochondria wear down with age. However, by itself, this functional decline appears to be insufficient to cause aging.”

this treatment has no effect on the long-lived ETC mutants (28). This supports the notion that increased mtROS generation with aging does not mean that ROS cause aging, but rather that mtROS are part of a stress response that combats the damage accumulation that accompanies aging (Box 2) (29).

Recent findings suggest that one of the principal mechanisms by which mtROS act as pro-longevity signaling molecules is via the intrinsic apoptosis signaling pathway, by activating a specific pattern of changes in gene expression without inducing cell death (Fig. 2A) (30). The intrinsic pathway of apoptosis is physically associated with mitochondria and is sensitive to mtROS in vertebrates, where it contributes to homeostasis by eliminating unwanted or dysfunctional cells. In *C. elegans*, this signaling pathway can be used in two ways: either to stimulate apoptosis when it is triggered by expression of EGL-1 or to stimulate greater survival when it is triggered by expression of CED-13 and mtROS. The mtROS presumably act on CED-9 (BCL2-like), which is tethered to the mitochondrial outer membrane, or CED-4 (APAF1-like), which is bound by CED-9 (Fig. 2A). The expression of the *ced-13* gene is known to be controlled by the p53 *C. elegans* homolog CEP-1, which also affects mtROS pro-longevity signaling (31, 32). Studies in yeast

have suggested that mtROS can also affect longevity by triggering a noncanonical activation of DNA damage pathways (33).

Altered energy metabolism in the long-lived ETC mutants (low oxygen consumption and ATP levels) might also play a role in their longevity, because mtROS in these mutants alters ATP-dependent behaviors and developmental processes, possibly by redirecting ATP use toward protective processes (30). This is consistent with findings that the metabolic regulators adenosine 5'-monophosphate (AMP) kinase and HIF-1 α modulate the effects of the mtROS pathway (34, 35).

Activating the UPR^{mt}

The UPR^{mt} allows cells to cope with the presence of unfolded or misfolded proteins in mitochondria by conveying a stress signal to the nucleus and up-regulating mitochondrial chaperones and proteases (36). It has been proposed that UPR^{mt} activation promotes longevity and is responsible for the life-span extension induced by resveratrol and rapamycin treatments (17), as well as for the life-span extension that follows the mitochondrial dysfunction induced by RNAi knockdown of ETC components (23, 37) or components of the mitochondrial translation machinery (Fig. 2B) (18). However, the mechanisms induced by RNAi and by the long-lived ETC point mutations appear to be fully distinct, in particular because their effects on life span are additive (23).

Nevertheless, the question of whether activation of the UPR^{mt} is sufficient for life-span extension remains open. Activation of the UPR^{mt} can be uncoupled from life-span extension in *C. elegans* (38). For example, gain-of-function alleles of *atfs-1*, which encodes the nuclear transcription factor that turns on the UPR^{mt} by sensing mitochondrial stress, do not lengthen life span. Furthermore, loss-of-function *atfs-1* alleles do not always prevent the longevity induced by RNAi knockdown of ETC subunits.

Even though the ATFS-1-dependent UPR^{mt} and other mechanisms of mitochondrial protein homeostasis (39) might not confer longevity by themselves, they might be needed to permit life-span extension in long-lived mutants with stressed mitochondria, such as *clk-1* and *isp-1* mutants (37, 39). The extended life spans of the mutants were abolished when the activation of these pathways, which shield mitochondria from the consequences of dysfunction, was prevented, because this intervention resulted in very severe synthetic phenotypes.

There are thus two distinct mechanisms of life-span extension by dysfunctional mitochondria: one mechanism induced by point mutations in ETC subunits, which increases mtROS generation and engages the apoptotic pathway, and one mechanism induced by RNAi knockdown of components of the ETC and of the mitochondrial translation machinery. The role of mitochondrial protein homeostasis in either mechanism is less clear, but it might be protective and thus facilitate life-span extensions induced by mitochondrial stress (Fig. 2B).

Conclusions

Studies in both vertebrates and invertebrates demonstrate the intimate connection between mitochondria and longevity. On the one hand, there is no doubt that mitochondria wear down with age. However, by itself, this functional decline appears to be insufficient to cause aging. On the other hand, some deviations from normal mitochondrial states can elicit responses that are protective and extend longevity. These findings point to unexpectedly complex links between mitochondria and longevity.

REFERENCES AND NOTES

1. M. Picard et al., *Aging Cell* **9**, 1032–1046 (2010).
2. S. DiMauro, E. A. Schon, V. Carelli, M. Hirano, *Nat. Rev. Neurol.* **9**, 429–444 (2013).
3. D. C. Wallace, W. Fan, *Genes Dev.* **23**, 1714–1736 (2009).
4. G. C. Kujoth, P. C. Bradshaw, S. Haroon, T. A. Prolla, *PLoS Genet.* **3**, e24 (2007).
5. A. Trifunovic et al., *Nature* **429**, 417–423 (2004).
6. G. C. Kujoth et al., *Science* **309**, 481–484 (2005).
7. A. Logan et al., *Aging Cell* **13**, 765–768 (2014).
8. D. F. Dai et al., *Aging Cell* **9**, 536–544 (2010).
9. S. R. Kennedy, J. J. Salk, M. W. Schmitt, L. A. Loeb, *PLoS Genet.* **9**, e1003794 (2013).
10. L. S. Itsara et al., *PLoS Genet.* **10**, e1003974 (2014).
11. M. Vermulst et al., *Nat. Genet.* **39**, 540–543 (2007).
12. H. Tynymäa et al., *Proc. Natl. Acad. Sci. U.S.A.* **102**, 17687–17692 (2005).
13. S. Hekimi, *Oncotarget* **2**, e23793 (2013).
14. C. Dell'Agnello et al., *Hum. Mol. Genet.* **16**, 431–444 (2007).
15. D. A. Pulliam et al., *Biochem. J.* **462**, 359–371 (2014).
16. S. S. Deeba et al., *FASEB J.* **27**, 1371–1380 (2013).
17. L. Mouchiroud et al., *Cell* **154**, 430–441 (2013).
18. R. H. Houtkooper et al., *Nature* **497**, 451–457 (2013).
19. H. Van Remmen et al., *Physiol. Genomics* **16**, 29–37 (2003).
20. Y. Wang, D. Oxer, S. Hekimi, *Nat. Commun.* **6**, 6393 (2015).
21. L. X. Xie et al., *J. Biol. Chem.* **287**, 23571–23581 (2012).
22. S. Felkai et al., *EMBO J.* **18**, 1783–1792 (1999).
23. W. Yang, S. Hekimi, *Aging Cell* **9**, 433–447 (2010).
24. J. Feng, F. Bussière, S. Hekimi, *Dev. Cell* **1**, 633–644 (2001).
25. A. Dillin et al., *Science* **298**, 2398–2401 (2002).
26. S. S. Lee et al., *Nat. Genet.* **33**, 40–48 (2002).
27. J. M. Copeland et al., *Curr. Biol.* **19**, 1591–1598 (2009).
28. W. Yang, S. Hekimi, *PLoS Biol.* **8**, e1000556 (2010).
29. S. Hekimi, J. Lapointe, Y. Wen, *Trends Cell Biol.* **21**, 569–576 (2011).
30. C. Yee, W. Yang, S. Hekimi, *Cell* **157**, 897–909 (2014).
31. B. Schumacher et al., *Cell Death Differ.* **12**, 153–161 (2005).
32. A. Baruah et al., *PLoS Genet.* **10**, e1004097 (2014).
33. E. A. Schroeder, N. Raimundo, G. S. Shadel, *Cell Metab.* **17**, 954–964 (2013).
34. A. B. Hwang et al., *Proc. Natl. Acad. Sci. U.S.A.* **111**, E4458–E4467 (2014).
35. L. Walter, A. Baruah, H. W. Chang, H. M. Pace, S. S. Lee, *PLoS Biol.* **9**, e1001084 (2011).
36. C. M. Haynes, C. J. Fiorese, Y. F. Lin, *Trends Cell Biol.* **23**, 311–318 (2013).
37. J. Durieux, S. Wolff, A. Dillin, *Cell* **144**, 79–91 (2011).
38. C. F. Bennett et al., *Nat. Commun.* **5**, 3483 (2014).
39. B. M. Baker, A. M. Nargund, T. Sun, C. M. Haynes, *PLoS Genet.* **8**, e1002760 (2012).
40. L. M. Dillon, A. P. Rebelo, C. T. Moraes, *IUBMB Life* **64**, 231–241 (2012).
41. M. Rera et al., *Cell Metab.* **14**, 623–634 (2011).
42. A. P. Gomes et al., *Cell* **155**, 1624–1638 (2013).
43. K. Zarse et al., *Cell Metab.* **15**, 451–465 (2012).
44. T. J. Schulz et al., *Cell Metab.* **6**, 280–293 (2007).
45. J. Paek et al., *Cell Metab.* **16**, 526–537 (2012).

ACKNOWLEDGMENTS

We thank C. Yee for useful discussions and R. Branicky for reading the manuscript. Our laboratory is funded by grants from the Canadian Institutes of Health Research (grants MOP-114891, MOP-123295, and MOP-97869) and by McGill University, S.H. holds the Strathcona Chair of Zoology and the Campbell Chair in Developmental Biology.

10.1126/science.aac4357

REVIEW

NAD⁺ in aging, metabolism, and neurodegeneration

Eric Verdin

Nicotinamide adenine dinucleotide (NAD⁺) is a coenzyme found in all living cells. It serves both as a critical coenzyme for enzymes that fuel reduction-oxidation reactions, carrying electrons from one reaction to another, and as a cosubstrate for other enzymes such as the sirtuins and poly(adenosine diphosphate-ribose) polymerases. Cellular NAD⁺ concentrations change during aging, and modulation of NAD⁺ usage or production can prolong both health span and life span. Here we review factors that regulate NAD⁺ and discuss how supplementation with NAD⁺ precursors may represent a new therapeutic opportunity for aging and its associated disorders, particularly neurodegenerative diseases.

Nicotinamide adenine dinucleotide (NAD⁺) is a key cellular factor for intermediary metabolism. Originally defined as a molecular fraction ("cozymase") that accelerated fermentation in yeast extracts, its chemical structure was resolved as a nucleotide sugar phosphate. The nicotinamide portion of NAD⁺ is the site of reduction-oxidation (redox) reactions, and its reduced form (NADH) serves as a key energy-transfer intermediate between different metabolic pathways (Fig. 1).

The medical importance of NAD⁺ was established early with the discovery of pellagra, a disease characterized by four "Ds": dermatitis, diarrhea, dementia, and death. A heat-stable dietary factor (known as pellagra-preventing factor) that cured pellagra was determined to be a NAD⁺ precursor called niacin. This provided the first evidence of a therapeutic role for what is now vitamin B₃ (7).

Although pellagra is rare in the developed world, decreased cellular NAD⁺ concentrations occur under defined conditions, including aging, and supplementation with NAD⁺ precursors may be useful against aging and its chronic diseases. Here we review recent findings on NAD⁺ biology and their implications for normal aging and age-associated diseases.

NAD⁺ biosynthesis, degradation, and salvage

Beyond its role as a coenzyme in redox reactions, NAD⁺ is an important cosubstrate for three classes of enzymes: (i) the sirtuins (SIRT), (ii) the adenosine diphosphate (ADP)-ribose transferases (ARTs) and poly(ADP-ribose) polymerases (PARPs), and (iii) the cyclic ADP-ribose (cADPR) synthases (CD38 and CD157). NAD⁺ is consumed by these enzymes and continuously degraded (Fig. 1). To maintain stable cellular concentrations of NAD⁺, organisms

primarily use a nicotinamide salvage pathway but also rely on several biosynthetic pathways.

NAD⁺ biosynthetic pathways

Nicotinamide adenine dinucleotide can be synthesized from diverse dietary sources, including nicotinic acid and nicotinamide, tryptophan, and nicotinamide riboside (NR). The major dietary source of NAD⁺ is nicotinic acid, a form of niacin (i.e., vitamin B₃) that can be transformed

by indoleamine 2,3-dioxygenase (IDO) or tryptophan 2,3-dioxygenase (TDO). IDO and TDO activities lead to metabolites in the kinurenine pathway that modulate the activity of the mammalian immune, reproductive, and central nervous systems. This is a rate-limiting step in the pathway, and both enzymes are frequently over-expressed in cancer and may contribute to immune tolerance to cancer cells through their immunomodulatory activities. Another key step is transformation of 2-amino-3-carboxymuconate semialdehyde (ACMS). This compound spontaneously condenses and rearranges into quinolinate, which serves as a precursor to NAD⁺ synthesis (Fig. 2). However, under most circumstances, ACMS is decarboxylated by ACMS decarboxylase into 2-amino-3-muconate semialdehyde (AMS), leading to its oxidation into acetyl-coenzyme A (CoA) via the tricarboxylic acid (TCA) cycle. If the ACMS decarboxylase enzymatic capacity is exceeded by an excess of tryptophan (6), quinolinate is transformed into NAMN, thus linking with the Preiss-Handler pathway (Fig. 2).

NAD⁺ salvage pathway

This is the key pathway for maintaining cellular NAD⁺ levels. The NAD⁺-consuming enzymes—the SIRTs, ARTs, and PARPs—all generate nicotinamide as a by-product of their enzymatic activities.

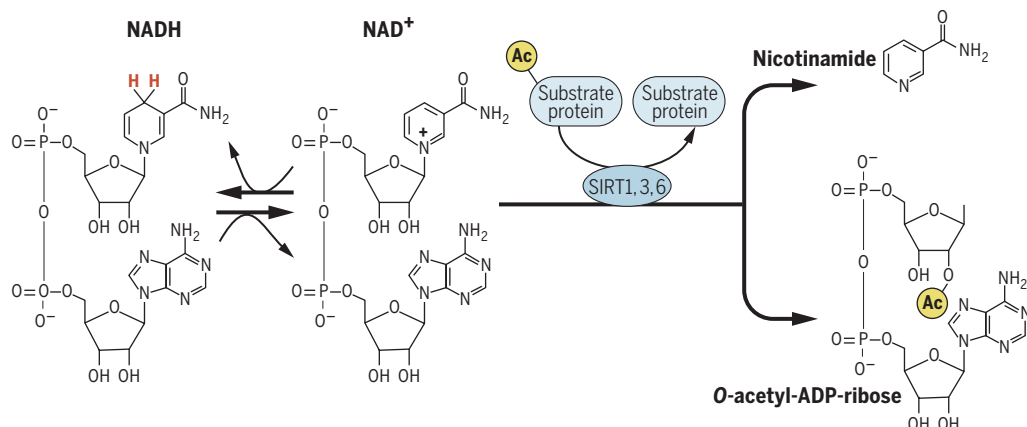


Fig. 1. NAD⁺ can be used as both a cosubstrate and a coenzyme. The structures of NAD in its reduced (NADH) and oxidized (NAD⁺) forms are shown (hydrides in red). Sirtuins remove acetyl and acyl groups from target proteins. This reaction is coupled to NAD⁺ cleavage into nicotinamide, and the ADP-ribose serves as the acceptor for the removed acetyl (or acyl) group (in yellow).

into NAD⁺ through three steps in the Preiss-Handler pathway (Fig. 2). A key enzyme in this pathway is nicotinamide mononucleotide adenylyl-transferase (NMNAT), which transforms nicotinic acid mononucleotide (NAMN) into nicotinic acid adenine dinucleotide (NAAD) in the presence of adenosine triphosphate (ATP). Three forms of the enzyme have distinct subcellular localizations: NMNAT1 in the nucleus, NMNAT2 in the cytosol and Golgi, and NMNAT3 in the cytosol and mitochondria (2–4). This enzyme is also important in the NAD⁺ salvage pathway.

Synthesis of NAD⁺ from tryptophan occurs in the kinurenine pathway (5) (Fig. 2). The first step is conversion of tryptophan to *N*-formylkinurenine

Nicotinamide regulates their activities as an inhibitory factor by binding in a conserved NAD⁺ pocket and also as a biosynthetic precursor to NAD⁺ via activity of nicotinamide phosphoribosyltransferase (NAMPT). This enzyme recycles nicotinamide into nicotinamide mononucleotide (NMN), which is converted into NAD⁺ by the various NMNATs (discussed above). This pathway leads to recycling of nicotinamide into NAD⁺ and relieves nicotinamide inhibition of NAD⁺-consuming enzymes. NAMPT is expressed in low amounts in pancreatic β cells and neurons, which might allow it to become more rapidly limiting in these cells (7). NAMPT can be either intracellular (iNAMPT) or extracellular (eNAMPT).

NAD⁺ as an enzyme cosubstrate

Nicotinamide adenine dinucleotide is a critical cofactor for other enzymes, including the sirtuin protein deacetylases, the ADP-ribose transferases and PARP, and the cADPR synthases (CD38 and CD157).

The sirtuin protein deacetylases

These proteins are conserved from bacteria to humans. They remove acyl groups from lysine residues on proteins in a NAD-dependent manner. NAD⁺ is cleaved between nicotinamide and ADP-ribose, and the latter serves as an acyl acceptor, generating acyl-ADP-ribose (Fig. 1). The demonstration that Sir2 is an NAD⁺-dependent protein deacetylase (8) suggested that Sir2 enzymatic activity could be coupled to metabolic status, a model supported by the observation that, in *Saccharomyces cerevisiae*, Sir2 is necessary for life-span extension in response to calorie restriction (9).

Sirtuins sense intracellular NAD⁺ concentrations and transduce a signal via protein deacetylation, predominantly modifying acetyl but also succinyl, malonyl, glutaryl, palmitoyl, and other fatty acids (10, 11). Yeast sirtuin Sir2 was identified as a gene controlling aging in yeast, and this function was confirmed in worms and *Drosophila melanogaster* (12–14). After questions were raised as to the robustness of these effects and confounding variables in the genetic background of the strains used (15), follow-up studies have confirmed the life-span-extending effects of Sir2 orthologs in flies and worms (16–18) and for SIRT1 and SIRT6 in mice (19, 20).

There are seven sirtuins in mammals in different subcellular compartments: nuclear for SIRT1, SIRT6, and SIRT7; cytoplasmic for SIRT2; and mitochondrial for SIRT3, SIRT4, and SIRT5. The possibility that NAD⁺ concentrations are regulated semi-independently in different cellular compartments could allow local changes in NAD⁺ concentrations to differentially affect the activity of distinct sirtuins.

Calorie restriction, a decrease in caloric intake (by 10 to 40%) without malnutrition, has been shown to increase life span and health span in all organisms in which it has been tested. The benefits of calorie restriction on metabolism and other cellular functions, such as cognition, depend on NAD⁺ sensing by SIRT1. The protein deacetylase of SIRT1 functions as an epigenetic regulator by targeting specific histone-acetylated residues (e.g., H3K9, H3K14, and H4K16) but also regulates transcription by deacetylating transcription factors (such as TP53, NF- κ B, PGC-1 α , and FOXO3a) (21). As discussed above, NAD⁺ concentrations fluctuate in a circadian manner and thereby link the peripheral clock to the transcriptional regulation of metabolism by epigenetic mechanisms through SIRT1. The core components of the circadian clock, BMAL1 and CLOCK, directly regulate expression of NAMPT in the NAD⁺ salvage pathway in mice. SIRT1 protein abundance is relatively stable, but its deacetylase activity depends on NAMPT to generate NAD⁺, and SIRT1 enzymatic activity oscillations correlate with the

circadian production of NAD⁺. Key targets of SIRT1 include lysines 9 and 14 of histone 3 at multiple loci of genes that oscillate under circadian control (22). SIRT1 also regulates ribosomal biogenesis, an energy-consuming process in eukaryotes, particularly in proliferative tissues. SIRT1 is presumably activated through increased levels of NAD⁺ during the transition to glucose starvation, and it deacetylates histone H3K9 at ribosomal DNA loci, in cooperation with a protein complex that contains nucleomethilin, the heterochromatin methyltransferase SUV39H1, and SIRT1 (23).

Sirtuin 1 is phosphorylated by protein kinase A as a consequence of adrenergic receptor activation during fasting. This induces a shift in its Michaelis constant (K_m) for NAD⁺ that sensitizes the enzyme for fluctuations in NAD⁺ concentrations (24). SIRT6, which is also localized in the nucleus, is linked to aging by regulating telomere stability and inflammation through NF- κ B signaling. Deacetylation of histone H3K9 appears to be the modification connecting SIRT6 activity with these aging pathways. Loss of SIRT6 leads to progeria, whereas gain of function extends life span in male mice by 15% (19, 25–27).

Sirtuin 3 is the major mitochondrial protein deacetylase (28). Its expression is enhanced by fasting and calorie restriction and is decreased during aging and by a high-fat diet (29). SIRT3 deacetylates and thereby increases the enzymatic activity of key mitochondrial proteins involved in the protection against oxidative stress and in intermediary metabolic pathways, such as fatty acid oxidation, the urea cycle, and oxidative phosphorylation (30–35). SIRT3 is necessary for the protective effect of calorie restriction on age-associated hearing loss (30). Without SIRT3, mice develop a syndrome similar to the metabolic syndrome in humans, which results in glucose intolerance, mild obesity, chronic inflammation, dyslipidemia, and steatohepatitis (29). Mitochondrial NAD⁺ concentrations fluctuate in a diurnal manner and mediate a change in mitochondrial oxidative activity in a SIRT3-dependent manner (36).

In worms, nicotinamide is metabolized into 1-methylnicotinamide (MNA) by a nicotinamide-N-methyltransferase (anmt-1). Loss of anmt-1 suppresses the life-span effect of Sir2.1. Thus, Sir2.1 might increase life span by generating nicotinamide, which is then transformed into MNA. MNA serves as a substrate for the aldehyde oxidase

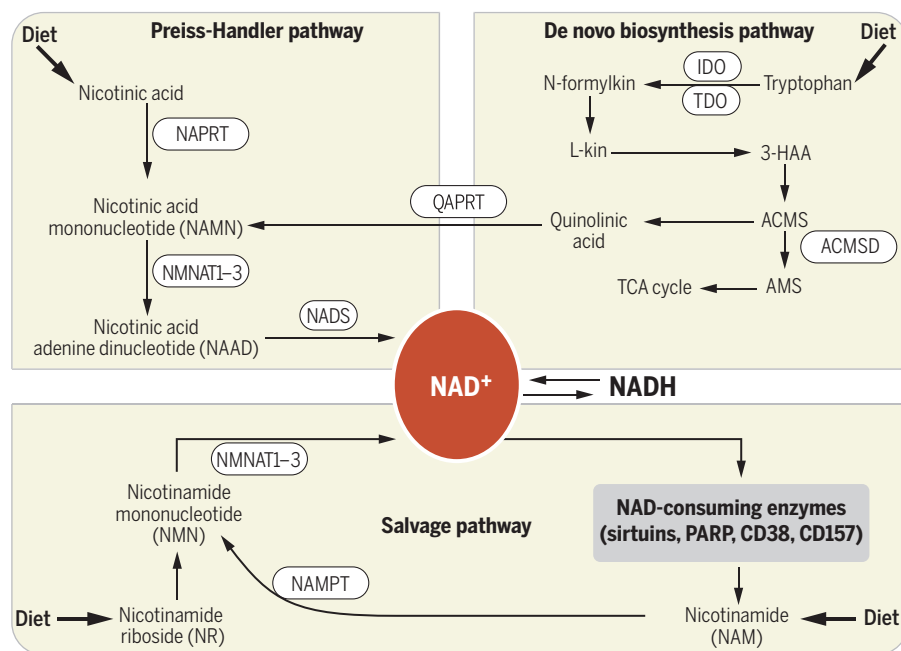


Fig. 2. NAD⁺ biosynthetic pathways. NAD⁺ levels are maintained by three independent pathways. First, the Preiss-Handler pathway uses dietary nicotinic acid and the enzyme nicotinic acid phosphoribosyltransferase (NAPRT) to generate NAMN, which is then transformed into NAAD by NAMN transferase (NMNAT). Three forms of this enzyme (NMNAT1, -2, and -3) have distinct subcellular localizations. The process is completed by the transformation of NAAD into NAD⁺ by NAD⁺ synthase (NADS). Second, the de novo synthesis pathway of NAD from tryptophan occurs through the kinurenine pathway (5). The first step in this pathway is the rate-limiting conversion of tryptophan to *N*-formylkinurenine (*N*-formylkin) by either IDO or TDO. Formylkinurenine is transformed into *L*-kinurenine (*L*-kin), 3-hydroxykinurenine, and 3-hydroxyanthranilic acid (3-HAA) and finally to ACMS. This compound can spontaneously condense and rearrange into quinolinic acid, which is transformed into NAMN, at which point it converges with the Preiss-Handler pathway. ACMS can also be decarboxylated into AMS by ACMS decarboxylase (ACMSD), leading to its oxidation into acetyl-CoA via the TCA cycle. Third, the NAD⁺ salvage pathway recycles the nicotinamide generated as a by-product of the enzymatic activities of NAD⁺-consuming enzymes: sirtuins, PARPs, and the cADPR synthases (CD38 and CD157). Initially, NAMPT recycles nicotinamide into NMN, which is then converted into NAD⁺ via the different NMNATs.

GAD-3 to generate hydrogen peroxide, which may promote a mitohormesis response, in which a mild stress in mitochondria promotes a protective response in the whole cell (37, 38). The implications for the mammalian NAD⁺-sirtuin-aging link and its relevance to mammalian systems are not clear but warrant further study.

Poly(ADP-ribose) polymerases

There are 17 genes encoding PARP-related proteins (39). Activated PARP1 and PARP2 catalyze the transfer of multiple ADP-ribose moieties from NAD^+ to protein acceptors, generating long poly(ADP-ribose) (PAR) chains. Other PARPs are enzymatically inactive or catalyze the transfer of mono-ADP ribose to acceptor proteins and are less important for modulating cellular NAD^+ concentrations. PARP1 is the most abundant PARP and is expressed ubiquitously. This DNA-dependent nuclear PARP is strongly activated by DNA damage, leading to consumption of a large amount of cellular NAD^+ . In fact, DNA damage leads to a decrease (up to 80%) in cellular NAD^+ concentrations. PARP1 is important in DNA damage detection and repair, as well as in a cell's decision to repair itself or die after a genotoxic insult (40). PARP1 also promotes ribosomal RNA biogenesis by PARylation of several nucleolar proteins and is required for assembly of cytoplasmic stress granules that regulate the stability and translation of mRNA in response to stress (41).

Selective PARP inhibitors are in development or are already approved for cancer treatment. They show synthetic lethality with defects in homologous replication or are tested in combination therapy with chemotherapy or radiation therapy (42). These inhibitors are also being tested as anti-inflammatory drugs in stroke and myocardial infarction.

NAD⁺ as an enzyme cofactor

Nicotinamide adenine dinucleotide and its phosphorylated derivative, nicotinamide adenine dinucleotide phosphate (NADP), serve as essential coenzymes for hydride-transfer enzymes (Fig. 3). They participate in redox reactions as hydride acceptors (NAD^+ and NADP^+) or donors [NADH or NADPH (reduced forms)]. These two redox pairs are kept in chemical opposition: NAD^+ is mostly maintained in its oxidized form; NADP is mostly in its reduced form, NADPH. As a coenzyme, NAD^+ is essential for energy generation by transferring reducing equivalents from glycolysis (from the activity of glyceraldehyde-3-phosphate dehydrogenase) and from the TCA cycle under the form of NADH. When oxygen is limiting, NADH is converted to NAD^+ by reduction of pyruvate

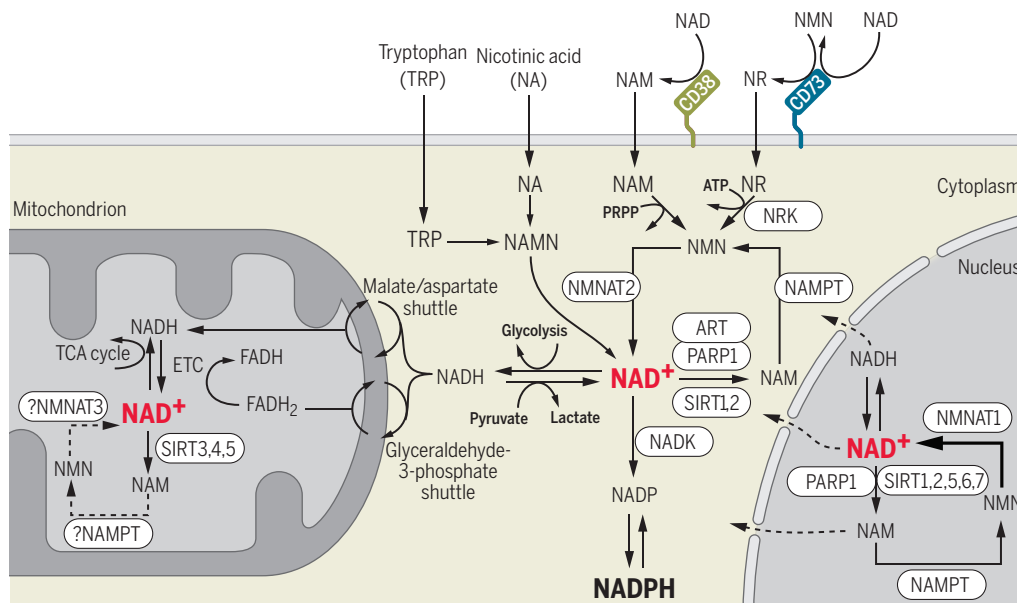


Fig. 3. NAD⁺ metabolism in different cellular compartments. The different precursors to intracellular NAD metabolism—tryptophan, nicotinic acid (NA), nicotinamide, NR, and NMN—are shown, along with their extracellular metabolism by CD38 and CD73. The cytoplasmic and nuclear NAD⁺ pools probably equilibrate by diffusion through the nuclear pore. However, the mitochondrial membrane is impermeable to both NAD⁺ and NADH. Reducing equivalents generated by glycolysis are transferred to the mitochondrial matrix via the malate/aspartate shuttle and the glyceraldehyde-3-phosphate shuttle. The resulting mitochondrial NADH (malate/aspartate shuttle) is oxidized by complex I in the respiratory chain (ETC), whereas the resulting FADH₂ (glyceraldehyde-3-phosphate shuttle) is oxidized by complex II. In each of the three compartments, different NAD⁺-consuming enzymes lead to the generation of nicotinamide, which is recycled via the NAD⁺ salvage pathway. Different forms of the NMNAT enzyme and sirtuins are localized in different compartments. The nature of the salvage pathway for NAD⁺ in mitochondria has not been fully resolved, although NMNAT3 has been found in mitochondria. NADK, NAD⁺ kinase.

into lactate. With oxygen, cytoplasmic NADH transfers its reducing equivalent through the malate-aspartate shuttle or the glycerol-3-phosphate shuttle to the mitochondrial matrix (Fig. 3). These reducing equivalents are oxidized by complex I of the electron-transport chain (ETC), thereby coupling glycolysis and the TCA cycle to ATP synthesis via oxidative phosphorylation. NADP is critical in several pathways, including fatty acid oxidation and cholesterol synthesis, as well as in redox protection. In these reactions, NAD^+ and NADH (or NADP and NADPH) interconvert but are not consumed.

Deterioration of mitochondrial function and the accompanying cellular energy deficit have emerged as critical factors in aging and diseases of aging (particularly neurodegenerative diseases). A number of pathways that extend life span help to maintain mitochondrial function, including mitochondrial biogenesis (43). The critical role of NAD^+ in mitochondrial intermediary metabolism suggests that variations in NAD^+ concentrations in this compartment may affect metabolic efficiency, aging, and aging-associated diseases. This model is supported by the observation that components of the malate-aspartate NADH shuttle, which transfers reducing equivalent from NADH in the cytoplasm to NADH in the mitochondrial matrix, are required for lifespan extension in response to dietary restriction in yeast (44).

Competition between NAD⁺-consuming enzymes for shared NAD⁺ pools

Although three classes of enzymes use NAD^+ , they have distinct roles in aging. Sirtuins are emerging as key mediators of increased life span, and PARPs and NAD^+ hydrolases exhibit the opposite effect. The evidence supporting this emerging model is detailed below (Fig. 4). An interesting competitive relationship exists between SIRT1 and PARP1 or CD38 for NAD^+ (45). For example, PARP1 activity increases during aging, as DNA damage accumulates, and in response to high-energy intake (46–48). Because PARP1 and SIRT1 have relatively similar values of K_m for NAD [50 to 97 μM for PARP1 versus 94 to 96 μM for SIRT1 (24, 49–52)], the decrease in NAD^+ concentrations that occurs when PARP1 is activated (up to an 80% decrease, starting from 200 to 500 μM under basal conditions) leads to a decrease in SIRT1 activity.

The antagonistic relationship between SIRT1 and PARP1 goes beyond competition for NAD: SIRT1 also inhibits PARP1 through deacetylation and at the transcriptional level (53, 54), and their activities on key cellular proteins are opposing. For example, activity of the transcription factor NF- κ B is suppressed by SIRT1-mediated deacetylation of its component p65/RelaA, whereas NF- κ B is transcriptionally activated by PARP1. In the case of tumor protein p53, it is activated by PARP1 under conditions of genotoxic stress

and inactivated by SIRT1 through deacetylation (55–57).

An extreme example of PARP1 activation occurs in patients with xeroderma pigmentosum group A (XPA), a nucleotide excision DNA repair disorder with severe neurodegeneration. The clinical neurological features of XPA (progressive cerebellar degeneration, peripheral neuropathy, and sensorineural hearing loss) are similar to those in two other DNA damage disorders: ataxia telangiectasia (AT) and Cockayne syndrome (CS). Further, hierarchical clustering of primary mitochondrial diseases with DNA repair disorders based on shared symptoms and manifestations shows a clustering of these DNA damage disorders (CS, XPA, AT) with several primary mitochondrial disorders [such as MEGDEL syndrome, Charcot-Marie-Tooth disease type 2A2, and NARP (neuropathy, ataxia, and retinitis pigmentosa) syndrome] and also with Friedreich ataxia, a disorder associated with defective mitochondrial SIRT3 activity, suggesting a shared pathogenic mechanism, perhaps driven by NAD⁺ depletion (58, 59).

Patients with XPA show PARP1 hyperactivation, NAD⁺ depletion, and decreased SIRT1 activity (Fig. 4). They also show mitochondrial abnormalities, including decreased mitochondrial autophagy (mitophagy), presumably as a consequence of decreased activity of the NAD⁺-SIRT1-PGC-1 α axis (60). This mitophagy defect in XPA, CS, and AT can be suppressed by treatment with PARP inhibitors or by supplementation with NAD⁺ precursors, such as NMN and NR (60). This concept was validated in a mouse CS model (*csb^{tm/m}*) that carries a mutation in the ortholog of human Cockayne syndrome B, *csb*. These mice display features characteristic of human Cockayne syndrome—for instance, decreased life span, mitochondrial abnormalities (hyperpolarized, increased O₂ consumption), and neuronal damage in the cerebellum and inner ear. As with XPA, PARP inhibitors or NAD⁺ precursors suppressed these phenotypes (61). A high-fat diet associated with a small increase in the ketone body β -hydroxybutyrate also suppressed these abnormalities. Intact SIRT1 was necessary for each of these interventions (high-fat diet, NAD⁺ precursors, or PARP inhibitors), which suggests that hyperactive PARP leads to decreased NAD⁺, decreased SIRT1 activity, and defective mitochondrial function, thus resulting in an energy deficit and increased oxidative stress (Fig. 4). The ketone body β -hydroxybutyrate inhibits class I histone deacetylases (HDAC1, HDAC2, and HDAC3) and increases expression of MT2 and FOXO3A (62). Because FOXO proteins regulate NAMPT, oxidative stress, and aging, β -hydroxybutyrate may indirectly regulate NAD⁺ concentrations, sirtuin function, and aging.

A similar model based on PARP activation and NAD⁺ depletion was invoked for aging in mice and worms. NAD⁺ concentrations are reduced in aged mice and worms, and restoring NAD with nicotinamide riboside or PARP inhibitors prevents age-associated metabolic decline and promotes longevity in worms. These effects depend on the SIRT1 worm ortholog, *sir-2.1*, and induction of mitonuclear protein imbalance (48).

Another parallel situation has been described in the case of cyclic ADP-ribose synthases (CD38, CD157) and brings further support for the model proposed above. Both proteins produce cyclic ADP-ribose from NAD⁺ and were initially described as lymphocyte-specific ectoenzymes. However, they occur in other tissues, both inside and outside cells. CD38 is a major NAD⁺-consuming enzyme, and mice lacking CD38 show increased NAD⁺ concentrations in the brain, liver, and muscles. Furthermore, due to their resulting enhanced energy expenditure and higher metabolic rates, these animals are protected against obesity, despite a high-fat diet (63–65).

Their resistance to obesity is mediated in part through an NAD⁺-dependent activation of the SIRT-PGC1 α axis (65). In contrast, CD38 overexpression in a cell line that resulted in a 35%

synthesis pathway and could be an important precursor for NAD⁺, but the activity of ACMS decarboxylase diverts ACMS from NAD synthesis and may explain why tryptophan is a relatively poor NAD⁺ precursor (6).

Intestinal brush border cells hydrolyze NAD⁺ into NMN and 5'-AMP. NMN is hydrolyzed to NR and nicotinamide (67). Nicotinic acid can be derived directly from diet or the activity of nicotinamide deamidase in the gut microbial community. Inside the cell, nicotinic acid feeds into the Preiss-Handler pathway. NR can also be obtained from the diet (milk) and from partial digestion of NAD⁺ and NMN. The fate of NMN and NR after ingestion as supplements or after injection is not clear. The cell-surface protein CD73 processes NAD⁺ into NMN and NMN into NR, therefore providing a possible

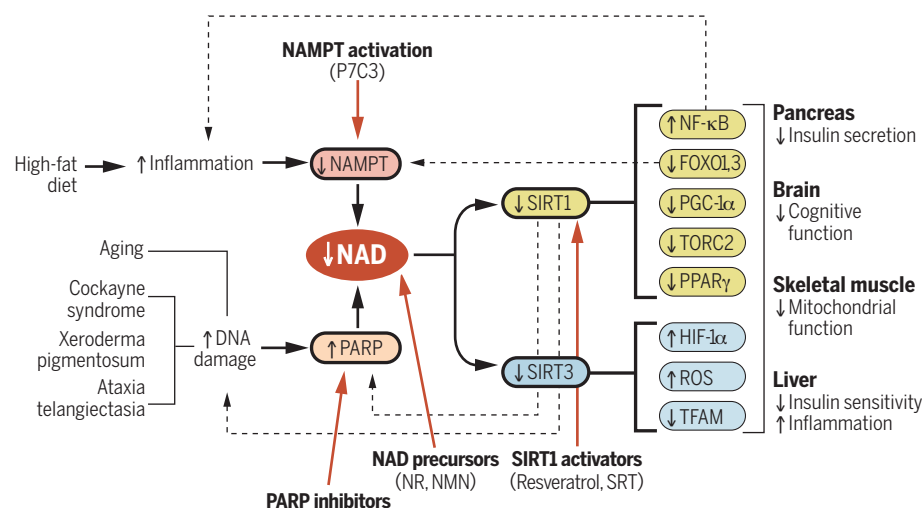


Fig. 4. A model for DNA damage, inflammation, NAD⁺, and aging. Two key events, the activation of PARP by DNA damage and the decreased NAMPT expression associated with inflammation, lead to decreased SIRT1 and SIRT3 activity in the nucleus and mitochondria, respectively. Decreased SIRT1 activity is associated with further PARP activation and increased DNA damage. Decreased SIRT1 also leads to NF- κ B activation and decreased FOXO3a activity, two factors that lead to increased inflammation. These contribute to the establishment of two parallel feed-forward self-reinforcing loops that further accelerate the aging process. This process is initiated earlier and faster in patients with DNA damage repair defects (such as CS, XPA, and AT). Mitochondrial function is diminished as a result of decreased SIRT3 activity, leading to mitochondrial protein hyperacetylation, whereas decreased SIRT1 is associated with decreased TFAM (necessary for mitochondrial DNA replication and transcription) and decreased PGC-1 α (necessary for mitochondrial biogenesis). Possible therapeutic interventions to restore NAD⁺ levels are illustrated for each of the key enzymes (red arrows).

decrease of cellular NAD⁺ concentrations was associated with a lower growth rate, increased oxidative stress, and decreased expression of proteins that function in glycolysis, antioxidant response, and DNA repair (66).

Nutritional precursors for NAD⁺ synthesis

As the field focuses on supplementing NAD precursors to remedy the decrease in NAD⁺ that occurs with aging, our understanding of the mechanisms of precursor import and conversion is still rudimentary. Precursors for NAD⁺ synthesis can be provided by the diet in several forms (Figs. 2 and 3). Tryptophan feeds into the de novo

mechanism for entry of NMN and NAD⁺ into cells (68, 69) (Fig. 3).

NAD⁺, mitochondrial function, and aging

Loss of mitochondrial function is a hallmark of aging and age-associated diseases (70). An interesting link has emerged between NAD⁺ metabolism, SIRT1, SIRT3, and mitochondrial function. NR and PARP inhibitors increased life span in worms via activation of the mitochondrial unfolded protein response UPR^{mt} by *sir-2.1* (48). Because the ETC is a multiprotein complex made up of proteins encoded by both the nuclear and mitochondrial genomes, unbalanced gene expression from both genomes results in stoichiometric

variations between different subunits in complex I of the respiratory chain. These partially unfolded proteins activate the mitochondrial unfolded protein response UPR^{mt}. In a separate study, decreased nuclear NAD⁺ was associated with defective SIRT1 activity and down-regulation of TFAM, the main transcription-replication factor for the mitochondrial genome. This resulted in an early decrease in the expression of mitochondrial genome-encoded proteins in the ETC and a pseudohypoxic state resembling the Warburg effect, with increased glycolysis and decreased activity of complexes I, III, and IV but not complex II, which is composed of only nuclear-encoded proteins (71). Short-term (1 week) supplementation of these mice with NMN restored mitochondrial homeostasis in muscles, which suggests that NAD⁺ supplementation can restore some reversible aspects of the aging process (71). Both observations are consistent with the model indicating that an imbalance in the relative stoichiometries of mitochondria- versus nucleus-encoded ETC proteins may induce life-span extension via activation of the UPR^{mt}. In support of such a mechanism, mutation or reduced function in nuclear genes encoding ETC components in yeast, *Caenorhabditis elegans*, *Drosophila*, and mice increase life span through activation of the mitochondrial unfolded protein response UPR^{mt} (72).

Although SIRT1 has emerged as a key NAD⁺ target in mediating its beneficial effects, mitochondrial NAD⁺ metabolism and SIRT3 are also important in aging. SIRT3 is necessary for the protective effect of calorie restriction against age-associated hearing loss and oxidative stress (30, 34). Furthermore, loss of SIRT3 is associated with induction of a pseudohypoxic state similar to that detected in aging (71). Loss of SIRT3 is associated with accelerated development of the metabolic syndrome in mice on a high-fat diet, and a SIRT3 polymorphism in humans is associated with decreased SIRT3 enzymatic activity and increased risk for the metabolic syndrome (29). Complex I is the major hydride acceptor from NADH in mitochondria, and inhibition of its activity traps the NADH in its reduced form (Fig. 3). Thus, loss of complex I of the respiratory chain through inactivation of one of its subunits (Ndufs4) is associated with an increase in NADH and a relative decrease in NAD⁺. This decrease in NAD⁺ leads to decreased SIRT3 activity, pronounced mitochondrial protein acetylation, and accelerated heart failure in response to chronic stress (73). Most of these consequences are rectified after supplementation with NMN (73). SIRT3 is also necessary for the protective effect of NR and *Wld^Δ* (a fusion protein encompassing NMNAT1, see below) against noise-induced hearing loss (29).

Defects of the mitochondrial ETC are one of the most frequent forms of human heritable metabolic diseases. Two recent studies tested NR supplementation in two mouse models of mitochondrial myopathy: Deletor mice carry a patient mutation in Twinkle, a mitochondrial replicative DNA helicase, and Sco2 knockout mice are characterized by impaired cytochrome c oxidase biogenesis (74, 75).

In both mouse lines, NR supplementation increased NAD⁺ concentrations and mitochondrial biogenesis and also delayed disease progression (74, 75), suggesting a protective role for NR against mitochondrial diseases and dysfunction associated with aging (22, 76–81).

Variation in NAD⁺ concentrations during aging

Nicotinamide adenine dinucleotide concentrations depend on several variables, including the cellular redox state (NAD⁺/NADH ratio) and the rates of NAD⁺ synthesis and NAD⁺ consumption. NAD⁺ is much more abundant than NADH, so we expect that variations in total NAD⁺ concentration, rather than in the NAD⁺/NADH ratio, are the main factor affecting sirtuin activity. However, changes in the NAD⁺/NADH ratio have been reported in muscle during the aging process (82). Although classical experiments have suggested that NAD⁺ concentrations were held constant (83), recent evidence indicates that cellular NAD⁺ concentrations change under various conditions. Importantly, they fluctuate in a circadian manner, through activation of the NAD⁺ salvage pathway (22, 80).

Nicotinamide adenine dinucleotide concentrations increase in response to conditions associated with lower energy loads, such as fasting, glucose deprivation, calorie restriction, and exercise (22, 76–81). In contrast, NAD⁺ concentrations decrease in animals on high-fat diets (46, 84–88) and during aging and senescence (47, 48, 71, 75, 82, 88–90).

The fact that NAD⁺ concentrations increase under conditions that increase life span or health span and decrease during aging or under conditions that decrease life span or health span supports the working model that decreased NAD⁺ levels contribute to the aging process and that NAD⁺ supplementation might exert protective effects during aging. Indeed, NAD⁺ supplementation increases life span in yeast and worms (48, 91).

Why do concentrations of NAD⁺ decrease during the aging process (47, 48, 71, 75, 82, 88–90)? The fact that supplementation with NMN (a product of NAMPT) corrects defects associated with aging may indicate that the NAD salvage pathway is deficient in aging. Decreased NAMPT expression occurs in several tissues (e.g., pancreas, white adipose tissue, and skeletal muscle) during aging (89), resulting from defective circadian rhythm regulation by CLOCK and BMAL (22) or from the oxidative stress and chronic inflammation associated with aging (7) (Fig. 4). NAD⁺ might be consumed through hyperstimulation of NAD-consuming enzymes, particularly PARP1, the activity of which increases during aging as DNA damage accumulates (47, 48).

Several key experiments highlight the protective role of NAD⁺ and sirtuins in aging. First, NAD⁺ and *SIR2* are critical for the life-span extension in response to calorie restriction in yeast (9). NAD⁺ supplementation with NR increases life span in yeast and is dependent on NR kinases and *SIR2* (92). NR also increases NAD⁺ concentrations in mammalian cells and mice, activates SIRT1 and SIRT3, and causes increased oxidative metabo-

lism and protection against metabolic abnormalities induced by consumption of a high-fat diet (84). NR promotes longevity in worms in a sir-2.1-dependent manner (48).

NAD⁺ metabolism in obesity, fatty liver disease, and type 2 diabetes

Pancreatic β cells and neurons may represent distinct frailty points in NAD⁺ metabolism: These tissues express the lowest amount of NAMPT, the rate-limiting enzyme in the NAD⁺ salvage pathway (7). The roles of the two forms appear contradictory: Increased eNAMPT is linked with obesity, nonalcoholic fatty liver disease, and type 2 diabetes (93, 94); in contrast, iNAMPT appears to decrease in abundance with age or in response to the inflammatory cytokine tumor necrosis factor α (88). Nutritional supplementation with the NAD⁺ precursor NMN restores NAD⁺ levels in mice with high-fat diet-induced type 2 diabetes and improves glucose intolerance and lipid profiles in older mice (88).

NAD⁺ metabolism and neurodegeneration

Several key observations support a role for the NAD⁺-sirtuin axis in neuroprotection. Axon degeneration has a key role in peripheral neuropathies; often precedes neuronal cell death in neurodegenerative disorders, such as Alzheimer's and Parkinson's disease; and can be induced directly by nerve injury in a process called Wallerian degeneration. A mouse strain called Wallerian degeneration slow mice (*Wld^Δ*) contains a spontaneous dominant mutation that delays this degeneration (95, 96). In the *Wld^Δ* mouse, a 85-kb tandem triplication generates a fusion protein between Ufd2a (ubiquitin fusion degradation protein 2a) and the Nmnat1 protein, a key enzyme in the NAD⁺ salvage pathway and the Preiss-Handler pathway (Fig. 2) (97). The *Wld^Δ* mutation protects against neuronal insults, including Parkinson's disease, hypoxic-ischemic injury, toxic neuropathy (taxol), and others (97). Although the native Nmnat1 is a predominantly nuclear protein, it is unclear whether the *Wld^Δ* fusion protein exerts its neuroprotective activity in the nucleus, axon, or mitochondria (97). The enzymatic activities of Nmnat1 and SIRT1 are necessary for the neuroprotective activity of *Wld^Δ* (98). *Wld^Δ* also protects against noise-induced hearing loss (99). Intense noise exposure causes hearing loss by inducing degeneration of spiral ganglia neurites that innervate cochlear hair cells. Administration of NR prevents noise-induced hearing loss and degeneration of spiral ganglia neurites, even after noise exposure. These effects appear to be mediated in the mitochondria, because SIRT3-overexpressing mice are resistant to noise-induced hearing loss and SIRT3 deletion abrogates the protective effects of NR and *Wld^Δ* in mice (99).

Further evidence for a role of NAD⁺ metabolism in neuroprotection comes from a screen conducted in vivo to identify small molecules that enhance hippocampal neurogenesis in adult mice (100). An aminopropyl carbazole compound called P7C3 appeared to mitigate the death of newborn neurons. P7C3 was improved to yield derivatives

with marked neuroprotective activity in animal models of Parkinson's disease, amyotrophic lateral sclerosis, and concussive injury (101–103). This compound was identified as an allosteric activator of NAMPT, the rate-limiting factor in NAD⁺ salvage, and was shown to protect cells treated with the NAD⁺-depleting drug doxorubicin (104). Studies involving this compound have been limited to its neuroprotective effects, but aging rats treated with P7C3 maintained their body weight when compared to aged vehicle-treated rats (104). Thus, PC73 might influence other age-related conditions, such as frailty.

Conclusions

The body of work reviewed above indicates that decreased NAD⁺ concentrations contribute to the aging process and to the pathogenesis of the chronic diseases of aging. These results also support the idea that NAD⁺ supplementation protects against aging and its associated conditions. The experiments reviewed here also raise expectations that NAD⁺ supplementation might be useful during normal human aging. Although such a prospect is clearly exciting, our understanding of NAD⁺ metabolism and its regulation during aging in humans remain fragmentary. In particular, little is understood about the pharmacological properties of NR or NMN as drugs: How are NR and NMN modified by the gut microbiome? How are they absorbed? What is their fate in the blood and in different organs? What sirtuins are they activating and in which tissues? Most experiments with NR involved large amounts of this compound (400 mg/kg of body weight in mice, corresponding to 28 g for a 70-kg adult). This raises important concerns about the exact mode of action of NR or its absorption.

For clinical applications, it will be critical to conduct rigorous double-blind and placebo-controlled clinical trials in humans. More work will also be necessary to gain a full understanding of the role of sirtuin activation against aging. SIRT1 increases life span in mice only when overexpressed in a distinct region of the brain but not when overexpressed in the whole organism (20, 105). Resveratrol and other sirtuin activators protect against the deleterious metabolic effects of the Western diet but initially did not appear to increase life span in mice (106–109). However, two recent studies show that SIRT1 activators can also modestly increase life span in mice on a regular chow diet (110, 111).

Although SIRT1 activation is clearly protective in terms of metabolism, its increased activity might pose considerable risk in other organs. For example, SIRT1 is a key factor in T helper 17 CD4 cells that contribute to autoimmune disease when hyperactivated (112). Similarly, loss of SIRT1 or inhibition of its activity promotes the development of another CD4 T cell subset, the regulatory T cells, which protects against autoimmunity (113, 114). Global SIRT1 activation, induced by SIRT1 activators or via an increase in NAD⁺ concentration, might therefore place susceptible individuals at increased risk of autoimmune diseases. Similarly, because some tumors show increased NAMPT expression, interventions that

increase NAD⁺ might enhance or promote tumor development (115).

These concerns notwithstanding, the studies reviewed here have ignited considerable interest in manipulating NAD⁺ concentrations in therapeutic efforts aimed at disease prevention and life-span extension. Future rigorous clinical testing in humans will tell us whether this early promise will become a reality.

REFERENCES AND NOTES

- D. J. Lanska, *Ann. Nutr. Metab.* **61**, 246–253 (2012).
- F. Berger, C. Lau, M. Dahlmann, M. Ziegler, *J. Biol. Chem.* **280**, 36334–36341 (2005).
- R. Felici, A. Lapucci, M. Ramazzotti, A. Chiarugi, *PLOS ONE* **8**, e76938 (2013).
- X. Zhang *et al.*, *J. Biol. Chem.* **278**, 13503–13511 (2003).
- K. L. Bogan, C. Brenner, *Annu. Rev. Nutr.* **28**, 115–130 (2008).
- M. Ikeda *et al.*, *J. Biol. Chem.* **240**, 1395–1401 (1965).
- S. Imai, J. Yoshino, *Diabetes Obes. Metab.* **15** (suppl. 3), 26–33 (2013).
- S. Imai, C. M. Armstrong, M. Kaeberlein, L. Guarente, *Nature* **403**, 795–800 (2000).
- S. J. Lin, P. A. Defosse, L. Guarente, *Science* **289**, 2126–2128 (2000).
- W. He, J. C. Newman, M. Z. Wang, L. Ho, E. Verdin, *Trends Endocrinol. Metab.* **23**, 467–476 (2012).
- J. L. Feldman, J. Baeza, J. M. Denu, *J. Biol. Chem.* **288**, 31350–31356 (2013).
- H. A. Tissenbaum, L. Guarente, *Nature* **410**, 227–230 (2001).
- B. Rogina, S. L. Helfand, *Proc. Natl. Acad. Sci. U.S.A.* **101**, 15998–16003 (2004).
- B. Rogina, S. L. Helfand, S. Frankel, *Science* **298**, 1745 (2002).
- C. Burnett *et al.*, *Nature* **477**, 482–485 (2011).
- K. K. Banerjee *et al.*, *Cell Reports* **2**, 1485–1491 (2012).
- J. H. Bauer *et al.*, *Aging* **1**, 38–48 (2009).
- M. Viswanathan, L. Guarente, *Nature* **477**, E1–E2 (2011).
- Y. Kanfi *et al.*, *Nature* **483**, 218–221 (2012).
- A. Satoh *et al.*, *Cell Metab.* **18**, 416–430 (2013).
- P. J. Fernandez-Marcos, J. Auwerx, *Am. J. Clin. Nutr.* **93**, 884S–890S (2011).
- Y. Nakahata, S. Sahar, G. Astarita, M. Kaluzova, P. Sassone-Corsi, *Science* **324**, 654–657 (2009).
- A. Murayama *et al.*, *Cell* **133**, 627–639 (2008).
- Z. Gerhart-Hines *et al.*, *Mol. Cell* **44**, 851–863 (2011).
- T. L. A. Kawahara *et al.*, *Cell* **136**, 62–74 (2009).
- E. Michishita *et al.*, *Nature* **452**, 492–496 (2006).
- R. Mostoslavsky *et al.*, *Cell* **124**, 315–329 (2006).
- D. Lombard *et al.*, *Mol. Cell Biol.* **27**, 8807–8814 (2007).
- M. D. Hirschey *et al.*, *Mol. Cell* **44**, 177–190 (2011).
- S. Someya *et al.*, *Cell* **143**, 802–812 (2010).
- W. C. Hallows *et al.*, *Mol. Cell* **41**, 139–149 (2011).
- A. S. Hebert *et al.*, *Mol. Cell* **49**, 186–199 (2013).
- M. D. Hirschey *et al.*, *Nature* **464**, 121–125 (2010).
- X. Qiu, K. Brown, M. D. Hirschey, E. Verdin, D. Chen, *Cell Metab.* **12**, 662–667 (2010).
- M. J. Rardin *et al.*, *Proc. Natl. Acad. Sci. U.S.A.* **110**, 6601–6606 (2013).
- C. B. Peek *et al.*, *Science* **342**, 1243417 (2013).
- K. Schmeisser *et al.*, *Nat. Chem. Biol.* **9**, 693–700 (2013).
- M. Ristow, S. Schmeisser, *Free Radic. Biol. Med.* **51**, 327–336 (2011).
- W. L. Kraus, *Mol. Cell* **58**, 902–910 (2015).
- R. H. Houtkooper, C. Cantó, R. J. Wanders, J. Auwerx, *Endocr. Rev.* **31**, 194–223 (2010).
- F. J. Bock, T. T. Todorova, P. Chang, *Mol. Cell* **58**, 959–969 (2015).
- F. Y. Feng, J. S. de Bono, M. A. Rubin, K. E. Knudsen, *Mol. Cell* **58**, 925–934 (2015).
- C. López-Otin, M. A. Blasco, L. Partridge, M. Serrano, G. Kroemer, *Cell* **153**, 1194–1217 (2013).
- E. Eason, F. Tsang, C. Skinner, C. Wang, S. J. Lin, *Genes Dev.* **22**, 931–944 (2008).
- C. Cantó, K. J. Menzies, J. Auwerx, *Cell Metab.* **22**, 31–53 (2015).
- P. Bai *et al.*, *Cell Metab.* **13**, 461–468 (2011).
- N. Braidy *et al.*, *PLOS ONE* **6**, e19194 (2011).
- L. Mouchiroud *et al.*, *Cell* **154**, 430–441 (2013).
- J.-C. Amé *et al.*, *J. Biol. Chem.* **274**, 17860–17868 (1999).
- H. Jiang, J. H. Kim, K. M. Frizzell, W. L. Kraus, H. Lin, *J. Am. Chem. Soc.* **132**, 9363–9372 (2010).
- H. Mendoza-Alvarez, R. Alvarez-Gonzalez, *J. Biol. Chem.* **268**, 22575–22580 (1993).
- M. Pacholec *et al.*, *J. Biol. Chem.* **285**, 8340–8351 (2010).

- U. Kolthur-Seetharam, F. Dantzer, M. W. McBurney, G. de Murcia, P. Sassone-Corsi, *Cell Cycle* **5**, 873–877 (2006).
- S. B. Rajamohan *et al.*, *Mol. Cell Biol.* **29**, 4116–4129 (2009).
- J. Luo *et al.*, *Cell* **107**, 137–148 (2001).
- M. T. Valenzuela *et al.*, *Oncogene* **21**, 1108–1116 (2002).
- H. Vaziri *et al.*, *Cell* **107**, 149–159 (2001).
- M. Scheibye-Knudsen, E. F. Fang, D. L. Croteau, D. M. Wilson III, V. A. Bohr, *Trends Cell Biol.* **25**, 158–170 (2015).
- G. R. Wagner, P. M. Pride, C. M. Babbey, R. M. Payne, *Hum. Mol. Genet.* **21**, 2688–2697 (2012).
- E. F. Fang *et al.*, *Cell* **157**, 882–896 (2014).
- M. Scheibye-Knudsen *et al.*, *Cell Metab.* **20**, 840–855 (2014).
- T. Shimazu *et al.*, *Science* **339**, 211–214 (2013).
- P. Aksoy *et al.*, *Biochem. Biophys. Res. Commun.* **349**, 353–359 (2006).
- P. Aksoy, T. A. White, M. Thompson, E. N. Chini, *Biochem. Biophys. Res. Commun.* **345**, 1386–1392 (2006).
- M. T. Barbosa *et al.*, *FASEB J.* **21**, 3629–3639 (2007).
- Y. Hu, H. Wang, Q. Wang, H. Deng, *J. Proteome Res.* **13**, 786–795 (2014).
- C. J. Gross, L. M. Henderson, *J. Nutr.* **113**, 412–420 (1983).
- S. Garavaglia *et al.*, *Biochem. J.* **441**, 131–141 (2012).
- A. Grozio *et al.*, *J. Biol. Chem.* **288**, 25938–25949 (2013).
- D. C. Wallace, *Annu. Rev. Genet.* **39**, 359–407 (2005).
- A. P. Gomes *et al.*, *Cell* **155**, 1624–1638 (2013).
- J. Durieux, S. Wolff, A. Dillin, *Cell* **144**, 79–91 (2011).
- G. Karamanlidis *et al.*, *Cell Metab.* **18**, 239–250 (2013).
- R. Cerutti *et al.*, *Cell Metab.* **19**, 1042–1049 (2014).
- N. A. Khan *et al.*, *EMBO Mol. Med.* **6**, 721–731 (2014).
- C. Cantó *et al.*, *Nature* **458**, 1056–1060 (2009).
- D. Chen *et al.*, *Genes Dev.* **22**, 1753–1757 (2008).
- S. R. Costford *et al.*, *Am. J. Physiol. Endocrinol. Metab.* **298**, E117–E126 (2010).
- M. Fulco *et al.*, *Dev. Cell* **14**, 661–673 (2008).
- K. M. Ramsey *et al.*, *Science* **324**, 651–654 (2009).
- J. T. Rodgers *et al.*, *Nature* **434**, 113–118 (2005).
- T. D. Pugh *et al.*, *Aging Cell* **12**, 672–681 (2013).
- W. G. Kaelin Jr., S. L. McKnight, *Cell* **153**, 56–69 (2013).
- C. Cantó *et al.*, *Cell Metab.* **15**, 838–847 (2012).
- D. Kraus *et al.*, *Nature* **508**, 258–262 (2014).
- E. Pirinen *et al.*, *Cell Metab.* **19**, 1034–1041 (2014).
- S. J. Yang *et al.*, *J. Nutr. Biochem.* **25**, 66–72 (2014).
- J. Yoshino, K. F. Mills, M. J. Yoon, S. Imai, *Cell Metab.* **14**, 528–536 (2011).
- H. Massudi *et al.*, *PLOS ONE* **7**, e42357 (2012).
- K. M. Ramsey, K. F. Mills, A. Satoh, S. Imai, *Aging Cell* **7**, 78–88 (2008).
- P. Benleny, K. L. Bogan, C. Brenner, *Trends Biochem. Sci.* **32**, 12–19 (2007).
- P. Benleny *et al.*, *Cell* **129**, 473–484 (2007).
- A. Garten, S. Petzold, A. Körner, S. Imai, W. Kiess, *Trends Endocrinol. Metab.* **20**, 130–138 (2009).
- A. Garten *et al.*, *Nat. Rev. Endocrinol.* **11**, 535–546 (2015).
- E. R. Lunn, V. H. Perry, M. C. Brown, H. Rosen, S. Gordon, *Eur. J. Neurosci.* **1**, 27–33 (1989).
- T. G. Mack *et al.*, *Nat. Neurosci.* **4**, 1199–1206 (2001).
- L. Conforti, J. Gilley, M. P. Coleman, *Nat. Rev. Neurosci.* **15**, 394–409 (2014).
- T. Araki, Y. Sasaki, J. Milbrandt, *Science* **305**, 1010–1013 (2004).
- K. D. Brown *et al.*, *Cell Metab.* **20**, 1059–1068 (2014).
- A. A. Pieper *et al.*, *Cell* **142**, 39–51 (2010).
- H. De Jesús-Cortés *et al.*, *Proc. Natl. Acad. Sci. U.S.A.* **109**, 17010–17015 (2012).
- R. Tesla *et al.*, *Proc. Natl. Acad. Sci. U.S.A.* **109**, 17016–17021 (2012).
- T. C. Yin *et al.*, *Cell Reports* **8**, 1731–1740 (2014).
- G. Wang *et al.*, *Cell* **158**, 1324–1334 (2014).
- D. Herranz *et al.*, *Nat. Commun.* **1**, 3 (2010).
- J. A. Baur *et al.*, *Nature* **444**, 337–342 (2006).
- M. Lagouge *et al.*, *Cell* **127**, 1109–1122 (2006).
- J. N. Feige *et al.*, *Cell Metab.* **8**, 347–358 (2008).
- N. L. Price *et al.*, *Cell Metab.* **15**, 675–690 (2012).
- S. J. Mitchell *et al.*, *Cell Reports* **6**, 836–843 (2014).
- E. M. Mercken *et al.*, *Aging Cell* **13**, 787–796 (2014).
- H. W. Lim *et al.*, *J. Exp. Med.* **212**, 607–617 (2015).
- H. S. Kwon *et al.*, *J. Immunol.* **188**, 2712–2721 (2012).
- J. van Loosdregt *et al.*, *Blood* **115**, 965–974 (2010).
- R. E. Shackelford, K. Mayhall, N. M. Maxwell, E. Kandil, D. Coppola, *Genes Cancer* **4**, 447–456 (2013).

ACKNOWLEDGMENTS

We thank G. Howard for editing, J. Carroll and T. Roberts for graphics, and V. Fonseca for clerical assistance. We apologize to colleagues whose work we could not cite due to space constraints.

10.1126/science.aac4854

PERSPECTIVE

Gut microbiota and aging

Paul W. O'Toole* and Ian B. Jeffery

The potential for the gut microbiota to affect health has a particular relevance for older individuals. This is because the microbiota may modulate aging-related changes in innate immunity, sarcopaenia, and cognitive function, all of which are elements of frailty. Both cell culture-dependent and -independent studies show that the gut microbiota of older people differs from that of younger adults. There is no chronological threshold or age at which the composition of the microbiota suddenly alters; rather, changes occur gradually with time. Our detailed analyses have separated the microbiota into groups associated with age, long-term residential care, habitual diet, and degree of retention of a core microbiome. We are beginning to understand how these groups change with aging and how they relate to clinical phenotypes. These data provide a framework for analyzing microbiota-health associations, distinguishing correlation from causation, identifying microbiota interaction with physiological aging processes, and developing microbiota-based health surveillance for older adults.

Prolongation of life span is a triumph of modern medicine, with most citizens of developed countries now looking forward to four-score-years-plus on the planet. The challenge now is to promote health span and to reduce the duration and severity of morbidity that precedes death. Simultaneously, changes in family and societal structures mean that an increasing proportion of older people desire, or are required to be capable of, independent living. The greatest barrier to independent living is frailty. Frailty occurs because of the accumulation of disorders rather than the chronological age of an individual. An "organ" in the human body that might not be expected to follow the general trajectory of physiological decline is that consisting of the microorganisms in the gut. Bacterial cells in the gut do not age per se, but people growing older may begin to experience comorbidities associated with the gut and with gut bacteria. So the question naturally arises as to how the microbiota in the human gut might affect the aging process, or if the gut microbiota simply changes as a function of age.

The gut microbiota composition of the elderly differs considerably between individuals in the ELDERMET cohort that we have studied most extensively (1). We observed a shift in the microbiota toward a *Bacteroidetes*-predominated population in frailer older individuals compared to younger individuals (1). However the variation in the microbiota profiles of these elderly subjects is large, so this trend is minimally informative in terms of prediction of the phenotype. This large variance can be explained by external factors influencing the microbiota, such as diet, exercise and mobility, medication, and cohabitation patterns (2), even after adjusting for the inferior health of residential care subjects. To identify associations with the phenotype and external influencing factors, we need to identify patterns in the other-

wise heterogeneous microbiota populations within aging individuals. We have therefore performed a fine-detail analysis using model microbiota associations generated through the use of a data-mining technique that successfully identified four subpopulations within the microbiota that are associated with biological phenotypes (3).

Although not significantly associated with chronological aging, loss of diversity in the core microbiota groups is associated with increased frailty.

These subpopulations, or microbiota profiles, were operationally defined as core, reduced core, diversity-associated, and longstay/age associated. A single individual's microbiota profile can consist of one or more of these subprofiles, as well as a number of rare species and strains. Age-related changes in the microbiota that are least influenced by other environmental factors can be identified in a relatively homogeneous data set of community-dwelling people (Fig. 1A, top), and this gradient is mirrored by length of stay in residential care (Fig. 1B, top).

The mechanism of microbiota change with age is not totally understood because the importance of senescence of the gut and the altered physical environment therein has not yet been systematically investigated. Extreme-age people (centenarians) have a microbiota that differs from those of older adults (4), consistent with general age-related microbiota trends (Fig. 1). Lifestyle, and particularly diet, play a large role, since aging is often accompanied by a reduction in the amount and variety of fiber-containing foods, and there is

often a risk of malnutrition (2). Lower fiber intake leads to a decrease in microbiota diversity, which may be detrimental to gut health (5). The risk of malnutrition is associated with increased microbiota diversity, particularly with a coabundant *Clostridiales* subpopulation. This is admittedly a counterintuitive idea, because many studies have shown that in adults, higher microbiota diversity correlates with being healthier. However, the composition of the microbiota associated with the risk of malnutrition is also associated with age in the community-dwelling people and their duration of stay in residential care (3). The *Clostridiales* subpopulation is also significantly associated with increased frailty, even after adjusting for age, to a much greater degree than loss of gut microbiota diversity.

There is evidence that loss of gut microbiota diversity can occur and does affect the aging process. Although not significantly associated with chronological aging, loss of diversity in the core microbiota groups is associated with increased frailty and reduced cognitive performance. The microbiota changes associated with duration in long-term care can be treated as a proxy for the changes associated with biological aging (Fig. 1) and the known deterioration in health that occurs when people enter long-term care. The group of organisms that are affected the most by aging are the diversity-associated taxa, comprising *Prevotella* and associated genera (Fig. 1). Their abundance also declines rapidly once individuals enter long-term care (2), but these organisms occur in high proportions in less than half the community-dwelling subjects of the ELDERMET cohort to begin with (3). The core microbiota are those taxa that are present in the vast majority of the subjects in appreciable proportions and, thus in our study, any loss of these taxa defines a microbiota profile as low diversity (3). The core microbiota may decline and be supplanted by highly abundant species, but the full core microbiota is rarely lost. Thus, the microbiota associated with low diversity is a subset of the core microbiota.

The age-related changes in the microbiota that we observed in the ELDERMET data sets can largely be associated with diet and reduced abundance of taxa from the diversity-associated core group. However, several specific coabundant taxa do seem to be associated with old age and risk of malnutrition. In the fruit fly, *Drosophila melanogaster*, the composition and diversity of the microbiota are correlated with food intake and the bacteria associated with the food (6). Diet and the microbiota of *Drosophila* act in concert on the health of the fly (7); for example, the microbiota associated with young flies promotes amino acid harvest during undernutrition. In a *Drosophila* model of aging (6), an age-related taxonomic profile develops that is characterized by bacterial overgrowth, and acquisition of aging-related taxa associates with subsequent mortality (6). Targeting of aging-related taxa in *Drosophila* using antibiotics increased fly life span. Obviously one cannot directly extrapolate these findings to humans, but the fruit fly could still be a useful discovery tool and model for investigating

School of Microbiology and APC Microbiome Institute, University College Cork, Cork T12 Y337, Ireland.

*Corresponding author. E-mail: pwotoole@ucc.ie

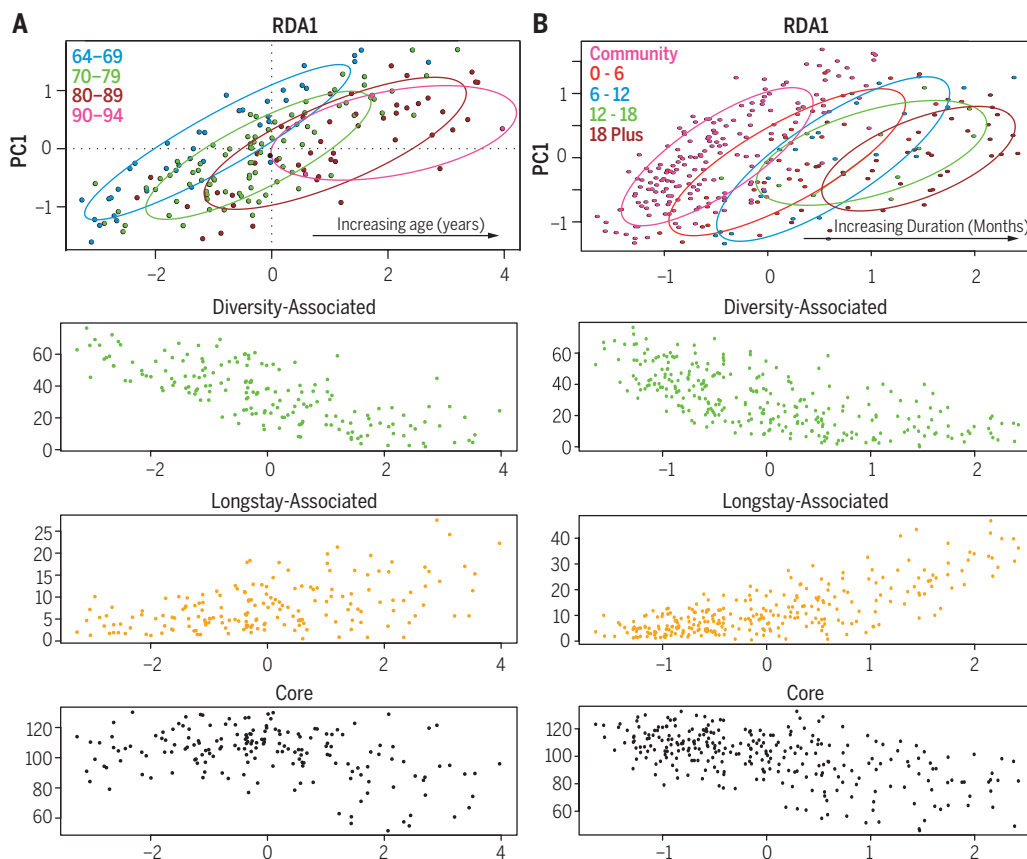


Fig. 1. Microbiota and aging. Top panels: Redundancy analysis plot of microbiota composition [log-transformed operational taxonomic unit (OTU) data set] of (A) community-dwelling individuals by age (in years), $n = 176$; $P < 0.002$. (B) Full data set of community and long-term residential care individuals by duration in care (logarithm of days), $n = 282$; $P < 0.001$. Lower panels indicate corresponding values for the OTUs of the indicated microbiota modules (sum of the log-transformed OTU abundances). Analysis was performed on ELDERMET microbiota data (3).

the drivers, consequences, and mechanisms of age-related microbiota change.

Our most detailed analysis of microbiota composition changes over time in the elderly was based on multiple time points and samples per individual (2). Previously we assumed that because the diversity in the long-stay subjects was lower than that of community dwellers, this led to instability of the microbiota, and when combined with the high-frequency use of antibiotics in the elderly population, the composition of the microbiota would be vulnerable to change (2). However, detailed investigation of the microbiota over time did not support a model of unstable low diversity. Over a 3-month period, a similar level of microbiota instability was seen among people living in the community and in those in long-stay residential homes, and antibiotic treatment increased instability in both subject groups. The real difference between community and long-stay microbiota types was detected when the microbiota was monitored for more than 6 months. In the community, these differences were similar to those occurring during the initial 3 months, whereas in the residential care population, this change was significantly

greater, indicating that changes were at least partially cumulative (3). The most unstable microbiota profiles, showing the largest shifts in composition, tended to be low-diversity profiles. After an initial change, diversity tended to recover best among people living in the community and less well in those in long-stay residential care.

Conclusion

Diet-microbiota-health interactions must be viewed in the broader context of the genetic and lifestyle changes that accompany aging, and the notable and sometimes conflicting effects of diet alone. For example, dietary restriction extends life span in a wide range of animal models from nematodes to Rhesus monkeys [reviewed in (7)], by mechanisms that include modulation of key pathways involved in nutrient sensing, metabolism, and inflammation. Restriction of specific amino acids can also be effective in increasing longevity. The activity of the innate immune system may also be directly influenced by members of the microbiota (8), making it challenging to dissect these mechanisms, especially in humans. As elderly people age and/or spend time in a long-stay res-

idential facility, they gain a long-stay-associated defined population of bacteria that are associated with increased frailty (Fig. 1). Centenarians also experience an overall decline in microbiome function (9), and these changes occur simultaneously with physiological loss of function. Considering the weight of evidence summarized elsewhere in this issue that the gut microbiota modulates or affects cardiometabolic and inflammatory processes, then the microbiota alterations that occur during aging may mean that some subjects are more prone to accelerated aging-related health loss. However, as some frailty-associated alterations may increase the diversity of the age-related microbiome, the assessment of diversity or stability by longitudinal sampling may be a less useful parameter to monitor than the phylogenetic composition of the microbiota. Several ongoing national and international studies, such as the NuAge project (10), will apply multi-omics analysis to determine if microbiota changes are correlative or causative of health loss and how other physiological processes are involved. This will establish if the microbiota could be a target for diagnostics that characterize aging health status, or could be a direct target for interventions that promote healthier aging by modulating the microbiota composition and function.

REFERENCES AND NOTES

1. M. J. Claesson *et al.*, *Proc. Natl. Acad. Sci. U.S.A.* **108** (suppl. 1), 4586–4591 (2011).
2. M. J. Claesson *et al.*, *Nature* **488**, 178–184 (2012).
3. I. B. Jeffery, D. B. Lynch, P. W. O'Toole, *ISME J.* 10.1038/ismej.2015.88 (2015).
4. E. Biagi *et al.*, *PLOS ONE* **5**, e10667 (2010).
5. H. J. Flint, K. P. Scott, P. Louis, S. H. Duncan, *Nat. Rev. Gastroenterol. Hepatol.* **9**, 577–589 (2012).
6. R. I. Clark *et al.*, *Cell Reports* **12**, 1656–1667 (2015).
7. L. Fontana, L. Partridge, *Cell* **161**, 106–118 (2015).
8. A. N. Hegazy, F. Powrie, *Science* **349**, 929–930 (2015).
9. S. Rampelli *et al.*, *Aging* **5**, 902–912 (2013).
10. A. Santoro *et al.*, *Mech. Ageing Dev.* **136–137**, 3–13 (2014).

ACKNOWLEDGMENTS

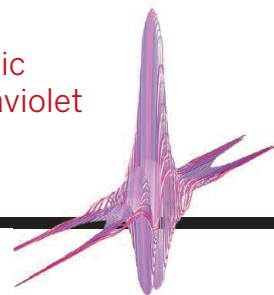
Work in the I.B.J. and P.W.O.T. laboratories is funded by awards from Science Foundation Ireland and the Department of Agriculture, Food, and the Marine of the government of Ireland and by General Mills International and the Kerry Group, who had no influence on the content of this review.

10.1126/science.aac8469

RESEARCH

Efficient high-harmonic generation in the ultraviolet

Popmintchev et al., p. 1225



IN SCIENCE JOURNALS

Edited by Stella Hurtley



Vulnerable short-tailed albatross (*Phoebastria albatrus*) nest in Japan and are responding to protection measures in Japan, Canada and the USA

PROTECTED AREAS

Not enough protection for migrating birds

Animals that migrate pass through a varying number of regions. Each of these regions contributes to a different component of their life cycles. Runge *et al.* looked at the degree of protection migratory birds receive, globally, across their breeding and wintering ranges. A remarkably low percentage of migratory birds receive adequate protection across their entire ranges. Given that over half the world's migratory bird populations are declining, these results emphasize the urgency with which we must act to protect birds across their entire migratory cycle. — SNV

Science, this issue p. 1255

SOLAR PHYSICS

Electron acceleration in solar flares

Magnetic reconnection during a solar flare releases energy into the Sun's atmosphere, some of which is converted

into accelerated particles in the plasma. Chen *et al.* combined radio and ultraviolet observations of a solar flare to identify the termination shock region where electrons are accelerated to relativistic speeds. They confirmed these results

with magneto-hydrodynamic simulations. This improved knowledge of the mechanism behind flares improves our understanding of the solar wind and space weather. — KTS

Science, this issue p. 1238

CATALYSIS

Faster elimination inside a cavity

Metals are adept at shuffling molecular bonds. They pry apart two atoms and then pair each one with a different partner. Sometimes the atoms get stuck on the metal, though, and the newly partnered products aren't released. Kaphan *et al.* designed a strategy for accelerating this elimination process (see the Perspective by Yan and Fujita). A hollow supramolecular capsule captured a gold or platinum complex and induced rapid bond formation between the carbon atoms in methyl groups bound to the metal. Generalization of this strategy could open the door to a wide range of chemical transformations that are currently held up by slow eliminations. — JSY

Science, this issue p. 1235; see also p. 1165

PALEOCLIMATOLOGY

Climate change and Norse migration patterns

It has been suggested that conditions of the Medieval Warm Period (~950–1250 CE) enabled the westward expansion of the Norse from Europe to Greenland and North America. The subsequent Little Ice Age (~1300–1850 CE) eventually drove their retreat from the western North Atlantic. Young *et al.* present chronological data for alpine glacial moraines on Baffin Island and western Greenland. Their findings suggest that cold conditions prevailed during the Medieval Warm Period in the eastern North Atlantic. This calls into question the notion that climate change alone led

to the retreat of the Norse from Greenland. — KVH

Sci. Adv. 10.1126/sciadv.1500806 (2015).

NEURODEVELOPMENT

Maturation of olfactory neurons

The sense of smell depends on neurons in the olfactory epithelium to perceive chemical scents. Each neuron specializes with one receptor. Hanchate *et al.* now show that the one-for-one relationship is not as simple as thought. As new neurons develop to replenish the olfactory epithelium, they initially express several different alleles of olfactory receptors. Then, as each neuron matures, they specialize to express a single receptor. — PJH

Science, this issue p. 1251

HUMAN GENETICS

Putting both heart and brain at risk

For reasons that are unclear, newborns with congenital heart disease (CHD) have a high risk of neurodevelopmental disabilities. Homsy *et al.* performed exome sequence analysis of 1200 CHD patients and their parents to identify spontaneously arising (de novo) mutations. Patients with both CHD and neurodevelopmental disorders had a much higher burden of damaging de novo mutations, particularly in genes with likely roles in both heart and brain development. Thus, clinical genotyping of patients with CHD may help to identify those at greatest risk of neurodevelopmental disabilities, allowing surveillance and early intervention. — PAK

Science, this issue p. 1262

EDUCATION

Toward a level playing field?

Do free learning resources benefit the disadvantaged and decrease gaps between rich and poor? Hansen and Reich studied the relationships between

socioeconomic status (SES) and enrollment in and completion of free Massive Open Online Courses (MOOCs) offered by Harvard and MIT. Students from low-SES backgrounds were less likely to enroll in MOOCs and earn a certificate than their high-SES peers. Thus, although there are many free online learning opportunities, it is not safe to assume that they will “level the playing field.” — BJ

Science, this issue p. 1245

WATER RESOURCES

Local decisions with global consequences

Some estimates suggest that humanity has already exceeded our sustainable global water footprint: the balance between fresh water use and supply. It seems that the situation may be more unsustainable than we realize. Jaramillo and Destouni analyzed hydroclimatic data for 100 large basins dating back to 1901. Better accounting of local water use revealed larger than anticipated effects on the global water cycle. For example, local regulation of surface water flow and expanded regional irrigation activities have increased global evapotranspiration rates. — NW

Science, this issue p. 1248

IMMUNOLOGY

When inhibitors don't mimic knockouts

The T helper 2 (T_H2) subset of lymphocytes releases cytokines implicated in the pathogenesis of asthma, a process that requires the kinase ITK. ITK-knockout mice are resistant to airway inflammation, suggesting that ITK inhibitors might be used to treat human asthma. However, Sun *et al.* found that an ITK-specific inhibitor aggravated disease symptoms in a mouse model of asthma. The airways of these mice had more T cells and higher levels of cytokines that are typically released by T_H2 lymphocytes. Thus, targeting ITK activity in asthma patients may exacerbate disease. — JFF

Sci. Signal. **8**, ra122 (2015).

IN OTHER JOURNALS

Edited by Kristen Mueller and Jesse Smith



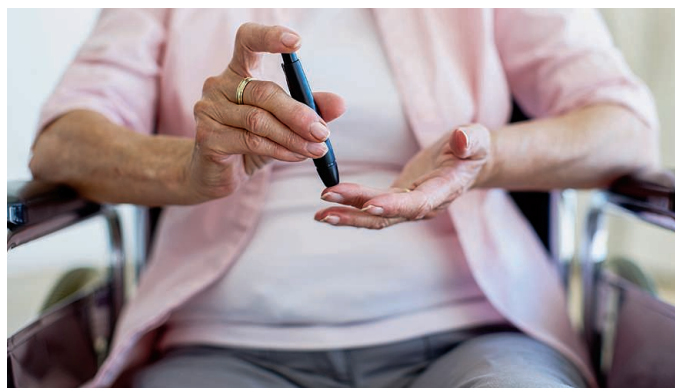
Airplane applying oil dispersant off the Louisiana coast

METABOLIC DISEASE

Inflammation improves insulin resistance

One of the hallmarks of diabetes is insulin resistance, a condition in which insulin accumulates because the body cannot effectively use it. Although insulin resistance occurs in both age- and obesity-associated diabetes, Bapat *et al.* now report that

the underlying cellular mechanisms that drive these diseases differ. An overzealous inflammatory response contributes to obesity-associated insulin resistance. In contrast, an immunosuppressive subset of T cells, called regulatory T cells (T_{reg}), promoted insulin resistance in aging mice. Aged but not obese mice that lacked these cells experienced improvement in



Suppressor T cells in fat tissue promote metabolic disease in aging mice

PHOTO: (FROM TOP) PATRICK SEMANSKY/AP IMAGES; STEEX/ISTOCK PHOTO

OIL SPILLS

Dispersants suppressed oil degradation

The 2010 Deepwater Horizon blowout released hundreds of millions of liters of oil into the Gulf of Mexico. One of the main mitigation strategies to prevent oil from reaching the shore—and potentially to stimulate natural bacterial communities capable of degrading oil and gas—was the application of 7 million liters of chemical dispersant. At the time, little was known about the effect these dispersants might have on hydrocarbon biodegradation rates. In a series of laboratory experiments, Kleindienst *et al.* observed that the same dispersant used in 2010 actually suppresses the major hydrocarbon-degrading groups in favor of dispersant-degrading bacteria. This confounding effect of dispersants therefore may explain why field data collected during the spill showed lower than expected biodegradation of oil and gas. — NW

Proc. Natl. Acad. Sci. U.S.A. 10.1073/pnas.1507380112 (2015).



multiple metabolic parameters. Scientists will need to determine whether T_{reg} in adipose tissue contribute to age-associated insulin resistance in humans and how they may do so. — KLM

Nature 10.1038/nature16151 (2015).

PROTEIN ENGINEERING

Engineering enzymes to stand alone

Enzymes efficiently synthesize many useful compounds. However, in many cases, their need to associate with other proteins limits their biosynthetic utility outside of cells. Buller *et al.* used directed evolution (a method of protein engineering that mimics of the process of natural selection) to increase the catalytic activity of the β subunit of the tryptophan synthase complex (TrpB). TrpB makes l-tryptophan from l-serine and indole but is inefficient on its

own. Mutations that restored activity to TrpB alone act through the same mechanism as partner protein binding. Both use a mechanism called allostery, in which changes distant from the active site affect enzymatic activity. The stand-alone TrpB provides a simplified platform to produce noncanonical amino acids. — VV

Proc. Natl. Acad. Sci. U.S.A. 10.1073/pnas.1516401112 (2015).

TRANSCRIPTION

Plants chemically modify their mRNAs

When *Arabidopsis* plants respond to stress, they often chemically modify their RNA transcripts; for instance, adding methyl groups to specific ribonucleotides. Such changes can alter RNA function and stability. In order to characterize such modifications on

RNAs transcribed from genes, Vandivier *et al.* performed a high-throughput annotation of modified ribonucleotides within mRNA. They found that modifications were not random but rather distributed to specific types of RNAs, such as on degrading transcripts and long noncoding RNAs, or specific sites within transcripts, such as regions that regulate RNA splicing. Overall, their studies suggest that marks regulate the stability of mRNA transcripts. — LMZ

Plant Cell 10.1105/tpc.15.00591 (2015).

X-RAY OPTICS

Guiding x-rays on a chip

For visible, infrared, and ultraviolet wavelengths of light, the ability to guide the light is very well served by a variety of mature platforms such as waveguides, optic fibers, and photonic crystals. Going to shorter wavelengths such as x-rays, however, provides a formidable challenge, because the light is penetrating and readily escapes attempts at confinement. By fabricating engineered channels in a layer of tantalum using electron beam lithography, Salditt *et al.* demonstrate the ability to guide hard x-rays in the curved waveguides and show that they can do so with channels of surprisingly small radii of curvature. The demonstration shows the possibility of extending the functionality of integrated optics to the x-ray regime. — ISO

Phys. Rev. Lett. **115**, 203902 (2015).

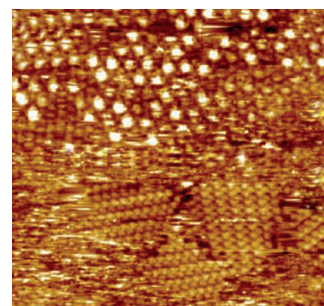
CANCER

Tumors evolve free of Darwinian constraints

Mutations help shape how tumors evolve. What constrains the diversity of these mutations is less clear. Ling *et al.* determined the spectrum of single-nucleotide variations in 286 samples from a single hepatocellular carcinoma tumor. They then modeled how mutations accumulated in tumors

using population genetic theory. Their analysis predicted that the tumor harbored more than 100 million mutations. Such high genetic diversity suggests that the tumors evolve in a non-Darwinian manner, because Darwinian evolution generally reduces genetic diversity within a population. These results imply that microscopic tumors are likely to be highly diverse, suggesting that even these tumors could quickly develop resistance in the face of therapy. — GR

Proc. Natl. Acad. Sci. U.S.A. 10.1073/pnas.1519556112 (2015).



Reversible surface configurations in a two-component network

MATERIALS SCIENCE

Switching locally or globally

Dynamic materials that can switch between two or more states have found a range of applications, from shape-memory materials to those with changeable surface adhesion properties. Lee *et al.* explore the properties of 1,3,5-tris(4-carboxyphenyl)benzene (BTB) absorbed from solution onto the surface of freshly cleaved, highly oriented pyrolytic graphite. BTB forms an open network structure and is able to accommodate polyaromatic guest molecules. However, though the application of a voltage bias, the network structure collapses, squeezing out the guest molecules in the local region. The same squeezing effect can also be achieved globally, by changing the temperature, thus giving two ways to tune the overall surface properties. — MSL

ACS Nano 10.1021/acsnano.5b06081 (2015).

ALSO IN SCIENCE JOURNALS

Edited by Stella Hurtley

HEART MITOCHONDRIA

A change of heart (mitochondria)

Mitochondria provide an essential source of energy to drive cellular processes and are particularly important in heart muscle cells (see the Perspective by Gottlieb and Bernstein). After birth, the availability of oxygen and nutrients to organs and tissues changes. This invokes changes in metabolism. Gong *et al.* studied the developmental transitions in mouse heart mitochondria soon after birth. Mitochondria were replaced wholesale via mitophagy in cardiomyocytes over the first 3 weeks after birth. Preventing this turnover by interfering with parkin-mediated mitophagy specifically in cardiomyocytes prevented the normal metabolic transition and caused heart failure. Thus, the heart has coopted a quality-control pathway to facilitate a major developmental transition after birth. Wai *et al.* examined the role of mitochondrial fission and fusion in mouse cardiomyocytes. Disruption of these processes led to “middle-aged” death from a form of dilated cardiomyopathy. Mice destined to develop cardiomyopathy were protected by feeding with a high-fat diet, which altered cardiac metabolism. — SMH

Science, this issue p. 1220, p. 1221;
see also p. 1162

PEROVSKITE LEDS

Brighter perovskite LEDs

Organic-inorganic hybrid perovskites such as methylammonium lead halides are attractive as low-cost light-emitting diode (LED) emitters. This is because, unlike many inorganic nanomaterials, they have very high color purity. Cho *et al.* made two modifications to address the main drawback of these materials, their low luminescent efficiency. They created nanograin materials lacking free

metallic lead, which helped to confine excitons and avoid their quenching. The perovskite LEDs had a current efficiency similar to that of phosphorescent organic LEDs. — PDS

Science, this issue p. 1222

LASER PHYSICS

Short wavelengths birth shorter ones

The shortest laser pulses—with durations measured in attoseconds—arise from a process termed high-harmonic generation (HHG). Essentially, a longer, “driving” pulse draws electrons out of gaseous atoms like a slingshot, and, when they ricochet back, light emerges at shorter wavelengths. Most HHG has been carried out using light near the visible/infrared boundary for the driving pulse. Popmintchev *et al.* used an ultraviolet driving pulse instead, which yielded an unexpectedly efficient outcome. These results could presage a more generally efficient means of creating x-ray pulses for fundamental dynamics studies as well as technological applications. — JSY

Science, this issue p. 1225

QUANTUM HALL EFFECT

Mixing interactions and superlattices

Under the influence of an external magnetic field, the energies of electrons in two-dimensional systems group into the so-called Landau levels. In the cleanest samples, interactions among electrons lead to fractional quantum Hall (FQH) states. If such a system is then subjected to a superlattice potential, it is unclear whether the fragile FQH states will survive. To address this question, Wang *et al.* sandwiched graphene between two layers of hexagonal boron nitride. Transport measurements on the superlattice showed that some FQH states did survive.

Furthermore, the interplay between interactions and the superlattice potential produced additional, anomalous states. — JS

Science, this issue p. 1231

BLACK HOLES

Magnetic fields near the event horizon

Astronomers have long sought to examine a black hole’s event horizon—the boundary around the black hole within which nothing can escape. Johnson *et al.* used sophisticated interferometry techniques to combine data from millimeter-wavelength telescopes around the world. They measured polarization just outside the event horizon of Sgr A*, the supermassive black hole at the center of our galaxy, the Milky Way. The polarization is a signature of ordered magnetic fields generated in the accretion disk around the black hole. The results help to explain how black holes accrete gas and launch jets of material into their surroundings. — KTS

Science, this issue p. 1242

GENE REGULATION

Broad versus restricted expression

Color vision in fruit flies requires the restricted expression of light-sensing rhodopsins with different wavelength sensitivities in subsets of photoreceptors. However, all photoreceptors express factors that transduce and amplify the visual signal. Rister *et al.* found that the distinct expression patterns are determined by a highly tunable regulatory motif. Genes that are broadly expressed have a palindromic variant of the motif. Spatially restricted rhodopsin genes display single-base-pair changes that alter the symmetry of the palindrome and are critical for subtype-specific expression. These findings on the differential regulation of

gene expression in fly photoreceptors have implications for the evolution of neuronal subtype diversity. — BAP

Science, this issue p. 1258

SOCIAL SCIENCE

Individuals, together against climate change

Can the actions of individuals play a role in preventing dangerous climate change? In a Perspective, O’Brien argues that both the speed and scale of the changes required to address climate change are so substantial that they cannot be left to governments and existing institutions. Individuals have tended to be overlooked as agents of such transformative change. Yet seemingly small actions of individuals and networks can have widespread global effects. Individuals can challenge deeply held notions that maintain habits and the status quo. By leading change, the actions of individuals can be a key part of effective mitigation of climate change, alongside technological and policy advances. — JFU

Science, this issue p. 1170

INFLUENZA

Stalking a flu vaccine

A universal flu vaccine has been a Sisyphean trial—despite successful seasonal vaccines, the immune system must start over when meeting newly mutated influenza strains. Andrews *et al.* took an in-depth look, over time, at the B cell response to the pandemic 2009 H1N1 vaccine. People with low titers of pre-existing antibodies were more likely to generate a broadly reactive response that targets the more conserved hemagglutinin (HA) stalk region, whereas those with higher levels of pre-existing antibodies responded by targeting the more variable HA head. The preexisting head antibodies were immunodominant and prevented clear access

to the stalk. These data suggest that recipients' exposure history will be critical in designing a universal flu vaccine. — ACC

Sci. Transl. Med. **7**, 316ra192 (2015).

ECOLOGY

Roads, roads everywhere

Over the past century, an ever-expanding network of roads has spread over our planet. In a Perspective, Haddad considers the environmental impacts of this network. Roads often lead to land-use change as people clear newly accessible land for agriculture or housing. Roads also fragment ecosystems and cause widespread wildlife losses through collisions with vehicles. Road planning and construction can help to protect wildlife from the worst effects of roads; for example, through the construction of wildlife corridors. However, these measures are not enough to prevent the habitat fragmentation and land-use change that accompany the growing global road network.

— JFU

Science, this issue p. 1166

RESEARCH ARTICLE SUMMARY

HEART MITOCHONDRIA

Parkin-mediated mitophagy directs perinatal cardiac metabolic maturation

Guohua Gong, Moshi Song, Gyorgy Csordas, Daniel P. Kelly, Scot J. Matkovich, Gerald W. Dorn II*

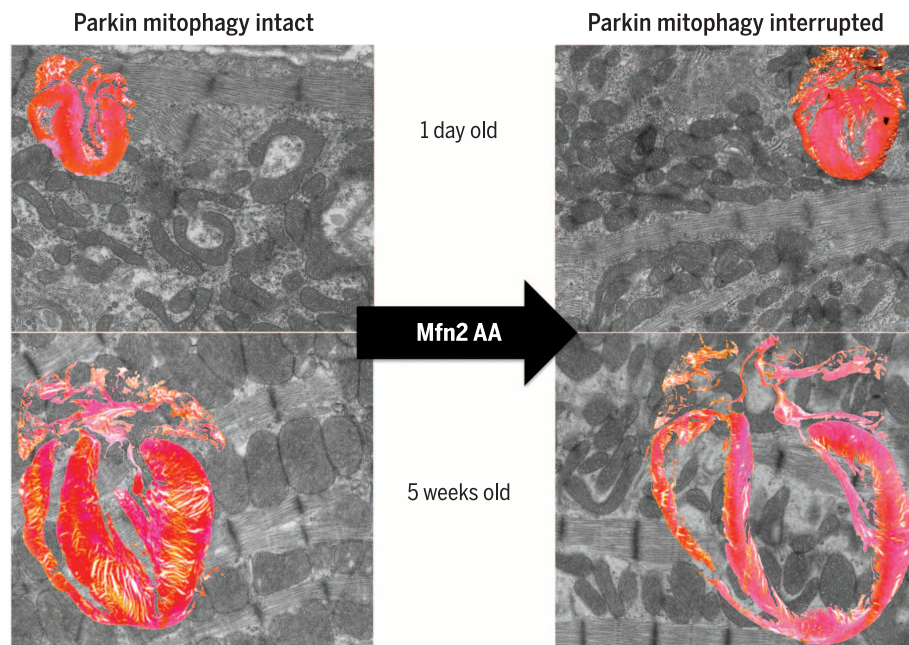
INTRODUCTION: During heart development, increased oxygenation during the early perinatal period and a change in nutrient availability evokes a switch in mitochondrial substrate preference from carbohydrates to fatty acids. This metabolic switching is reversed in adult heart disease. Genetic “reprogramming” of mitochondria plays a role in developmental and disease-related metabolic transitioning, but how mitochondrial plasticity is governed is unclear. Here, we found that mitophagy induced by PINK1-mitofusin 2 (Mfn2)–Parkin signaling was central to perinatal switching from glycolytic to fatty acid metabolism in mouse hearts. The Mfn2–Parkin interaction provoked generalized mitophagic removal of fetal cardiomyocyte mitochondria during the first 3 weeks of life and was a prerequisite for

introduction of mature cardiac mitochondria optimized for fatty acid metabolism.

RATIONALE: We considered that the highly ordered paracrystalline structure of ATP biosynthetic pathways makes it unlikely that mitochondria can behave as flexible fuel organelles, readily adjusting their metabolism to differing substrate availability. Rather, we posited that mitochondria optimized for a given metabolic milieu must be replaced when conditions change, as during the perinatal period. In support of this notion, late fetal and adult cardiomyocyte mitochondria have distinct morphologies as well as metabolic preferences. Because targeted autophagic elimination of individual damaged mitochondria (mitophagy) is mediated by the Parkinson’s disease factors

ON OUR WEB SITE

Read the full article at <http://dx.doi.org/10.1126/science.aad2459>



Mitochondrial maturation fails when mitophagy is interrupted. Normal perinatal mitochondrial maturation is shown on the left: Heart sections from neonatal and 5-week-old hearts are superimposed on their electron micrographs. To the right are similar images from hearts expressing the dominant negative mitochondrial Parkin receptor, Mfn2 AA. Retention of fetal cardiomyocyte mitochondria in mitophagically impaired hearts was lethal.

PINK1 and Parkin, we examined the consequences of cardiac-specific Parkin loss-of-function on perinatal mitochondrial maturation and metabolic transitioning in mouse hearts. Whereas Parkin deletion from adult hearts had no discernible adverse effects, cardiomyocyte-specific Parkin ablation from the first day of life was lethal in most mice before 3 weeks of age; in surviving mice, mitochondrial maturation was arrested at the fetal stage.

RESULTS: To interrupt Parkin-mediated mitophagy with more precision than gene ablation, we expressed PINK1 T111 and S442 phosphorylation site Mfn2 mutants. In cultured fibroblasts, the glutamic acid (E) substituted phosphomimetic mutant Mfn2 EE spontaneously recruited Parkin to mitochondria and promoted mitophagy, whereas alanine (A) substituted nonphosphorylatable Mfn2 AA prevented Parkin translocation and interrupted mitophagy stimulated by mitochondrial depolarization.

We expressed wild-type Mfn2, Mfn2 EE, and Mfn2 AA in mouse hearts. Mfn2 AA, when expressed perinatally but not at or after weaning, provoked cardiomyopathy that was lethal by 7 to 8 weeks. Cardiomyocyte mitochondria of surviving young adult Mfn2 AA mice had an eccentric morphology and impaired palmitoylcarnitine use, which are typical features of fetal heart mitochondria. The transcriptional signature of juvenile Mfn2 AA hearts was distinguished from age-matched controls by depressed abundance of fatty acid and branched chain amino acid metabolism messenger RNAs, again resembling fetal hearts. Mitochondrial biogenesis was impaired, and metabolite profiling of young adult Mfn2 AA hearts revealed developmental metabolic arrest at the perinatal stage—that is, impaired fatty acid use and preserved glycolytic function. Thus, interrupting Parkin-mediated mitophagy in perinatal mouse hearts prevented normal maturational metabolic transitioning to fatty acids through retention of fetal cardiomyocyte mitochondria. Mitophagy was a prerequisite for mitochondrial biogenesis in this context.

CONCLUSION: Fetal cardiomyocyte mitochondria undergo perinatal PINK1–Mfn2–Parkin-mediated mitophagy and replacement by mature adult mitochondria, rather than transcriptional reprogramming. Mitophagic mitochondrial removal underlies developmental cardiomyocyte mitochondrial plasticity and metabolic transitioning. Facilitating developmentally programmed mitochondrial turnover is functionally distinct from canonical selective targeting and removal of damaged mitochondria by Parkin in other contexts. ■

The list of author affiliations is available in the full article online.

*Corresponding author. E-mail: gdorn@dom.wustl.edu
Cite this article as G. Gong et al., *Science* 350, aad2459 (2015). DOI: 10.1126/science.aad2459

RESEARCH ARTICLE

HEART MITOCHONDRIA

Parkin-mediated mitophagy directs perinatal cardiac metabolic maturation in mice

Guohua Gong,^{1*} Moshi Song,^{1*} Gyorgy Csordas,² Daniel P. Kelly,³ Scot J. Matkovich,¹ Gerald W. Dorn II^{1†}

In developing hearts, changes in the cardiac metabolic milieu during the perinatal period redirect mitochondrial substrate preference from carbohydrates to fatty acids. Mechanisms responsible for this mitochondrial plasticity are unknown. Here, we found that PINK1-Mfn2-Parkin-mediated mitophagy directs this metabolic transformation in mouse hearts. A mitofusin (Mfn) 2 mutant lacking PINK1 phosphorylation sites necessary for Parkin binding (Mfn2 AA) inhibited mitochondrial Parkin translocation, suppressing mitophagy without impairing mitochondrial fusion. Cardiac Parkin deletion or expression of Mfn2 AA from birth, but not after weaning, prevented postnatal mitochondrial maturation essential to survival. Five-week-old Mfn2 AA hearts retained a fetal mitochondrial transcriptional signature without normal increases in fatty acid metabolism and mitochondrial biogenesis genes. Myocardial fatty acylcarnitine levels and cardiomyocyte respiration induced by palmitoylcarnitine were concordantly depressed. Thus, instead of transcriptional reprogramming, fetal cardiomyocyte mitochondria undergo perinatal Parkin-mediated mitophagy and replacement by mature adult mitochondria. Mitophagic mitochondrial removal underlies developmental cardiomyocyte mitochondrial plasticity and metabolic transitioning of perinatal hearts.

Mammalian hearts depend on mitochondrial oxidative phosphorylation to fuel myocardial contraction and pump function; catabolism of carbohydrates or fats generates adenosine triphosphate (ATP) that powers excitation-contraction coupling. Under conditions of optimal intrinsic mitochondrial functioning—i.e., when mitochondria are “fit”—energy demands and access to metabolic substrates and oxygen are central determinants of mitochondrial respiration. During organism development, both substrate availability and tissue oxygen content change. Accordingly, the increase in transplacental oxygen exchange in early embryos provokes a shift from anaerobic glycolysis to aerobic mitochondrial respiration (1). After birth, loss of transplacental carbohydrate substrates promotes a further transition to fatty acid metabolism (2) as small, fetal cardiomyocyte mitochondria are supplanted by adult organelles (3). The normal perinatal developmental conversion from glucose to fatty acid cardiac metabolism, and its maladaptive reversal back toward glucose in diseased adult hearts, have been linked

to changes in metabolic gene expression, so-called “metabolic reprogramming” (4). Cellular mechanisms underlying these cardiac metabolic transitions are poorly described, and conventional wisdom has been that mitochondria are “flexible fuel” organelles capable of switching back and forth between carbohydrate and fatty acid metabolism (5).

Stochastic damage to cardiomyocyte mitochondria places hearts at risk from bioenergetic insufficiency or reactive oxygen species (ROS)-mediated cytotoxicity (6). It is believed that maintaining mitochondrial functional integrity requires continuous surveillance and culling of dysfunctional organelles. In cultured fibroblasts, depolarized mitochondria are identified, sequestered, and eliminated through directed autophagy followed by lysosomal destruction (mitophagy). This form of mitochondrial quality control is mediated in part by two Parkinson’s disease factors, the E3 ubiquitin ligase Parkin and its upstream activating kinase, phosphatase and tensin homolog (PTEN)-induced putative kinase 1 (PINK1) (7, 8). By removing impaired organelles, the overall fitness of the mitochondrial collective is preserved.

The observation that glycolytic metabolism is preferred in fetal hearts, but is maladaptive in diseased adult hearts (4), indicates that mitochondrial fitness is neither a specific nor a unique condition. Rather, mitochondria are “fit” when they demonstrate optimal functional compatibility for a given developmental or pathophysiological milieu. In this context, the idea that mitochon-

drial quality must be actively controlled applies not just to selective culling of individual damaged mitochondria but also to generalized cell- and organ-wide promotion of mitochondrial turnover during developmental or disease-related transitions of cellular fuel and energy metabolism. A possible role for mitophagic mitochondrial replacement during metabolic transitions has not been addressed, in part because developmental phenotypes are not observed in otherwise normal mice systemically lacking Parkin (9, 10). However, absence of phenotypes in Parkin-deficient mice may simply reflect opportunistic compensation by Parkin-independent mitophagy pathways (11).

Here, we set out to clarify the role of Parkin-mediated mitochondrial turnover in the normal developmental switch from carbohydrate to fatty acid-based metabolism in perinatal mouse hearts. To avoid confounding effects of germline and cardiac-specific Parkin ablation, we developed and deployed *in vitro* and *in vivo* systems in which expression of a mitofusin 2 (Mfn2) mutant lacking PINK1 phosphorylation sites essential for its binding of Parkin suppressed Parkin translocation to mitochondria, thus specifically interrupting Parkin-dependent mitophagy.

Parkin is essential for perinatal mitochondrial maturation in cardiomyocytes

Cardiomyocyte mitochondria of 1-day-old mice exhibit the typical elongated, curvilinear morphology of human fetal heart mitochondria (3) but mature over 3 weeks into the larger ovoid mitochondrial structure and denser collective that is characteristic of adult mammalian hearts (Fig. 1A). Cardiomyocyte-specific ablation of *Park2*, encoding Parkin, on perinatal day 1 (P1) was rapidly lethal in most mice. However, a small number of “escapers” survived until P21. Polymerase chain reaction (PCR) analysis revealed incomplete Cre-mediated *Park2* gene recombination in the hearts of these mice (Fig. 1B), suggesting that partial Parkin insufficiency induced a *forme fruste* of the early lethal cardiac Parkin deletion phenotype. Compared with normal littermates, P21 Parkin-insufficient hearts appeared slightly smaller (Fig. 1, C and D). Myocardial histology of Parkin-deficient hearts was unremarkable (Fig. 1, C and D), but ultrastructural imaging of myocardium from surviving 3-week-old perinatal cardiac Parkin-insufficient mice revealed mitochondria having a morphology typical of fetal hearts (Fig. 1C), whereas control (*Park2* *fl/fl*) littermate mitochondria had the morphology of normal adult hearts (Fig. 1D). Furthermore, perinatal Parkin-deficient hearts had abundant homogeneous inclusions with smooth borders, characteristic of lipid droplets (Fig. 1C). Lethality of perinatal cardiac-specific *Park2* ablation, together with findings of surviving escaper mice, suggested that Parkin may be essential for maturational development of cardiomyocyte mitochondria. However, the aggressive phenotype confounded attempts to determine underlying mechanisms. Accordingly, we built upon previous

¹Center for Pharmacogenomics, Department of Internal Medicine, Washington University School of Medicine, St. Louis, MO, USA. ²Department of Pathology, Anatomy, and Cell Biology, Thomas Jefferson University, Philadelphia, PA, USA. ³Center for Metabolic Origins of Disease, Cardiovascular Metabolism Program, Sanford Burnham Prebys Medical Discovery Institute, Orlando, FL, USA.

*These authors contributed equally to this work. †Corresponding author. E-mail: gdorn@dom.wustl.edu

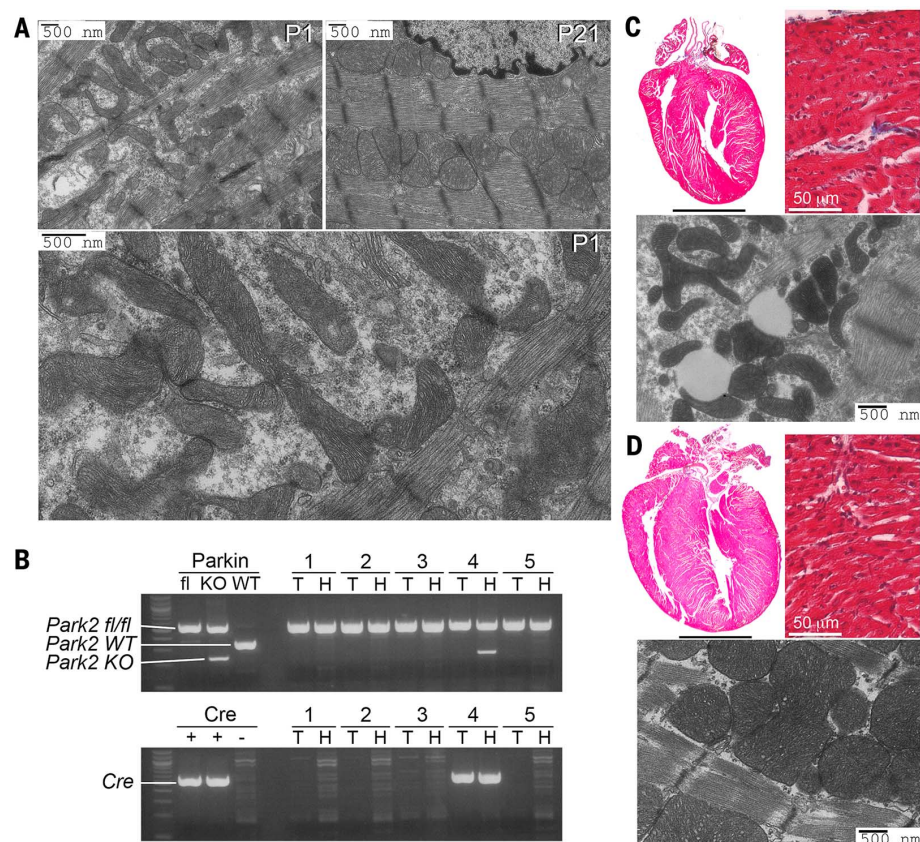


Fig. 1. Early lethality of perinatal cardiomyocyte-specific Parkin-deficient mice. (A) Transmission electron microscopy (TEM) showing normal cardiomyocyte mitochondria on the first (P1) and 21st (P21) day of life. Enlargement shows structural details at P1. (B) PCR genotyping of floxed *Parkin* gene (top) and tamoxifen-inducible cardiac Cre (bottom) of surviving mice from a representative litter at P21; three mice died before weaning. KO indicates Cre recombined *Parkin* fl/fl allele. T is tail DNA; H is heart DNA. (C and D) Representative (of three) hearts, histological sections, and TEMs from P21 cardiac Parkin-deficient (top) and control (bottom) mice. Scale bars for hearts are 2 mm.

observations that Parkin fails to translocate to depolarized mitochondria of Mfn2-deficient mice (12, 13), and the discovery that PINK1 phosphorylation of Mfn2 promotes Mfn2-Parkin binding (12), to develop a system in which Parkin-mediated mitophagy could be conditionally interrupted in vitro or in vivo without primarily targeting either Parkin or PINK1.

Mutational interdiction of Mfn2 phosphorylation by PINK1 inhibits Parkin-mediated mitophagy

PINK1 is stabilized and accumulates in depolarized mitochondria (14) and phosphorylates Mfn2 (Fig. 2A), enabling its binding to Parkin (12). Mimicking Mfn2 phosphorylation by substituting glutamic acid (E) for the critical threonine and serine (Mfn2 T111E/S442E; Mfn2 EE) induces PINK1-independent Mfn2-Parkin association (12) and promotes spontaneous Parkin recruitment to mitochondria of cultured fibroblasts (Fig. 2B and fig. S1). Nonphosphorylatable alanine (A) substitution at the same sites (Mfn2 AA) had reciprocal effects, preventing PINK1-mediated Mfn2-Parkin binding (12) and suppressing Parkin translocation provoked by the

mitochondrial uncoupling agent carbonyl cyanide *p*-trifluoromethoxyphenylhydrazone (FCCP) (Fig. 2B and fig. S1). Effects of Mfn2 EE and Mfn2 AA on Parkin translocation were concordant with stimulation or inhibition, respectively, of mitochondrial-lysosomal interactions (Fig. 2C and fig. S1). In agreement with Mfn2 EE functioning as a constitutive mitochondrial Parkin receptor, it failed to evoke mitophagy in Parkin-deficient cells (fig. S2). Although the mitophagy response to FCCP was reduced in PINK1-deficient cells, Mfn2 EE nevertheless promoted spontaneous Parkin translocation (fig. S3). Because nonphosphorylatable Mfn2 AA inhibited Parkin localization to mitochondria without primarily affecting PINK1 or Parkin, we used it to interrupt PINK1-Parkin-mediated mitophagy without adversely affecting nonmitophagic Parkin functionality (15).

We asked whether Mfn2 phosphorylation of T111 and S442 modified other cellular actions of Mfn2. Mfn2 promotes outer mitochondrial membrane tethering and fusion (16). Nonphosphorylatable Mfn2 AA was as effective as wild-type (WT) Mfn2 for inducing mitochondrial fusion in either WT or Mfn2-deficient fibroblasts; pseudo-phosphorylated Mfn2 EE did not promote fusion,

instead evoking mitochondrial shortening (Fig. 2D and figs. S1 to S3). Thus, Parkin binding and mitochondrial outer membrane fusion are mutually exclusive functions of Mfn2 regulated by PINK1-mediated phosphorylation.

Mitochondrial fragmentation is functionally linked to mitophagy (17). We asked whether the absence of fusion-promoting activity for the phosphomimic Mfn2 EE was sufficient to provoke mitophagy. FCCP-stimulated Parkin translocation and lysosomal-mitochondrial colocalization were examined in cells expressing a naturally occurring fusion-defective human Mfn2 mutant, R400Q, in which PINK1 phosphorylation sites are intact (18). Mfn2 R400Q induced mitochondrial shortening similar to Mfn2 EE but did not promote Parkin translocation or mitophagy (fig. S4). Thus, inhibition of mitochondrial fusion and mitochondrial recruitment of Parkin by Mfn2 are not functionally coupled, except through PINK1-mediated Mfn2 phosphorylation. Finally, we determined whether phosphorylation of Mfn2 on T111 and S442 affected its binding of Miro mitochondrial transport proteins (19). WT Mfn2, Mfn2 AA, and Mfn2 EE each bound Miro1 and Miro2, exhibiting the previously reported preference for Miro2 (fig. S5). Mitochondrial fusion and Parkin translocation are therefore reciprocally and uniquely regulated by PINK1-mediated phosphorylation of Mfn2 on T111 and S442.

Perinatal inhibition of Parkin-mediated mitophagy induces lethal cardiomyopathy

Because Mfn2 AA promoted mitochondrial fusion similar to WT Mfn2, but inhibited mitochondrial Parkin localization, we used it to dissect the role of Parkin-mediated mitophagy in mouse hearts. Both separation-of-function Mfn2 mutants (EE and AA) were expressed using a bitransgenic doxycycline-suppressible cardiomyocyte-specific *Myh6* promoter system (Fig. 3A); cardiac transgene expression can be suppressed with doxycycline, but in its absence, such expression begins shortly after birth (20). WT Mfn2 was expressed separately as a control for increased myocardial Mfn2 content (Fig. 3A, top). In vivo regulation of cardiac mitophagy by Mfn2 EE and Mfn2 AA was assessed by crossing Mfn2 EE and Mfn2 AA mice to mice conditionally expressing Parkin using the same doxycycline-suppressible *Myh6*-driven expression system (21) and concomitantly inducing the Mfn2 and Parkin transgenes in adult mice. Mitochondrial localization of Parkin, increased ubiquitination of mitochondrial proteins, and mitochondrial localization of the autophagosomal docking protein, p62/Sequestosome 1 (SQSTM1), were enhanced in Mfn2 EE/Parkin hearts but reduced in Mfn2 AA/Parkin hearts, compared with Parkin-overexpressing controls (Fig. 3A, bottom). These in vivo results recapitulate the in vitro effects of the Mfn2 phosphorylation mutants on mitophagy.

Mice expressing WT Mfn2 or Mfn2 EE from birth (i.e., those that never received doxycycline) appeared normal (Fig. 3, B to E, and fig. S6). In contrast, cardiac expression of Mfn2 AA at similar

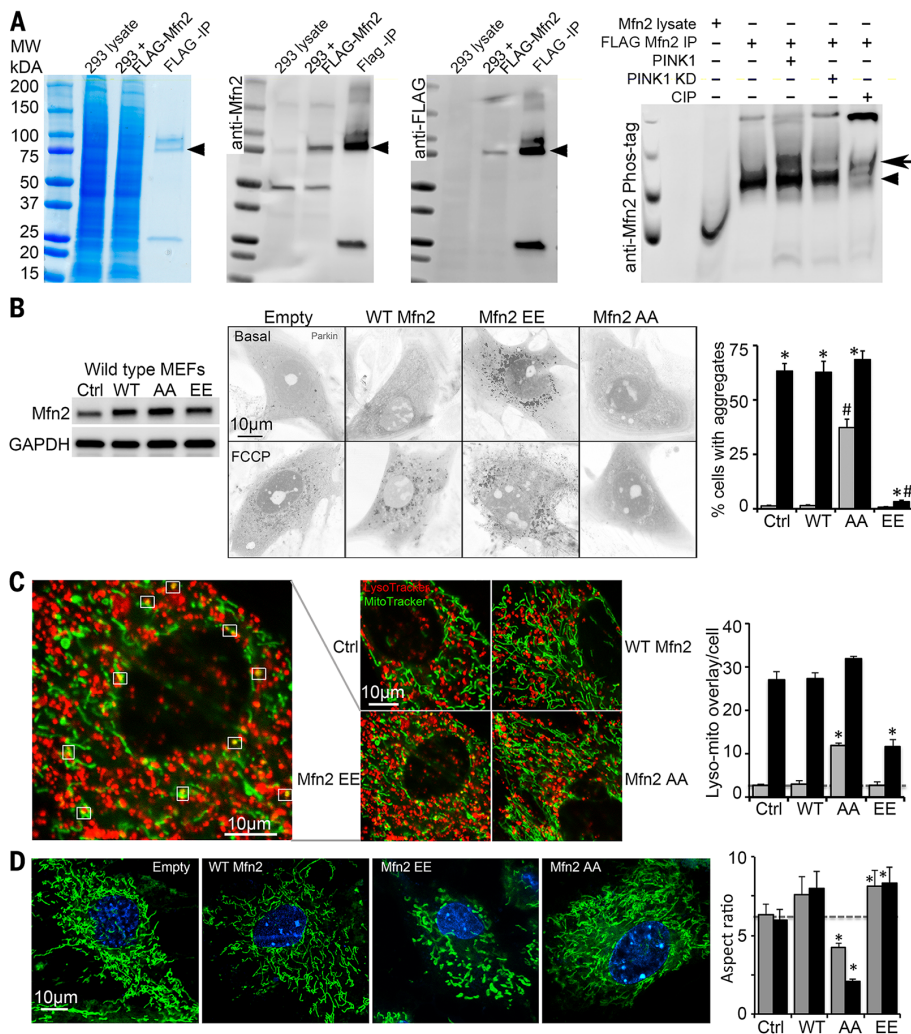


Fig. 2. Mitochondrial Parkin mobilization directed by pseudo-PINK1 phosphorylated Mfn2. (A) Phosphorylation of Mfn2 by recombinant PINK1 in a cell-free system. First three panels show enrichment of FLAG-Mfn2 by immunoprecipitation (IP) with antibody to FLAG (anti-FLAG); left is Coomassie blue stained gel, middle is anti-Mfn2 immunoblot, right is anti-FLAG immunoblot. Fourth panel shows anti-Mfn2 Phos-tag immunoblot of in vitro PINK1 phosphorylation reactants; KD is kinase dead PINK1; CIP is calf intestinal phosphatase. Arrowheads show FLAG-Mfn2; bold arrow indicates phospho-Mfn2. (B) Spontaneous maraschino cherry (mc) Parkin translocation in MEFs provoked by adeno-Mfn2 EE, and FCCP-mediated mcParkin translocation suppressed by adeno-Mfn2 AA. To the left is an immunoblot of Mfn2. (C) Lysosomal-mitochondrial interactions (white squares) provoked by adeno-Mfn2 EE and suppressed by adeno-Mfn2 AA. (D) Mitochondrial elongation (aspect ratio) inhibited by adeno-Mfn2 EE and stimulated by adeno-Mfn2 AA. WT is wild-type adeno-Mfn2. In (B) and (C), gray bars are basal; the black bars are 60 min after FCCP or antimycin A. In (D), gray bars are 24 hours and black bars are 48 hours after adeno-Mfn2 virus infection. *, $P < 0.05$ versus adeno β -gal control (Ctrl); #, $P < 0.05$ versus same condition WT adeno-Mfn2.

levels from birth (Fig. 3A) was uniformly lethal by 7 to 8 weeks of age in two independent transgenic lines (Fig. 3, B and C). Cardiac dilatation (Fig. 3, B and D), worsening pump function (Fig. 3D), and pulmonary congestion (Fig. 3E) identified progressive cardiomyopathy as the underlying process and heart failure as the terminal event. Myocardium from surviving 6-week-old Mfn2 AA mice exhibited cardiomyocyte enlargement and replacement fibrosis (Fig. 3F). TUNEL (terminal deoxynucleotidyl transferase-mediated deoxyuridine triphosphate nick end labeling) staining was

increased proportionally to in vivo Evans blue labeling without caspase 3 processing, revealing necrosis to be the likely mechanism for Mfn2 AA-induced cardiomyocyte dropout (fig. S7, A to C). However, there were no differences in the size of Mfn2-dependent mitochondrial-sarcoplasmic reticulum interfaces (22) in WT-Mfn2 and Mfn2 AA-expressing mice (fig. S7D), showing that interorganelle tethering by Mfn2 (23) was not perturbed by preventing T111 and S442 phosphorylation. Remarkably, cardiac Mfn2 AA induction at the time of weaning (~3 weeks) or in

young adult mice (8 weeks) evoked no cardiac pathology (fig. S8). Thus, Parkin localization to Mfn2 on cardiomyocyte mitochondria is essential only between birth and weaning.

Parkin-mediated mitophagy is essential for perinatal cardiomyocyte mitochondrial maturation

The only molecular differences between cardiac WT Mfn2 and Mfn2 AA mice were two nonphosphorylatable amino acids (fig. S9). Yet, the cardiac phenotype of the former was benign, whereas the latter developed lethal juvenile cardiomyopathy. Because Mfn2 AA promoted mitochondrial fusion as well as WT Mfn2 (Fig. 2D and fig. S1D), and the Mfn2 AA mutation did not affect other Mfn2 functions (figs. S5 and S7), we reasoned that the Mfn2 AA cardiomyopathy was caused by suppressing Parkin-mediated mitophagy. In agreement with this idea, mitochondria-associated Parkin and p62/SQSTM1 were both reduced in the hearts of 2- to 3-week-old Mfn2 AA mice, compared with age-matched WT Mfn2 mice (Fig. 4A, top). Mitochondrial Parkin association was likewise depressed by Mfn2 AA in hearts of 2- to 3-week-old food-deprived mice, but mitochondrial-associated p62/SQSTM1 was increased (Fig. 4A, bottom). Thus, Mfn2 AA inhibits developmentally programmed Parkin-mediated mitophagy, but not Parkin-independent mitochondrial autophagy provoked by starvation.

Multiple lines of evidence revealed a deterioration in mitochondrial quality specific to Mfn2 AA hearts, including impaired maximal mitochondrial respiration (Fig. 4B), increased mitochondrial production of O_2^- and H_2O_2 (Fig. 4C), and modest increases in levels of the mitochondrial stress proteins fibroblast growth factor 21 (FGF21), heat shock protein 60 (Hsp60), Lon peptidase 1 (LONP1), and adenosine triphosphatase family gene 3-like 2 (AFG3L2) (fig. S10). By comparison, liver and skeletal muscle mitochondria from cardiac-expressing Mfn2 AA mice were normal (fig. S11).

Reduced myocardial content of mitochondrial proteins (Fig. 4D and fig. S12) and decreased flow cytometric forward scatter (Fig. 4E) pointed to abnormalities in the abundance and morphology of cardiac mitochondria of 6-week-old Mfn2 AA mice. Ultrastructural examination revealed small, unusually shaped cardiomyocyte mitochondria (Fig. 4F and fig. S13). Decreased respiratory complex protein abundance reflected lower mitochondrial content in Mfn2 AA hearts (Fig. 4G). In agreement with absence of cardiac phenotypes when Mfn2 AA expression was induced at or after weaning (fig. S8A), mitochondrial respiration, morphometry, and ROS production were normal in those mice (fig. S14).

Mitochondrial morphology of young adult Mfn2 AA mouse hearts resembled that of both normal postnatal (P1) mouse hearts and P21 cardiac Parkin-deficient mouse hearts (compare Fig. 4F to Fig. 1, A and D). The transition of mouse cardiac mitochondria from fetal to adult morphology normally occurs within the first 3 weeks of life (Fig. 1), concurrent with a functional

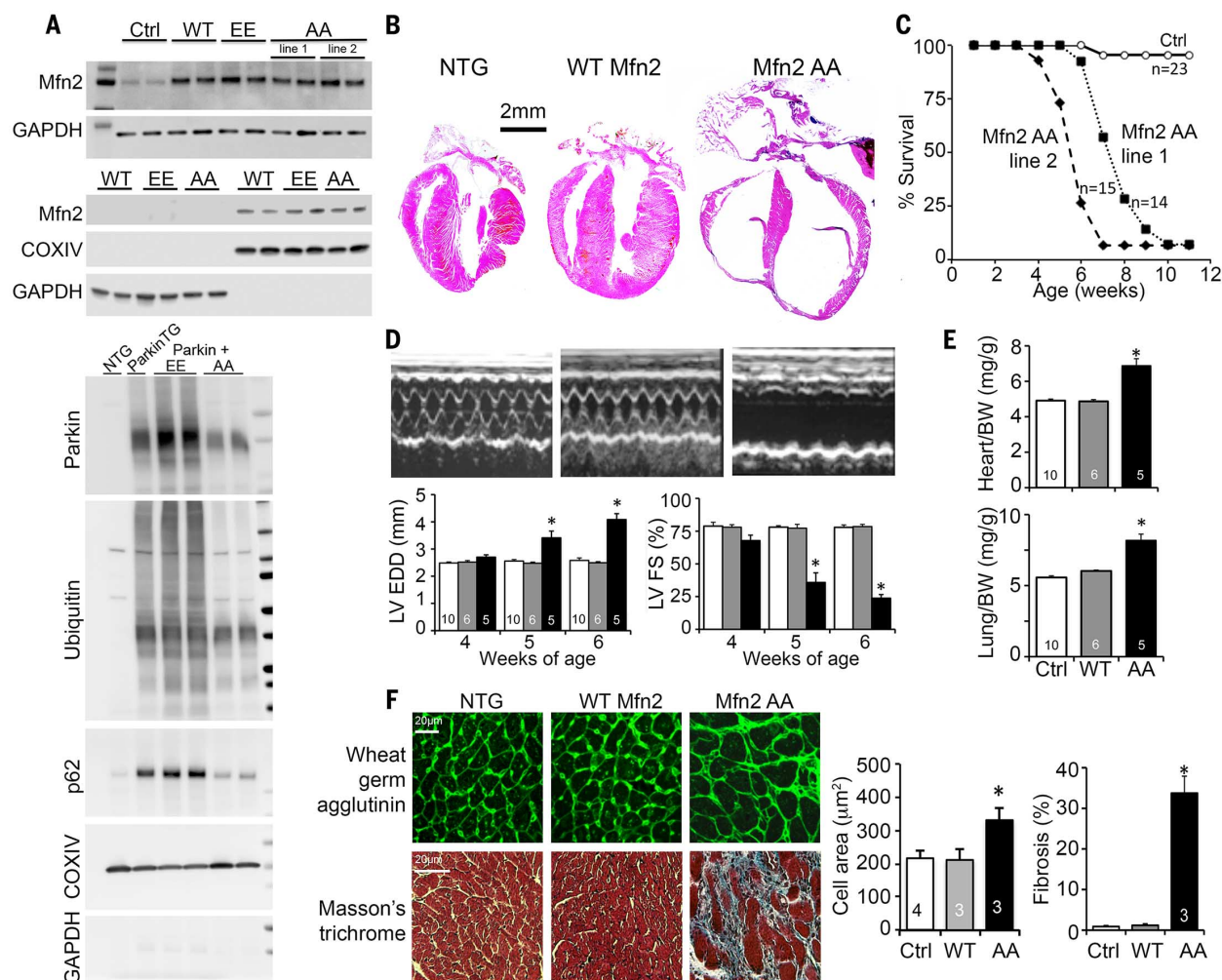


Fig. 3. Perinatal cardiomyopathy evoked by nonphosphorylated Mfn2 AA.

(A) Immunoblot analysis of Mfn2 expression (top) and mitochondrial Parkin localization (bottom) in transgenic mouse hearts. (Top) Top pair is cardiac homogenate; bottom pair is mitochondrial-enriched 10,000 g pellet (cytochrome oxidase IV; COX IV) and postmitochondrial supernatant [glyceraldehyde-3-phosphate dehydrogenase (GAPDH)]. (Bottom) Immunoblot analysis of mitochondrial-associated Parkin and downstream mitophagy events and their

modulation by cardiac-expressed Mfn2 EE and Mfn2 AA. (B) Representative hearts of 6-week-old mice. (C) Survival. (D) Serial echocardiographic data of 4- to 6-week-old mice; white bars are Ctrl, gray is WT Mfn2, and black is Mfn2 AA. (E) Heart (top) and lung (bottom) weights of 6-week-old mice indexed to body weight (BW). (F) Histological studies of cardiomyocyte cross-sectional area (top) and myocardial fibrosis (bottom); quantitative data are on the right. * $P < 0.05$ versus WT Mfn2 and nontransgenic (NTG) control.

shift favoring fatty acid metabolism (5, 24, 25). We posited that suppression of Parkin-mediated mitophagy by Mfn2 AA caused fetal mitochondria to be retained. Consistent with this idea, Mfn2 AA cardiac mitochondria did not undergo the time-dependent transformation in size and shape observed by P21 in WT Mfn2 and control hearts (Fig. 5A). Interruption of normal mitochondrial morphological maturation that is normally complete by P21 was associated with dilated cardiomyopathy that developed within 2 weeks thereafter (Figs. 3D and 5, B and C and fig. S15).

Mitophagy is essential for the perinatal transformation of cardiac metabolism

Cardiac metabolic transition after birth is linked to increased expression of mitochondrial replication and transcription factors—i.e., mitochondrial biogenesis (26). We measured the changes in transcript levels for more than 400 cardiac-

expressed mitochondrial proteins from late embryo through adulthood, thereby defining normal transcriptional reprogramming of cardiac metabolism (fig. S16). RNA sequencing of perinatal day 1 (P1), day 21 (P21), and 5-week-old hearts showed that WT Mfn2 did not perturb normal mitochondrial gene reprogramming. By contrast, the mitochondrial transcript profile of 5-week-old Mfn2 AA hearts cosegregated with P1 hearts (Fig. 6A), driven largely by failure of electron transport, fatty acid catabolism, and ketone body metabolism gene abundance to increase during the perinatal-to-adult transition (Fig. 6A and supplementary data sets 1 and 2). Hemodynamic stress in adult hearts did not fully recapitulate fetal metabolic gene expression (fig. S17), demonstrating that Mfn2 AA caused true retention of the embryonic metabolic transcriptome and not cardiomyopathy-related reexpression of embryonic genes (25). Suppression of

metabolic gene reprogramming in 5-week-old Mfn2 AA hearts affected genes encoding fatty acid (Fig. 6B) and branched chain amino acid (fig. S18) tricarboxylic acid (TCA) cycle entry factors and some TCA cycle enzymes themselves (Fig. 6B), while largely sparing glycolysis genes (Fig. 6B); effects on oxidative phosphorylation (OXPHOS) genes were variable (Fig. 6B). Characteristic perinatal increases in the abundance of transcriptional activators of metabolism and mitochondrial replication factors—i.e., mitochondrial biogenesis genes—were also suppressed in Mfn2 AA hearts (Fig. 6C).

To define the metabolic consequences of interrupting Parkin-mediated mitophagy in Mfn2 AA mouse hearts, we compared mitochondrial respiration stimulated by the fetal-preferred glycolytic substrate pyruvate to respiration stimulated by the adult-preferred fatty acid substrate palmitoylcarnitine (2, 4, 24). Oxygen consumption

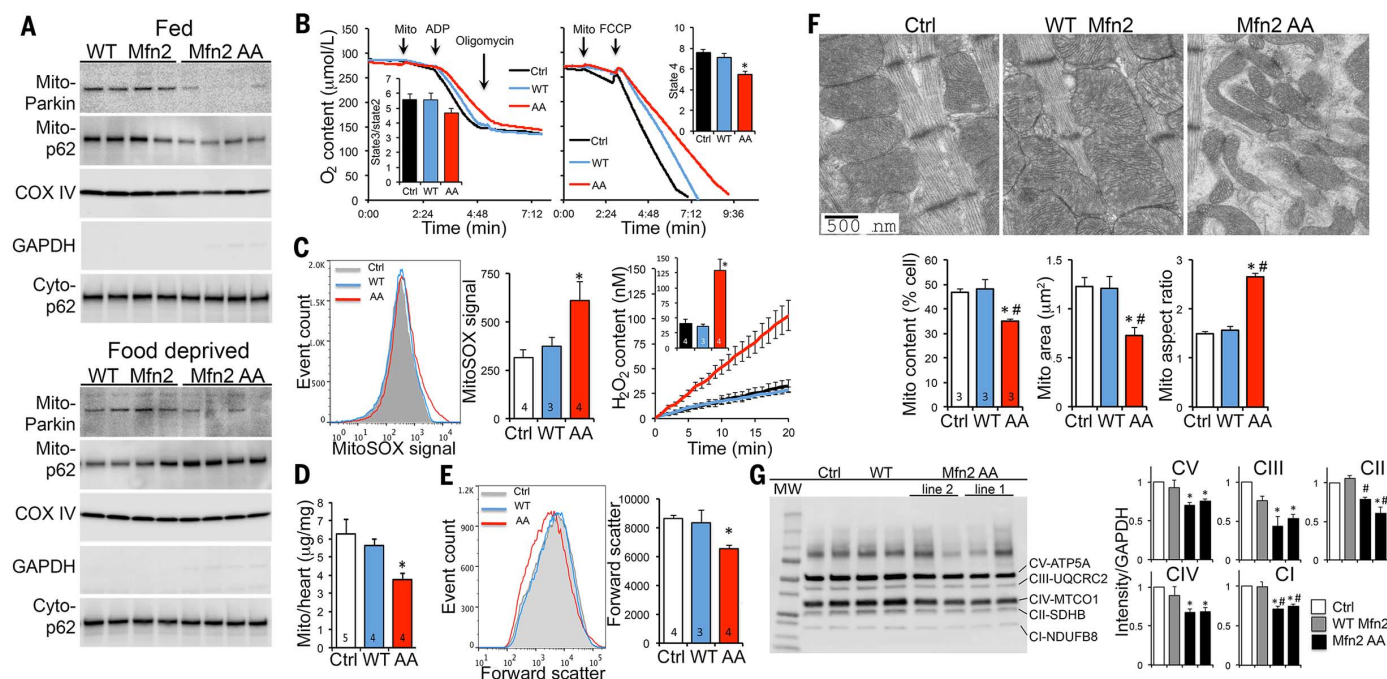


Fig. 4. Abnormalities in mitophagy and mitochondria induced by perinatal cardiac Mfn2 AA. (A) Immunoreactive Parkin and p62/SQSTM1 in 2- to 3-week-old mitochondrial-enriched mouse heart fractions (mito-) of fed mice (top) and food-deprived mice (bottom). Cyto-p62 is p62/SQSTM1 in the cytosolic fraction. (B) Substrate-stimulated (left) and maximum uncoupled (right) respiration of isolated cardiac mitochondria. (C) Isolated mitochondrial O₂⁻ (MitoSOX; left) and H₂O₂ (Amplex red; right) production studies. (D) Cardiac mitochondrial protein content. (E) Flow cytometric mitochondrial forward scatter. (F) Ultrastructural studies of cardiomyocyte mitochondria. Mitochondrial content is the percentage of cell area occupied by mitochondria; mitochondrial area is the mean area of individual organelles; mitochondrial aspect ratio is long axis/short axis. (G) Immunoblot analysis of respiratory complex proteins. Quantitative data to right are $n = 4$ individual mouse hearts. * $P < 0.05$ versus Ctrl; # $P < 0.05$ versus WT Mfn2.

by permeabilized cardiomyocytes was similar in control, WT-Mfn2, and Mfn2 AA cells given pyruvate. However, Mfn2 AA cardiomyocytes exhibited impaired respiration when provided with palmitoylcarnitine (Fig. 7A). Moreover, myocardial metabolite profiling revealed abnormally low levels of multiple fatty acid acylcarnitines, which are products of mitochondrial fatty acid oxidative flux, in comparison with age-matched control and WT-Mfn2 hearts. Specifically, acylcarnitine levels in 5-week-old Mfn2 AA hearts were comparable to those of normal P1 hearts (Fig. 7, B to D). By contrast, myocardial abundance of organic acids in young adult Mfn2 AA and control hearts was similar. The concordant abnormalities of mitochondrial gene expression, substrate preference for mitochondrial respiration, and metabolic profile exhibited by cardiac Mfn2 AA mice (fig. S19) illustrate the global effect of Parkin-mediated mitochondrial removal on normal developmental metabolic transitioning of the perinatal heart. Taken together, the data point to a mismatch between mitochondrial programming and metabolic substrate availability as the underlying cause of progressive cardiomyopathy in juvenile Mfn2 AA mice with defective cardiomyocyte mitophagy.

Discussion

We have shown that Parkin-mediated mitophagy is essential for normal perinatal cardiac mito-

chondrial and metabolic maturation. By expressing from birth an engineered Mfn2 AA mutant that cannot be PINK1-phosphorylated on T111 and S442 as required for Mfn2-Parkin binding (12), the normal developmental perinatal transformation of cardiac metabolism was disrupted. Persistence of fetal carbohydrate-metabolizing mitochondria in adult Mfn2 AA hearts revealed the requirement for organelle removal through the PINK1-Mfn2-Parkin mitophagy mechanism before mitochondrial transitioning to normal adult fatty acid metabolism. Even the genetic program encoding critical fatty acid metabolism pathways was repressed when fetal mitochondria were retained. Parkin thus promotes mitochondrial removal and suppresses biogenesis, consistent with previously described Parkin-dependent regulation of the mitochondrial biogenesis factors PARIS and PGC-1 α (17). Organelle replacement, rather than simple reprogramming, may be necessary because mitochondrial respiratory supercomplexes are organized as paracrystalline arrays (27, 28) whose disassembly, reorganization, and reassembly in preexisting embryonic cardiac mitochondria could be disruptive (7). An alternate means of mitochondrial transitioning might be through cycles of fission and fusion. However, the normal half-time for turning over adult cardiomyocyte mitochondria through mitochondrial dynamism is ~3 weeks (29), within which time our studies reveal the perinatal transformation from fetal to

adult mitochondria to be complete. Thus, we propose that the Parkin-Mfn2 interaction drives general mitophagic turnover of fetal mitochondria in the perinatal heart, enabling their replacement with mitochondria incorporating biogenically derived metabolic systems optimized for the high energetic demands of contracting adult hearts.

The metabolic preference for glycolysis in growing fetal hearts is reminiscent of the Warburg effect observed in cancer, wherein the transformation from restrained to malignant growth is associated with a transition to increased glycolysis and less dependence on aerobic mitochondrial ATP production (30). Although the specific molecular determinants of glycolytic metabolism in fetal hearts undoubtedly differ from those of tumors, in both instances, increased glycolysis is adaptive for a hypoxic environment and is optimized for increasing biomass—i.e., for promoting cell growth (31). Thus, the growing fetal heart derives two benefits from a predominantly glycolytic metabolism: (i) the ability to generate ATP sufficient for the comparatively modest needs of fetal heart contraction despite a relatively hypoxic environment; and (ii) a metabolism that facilitates uptake and incorporation of amino acids and fatty acids into new cellular structures for cell and organ growth, rather than metabolizing them for energy production. On the other hand, fatty acid metabolism in fully grown adult hearts provides more efficient ATP production to fuel increased

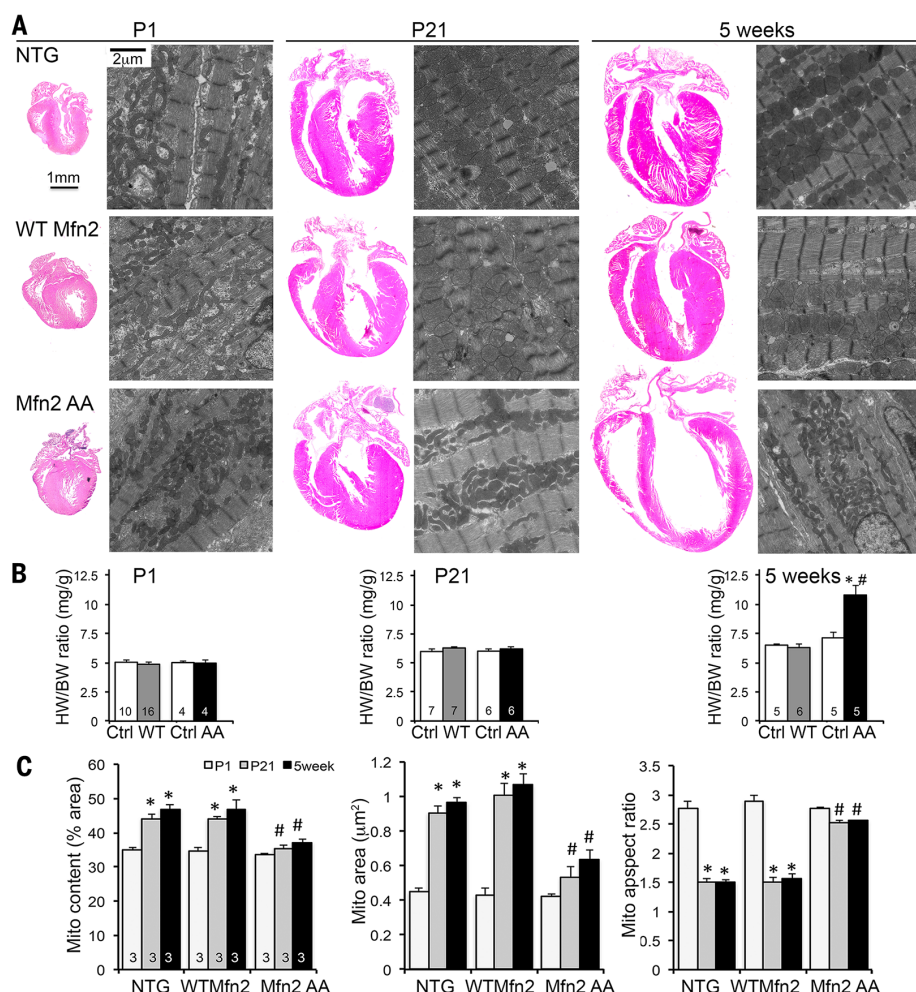


Fig. 5. Fetal mitochondria persist in young adult Mfn2 AA mouse hearts. (A) Representative four-chamber heart sections and transmission electron micrographs of cardiomyocyte mitochondria from P1, P21, and 5-week-old mouse hearts. NTG controls are top row, WT Mfn2 middle row, Mfn2 AA bottom row. Quantitative data for heart weights are in (B) and for mitochondrial ultrastructure in (C). *, $P < 0.05$ versus P1; #, $P < 0.05$ versus WT Mfn2 at the same stage.

contractile demand. Our findings reveal this cardiac metabolic transition to be an essential adaptation for extra-uterine life.

The developmental role for Parkin-dependent mitophagy described herein was unsuspected because germline Parkin gene ablation in mice has not produced robust phenotypes (9, 10). As deployed here, Mfn2 AA perturbed endogenous Parkin strictly by interdicting its localization to mitochondria—i.e., by acting as a nonfunctioning cardiomyocyte Parkin receptor. The lethal cardiomyopathy evoked by Mfn2 AA, but not WT Mfn2, exposed novel Parkin functionality specific to the postnatal period, during which myocardial carbohydrate-dependent metabolism transitions to fatty acid dependence. Early lethality after perinatal cardiomyocyte-specific Parkin gene deletion likewise demonstrated an essential role for Parkin in postnatal hearts. However, perinatal cardiomyocyte Parkin deficiency was generally fatal within the first 3 weeks of life, whereas perinatal cardiac Mfn2 AA expression provoked a slower-

progressing (but ultimately equally deadly) cardiomyopathy. The aggressive phenotype induced by cardiomyocyte-directed Parkin deletion likely results from complete disruption of Parkin activity that, in addition to promoting mitophagy, includes regulation of mitochondrial dynamism, modulation of subcellular mitochondrial motility, mediation of mitochondrial protein degradation, and stimulation of mitochondrial biogenesis (15). By comparison, expressing Mfn2 AA is a more precise intervention that only inhibits Parkin activity dependent upon its binding to PINK1-phosphorylated Mfn2—i.e., mitophagy. Indeed, because endogenous Mfn2, PINK1, and Parkin are still present, mitophagy was not entirely abrogated by Mfn2 AA. Accordingly, cardiomyocyte-specific perinatal Parkin gene deletion and Mfn2 AA expression had similar effects on mitochondrial maturation in the heart, but the Mfn2 AA phenotype was an attenuated form of the full-blown phenotypic dysfunction.

Our findings add to the evidence that in vivo Parkin functionality is underestimated from conventional systemic Parkin deletion. Whereas germline Parkin knockout mice exhibit few manifestations of Parkinson's disease or cardiac involvement at baseline (9, 10, 32), conditional Parkin ablation in the substantia nigra recapitulates a central pathological feature of Parkinson's disease, degeneration of dopaminergic neurons (11). Likewise, short hairpin RNA-mediated Parkin suppression reduces mitophagy in mouse livers, whereas mitophagy is intact in germline Parkin knockout mouse livers (33). Finally, cardiomyocyte-specific Parkin ablation alleviates the cardiomyopathy induced by dynamin-related protein 1 (Drp1) deficiency, whereas global Parkin deficiency fails to rescue a similar cardiac Drp1-deficient model (21, 34).

These results also clarify the specific function of PINK1-Mfn2-Parkin signaling in mitophagy. The need for PINK1-phosphorylated Mfn2 to function as a Parkin binding protein in mitophagic mitochondrial clearance is not absolute, because Parkin will translocate to mitochondria of FCCP-treated cells lacking Mfn2 (fig. S1). Thus, just as there are Parkin-independent pathways for mitochondrial elimination (35), we would infer one or more Mfn2-independent means of recruiting Parkin to depolarized mitochondria. Nonetheless, in normal and Mfn2-deficient fibroblasts, nonphosphorylatable Mfn2 AA abolished Parkin translocation to, and lysosomal engulfment of, depolarized mitochondria without affecting other Mfn2 activities such as mitochondrial fusion, mitochondrial-sarcoplasmic reticulum tethering, and Miro binding. These results define a central role for the PINK1-Mfn2 phosphorylation interaction in conventional mitochondrial quality control and suggest a mechanism whereby PINK1-phosphorylated Mfn2 induces primary mitochondrial Parkin binding, with PINK1-phosphorylated ubiquitin as the preferred substrate for mitochondrial localized Parkin (36).

The current findings suggest why Mfn2 and Parkin are present in hearts that seemingly have little use for the canonical functions assigned to both proteins. In adult hearts, cardiomyocyte mitochondria are static, distinct, rounded organelles. Lacking extensive interconnected mitochondrial networks, adult cardiomyocytes have little requirement for the mitochondrial remodeling that would be promoted by a redundant mitochondrial fusion protein. Indeed, in our hands, Mfn1 (but not Mfn2) is completely dispensable to adult mouse hearts (12). Likewise, the PINK1-Parkin pathway clearly mediates autophagic elimination of damaged mitochondria in cultured mammalian cells (14), but evidence from germline *Parkin* knockout mice (9), adult cardiomyocyte-specific Parkin-deficient mice (21), and from interrupting Parkin signaling in adult mice with Mfn2 AA (current study) does not support an important role for Parkin-mediated mitophagy as a homeostatic mitochondrial quality-control mechanism in hearts; normal surveillance and culling of individual damaged mitochondria seems to be accomplished through Parkin-independent

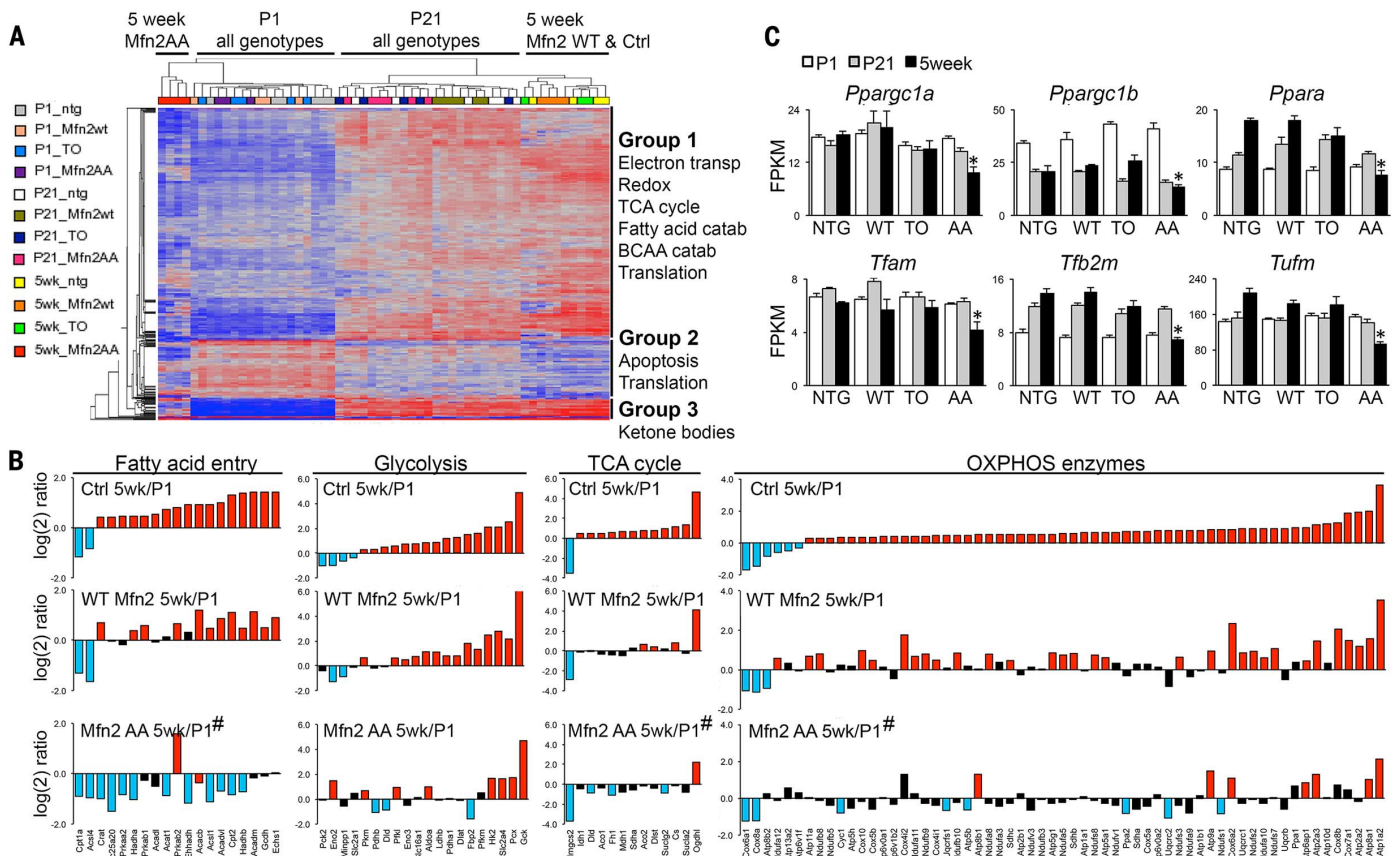


Fig. 6. Failure of metabolic gene reprogramming after perinatal Mfn2 AA expression. (A) Heat map of mitochondrial gene expression in P1, P21, and 5-week-old mouse hearts; functional annotation of Mfn2 AA gene clusters is to the right. (B) Postnatal reprogramming of mitochondrial genes by metabolic function. Bars are mean values from results in Fig. 4B; log(2) gene expression at 5 weeks versus P1 for Ctrl (top), WT Mfn2 (middle), and Mfn2 AA

(bottom) hearts. Blue and red bars are significantly down- and up-regulated, respectively [1.25-fold; false discovery (FDR) < 0.02]; black bars are not significantly regulated. (C) Regulated expression of mitochondrial biogenesis and replication genes during the perinatal-adult transition. *, FDR < 0.02 versus littermate control mice (TO); #, $P < 0.0001$ versus WT Mfn2 [two-way analysis of variance (ANOVA)].

mechanisms (35). Rather, Parkin-directed mitophagy is invoked as needed to accelerate generalized mitochondrial turnover during developmental transitions of myocardial metabolism (current study), after myocardial injury (9), and when mitochondrial homeostasis is disrupted (27).

Our findings demonstrate that mitochondria are not simply flexible fuel organelles readily switching between carbohydrate and fatty acid substrates. Rather, they have intrinsic metabolic and respiratory systems optimized for different substrate-specific metabolic pathways, and metabolic transitioning requires existing organelles to be mitophagically removed, enabling their replacement with mitochondria appropriate for a given biological context. Parkin and PINK1 gene mutations cause hereditary Parkinson's disease, and Mfn2 mutations cause Charcot-Marie-Tooth syndrome type IIa. These are chronic neuromuscular disorders in which cardiac involvement is uncommon (37). It remains to be determined whether PINK1-Parkin-Mfn2-mediated mitophagy regulates metabolic function in neurons or skeletal muscle as it does in perinatal hearts. The discovery that PINK1-Mfn2-Parkin directed-mitophagy is essential to cardiomyocyte metabolic remodeling

only during the brief period following birth supports intensive genetic evaluation of the Parkin signaling pathway in neonatal, in addition to adult, cardiomyopathy.

REFERENCES AND NOTES

1. G. A. Porter Jr. et al., Bioenergetics, mitochondria, and cardiac myocyte differentiation. *Prog. Pediatr. Cardiol.* **31**, 75–81 (2011). doi: [10.1016/j.pppedcard.2011.02.002](https://doi.org/10.1016/j.pppedcard.2011.02.002); pmid: [21603067](https://pubmed.ncbi.nlm.nih.gov/21603067/)
2. B. Bartelds et al., Perinatal changes in myocardial metabolism in lambs. *Circulation* **102**, 926–931 (2000). doi: [10.1161/01.CIR.102.8.926](https://doi.org/10.1161/01.CIR.102.8.926); pmid: [10952964](https://pubmed.ncbi.nlm.nih.gov/10952964/)
3. H. D. Kim et al., Human fetal heart development after mid-term: Morphometry and ultrastructural study. *J. Mol. Cell. Cardiol.* **24**, 949–965 (1992). doi: [10.1016/0022-2828\(92\)91862-Y](https://doi.org/10.1016/0022-2828(92)91862-Y); pmid: [1433323](https://pubmed.ncbi.nlm.nih.gov/1433323/)
4. W. C. Stanley, F. A. Recchia, G. D. Lopaschuk, Myocardial substrate metabolism in the normal and failing heart. *Physiol. Rev.* **85**, 1093–1129 (2005). doi: [10.1152/physrev.00006.2004](https://doi.org/10.1152/physrev.00006.2004); pmid: [15987803](https://pubmed.ncbi.nlm.nih.gov/15987803/)
5. H. Taegtmeyer, S. Sen, D. Vela, Return to the fetal gene program: A suggested metabolic link to gene expression in the heart. *Ann. N.Y. Acad. Sci.* **1188**, 191–198 (2010). doi: [10.1111/j.1749-6632.2009.05100.x](https://doi.org/10.1111/j.1749-6632.2009.05100.x); pmid: [20201903](https://pubmed.ncbi.nlm.nih.gov/20201903/)
6. M. Song, G. W. Dorn 2nd, Mitochondria: Noncanonical functioning of dynamism factors in static mitochondria of the heart. *Cell Metab.* **21**, 195–205 (2015). doi: [10.1016/j.cmet.2014.12.019](https://doi.org/10.1016/j.cmet.2014.12.019); pmid: [25651174](https://pubmed.ncbi.nlm.nih.gov/25651174/)
7. O. S. Shirihai, M. Song, G. W. Dorn 2nd, How mitochondrial dynamism orchestrates mitophagy. *Circ. Res.* **116**,

- 1835–1849 (2015). doi: [10.1161/CIRCRESAHA.116.306374](https://doi.org/10.1161/CIRCRESAHA.116.306374); pmid: [25999423](https://pubmed.ncbi.nlm.nih.gov/25999423/)
8. R. J. Youle, A. M. van der Blik, Mitochondrial fission, fusion, and stress. *Science* **337**, 1062–1065 (2012). doi: [10.1126/science.1219855](https://doi.org/10.1126/science.1219855); pmid: [22936770](https://pubmed.ncbi.nlm.nih.gov/22936770/)
9. D. A. Kubli et al., Parkin protein deficiency exacerbates cardiac injury and reduces survival following myocardial infarction. *J. Biol. Chem.* **288**, 915–926 (2013). doi: [10.1074/jbc.M112.411363](https://doi.org/10.1074/jbc.M112.411363); pmid: [23152496](https://pubmed.ncbi.nlm.nih.gov/23152496/)
10. Y. Lee, V. L. Dawson, T. M. Dawson, Animal models of Parkinson's disease: Vertebrate genetics. *Cold Spring Harb. Perspect. Med.* **2**, a009324 (2012). doi: [10.1101/cshperspect.a009324](https://doi.org/10.1101/cshperspect.a009324); pmid: [22960626](https://pubmed.ncbi.nlm.nih.gov/22960626/)
11. J. H. Shin et al., PARIS (ZNF746) repression of PGC-1 α contributes to neurodegeneration in Parkinson's disease. *Cell* **144**, 689–702 (2011). doi: [10.1016/j.cell.2011.02.010](https://doi.org/10.1016/j.cell.2011.02.010); pmid: [21376232](https://pubmed.ncbi.nlm.nih.gov/21376232/)
12. Y. Chen, G. W. Dorn 2nd, PINK1-phosphorylated mitofusins 2 is a Parkin receptor for culling damaged mitochondria. *Science* **340**, 471–475 (2013). doi: [10.1126/science.1231031](https://doi.org/10.1126/science.1231031); pmid: [23620051](https://pubmed.ncbi.nlm.nih.gov/23620051/)
13. S. Lee et al., Mitofusins 2 is necessary for striatal axonal projections of midbrain dopamine neurons. *Hum. Mol. Genet.* **21**, 4827–4835 (2012). doi: [10.1093/hmg/dd3352](https://doi.org/10.1093/hmg/dd3352); pmid: [22914740](https://pubmed.ncbi.nlm.nih.gov/22914740/)
14. D. P. Narendra et al., PINK1 is selectively stabilized on impaired mitochondria to activate Parkin. *PLoS Biol.* **8**, e1000298 (2010). doi: [10.1371/journal.pbio.1000298](https://doi.org/10.1371/journal.pbio.1000298); pmid: [20126261](https://pubmed.ncbi.nlm.nih.gov/20126261/)
15. L. A. Scarffe, D. A. Stevens, V. L. Dawson, T. M. Dawson, Parkin and PINK1: Much more than mitophagy. *Trends Neurosci.* **37**, 315–324 (2014). doi: [10.1016/j.tins.2014.03.004](https://doi.org/10.1016/j.tins.2014.03.004); pmid: [24735649](https://pubmed.ncbi.nlm.nih.gov/24735649/)

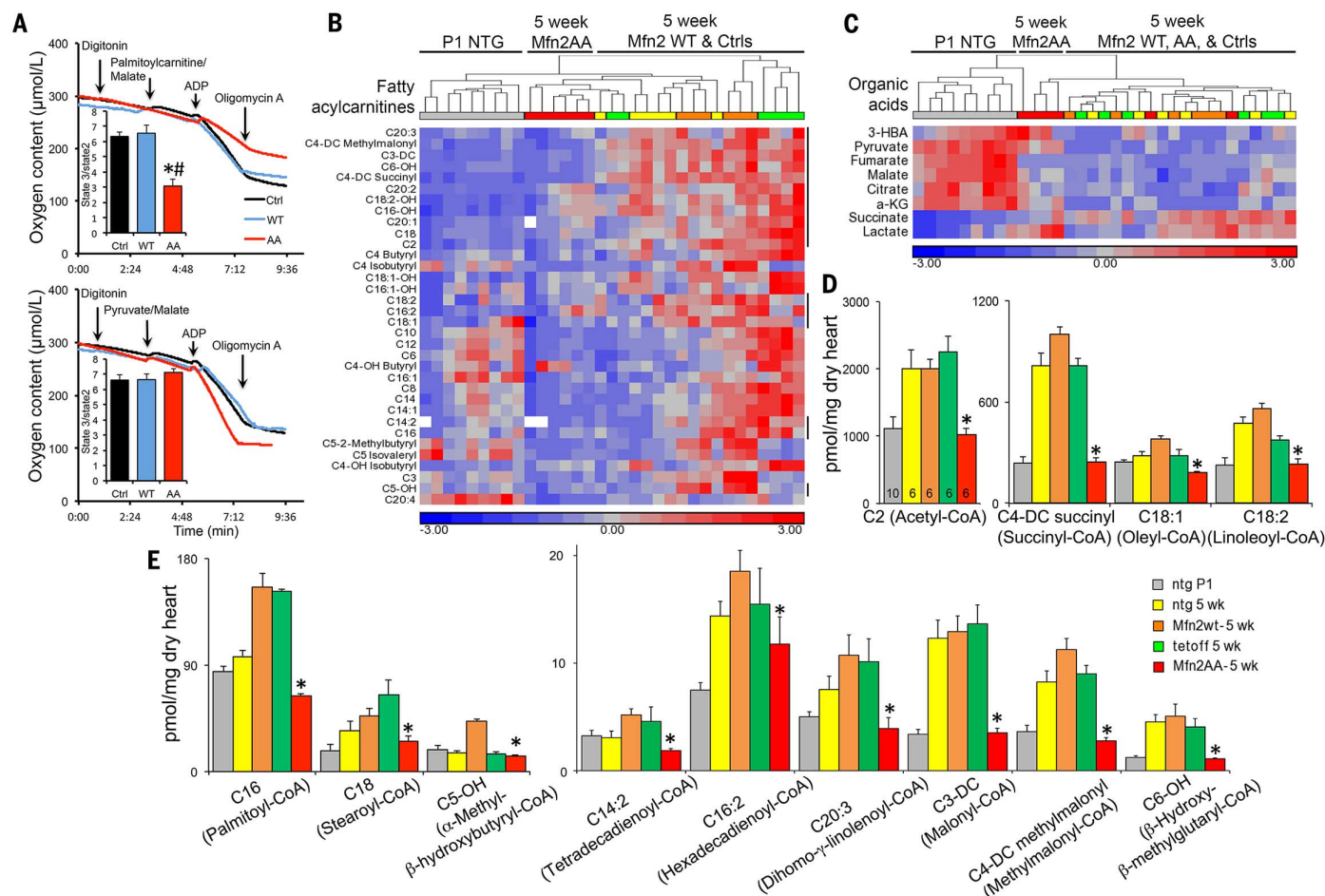


Fig. 7. Adult Mfn2 AA hearts retain a fetal-like glycolytic metabolism.

(A) Palmitoyl carnitine-stimulated (top) and pyruvate-stimulated (bottom) respiration of isolated permeabilized cardiomyocytes. (B and C) Standardized heat map showing unsupervised clustering of myocardial acylcarnitine (B) and organic acid (C) metabolite content in P1 NTG and 5-week-old NTG, WT Mfn2, and Mfn2 AA mouse hearts. Vertical lines to the right of (B) indicate sig-

nificantly dysregulated metabolites in 5-week-old Mfn2 AA hearts versus contemporaneous controls. (D) Quantitative data for absolute myocardial content of dysregulated metabolites in (B). -DC and -OH designate mono-hydroxylated and dicarboxylic acid acylcarnitine species, respectively. Common names for parent species are in parentheses. *, $P < 0.05$ versus WT Mfn2 (ANOVA).

- Koshiba et al., Structural basis of mitochondrial tethering by mitofusin complexes. *Science* **305**, 858–862 (2004). doi: [10.1126/science.1099793](https://doi.org/10.1126/science.1099793); pmid: [15297672](https://pubmed.ncbi.nlm.nih.gov/15297672/)
- Twig et al., Fission and selective fusion govern mitochondrial segregation and elimination by autophagy. *EMBO J.* **27**, 433–446 (2008). doi: [10.1038/sj.emboj.7601963](https://doi.org/10.1038/sj.emboj.7601963); pmid: [18200046](https://pubmed.ncbi.nlm.nih.gov/18200046/)
- W. H. Eschenbacher et al., Two rare human mitofusin 2 mutations alter mitochondrial dynamics and induce retinal and cardiac pathology in Drosophila. *PLOS ONE* **7**, e44296 (2012). doi: [10.1371/journal.pone.0044296](https://doi.org/10.1371/journal.pone.0044296); pmid: [22957060](https://pubmed.ncbi.nlm.nih.gov/22957060/)
- A. Misko, S. Jiang, I. Wegorzewska, J. Milbrandt, R. H. Baloh, Mitofusin 2 is necessary for transport of axonal mitochondria and interacts with the Miro/Milton complex. *J. Neurosci.* **30**, 4232–4240 (2010). doi: [10.1523/JNEUROSCI.6248-09.2010](https://doi.org/10.1523/JNEUROSCI.6248-09.2010); pmid: [20335458](https://pubmed.ncbi.nlm.nih.gov/20335458/)
- Syed et al., Physiological growth synergizes with pathological genes in experimental cardiomyopathy. *Circ. Res.* **95**, 1200–1206 (2004). doi: [10.1161/01.RES.0000150366.08972.7f](https://doi.org/10.1161/01.RES.0000150366.08972.7f); pmid: [15539635](https://pubmed.ncbi.nlm.nih.gov/15539635/)
- M. Song et al., Interdependence of Parkin-mediated mitophagy and mitochondrial fission in adult mouse hearts. *Circ. Res.* **117**, 346–351 (2015). doi: [10.1161/CIRCRESAHA.117.306859](https://doi.org/10.1161/CIRCRESAHA.117.306859); pmid: [26038571](https://pubmed.ncbi.nlm.nih.gov/26038571/)
- Y. Chen et al., Mitofusin 2-containing mitochondrial-reticular microdomains direct rapid cardiomyocyte bioenergetic responses via interorganelle Ca²⁺ crosstalk. *Circ. Res.* **111**, 863–875 (2012). doi: [10.1161/CIRCRESAHA.112.266585](https://doi.org/10.1161/CIRCRESAHA.112.266585); pmid: [22777004](https://pubmed.ncbi.nlm.nih.gov/22777004/)
- O. M. de Brito, L. Scorrano, Mitofusin 2 tethers endoplasmic reticulum to mitochondria. *Nature* **456**, 605–610 (2008). doi: [10.1038/nature07534](https://doi.org/10.1038/nature07534); pmid: [19052620](https://pubmed.ncbi.nlm.nih.gov/19052620/)
- G. D. Lopaschuk, M. A. Spafford, D. R. Marsh, Glycolysis is predominant source of myocardial ATP production immediately after birth. *Am. J. Physiol.* **261**, H1698–H1705 (1991). pmid: [1750528](https://pubmed.ncbi.nlm.nih.gov/1750528/)
- P. Razeghi et al., Metabolic gene expression in fetal and failing human heart. *Circulation* **104**, 2923–2931 (2001). doi: [10.1161/hc4901.100526](https://doi.org/10.1161/hc4901.100526); pmid: [11739307](https://pubmed.ncbi.nlm.nih.gov/11739307/)
- J. J. Lehman et al., Peroxisome proliferator-activated receptor gamma coactivator-1 promotes cardiac mitochondrial biogenesis. *J. Clin. Invest.* **106**, 847–856 (2000). doi: [10.1172/JCI10268](https://doi.org/10.1172/JCI10268); pmid: [11018072](https://pubmed.ncbi.nlm.nih.gov/11018072/)
- N. V. Dudkina, R. Kouril, K. Peters, H. P. Braun, E. J. Boekema, Structure and function of mitochondrial supercomplexes. *Biochim. Biophys. Acta* **1797**, 664–670 (2010). doi: [10.1016/j.bbabi.2009.12.013](https://doi.org/10.1016/j.bbabi.2009.12.013); pmid: [20036212](https://pubmed.ncbi.nlm.nih.gov/20036212/)
- E. Lapuente-Brun et al., Supercomplex assembly determines electron flux in the mitochondrial electron transport chain. *Science* **340**, 1567–1570 (2013). doi: [10.1126/science.1230381](https://doi.org/10.1126/science.1230381); pmid: [23812712](https://pubmed.ncbi.nlm.nih.gov/23812712/)
- Y. Chen, Y. Liu, G. W. Dorn 2nd, Mitochondrial fusion is essential for organelle function and cardiac homeostasis. *Circ. Res.* **109**, 1327–1331 (2011). doi: [10.1161/CIRCRESAHA.111.258723](https://doi.org/10.1161/CIRCRESAHA.111.258723); pmid: [22052916](https://pubmed.ncbi.nlm.nih.gov/22052916/)
- H. R. Christofk et al., The M2 splice isoform of pyruvate kinase is important for cancer metabolism and tumour growth. *Nature* **452**, 230–233 (2008). doi: [10.1038/nature06734](https://doi.org/10.1038/nature06734); pmid: [18337823](https://pubmed.ncbi.nlm.nih.gov/18337823/)
- M. G. Vander Heiden, L. C. Cantley, C. B. Thompson, Understanding the Warburg effect: The metabolic requirements of cell proliferation. *Science* **324**, 1029–1033 (2009). doi: [10.1126/science.1160809](https://doi.org/10.1126/science.1160809); pmid: [19460998](https://pubmed.ncbi.nlm.nih.gov/19460998/)
- P. Bhandari, M. Song, Y. Chen, Y. Burelle, G. W. Dorn 2nd, Mitochondrial contagion induced by Parkin deficiency in Drosophila hearts and its containment by suppressing mitofusin. *Circ. Res.* **114**, 257–265 (2014). doi: [10.1161/CIRCRESAHA.114.302734](https://doi.org/10.1161/CIRCRESAHA.114.302734); pmid: [24192653](https://pubmed.ncbi.nlm.nih.gov/24192653/)
- J. A. Williams et al., Chronic deletion and acute knockdown of Parkin have differential responses to acetaminophen-induced mitophagy and liver injury in mice. *J. Biol. Chem.* **290**, 10934–10946 (2015). doi: [10.1074/jbc.M114.602284](https://doi.org/10.1074/jbc.M114.602284); pmid: [25752611](https://pubmed.ncbi.nlm.nih.gov/25752611/)
- Y. Kageyama et al., Parkin-independent mitophagy requires Drp1 and maintains the integrity of mammalian heart and brain. *EMBO J.* **33**, 2798–2813 (2014). doi: [10.15252/embj.201488658](https://doi.org/10.15252/embj.201488658); pmid: [25349190](https://pubmed.ncbi.nlm.nih.gov/25349190/)
- M. Song et al., Super-suppression of mitochondrial reactive oxygen species signaling impairs compensatory autophagy in primary mitophagic cardiomyopathy. *Circ. Res.* **115**, 348–353 (2014). doi: [10.1161/CIRCRESAHA.115.304384](https://doi.org/10.1161/CIRCRESAHA.115.304384); pmid: [24874428](https://pubmed.ncbi.nlm.nih.gov/24874428/)

36. A. M. Pickrell, R. J. Youle, The roles of PINK1, parkin, and mitochondrial fidelity in Parkinson's disease. *Neuron* **85**, 257–273 (2015). doi: [10.1016/j.neuron.2014.12.007](https://doi.org/10.1016/j.neuron.2014.12.007); pmid: [25611507](https://pubmed.ncbi.nlm.nih.gov/25611507/)
37. G. W. Dorn 2nd, Mitochondrial dynamism and heart disease: Changing shape and shaping change. *EMBO Mol. Med.* **7**, 865–877 (2015). doi: [10.15252/emmm.201404575](https://doi.org/10.15252/emmm.201404575); pmid: [25861797](https://pubmed.ncbi.nlm.nih.gov/25861797/)

ACKNOWLEDGMENTS

We gratefully acknowledge the invaluable contributions of S. J. Gardell of the Sanford Burnham Prebys Medical Discovery Institute for liquid

chromatography tandem mass spectrometry studies; and M. Levy of the Laboratory of Electron Microscopy Sciences, Department of Cell Biology, Washington University School of Medicine, S. de la Fuente, J. Mishra, and D. Weaver of the Thomas Jefferson University Mito Care Center for TEM analyses. *Park2* floxed allele mice were obtained from and used under a Materials Transfer Agreement with Lexicon Pharmaceuticals. The authors declare no conflicts. The data presented in this manuscript are tabulated in the supplementary materials. Both unprocessed and transcriptome-aligned RNA-sequencing reads have been deposited in the National Center for Biotechnology Information Gene Expression Omnibus with accession number GSE68921. This work was supported by NIH HL59888, HL108943, HL128071 (G.W.D.),

HL122124 (G.C.), HL058493 (D.P.K.), and American Heart Association grants 14PRE18970093 (M.S.) and 14GRNT20410000 (S.J.M.).

SUPPLEMENTARY MATERIALS

www.sciencemag.org/content/350/6265/aad2459/suppl/DC1
Materials and Methods
Figs. S1 to S19
Data sets S1 and S2
References (38–50)

13 August 2015; accepted 16 October 2015
10.1126/science.aad2459

RESEARCH ARTICLE SUMMARY

HEART MITOCHONDRIA

Imbalanced OPA1 processing and mitochondrial fragmentation cause heart failure in mice

Timothy Wai, Jaime García-Prieto, Michael J. Baker, Carsten Merkwirth, Paule Benit, Pierre Rustin, Francisco Javier Rupérez, Coral Barbas, Borja Ibañez,* Thomas Langer*

INTRODUCTION: Mitochondria are essential organelles whose form and function are inextricably linked. Balanced fusion and fission events shape mitochondria to meet metabolic demands and to ensure removal of damaged organelles. A fragmentation of the mitochondrial network occurs in response to cellular stress and is observed in a wide variety of disease conditions, including heart failure, neurodegenerative disorders, cancer, and obesity. However, the physiological relevance of stress-induced mitochondrial fragmentation remains unclear.

RATIONALE: Proteolytic processing of the dynamin-like guanosine triphosphatase (GTPase) OPA1 in the inner membrane of mitochondria is emerging as a critical regulatory step to balance mitochondrial fusion and fission. Two mitochondrial proteases, OMA1 and the AAA protease

YME1L, cleave OPA1 from long (L-OPA1) to short (S-OPA1) forms. L-OPA1 is required for mitochondrial fusion, but S-OPA1 is not, although accumulation of S-OPA1 in excess accelerates fission. In cultured mammalian cells, stress conditions activate OMA1, which cleaves L-OPA1 and inhibits mitochondrial fusion resulting in mitochondrial fragmentation. In this study, we generated conditional mouse models for both YME1L and OMA1 and examined the role of OPA1 processing and mitochondrial fragmentation in the heart, a metabolically demanding organ that depends critically on mitochondrial functions.

RESULTS: Deletion of *Yme1l* in cardiomyocytes did not grossly affect mitochondrial respiration but induced the proteolytic cleavage of OPA1 by the stress-activated peptidase OMA1 and drove fragmentation of mitochondria in vivo. These mice suffered from dilated

cardiomyopathy characterized by well-established features of heart failure that include necrotic cell death, fibrosis and ventricular remodelling, and a metabolic switch away from fatty acid oxidation and toward glucose use. We discovered that additional deletion of *Oma1* in cardiomyocytes prevented OPA1 processing

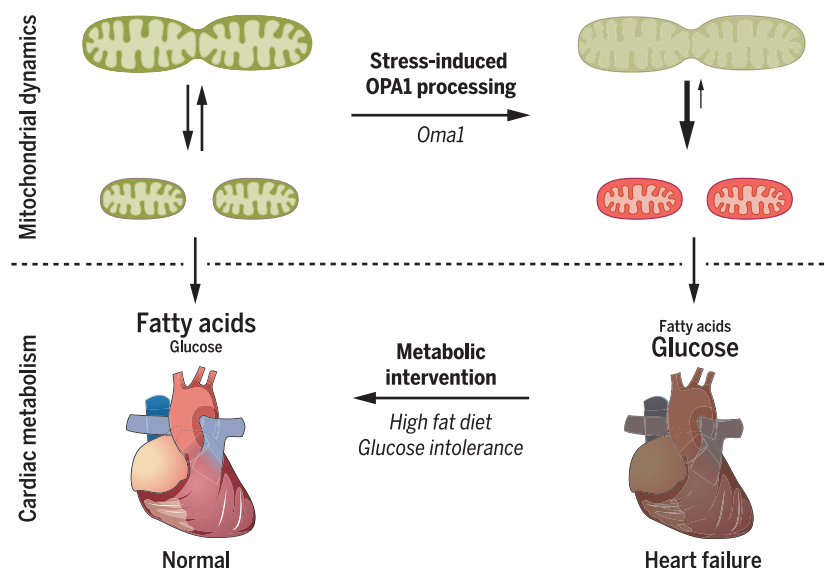
ON OUR WEB SITE

Read the full article at <http://dx.doi.org/10.1126/science.aad0116>

altogether and restored normal mitochondrial morphology and cardiac health. On the other hand, mice lacking YME1L in both skeletal muscle and cardio-

myocytes exhibited normal cardiac function and life span despite mitochondrial fragmentation in cardiomyocytes. Imbalanced OPA1 processing in skeletal muscle, which is an insulin signaling tissue, induced systemic glucose intolerance and prevented cardiac glucose overload and cardiomyopathy. We observed a similar effect on cardiac metabolism upon feeding mice lacking *Yme1l* in cardiomyocytes a high-fat diet, which preserved heart function despite mitochondrial fragmentation.

CONCLUSION: Our work highlights the importance of balanced fusion and fission of mitochondria for cardiac function and unravels an intriguing link between mitochondrial dynamics and cardiac metabolism in the adult heart in vivo. Mitochondrial fusion mediated by L-OPA1 preserves cardiac function, whereas its stress-induced processing by OMA1 and mitochondrial fragmentation triggers dilated cardiomyopathy and heart failure. In contrast to previous genetic models of the mitochondrial fusion machinery, mice lacking *Yme1l* in cardiomyocytes do not show pleiotropic respiratory deficiencies and thus provide a tool to directly assess the physiological importance of mitochondrial dynamics. Preventing mitochondrial fragmentation by deleting *Oma1* protects against cell death and heart failure. The identification of OMA1 as a critical regulator of mitochondrial morphology and cardiomyocyte survival holds promise for translational applications in cardiovascular medicine. Mitochondrial fragmentation induces a metabolic switch from fatty acid to glucose utilization in the heart. It turns out that reversing this switch and restoring normal cardiac metabolism is sufficient to preserve heart function despite mitochondrial fragmentation. These findings raise the intriguing possibility that the switch in fuel usage that occurs in the failing adult heart may, in fact, be maladaptive and could contribute to the pathogenesis of heart failure. ■



Critical role of balanced mitochondrial fusion and fission for cardiac metabolism and heart function. Induced processing of the dynamin-like GTPase OPA1 in the inner membrane by the stress-activated peptidase OMA1 leads to mitochondrial fragmentation, cardiomyopathy and heart failure, which is characterized by a switch in fuel utilization. Heart function can be preserved by reversing this metabolic switch without suppressing mitochondrial fragmentation.

The list of author affiliations is available in the full article online.

*Corresponding author. E-mail: thomas.langer@uni-koeln.de

(T.L.); bibanez@cnic.es (B.I.)

Cite this article as T. Wai et al., *Science* 350, aad0116 (2015).

DOI: 10.1126/science.aad0116

RESEARCH ARTICLE

HEART MITOCHONDRIA

Imbalanced OPA1 processing and mitochondrial fragmentation cause heart failure in mice

Timothy Wai,^{1,2*} Jaime García-Prieto,^{3*} Michael J. Baker,¹ Carsten Merkwirth,¹ Paule Benit,^{4,5} Pierre Rustin,^{4,5} Francisco Javier Rupérez,⁶ Coral Barbas,⁶ Borja Ibañez,^{3,7†} Thomas Langer^{1,2,8,9†}

Mitochondrial morphology is shaped by fusion and division of their membranes. Here, we found that adult myocardial function depends on balanced mitochondrial fusion and fission, maintained by processing of the dynamin-like guanosine triphosphatase OPA1 by the mitochondrial peptidases YME1L and OMA1. Cardiac-specific ablation of *Yme1l* in mice activated OMA1 and accelerated OPA1 proteolysis, which triggered mitochondrial fragmentation and altered cardiac metabolism. This caused dilated cardiomyopathy and heart failure. Cardiac function and mitochondrial morphology were rescued by *Oma1* deletion, which prevented OPA1 cleavage. Feeding mice a high-fat diet or ablating *Yme1l* in skeletal muscle restored cardiac metabolism and preserved heart function without suppressing mitochondrial fragmentation. Thus, unprocessed OPA1 is sufficient to maintain heart function, OMA1 is a critical regulator of cardiomyocyte survival, and mitochondrial morphology and cardiac metabolism are intimately linked.

The dynamic behavior of mitochondria preserves mitochondrial integrity and distribution and allows mitochondrial shape and function to be adapted to altered physiological demands (1, 2). Disturbed mitochondrial dynamics is associated with a number of neurodegenerative disorders and cardiac hypertrophy in mice (3, 4). Dynamin-like guanosine triphosphatases (GTPases) mediate the fusion and fission of mitochondrial membranes. Mitofusins 1 and 2 (MFN1 and MFN2) orchestrate outer mitochondrial membrane fusion, whereas OPA1 is required for inner mitochondrial membrane fusion. Fission, on the other hand, is executed by dynamin-related protein 1 (DRP1), a cytosolic protein that is recruited to the mitochondrial surface in response to various physiological cues. This complex machinery, including DRP1-specific receptor proteins and cytoskeletal

components, assembles at contact sites between the mitochondria and the endoplasmic reticulum, which mark mitochondrial division sites (5, 6).

Fusion and fission of mitochondrial membranes occur in a coordinated manner. Balanced cycles of fusion and fission determine the shape, size, and number of mitochondria, which leads to a large variability in the morphology of mitochondria in different cell types. Although mitochondria form interconnected, tubular networks in cultured fibroblasts, they appear as distinct entities in tissues, such as heart and skeletal muscle, that are characterized by low fusion and fission rates (7). Moreover, coordinated mitochondrial dynamics is critical for the bioenergetic function of mitochondria and is closely linked to metabolism. Changes in mitochondrial ultrastructure and dynamics occur in response to altered metabolic demands (8–11), and components involved in mitochondrial fusion are central regulators of cellular metabolism (12). Coordinated fusion and fission events are crucial for mitochondrial quality-control. Fusion contributes to mitochondrial maintenance, whereas excessive fission causes mitochondrial fragmentation, which allows removal of irreversibly damaged mitochondria by mitophagy and is associated with cell death (13, 14). Fragmentation of the mitochondrial network is observed in a wide variety of diseases.

The dynamin-like GTPase OPA1 mediates mitochondrial fusion and orchestrates mitochondrial cristae morphogenesis and resistance to apoptosis in response to physiological demands (15–17). The processing of OPA1 is emerging as a central regulatory step coordinating fusion and fission of mitochondria (18, 19). Two peptidases in the

inner membrane, OMA1 and the *i*-AAA protease YME1L, convert long OPA1 forms (L-OPA1) into short forms (S-OPA1) (20–23). The balanced accumulation of both forms maintains normal mitochondrial morphology. Fusion depends on L-OPA1 only, whereas S-OPA1 is associated with mitochondrial fission (Fig. 1A) (24–26). Cellular stress, mitochondrial dysfunction, or genetic interventions (such as deletion of *Yme1l*) can activate OMA1, which results in the increased conversion of L-OPA1 into S-OPA1 and mitochondrial fragmentation (25, 27–30). Loss of *Yme1l* in cultured fibroblasts does not impair fusion but triggers mitochondrial fragmentation (22, 25, 31), which can be suppressed by deletion of *Oma1* (22, 25, 31). Thus, although OPA1 processing is dispensable for mitochondrial fusion per se, an increased oxidative phosphorylation promotes cleavage of OPA1 by YME1L (10). It thus appears that different stimuli modulate OPA1 processing by YME1L or OMA1, which allows the coordination of mitochondrial fusion and division under various physiological conditions.

In agreement with its role for stress-induced OPA1 processing, ablation of *Oma1* in mice causes impaired thermogenesis and diet-induced obesity and protects against ischemic kidney injury (29, 32). Here, we generated tissue-specific mouse models for the OPA1-processing peptidases YME1L and OMA1 and examined the role of OPA1 processing in myocardial function.

Results

YME1L is essential for embryonic development

To study the importance of balanced mitochondrial dynamics (Fig. 1A), we generated conditional mouse models of the OPA1-processing peptidases *Yme1l* and *Oma1* (fig. S1, A to D, and table S1). We used a mouse line expressing Cre recombinase under the control of the β -actin promoter to delete *Yme1l* or *Oma1* by Cre/loxP-mediated recombination in all tissues. As expected (29), *Oma1*^{−/−} mice were born at the expected Mendelian ratio (fig. S1E). *Yme1l*^{+/−} mice were viable and exhibited no obvious phenotypes, but heterozygous intercrosses did not yield viable null offspring (Fig. 1B). We observed a generalized developmental delay in *Yme1l*^{−/−} embryos isolated from embryonic day 8.5 (E8.5) to E12.5 (Fig. 1C). Hearts from *Yme1l*^{−/−} embryos isolated at E9.5 and E10.5 failed to beat properly, and we did not recover any null embryos after E13.5. Thus, YME1L is essential for embryogenesis.

Cardiomyocyte-specific deletion of Yme1l causes dilated cardiomyopathy

We next examined the requirement of YME1L for the function of the heart, a metabolically demanding organ sensitive to disruption of mitochondrial shape (7, 33). We crossed *Yme1l*^{LoxP/LoxP} mice to mice expressing Cre recombinase specifically in cardiomyocytes (Myh6-Cre; cYKO) (34). cYKO mice were viable but had a significantly shortened life span (median life span: 46 weeks) (Fig. 1, D and E) punctuated by weight loss before their demise (Fig. 1F), which suggested that YME1L is required for normal heart function.

¹Institute for Genetics, University of Cologne, 50674 Cologne, Germany. ²Max-Planck-Institute for Biology of Aging, Cologne, Germany. ³Myocardial Pathophysiology Area, Centro Nacional de Investigaciones Cardiovasculares Carlos III (CNIC), Madrid, Spain. ⁴INSERM UMR 1141, Hôpital Robert Debré, Paris, France. ⁵Université Paris 7, Faculté de Médecine Denis Diderot, Paris, France. ⁶Centre for Metabolomics and Bioanalysis (CEMBIO), Faculty of Pharmacy, Universidad San Pablo CEU, Campus Monteprincipe, Boadilla del Monte, 28668 Madrid, Spain. ⁷Department of Cardiology, Instituto de Investigación Sanitaria (IIS), Fundación Jiménez Díaz Hospital, Madrid, Spain. ⁸Cologne Excellence Cluster on Cellular Stress Responses in Aging-Associated Diseases (CECAD), University of Cologne, Cologne, Germany. ⁹Center for Molecular Medicine (CMMC), University of Cologne, Cologne, Germany.

*These authors contributed equally to this work.

†Corresponding author. E-mail: thomas.langer@uni-koeln.de (T.L.); bibanez@cnic.es (B.I.)

We examined heart function from an early age up to 40 weeks of age in cYKO mice (Fig. 2A). Longitudinal echocardiographic (echo) analyses (fig. S2A) revealed progressive cardiac dysfunction (table S2), which became apparent at 20 weeks and was characterized by hallmarks of dilated cardiomyopathy (DCM): a reduced percentage of LVEF (% LVEF) (Fig. 2B and fig. S2A), a dilated left ventricular chamber (Fig. 2C), and a preserved left ventricular mass (fig. S2B). We observed myocardial fibrosis (Fig. 2D), increased serum levels of cardiac troponin T (Fig. 2E), and evidence of ongoing necrotic cell death (Fig. 2, F and G) in cYKO mice.

The failing adult heart is commonly characterized by an altered metabolism where glucose

use is increased and β oxidation is decreased (35, 36). We monitored in vivo cardiac uptake of 18 F-fluorodeoxyglucose (18 F]FDG) in cYKO mice by hybrid positron emission tomography-computed tomography (PET-CT). The loss of YME1L in cardiomyocytes caused an increase in in vivo cardiac glucose uptake (Fig. 2, H and I) and in vitro glycolysis rates (fig. S2C). Gas chromatography-mass spectrometry analyses revealed increased endogenous glucose levels and decreased lactate levels in cYKO hearts, whereas the levels of citric acid cycle intermediates were not altered (fig. S2D) nor were the levels and use of pyruvate (fig. S2E). However, we observed a global reduction of total cardiac acylcarnitines (fig. S2F), which indicated reduced β oxidation in

YME1L-deficient cardiomyocytes. Thus, loss of YME1L in cardiomyocyte mitochondria can induce a metabolic shift from lipid utilization to carbohydrate utilization that is typically observed in the failing heart (37). In conclusion, cYKO mice develop DCM, which progresses to heart failure and middle-aged death.

Loss of YME1L impairs mitochondrial morphology in cardiomyocytes

To define the molecular basis of DCM in cYKO mice, we first analyzed mitochondrial respiration. Ex vivo cardiac respiration measurements revealed no differences between resting hearts isolated from cYKO mice and controls (Fig. 3A). Specific activities of mitochondrial complexes II, III,

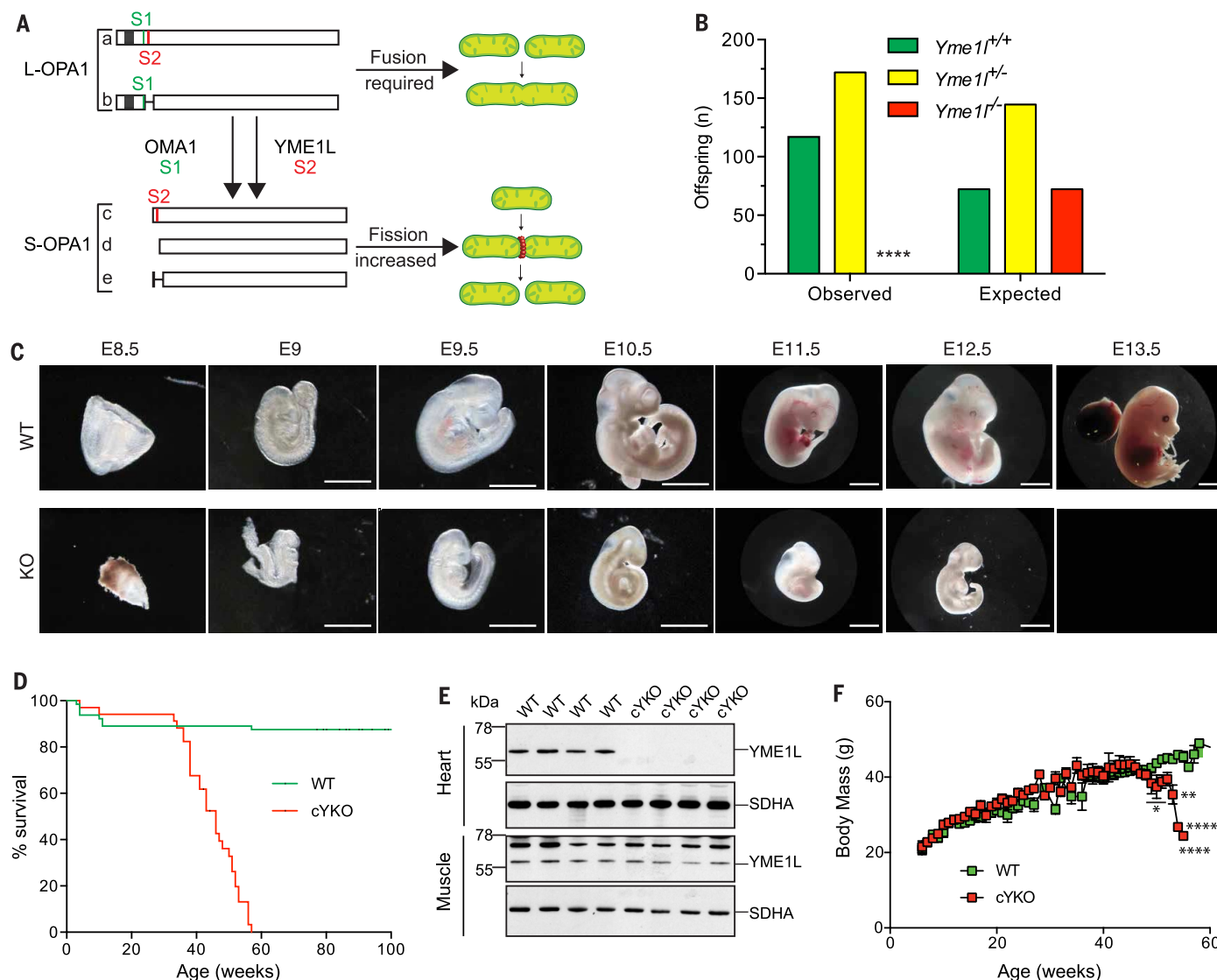


Fig. 1. YME1L is required in the developing embryo and the adult heart. (A) The mitochondrial proteases OMA1 and YME1L cleave L-OPA1 (a and b) at S1 and S2, respectively, to yield S-OPA1 forms (c, d, and e). (B) No viable *Yme1l*^{-/-} mice were recovered from intercrosses of *Yme1l*^{+/-} mice (0 out of 289 offspring). Chi-squared test, *****P* < 0.0001. (C) Postimplantation developmental delay of *Yme1l*^{-/-} embryos scaled relative to WT. Scale bar, 2 mm. (D) Life span of cardiomyocyte-specific cYKO mice (Myh6-Cre red; median

of 46 weeks, *n* = 69) is reduced relative to WT littermates (green; *n* = 74). Log-rank (Mantel-Cox) test, *****P* < 0.0001. (E) Immunoblots of tissues isolated from 18-week-old WT and cYKO mice. Antibodies directed against succinate dehydrogenase subunit A (SDHA) were used to control for gel loading. (F) Mean body weight (g) of cYKO males (red; *n* = 30) declines relative to WT (green; *n* = 30). Multiple *t* test, **P* < 0.05, *****P* < 0.0001. Data are means \pm SEM.

and IV were increased, although we observed only moderately impaired adenosine 5'-triphosphate (ATP) synthesis by complex V in cYKO hearts (Fig.

3B) and no significant differences in the assembly of respiratory chain complexes and supercomplexes (fig. S3A). Respiratory deficiencies thus

appeared unlikely to be the major cause for DCM in cYKO mice.

We next examined the morphology of mitochondria and performed transmission electron microscopy (TEM) of cYKO hearts (Fig. 3C). Smaller mitochondria with normal architecture of cristae accumulated in the absence of YME1L, which indicated impaired mitochondrial dynamics (Fig. 3, C and D). Similar results were seen in primary adult cardiomyocytes isolated from 8-week-old (before DCM development) and 40-week-old cYKO hearts (Fig. 3, E and F, and fig. S3B). Consistent with our TEM data, we observed distorted mitochondrial morphology in *Yme1l*^{-/-} cardiomyocytes, as seen previously in noncardiac cell types lacking YME1L (20, 22, 25). Loss of YME1L in cardiomyocytes abolished formation of S-OPA1 form d and led to the accumulation of S-OPA1 forms c and e, which are generated by OMA1 (Fig. 3, G and H). Moreover, the mitochondrial lipid transfer protein PRELID1, normally degraded by YME1L, accumulated (Fig. 3G) (38). Notably, *Yme1l* is specifically deleted in cardiomyocytes and was not lost in cardiac fibroblasts isolated from cYKO mice. However, in vitro deletion of *Yme1l* in adult cardiac fibroblasts did recapitulate fragmentation of the mitochondrial network (fig. S3, C and D) and impaired OPA1 processing (fig. S3E) as observed in *Yme1l*^{-/-} cardiomyocytes. Thus, YME1L deficiency in cardiomyocytes induces OPA1 processing and mitochondrial fragmentation, which raises the possibility that disturbed mitochondrial morphology could cause heart failure in cYKO mice.

Deletion of *Oma1* restores mitochondrial morphology and myocardial function in the absence of YME1L

The accumulation of OPA1 forms c and e in cardiomyocytes lacking YME1L indicated activation of OMA1, as previously observed in YME1L-deficient mouse embryonic fibroblasts (MEFs) in vitro (25). Because additional deletion of *Oma1* in *Yme1l*^{-/-} MEFs restores tubular mitochondria and apoptotic resistance (25), we reasoned that ablation of *Oma1* may preserve the mitochondrial network in cardiomyocytes lacking YME1L. To examine the role of disturbed mitochondrial morphology in DCM and heart failure in cYKO mice, we generated double-knockout mice lacking both YME1L and OMA1 specifically in cardiomyocytes (cDKO; *Myh6-Cre*^{tg/wt}*Yme1l*^{LoxP/LoxP}*Oma1*^{LoxP/LoxP}) and monitored heart function (Fig. 4A). In contrast to cYKO mice, cDKO mice showed normal cardiac function and normal exercise tolerance in treadmill tests (Fig. 4, B to D). Myocardial fibrosis present in cYKO mice (Fig. 2E) was absent in cDKO hearts (Fig. 4E). Moreover, TEM analysis of cDKO hearts revealed that mitochondrial fragmentation was largely suppressed (Fig. 4, F and G). Similarly, mitochondrial morphology was restored in primary adult cardiomyocytes isolated from cDKO mice (Fig. 4, H and I). L-OPA1 processing was prevented in these cells, whereas other YME1L substrates such as PRELID1 continued to accumulate to

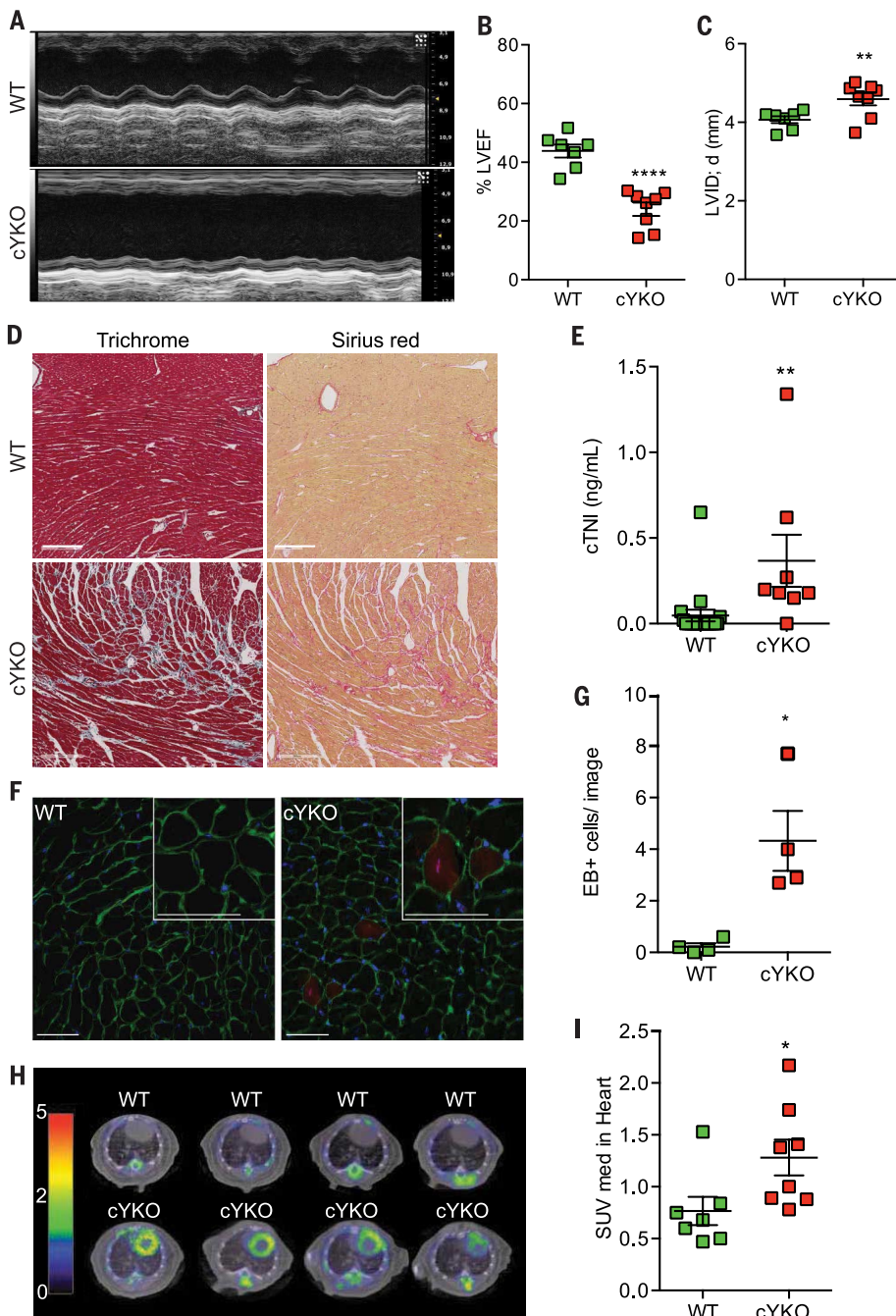
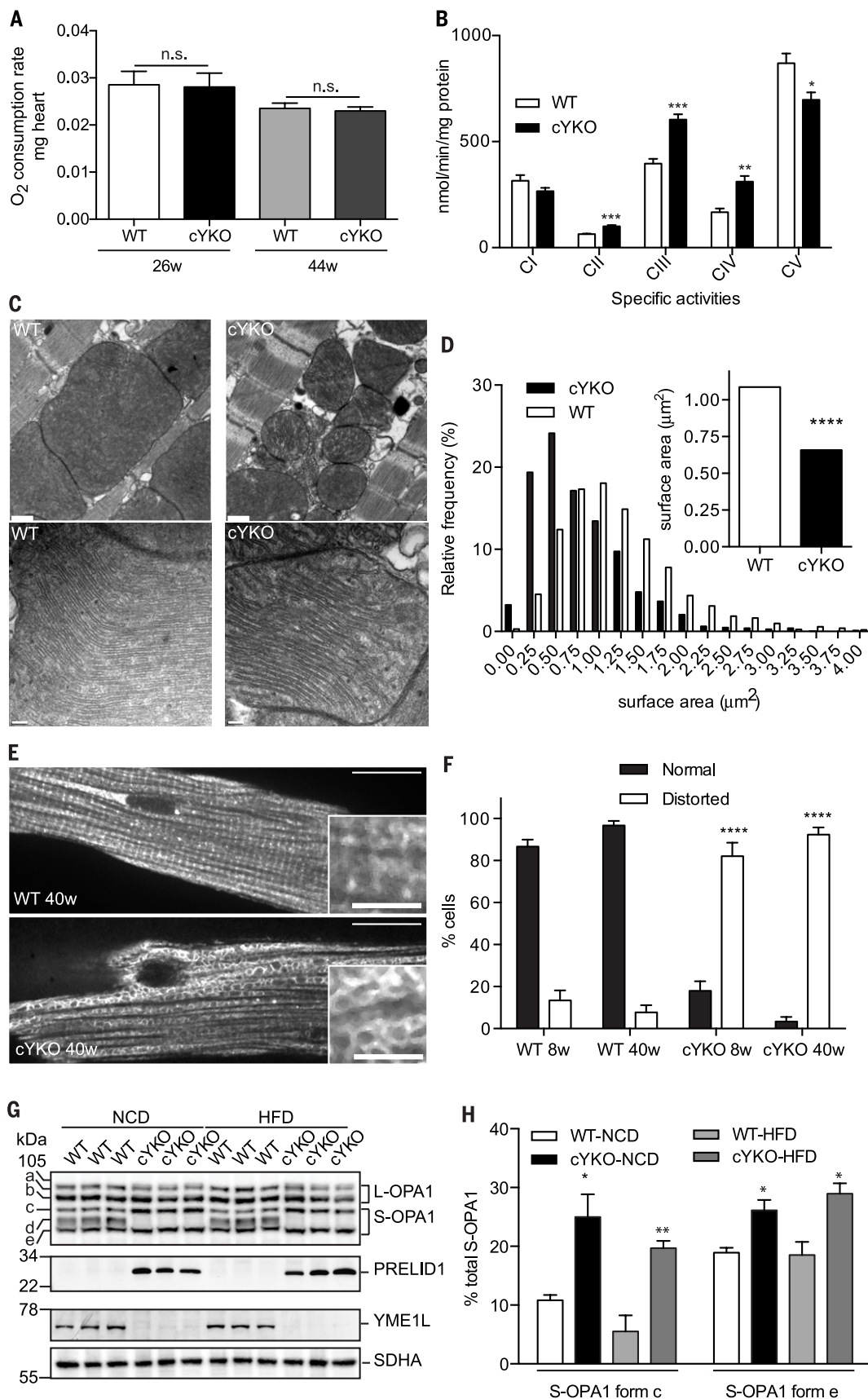


Fig. 2. Deletion of *Yme1l* causes dilated cardiomyopathy and heart failure. (A to C) Echocardiographic evaluation of cardiac function (by M-mode) of randomized 40-week-old WT ($n = 8$) and cYKO ($n = 8$) males reveals DCM characterized by (B) reduced LVEF (**** $P < 0.0001$) and (C) increased left ventricular internal dimension (LVID) [d (mm), ** $P = 0.0154$]. (D) Cardiac fibrosis in cYKO mice monitored by trichrome and sirius red staining of heart sections [40 weeks old (40w), $n = 3$; scale bar, 200 μ m]. (E) Increased serum levels of cardiac troponin (cTNI ng/ml) in 30-week-old cYKO mice ($n = 8$) relative to WT ($n = 19$). Mann-Whitney test, ** $P = 0.0027$. (F and G) Cardiomyocyte necrosis analysis of 20-week-old cYKO ($n = 4$) and WT ($n = 4$) hearts stained with Evans Blue (EB red), wheat germ agglutinin (green), and DAPI (blue). Individual t test, * $P = 0.0286$; scale bar, 50 μ m. (H) PET-CT of 40-week-old cYKO ($n = 8$) and WT ($n = 7$) animals after [18 F]FDG injections. Representative images of four cYKO and four WT thoracic scans are shown. (I) Average standardized uptake value (SUV) in WT ($n = 7$) and cYKO hearts ($n = 8$); unpaired t test, * $P = 0.0140$. In graphs, data are means \pm SEM.

Fig. 3. Stress-induced OPA1 processing in cardiomyocytes perturbs mitochondrial morphology.

(A) Ex vivo respiration measured in resting hearts ($n = 3$ to 5) from 26- and 44-week-old WT (white or pale gray) and cYKO (black or dark gray) mice. Linear oxygen uptake rates are presented as nmol O_2 /min per mg (weight, heart weight). Differences were not significant. (B) Respiratory chain activity measurements of complex I to V (CI to CV) in 44-week-old hearts of WT (white) and cYKO (black) mice. Individual unpaired t tests ($n = 3$ to 5); CI ($P = 0.1442$), CII ($***P = 0.0003$), CIII ($***P = 0.0003$), CIV ($**P = 0.0020$), and CV ($*P = 0.0172$). (C) TEM of 20-week-old WT and cYKO hearts (thick scale bar, 500 nm; thin scale bar, 100 nm). (D) Mitochondrial size was represented as median surface area, and frequency distributions of mitochondrial surface were calculated from 20-week-old WT ($n = 4224$) and cYKO ($n = 2308$) mitochondria imaged by TEM. Kruskal-Wallis test, $****P < 0.0001$. Data are median values. (E) Indirect immunocytochemistry with antibodies directed against TOMM20 (a rabbit-specific antibody) in cardiomyocytes isolated from WT ($n = 3$) and cYKO ($n = 3$) mice (thin scale bar, 30 μm ; thick scale bar, 75 μm). 40w, 40 weeks old. (F) Mitochondrial morphology in WT (8w, $n = 2$; 40w, $n = 3$) and cYKO (8w, $n = 2$; 40w, $n = 3$) cardiomyocytes ($****P < 0.0001$). Cells (>100) were counted. 8w, 8 weeks old. (G) Immunoblot analysis of cardiomyocytes isolated from 40-week-old mice fed a normal chow diet (NCD) or high-fat diet (HFD). SDHA was used as a loading control. (H) Quantification of OPA1 processing in hearts of WT and cYKO mice (Fig. 3F). (Pairwise t test, $*P < 0.05$, $**P < 0.01$) relative to WT-NCD controls. In graphs (B), (F), and (H), data are means \pm SEM.



similar levels as in cardiomyocytes of cYKO mice (Fig. 4J).

Thus, YME1L ablation in cardiomyocytes activates OMA1 and promotes OPA1 processing and mitochondrial fragmentation, which causes DCM and heart failure.

Loss of YME1L in skeletal muscle preserves the function of YME1L-deficient hearts

The results obtained from cardiomyocyte-specific knockout mice establish an essential role of YME1L for normal cardiac function in vivo. We

observed, to our surprise, the normal life span of mice lacking YME1L both in cardiomyocytes and skeletal muscle (hmYKO for heart and muscle-specific YME1L knockout; median life span 125 weeks) (Fig. 5A, fig. S5A, and table S1). hmYKO mice were obtained by crossing *Yme1L^{LoxP/LoxP}*

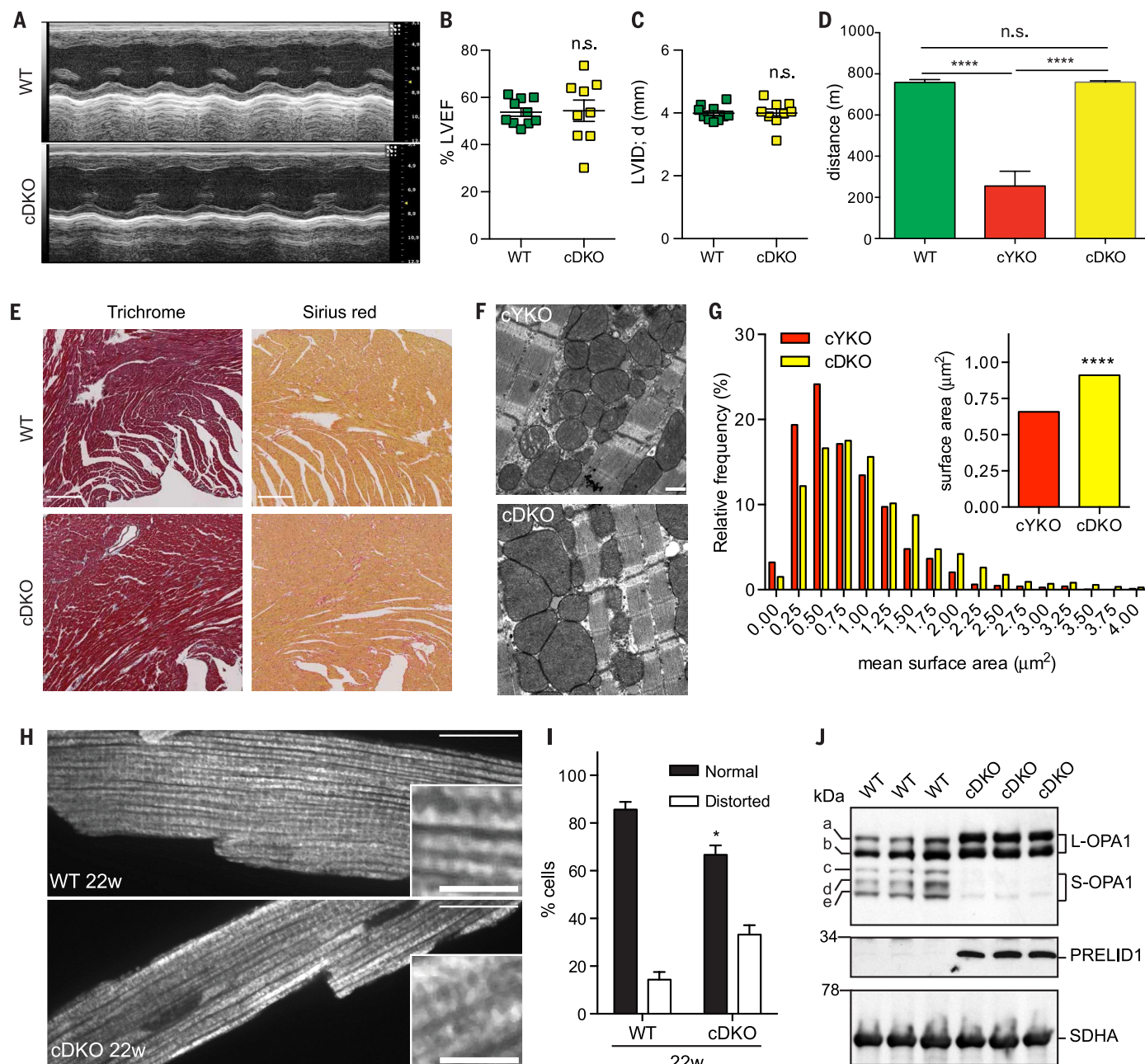


Fig. 4. *Oma1* ablation restores mitochondrial morphology and protects cYKO mice against DCM and heart failure. (A) Echocardiographic evaluation of cardiac function (by M-mode) of 22-week-old WT and cDKO mice. (B and C) Percentage LVEF and (C) diastolic LVID of 22-week-old WT ($n = 10$) and cDKO ($n = 9$) mice. n.s., not significant. (D) Treadmill endurance of 20-week-old WT ($n = 10$), cYKO ($n = 10$), and cDKO ($n = 5$) mice (5% incline). cYKO mice versus WT, **** $P = 0.0003$; cYKO versus cDKO, **** $P = 0.0001$. (E) Suppression of cardiac fibrosis in cDKO mice. Trichrome and sirius red staining of heart sections of 22-week-old WT and cDKO mice ($n = 3$). Scale bar, 200 μm. (F) TEM of 20-week-old cYKO and cDKO hearts (thick scale bar, 500 nm).

(G) Mitochondrial size represented as median surface area and frequency distributions of mitochondrial surface calculated from 20-week-old cYKO ($n = 2308$) and cDKO ($n = 3122$) mitochondria imaged by TEM. Kruskal-Wallis test, **** $P < 0.0001$. Data are median values. (H) Indirect immunocytochemistry with TOMM20-specific antibodies in cardiomyocytes isolated from 22-week-old WT and cDKO mice (thin scale bar, 30 μm; thick scale bar, 7.5 μm). (I) Quantification of mitochondrial morphology from (H) ($n = 3$, $n > 100$ cells; * $P = 0.0112$). In (B) to (D) and (I), data are means \pm SEM. (J) Immunoblot analysis of cardiomyocytes from 22-week-old WT ($n = 3$) and cDKO ($n = 3$) mice. SDHA was used as a loading control.

mice to mice expressing Cre recombinase under the control of the muscle creatine kinase (*Ckmm*) promoter, which is active in cardiomyocytes and additionally in skeletal muscle (39). Note that differences in life span could not be explained by differences in the efficiency of *Yme1l* deletion: mRNA (fig. S5B) and protein (fig. S5C) levels were pro-

foundly depleted in adult hearts of both *cYKO* and *hmYKO* mice. *YME1L* was lost with similar efficiencies and kinetics upon Cre recombinase-mediated deletion of *Yme1l* both in postnatal hearts of *cYKO* and *hmYKO* mice (fig. S5, D to G). Unlike *cYKO* mice, however, myocardial activity was preserved in *hmYKO* mice. We observed normal

heart function by echocardiography and normal cardiac uptake of [18 F]FDG in these mice (Fig. 5, B to D, and fig. S5, H and I).

We analyzed the morphology of mitochondria in *hmYKO* hearts by TEM. Smaller mitochondria accumulated in hearts of *hmYKO* mice as observed in *cYKO* mice, which indicated mitochondrial

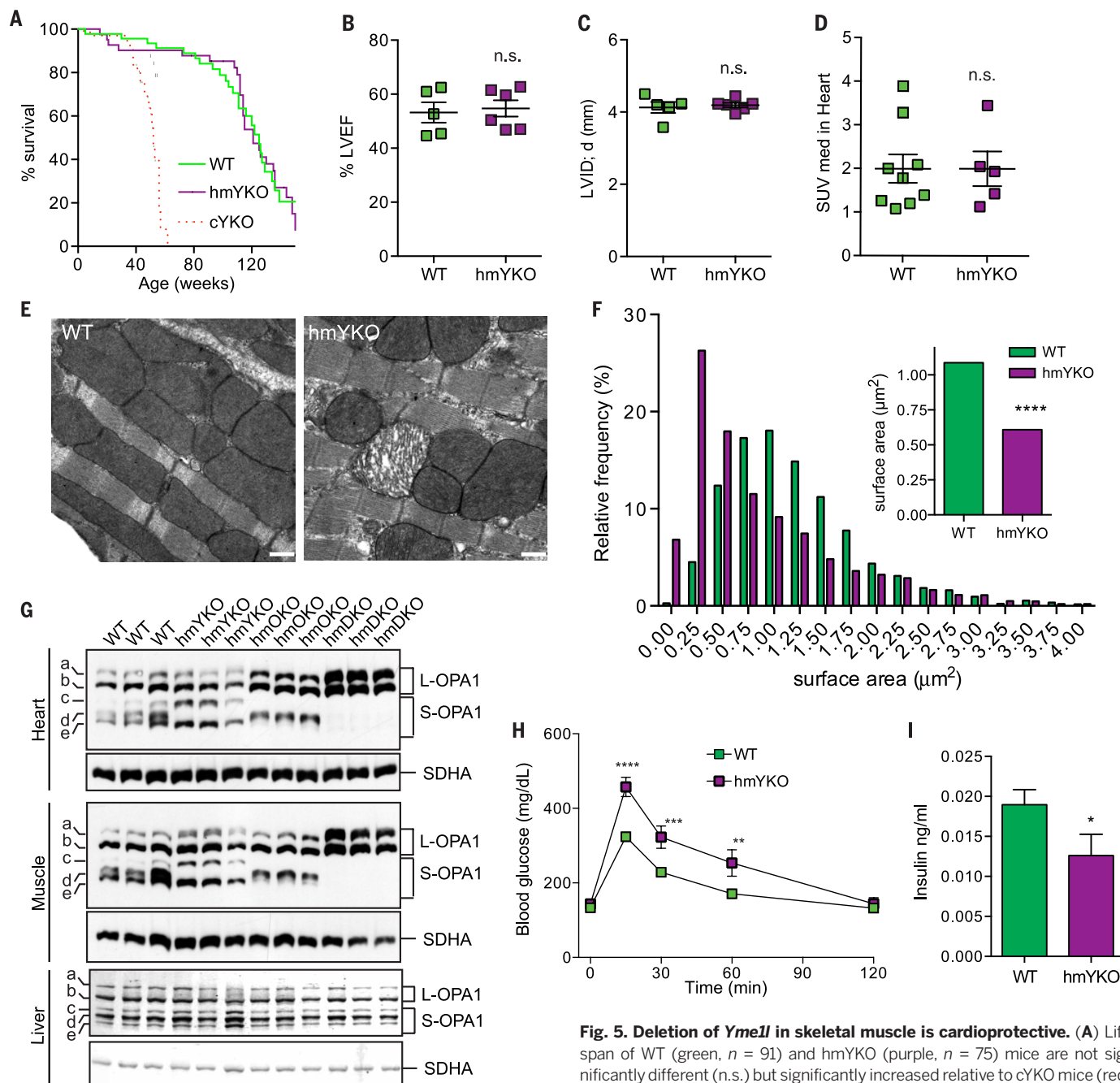


Fig. 5. Deletion of *Yme1l* in skeletal muscle is cardioprotective. (A) Life span of WT (green, $n = 91$) and *hmYKO* (purple, $n = 75$) mice are not significantly different (n.s.) but significantly increased relative to *cYKO* mice (red, $n = 69$; log-rank Mantel-Cox test, **** $P < 0.0001$).

(B and C) Percentage LVEF and diastolic LVID in 46-week-old WT ($n = 5$) and *hmYKO* ($n = 6$) mice analyzed by echocardiography (fig. S5A). (D) PET-CT average standardized cardiac glucose uptake in 46-week-old WT (green, $n = 8$) and *hmYKO* (purple, $n = 5$) mice fed normal chow. (E) TEM of 20-week-old WT and *hmYKO* hearts (thick scale bar, 500 nm).

(F) Mitochondrial size represented as median surface area and frequency distributions of mitochondria surface calculated from 20-week-old WT ($n = 4224$) (Fig. 3, C and D) and *hmYKO* ($n = 3246$) mitochondria imaged by TEM. Kruskal-Wallis test, **** $P < 0.0001$. Data are median values. (G) Immunoblot analysis of lysates from heart skeletal muscle and liver of 18-week-old *hmYKO* mice ($n = 3$), *hmOKO* mice (*Ckmm*-Cre; *Oma1*^{LoxP/LoxP}, $n = 3$), and *hmDKO* mice (*Ckmm*-Cre; *Oma1*^{LoxP/LoxP} *Yme1l*^{LoxP/LoxP}, $n = 3$) reveals altered OPA1 processing. (H) Intraperitoneal glucose tolerance tests in 18-week-old WT ($n = 18$) and *hmYKO* ($n = 13$) mice. Two-way ANOVA (** $P < 0.01$, *** $P < 0.001$, **** $P < 0.0001$) relative to WT controls. (I) Fasting insulin levels in 20-week-old WT ($n = 6$) and *hmYKO* ($n = 7$) mice. (* $P = 0.0357$). In (A), (C), (F), (H), and (I), data are means \pm SEM.

fragmentation (Fig. 5, E and F). These morphological changes corresponded to defects in OPA1 processing that were similar in cardiomyocytes isolated from hmYKO and cYKO mice (Figs. 3G and 5G). In both models, deletion of *Yme1l* in cardiomyocytes prevented formation of S-OPA1 form d, whereas S-OPA1 forms c and e accumulated, which was indicative of OMA1 activation (fig. S5F). OPA1 processing was affected similarly upon loss of YME1L in skeletal muscle of hmYKO mice (Fig. 5G) but normal in skeletal muscle of cYKO mice harboring YME1L (Fig. 1E). Thus, loss of YME1L impairs OPA1 processing and induces mitochondrial fragmentation in cardiomyocytes of both cYKO and hmYKO mice. Furthermore, additional deletion of *Yme1l* in skeletal muscle maintains heart function and life span without

restoring mitochondrial morphology defects in cardiomyocytes lacking YME1L.

Mitochondrial dysfunction in skeletal muscle is associated with impaired insulin signaling and glucose intolerance (40–42). Thus, possible endocrine effects owing to the loss of YME1L in skeletal muscle may cause metabolic alterations in cardiomyocytes; this preserves heart function downstream of mitochondrial deficiencies. We thus investigated systemic glucose homeostasis and performed intraperitoneal glucose tolerance tests (GTT) in both hmYKO and cYKO mice (Figs. 5H and 6A). We observed glucose intolerance in hmYKO mice but not in cYKO mice (Figs. 5H and 6A), which suggested that deletion of *Yme1l* in skeletal muscle impaired glucose homeostasis systemically. Additional ablation of *Oma1* in hmYKO

mice (hmDKO; table S1) prevented OPA1 processing in both heart and skeletal muscle (Fig. 5G) and restored normal glucose tolerance (fig. S5F). Thus, stress-induced OPA1 processing by OMA1 in skeletal muscle impairs glucose homeostasis in hmYKO mice.

Deletion of *Pgc1a* in skeletal muscle significantly impairs glucose-stimulated insulin secretion, which suggests a cytokine-mediated cross-talk between skeletal muscle and pancreatic islets (41). In agreement with these findings, we observed lowered fasting insulin concentration in the serum of hmYKO mice (Fig. 5I), although *Yme1l* was not deleted in the pancreas of these mice. hmYKO mice had normal fasting blood glucose (fig. S5G), normal weight gains (fig. S5H), and body composition as normal lean and fat mass (fig. S5I).

Fig. 6. Suppression of DCM and heart failure by dietary intervention. (A)

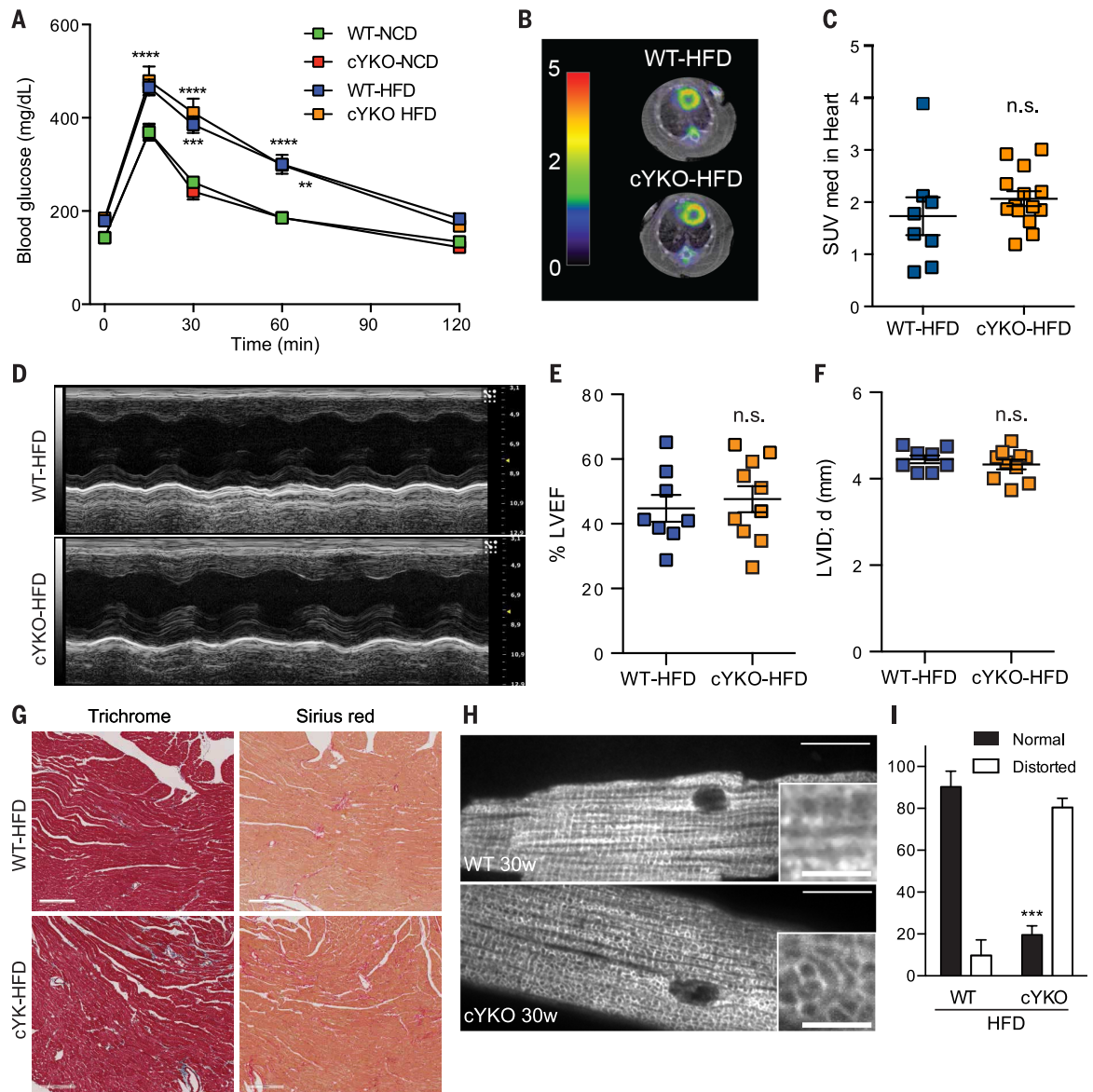
Intraperitoneal glucose tolerance tests in WT (green, $n = 30$; blue, $n = 13$) and cYKO (orange, $n = 5$; red, $n = 14$) mice fed HFD or NCD. Two-way ANOVA ($*P < 0.05$, $**P < 0.01$, $***P < 0.001$, $****P < 0.0001$) relative to WT-NCD controls.

(B) PET-CT in 30-week-old WT and cYKO mice treated with HFD starting at 9 weeks of age. Representative images of 2 cYKO and 2 WT mice are shown.

(C) Average standardized cardiac glucose uptake in 30-week-old WT ($n = 8$; blue) and cYKO mice ($n = 14$; orange) treated with HFD starting at 9 weeks of age.

(D) Echocardiographic M-mode images of 30-week-old WT and cYKO mice fed with HFD starting at 9 weeks of age. (E and F) Percentage LVEF and diastolic LVID of WT ($n = 14$) and cYKO ($n = 10$) mice. n.s., not significant. (G) Trichrome and sirius red stainings of heart sections of 40-week-old HFD-fed

WT ($n = 3$) and cYKO ($n = 3$) mice. Scale bar, 200 μm . (H) Indirect immunocytochemistry using antibodies directed against TOMM20 in cardiomyocytes isolated from 30-week-old HFD-fed WT ($n = 3$) and cYKO ($n = 3$) mice (thin scale bar, 30 μm ; thick scale bar, 7.5 μm). OPA1 processing in these cells is shown in Fig. 3G. (I) Quantification of mitochondrial morphology from (H) (WT, $n \geq 100$ cells; cYKO, $n = 3$; $***P = 0.001$). In graphs, data are means \pm SEM.



Thus, loss of YME1L in skeletal muscle induces systemic glucose intolerance and lowers insulin levels, which blunts increased cardiac glucose uptake and alters cardiac metabolism. Furthermore, cell nonautonomous metabolic alleviation can preserve cardiac function and prevent DCM and heart failure despite mitochondrial fragmentation in cardiomyocytes.

Feeding a high-fat diet suppresses heart failure and restores the life span of cYKO mice

The protective effect of systemic glucose intolerance on the heart suggests that deleterious effects of mitochondrial fragmentation in cardiomyocytes can be circumvented by metabolic intervention. To provide further support for this notion, we subjected wild-type (WT) and cYKO mice to a high-fat diet. This diet is commonly used to dysregulate systemic glucose homeostasis. It impairs insulin signaling in target tissues and compromises glucose-stimulated insulin secretion by pancreatic β cells triggering obesity. Mice were fed a high-fat diet beginning at 9 weeks of age, at a time when cardiac function was normal. Both WT and cYKO mice fed a high-fat diet gained weight significantly more rapidly than mice fed normal chow (fig. S6A) and exhibited reduced glucose tolerance (Fig. 6A).

To determine whether this dietary intervention could influence cardiac metabolism, we examined the cardiac uptake of [18 F]FDG by PET-CT and determined levels of endogenous glucose and acylcarnitine in the hearts of high fat-fed cYKO mice. In contrast to mice fed normal chow, we did not observe significant differences in cardiac glucose uptake (Fig. 6, B and C) nor in the levels of endogenous cardiac glucose or acylcarnitine between high fat-fed WT and cYKO mice (fig. S2, D and

F). The adjustment of the levels of these cardiac metabolites was accompanied by restoration of cardiac function in cYKO mice (Fig. 6, D to F, and fig. S5B): left ventricular ejection fraction (LVEF) and left ventricular chamber diameter values were indistinguishable from those of high fat-fed littermate controls. Treatment with the high-fat diet also prevented cardiac fibrosis (Fig. 6G) and suppressed differences in exercise tolerance previously observed between WT and cYKO mice fed normal chow (fig. S6, C and D).

Similar to normally fed cYKO mice (Fig. 3, F and G), cardiomyocytes isolated from high fat-fed cYKO mice still contained distorted mitochondria (Fig. 6, H and I), because the high-fat diet had not rescued the proteolytic activity of YME1L or OMA1-dependent, stress-induced processing of OPA1 (Fig. 3G, H). High-fat feeding did not markedly alter oxygen consumption or the activity of respiratory complexes in cYKO mice (fig. S6, E and F). Thus, the consequences of mitochondrial defects in cYKO mice can be metabolically circumvented to suppress cardiomyopathy.

Discussion

In these experiments, we observed the deleterious effects of stress-induced OPA1 processing and mitochondrial fragmentation on myocardial function, which revealed an unexpected functional link between systemic glucose homeostasis, cardiac metabolism, and mitochondrial dynamics in vivo.

Uncleaved, fusion-active L-OPA1 is sufficient to maintain cardiac activity. Mice lacking both YME1L and OMA1 in cardiomyocytes exhibited normal heart function, which demonstrates that proteolytic cleavage of OPA1 by YME1L and OMA1 is dispensable. The previously described, essential role of OPA1 for normal cardiac functioning can

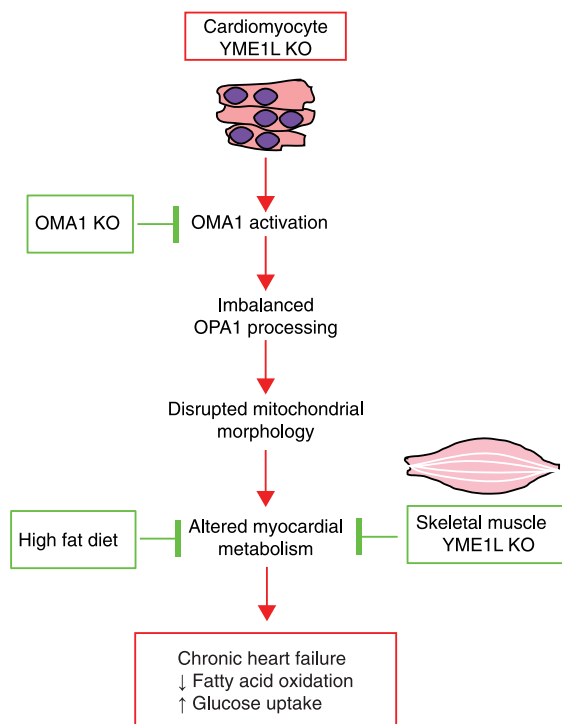
thus be attributed to the loss of L-OPA1 (43, 44). L-OPA1 is sufficient to mediate mitochondrial fusion, which serves a prosurvival function (24–26). Mitochondrial fusion protects against mitophagy (4, 45) and is thought to serve a repair function by allowing content mixing and by preventing the accumulation of mitochondrial damage in cultured cells (46). Although mitochondrial fusion occurs infrequently in adult cardiomyocytes (7), it is required for cardiomyocyte differentiation and cardiac development (7, 47–51).

Whereas L-OPA1 is sufficient to preserve cardiac function, accumulation of S-OPA1 and unopposed fission is deleterious for the heart. Our results establish cardiomyocyte-specific YME1L-deficient mice as a model for DCM and heart failure, which culminates in middle-aged death (Fig. 7). The loss of YME1L activates OMA1 and triggers stress-induced OPA1 processing, which unbalances fusion and fission of mitochondria and impairs mitochondrial morphology in cardiomyocytes. In the absence of YME1L, we observed the accumulation of smaller mitochondria in the heart and mitochondrial fragmentation in cardiomyocytes and cardiac fibroblasts in vitro. Mitochondrial fragmentation is caused by the loss of L-OPA1 forms mediating fusion and the concomitant accumulation of S-OPA1 forms c and e that are generated by OMA1 and are associated with fission (21, 23–26). Deletion of *Oma1* restores normal mitochondrial morphology in cardiomyocytes lacking YME1L and myocardial activity in vivo, which demonstrates that accelerated OPA1 processing and mitochondrial fragmentation cause heart failure (Fig. 7). Consistent with a deleterious effect of unopposed fission in the heart (7), pharmacological inhibition of mitochondrial fission protects against ischemia and reperfusion injury (52). Notably, germline deletion of *Oma1* does not impair embryogenesis and is not able to suppress postimplantation embryonic lethality of *Yme1l*^{−/−} embryos (fig. S1F), which indicates that stress-induced OPA1 processing is not deleterious for prenatal organogenesis in these mice.

How does stress-induced OPA1 processing and mitochondrial fragmentation affect cardiac function? Mitochondria are vital for the beating heart, and defects in mitochondrial respiration cause cardiac dysfunction (36, 53, 54). However, we observed only a minor impairment of respiratory activities and ATP synthesis and no accumulation of lactate in YME1L-deficient hearts, unlike other animal models of mitochondrial cardiomyopathy (7, 36, 51, 54). Whereas severe and lethal cardiomyopathies manifest not long after birth in most of these models, cardiac ablation of YME1L causes DCM and death at ~1 year of age.

Unrestrained autophagy can also cause cardiomyocyte loss and heart failure (55), which raises the possibility that stress-induced OPA1 processing and the accumulation of S-OPA1 affects the autophagic disposal of mitochondria. The analysis of heart-specific DRP1 knockout mice indeed pointed to a major role of DRP1 and fission for mitochondrial quality-control and autophagy in the heart (56–58). However, autophagic marker proteins such as p62/SQSTM1 or microtubule-associated

Fig. 7. Unbalanced mitochondrial dynamics in cardiomyocytes upon loss of YME1L causes DCM and heart failure. Unregulated OPA1 processing by OMA1 causes metabolic alterations triggering DCM and heart failure in cardiomyocyte-specific *Yme1l*^{−/−} mice. Heart function is preserved upon restoration of mitochondrial morphology by *Oma1* ablation or without suppressing mitochondrial morphology defects by metabolic intervention bypassing deleterious effects of disturbed mitochondrial dynamics on cardiac metabolism.



protein 1 light chain 3 did not accumulate in YME1L-deficient heart nor were myocardial amino acid levels altered (fig. S7, A and B). Thus, increased autophagy is unlikely to cause the loss of cardiomyocytes in this model. In contrast, our results suggest that stress-induced OPA1 processing by OMA1 promotes cardiomyocyte death in the absence of YME1L (fig. S7, C and D). We observed increased serum levels of cardiac troponin, fibrotic remodeling, and necrotic cell death, as well as the dysregulation of genes functionally linked to cell death in YME1L-deficient hearts (fig. S7, C and D). These results identify OMA1 as a critical regulator of cardiomyocyte survival in vivo, consistent with an antiapoptotic effect of OMA1 in cultured cells (21, 25, 29). Note that cardiac mitochondria form normal cristae in the absence of YME1L. Thus, cristae remodeling and facilitated cytochrome c release does not drive cell death in these mice, which instead is triggered by the loss of L-OPA1 and the impairment of mitochondrial fusion. In light of these observations, it is conceivable that the recently reported, protective effect of OPA1 overexpression in various mouse models for mitochondrial disease (59, 60) can be attributed to L-OPA1 alone, which drives fusion and can support cell survival independent of cristae morphogenesis.

Similar to previous models for the failing heart (36, 61), the cardiomyocyte-specific loss of YME1L and disturbed mitochondrial dynamics provoked a downstream metabolic shift from lipid to glucose metabolism in the myocardium. We observed reduced levels of acylcarnitine and increased glucose uptake that indicated reinforced myocardial glucose utilization, which is known to be associated with heart failure when combined with disturbed fatty acid metabolism (37). These alterations occur in the absence of overt respiratory deficiencies, which were previously observed to enhance cardiac glucose metabolism (36, 61), which highlights the regulatory role of mitochondrial dynamics in cardiac metabolism. Increasing evidence indeed supports a close link between energy metabolism and mitochondrial fusion and fission in various tissues, including the central nervous system and brown adipose tissue, and suggests an association between mitochondrial fission, lipid metabolism, and energy expenditure (62–64).

Our experiments provide strong evidence that alterations in metabolism cause heart failure in cYKO mice. Additional deletion of *Yme1l* in skeletal muscle preserved cardiac function and normal life span of mice lacking YME1L in cardiomyocytes without restoring defects in mitochondrial morphology (Fig. 7). This is likely due to an endocrine effect by the skeletal muscle on glucose uptake in the heart. Dysfunction of mitochondria in skeletal muscle was previously reported to affect systemic glucose metabolism by impairing insulin secretion by pancreatic β cells and glucose uptake in target tissues (41). Similarly, we observed lowered fasting-insulin concentrations, systemic glucose intolerance, and normalized heart glucose uptake in mice upon additional deletion of *Yme1l* in skeletal muscle. Loss of YME1L appears to impair insulin

signaling via its effect on mitochondrial dynamics and stress-induced OPA1 processing by OMA1, because we observed normal systemic glucose homeostasis in mice lacking both OMA1 and YME1L in skeletal muscle. These results highlight the physiological importance of tissue cross-talk that must be taken into consideration when analyzing tissue-specific models for mitochondrial disease.

Further support for a critical role of disturbed cardiomyocyte metabolism for heart failure came from the observation that feeding a high-fat diet preserved normal cardiac function of cardiomyocyte-specific YME1L knockout mice (Fig. 7). Similar to ablation of *Yme1l* in skeletal muscle, this metabolic intervention did not circumvent the primary mitochondrial defects in cardiomyocytes because the catalytic activity of YME1L, OMA1 activation, mitochondrial morphology, and respiratory chain profiles were unaffected by diet. However, it did blunt downstream metabolic disruptions and normalized cardiac glucose uptake in cardiomyocyte-specific YME1L knockout mice, which suppressed cell death and preserved cardiac function. Remarkably, feeding of cardiomyocyte-specific YME1L knockout mice with a high-fat diet prevents cardiomyopathy at least at early stages despite normal weight gain of the mice. Echocardiographic analyses of failing cYKO hearts demonstrate that these mice have reduced contractile function but normal left ventricular mass, which suggests that YME1L ablation does not result in a concentric hypertrophic response, and thus cardiac dysfunction can be improved by metabolic intervention. In this sense, some forms of DCM in humans can be treated by pharmacological means (65). Consistent with previous reports (37), high-fat feeding of WT mice did not incite contractile dysfunction (table S2). In contrast, feeding mice manifesting cardiomyopathy associated with ventricular hypertrophy a high-fat diet exacerbates myocardial dysfunction (66, 67). It is thus an intriguing possibility that this metabolic intervention is beneficial exclusively in the context of DCM. Our results reveal an intimate relation between alterations in mitochondrial morphology and metabolism in the heart, which may underlie myocardial disease in humans. Metabolic interventions can preserve cardiac function even if mitochondrial morphology is disturbed, which opens potential avenues for therapeutic interventions in myocardial disease.

Methods

Echocardiography and PET-CT

Echocardiography and functional examination in mice was performed as previously described (68). All PET-CT studies were performed with a small-animal PET-CT device. Briefly, animals were fasted overnight, and anatomic thorax CT scanning was performed 1 hour after [^{18}F]FDG injections, followed by metabolic PET static acquisition for 15 min. Image analysis was performed in prefused and prereconstructed images with Osirix (Aycam Medical Systems, LLC); we selected myocardium of the whole left ventricle and calculated mean myocardial standardized uptake value (SUV

med) for each animal. See supplemental methods for full methods description.

Incline treadmill

Treadmill experiments were conducted using a TSE treadmill and up to six randomized mice assessed simultaneously. Low-intensity incline (5%) experiments began at 0.05 m/s and increasing to 0.1 m/s for 60 s, 0.1 m/s for 600 s, then increasing to 0.28 m/s for 3100 s by 172-s increments. Blinded determination of exercise exhaustion was assessed and plotted as a function of total distance (m).

Histology and immunochemistry

Paraffin-embedded sections (4 μm) were subjected to hematoxylin and eosin, picrosirius red, or Masson's trichrome staining. Images were acquired using a Leica SCN400 automated slide scanner at 40 \times .

Generation of primary cardiomyocytes and cardiac fibroblasts

Adult cardiomyocytes were isolated by retrograde Langerdorff perfusion with an enzymatic digestion buffer containing trypsin and Liberase (Roche Applied Science) (68). Primary cardiac fibroblasts obtained during cardiomyocyte isolations were immortalized using a plasmid encoding SV40 large T antigen and deleted for *Yme1l* in vitro. See supplemental methods for full methods description.

Transmission electron microscopy (TEM)

Left ventricle samples of hearts perfused with paraformaldehyde [2% (w/v) in phosphate-buffered saline (PBS)] and glutaraldehyde [2% (w/v) in PBS] hearts were fixed for 3 days in 2% (v/v) glutaraldehyde, 2.5% (w/v) sucrose, 3 mM CaCl_2 , and 100 mM HEPES-KOH, pH 7.4, at 4°C. After washes, samples were fixed using reduced OsO_4 [1% (w/v) OsO_4 , 10 mg/ml potassium ferrocyanide, 1.25% (w/v) sucrose, and 100 mM sodium cacodylate, pH 7.4] for 1 hour on ice. After washes in water, cells were incubated in 2% (w/v) uranyl acetate for 30 min. After dehydration with 50, 70, 90, and 100% ethanol, samples were embedded in epon resin. Samples were observed under a transmission electron microscope (EM902; Carl Zeiss) at an acceleration voltage of 80 kV.

Confocal fluorescence microscopy

To monitor mitochondrial morphology by immunofluorescence microscopy, primary cardiomyocytes were fixed and stained with antibodies directed against TOMM20 (rabbit-specific antibody 1:1000, Santa Cruz Biotechnology). Fluorescently coupled secondary antibody Alexa Fluor 568 (a goat antibody directed against a rabbit secondary antibody) was used at 1:1000 dilution (Invitrogen). Images were acquired using an UltraVIEW VoX spinning disc microscope (CSU-X1; Yokogawa Corporation of America). Quantification of mitochondrial morphology in primary cardiomyocytes was performed by blinded, randomized examination of z-stack images. Cardiac necrosis was assessed by Evans Blue diffusion as previously described (57). Paraffin-embedded cardiac sections were stained with

fluorescein isothiocyanate-conjugated wheat germ agglutinin (Invitrogen, W834) for 30 min before nuclear counterstaining with 4',6'-diamidino-2-phenylindole (DAPI). Evans Blue-positive cardiomyocytes fluorescence is in red. Images were acquired using a Leica SP8 confocal microscope at 40 \times .

Blood glucose and serum analyses

Intraperitoneal GTTs were carried out in mice after they were fasted for 6 hours. After determination of fasted blood glucose levels, an intraperitoneal bolus of 2 g glucose/kg body weight [20% (w/v) glucose]. Blood glucose levels were determined after 15, 30, 60, and 120 min using Contour test strips (Bayer, Germany). Serum insulin levels were measured from blood collected from 6 hours fasted mice, by enzyme-linked immunosorbent assays (ELISAs), according to the manufacturer's instructions (Mouse/Rat Insulin ELISA, Mouse Leptin ELISA; Crystal Chem Inc.). Serum levels of cardiac troponin assayed by auto-analyzer Dimension RxL Max HM (Siemens).

Oxygen consumption measurements

Oxygen consumption of WT and cYKO hearts, fed normal chow diet (NCD) or high-fat diet (HFD), was measured using a fluorescence-based micro-optode that consisted of an optic fiber equipped with an oxygen-sensitive fluorescent terminal sensor (FireSting O₂; Bionef, Paris, France) as described previously (69). Hearts were perfused in buffer (10 mM KH₂PO₄, 300 mM mannitol, 10 mM KCl, 5 mM MgCl₂, 5 mM bovine serum albumin, pH 7.4), dissected, weighted, and assayed at rest, precisely 3 min after mice were killed by cervical dislocation. Oxygen uptake rates (nmol O₂/min) were adjusted relative to wet heart weight.

Respiratory chain measurements

Activity of respiratory chain complexes and citrate synthase was spectrophotometrically assayed as previously described (70).

Statistical analysis

Statistical analyses were performed using Prism (GraphPad Software Inc., San Diego, CA). All values are expressed as means \pm SEM. Statistical significance was assessed by using a two-tailed unpaired Student's *t* test or the Mann-Whitney test for two-group comparisons. Two-way analysis of variance (ANOVA) with Bonferroni post hoc tests (corrected *P* values are given for comparison between genotypes at specific time points) were used to evaluate multiple pairwise comparisons of groups. Life span survival curves were compared by using a log-rank Mantel-Cox test. Differences were considered statistically significant at a value of *P* < 0.05. **P* < 0.05, ***P* < 0.01, ****P* < 0.001, *****P* < 0.0001.

REFERENCES AND NOTES

- J. R. Friedman, J. Nunnari, Mitochondrial form and function. *Nature* **505**, 335–343 (2014). doi: [10.1038/nature12985](https://doi.org/10.1038/nature12985); pmid: [24429632](https://pubmed.ncbi.nlm.nih.gov/24429632/)
- P. Mishra, D. C. Chan, Mitochondrial dynamics and inheritance during cell division, development and disease. *Nat. Rev. Mol. Cell Biol.* **15**, 634–646 (2014). doi: [10.1038/nrm3877](https://doi.org/10.1038/nrm3877); pmid: [25237825](https://pubmed.ncbi.nlm.nih.gov/25237825/)
- F. Burté, V. Carelli, P. F. Chinnery, P. Yu-Wai-Man, Disturbed mitochondrial dynamics and neurodegenerative disorders. *Nat. Rev. Neurol.* **11**, 11–24 (2015). doi: [10.1038/nrneuro.2014.228](https://doi.org/10.1038/nrneuro.2014.228); pmid: [25486875](https://pubmed.ncbi.nlm.nih.gov/25486875/)
- G. W. Dorn 2nd, R. N. Kitsis, The mitochondrial dynamism-mitophagy-cell death interaction: Multiple roles performed by members of a mitochondrial molecular ensemble. *Circ. Res.* **116**, 167–182 (2015). doi: [10.1161/CIRCRESAHA.116.303554](https://doi.org/10.1161/CIRCRESAHA.116.303554); pmid: [25323859](https://pubmed.ncbi.nlm.nih.gov/25323859/)
- J. R. Friedman *et al.*, ER tubules mark sites of mitochondrial division. *Science* **334**, 358–362 (2011). doi: [10.1126/science.1207385](https://doi.org/10.1126/science.1207385); pmid: [21885730](https://pubmed.ncbi.nlm.nih.gov/21885730/)
- F. Korobova, V. Ramabhadran, H. N. Higgs, An actin-dependent step in mitochondrial fission mediated by the ER-associated formin INF2. *Science* **339**, 464–467 (2013). doi: [10.1126/science.1228360](https://doi.org/10.1126/science.1228360); pmid: [23349293](https://pubmed.ncbi.nlm.nih.gov/23349293/)
- Y. Chen, Y. Liu, G. W. Dorn 2nd, Mitochondrial fusion is essential for organelle function and cardiac homeostasis. *Circ. Res.* **109**, 1327–1331 (2011). doi: [10.1161/CIRCRESAHA.111.258723](https://doi.org/10.1161/CIRCRESAHA.111.258723); pmid: [22052916](https://pubmed.ncbi.nlm.nih.gov/22052916/)
- L. C. Gomes, L. Scorrano, Mitochondrial elongation during autophagy: A stereotypical response to survive in difficult times. *Autophagy* **7**, 1251–1253 (2011). doi: [10.4161/auto.7.10.16771](https://doi.org/10.4161/auto.7.10.16771); pmid: [21743300](https://pubmed.ncbi.nlm.nih.gov/21743300/)
- D. A. Patten *et al.*, OPA1-dependent cristae modulation is essential for cellular adaptation to metabolic demand. *EMBO J.* **33**, 2676–2691 (2014). doi: [10.15252/embj.201488349](https://doi.org/10.15252/embj.201488349); pmid: [25298396](https://pubmed.ncbi.nlm.nih.gov/25298396/)
- P. Mishra, V. Carelli, G. Manfredi, D. C. Chan, Proteolytic cleavage of Opa1 stimulates mitochondrial inner membrane fusion and couples fusion to oxidative phosphorylation. *Cell Metab.* **19**, 630–641 (2014). doi: [10.1016/j.cmet.2014.03.011](https://doi.org/10.1016/j.cmet.2014.03.011); pmid: [24703695](https://pubmed.ncbi.nlm.nih.gov/24703695/)
- C. R. Hackenbrock, Ultrastructural bases for metabolically linked mechanical activity in mitochondria. I. Reversible ultrastructural changes with change in metabolic steady state in isolated liver mitochondria. *J. Cell Biol.* **30**, 269–297 (1966). doi: [10.1083/jcb.30.2.269](https://doi.org/10.1083/jcb.30.2.269); pmid: [5968972](https://pubmed.ncbi.nlm.nih.gov/5968972/)
- D. Sebastián *et al.*, Mitofusin 2 (Mfn2) links mitochondrial and endoplasmic reticulum function with insulin signaling and is essential for normal glucose homeostasis. *Proc. Natl. Acad. Sci. U.S.A.* **109**, 5523–5528 (2012). doi: [10.1073/pnas.1108220109](https://doi.org/10.1073/pnas.1108220109); pmid: [22427360](https://pubmed.ncbi.nlm.nih.gov/22427360/)
- R. J. Youle, A. M. van der Bliek, Mitochondrial fission, fusion, and stress. *Science* **337**, 1062–1065 (2012). doi: [10.1126/science.1219855](https://doi.org/10.1126/science.1219855); pmid: [22936770](https://pubmed.ncbi.nlm.nih.gov/22936770/)
- G. Twig *et al.*, Fission and selective fusion govern mitochondrial segregation and elimination by autophagy. *EMBO J.* **27**, 433–446 (2008). pmid: [18200046](https://pubmed.ncbi.nlm.nih.gov/18200046/)
- A. Olichon *et al.*, Loss of OPA1 perturbs the mitochondrial inner membrane structure and integrity, leading to cytochrome c release and apoptosis. *J. Biol. Chem.* **278**, 7743–7746 (2003). doi: [10.1074/jbc.C200677200](https://doi.org/10.1074/jbc.C200677200); pmid: [12509422](https://pubmed.ncbi.nlm.nih.gov/12509422/)
- S. Cipolat, A. Martins de Brito, B. Dal Zilio, L. Scorrano, OPA1 requires mitofusin 1 to promote mitochondrial fusion. *Proc. Natl. Acad. Sci. U.S.A.* **101**, 15927–15932 (2004). doi: [10.1073/pnas.0407043101](https://doi.org/10.1073/pnas.0407043101); pmid: [15509649](https://pubmed.ncbi.nlm.nih.gov/15509649/)
- C. Frezza *et al.*, OPA1 controls apoptotic cristae remodeling independently from mitochondrial fusion. *Cell* **126**, 177–189 (2006). doi: [10.1016/j.cell.2006.06.025](https://doi.org/10.1016/j.cell.2006.06.025); pmid: [16839885](https://pubmed.ncbi.nlm.nih.gov/16839885/)
- P. M. Quirós, T. Langer, C. López-Otin, New roles for mitochondrial proteases in health, ageing and disease. *Nat. Rev. Mol. Cell Biol.* **16**, 345–359 (2015). doi: [10.1038/nrm3984](https://doi.org/10.1038/nrm3984); pmid: [25970558](https://pubmed.ncbi.nlm.nih.gov/25970558/)
- M. Roy, P. H. Reddy, M. Iijima, H. Sesaki, Mitochondrial division and fusion in metabolism. *Curr. Opin. Cell Biol.* **33**, 111–118 (2015). doi: [10.1016/j.cob.2015.02.001](https://doi.org/10.1016/j.cob.2015.02.001); pmid: [25703628](https://pubmed.ncbi.nlm.nih.gov/25703628/)
- L. Griparic, T. Kanazawa, A. M. van der Bliek, Regulation of the mitochondrial dynamin-like protein Opa1 by proteolytic cleavage. *J. Cell Biol.* **178**, 757–764 (2007). doi: [10.1083/jcb.200704112](https://doi.org/10.1083/jcb.200704112); pmid: [17709430](https://pubmed.ncbi.nlm.nih.gov/17709430/)
- B. Head, L. Griparic, M. Amiri, S. Gandre-Babbe, A. M. van der Bliek, Inducible proteolytic inactivation of OPA1 mediated by the OMA1 protease in mammalian cells. *J. Cell Biol.* **187**, 959–966 (2009). doi: [10.1083/jcb.200906083](https://doi.org/10.1083/jcb.200906083); pmid: [20038677](https://pubmed.ncbi.nlm.nih.gov/20038677/)
- Z. Song, H. Chen, M. Fiket, C. Alexander, D. C. Chan, OPA1 processing controls mitochondrial fusion and is regulated by mRNA splicing, membrane potential, and Yme1L. *J. Cell Biol.* **178**, 749–755 (2007). doi: [10.1083/jcb.200704110](https://doi.org/10.1083/jcb.200704110); pmid: [17709429](https://pubmed.ncbi.nlm.nih.gov/17709429/)
- S. Ehses *et al.*, Regulation of OPA1 processing and mitochondrial fusion by m-AAA protease isoenzymes and OMA1. *J. Cell Biol.* **187**, 1023–1036 (2009). doi: [10.1083/jcb.200906084](https://doi.org/10.1083/jcb.200906084); pmid: [20038678](https://pubmed.ncbi.nlm.nih.gov/20038678/)
- D. Tondera *et al.*, SLP-2 is required for stress-induced mitochondrial hyperfusion. *EMBO J.* **28**, 1589–1600 (2009). doi: [10.1038/emboj.2009.89](https://doi.org/10.1038/emboj.2009.89); pmid: [19360003](https://pubmed.ncbi.nlm.nih.gov/19360003/)
- R. Anand *et al.*, The i-AAA protease YME1L and OMA1 cleave OPA1 to balance mitochondrial fusion and fission. *J. Cell Biol.* **204**, 919–929 (2014). doi: [10.1083/jcb.201308006](https://doi.org/10.1083/jcb.201308006); pmid: [24616225](https://pubmed.ncbi.nlm.nih.gov/24616225/)
- N. Ishihara, Y. Fujita, T. Oka, K. Mihara, Regulation of mitochondrial morphology through proteolytic cleavage of OPA1. *EMBO J.* **25**, 2966–2977 (2006). doi: [10.1038/sj.emboj.7601184](https://doi.org/10.1038/sj.emboj.7601184); pmid: [16778770](https://pubmed.ncbi.nlm.nih.gov/16778770/)
- M. J. Baker *et al.*, Stress-induced OMA1 activation and autocatalytic turnover regulate OPA1-dependent mitochondrial dynamics. *EMBO J.* **33**, 578–593 (2014). doi: [10.1002/embj.201386474](https://doi.org/10.1002/embj.201386474); pmid: [24550258](https://pubmed.ncbi.nlm.nih.gov/24550258/)
- K. Zhang, H. Li, Z. Song, Membrane depolarization activates the mitochondrial protease OMA1 by stimulating self-cleavage. *EMBO Rep.* **15**, 576–585 (2014). doi: [10.1002/embr.201338240](https://doi.org/10.1002/embr.201338240); pmid: [24719224](https://pubmed.ncbi.nlm.nih.gov/24719224/)
- P. M. Quirós *et al.*, Loss of mitochondrial protease OMA1 alters processing of the GTPase OPA1 and causes obesity and defective thermogenesis in mice. *EMBO J.* **31**, 2117–2133 (2012). doi: [10.1038/emboj.2012.70](https://doi.org/10.1038/emboj.2012.70); pmid: [22433842](https://pubmed.ncbi.nlm.nih.gov/22433842/)
- X. Jiang, H. Jiang, Z. Shen, X. Wang, Activation of mitochondrial protease OMA1 by Bax and Bak promotes cytochrome c release during apoptosis. *Proc. Natl. Acad. Sci. U.S.A.* **111**, 14782–14787 (2014). doi: [10.1073/pnas.1417253111](https://doi.org/10.1073/pnas.1417253111); pmid: [25275009](https://pubmed.ncbi.nlm.nih.gov/25275009/)
- Y. Ruan *et al.*, Loss of Yme1L perturbs mitochondrial dynamics. *Cell Death Dis.* **4**, e896 (2013). doi: [10.1038/cddis.2013.414](https://doi.org/10.1038/cddis.2013.414); pmid: [24176854](https://pubmed.ncbi.nlm.nih.gov/24176854/)
- X. Xiao *et al.*, OMA1 mediates OPA1 proteolysis and mitochondrial fragmentation in experimental models of ischemic kidney injury. *Am. J. Physiol. Renal Physiol.* **306**, F1318–F1326 (2014). doi: [10.1152/ajprenal.00036.2014](https://doi.org/10.1152/ajprenal.00036.2014); pmid: [24671334](https://pubmed.ncbi.nlm.nih.gov/24671334/)
- K. N. Papanicolaou *et al.*, Mitofusins 1 and 2 are essential for postnatal metabolic remodeling in heart. *Circ. Res.* **111**, 1012–1026 (2012). doi: [10.1161/CIRCRESAHA.112.274142](https://doi.org/10.1161/CIRCRESAHA.112.274142); pmid: [22904094](https://pubmed.ncbi.nlm.nih.gov/22904094/)
- R. Agah *et al.*, Gene recombination in postmitotic cells. Targeted expression of Cre recombinase provokes cardiac-restricted, site-specific rearrangement in adult ventricular muscle in vivo. *J. Clin. Invest.* **100**, 169–179 (1997). doi: [10.1172/JCI119509](https://doi.org/10.1172/JCI119509); pmid: [9202069](https://pubmed.ncbi.nlm.nih.gov/9202069/)
- S. C. Kolwicz Jr., R. Tian, Glucose metabolism and cardiac hypertrophy. *Cardiovasc. Res.* **90**, 194–201 (2011). doi: [10.1093/cvr/cvr071](https://doi.org/10.1093/cvr/cvr071); pmid: [21502371](https://pubmed.ncbi.nlm.nih.gov/21502371/)
- A. Hansson *et al.*, A switch in metabolism precedes increased mitochondrial biogenesis in respiratory chain-deficient mouse hearts. *Proc. Natl. Acad. Sci. U.S.A.* **101**, 3136–3141 (2004). doi: [10.1073/pnas.0308701010](https://doi.org/10.1073/pnas.0308701010); pmid: [14978272](https://pubmed.ncbi.nlm.nih.gov/14978272/)
- J. Yan *et al.*, Increased glucose uptake and oxidation in mouse hearts prevent high fatty acid oxidation but cause cardiac dysfunction in diet-induced obesity. *Circulation* **119**, 2818–2828 (2009). doi: [10.1161/CIRCULATIONAHA.108.832915](https://doi.org/10.1161/CIRCULATIONAHA.108.832915); pmid: [19451348](https://pubmed.ncbi.nlm.nih.gov/19451348/)
- C. Potting *et al.*, TRIAP1/PRELI complexes prevent apoptosis by mediating intramitochondrial transport of phosphatidic acid. *Cell Metab.* **18**, 287–295 (2013). doi: [10.1016/j.cmet.2013.07.008](https://doi.org/10.1016/j.cmet.2013.07.008); pmid: [23931759](https://pubmed.ncbi.nlm.nih.gov/23931759/)
- J. C. Brüning *et al.*, A muscle-specific insulin receptor knockout exhibits features of the metabolic syndrome of NIDDM without altering glucose tolerance. *Mol. Cell* **2**, 559–569 (1998). doi: [10.1016/S1097-2765\(00\)80155-0](https://doi.org/10.1016/S1097-2765(00)80155-0); pmid: [9844629](https://pubmed.ncbi.nlm.nih.gov/9844629/)
- K. T. Chambers *et al.*, Chronic inhibition of pyruvate dehydrogenase in heart triggers an adaptive metabolic response. *J. Biol. Chem.* **286**, 11155–11162 (2011). doi: [10.1074/jbc.M110.213419](https://doi.org/10.1074/jbc.M110.213419); pmid: [21321124](https://pubmed.ncbi.nlm.nih.gov/21321124/)
- C. Handschin *et al.*, Abnormal glucose homeostasis in skeletal muscle-specific PGC-1 α knockout mice reveals skeletal muscle-pancreatic beta cell crosstalk. *J. Clin. Invest.* **117**, 3463–3474 (2007). doi: [10.1172/JCI31785](https://doi.org/10.1172/JCI31785); pmid: [17932564](https://pubmed.ncbi.nlm.nih.gov/17932564/)
- E. Jing *et al.*, Sirtuin-3 (Sirt3) regulates skeletal muscle metabolism and insulin signaling via altered mitochondrial oxidation and reactive oxygen species production. *Proc. Natl. Acad. Sci. U.S.A.* **108**, 14608–14613 (2011). doi: [10.1073/pnas.1111308108](https://doi.org/10.1073/pnas.1111308108); pmid: [21873205](https://pubmed.ncbi.nlm.nih.gov/21873205/)
- L. Chen *et al.*, OPA1 mutation and late-onset cardiomyopathy: Mitochondrial dysfunction and mtDNA instability. *J. Am. Heart Assoc.* **1**, e003012 (2012). doi: [10.1161/JAHA.112.003012](https://doi.org/10.1161/JAHA.112.003012); pmid: [23316298](https://pubmed.ncbi.nlm.nih.gov/23316298/)

44. J. Piquereau *et al.*, Down-regulation of OPA1 alters mouse mitochondrial morphology, PTP function, and cardiac adaptation to pressure overload. *Cardiovasc. Res.* **94**, 408–417 (2012). doi: [10.1093/cvr/cvs117](https://doi.org/10.1093/cvr/cvs117); pmid: [22406748](https://pubmed.ncbi.nlm.nih.gov/22406748/)
45. L. C. Gomes, G. Di Benedetto, L. Scorrano, During autophagy mitochondria elongate, are spared from degradation and sustain cell viability. *Nat. Cell Biol.* **13**, 589–598 (2011). doi: [10.1038/ncb2220](https://doi.org/10.1038/ncb2220); pmid: [21478857](https://pubmed.ncbi.nlm.nih.gov/21478857/)
46. H. Chen, A. Chomyn, D. C. Chan, Disruption of fusion results in mitochondrial heterogeneity and dysfunction. *J. Biol. Chem.* **280**, 26185–26192 (2005). doi: [10.1074/jbc.M503062200](https://doi.org/10.1074/jbc.M503062200); pmid: [15899901](https://pubmed.ncbi.nlm.nih.gov/15899901/)
47. K. N. Papanicolaou *et al.*, Mitofusin-2 maintains mitochondrial structure and contributes to stress-induced permeability transition in cardiac myocytes. *Mol. Cell. Biol.* **31**, 1309–1328 (2011). doi: [10.1128/MCB.00911-10](https://doi.org/10.1128/MCB.00911-10); pmid: [21245373](https://pubmed.ncbi.nlm.nih.gov/21245373/)
48. Y. Chen *et al.*, Mitofusin 2-containing mitochondrial-reticular microdomains direct rapid cardiomyocyte bioenergetic responses via interorganelle Ca(2+) crosstalk. *Circ. Res.* **111**, 863–875 (2012). doi: [10.1161/CIRCRESAHA.112.266585](https://doi.org/10.1161/CIRCRESAHA.112.266585); pmid: [22777004](https://pubmed.ncbi.nlm.nih.gov/22777004/)
49. G. W. Dorn 2nd, M. Song, K. Walsh, Functional implications of mitofusin 2-mediated mitochondrial-SR tethering. *J. Mol. Cell. Cardiol.* **78**, 123–128 (2015). doi: [10.1016/j.jmcc.2014.09.015](https://doi.org/10.1016/j.jmcc.2014.09.015); pmid: [25252175](https://pubmed.ncbi.nlm.nih.gov/25252175/)
50. A. Kasahara, S. Cipolat, Y. Chen, G. W. Dorn 2nd, L. Scorrano, Mitochondrial fusion directs cardiomyocyte differentiation via calcineurin and Notch signaling. *Science* **342**, 734–737 (2013). doi: [10.1126/science.1241359](https://doi.org/10.1126/science.1241359); pmid: [24091702](https://pubmed.ncbi.nlm.nih.gov/24091702/)
51. A. Mourier *et al.*, Mitofusin 2 is required to maintain mitochondrial coenzyme Q levels. *J. Cell Biol.* **208**, 429–442 (2015). doi: [10.1083/jcb.201411100](https://doi.org/10.1083/jcb.201411100); pmid: [25688136](https://pubmed.ncbi.nlm.nih.gov/25688136/)
52. S. B. Ong *et al.*, Inhibiting mitochondrial fission protects the heart against ischemia/reperfusion injury. *Circulation* **121**, 2012–2022 (2010). doi: [10.1161/CIRCULATIONAHA.109.906610](https://doi.org/10.1161/CIRCULATIONAHA.109.906610); pmid: [20421521](https://pubmed.ncbi.nlm.nih.gov/20421521/)
53. C. B. Park *et al.*, MTERF3 is a negative regulator of mammalian mtDNA transcription. *Cell* **130**, 273–285 (2007). doi: [10.1016/j.cell.2007.05.046](https://doi.org/10.1016/j.cell.2007.05.046); pmid: [17662942](https://pubmed.ncbi.nlm.nih.gov/17662942/)
54. B. Ruzzenente *et al.*, LRPPRC is necessary for polyadenylation and coordination of translation of mitochondrial mRNAs. *EMBO J.* **31**, 443–456 (2012). doi: [10.1038/emboj.2011.392](https://doi.org/10.1038/emboj.2011.392); pmid: [22045337](https://pubmed.ncbi.nlm.nih.gov/22045337/)
55. C. Riehle *et al.*, Insulin receptor substrate signaling suppresses neonatal autophagy in the heart. *J. Clin. Invest.* **123**, 5319–5333 (2013). doi: [10.1172/JCI71171](https://doi.org/10.1172/JCI71171); pmid: [24177427](https://pubmed.ncbi.nlm.nih.gov/24177427/)
56. Y. Kageyama *et al.*, Parkin-independent mitophagy requires Drp1 and maintains the integrity of mammalian heart and brain. *EMBO J.* **33**, 2798–2813 (2014). doi: [10.15252/emboj.201488658](https://doi.org/10.15252/emboj.201488658); pmid: [25349190](https://pubmed.ncbi.nlm.nih.gov/25349190/)
57. M. Song, K. Mihara, Y. Chen, L. Scorrano, G. W. Dorn 2nd, Mitochondrial fission and fusion factors reciprocally orchestrate mitophagic culling in mouse hearts and cultured fibroblasts. *Cell Metab.* **21**, 273–285 (2015). doi: [10.1016/j.cmet.2014.12.011](https://doi.org/10.1016/j.cmet.2014.12.011); pmid: [25600785](https://pubmed.ncbi.nlm.nih.gov/25600785/)
58. Y. Ikeda *et al.*, Endogenous Drp1 mediates mitochondrial autophagy and protects the heart against energy stress. *Circ. Res.* **116**, 264–278 (2015). doi: [10.1161/CIRCRESAHA.116.303356](https://doi.org/10.1161/CIRCRESAHA.116.303356); pmid: [25332205](https://pubmed.ncbi.nlm.nih.gov/25332205/)
59. G. Civiletto *et al.*, Opa1 overexpression ameliorates the phenotype of two mitochondrial disease mouse models. *Cell Metab.* **21**, 845–854 (2015). doi: [10.1016/j.cmet.2015.04.016](https://doi.org/10.1016/j.cmet.2015.04.016); pmid: [26039449](https://pubmed.ncbi.nlm.nih.gov/26039449/)
60. T. Varanita *et al.*, The OPA1-dependent mitochondrial cristae remodeling pathway controls atrophic, apoptotic, and ischemic tissue damage. *Cell Metab.* **21**, 834–844 (2015). doi: [10.1016/j.cmet.2015.05.007](https://doi.org/10.1016/j.cmet.2015.05.007); pmid: [26039448](https://pubmed.ncbi.nlm.nih.gov/26039448/)
61. J. M. Huss, D. P. Kelly, Mitochondrial energy metabolism in heart failure: A question of balance. *J. Clin. Invest.* **115**, 547–555 (2005). doi: [10.1172/JCI24405](https://doi.org/10.1172/JCI24405); pmid: [15765136](https://pubmed.ncbi.nlm.nih.gov/15765136/)
62. C. M. Nasrallah, T. L. Horvath, Mitochondrial dynamics in the central regulation of metabolism. *Nat. Rev. Endocrinol.* **10**, 650–658 (2014). doi: [10.1038/nrendo.2014.160](https://doi.org/10.1038/nrendo.2014.160); pmid: [25200564](https://pubmed.ncbi.nlm.nih.gov/25200564/)
63. M. O. Dietrich, Z. W. Liu, T. L. Horvath, Mitochondrial dynamics controlled by mitofusins regulate AgRP neuronal activity and diet-induced obesity. *Cell* **155**, 188–199 (2013). doi: [10.1016/j.cell.2013.09.004](https://doi.org/10.1016/j.cell.2013.09.004); pmid: [24074868](https://pubmed.ncbi.nlm.nih.gov/24074868/)
64. J. D. Wikstrom *et al.*, Hormone-induced mitochondrial fission is utilized by brown adipocytes as an amplification pathway for energy expenditure. *EMBO J.* **33**, 418–436 (2014). doi: [10.1002/emboj.201385014](https://doi.org/10.1002/emboj.201385014); pmid: [24431221](https://pubmed.ncbi.nlm.nih.gov/24431221/)
65. B. D. Lowes *et al.*, Myocardial gene expression in dilated cardiomyopathy treated with beta-blocking agents. *N. Engl. J. Med.* **346**, 1357–1365 (2002). doi: [10.1056/NEJMoa012630](https://doi.org/10.1056/NEJMoa012630); pmid: [11986409](https://pubmed.ncbi.nlm.nih.gov/11986409/)
66. S. Sankaralingam *et al.*, Lowering body weight in obese mice with diastolic heart failure improves cardiac insulin sensitivity and function: Implications for the obesity paradox. *Diabetes* **64**, 1643–1657 (2015). doi: [10.2337/db14-1050](https://doi.org/10.2337/db14-1050); pmid: [25524917](https://pubmed.ncbi.nlm.nih.gov/25524917/)
67. Z. Sun *et al.*, Diet-induced lethality due to deletion of the Hdac3 gene in heart and skeletal muscle. *J. Biol. Chem.* **286**, 33301–33309 (2011). doi: [10.1074/jbc.M111.277707](https://doi.org/10.1074/jbc.M111.277707); pmid: [21808063](https://pubmed.ncbi.nlm.nih.gov/21808063/)
68. J. Garcia-Prieto *et al.*, β_3 Adrenergic receptor selective stimulation during ischemia/reperfusion improves cardiac function in translational models through inhibition of mPTP opening in cardiomyocytes. *Basic Res. Cardiol.* **109**, 422 (2014). doi: [10.1007/s00395-014-0422-0](https://doi.org/10.1007/s00395-014-0422-0); pmid: [24951958](https://pubmed.ncbi.nlm.nih.gov/24951958/)
69. R. El-Khoury *et al.*, Alternative oxidase expression in the mouse enables bypassing cytochrome c oxidase blockade and limits mitochondrial ROS overproduction. *PLOS Genet.* **9**, e1003182 (2013). doi: [10.1371/journal.pgen.1003182](https://doi.org/10.1371/journal.pgen.1003182); pmid: [23300486](https://pubmed.ncbi.nlm.nih.gov/23300486/)
70. P. B  nit *et al.*, Three spectrophotometric assays for the measurement of the five respiratory chain complexes in minuscule biological samples. *Clin. Chim. Acta* **374**, 81–86 (2006). doi: [10.1016/j.cca.2006.05.034](https://doi.org/10.1016/j.cca.2006.05.034); pmid: [16828729](https://pubmed.ncbi.nlm.nih.gov/16828729/)

ACKNOWLEDGMENTS

We thank K. Lemke, H. Bank, E. Barth, V. Zorita, and M. G  mez for technical assistance; A. Polykratis and C. Uthoff-Hachenberg for genetic engineering assistance; A. Pun-Garc  a and R. Villena-Guti  rrez for cardiomyocyte isolations; A. V. Alonso L  pez, L. Flores Ruiz, and J. Jim  nez-Borreguero for echocardiography evaluation; I. Bilbao, C. Velasco, and J. Ruiz-Cabello for PET-CT evaluation; A. Ferrarini and D. Dudzik for help in metabolomics; G. Rapl for single-cell sorting of cardiac fibroblasts; P. Frommolt for microarray quality control; and J. Br  uning for discussion. This work was supported by a fellowship of the Human Frontiers Science Program to T.W., by grants of the Deutsche Forschungsgemeinschaft and the European Research Council to T.L., and by a grant from the Spanish Ministry of Economy and Competitiveness (MINECO) through the Carlos III Institute of Health–Fondo de Investigaci  n Sanitaria and European Regional Development Fund (ERDF/FEDER) funds (PI13/01979) and Networks for Cooperative Research in Health (RETIC) (RD12/0042/0054) to B.I. The CNIC is supported by the Ministry of Economy and Competitiveness and the Pro-CNIC Foundation. B.I. is Princess of Girona awardee in science. F.J.R. and C.B. acknowledge MINECO CTQ 2014-55279-R. The authors declare no competing or financial interests. The mice used in this study are available under a materials transfer agreement from the authors. The data are included in the main manuscript and the supplementary materials. Author contributions: M.J.B. generated the floxed *Oma1* mouse, T.W. generated the floxed *Yme1l* mouse, hmYKO mice, hmOKO mice, hmDKO mice, cYKO mice, and cDKO mice. C.M. designed targeting constructs. P.B. and P.R. performed oxygen consumption measurements. F.J.R. and C.B. performed the acylcarnitine profiling, and T.W. and J.G.-P. performed all other experiments. T.W., J.G.-P., B.I., and T.L. drafted the manuscript.

SUPPLEMENTARY MATERIALS

www.sciencemag.org/content/350/6265/aad0116/suppl/DC1

Additional Materials and Methods

Figs. S1 to S7

Tables S1 and S2

References (71, 72)

13 July 2015; accepted 2 October 2015

10.1126/science.aad0116

REPORTS

PEROVSKITE LEDs

Overcoming the electroluminescence efficiency limitations of perovskite light-emitting diodes

Himchan Cho,^{1*} Su-Hun Jeong,^{1*} Min-Ho Park,^{1*} Young-Hoon Kim,¹ Christoph Wolf,¹ Chang-Lyoul Lee,² Jin Hyuck Heo,³ Aditya Sadhanala,⁴ NoSoung Myoung,² Seunghyup Yoo,⁵ Sang Hyuk Im,³ Richard H. Friend,⁴ Tae-Woo Lee^{1,6†}

Organic-inorganic hybrid perovskites are emerging low-cost emitters with very high color purity, but their low luminescent efficiency is a critical drawback. We boosted the current efficiency (CE) of perovskite light-emitting diodes with a simple bilayer structure to 42.9 candelas per ampere, similar to the CE of phosphorescent organic light-emitting diodes, with two modifications: We prevented the formation of metallic lead (Pb) atoms that cause strong exciton quenching through a small increase in methylammonium bromide (MABr) molar proportion, and we spatially confined the exciton in uniform MAPbBr₃ nanograins (average diameter = 99.7 nanometers) formed by a nanocrystal pinning process and concomitant reduction of exciton diffusion length to 67 nanometers. These changes caused substantial increases in steady-state photoluminescence intensity and efficiency of MAPbBr₃ nanograin layers.

Organic-inorganic hybrid perovskites (OIPs) have recently been established as an important class of materials in photovoltaic devices, and there has been rapid progress in increasing their power conversion efficiency (1–5). OIPs are emerging also as promising light emitters because they can provide very high color purity (full width at half maximum ~ 20 nm) irrespective of the crystal size, unlike conventional inorganic quantum dots, because their intrinsic crystal structure is similar to a multiple quantum well (6, 7). Also, OIPs have low material cost and a simply tunable band gap, with a reasonable ionization energy (IE) comparable to that of common hole-injection materials (7–11). Thus, OIPs are attractive materials as alternative emitters that can overcome the disadvantages of organic light-emitting diodes (OLEDs) (e.g., com-

plex synthesis, high cost, and poor color purity) and inorganic quantum dot LEDs (e.g., complex synthesis, high cost, and high IE).

Bright electroluminescence (EL) (>100 cd m⁻²) at room temperature from perovskite light-emitting diodes (PeLEDs) with a methylammonium lead halide (MAPbX₃, where X is I, Br, or Cl) emission layer was demonstrated recently (6, 7, 12–18). As an emission layer, MAPbBr₃ has higher air stability (7, 19) and exciton binding energy (76 or 150 meV) than does MAPbI₃ (30 or 50 meV) (20, 21). However, PeLEDs have much lower current efficiency (CE) at room temperature than do OLEDs or quantum dot LEDs. Existing methods have not overcome the substantial luminescence quenching in MAPbX₃ caused by facile thermal ionization of excitons generated in the OIP layer, which has a low exciton binding energy. Spin-coating of MAPbBr₃ solution creates a rough, nonuniform surface with many cuboids of large grain size (22), which leads to a substantial leakage current and large exciton diffusion length, L_D , that reduces CE in PeLEDs. To improve the CE of PeLEDs, the OIP grain size must be decreased, and OIP films should be flat and uniform. Smaller grains can spatially limit the L_D of excitons or charge carriers and reduce the possibility of exciton dissociation into carriers. This fabrication goal differs from that of the OIP layers in solar cells, which should be dense films with large grain size to achieve facile exciton diffusion and dissociation. Thus, processes designed to achieve uniform OIP film morphology with large grain size in solar cells, such as solvent engineering (23, 24), are not applicable to PeLEDs, which require a small L_D .

Here, we report a systematic approach for achieving highly bright and efficient green PeLEDs with CE = 42.9 cd A⁻¹ and external quantum efficiency (EQE) = 8.53%, even in a simplified bilayer structure. These high efficiencies represent a >20,000-fold increase compared with that of the control devices and are higher than the best EQEs of a previous report regarding visible PeLEDs using OIP films by factors of >10.6 (table S1 and fig. S1) (15). The high-efficiency PeLEDs were constructed on the basis of effective management of exciton quenching by a modified MAPbBr₃ emission layer that was achieved with (i) fine and controllable stoichiometry modification and (ii) optimized nanograin engineering by nanocrystal pinning (NCP) (fig. S2). Furthermore, we demonstrated a flexible PeLED using a self-organized conducting polymer (SOCP) anode and the first large-area PeLED (2 cm by 2 cm pixel).

A fundamental problem that must be solved to achieve high CE in PeLEDs is minimizing the presence of metallic Pb atoms in MAPbBr₃ that limits the efficiency of PeLEDs. Metallic Pb atoms can emerge in MAPbBr₃ even if MABr and PbBr₂ are mixed in 1:1 (mol:mol) ratios because of the unintended losses of Br atoms or incomplete reaction between MABr and PbBr₂ (25). Excess Pb atoms degrade luminescence by increasing the non-radiative decay rate and decreasing the radiative decay rate (26). Preventing the formation of metallic Pb atoms was achieved by finely increasing the molar proportion of MABr by 2 to 7% in MAPbBr₃ solution (fig. S2A). Use of excess MABr suppressed exciton quenching and reduced the hole-injection barrier from SOCP layers (table S2) to MAPbBr₃ layers with decreased IE and greatly increased the steady-state photoluminescence (PL) intensity and PL lifetime of MAPbBr₃ films. We propose that the PL process in MAPbBr₃ nanograins depends on trap-assisted recombination at grain boundaries and radiative recombination inside the grains. Second, the CE in PeLEDs can be increased by decreasing MAPbBr₃ grain sizes, which improves uniformity and coverage of MAPbBr₃ nanograin layers and radiative recombination by confining the excitons in the nanograins (leading to small L_D). An optimized NCP process (fig. S3) helped to change the morphology of MAPbBr₃ layers from scattered micrometer-sized cuboids to well-packed nanograins with uniform coverage, which greatly reduced leakage current and increased CE.

We fabricated MAPbBr₃ films by spin-coating with stoichiometrically modified perovskite solutions on prepared glass/SOCs or silicon wafer/SOCs substrates later used in devices (Fig. 1, A and B), and then characterized the films' morphologies and optoelectronic properties. The solutions had different molar ratios of MABr to PbBr₂ (MABr:PbBr₂ = 1.05:1, 1:1, or 1:1.05). To achieve uniform surface coverage and reduced grain size, we used NCP instead of normal spin coating (fig. S3). This process washed out the "good" solvents [dimethylformamide or dimethyl sulfoxide (DMSO)] and causes pinning of NCs by inducing fast crystallization. Chloroform was

¹Department of Materials Science and Engineering, Pohang University of Science and Technology (POSTECH), 77 Cheongam-Ro, Pohang, Gyeongbuk 790-784, Republic of Korea.

²Advanced Photonics Research Institute (APRI), Gwangju Institute of Science and Technology (GIST), 1 Oryong-dong, Buk-gu, Gwangju 500-712, Republic of Korea. ³Department of Chemical Engineering, College of Engineering, Kyung Hee University, 1 Seochon-dong, Giheung-gu, Youngin-si, Gyeonggi-do 446-701, Republic of Korea. ⁴Cavendish Laboratory, University of Cambridge, J J Thomson Avenue, Cambridge CB3 0HE, UK. ⁵Department of Electrical Engineering, Korea Advanced Institute of Science and Technology (KAIST), 373-1 Guseong-dong, Yuseong-gu, Daejeon 305-701, Republic of Korea. ⁶Department of Chemical Engineering, Division of Advanced Materials Science, School of Environmental Science and Engineering, Pohang University of Science and Technology (POSTECH), 77 Cheongam-Ro, Nam-Gu, Pohang, Gyeongbuk 790-784, Republic of Korea.

*These authors contributed equally to this work. †Corresponding author. E-mail: twlee@postech.ac.kr, taewlees@gmail.com

chosen as the solvent for NCP because a highly volatile nonpolar solvent is suitable to reduce the size and increase the uniformity of MAPbBr₃ grains by reducing solvent evaporation time. In addition, to further reduce grain size, we devised additive-based NCP (A-NCP), which uses an organic small molecule, 2,2',2''-(1,3,5-benzinetriyl)-tris(1-phenyl-1-H-benzimidazole) (TPBI), as an additive to chloroform, whereas pure chloroform is used in solvent-based NCP (S-NCP).

The use of NCP affected film morphology (Fig. 2). Without NCP, micrometer-sized MAPbBr₃ cuboids were scattered on the SOCP layer (Fig. 2A). They were only interconnected with a few other cuboids, so a large amount of space remained uncovered. This high surface roughness and the formation of pinholes in OIP films result in formation of a bad interface with the electron transport layer and electrical shunt paths, and thus severely limit CE in PeLEDs. In contrast, when NCP was used, perfect surface coverage was obtained, and the MAPbBr₃ crystal morphology changed to a well-packed assembly of tiny grains ranging from 100 to 250 nm (Fig. 2, B to E, and fig. S4). MAPbBr₃ grain size was very slightly affected by the stoichiometric modification of MAPbBr₃ solutions (Fig. 2, B to D, and fig. S4, A to C). Furthermore, MAPbBr₃ grain size was greatly reduced to 50 to 150 nm (average = 99.7 nm) by A-NCP (Fig. 2E and fig. S4D). This reduction can be attributed to hindrance of crystal growth by TPBI molecules during crystal pinning. The thickness of MAPbBr₃ layer was ~400 nm (Fig. 1B).

The crystal structures of MAPbBr₃ films were analyzed by measuring x-ray diffraction (XRD) patterns (Fig. 2F, fig. S5, and table S3). The XRD patterns of MAPbBr₃ films (1:1) exhibit peaks at 15.02°, 21.3°, 30.28°, 33.92°, 37.24°, 43.28°, and 46.00° that can be assigned to (100), (110), (200), (210), (211), (220), and (300) planes, respectively, by using Bragg's law to convert the peak positions to interplanar spacings (Fig. 2F). The lattice parameter is in accordance with a previous report (19) and demonstrates that MAPbBr₃ films had a stable cubic *Pm3m* phase. Using the Scherrer equation, we calculated the crystallite size to be 24.4 ± 2.4 nm, and the variation with stoichiometric change was not large (table S3). Because the crystallite sizes were much smaller than the apparent grain sizes (Fig. 2, A to E), we conclude that all grains consisted of many crystallites. The stoichiometric changes had very little effect on the peak positions (fig. S5A). Furthermore, A-NCP did not change the peak positions when compared to S-NCP (fig. S5); this stability in positions indicates that the stoichiometric changes of MAPbBr₃ solution and the use of TPBI additive did not affect the crystal structure of MAPbBr₃ films.

To study chemical changes in the MAPbBr₃ layers fabricated with perovskite solutions of different stoichiometries, we conducted x-ray photoelectron spectroscopy (XPS). The survey spectra showed strong peaks of Br (~68 eV), Pb (~138 and 143 eV), C (~285 eV), and N (~413 eV); these results agree with values in previous reports

(fig. S6A) (7, 25, 27, 28). Systematic deconvolution of Pb4f, Br3d, and N1s spectra into summations of Gaussian-Lorentzian curves revealed the nature of chemical bonds in MAPbBr₃ (figs. S6, B to D, and S7). We confirmed the gradual increase in MABr molar proportion in the films by observing the gradual increase in N1s peak intensities as MABr:PbBr₂ increased from 1:1.05 to 1.05:1 (fig. S7, C and D) and the gradual decrease in Br:Pb atomic ratio (supplementary text F). In the Pb4f spectra (fig. S6, B to F), large peaks were observed at ~138.8 and ~143.6 eV (caused by the spin orbit split) that correspond to Pb4f_{7/2} and Pb4f_{5/2} lev-

els, respectively (25, 27, 28). Each of these peaks was associated with a smaller peak that was shifted to 1.8-eV lower binding energy; these small peaks can be assigned to metallic Pb (25, 27, 28). The height of peaks that represent metallic Pb decreased as MABr:PbBr₂ increased from 1:1.05 to 1:1 (fig. S6, E and F); this peak was absent in the film with MABr:PbBr₂ = 1.05:1 (fig. S6F). This trend indicates that the presence of metallic Pb atoms on the films was successfully prevented by fine stoichiometry control. In contrast, the high peak intensity of the metallic Pb peak in the films with MABr:PbBr₂ = 1:1 and 1:1.05 suggests that numerous

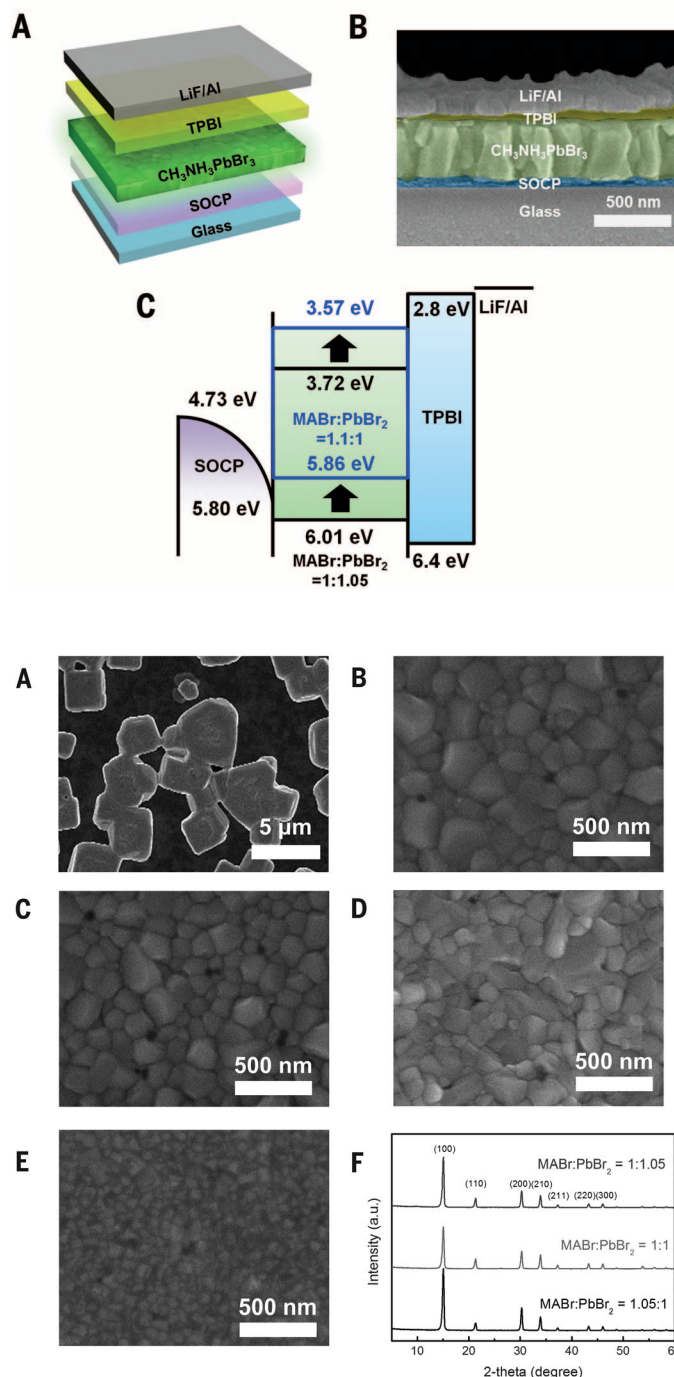


Fig. 1. Schematic illustrations of device structure and its cross-sectional scanning electron microscope (SEM) image, and energy band structure. (A) The device structure. (B) Cross-sectional SEM image of PeLEDs. (C) Energy band diagram of PeLEDs, showing a decrease in IE with increasing MABr molar proportion.

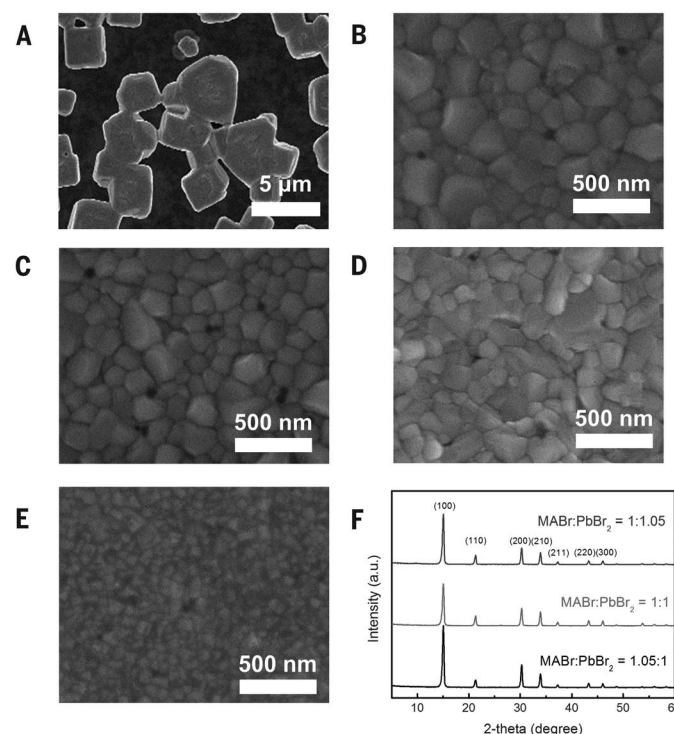


Fig. 2. SEM images and XRD patterns of MAPbBr₃ layers. SEM images of MAPbBr₃ layers of (A) MABr:PbBr₂ = 1:1 without NCP, (B) 1:1.05, (C) 1:1, (D) 1:1.05:1 with S-NCP, and (E) 1:1.05:1 with A-NCP. (F) XRD patterns of MAPbBr₃ nanograin layers with MABr:PbBr₂ = 1:1.05, 1:1, and 1:1.05:1.

metallic Pb atoms were formed on the film surfaces.

We measured the work functions (WFs) and IEs of the MAPbBr₃ films using ultraviolet photoelectron spectroscopy (UPS) (fig. S8). The WFs were obtained by subtracting the energies at secondary cut-offs of the UPS spectra from the ultraviolet radiation energy of 21.2 eV when a Fermi level of 0 eV was the common reference for all energies. The IEs were determined by adding the WF (fig. S8A) to the energy offset between WFs and IEs of MAPbBr₃ (fig. S8B) (29). The IE gradually decreased with increasing MABr molar proportion from 6.01 eV in the film with MABr:PbBr₂ = 1:1.05 to 5.86 eV in the film with MABr:PbBr₂ = 1:1 (Fig. 1C and table S4).

Table 1. Maximum CE of PeLEDs depending on NCP and the molar ratio of MABr:PbBr₂.

MABr:PbBr ₂	NCP type	Max. CE (cd A ⁻¹)
1.05:1	A-NCP	42.9
1.07:1	S-NCP	19.3
1.05:1	S-NCP	21.4
1.03:1	S-NCP	4.03
1.02:1	S-NCP	0.457
1:1	S-NCP	0.183
1:1.05	S-NCP	4.87×10^{-2}
1:1	Without NCP	2.03×10^{-3}

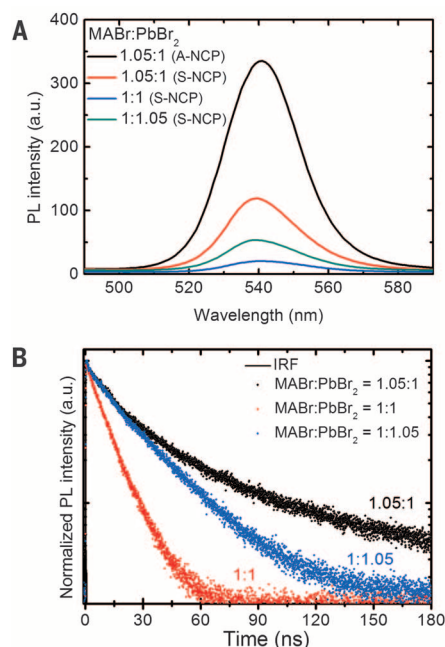


Fig. 3. Steady-state PL spectra and lifetime.

(A) Steady-state PL spectra of MAPbBr₃ nanograin layers with NCP type and varying molar ratio of MABr:PbBr₂. (B) PL lifetime curves of MAPbBr₃ nanograin layers with varying molar ratio of MABr:PbBr₂. Black line: instrument response function (IRF).

The gradual decrease in IEs with decreasing PbBr₂ molar proportion can be understood on the basis of the IE being greater in PbBr₂ than in MAPbBr₃ (30). In PeLEDs, this decrease can help alleviate hole-injection barriers from SOCP layers to MAPbBr₃ layers (Fig. 1C).

The luminescent properties of the MAPbBr₃ films were investigated by steady-state PL measurement (Fig. 3A). We carried out the measurement using a spectrofluorometer with excitation from monochromatic light with a wavelength of 405 nm (xenon lamp). The MAPbBr₃ films fabricated from MABr:PbBr₂ = 1.05:1 had a ~5.8 times increase in PL intensity (Fig. 3A) compared with 1:1 films and had much higher PL quantum efficiency (PLQE; 36% versus 3%). In addition, the reduction in grain size with A-NCP versus S-NCP increased the PL intensity by ~2.8 times. The PL intensity of the films with MABr:PbBr₂ = 1:1.05 was greater than in those with MABr:PbBr₂ = 1:1, although the PbBr₂ molar propor-

tion had increased in the former. We suspect that this departure from the expected trend is due to PbBr₂-induced surface passivation of the film, which reduces nonradiative recombination at the trap sites (31).

To understand the kinetics of excitons and free carriers in MAPbBr₃ films and how the presence of metallic Pb atoms affects the PL lifetime, we conducted time-correlated single-photon counting measurements (Fig. 3B). The PL decay curves were fitted with a bi-exponential decay model, in which the PL lifetime is considered as the summation of fast- and slow-decay components that give a short lifetime τ_1 and a long lifetime τ_2 , respectively. To investigate the quality of quenching sites, we prepared the layers (MABr:PbBr₂ = 1.05:1) with and without sealing with a 50-nm-thick poly(methyl methacrylate) (PMMA) layer. The fraction f_2 of τ_2 decreased from 91 to 77% in the film without sealing (table S5). Oxygen and moisture can diffuse quickly into grain boundaries when the top

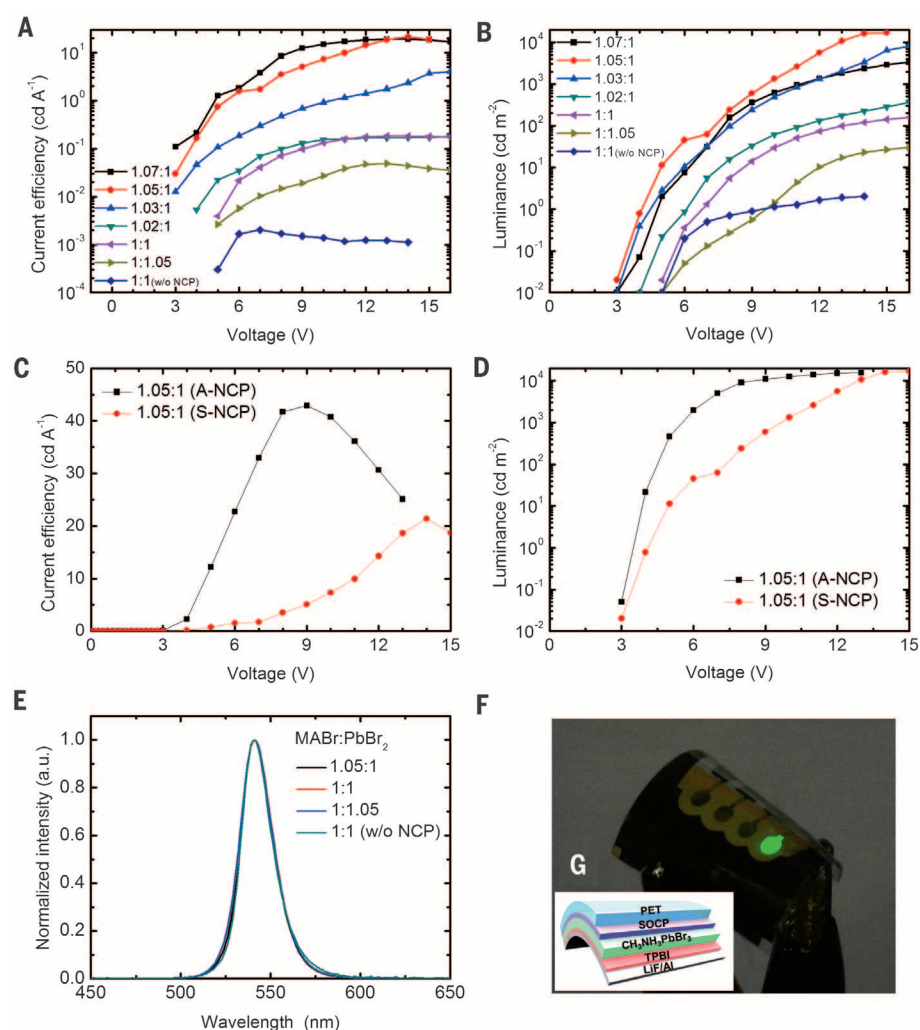


Fig. 4. PeLED characteristics, EL spectra, and photograph of PeLED. (A and B) CE and luminance of PeLEDs based on S-NCP and MAPbBr₃ nanograin emission layers with varying molar ratio of MABr:PbBr₂ (■ 1.07:1, ● 1.05:1, ▲ 1.03:1, ▼ 1.02:1, ◆ 1:1, ▴ 1:1.05, ◆ 1:1 without NCP). (C and D) CE and luminance of PeLEDs based on A-NCP and MAPbBr₃ nanograin emission layers. (E) EL spectra of PeLEDs. (F) Photograph of a flexible PeLED, and (G) its device structure.

PMMA layer is not used; oxygen or moisture at grain boundaries provides quenching sites. The fast decay is related to trap-assisted recombination at grain boundaries, whereas the slow decay is related to radiative recombination inside the grains (fig. S9) (32).

This proposition was supported by analyzing the change in τ and f of MAPbBr₃ films with varying stoichiometric ratio. As MABr:PbBr₂ increased from 1:1 to 1.05:1, the average lifetime τ_{avg} gradually increased from 12.2 to 51.0 ns (table S5). The short τ_{avg} (12.2 ns) in the film with MABr:PbBr₂ = 1:1 originated from the substantial reduction in τ_2 . This implies that uncoordinated metallic Pb atoms at grain boundaries inhibit radiative recombination and cause strong non-radiative recombination (fig. S9). The MAPbBr₃ films fabricated with PbBr₂-rich perovskite solution (MABr:PbBr₂ = 1:1.05) had a longer lifetime than films with MABr:PbBr₂ = 1:1, possibly through PbBr₂-induced surface passivation (31). We calculated the average L_D using a model similar to that in a previous report (fig. S10) (33). The films (MABr:PbBr₂ = 1.05:1) underneath a PMMA layer exhibited a much smaller L_D (67 nm) than those previously reported (>1 μm) (34). We attribute this reduction in L_D to the reduced grain sizes in which excitons are under stronger spatial confinement, thereby reducing dissociation and enhancing radiative recombination; this compensates the plausible adverse effect of larger grain boundary area (6).

The PeLED fabricated from the MAPbBr₃ solution (MABr:PbBr₂ = 1:1) without using NCP showed poor luminous characteristics (maximum CE = 2.03×10^{-3} cd A⁻¹), mainly owing to high leakage current (fig. S11). In contrast, maximum CE was substantially increased (0.183 cd A⁻¹) when a full-coverage uniform MAPbBr₃ nanograin layer (MABr:PbBr₂ = 1:1) with decreased grain size was achieved with S-NCP, without stoichiometric modifications to avoid metallic Pb atoms (Fig. 4, A and B, and Table 1). The maximum CE was boosted to 21.4 cd A⁻¹ in the PeLEDs fabricated with perovskite solutions with excess MABr (1.07:1, 1.05:1, 1.03:1 and 1.02:1) (Fig. 4A and Table 1). As MABr:PbBr₂ increased from 1:1 to 1.05:1, the maximum CE varied from 0.183 to 21.4 cd A⁻¹.

We further increased the CE of PeLEDs by using A-NCP. The PeLEDs based on A-NCP had a maximum CE of 42.9 cd A⁻¹ (Fig. 4, C and D, and Table 1), which represents an EQE of 8.53% when the angular emission profile is considered (fig. S12). The EL spectra of PeLEDs were very narrow; full width at half maximum was ~20 nm for all spectra. This high color purity of OIP emitters shows great potential when used in displays (Fig. 4E). A pixel of the PeLED based on MABr:PbBr₂ = 1.05:1 exhibited strong green-light emission (fig. S13A). Furthermore, the proposed processes and materials used therein are compatible with flexible and large-area devices; a high-brightness flexible PeLED (Fig. 4, F and G) and a large-area (2 cm by 2 cm pixel) PeLED (fig. S13B) were fabricated. Our study reduces the technical gap between PeLEDs and OLEDs or quantum dot LEDs and is a big step toward the development of efficient

next-generation emitters with high color purity and low fabrication cost based on perovskites.

REFERENCES AND NOTES

- W. S. Yang *et al.*, *Science* **348**, 1234–1237 (2015).
- M. Liu, M. B. Johnston, H. J. Snaith, *Nature* **501**, 395–398 (2013).
- N. J. Jeon *et al.*, *Nature* **517**, 476–480 (2015).
- J.-H. Im, I.-H. Jang, N. Pellet, M. Grätzel, N.-G. Park, *Nat. Nanotechnol.* **9**, 927–932 (2014).
- H. Kim, K.-G. Lim, T.-W. Lee, *Energy Environ. Sci.* 10.1039/c5ee02194d (2015).
- Z.-K. Tan *et al.*, *Nat. Nanotechnol.* **9**, 687–692 (2014).
- Y.-H. Kim *et al.*, *Adv. Mater.* **27**, 1248–1254 (2015).
- D. B. Mitzi, *Chem. Mater.* **8**, 791–800 (1996).
- M. R. Filip, G. E. Eperon, H. J. Snaith, F. Giustino, *Nat. Commun.* **5**, 5757 (2014).
- T. M. Koh *et al.*, *J. Phys. Chem. C* **118**, 16458–16462 (2014).
- G. E. Eperon *et al.*, *Energy Environ. Sci.* **7**, 982–988 (2014).
- R. L. Z. Hoyer *et al.*, *Adv. Mater.* **27**, 1414–1419 (2015).
- N. K. Kumawat, A. Dey, K. L. Narasimhan, D. Kabra, *ACS Photonics* **2**, 349–354 (2015).
- G. Li *et al.*, *Nano Lett.* **15**, 2640–2644 (2015).
- J. Wang *et al.*, *Adv. Mater.* **27**, 2311–2316 (2015).
- A. Sadhanala *et al.*, *Adv. Electron. Mater.* **1**, 1500008 (2015).
- J. C. Yu *et al.*, *Adv. Mater.* **27**, 3492–3500 (2015).
- N. K. Kumawat *et al.*, *ACS Appl. Mater. Interfaces* **7**, 13119–13124 (2015).
- J. H. Noh, S. H. Im, J. H. Heo, T. N. Mandal, S. I. Seok, *Nano Lett.* **13**, 1764–1769 (2013).
- I. B. Koutselas, L. Ducasse, G. C. Papavassiliou, *J. Phys. Condens. Matter* **8**, 1217–1227 (1996).
- K. Tanaka *et al.*, *Solid State Commun.* **127**, 619–623 (2003).
- J. H. Heo, D. H. Song, S. H. Im, *Adv. Mater.* **26**, 8179–8183 (2014).
- Z. Xiao *et al.*, *Adv. Mater.* **26**, 6503–6509 (2014).
- N. J. Jeon *et al.*, *Nat. Mater.* **13**, 897–903 (2014).
- R. Lindblad *et al.*, *J. Phys. Chem. C* **119**, 1818–1825 (2015).
- E. Dulkeith *et al.*, *Nano Lett.* **5**, 585–589 (2005).
- S. Gonzalez-Carrero, R. E. Galian, J. Pérez-Prieto, *J. Mater. Chem. A* **3**, 9187–9193 (2015).
- I. A. Shkrob, T. W. Marin, *J. Phys. Chem. Lett.* **5**, 1066–1071 (2014).
- P. Schulz *et al.*, *Energy Environ. Sci.* **7**, 1377–1381 (2014).
- J. Kanbe, H. Onuki, R. Onaka, *J. Phys. Soc. Jpn.* **43**, 1280–1285 (1977).
- Q. Chen *et al.*, *Nano Lett.* **14**, 4158–4163 (2014).
- D. Shi *et al.*, *Science* **347**, 519–522 (2015).
- S. D. Stranks *et al.*, *Science* **342**, 341–344 (2013).
- R. Sheng *et al.*, *J. Phys. Chem. C* **119**, 3545–3549 (2015).

ACKNOWLEDGMENTS

This work was partially supported by Samsung Research Funding Center of Samsung Electronics under Project Number SRFC-MA-1402-07. A.S. was partially supported by the Engineering and Physical Sciences Research Council (UK). All data are available in the main text and the supplementary materials.

SUPPLEMENTARY MATERIALS

www.sciencemag.org/content/350/6265/1222/suppl/DC1
Materials and Methods
Supplementary Text
Figs. S1 to S13
Tables S1 to S5
References (35–43)

4 August 2015; accepted 22 October 2015
10.1126/science.aad1818

LASER PHYSICS

Ultraviolet surprise: Efficient soft x-ray high-harmonic generation in multiply ionized plasmas

Dimitar Popmintchev,¹ Carlos Hernández-García,^{1,2} Franklin Dollar,¹ Christopher Mancuso,¹ Jose A. Pérez-Hernández,³ Ming-Chang Chen,⁴ Amelia Hankla,¹ Xiaohui Gao,⁵ Bonggu Shim,⁵ Alexander L. Gaeta,⁵ Maryam Tarazkar,⁶ Dmitri A. Romanov,⁷ Robert J. Levis,⁶ Jim A. Gaffney,⁸ Mark Foord,⁸ Stephen B. Libby,⁸ Agnieszka Jaron-Becker,¹ Andreas Becker,¹ Luis Plaja,² Margaret M. Murnane,¹ Henry C. Kapteyn,¹ Tenio Popmintchev^{1*}

High-harmonic generation is a universal response of matter to strong femtosecond laser fields, coherently upconverting light to much shorter wavelengths. Optimizing the conversion of laser light into soft x-rays typically demands a trade-off between two competing factors. Because of reduced quantum diffusion of the radiating electron wave function, the emission from each species is highest when a short-wavelength ultraviolet driving laser is used. However, phase matching—the constructive addition of x-ray waves from a large number of atoms—favors longer-wavelength mid-infrared lasers. We identified a regime of high-harmonic generation driven by 40-cycle ultraviolet lasers in waveguides that can generate bright beams in the soft x-ray region of the spectrum, up to photon energies of 280 electron volts. Surprisingly, the high ultraviolet refractive indices of both neutral atoms and ions enabled effective phase matching, even in a multiply ionized plasma. We observed harmonics with very narrow linewidths, while calculations show that the x-rays emerge as nearly time-bandwidth-limited pulse trains of ~100 attoseconds.

High-order harmonic generation (HHG) results from the extreme quantum nonlinear response of atoms to intense laser fields: Atoms in the process of being ionized by an intense femtosecond laser pulse

coherently emit short-wavelength light that can extend well into the soft x-ray region (1–6). When implemented in a phase-matched geometry to ensure that the laser and HHG fields both propagate at the same speed $\sim c$, HHG from

many atoms adds constructively to generate bright, coherent beams (7). The high temporal coherence of HHG supports ultrabroad bandwidths ($\Delta\lambda/\lambda \approx 1$) that simultaneously span many characteristic elemental absorption edges, as well as pulse durations from femtoseconds to attoseconds (8–11), making it possible to capture the fastest electron dynamics in atoms, molecules, nanosystems, and materials (12–23). Moreover, the high spatial coherence of HHG makes it possible to image with spatial resolution near the wavelength limit (24, 25). Recently, the use of mid-infrared (IR) femtosecond driving lasers enabled the generation of bright x-ray supercontinua extending to photon energies greater than 1.6 keV (26).

To date, however, generating bright harmonics demanded a trade-off between two competing factors. High harmonics are radiated as a result of a laser-driven quantum-coherent electron recollision process that occurs while an atom is ionizing. This physics dictates that the HHG emission per atom is brightest for short-wavelength ultraviolet (UV) driving lasers, because the short laser cycle minimizes quantum diffusion of the electron wave packet as it propagates away from, and then back to, its parent ion. This maximizes the probability of the recollision HHG event and hence the HHG yield per atom (27). In contrast, generating and phase-matching HHG in the soft x-ray region favors long-wavelength, mid-IR lasers ($>0.8 \mu\text{m}$) (26, 28–30). This can be understood from simple arguments. First, the maximum HHG photon energy emitted by a single atom scales quadratically with laser wavelength and is given by $h\nu_{\text{SA}} \approx I_p + 3.17 U_p$ (4), where $U_p \propto I_L \lambda_L^2$ is the average quiver energy of the electron in a laser field of intensity I_L and wavelength λ_L . Second, phase matching is achieved by balancing the positive dispersion of the neutral gas with the negative contribution of the free electrons and is only possible for ionization levels of $<5\%$ for argon. Fortunately, the lower laser intensity required for long-wavelength driving lasers means that the medium is only weakly ionized, thereby enabling phase matching.

Very weak HHG emission at high photon energies of ~ 200 to 500 eV at very low (few torr) gas pressures has been observed using intense UV and near-IR lasers (1, 31, 32). In those studies, the HHG emission emerged from ionization of a small number of ions, which emit harmonics with comparable efficiency to neutral atoms (33). Moreover, the inability to phase-match the HHG

process in plasmas, combined with strong plasma-induced defocusing of the laser, meant that the HHG flux was weaker than theoretically possible in a phase-matched geometry by a factor of 10^{-4} to 10^{-11} .

Here, we demonstrate a regime of bright high-harmonic emission in multiply ionized plasmas

(Figs. 1 and 2). Using intense UV driving lasers at a wavelength of $0.27 \mu\text{m}$, bright discrete HHG peaks extend well into the soft x-ray region of the spectrum. It is well established that low quantum diffusion of the electron wave packet (due to the shorter time the electron spends away from the ion) maximizes the single-atom yield for UV

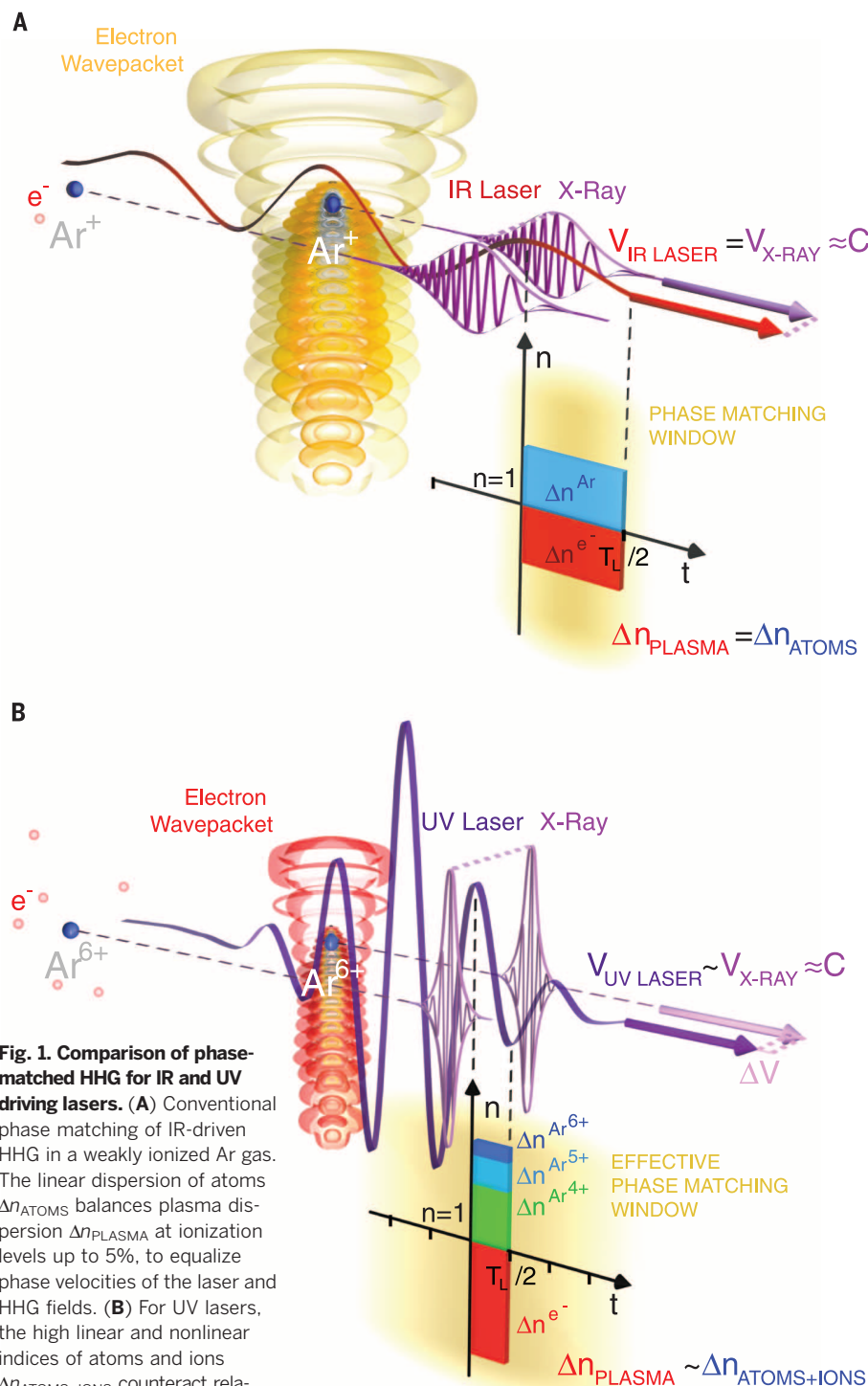


Fig. 1. Comparison of phase-matched HHG for IR and UV driving lasers. (A) Conventional phase matching of IR-driven HHG in a weakly ionized Ar gas.

The linear dispersion of atoms Δn_{ATOMS} balances plasma dispersion Δn_{PLASMA} at ionization levels up to 5%, to equalize phase velocities of the laser and HHG fields. (B) For UV lasers, the high linear and nonlinear indices of atoms and ions $\Delta n_{\text{ATOMS+IONS}}$ counteract relatively low plasma dispersion, ensuring a good HHG yield even in a multiply ionized plasma (500% ionization).

Δv is the small offset from the speed of light c . The large single-atom yield, coupled with coherence lengths ranging from several micrometers to ∞ , as well as low harmonic orders, result in full to effective phase matching over many laser cycles.

¹JILA, University of Colorado, Boulder, CO 80309, USA.

²Grupo de Investigación en Óptica Extrema, Universidad de Salamanca, E-37008 Salamanca, Spain. ³Centro de Lasers Pulsados, E-37008 Salamanca, Spain. ⁴Institute of Photonics Technologies, National Tsing Hua University, Hsinchu 30013, Taiwan. ⁵School of Applied and Engineering Physics, Cornell University, Ithaca, NY 14853, USA. ⁶Department of Chemistry, Temple University, Philadelphia, PA 19122, USA. ⁷Department of Physics, Temple University, Philadelphia, PA 19122, USA. ⁸Physics Division, Physical and Life Sciences, Lawrence Livermore National Laboratory, Livermore, CA 94550, USA.

*Corresponding author. E-mail: tenio.popmintchev@jila.colorado.edu

driving lasers. However, in this new regime of intense UV-driven HHG, the higher linear and nonlinear indices of atoms and ions contribute substantially to the dispersion experienced by the driving laser and serve to counteract plasma dispersion (Fig. 1B). This enables coherent build-up of the HHG signal in multiply ionized plasmas at very high gas pressures (i.e., effective phase matching) to photon energies greater than 280 eV, corresponding to harmonic orders of only ~ 61 .

We observed high conversion efficiencies of $\sim 10^{-3}$ to 10^{-7} throughout the extreme UV (EUV) and soft x-ray regions; these values are orders of magnitude brighter than has been observed to date from ions. The well-separated (~ 9 eV) narrowband HHG peaks, with linewidths of 70 to 700 meV ($\lambda/\Delta\lambda \approx 350$ to 450) in the vacuum UV (VUV) to soft x-ray regions, are ideal for applications in imaging and photoelectron spectroscopies. The high HHG efficiency and narrow linewidths arise from a long phase-matching window as well as low group velocity walk-off, so that group and phase velocity matching are possible over many laser cycles. Moreover, in contrast to the strongly chirped HHG emission driven by near- and mid-IR driving lasers, simulations show that UV-driven harmonics emerge as nearly time-bandwidth-limited series of ~ 100 -as bursts. Our predictions indicate that bright UV-driven harmonics can extend into the multi-keV region. This leads to the surprising conclusion that the fundamental of Ti:sapphire lasers may be the most limited for generating bright soft x-ray harmonics, relative to using longer- or shorter-wavelength driving lasers.

In our experiment, high harmonics were produced by focusing the third harmonic (0.27 μm) of a Ti:sapphire laser into an Ar-filled waveguide (diameter 150 to 400 μm , length 1 to 15 mm) at pressures between 1 and 1500 torr (see supplementary materials). The pulse energy and duration were 2.6 mJ and 35 fs [full width at half maximum (FWHM)], respectively. By focusing to a spot size less than 55 μm in diameter, the peak laser intensity was $>6 \times 10^{15}$ W/cm², with a confocal parameter less than 17 mm.

Figure 2A shows that bright HHG emission from Ar extends far beyond the ~ 30 -eV limit predicted using only the dispersion of atoms, to photon energies of >280 eV (see fig. S1 for HHG plotted on a linear scale). The high laser intensity required for UV-driven soft x-ray HHG (at $>6 \times 10^{15}$ W/cm²) is well above the barrier suppression ionization for atoms; thus, neutral atoms will be fully ionized well before the peak intensity of the pulse. However, this intensity is in the tunneling regime for ions. Moreover, time-dependent Schrödinger equation (TDSE) calculations (Fig. 2B and fig. S3) show that HHG from Ar in this energy range must emerge from ions (Ar⁺ to Ar⁵⁺) with relatively high ionization potentials ($I_p^{\text{Ar}^+} = 27.6$ eV to $I_p^{\text{Ar}^{5+}} = 90.1$ eV).

Phase matching in UV-driven VUV and soft x-ray HHG optimizes at higher gas pressures of ~ 100 to 400 torr, as shown in Fig. 2A, fig. S1,

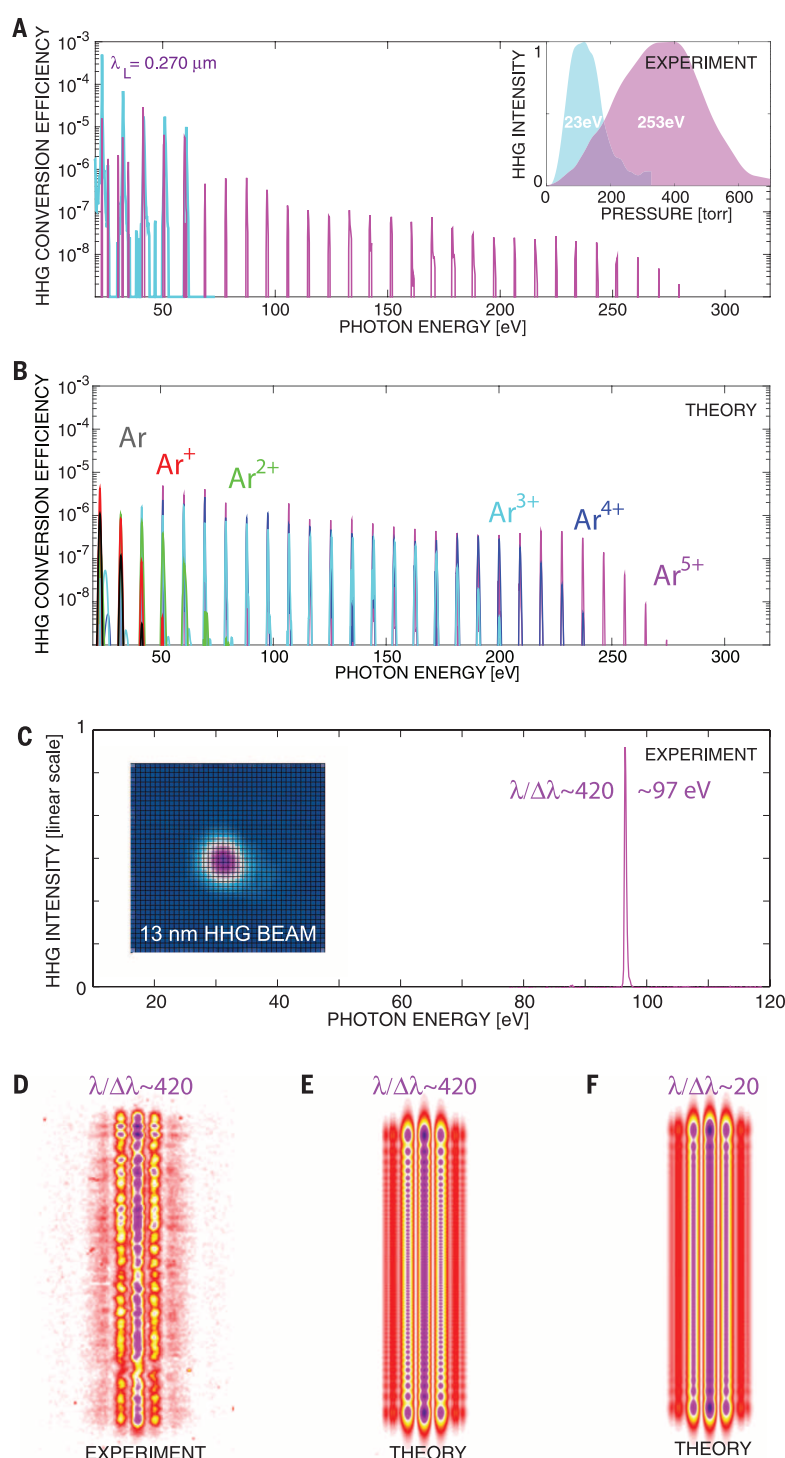


Fig. 2. UV-driven HHG gives bright discrete peaks and isolated harmonics into the soft x-ray region.

(A) Experimentally observed UV-driven HHG from multiply ionized Ar, optimized in the EUV (blue spectrum) and soft x-ray (purple spectrum) regions. Inset: VUV HHG optimizes at <100 torr and low laser intensities ($>10^{15}$ W/cm²), while soft x-ray HHG optimizes at 400 torr and high intensities ($>6 \times 10^{15}$ W/cm²). (B) Predicted HHG yield from single Ar atoms and ions using TDSE calculations. Above 30 eV, the extended UV-driven HHG must originate from highly charged ions. The emission from different ionic species is plotted separately (not integrated). (C) Experimentally isolated 13-nm harmonic with ultranarrow linewidth of $\lambda/\Delta\lambda \approx 420$ or 230 meV. Adjacent harmonic orders were eliminated using Rh + Si + Be filters. The inset shows the 13-nm HHG beam. (D to F) Experimental and theoretical Young's double-slit diffraction patterns showing full spatial coherence, from a slit of width of 20 μm and height 1.5 mm. The spatial modulations perpendicular to the slit in (D) and (E) are due to the high spectral purity that generates observable interferences in (D). For broad harmonic linewidths (F), the vertical spatial modulations are not present.

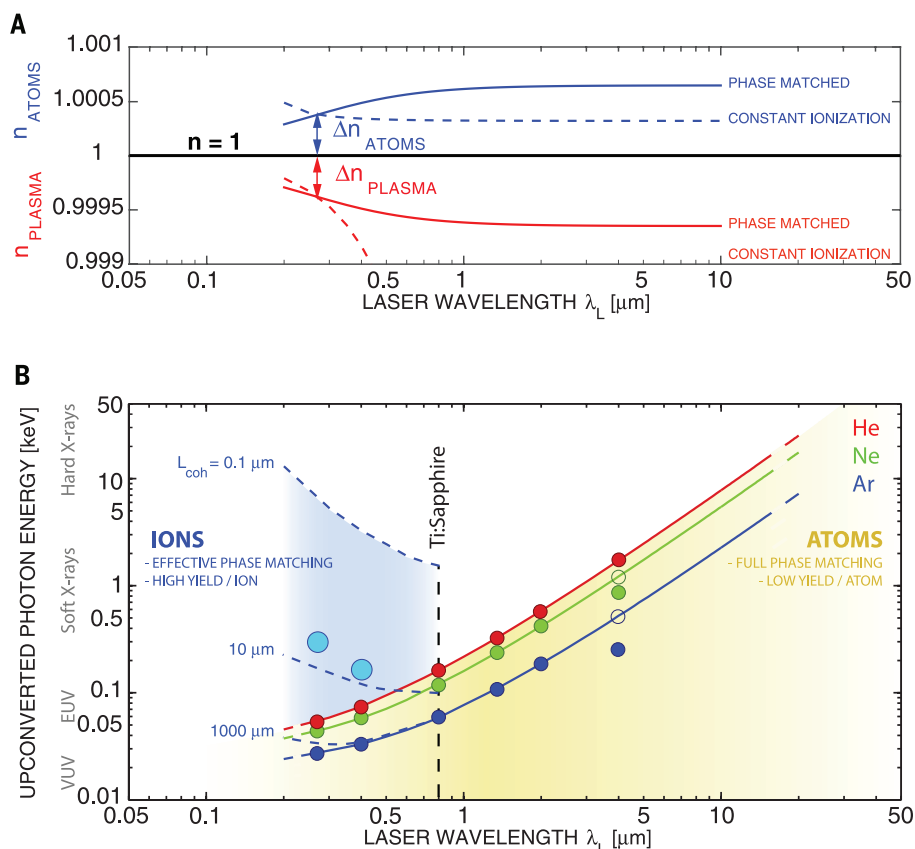


Fig. 3. Phase matching of HHG using UV to mid-IR lasers. (A) Refractive index of Ar atoms (blue dashed) compared with that of free electron plasma (red dashed) as a function of wavelength, for constant ionization conditions of 40%. The solid lines plot the indices under phase-matching conditions near cutoff, where IR-driven HHG needs multi-atmospheres of gently ionized gas, whereas UV-driven HHG occurs in a multiply ionized plasma. (B) Bright HHG from atoms and ions for UV to mid-IR driving lasers. The experimental data are plotted as circles. The solid lines plot the theoretical full phase-matching limits, including only the index of neutral atoms. The dashed lines also include the refractive indices of ions, which extend UV-driven HHG effective phase matching into the soft x-ray region.

and table S1. This is in contrast to all previous observations of HHG x-rays from ions in a non-phase-matched regime, where very high harmonic orders can be observed only at pressures that are lower by about two orders of magnitude (1 to 3 torr) (31, 33). In general, only harmonic orders that are phase-matched will increase in intensity with increasing gas pressure. The optimal pressures increase with harmonic order to compensate for increasing plasma dispersion. Furthermore, the increasing HHG yield with pressure indicates that ionization-induced defocusing of the laser is not a dominant limitation. Other evidence of good coherent HHG signal buildup over many laser cycles is the narrow spectral width of UV-driven HHG, shown in Figs. 1 and 2 and fig. S1. The linewidths decrease from >900 meV (at ~ 50 eV) for Ti:sapphire lasers, to ~ 70 meV (at ~ 30 eV) and 400 meV (at ~ 180 eV) for UV driving lasers. These narrow-linewidth HHG peaks, with spectral purity up to $\lambda/\Delta\lambda > 450$, are observed despite strong ionization that must occur on the leading edge of the driving laser pulse and that would normally result in strong spectral broadening and blue shifting of both the driving

laser and HHG emission. Fortunately, because this frequency shift scales as $\Delta\lambda_{\text{LASER}} \sim -\lambda_{\text{LASER}}^3$ at similar rates of ionization (34, 35), this shift is smaller for UV lasers, which preserves narrow harmonic linewidths.

Because the HHG spectra consist of odd-harmonic peaks that are well separated in energy (>9 eV), UV-driven HHG also provides a practical way to isolate a single harmonic order. Figure 2 plots a single harmonic near the technologically relevant 13.5-nm wavelength for lithography, highlighting the excellent beam quality (Fig. 2C, inset) and high spatial and temporal coherence. Lower harmonic orders were eliminated by the same thin-film filters used to reject the fundamental laser light, whereas higher cutoff harmonics were excluded by adjusting the intensity of the UV laser. Figure 2, D to F, plots the experimental and theoretical double-slit diffraction patterns for a slit of width 20 μm , slit separation of 50 μm , and height of 1.5 mm. The spatial modulations perpendicular to the slit in Fig. 2, D and E, are due to the high spectral purity of the HHG beam and generate observable interference both along and perpendicular to the slit.

At 13 nm, the estimated HHG flux of Fig. 2C corresponds to $>10^{11}$ photons/s (peak brightness $>10^{29}$ photons $\text{s}^{-1} \text{mm}^{-2} \text{mrad}^{-2}$) at the exit of the waveguide under optimal conditions for generating 280-eV harmonics. Over the whole spectral range, the efficiencies into a single harmonic order are estimated to approach 10^{-3} to 10^{-7} in the VUV, EUV, and soft x-ray regions. The HHG flux was measured to be consistent using three different methods. First, we compared HHG driven by 0.8- μm and 0.27- μm lasers in the same spectral region. Second, we estimated the efficiency from known spectrometer, x-ray filter, and charge-coupled device efficiencies. Third, we used a NIST-calibrated vacuum diode to measure the flux in the VUV and EUV regions. We observed good HHG signal—comparable to or greater than phase-matched HHG at 100 eV driven by 0.8- μm lasers—throughout the EUV and soft x-ray regions (Fig. 2 and fig. S1).

High harmonics were first observed in 1987 using a UV driving laser (1). That work used longer pulses (by a factor of ~ 10) in a tight focus geometry, and HHG up to 85 eV (14.6 nm) was observed with estimated efficiency of 10^{-11} . Subsequent work observed HHG from ions (also using long-pulse UV lasers in a tight focus geometry with limited interaction length), with conversion efficiencies around 10^{-10} or 10^{-12} at photon energies from 100 to 180 eV (32). More recently, broadband HHG from Ar ions up to 500 eV was observed for 0.8- μm driving lasers in a few-torr gas-filled hollow waveguide (31). However, this emission was also extremely weak because of the low pressures (few torr) and poor phase-matching conditions (see table S1 for comparison).

To quantitatively explain why bright harmonics from Ar driven by UV lasers can extend into the soft x-ray region, we used simple numerical models, which have been extensively validated for near and mid-IR driving lasers, as well as exact integration of the time-dependent Schrödinger equation (26, 28–30). To aid with physical insight, Fig. 3A (dashed lines) plots the calculated index of refraction contribution of an Ar atom compared with that of a free electron. As expected, the refractive indices of neutral atoms are largest in the UV region of the spectrum.

On the other hand, the free electron plasma contribution to the refractive index scales as $n_{\text{plasma}} = [(1 - \omega_p^2)/\omega_{\text{LASER}}^2]^{1/2}$, where $\omega_p = (n_e e^2/m_e \epsilon_0)^{1/2}$ is the plasma frequency corresponding to an electron density n_e , and where e and m_e are the charge and mass of the electron. Hence, lower frequencies (i.e., longer laser wavelengths) will experience much higher plasma dispersion, and therefore phase matching occurs only at low ionization levels below the critical ionization (7, 36) (table S1).

In contrast, for wavelengths in the visible and UV spectral regions, the positive refractive index contribution of a neutral Ar atom exceeds the negative contribution of a free electron. This corresponds to a critical ionization level of $\sim 40\%$ for UV-driven HHG at ~ 40 eV. Moreover, the

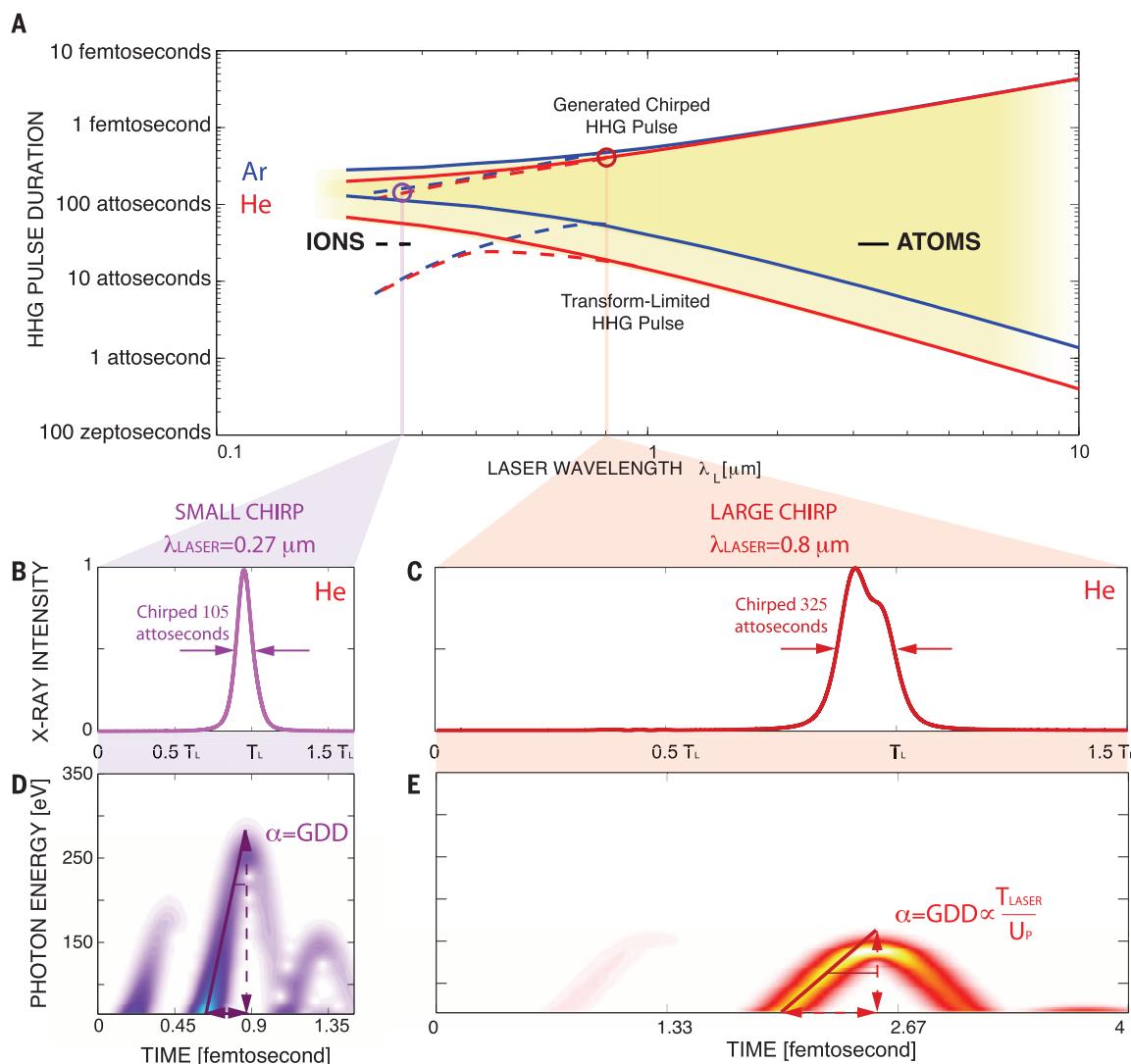


Fig. 4. Theoretical UV-driven HHG gives shorter duration and lower chirp pulses than mid-IR-driven HHG. (A) The pulse duration of HHG soft x-ray bursts converges to the transform limit for UV driving lasers. (B to E) Chirp [group delay dispersion (GDD)] of the HHG pulses in He driven by intense three-cycle UV and near-IR lasers, respectively. For UV lasers, the HHG chirp is reduced as a result of the shorter laser cycle duration T_{LASER} and

the higher ponderomotive potential U_p (higher HHG cutoff). The highest harmonics with a 280-eV cutoff (spectrally filtered by a Rh thin film) have a pulse duration of 105 as (even shorter 45- to 75-as pulses could be generated from He and He^+ ; see supplementary materials). In comparison, for a 0.8- μm driver and a phase-matching cutoff of 160 eV, the pulse durations are 325 as (>3 times as long).

refractive indices of ions in the UV are comparable to that of neutral Ar (see supplementary materials), as the ionization potential of each successive ionization stage increases only modestly. Thus, for UV driving lasers, good buildup of the HHG signal is possible even in a multiply ionized plasma. This enables extension of effective phase matching into the soft x-ray region and, in theory, even to hard x-rays. Note that for UV-driven HHG, full phase matching is possible in the VUV-EUV, while efficient HHG is possible in soft x-ray region at high pressures, with high photon flux.

In our simple phase-matching model, we consider a one-dimensional geometry, which corresponds to the general case of a large waveguide diameter or large focal spot size (near-plane wave propagation). To calculate the phase mis-

match to a first approximation, we need to consider a generalized set of multispecies time-dependent equations, given by

$$\begin{aligned} \Delta k(t) &= qk_{\omega}(t) - k_{q\omega}(t) \\ &\approx -qP\eta_0(t) \frac{2\pi}{\lambda_L} [\delta_L^0(t) + \tilde{n}_2^0(t)I_L(t)] \\ &\quad - \sum_{i=1,2,\dots} qP\eta_i(t) \frac{2\pi}{\lambda_L} [\delta_L^i(t) + \tilde{n}_2^i(t)I_L(t)] \\ &\quad + \underbrace{qP\eta_{\text{total}}(t)N_{\text{atm}}r_e\lambda_L}_{\text{free electrons}} + \Delta k_{\text{geometry}} \end{aligned} \quad (1)$$

where $\eta_i(t)$ is the fractional population of the various gas species present at a given moment ($i=0$ denotes

neutral atoms, $i=1, 2, 3, \dots$ denote various ion states), $\eta_{\text{total}}(t)$ is the cumulative fractional ionization [$\eta_{\text{total}}(t) > 100\%$ for multiply charged ions], r_e is the classical electron radius, N_{atm} is the number density of atoms at 1 atm, P is the pressure, and $\delta_L^i(t)$ is the difference between the indices of refraction at the fundamental and harmonic wavelengths (which is very large in the UV). Although in general the nonlinear index contributions are estimated to play a rather small role, for high UV laser intensities $>6 \times 10^{15} \text{ W/cm}^2$, an additional term due to the nonlinear index of refraction (t) must also be included, estimated by multiconfigurational self-consistent field calculations (table S2). For $\eta_{\text{total}}(t) > 10\%$, one must include the dispersion of ions as well as a cumulative total ionization level η_{total} resulting from all ions of higher charge. The phase-matching photon energy limits

are determined by the ionization level at which a dispersion balance is achieved and are independent of HHG geometry (the geometrical dispersion sets only an optimal pressure for a wave-guiding geometry) (7, 29). For our experimental conditions, at any time during the HHG emission, two to three species contribute strongly to the HHG signal (Fig. 2B and fig. S2). Fortunately, for a given HHG photon energy, the harmonic order q is lower for UV-driven versus mid-IR-driven HHG, naturally leading to longer coherence lengths even at very high ionization levels and pressures as $\Delta k \propto q$.

Figure S6 plots the estimated dynamic phase mismatch ratio due to plasma and to atoms and ions for Ar driven by 10-cycle 0.27- and 0.8- μm lasers. The dashed black horizontal lines show the high-flux HHG region with coherence lengths $L_{\text{coh}} = \pi/\Delta k$ from infinity to 10 μm . This time window is substantially longer for UV driving lasers than for near-IR driving lasers, extending effective phase matching over ~ 5 to 40 half-cycles or a time interval of ~ 2 to 18 fs. This picture is also consistent with the observed narrow spectral linewidths in the VUV to x-ray regime at high phase-matching pressures (Fig. 2 and fig. S1). Under our conditions, at a photon energy of 250 eV, $L_{\text{coh}} > 3 \mu\text{m}$, the absorption length $L_{\text{abs}} \approx 1 \text{ mm}$ at 400 torr (for ions see fig. S7), whereas the medium length $L_{\text{med}} \approx 1$ to 15 mm. At 40 eV, $L_{\text{coh}} \approx \infty$.

Additional nonlinear effects—for example, due to laser pulse self-guiding or filamentation, which are likely present—would further enhance effective HHG phase matching in plasmas, because the nonlinear index induced by the laser will increase further to compensate for plasma-induced dispersion. Figure S10 shows blue-shifting and broadening of the fundamental spectrum that is characteristic also for self-effects in efficient HHG at other laser wavelengths, at 0.8 μm and in the mid-IR phase-matching regimes (26, 31, 37). This is also supported by our observation that in a short gas cell geometry the HHG spectrum extends to only ~ 180 eV in Ar, Ne, or He.

Decreased medium opacity due to removal of several valence electrons can also increase the yield, particularly for intense UV-driven HHG, where the single-atom yield is already very high. However, we calculate that increasing transparency of the medium is not sufficient to explain the observed increase in HHG yield, especially when the coherence length is smaller than the absorption length. As shown in fig. S6, while the transparency increases as expected at photon energies around 100 eV, in the soft x-ray region the transparency does not change substantially. Thus, in the future, all-optical quasi-phase-matching HHG techniques could be applied to take advantage of the full x-ray absorption length to enhance the yield further (38–41).

We also modeled UV-driven HHG using the TDSE. Figure 2B plots the TDSE predictions for strong field ionization in Ar for a peak laser intensity similar to the experiment, which shows that HHG in the 30- to 280-eV photon energy range must be generated from multiply ionized

species, up to Ar^{5+} , at ionization levels above 500% (on axis of the waveguide). This far exceeds the 5% critical ionization limit for fully phase-matched HHG in Ar using 0.8- μm lasers. Our TDSE calculations show that the single-atom yield scales more strongly than $\sim \lambda_L^{-7.5}$ (42) for a single harmonic of He, corresponding to a factor of ~ 4000 greater yield for 0.27- μm relative to 0.8- μm driving lasers. A similar scaling is expected for Ar species, although with a slightly modified exponent.

These TDSE calculations also show that HHG driven by UV is particularly suitable for generating nearly transform-limited isolated attosecond bursts (or pulse trains), with very low temporal chirp that should be straightforward to compensate. It is already known that the atto-chirp of each individual attosecond burst will be reduced as the driving laser wavelength is reduced in the UV, because of the shorter time the electron spends in the continuum (~ 300 as). However, for higher photon energies using more intense UV driving lasers, the pulse duration and atto-chirp will be reduced even further as a result of the larger phase-matched bandwidth (i.e., large U_p). Figure 4 plots a time-frequency analysis for HHG in He driven by intense three-cycle UV and 0.8- μm lasers, where the reduction in the temporal chirp is very apparent. This effect is dictated by the duration of an individual laser cycle, independent of the number of cycles in the laser pulse. In the case of UV driving lasers, the FWHM duration of the highest harmonics naturally emerges as slightly chirped ~ 105 -as bursts, compared with strongly chirped 325-as pulses for an 0.8- μm driving laser in the same photon energy range. For comparison, for 2- to 4- μm mid-IR-driven HHG, the emission is brightest when the HHG pulse emerges as an isolated, very strongly chirped, 300- to 1200-as burst (26). The experimental HHG emission from Ar is predicted to emerge as a long 10-fs train of nearly transform-limited ~ 100 -as pulses.

Another advantage of UV driving lasers is the low group velocity walk-off. This is in contrast to mid-IR ($>2 \mu\text{m}$)-driven HHG, where group velocity walk-off limits the coherent buildup length and conversion efficiency (29, 43). Using UV lasers, the temporal window for phase matching increases while the walk-off decreases (see supplementary materials). Both the group and phase velocities of the driving laser and HHG light can be nearly matched, so that the electron wave packets of different atoms in the medium rescatter in a coherent way (i.e., electron wave packets have the same quantum paths and same quantum phases, resulting in highly temporally coherent HHG). Furthermore, because the coherence length for effective phase matching in the soft x-ray region is smaller than the characteristic group velocity walk-off length (see supplementary materials and table S1), intense UV-driven HHG is also effectively group velocity-matched.

As shown in Fig. 3B, our best current experimental and theoretical understanding indicates that shorter UV laser wavelengths and

intensities $>10^{16} \text{ W/cm}^2$ will produce bright HHG emission at even higher soft x-ray photon energies $\gg 280$ eV, which would be ideal for coherent imaging. The phase mismatch decreases more slowly using UV lasers compared with near-IR or mid-IR lasers; this is due to the lower harmonic orders and pressures required (i.e., lower q and P in Eq. 1). To a first approximation under ideal phase-matching conditions, every term in Eq. 1 scales linearly with the laser wavelength. Because lower harmonic orders correspond to much higher photon energies in the case of UV driving lasers, the coherence length is relatively long compared to the coherence length at the same photon energy generated with a longer-wavelength UV-visible laser (Fig. 3B). This ensures strong constructive buildup over the interaction region in an effectively phase-matched geometry even in the presence of a finite phase mismatch—and also ensures HHG emission that is as bright as fully phase-matched HHG at 13 nm in He driven by 0.8- μm lasers. This strongly contrasts with longer-wavelength mid-IR lasers, where the order of the upconversion process is higher, with $q > 5000$ for a 4- μm driver.

Using intense UV driving lasers, effective phase matching of the HHG process extends the bright emission in the VUV, EUV, and soft x-ray regions. This regime provides coherent light with contrasting and complementary spectral and temporal properties, compared to the mid-IR-driven HHG x-rays: These exhibit ultrabroad supercontinuum spectra that can be used to probe multiple elements over a spectral range of >1 keV. Remarkably, the UV-driven HHG linewidths decrease to fractional bandwidths of $\lambda/\Delta\lambda \approx 450$ that are ideal for a complementary set of scientific and technological applications, such as in photoemission spectroscopy with very high energy resolution and coherent diffraction imaging with very high spatial resolution (44, 45). In terms of laser technology, the availability of intense femtosecond UV lasers (e.g., harmonics of Yb:YAG, Ti:sapphire, or excimer lasers) makes this approach ideal for many applications. Finally, there is a strong potential to produce much brighter HHG beams at even higher multi-keV x-ray photon energies than would be possible with other approaches.

REFERENCES AND NOTES

1. A. McPherson *et al.*, *J. Opt. Soc. Am. B* **4**, 595–601 (1987).
2. M. Y. Kuchiev, *JETP Lett.* **45**, 404–406 (1987).
3. J. L. Krause, K. J. Schafer, K. C. Kulander, *Phys. Rev. Lett.* **68**, 3535–3538 (1992).
4. K. C. Kulander, K. J. Schafer, J. L. Krause, in *Super-Intense Laser-Atom Physics*, B. Piraux, A. L'Huillier, K. Rzaewski, Eds. (Plenum, New York, 1993), pp. 95–110.
5. M. Lewenstein, P. Balcou, M. Y. Ivanov, A. L'Huillier, P. B. Corkum, *Phys. Rev. A* **49**, 2117–2132 (1994).
6. M. Ferray *et al.*, *J. Phys. At. Mol. Opt. Phys.* **21**, L31–L35 (1988).
7. A. Rundquist *et al.*, *Science* **280**, 1412–1415 (1998).
8. I. P. Christov, M. M. Murnane, H. C. Kapteyn, *Phys. Rev. Lett.* **78**, 1251–1254 (1997).
9. P. Antoine *et al.*, *Phys. Rev. A* **56**, 4960–4969 (1997).
10. P. B. Corkum, N. H. Burnett, M. Y. Ivanov, *Opt. Lett.* **19**, 1870 (1994).
11. G. Sansone *et al.*, *Science* **314**, 443–446 (2006).

12. M. E. Siemens *et al.*, *Nat. Mater.* **9**, 26–30 (2010).
13. S. Mathias *et al.*, *Proc. Natl. Acad. Sci. U.S.A.* **109**, 4792–4797 (2012).
14. E. Turgut *et al.*, *Phys. Rev. Lett.* **110**, 197201 (2013).
15. M. Bauer *et al.*, *Phys. Rev. Lett.* **87**, 025501 (2001).
16. T. Rohwer *et al.*, *Nature* **471**, 490–493 (2011).
17. P. Salieres, A. Maquet, S. Haessler, J. Caillat, R. Taieb, *Rep. Prog. Phys.* **75**, 062401 (2012).
18. R. Haight, *Surf. Sci. Rep.* **21**, 275–325 (1995).
19. M. Probst, R. Haight, *Appl. Phys. Lett.* **71**, 202–204 (1997).
20. A. Rettenberger, P. Leiderer, M. Probst, R. Haight, *Phys. Rev. B* **56**, 12092–12095 (1997).
21. A. L. Cavalieri *et al.*, *Nature* **449**, 1029–1032 (2007).
22. G. Sansone *et al.*, *Nature* **465**, 763–766 (2010).
23. M. Drescher *et al.*, *Nature* **419**, 803–807 (2002).
24. M. D. Seaberg *et al.*, *Opt. Express* **19**, 22470–22479 (2011).
25. J. Miao, T. Ishikawa, I. K. Robinson, M. M. Murnane, *Science* **348**, 530–535 (2015).
26. T. Popmintchev *et al.*, *Science* **336**, 1287–1291 (2012).
27. M. V. Frolov, N. L. Manakov, A. F. Starace, *Phys. Rev. Lett.* **100**, 173001 (2008).
28. T. Popmintchev *et al.*, *Opt. Lett.* **33**, 2128–2130 (2008).
29. T. Popmintchev *et al.*, *Proc. Natl. Acad. Sci. U.S.A.* **106**, 10516–10521 (2009).
30. M. C. Chen *et al.*, *Phys. Rev. Lett.* **105**, 173901 (2010).
31. P. Arpin *et al.*, *Phys. Rev. Lett.* **103**, 143901 (2009).
32. S. G. Preston *et al.*, *Phys. Rev. A* **53**, R31–R34 (1996).
33. E. A. Gibson *et al.*, *Phys. Rev. Lett.* **92**, 033001 (2004).
34. S. C. Rae, *Opt. Commun.* **104**, 330–335 (1994).
35. S. C. Rae, K. Burnett, *Phys. Rev. A* **46**, 1084–1090 (1992).
36. C. G. Durfee *et al.*, *Phys. Rev. Lett.* **83**, 2187–2190 (1999).
37. N. L. Wagner *et al.*, *Phys. Rev. Lett.* **93**, 173902 (2004).
38. X. Zhang *et al.*, *Nat. Phys.* **3**, 270–275 (2007).
39. O. Cohen *et al.*, *Phys. Rev. Lett.* **99**, 053902 (2007).
40. S. L. Voronov *et al.*, *Phys. Rev. Lett.* **87**, 133902 (2001).
41. P. L. Shkolnikov, A. Lago, A. E. Kaplan, *Phys. Rev. A* **50**, R4461–R4464 (1994).
42. D. Popmintchev *et al.*, in *Conference on Lasers and Electro-optics (CLEO)* (Optical Society of America, San Jose, CA, 2013), p. QW1A.5.
43. M.-C. Chen *et al.*, *Proc. Natl. Acad. Sci. U.S.A.* **111**, E2361–E2367 (2014).
44. J. Miao, T. Ishikawa, I. K. Robinson, M. M. Murnane, *Science* **348**, 530–535 (2015).
45. B. Zhang *et al.*, *Ultramicroscopy* **158**, 98–104 (2015).

ACKNOWLEDGMENTS

The experimental work was done at JILA, supported by Army Research Office grant WN11NF-13-1-0259, an NSF PFI AIR award, and U.S. Department of Energy (DOE) grant DE-SC0008803 (M.M.M., T.P., and H.C.K.). Theory was supported by a Marie Curie International Outgoing Fellowship within the EU Seventh Framework Programme for Research and Technological Development (2007–2013) under REA

grant agreement 328334 (C.H.-G.); Junta de Castilla y León (SA116U13, UIC016) and MINECO (FIS2013-44174-P) (C.H.-G. and L.P.); NSF grants PHY-1125844 and PHY-1068706 and AFOSR MURI “Mathematical Modeling and Experimental Validation of Ultrafast Light-Matter Coupling associated with Filamentation in Transparent Media” grant FA9550-10-1-0561 (A.J.-B., R.J.L., X.G., A.L.G., M.M.M., and H.C.K.); Ministry of Science and Technology, Taiwan, grant 102-2112-M-007-025-MY3 (M.-C.C.); U.S. Department of Energy, Division of Chemical Sciences, Atomic, Molecular and Optical Sciences Program (A.B.); and DOE Office of Fusion Energy, HED Laboratory Plasmas program, grant AT5015033 (S.B.L., M.F., and J.A.G.). Lawrence Livermore National Laboratory is operated by Lawrence Livermore National Security LLC for DOE, National Nuclear Security Administration, under contract DE-AC52-07NA27344, LLNL-JRNL-676693. T.P., D.P., M.M.M., and H.C.K. have filed a patent on “Generation of VUV, EUV, X-ray Light Using VUV-UV-VIS Lasers.” U.S. patent application 61873794 (2013)/US 20150063385 (2015).

SUPPLEMENTARY MATERIALS

www.sciencemag.org/content/350/6265/1225/suppl/DC1
Supplementary Text
Figs. S1 to S10
Tables S1 to S3
References (46–65)

7 July 2015; accepted 19 October 2015
10.1126/science.aac9755

QUANTUM HALL EFFECT

Evidence for a fractional fractal quantum Hall effect in graphene superlattices

Lei Wang,^{1,2} Yuanda Gao,¹ Bo Wen,³ Zheng Han,³ Takashi Taniguchi,⁴ Kenji Watanabe,⁴ Mikito Koshino,⁵ James Hone,¹ Cory R. Dean^{3*}

The Hofstadter energy spectrum provides a uniquely tunable system to study emergent topological order in the regime of strong interactions. Previous experiments, however, have been limited to low Bloch band fillings where only the Landau level index plays a role. We report measurements of high-mobility graphene superlattices where the complete unit cell of the Hofstadter spectrum is accessible. We observed coexistence of conventional fractional quantum Hall effect (QHE) states together with the integer QHE states associated with the fractal Hofstadter spectrum. At large magnetic field, we observed signatures of another series of states, which appeared at fractional Bloch filling index. These fractional Bloch band QHE states are not anticipated by existing theoretical pictures and point toward a distinct type of many-body state.

In a two-dimensional electron gas (2DEG) subjected to a magnetic field, the Hall conductivity is generically quantized whenever the Fermi energy lies in a gap (*I*). The integer quantum Hall effect (IQHE) results from the cyclotron gap that separates the Landau energy levels (LLs). The longitudinal resistance drops to zero, and the Hall conductivity develops plateaus

quantized to $\sigma_{xy} = \nu e^2/h$, where ν , the Landau level filling fraction, is an integer; h is Planck's constant; and e is the electron charge. When the 2DEG is modified by a spatially periodic potential, the LLs develop additional subbands separated by minigaps, resulting in the fractal energy diagram known as the Hofstadter butterfly (2). When plotted against normalized magnetic flux ϕ/ϕ_0 and normalized density n/n_0 (representing the magnetic flux quanta and electron density per unit cell of the superlattice, respectively), the fractal minigaps follow linear trajectories (3) according to a Diophantine equation, $n/n_0 = t\phi/\phi_0 + s$, where s and t are integers; s is the Bloch band-filling index associated with the superlattice, and t is a similar index related to the gap structure

along the field axis (4) (in the absence of a superlattice, t reduces to the LL filling fraction). The fractal minigaps give rise to QHE features at partial Landau level filling, but in this case t , rather than the filling fraction, determines the quantization value (*I*, 5) and the Hall plateaus remain integer-valued.

In very-high-mobility 2DEGs, strong Coulomb interactions can give rise to many-body gapped states also appearing at partial Landau fillings (6–8). Again, the Hall conductivity exhibits a plateau, but in this case quantized to fractions of e^2/h . This effect, termed the fractional quantum Hall effect (FQHE), represents an example of emergent behavior in which electron interactions give rise to collective excitations with properties fundamentally distinct from the fractal IQHE states. A natural theoretical question arises regarding how interactions manifest in a patterned 2DEG (9–12). In particular, because both the FQHE many-body gaps and the single-particle fractal minigaps can appear at the same filling fraction, it remains unclear whether the FQHE is even possible within the fractal Hofstadter spectrum (13–15). Experimental effort to address this question has been limited, owing to the requirement of imposing a well-ordered superlattice potential while preserving a high carrier mobility (16–18).

Here, we report a low-temperature magnetotransport study of fully encapsulated hexagonal boron nitride (h-BN)/graphene/h-BN heterostructures, fabricated by van der Waals assembly with edge contact (19, 20). A key requirement to observe the Hofstadter butterfly is the capability to reach the commensurability condition in which the magnetic length $l_B = \sqrt{\hbar/eB}$ (where \hbar is Planck's constant divided by 2π , e is the electron charge, and B is the magnetic field) is comparable to the wavelength of the spatially periodic potential, λ . For experimentally accessible magnetic

¹Department of Mechanical Engineering, Columbia University, New York, NY 10027, USA. ²Kavli Institute at Cornell for Nanoscale Science, Ithaca, NY 14853, USA. ³Department of Physics, Columbia University, New York, NY 10027, USA. ⁴National Institute for Materials Science, 1-1 Namiki, Tsukuba 305-0044, Japan. ⁵Department of Physics, Tohoku University, Sendai 980-8578, Japan.

*Corresponding author. E-mail: cdean@phys.columbia.edu

fields, this requires a superlattice potential with wavelength on the order of tens of nanometers. In this regard, graphene/h-BN heterostructures provide an ideal system, because at near-zero angle mismatch, the slight difference in lattice constants between the graphene and BN crystal structures gives rise to a moiré superlattice with a period of ~ 14 nm (21–24). Moreover, we find that in our van der Waals assembly technique, in which the graphene-BN interface remains pristine (19), alignment between the graphene and BN can be achieved by simple application of heat. Figure 1A shows an example of a heterostructure that was assembled with random (and unknown) orientation of each material. After heating the sample to $\sim 350^\circ\text{C}$, the graphene flake translates and rotates through several micrometers, despite being fully encapsulated between two BN sheets. This behavior has been observed in several devices (20), in each case resulting in a moiré wavelength of 10 to 14 nm [indicating less than 2° angle mismatch

(21)]. We speculate that the thermally induced motion proceeds until the macroscale graphene flake finds a local energy minimum, corresponding to crystallographic alignment to one of the BN surfaces (25).

Figure 1A shows the resistance versus gate voltage at zero applied magnetic field for a device with moiré wavelength of ~ 10 nm. In addition to the usual peak in resistance at the zero-density charge neutrality point (CNP), two additional satellite peaks appear at equidistant positive and negative gate bias—characteristic signatures of electronic coupling to a moiré superlattice (21–23). The CNP peak resistance exhibits thermally activated behavior and exceeds 100 kilohms at low temperature, indicating a moiré coupling-induced band gap (24–26). The gap varies continuously with rotation angle, consistent with previous studies of nonencapsulated graphene (20, 24). At zero angle, the energy gap measured by transport is equivalent to the optical gap (27), indicating low disorder broadening of the energy band in our

devices, and consistent with the high electron mobility achievable by the van der Waals assembly technique (19, 20). Unlike previous studies of encapsulated devices (23, 25), we find that the gap remains robust despite the graphene being covered with a top BN layer. The precise origin of the gap in h-BN/graphene heterostructures remains uncertain (28), and further experimental and theoretical studies will be required to resolve the differences in the gap magnitude and correlation with twist angle that have been reported so far.

Figure 1B shows the longitudinal resistance and transverse Hall conductivity for the same device as in Fig. 1A. The low disorder in our samples allows smaller energy gap states to be resolved than previously possible, resulting in a rich complexity of observable transport features. A sequence of repeated minifans, resembling a repeated butterfly in the Hall conductivity map, shows evidence of the fractal nesting expected from the Hofstadter spectrum. In Fig. 1C, a simplified Wannier diagram

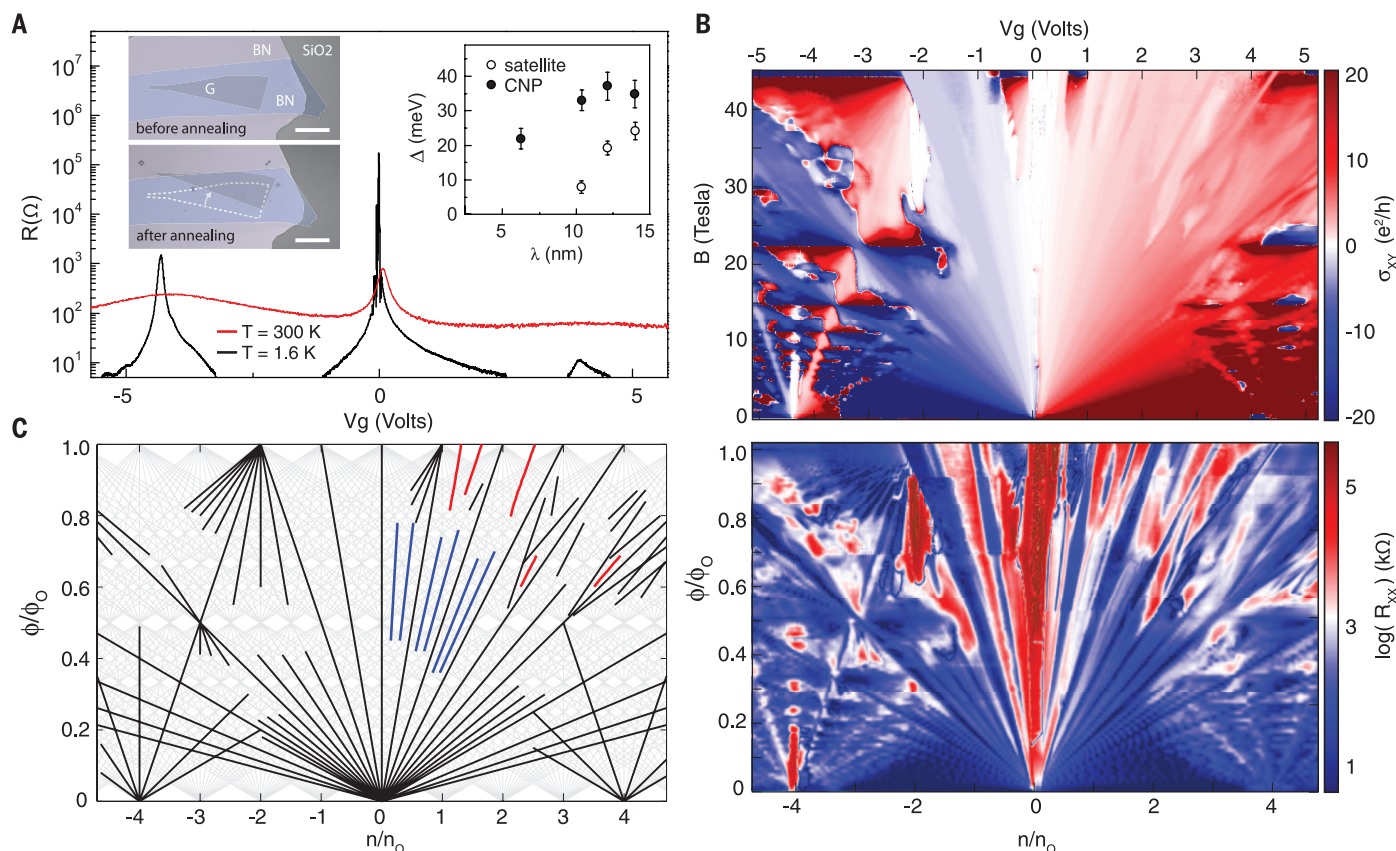


Fig. 1. Transport measurements in a BN-encapsulated graphene device with a ~ 10 -nm moiré superlattice. (A) Zero-field resistance versus gate bias. Left inset: False-colored optical image showing macroscopic motion of the graphene (G) after heating; scale bar, 15 μm . Right inset: Gap measured by thermal activation at the CNP and hole satellite peak positions, across four different devices (20). (Note that the satellite peak does not exhibit activated behavior, within the resolution of our measurement, for superlattice wavelengths less than ~ 10 nm.) Both gaps are observed to vary continuously with rotation angle. Error bars indicate the uncertainty in the gap deduced from a linear fit to the activated temperature response (20). (B) Hall conductivity plotted versus magnetic field and gate bias (top) and longitudinal resistance

versus normalized field and density (bottom) for the same device as in (A). (C) Simplified Wannier diagram labeling the QHE states identified in (B). Light gray lines indicate all possible gap trajectories according to the Diophantine equation, where we have assumed that both spin and valley degeneracy may be lifted such that s and t are allowed to take any integer value (for clarity, the range is restricted to $|s|, |t| = 0 \dots 10$). Families of states are identified by color as follows: Black lines indicate fractal IQHE states within the conventional Hofstadter spectrum, including complete lifting of spin and valley degrees of freedom. Blue lines indicate conventional FQHE states. Red lines indicate anomalous QHE states that do not fit either of these descriptions, exhibiting integer Hall quantization but corresponding to a fractional Bloch index (see text).

is shown in which the positions of the most prominent QHE states are plotted against normalized flux and normalized density axes. We focus our discussion on the FQHE and anomalous states.

FQHE states are characterized by a longitudinal resistance minimum occurring at a fractional Landau filling index, with the corresponding Hall

conductivity plateau quantized to the same fractional value, and with the gap trajectory in the Wannier diagram projecting to $n/n_0 = 0$. The FQHE states are observed at $m/3$ filling fractions in the lowest and first excited Landau level, where m is an integer. The observation of a well-developed $5/3$ state is consistent with previous

studies of monolayer graphene in which a zero-field band gap was reported (24, 26) and is presumably due to the lifting of the valley degeneracy that results from coupling to the moiré pattern (11). In the second Landau level, fractional states beyond $8/3$ are absent, apparently obscured by the appearance of the minigap states (Fig. 1B).

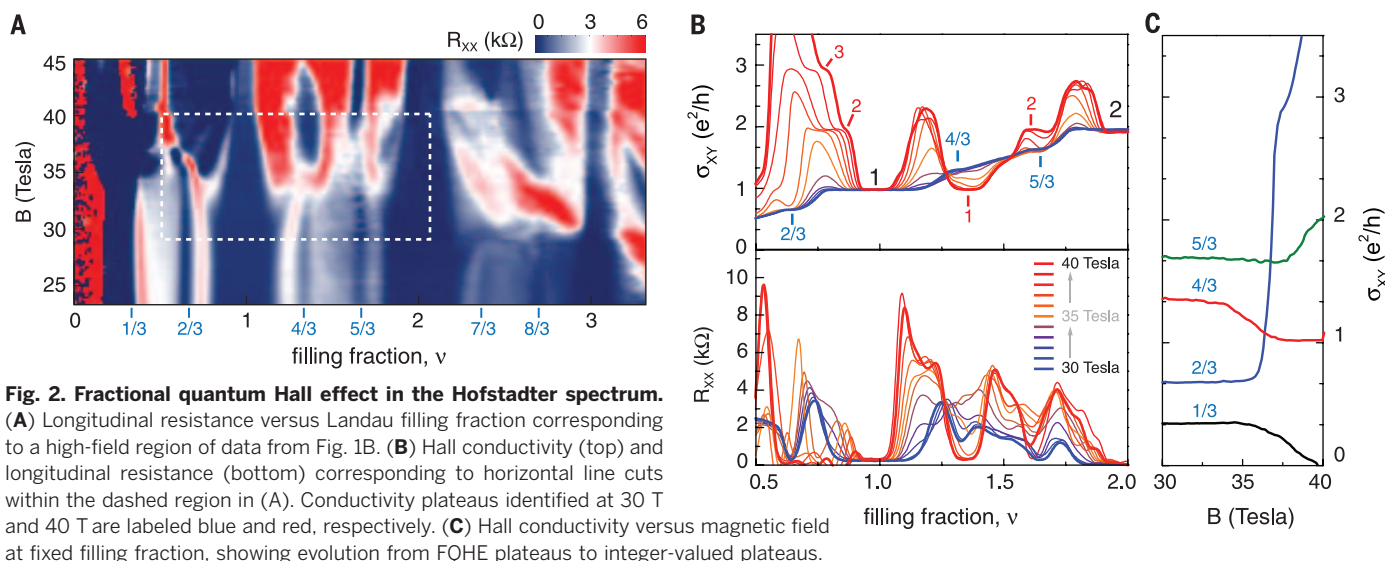
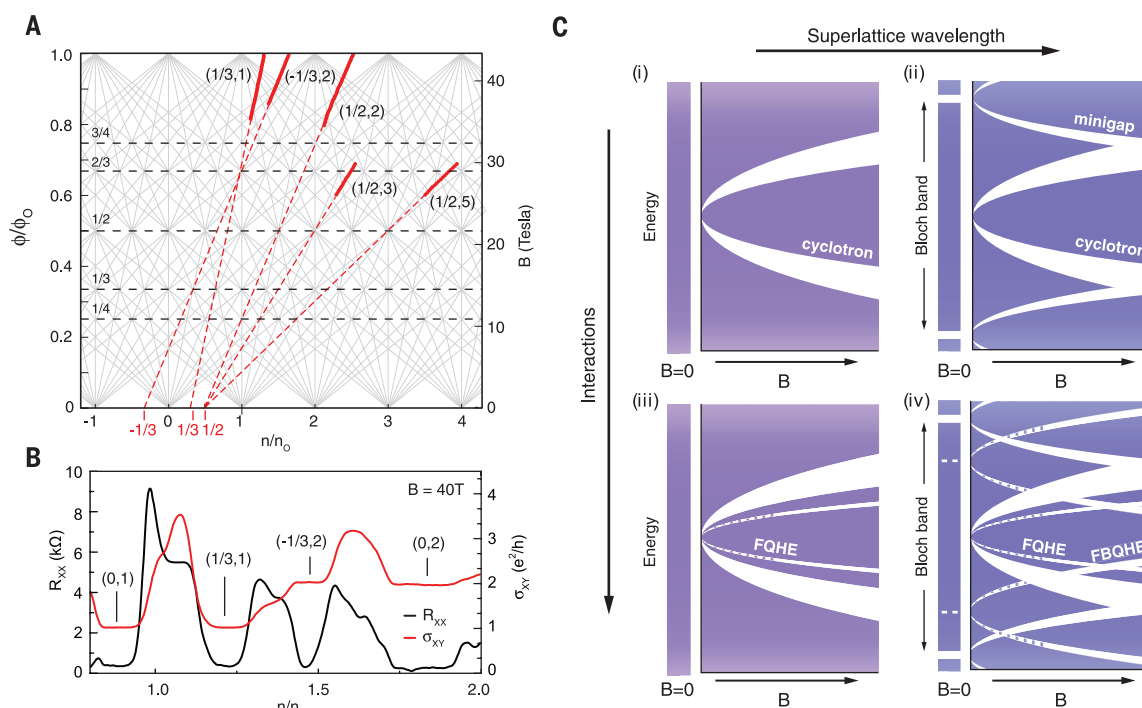


Fig. 3. The FBQHE states.

(A) Wannier diagram showing only the anomalous features from Fig. 1. Brackets label the corresponding Bloch band (s) and Landau band (t) numbers; dashed lines show linear projections to the n/n_0 axis. (B) Hall conductivity and longitudinal resistance versus normalized density, measured at fixed magnetic field $B = 40$ T, showing transport signatures of selected gap states from (A). The s and t numbers, determined respectively from the n/n_0 intercept and the Hall quantization value, are labeled for each QHE plateau. (C) Summary illustration of the energy band structure evolution with magnetic field in the case of no superlattice (left) and with a superlattice (right), and in the limit of no interactions (top) and strong interactions (bottom):



levels at large magnetic field. (iii) With no superlattice present, interactions give rise to the fractional quantum Hall effect, appearing also as subgaps within the Landau level but projecting to zero energy. (iv) In the regime of both strong interactions and large-wavelength superlattice, we observe a set of gaps that do not correspond to either the IQHE of single-particle gaps or the conventional many-body FQHE gaps. These are defined by integer-valued Hall quantization, but they project to fractional Bloch band-filling indices.

As can be seen in Fig. 1C, the visible FQHE states span only a finite range of the perpendicular magnetic field. This is shown in more detail in Fig. 2A, where a selected region of the longitudinal resistance from Fig. 1B is replotted against magnetic field on the vertical axis and Landau filling fraction along the horizontal axis. Select line traces from this diagram, corresponding to varying filling fraction at constant magnetic field, are shown in Fig. 2B. For clarity, we plot the Hall conductivity calculated from the measured longitudinal and Hall resistances (20). In the following, we focus on the $\frac{4}{3}$ state as a representative example of the general behavior.

At $B = 30$ T, the Hall conductivity at filling fraction $\frac{4}{3}$ is well quantized to $\sigma_{XY} = \frac{4}{3}(e^2/h)$. Upon increasing to $B = 34$ T, this FQHE state has completely disappeared; by $B = 40$ T, a Hall plateau has reemerged, but it is quantized to the integer-valued $\sigma_{XY} = 1(e^2/h)$ and with the plateau no longer precisely coincident with $\frac{4}{3}$ filling (Fig. 2B). We interpret the apparent phase transition to be the result of a competition with a fractal minigap state. This is supported by examining the relative strength of the QHE features on either side of the transition as a qualitative measure of relative gap size; the high-field integer-valued state exhibits a substantially better-developed longitudinal resistance minimum and wider Hall plateau (indicative of a larger gap) than the lower-field FQHE state. Taken together, these observations provide experimental evidence supporting two theoretical predictions (13–15): (i) The fractal Hofstadter spectrum can support Laughlin-like FQHE states even at field strengths approaching the commensurability condition, and (ii) at filling fractions in which a conventional FQHE and a Hofstadter minigap state coexist, the state with the larger associated band gap is the one that is observed.

We next discuss the anomalous QHE features associated with the red lines in Fig. 1C. In Fig. 3A, a reduced Wannier plot is shown in which only these anomalous features are replotted (solid red lines), together with a dashed line showing the projection to the n/n_0 axis. Linear fits to the R_{XX} minimum position versus magnetic field (20) indicate that these states follow a trajectory with an integer-valued slope, t , but project to non-integer-valued intercepts, s . Figure 3B demonstrates that these features correspond to QHE features with well-quantized Hall plateaus, and further that the quantization value corresponds to the t value, as expected from the Diophantine equation. Determining the fractional s number from the n/n_0 intercept of the Wannier plot is imprecise because this depends on calculating the density. Nonetheless, within experimental uncertainty (fig. S8), the fractional intercepts appear to cluster around values of $\frac{1}{3}$ and $\frac{1}{2}$ (Fig. 3A). We observe similar features in a second device (20) fabricated in the same way but with zero orientation angle between the graphene and BN lattices (moiré wavelength ~ 14 nm). Again, several anomalous features are present, characterized by integer Hall quantization and slope in the Wannier diagram but exhibiting fractional intercept (s

number). In the second device, which exhibits in general a more symmetric electron and hole response, these features appear on both the electron and hole side, and with both positive and negative Hall quantization. We note, however, that the fractional s numbers remain limited to multiples of $|\frac{1}{3}|$ and $|\frac{1}{2}|$ in both samples.

Figure 3C shows a cartoon summary of this result. In the regime of very large magnetic field, in addition to the conventional fractional quantum Hall effect, we observe a new series of states outside of the single-particle band structure as described by the Diophantine equation, and coinciding with a fractional Bloch band index. This so-called fractional Bloch band QHE (FBQHE), described by integer t numbers but fractional s numbers, may have several possible origins. We note that at $B = 30$ T, the Coulomb energy is ~ 80 meV ($E_{\text{Coulomb}} = e^2/\epsilon l_B$, where we assume the dielectric constant ϵ to be 4). This is similar in magnitude to the superlattice potential (29), which suggests that interactions play a comparable role. Recent theoretical consideration of graphene superlattices indeed showed (15) that electron interactions may open a gap consistent with a fractional s number. However, the nature of the associated ground state was not identified. Previously, it was predicted that electron interactions may drive a charge density wave (CDW)-type modulation of the electron density, commensurate to the superlattice but with a larger period (30). A superstructure with 3 times the moiré unit cell area (such as a $\sqrt{3} \times \sqrt{3}$ Kekulé distortion) could explain n/n_0 intercepts of $\frac{1}{3}$, whereas a doubling of the superlattice cell could explain $\frac{1}{2}$ intercepts. In this regard, our observation may resemble the reentrant QHE seen in high-mobility GaAs (31), also believed to result from a CDW phase. Alternatively, one interpretation of the Wannier diagram is to consider the minigaps as a sequence of mini-Landau fans, residing in a local reduced magnetic field $B' = B - B_0/\phi_0 = 1/m$, where $\phi_0 = 1/m$ (or equivalently $1 - 1/m$ by symmetry) labels regions of high density of minigap crossing. Recent band structure calculation of moiré-patterned graphene (11) indicates that the minifans are not exact replicas, but instead can exhibit a local degeneracy with additional Dirac points emerging near $\phi_0/\phi_0 = 1/m$. The FBQHE states may therefore result from an interaction-driven breaking of this degeneracy, similar to quantum Hall ferromagnetism.

Finally, we consider that within the minifan picture, the FBQHE states resemble the FQHE effect in that they follow trajectories that evolve along fractional filling of the minifan LLs, projecting to the $B' = 0$ center of the minifan (20). However, both the slope and the corresponding Hall conductivity plateaus are integer-valued. A complete understanding of our findings will require a theory that accounts for both the observed fractional Bloch band numbers and the associated Hall conductivity value. Experimentally, possible ground states could be distinguished by a local probe of the density of states, because (for example) a CDW phase exhibits

broken translation symmetry, unlike the Laughlin FQHE state.

REFERENCES AND NOTES

1. D. Thouless, M. Kohmoto, M. Nightingale, M. den Nijs, *Phys. Rev. Lett.* **49**, 405–408 (1982).
2. D. Hofstadter, *Phys. Rev. B* **14**, 2239–2249 (1976).
3. G. H. Wannier, *Phys. Status Solidi. B* **88**, 757–765 (1978).
4. A. MacDonald, *Phys. Rev. B* **28**, 6713–6717 (1983).
5. P. Streda, *J. Phys. C* **15**, L1299–L1303 (1982).
6. D. Tsui, H. Stormer, A. Gossard, *Phys. Rev. Lett.* **48**, 1559–1562 (1982).
7. R. Laughlin, *Phys. Rev. Lett.* **50**, 1395–1398 (1983).
8. C. R. Dean *et al.*, *Nat. Phys.* **7**, 693–696 (2011).
9. V. Gudmundsson, R. R. Gerhardt, *Phys. Rev. B* **52**, 16744–16752 (1995).
10. H. Doh, S.-H. Salk, *Phys. Rev. B* **57**, 1312–1315 (1998).
11. X. Chen *et al.*, *Phys. Rev. B* **89**, 075401 (2014).
12. V. M. Apalkov, T. Chakraborty, *Phys. Rev. Lett.* **112**, 176401 (2014).
13. A. Kol, N. Read, *Phys. Rev. B* **48**, 8890–8898 (1993).
14. D. Pfannkuche, A. H. MacDonald, *Phys. Rev. B* **56**, R7100–R7103 (1997).
15. A. Ghazaryan, T. Chakraborty, P. Pietiläinen, *J. Phys. Condens. Matter* **27**, 185301 (2015).
16. T. Schlösser, K. Ensslin, J. P. Kotthaus, M. Holland, *Semicond. Sci. Technol.* **11** (11S), 1582–1585 (1996).
17. C. Albrecht *et al.*, *Phys. Rev. Lett.* **86**, 147–150 (2001).
18. S. Melinte *et al.*, *Phys. Rev. Lett.* **92**, 036802 (2004).
19. L. Wang *et al.*, *Science* **342**, 614–617 (2013).
20. See supplementary materials on Science Online.
21. M. Yankowitz *et al.*, *Nat. Phys.* **8**, 382–386 (2012).
22. C. R. Dean *et al.*, *Nature* **497**, 598–602 (2013).
23. L. A. Ponomarenko *et al.*, *Nature* **497**, 594–597 (2013).
24. B. Hunt *et al.*, *Science* **340**, 1427–1430 (2013).
25. C. R. Woods *et al.*, *Nat. Phys.* **10**, 451–456 (2014).
26. F. Amet *et al.*, *Nat. Commun.* **6**, 5838 (2015).
27. Z.-G. Chen *et al.*, *Nat. Commun.* **5**, 4461 (2014).
28. J. Jung, A. M. DaSilva, A. H. MacDonald, S. Adam, *Nat. Commun.* **6**, 6308 (2015).
29. P. Moon, M. Koshino, *Phys. Rev. B* **90**, 155406 (2014).
30. A. H. MacDonald, D. B. Murray, *Phys. Rev. B* **32**, 2291–2295 (1985).
31. J. P. Eisenstein, K. B. Cooper, L. N. Pfeiffer, K. W. West, *Phys. Rev. Lett.* **88**, 076801 (2002).

ACKNOWLEDGMENTS

We thank A. MacDonald, T. Chakraborty, I. Aleiner, V. Falko, A. F. Young, and B. Hunt for helpful discussions. Supported by Office of Naval Research grant N000141310662 (L.W., Y.G., and J.H.), NSF grant DMR-1463465 (C.R.D.), and JSPS grant-in-aid for scientific research 25107005 (M.K.). A portion of this work was performed at the National High Magnetic Field Laboratory, which is supported by National Science Foundation Cooperative Agreement No. DMR-0654118, the State of Florida and the U.S. Department of Energy.

SUPPLEMENTARY MATERIALS

www.sciencemag.org/content/350/6265/1231/suppl/DC1
Materials and Methods
Supplementary Text
Figs. S1 to S13
References (32–34)

8 August 2015; accepted 2 November 2015
10.1126/science.aad2102

CATALYSIS

A supramolecular microenvironment strategy for transition metal catalysis

David M. Kaphan,^{1,2*} Mark D. Levin,^{2*} Robert G. Bergman,^{1,2,†} Kenneth N. Raymond,^{1,2,†} F. Dean Toste^{1,2,†}

A self-assembled supramolecular complex is reported to catalyze alkyl-alkyl reductive elimination from high-valent transition metal complexes [such as gold(III) and platinum(IV)], the central bond-forming elementary step in many catalytic processes. The catalytic microenvironment of the supramolecular assembly acts as a functional enzyme mimic, applying the concepts of enzymatic catalysis to a reactivity manifold not represented in biology. Kinetic experiments delineate a Michaelis-Menten-type mechanism, with measured rate accelerations ($k_{\text{cat}}/k_{\text{uncat}}$) up to 1.9×10^7 (here k_{cat} and k_{uncat} are the Michaelis-Menten enzymatic rate constant and observed uncatalyzed rate constant, respectively). This modality has further been incorporated into a dual catalytic cross-coupling reaction, which requires both the supramolecular microenvironment catalyst and the transition metal catalyst operating in concert to achieve efficient turnover.

Supramolecular catalysis was born from biological inspiration. By emulating the transition state binding of enzymatic active sites (1), chemists have developed synthetic non-covalent microenvironment catalysts that are capable of reproducing a range of enzymatic reaction motifs, from proton-catalyzed hydrolases

to constrictive terpene cyclases (2–9). However, due to the circumstances of evolutionary history, nature has selected for enzymes that mediate a narrow subset of chemistries employing Earth-abundant elements. Although the exploration of biomimetic chemistries has dominated supramolecular catalysis thus far, no such limitations

are inherent to fully synthetic systems, and as such, microenvironment catalysis is poised for expansion to abiotic mechanistic manifolds.

In many ways, the development of organic chemistry was born out of the same biological impetus, and many triumphs of the field are recaptulations of superior enzymatic systems (consider the excellent stereoselectivity of aldolases or the site selectivity in C-H functionalization by oxidases). In contrast, organotransition metal catalysis was developed in the absence of a preceding biological analog. The proliferation of such methods has relied on the judicious examination of catalyst structure-activity relationships, traditionally exploiting ligand architecture to provide a series of specialized catalyst systems for individual transformations and substrate classes (10). As an alternative strategy, we envisioned a marriage of transition metal and microenvironment catalysts for the expansion of the canon of accessible reactivity. This wedding of biomimetic and anthropogenic chemistries opens the door for a paradigmatic shift in strategic approaches to catalysis.

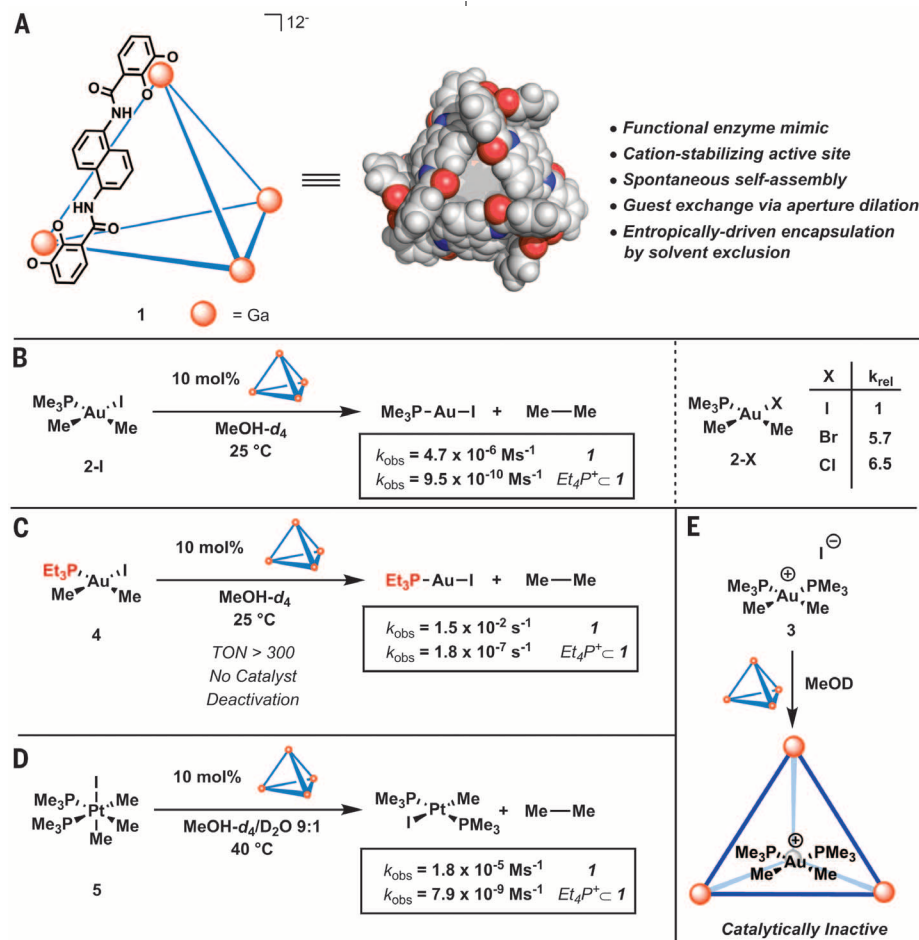


Fig. 1. Supramolecular catalysis of reactivity at a transition metal center. (A) Structure of the Ga₄L₆ catalyst. (B) Catalyzed reductive elimination from gold and halide series. Me, methyl; k_{obs} , observed rate; k_{rel} , relative rate. (C) Improved catalysis with a triethylphosphine analog. TON, turnover number. (D) Catalyzed reductive elimination from platinum. (E) Identification of a catalyst-deactivation pathway.

¹Chemical Sciences Division, Lawrence Berkeley National Laboratory, Berkeley, CA 94720, USA. ²Department of Chemistry, University of California, Berkeley, Berkeley, CA 94720, USA.

*These authors contributed equally to this work. †Corresponding author. E-mail: rbergman@berkeley.edu (R.G.B.); raymond@socrates.berkeley.edu (K.N.R.); fdtoste@berkeley.edu (F.D.T.)

Successful realization of catalytic cycles requires the careful orchestration of elementary steps: Should any step prove particularly slow, the overall rate will become retarded, and in extreme cases, reactivity can be precluded altogether. Although certain stoichiometric additives have been shown to accelerate elementary organometallic reactions (11–15), the catalysis of such reactions is less common (16–18). Rather than altering catalyst structure in a way that influences each elementary step, a synthetic microenvironment catalyst could be leveraged to specifically target one step without sacrificing reactivity elsewhere along the catalytic cycle, enabling an otherwise inaccessible catalytic process. One catalytically relevant yet particularly sluggish transformation is reductive elimination of sp^3 fragments from transition metals (10). As a result, alkyl-alkyl cross-coupling processes are often plagued by slow turnover and undesired side reactions (19).

In light of the known trends for reductive elimination, we envisioned that the tendency of $Ga_4L_6^{12-}$ (**1**) supramolecular assembly (Fig. 1A) [$L = N,N'$ -bis(2,3-dihydroxybenzoyl)-1,5-diaminonaphthalene] to encapsulate low-coordinate cationic transition

metal complexes was promising as a means to selectively recognize and stabilize the relevant transition state for C-C bond formation (20, 21). The highly anionic, tetrahedral metal-ligand cluster **1** assembles spontaneously in solution and has been shown to catalyze a range of reactions involving neutral and cationic substrates via encapsulation within its hydrophobic interior cavity (22). Thus, we hypothesized that **1** would be competent to act as a microenvironment catalyst for reductive elimination from an appropriate high-valent dialkyl metal complex. Initial realization of this reactivity in a stoichiometric sense would potentially inform the development of a dual catalytic process, wherein a microenvironment catalyst and a transition metal catalyst act in concert to achieve a challenging alkyl-alkyl cross-coupling.

To that end, we evaluated **1** as a catalyst for the elimination of ethane from the dialkyl Au(III) iodide complex **2-I** (23, 24). The observed half-life for reductive elimination under a 10 mol% loading of **1** decreased from 20 weeks to just 53 min, corresponding to a 4000-fold acceleration in the observed initial rate (Fig. 1B). Substitution of the compact trimethylphosphine ligand by its

more sterically demanding triphenyl congener resulted in no observable acceleration for the reductive elimination in the presence of **1**, which is indicative of size exclusion from the internal cavity of the catalyst. Likewise, blocking the interior cavity with the strongly encapsulated Et_4P^+ (Et, ethyl) cation eliminated the accelerating effect of **1**. Compared to observations for reactions with **2-I**, the corresponding chloride and bromide complexes **2-Br** and **2-Cl** showed similar behavior under cluster-catalyzed conditions, with relative rates of 5.7 and 6.5, respectively.

From the kinetic profile of the reductive elimination from **2-I** (fig. S1), it became clear that a catalyst-deactivation pathway was operative at extended reaction times. Although no product inhibition was observed, examination of the reaction mixture by 1H nuclear magnetic resonance (NMR) spectroscopy revealed a strongly encapsulated species, which was identified as the cationic bis(phosphine) complex **3** (25). Its identity was verified by independent synthesis, and **3-Cl** was shown to be incompetent as a catalyst for the elimination of ethane from **2-I** (Fig. 1E). To disfavor this deleterious pathway, we hypothesized that a

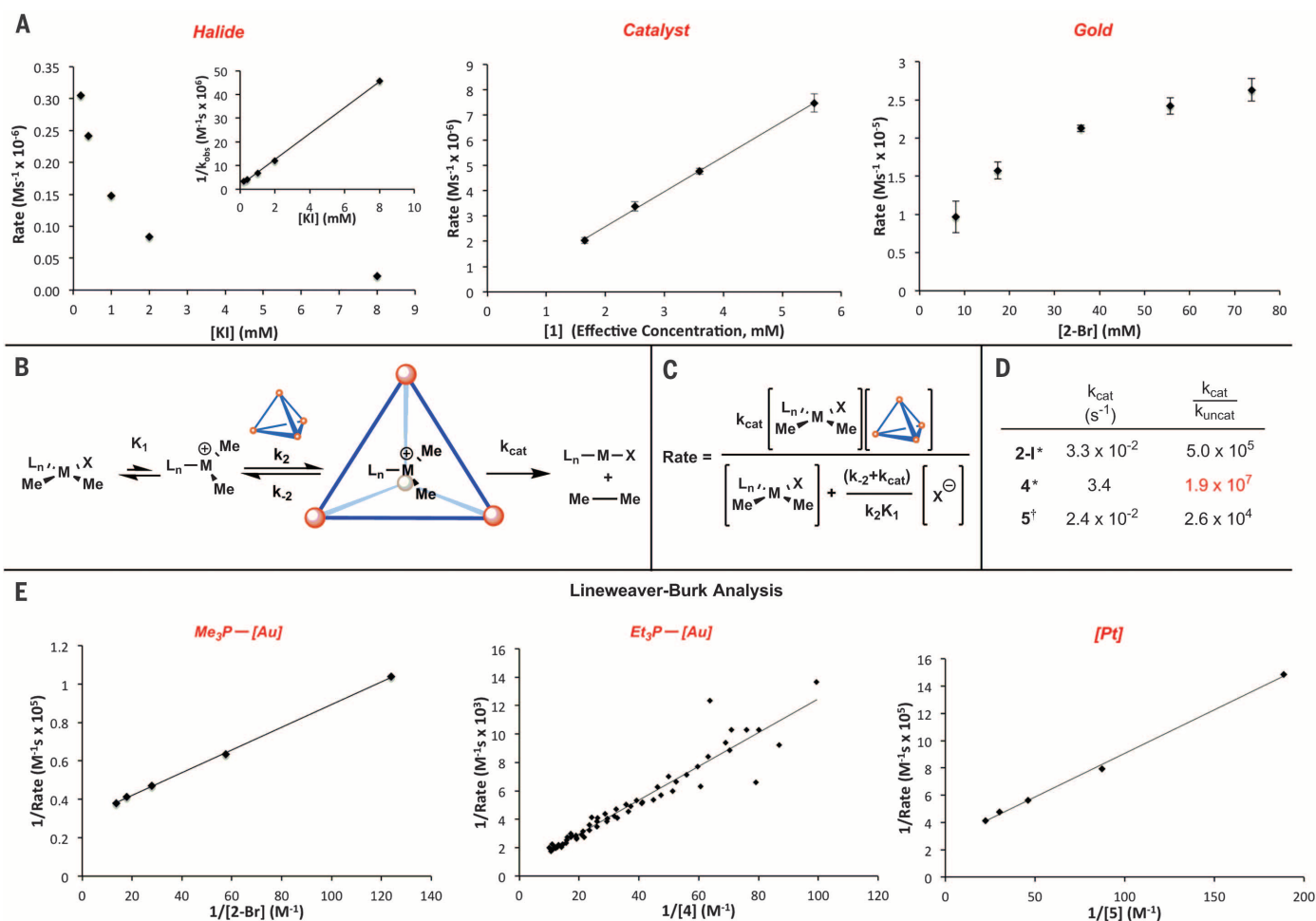


Fig. 2. Kinetic experiments and implications. (A) Determination of the order in each reactant in the rate law. (B) Proposed mechanism for catalysis by **1**. M, metal; X, halide. (C) Experimentally determined rate law. (D) Measured values for k_{cat} and overall acceleration. Asterisks denote 298 K in MeOH- d_4 ; the dagger symbol indicates 313 K in 9:1 MeOH- d_4 /D $_2$ O. (E) Lineweaver-Burk analysis. All error bars represent 1 SD, based on three replicates.

phosphine of intermediate steric demand would preclude the formation of the analogous bis (phosphine) cation while remaining sufficiently compact to allow encapsulation by **1**. In accordance with this hypothesis, triethylphosphine-ligated complex **4** exhibited rapid and complete reductive elimination in the presence of **1** (Fig. 1C). No catalyst deactivation was observed, and a turnover number in excess of 300 could be achieved. The catalyzed reaction of **4** exhibits a half-life of just 47 s compared with 45 days in the uncatalyzed reaction, corresponding to more than an 80,000-fold increase in the observed rate.

We then endeavored to evaluate whether this catalytic methodology could be generalized to reductive elimination from other dialkyl transition metal complexes bearing a labile X-type ligand. To that end, platinum complex **5** was prepared and subjected to catalysis by **1** (26). The observed half-life for reductive elimination of ethane decreased from 9 days in the absence of **1** to just 6 min in its presence, corresponding to a 2300-fold acceleration of the observed rate (Fig. 1D).

For a better understanding of the catalyzed reductive elimination process, we conducted kinetic experiments to determine the order in each reactant, using the method of initial rates. For the

reductive elimination of ethane from complex **2-I**, the reaction displayed first-order dependence on catalyst **1**, as measured by competitive inhibition with Et_4P^+ (a linear relation was observed between the rate of reductive elimination and the concentration of the unblocked cluster). Conversely, the rate of reductive elimination was found to be dramatically attenuated in the presence of exogenous iodide (Fig. 2A). The dependence on gold concentration showed saturation behavior, which could be linearized by plotting the double reciprocal of concentration and rate (27). These results are consistent with an overall Michaelis-Menten-type mechanism involving pre-equilibrium halide dissociation followed by a transient and reversible encapsulation of the nascent cationic species and, finally, an irreversible reductive elimination event within the cluster cavity (Fig. 2B).

Accordingly, from the aforementioned double reciprocal (i.e., Lineweaver-Burk) plot, the Michaelis-Menten parameter k_{cat} (Michaelis-Menten enzymatic rate constant) could be assessed (Fig. 2E). The measured k_{cat} for complex **2-I** was found to be $3.3 \times 10^{-2} \text{ s}^{-1}$, corresponding to an overall acceleration ($k_{\text{cat}}/k_{\text{uncat}}$) of 5.0×10^5 (where k_{uncat} is the rate constant for the uncatalyzed reaction). Gold complex **4** and pla-

tinum complex **5** showed analogous kinetic profiles consistent with a Michaelis-Menten mechanism (figs. S10 to S12 and S18 to S20). The corresponding Lineweaver-Burk plot for **5** provided a k_{cat} of $2.3 \times 10^{-2} \text{ s}^{-1}$, corresponding to a similar acceleration of 2.6×10^4 (Fig. 2D).

For complex **4**, however, the rapidity of the reaction introduced substantial error into the estimation of k_{cat} by the method of initial rates. Thus, we instead applied reaction progress kinetic analysis to generate a larger data set, affording an estimate for k_{cat} of 3.4 s^{-1} , corresponding to a $k_{\text{cat}}/k_{\text{uncat}}$ of 1.9×10^7 (28). The data obtained in this way are consistent with the initial rate data (fig. S12) while providing a more robust measurement due to the expanded data set. This rate acceleration is on par with that of many enzymatic processes; for comparison, chymotrypsin has been shown to accelerate amide bond hydrolysis with 10^7 -fold rate accelerations (29).

The extension of this phenomenon to a dual catalytic cross-coupling would represent a proof of principle for our initial hypothesis that a synthetic self-assembled supramolecular cocatalyst could be employed to overcome kinetically prohibitive barriers in otherwise desirable cross-coupling reactions (30). On the basis of the stoichiometric reactivity (see above), we envisioned a cocatalytic cross-coupling of a methyl electrophile with a complementary nucleophilic alkyl metal species. This goal presented several challenges: The supramolecular assembly **1** was found to decompose in the presence of methyl iodide, requiring the implementation of the previously reported analog **6**, which bears catechol ligands with diminished electron density (Fig. 3A) (31). Identification of a nucleophile capable of transmetalating to Pt^{II} while remaining tolerant of both a protic solvent and the supramolecular catalyst eliminated several typical candidates (32), but stannanes were found to be suitable partners under these criteria. Subsequently, we discovered that the Me_3SnI by-product formed upon transmetalation from tetramethyltin was a strong guest for **6**, requiring the use of fluoride to generate Me_3SnF and prevent catalyst inhibition. Under these conditions, we found that efficient C-C coupling occurred only in the presence of both the platinum and supramolecular catalysts (Fig. 3B). The presence of a radical trap (9,10-dihydroanthracene) did not inhibit the reaction, and an isotopic labeling study employing deuterated iodomethane indicated the incorporation of both coupling partners. An overall mechanism for this process is proposed in which the demonstrated microenvironment catalysis of reductive elimination from complex **5** is incorporated into a traditional organometallic catalytic cycle (Fig. 3C), enabling an otherwise prohibitively slow process. This strategy should prove general; a tailored synthetic microenvironment catalyst could be designed to recognize the rate-limiting transition state for other high-value catalytic processes.

REFERENCES AND NOTES

1. L. Pauling, *Nature* **161**, 707–709 (1948).
2. M. D. Pluth, R. G. Bergman, K. N. Raymond, *Science* **316**, 85–88 (2007).

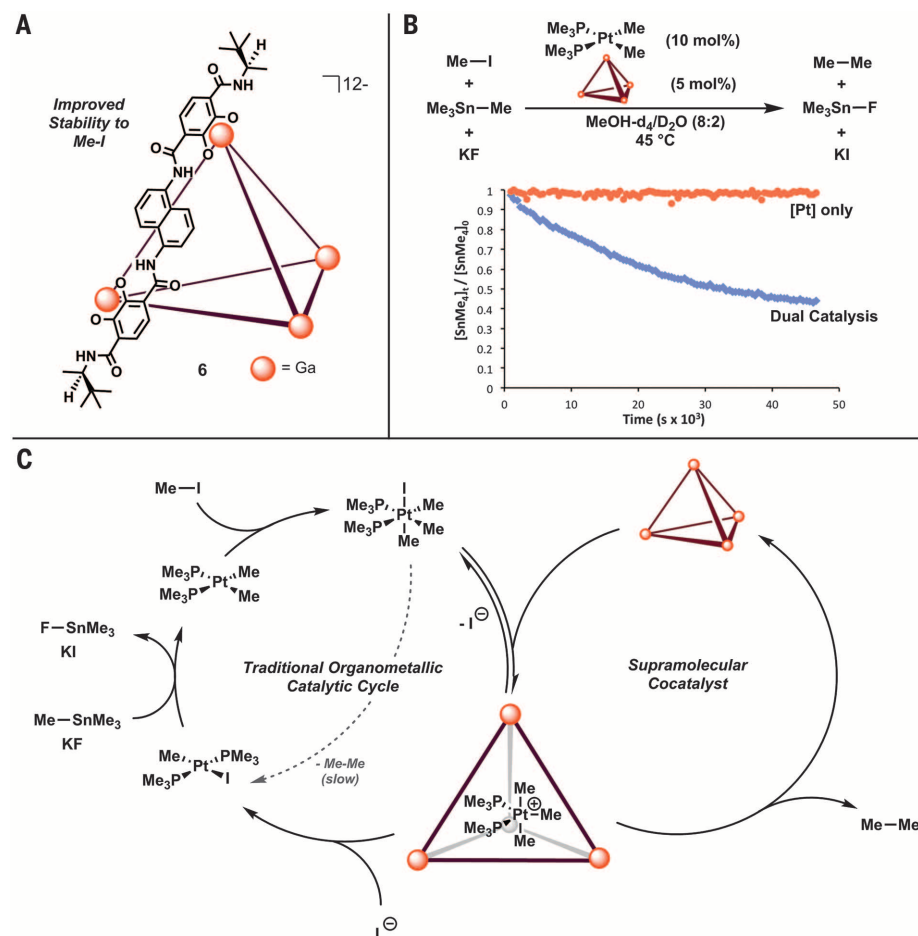


Fig. 3. Demonstration of dual catalysis. (A) Modified supramolecular assembly with improved stability to electrophiles. (B) Dual catalytic alkyl-alkyl cross-coupling enabled via supramolecular catalysis. (C) Proposed mechanism.

3. M. Yoshizawa, M. Tamura, M. Fujita, *Science* **312**, 251–254 (2006).
4. J. Kang, J. Rebek Jr., *Nature* **385**, 50–52 (1997).
5. Q. Zhang, K. Tiefenbacher, *Nat. Chem.* **7**, 197–202 (2015).
6. W. M. Hart-Cooper, K. N. Clary, F. D. Toste, R. G. Bergman, K. N. Raymond, *J. Am. Chem. Soc.* **134**, 17873–17876 (2012).
7. C. J. Hastings, M. D. Pluth, R. G. Bergman, K. N. Raymond, *J. Am. Chem. Soc.* **132**, 6938–6940 (2010).
8. M. L. Merlau, M. del Pilar Mejia, S. T. Nguyen, J. T. Hupp, *Angew. Chem. Int. Ed.* **40**, 4239–4242 (2001).
9. J. Meeuwissen, J. N. H. Reek, *Nat. Chem.* **2**, 615–621 (2010).
10. J. F. Hartwig, in *Organotransition Metal Chemistry: From Bonding to Catalysis* (University Science Books, Mill Valley, CA, 2010), pp. 321–348, 877–883.
11. A. L. Liberman-Martin, R. G. Bergman, T. D. Tilley, *J. Am. Chem. Soc.* **135**, 9612–9615 (2013).
12. A. Hazari, J. A. Labinger, J. E. Bercaw, *Angew. Chem. Int. Ed.* **51**, 8268–8271 (2012).
13. Q. Shen, J. F. Hartwig, *J. Am. Chem. Soc.* **129**, 7734–7735 (2007).
14. T. Yamamoto, A. Yamamoto, S. Ikeda, *J. Am. Chem. Soc.* **93**, 3350–3359 (1971).
15. W. Lau, J. C. Huffman, J. K. Kochi, *Organometallics* **1**, 155–169 (1982).
16. V. Lavallo, R. H. Grubbs, *Science* **326**, 559–562 (2009).
17. S. Takemoto, V. V. Grushin, *J. Am. Chem. Soc.* **135**, 16837–16840 (2013).
18. J. P. Collman, R. G. Finke, J. N. Cawse, J. I. Brauman, *J. Am. Chem. Soc.* **100**, 4766–4772 (1978).
19. R. Jana, T. P. Pathak, M. S. Sigman, *Chem. Rev.* **111**, 1417–1492 (2011).
20. D. Fiedler, R. G. Bergman, K. N. Raymond, *Angew. Chem. Int. Ed.* **45**, 745–748 (2006).
21. Z. J. Wang, C. J. Brown, R. G. Bergman, K. N. Raymond, F. D. Toste, *J. Am. Chem. Soc.* **133**, 7358–7360 (2011).
22. C. J. Brown, F. D. Toste, R. G. Bergman, K. N. Raymond, *Chem. Rev.* **115**, 3012–3035 (2015).
23. S. Komiya, J. K. Kochi, *J. Am. Chem. Soc.* **98**, 7599–7607 (1976).
24. P. Lawrence Kuch, R. Stuart Tobias, *J. Organomet. Chem.* **122**, 429–446 (1976).
25. O. Schuster, H. Schmidbaur, *Z. Naturforsch. B* **61**, 1–5 (2006).
26. K. I. Goldberg, J. Y. Yan, E. L. Winter, *J. Am. Chem. Soc.* **116**, 1573–1574 (1994).
27. **2-Br** was employed rather than **2** because it was expected to show a higher affinity for the interior of **1**, on the basis of previous observations in similar systems (19). The calculated value for k_{cat} is necessarily identical for **2** and **2-Br** because of the mechanistic convergence in the encapsulated intermediate.
28. D. G. Blackmond, *Angew. Chem. Int. Ed.* **44**, 4302–4320 (2005).
29. R. B. Silverman, in *The Organic Chemistry of Enzyme-Catalyzed Reactions* (Academic Press, San Diego, CA, 2002), p. 15.
30. A. E. Allen, D. W. C. Macmillan, *Chem. Sci.* **2012**, 633–658 (2012).
31. C. Zhao *et al.*, *J. Am. Chem. Soc.* **135**, 18802–18805 (2013).
32. C. C. C. Johansson Seechurn, M. O. Kitching, T. J. Colacot, V. Snieckus, *Angew. Chem. Int. Ed.* **51**, 5062–5085 (2012).

ACKNOWLEDGMENTS

This research was supported by the Director, Office of Science, Office of Basic Energy Sciences and the Division of Chemical Sciences, Geosciences, and Biosciences of the U.S. Department of Energy at Lawrence Berkeley National Laboratory (grant DE-AC02-05CH11231) and NIH National Institute of General Medical Sciences (grant R01 GM073932). D.M.K. was supported by an NSF Graduate Research Fellowship Program (GRFP) (grant DGE 1106400), and M.D.L. was supported by the ARCS Foundation and an NSF GRFP. We thank J. N. Brantley and M. S. Winston for helpful discussions and C. G. Canlas for assistance with NMR experiments.

SUPPLEMENTARY MATERIALS

www.sciencemag.org/content/350/6265/1235/suppl/DC1
Materials and Methods
Figs. S1 to S42
References

25 August 2015; accepted 23 October 2015
10.1126/science.aad3087

SOLAR PHYSICS

Particle acceleration by a solar flare termination shock

Bin Chen,^{1*} Timothy S. Bastian,² Chengcai Shen,¹ Dale E. Gary,³
Sām Krucker,^{4,5} Lindsay Glesener^{4,6}

Solar flares—the most powerful explosions in the solar system—are also efficient particle accelerators, capable of energizing a large number of charged particles to relativistic speeds. A termination shock is often invoked in the standard model of solar flares as a possible driver for particle acceleration, yet its existence and role have remained controversial. We present observations of a solar flare termination shock and trace its morphology and dynamics using high-cadence radio imaging spectroscopy. We show that a disruption of the shock coincides with an abrupt reduction of the energetic electron population. The observed properties of the shock are well reproduced by simulations. These results strongly suggest that a termination shock is responsible, at least in part, for accelerating energetic electrons in solar flares.

The acceleration of charged particles to high energies occurs throughout the universe. Understanding the physical mechanisms is a fundamental topic in many space, astrophysical, and laboratory contexts that involve magnetized plasma (1). For solar flares and the often-associated coronal mass ejections (CMEs), it is generally accepted that fast mag-

netic reconnection—the sudden reconfiguration of the magnetic field topology and the associated magnetic energy release—serves as the central engine driving these powerful explosions. However, the mechanism for converting the released magnetic energy into the kinetic energy in accelerated particles has remained uncertain (2, 3). Competing mechanisms include acceleration by the reconnection current sheet, turbulence, and shocks (2–5).

Of possible interest in this regard is the termination shock (TS), produced by super-magnetosonic reconnection outflows impinging upon dense, closed magnetic loops in a cusp-shaped reconnection geometry (6). Although often invoked in the standard picture of solar flares (7, 8) and predicted in numerical simulations (6, 9–11), its presence has yet to be firmly established observationally and, because of the paucity of direct observation-

al evidence, its role as a possible particle accelerator has received limited attention (2, 3). Previous reports of coronal hard x-ray (HXR) sources in some flares have shown convincing evidence of the presence of accelerated electrons at or above the top of flare loops (referred to as the “loop-top” hereafter, or LT) (7, 12), where a TS is presumably located. The often-cited observational evidence for a solar flare TS has been certain radio sources showing spectroscopic features similar to solar type II radio bursts (radio emission associated with propagating shocks in the outer corona), but with small drifts in their emission frequency as a function of time, which implies a standing shock wave (13–17). However, because of the limited spectral imaging capabilities of the previous observations, none of these have shown direct signatures of the TS in terms of its characteristic morphology and dynamics, as well as a clear relation to the reconnection outflows, so that a definitive association with a TS could be demonstrated.

We present observations of a TS in an eruptive solar flare using the Karl G. Jansky Very Large Array (VLA). This eruption occurred close to the east limb of the Sun on 3 March 2012 (Fig. 1A), producing a fast white light CME [~ 1000 km s^{−1}; observed by the Large Angle and Spectrometric Coronagraph Experiment (LASCO)] and a C1.9-class long-duration flare (18). It displayed a cusp-shaped reconnection geometry typical of the standard scenario of eruptive solar flares (7, 8), in which the eruption outward into the upper corona stretches magnetic field lines behind it and induces a vertical current sheet, where magnetic reconnection occurs. The reconnected field lines below the reconnection site are pulled downward by magnetic tension to form an arcade of magnetic loops anchored at the solar surface. The arcade of reconnected loops subsequently fills with hot plasma and becomes bright in extreme ultraviolet (EUV) and soft x-ray (SXR) wavelengths. For this event, the eruption, the current-sheet-like structure, and the

¹Harvard-Smithsonian Center for Astrophysics, 60 Garden Street, Cambridge, MA 02138, USA. ²National Radio Astronomy Observatory, 520 Edgemont Road, Charlottesville, VA 22903, USA. ³New Jersey Institute of Technology, 323 Martin Luther King Boulevard, Newark, NJ 07102, USA. ⁴University of California, Berkeley, 7 Gauss Way, Berkeley, CA 94720, USA. ⁵University of Applied Sciences and Arts Northwestern Switzerland, Bahnhofstrasse 6, 5210 Windisch, Switzerland. ⁶University of Minnesota, Twin Cities, 116 Church Street SE, Minneapolis, MN 55455, USA.
*Corresponding author. E-mail: bin.chen@njit.edu

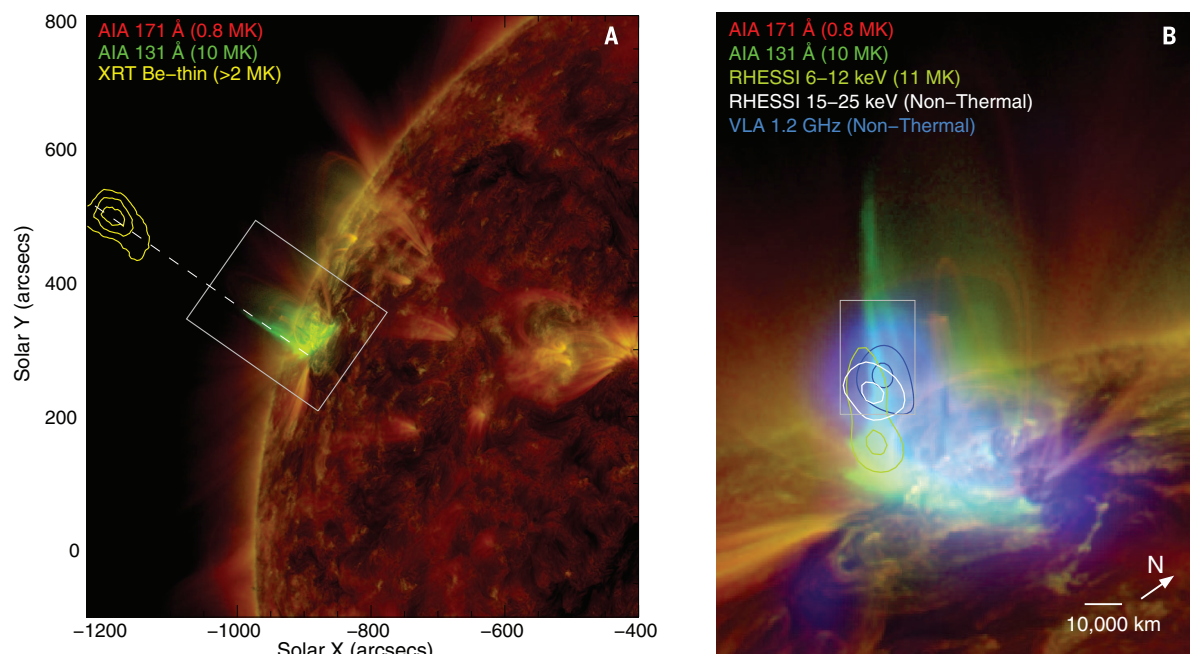


Fig. 1. Solar flare seen in multiple wavelengths. (A) The eruptive flare observed in EUV and x-ray wavelengths by the Atmospheric Imaging Assembly (AIA) 171 Å (red), X-Ray Telescope (XRT; aboard the Hinode satellite) Be-thin (yellow contours, showing the eruption), and AIA 131 Å (green, showing the newly reconnected flare loops) passbands, which are respectively sensitive to plasma temperatures of 0.8, >2, and 10 MK. (B) Closer view of the flaring region [box in (A), rotated clockwise to an upright orientation]. A radio source (blue; at 1.2 GHz) is observed at the top of hot flaring loops (~10 MK), which is nearly cospatial with a nonthermal HXR source (white contours; at 15 to 25 keV) seen by the Reuven Ramaty High Energy Solar Spectroscopic Imager (RHESSI).

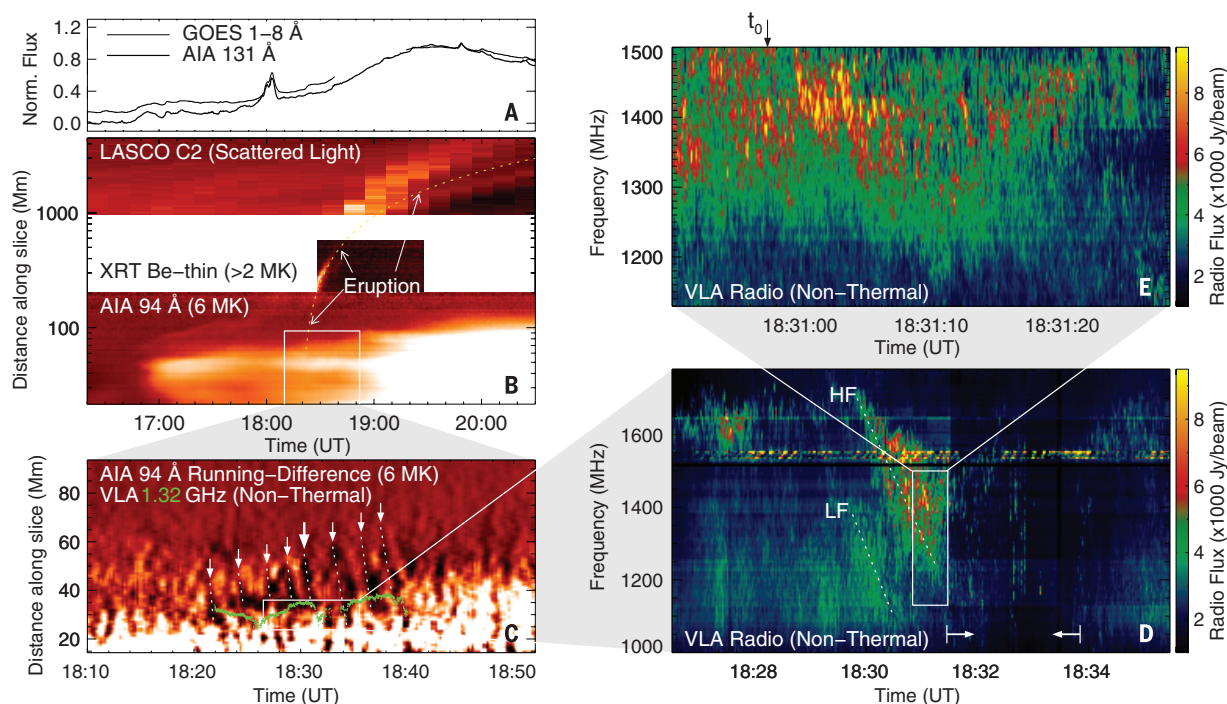


Fig. 2. Radio emission at the front of fast reconnection outflows. (A) EUV and x-ray light curves showing the time history of the radiating hot plasmas (≥ 10 MK) of the flare event. The TS is observed during the flare rise phase. (B) Time-distance plot of the EUV, x-ray, and white light intensities, showing the evolution of the eruption and the underlying flare loops, obtained at the slice in Fig. 1A (dashed line). (C) Running-difference space-time plot of EUV 94 Å zoomed in to the LT region. A series of fast PDs are visible as features with a negative slope (indicated by small white arrows; the PD

associated with the TS disruption in Fig. 3 is marked by a large white arrow). The stochastic spike bursts are located near the endpoint of these PDs (green dots). Its spectrotemporal intensity variation is shown in the spatially resolved, or “vector” dynamic spectrum of (D) and (E), manifesting as many short-lived, narrow-frequency-bandwidth radio bursts. Two dotted lines in (D) mark the split-band feature (HF and LF denote the high- and low-frequency branch, respectively). A pair of arrows brackets a period when the TS experiences a major disruption, starting from 18:31:27 UT (start time t_0).

cusp-shaped magnetic loops are all clearly visible in EUV and SXR passbands that are sensitive to plasma hotter than ~ 2 MK (Fig. 1A). A non-thermal HXR source appears at the LT during the rise phase of the flare, indicating the presence of accelerated electrons at this location (Fig. 1B).

VLA images at 1 to 1.8 GHz show a localized radio source nearly cospatial with the HXR LT source, in addition to two other sources located near the conjugate magnetic footpoints (FPs) of the flaring loops (Fig. 1B and fig. S1). The VLA's simultaneous high spectral and temporal resolution (1 MHz and 50 ms, respectively, enabling high-cadence radio imaging spectroscopy) reveals the highly dynamic and fragmented nature of this LT radio source. It consists of thousands of short-lived (< 50 ms) and narrow-frequency bandwidth (with spectral width $\delta\nu/\nu \approx 2\%$) brightenings (Fig. 2, D and E) (19). These observations strongly imply that many short-lived emission events, which we term stochastic radio spikes, are occurring at the LT, which, as we will demonstrate, are associated with a dynamic TS.

Difference imaging in the EUV 94 Å passband of the Atmospheric Imaging Assembly (AIA)

aboard the Solar Dynamics Observatory (20) reveals that many recurring plasma downflows (PDs) stream rapidly (at ~ 550 km/s in projection) along the current sheet from the reconnection site downward to the flaring, reconnected loops. They end near the same location as the LT radio and HXR sources (Fig. 2C). These fast PDs are thought to be associated with magnetic structures embedded in reconnection outflows, probably in the form of rapidly contracting magnetic loops (22). The relative locations of the PDs and the radio/HXR LT sources agree very well with the scenario in which a TS forms at the ending fronts of fast reconnection outflows and drives particle acceleration.

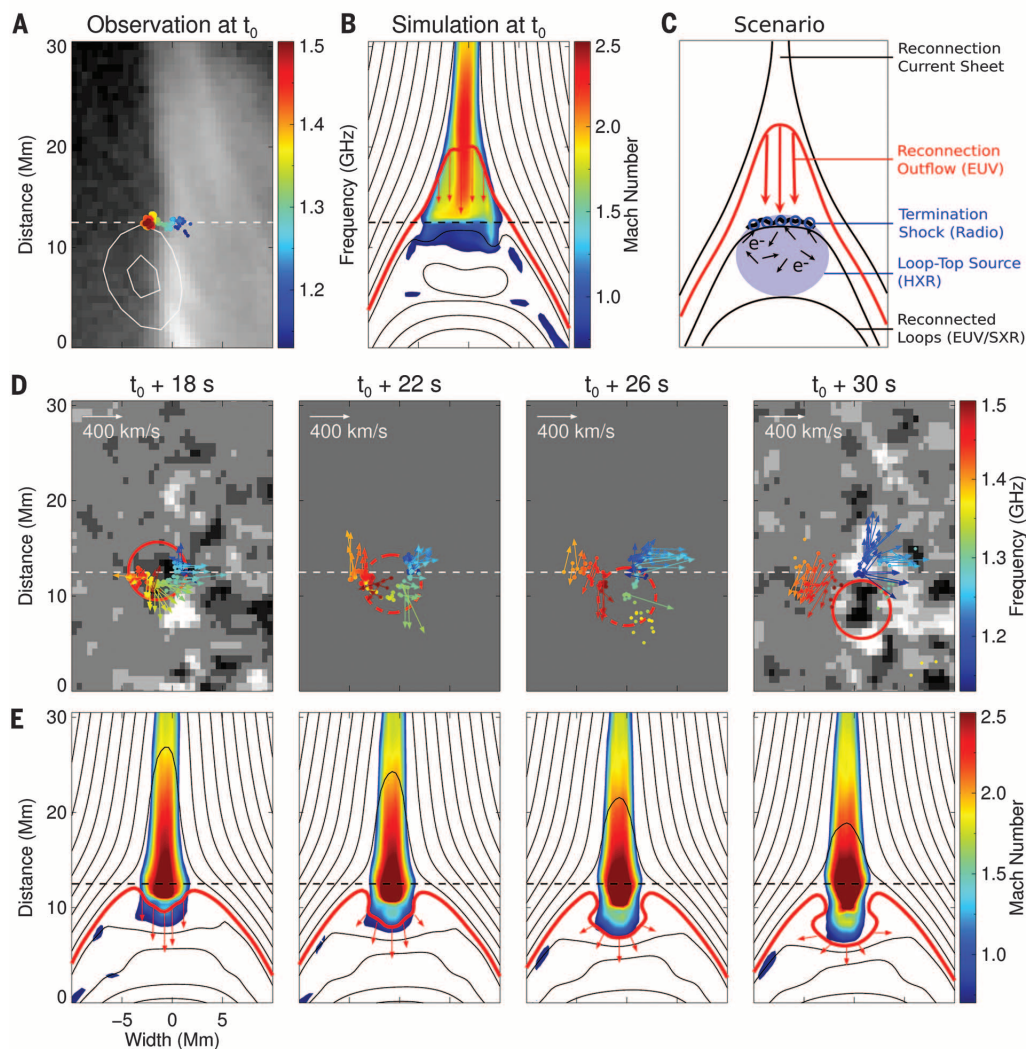
The most direct observational evidence of the TS comes from the instantaneous spatial distribution of the myriad radio spikes at different frequencies, which forms a narrow surface at the LT region (Fig. 3A). The location and morphology of this surface closely resemble those of a TS, as predicted in numerical simulations when viewed edge-on [(6, 9–11); see also Fig. 3B]. The coronal HXR source is located slightly below this surface and evolves coherently with it (Fig. 3A and fig. S4), suggesting that this is nonthermal

emission from accelerated electrons confined in the shock downstream region, possibly due to strong pitch-angle scattering and/or magnetic trapping in the turbulent environment (21). The TS is probably a weak quasi-perpendicular fast-mode shock, based on multiple lines of evidence (19). A Mach number of $M \approx 1.5$ can be inferred based on the interpretation of the split-band feature seen in the radio dynamic spectrum [marked HF (high-frequency) and LF (low-frequency) in Fig. 2D (19)].

The TS front, as outlined by the radio spikes, reacts dynamically to the arrival of the fast PDs. Some PDs cause only partial disruption of the TS front, and the shock is quickly restored to its original state. Some other PDs, however, cause a major disruption of the TS. This process starts with the quasi-flat TS front being first driven concave-downward by a PD, followed by a break-up of the TS (Fig. 3D and fig. S4). To understand the dynamic nature of the TS, we used a magnetohydrodynamics (MHD) model to simulate magnetic reconnection in a standard flare geometry based on physical values constrained by the observations (19). The model shows that reconnection outflows with super-magnetosonic speeds

Fig. 3. Observation and simulation of the dynamic TS. (A) A

closer view of the LT region (white box in Fig. 1B) at 18:30:57 UT (t_0 in Fig. 2E). The TS appears as a dynamic surface delineated by the many unresolved radio sources, each of which corresponds to a radio spike in the dynamic spectrum at a given time and frequency (colored dots indicate their centroid location). White contours show the coronal HXR source at 15 to 25 keV. The grayscale background is the AIA 94 Å intensity. (B) The TS is seen in the MHD simulation as a sharp layer of velocity discontinuity at the LT. The fast-mode magnetosonic Mach number is shown in color, overlaid with magnetic field lines. (C) Physical scenario of emission processes near the TS. Radio spikes are emitted as accelerated electrons impinge on density fluctuations at the shock (blue circles). These electrons also produce a HXR source in the shock downstream region (blue shadowed region). (D and E) Observation and simulation of the TS disruption. A fast PD identified in the AIA 94 Å running-difference images (red circles) arrives at the TS at $\sim 18:31:15$ UT ($t_0 + 18$ s) and disrupts the shock, which appears in the simulation as a rapidly contracting magnetic loop (red curve). Arrows show the velocity vectors.



can produce a TS in the LT region, and the observed morphology and dynamics of the TS are well reproduced by the simulations (Fig. 3, B and E, and movie S1). In the simulations, the observed PDs correspond to magnetic structures formed because of instabilities in the reconnection current sheet, which may facilitate the efficiency of the magnetic energy release that powers solar flares (22).

During the largest disruption of the TS, the intensities of all of the three widely separated radio sources decrease simultaneously. The HXR flux above 15 keV is also abruptly reduced, whereas the SXR flux (<12 keV) is largely unaffected, which is consistent with a temporarily softened x-ray photon spectrum (Fig. 4). Both phenomena suggest a temporary decrease of the number of energetic electrons. By fitting the observed x-ray spectrum using an isothermal plasma plus a nonthermal electron distribution with a power-law form, we confirmed that energetic electrons were much less abundant during the shock destruction: the total number of >18 keV electrons was reduced by ~62% (19). This is strong evidence that the TS plays a key role in accelerating the energetic electrons.

An important question is what emission mechanism is responsible for the multitudes of narrow-band stochastic radio spikes at the TS. An attractive possibility is linear mode conversion of Langmuir waves on small-scale density fluctuations (23, 24), a mechanism that has been explored in the context of radio bursts in the solar corona, in Earth's foreshock region, and near the heliospheric TS (24–26). This mechanism requires both a source of Langmuir waves and the presence of small-scale density fluctuations. We suggest that electrons are accelerated in the turbulent plasma environment at the TS (5, 16, 27, 28), an assumption supported by the HXR source at the LT (Fig. 3C). These accelerated electrons are unstable to the production of Langmuir waves, which impinge on the small-scale density fluctuations associated with the turbulent medium and convert to electromagnetic waves near the local plasma frequency $\nu_{pe} = (e^2 n_e / \pi m_e)^{1/2} \approx 8980 \sqrt{n_e}$ Hz, where n_e is the electron density (23, 24). The frequency range of 1 to 1.8 GHz over which the spike bursts appear then implies a density range of $n_e \approx 1.2 \times 10^{10}$ to $4 \times 10^{10} \text{ cm}^{-3}$, which is consistent with that from the x-ray spectral analysis (19). The level of the density fluctuations $\delta n_e / n_e$ is

related to the observed spike bandwidths as $\delta n_e / n_e \approx 2\delta\nu/\nu$, which is relatively small (4%). The spatial scales of the density fluctuations are also small, a few hundred kilometers at the maximum (19).

A major theoretical concern regarding electron acceleration by a fast-mode quasi-perpendicular shock (as for the case of a TS) has been the injection problem: Electrons need to cross the shock front multiple times and/or be pre-accelerated to suprathermal energies in order to gain energy efficiently (2, 3, 27). Our observations show strong evidence for the existence of many small-scale low-amplitude fluctuations at the TS front, which may serve as scattering agents that cause repeated passage of the electrons across the shock (5, 27–30). In addition, the nonthermal electron population is reduced but not eliminated during the TS disruption (Fig. 4 and fig. S5), which implies that electrons may have been pre-accelerated before they reach the shock, possibly at or near the reconnection site (2–4, 12). Both signatures may contribute to resolving the injection problem.

By confirming the existence of the previously controversial solar flare TS and providing strong evidence for it being a particle accelerator, we have obtained new insights into the long-standing problem of particle acceleration in solar flares.

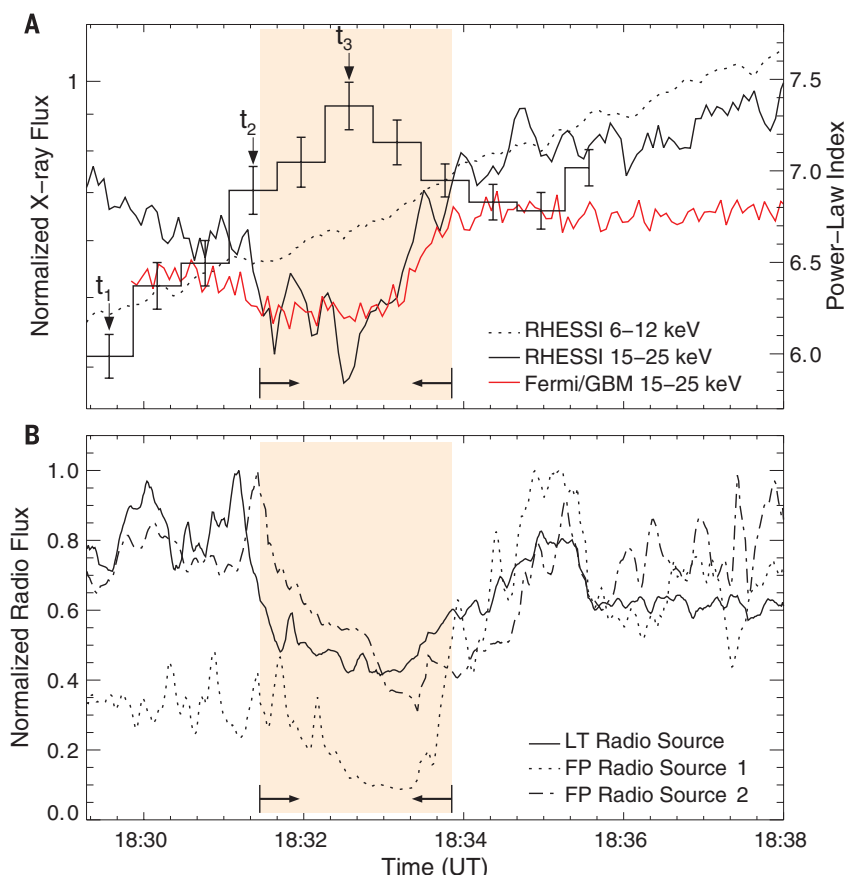


Fig. 4. Reduction of x-ray and radio flux during shock disruption. (A) Temporal evolution of total x-ray photon counts (curves) and power-law index of the x-ray photon spectrum (histogram). Examples of the observed and fitted x-ray spectra are shown in fig. S5 for selected times before and during the shock disruption (marked as t_1 , t_2 , and t_3). **(B)** Evolution of the spatially resolved radio flux of the LT source and the two FP sources, showing a co-temporal radio flux reduction (see also fig. S1C). Arrows bracket a period when the TS experiences a major disruption starting from 18:31:27 UT (or $t_0 + 30$ s, corresponding to the last panel of Fig. 3D).

REFERENCES AND NOTES

1. Y. Matsumoto, T. Amano, T. N. Kato, M. Hoshino, *Science* **347**, 974–978 (2015).
2. J. A. Miller et al., *J. Geophys. Res.* **102**, 14631–14660 (1997).
3. V. V. Zharkova et al., *Space Sci. Rev.* **159**, 357–420 (2011).
4. J. F. Drake, M. Swisdak, H. Che, M. A. Shay, *Nature* **443**, 553–556 (2006).
5. S. Tsuneta, T. Naito, *Astrophys. J.* **495**, L67–L70 (1998).
6. T. G. Forbes, *Astrophys. J.* **305**, 553–563 (1986).
7. S. Masuda, T. Kosugi, H. Hara, S. Tsuneta, Y. Ogawara, *Nature* **371**, 495–497 (1994).
8. K. Shibata et al., *Astrophys. J.* **451**, L83 (1995).
9. T. Yokoyama, K. Shibata, *Astrophys. J.* **494**, L113–L116 (1998).
10. J. C. Workman, E. G. Blackman, C. Ren, *Phys. Plasmas* **18**, 092902 (2011).
11. S. Takasao, T. Matsumoto, N. Nakamura, K. Shibata, *Astrophys. J.* **805**, 135 (2015).
12. W. Liu, Q. Chen, V. Petrosian, *Astrophys. J.* **767**, 168 (2013).
13. H. Aurass, B. Vršnak, G. Mann, *Astron. Astrophys.* **384**, 273–281 (2002).
14. H. Aurass, G. Mann, *Astrophys. J.* **615**, 526–530 (2004).
15. G. Mann, A. Warmuth, H. Aurass, *Astron. Astrophys.* **494**, 669–675 (2009).
16. A. Warmuth, G. Mann, H. Aurass, *Astron. Astrophys.* **494**, 677–691 (2009).
17. H. Aurass, G. Holman, S. Braune, G. Mann, P. Zlobec, *Astron. Astrophys.* **555**, A40 (2013).
18. B. Chen, T. S. Bastian, D. E. Gary, *Astrophys. J.* **794**, 149 (2014).
19. Materials and methods are available as supplementary materials on Science Online.
20. J. R. Lemen et al., *Sol. Phys.* **275**, 17–40 (2012).
21. P. J. A. Simões, E. P. Kontar, *Astron. Astrophys.* **551**, A135 (2013).
22. A. Bhattacharjee, Y.-M. Huang, H. Yang, B. Rogers, *Phys. Plasmas* **16**, 112102 (2009).
23. D. B. Melrose, *Space Sci. Rev.* **26**, 3–38 (1980).
24. E.-H. Kim, I. H. Cairns, P. A. Robinson, *Phys. Plasmas* **15**, 102110 (2008).
25. G. Thejappa, D. Lengyel-Frey, R. G. Stone, M. L. Goldstein, *Astrophys. J.* **416**, 831 (1993).

26. L. Yin, M. Ashour-Abdalla, M. El-Alaoui, J. M. Bosqued, J. L. Bougeret, *Geophys. Res. Lett.* **25**, 2609–2612 (1998).
 27. F. Guo, J. Giacalone, *Astrophys. J.* **753**, 28 (2012).
 28. G. Li, X. Kong, G. Zank, Y. Chen, *Astrophys. J.* **769**, 22 (2013).
 29. E. P. Carley *et al.*, *Nat. Phys.* **9**, 811–816 (2013).
 30. D. Burgess, *Astrophys. J.* **653**, 316–324 (2006).

ACKNOWLEDGMENTS

The authors thank the National Radio Astronomy Observatory (NRAO) staff for their support and E. DeLuca, K. Reeves, H. Tian, J. Lin, A. Warmuth, H. Hudson, A. Caspi, F. Guo, G. Nita, G. Fleishman, and X. Bai for helpful discussions. S. Bourke and G. Hallinan are acknowledged for making their fast radio imaging

software AIPSLite available for B.C. A. K. Tolbert and R. Schwartz are thanked for their help in providing the Fermi/GBM detector response for this flare. Z. Wang and M. DeRosa are thanked for their help on the Prss extrapolations. The NRAO is a facility of the National Science Foundation (NSF) operated under cooperative agreement by Associated Universities, Inc. The VLA data can be accessed at <https://archive.nrao.edu/archive/advquery.jsp>, using the observing times as the search criteria. The Solar Dynamics Observatory/AIA, RHESSI, Hinode/XRT, and Solar and Heliospheric Observatory/LASCO data are all available through the Virtual Solar Observatory (<http://sdac.virtualsolar.org/cgi/search>). B.C. acknowledges support by NASA under contract SP02H1701R from Lockheed-Martin to the Smithsonian Astrophysical Observatory (SAO) and contract NNM07AB07C to SAO, and by the NASA Living With a Star Jack Eddy Fellowship (administered by the University Corporation for

Atmospheric Research). C.S.'s work was supported by NSF SHINE grants AGS-1156076 and AGS-1358342 to SAO. D.E.G. acknowledges support from NSF grant AST-1312802 and NASA grant NNX14AK66G to the New Jersey Institute of Technology. S.K. and L.G. are supported by NASA contract NAS598033 for the RHESSI spacecraft.

SUPPLEMENTARY MATERIALS

www.sciencemag.org/content/350/6265/1238/suppl/DC1

Materials and Methods

Figs. S1 to S6

References (31–56)

Movie S1

24 June 2015; accepted 3 November 2015

10.1126/science.aac8467

BLACK HOLES

Resolved magnetic-field structure and variability near the event horizon of Sagittarius A*

Michael D. Johnson,^{1*} Vincent L. Fish,² Sheperd S. Doeleman,^{1,2} Daniel P. Marrone,³ Richard L. Plambeck,⁴ John F. C. Wardle,⁵ Kazunori Akiyama,^{2,6,7} Keiichi Asada,⁸ Christopher Beaudoin,² Lindy Blackburn,¹ Ray Blundell,¹ Geoffrey C. Bower,⁹ Christiaan Brinkerink,¹⁰ Avery E. Broderick,^{11,12} Roger Cappallo,² Andrew A. Chael,¹ Geoffrey B. Crew,² Jason Dexter,¹³ Matt Dexter,⁴ Robert Freund,³ Per Friberg,¹⁴ Roman Gold,¹⁵ Mark A. Gurwell,¹ Paul T. P. Ho,⁸ Mareki Honma,^{6,16} Makoto Inoue,⁸ Michael Kosowsky,^{1,2,5} Thomas P. Krichbaum,¹⁷ James Lamb,¹⁸ Abraham Loeb,¹ Ru-Sen Lu,^{2,17} David MacMahon,⁴ Jonathan C. McKinney,¹⁵ James M. Moran,¹ Ramesh Narayan,¹ Rurik A. Primiani,¹ Dimitrios Psaltis,³ Alan E. E. Rogers,² Katherine Rosenfeld,¹ Jason SooHoo,² Remo P. J. Tilanus,^{10,19} Michael Titus,² Laura Vertatschitsch,¹ Jonathan Weintraub,¹ Melvyn Wright,⁴ Ken H. Young,¹ J. Anton Zensus,¹⁷ Lucy M. Ziurys³

Near a black hole, differential rotation of a magnetized accretion disk is thought to produce an instability that amplifies weak magnetic fields, driving accretion and outflow. These magnetic fields would naturally give rise to the observed synchrotron emission in galaxy cores and to the formation of relativistic jets, but no observations to date have been able to resolve the expected horizon-scale magnetic-field structure. We report interferometric observations at 1.3-millimeter wavelength that spatially resolve the linearly polarized emission from the Galactic Center supermassive black hole, Sagittarius A*. We have found evidence for partially ordered magnetic fields near the event horizon, on scales of ~6 Schwarzschild radii, and we have detected and localized the intrahour variability associated with these fields.

Sagittarius A* (Sgr A*) emits most of its $\sim 10^{36}$ erg/s luminosity at wavelengths just short of 1 mm, resulting in a distinctive “submillimeter bump” in its spectrum (*1*). A diversity of models attribute this emission to synchrotron radiation from a population of relativistic thermal electrons in the innermost accretion flow (*2–4*). Such emission is expected to be strongly linearly polarized, ~70% in the optically thin limit for a highly ordered magnetic field configuration (*5*), with its direction tracing the underlying magnetic field. At 1.3-mm wavelength, models of magnetized accretion flows predict linear polarization fractions $> \sim 30\%$ (*6–9*), yet connected-element interferometers measure only a 5 to 10% polarization fraction for Sgr A*

(*10, 11*), which is typical for galaxy cores (*12*). However, the highest resolutions of these instruments, ~0.1 to 1", are insufficient to resolve the millimeter emission region, and linear polarization is not detected from Sgr A* at the longer wavelengths at which facility very-long-baseline interferometry (VLBI) instruments offer higher resolution (*13*). Thus, these low-polarization fractions could indicate any combination of low intrinsic polarization, depolarization from Faraday rotation or opacity, disordered magnetic fields within the turbulent emitting plasma, or ordered magnetic fields with unresolved structure, leading to a low beam-averaged polarization. The higher polarization seen during some near-infrared flares may support the last possibility (*14, 15*),

but the origin and nature of these flares is poorly understood and may probe a different emitting electron population than is responsible for the energetically dominant submillimeter emission.

To definitively study this environment, we are assembling the Event Horizon Telescope (EHT), a global VLBI array operating at 1.3-mm wavelength. Initial studies with the EHT have spatially resolved the ~40 micro-arc sec emission region of Sgr A* (*16, 17*), suggesting the potential for polarimetric VLBI with the EHT to resolve its magnetic field structure. For comparison, Sgr A* has a mass of $\sim 4.3 \times 10^6 M_{\odot}$ (M_{\odot} , solar mass) and lies at a distance of ~8 kpc, so its Schwarzschild radius ($R_{\text{Sch}} = 2GM/c^2$) is 1.3×10^{12} cm and subtends 10 micro-arc sec (*18, 19*). In March 2013, the EHT observed Sgr A* for five nights using sites in California, Arizona, and Hawaii. In California, we phased together eight antennas from the

¹Harvard-Smithsonian Center for Astrophysics, 60 Garden Street, Cambridge, MA 02138, USA. ²Haystack Observatory, Route 40, Massachusetts Institute of Technology, Westford, MA 01886, USA. ³Steward Observatory, University of Arizona, 933 North Cherry Avenue, Tucson, AZ 85721-0065, USA. ⁴Department of Astronomy, Radio Astronomy Laboratory, 501 Campbell, University of California Berkeley, Berkeley, CA 94720-3411, USA. ⁵Department of Physics MS-057, Brandeis University, Waltham, MA 02454-0911. ⁶National Astronomical Observatory of Japan, Osawa 2-21-1, Mitaka, Tokyo 181-8588, Japan. ⁷Department of Astronomy, Graduate School of Science, The University of Tokyo, 7-3-1 Hongo, Bunkyo-ku, Tokyo 113-0033, Japan. ⁸Institute of Astronomy and Astrophysics, Academia Sinica, Post Office Box 23-141, Taipei 10617, Taiwan. ⁹Academia Sinica Institute for Astronomy and Astrophysics (ASIAA), 645 N. A'ohoku Pl. Hilo, HI 96720, USA. ¹⁰Department of Astrophysics/Institute for Mathematics, Astrophysics and Particle Physics, Radboud University Nijmegen, Post Office Box 9010, 6500 GL Nijmegen, Netherlands. ¹¹Perimeter Institute for Theoretical Physics, 31 Caroline Street North, Waterloo, ON N2L 2Y5, Canada. ¹²Department of Physics and Astronomy, University of Waterloo, 200 University Avenue West, Waterloo, ON N2L 3G1, Canada. ¹³Max Planck Institute for Extraterrestrial Physics, Giessenbachstrasse 1, 85748 Garching, Germany. ¹⁴James Clerk Maxwell Telescope, East Asia Observatory, 660 N. A'ohoku Place, University Park, Hilo, HI 96720, USA. ¹⁵Department of Physics, Joint Space-Science Institute, University of Maryland at College Park, Physical Sciences Complex, College Park, MD 20742, USA. ¹⁶Graduate University for Advanced Studies, Mitaka, 2-21-1 Osawa, Mitaka, Tokyo 181-8588. ¹⁷Max-Planck-Institut für Radioastronomie, Auf dem Hügel 69, D-53121 Bonn, Germany. ¹⁸Owens Valley Radio Observatory, California Institute of Technology, 100 Leighton Lane, Big Pine, CA 93513-0968, USA. ¹⁹Leiden Observatory, Leiden University, Post Office Box 9513, 2300 RA Leiden, Netherlands.

*Corresponding author. E-mail: mjohnson@cfa.harvard.edu

Combined Array for Research in Millimeter-wave Astronomy (CARMA) to act as a single dual-polarization station, and we separately recorded dual-polarization data from an additional 10.4-m antenna. We also conducted normal observations with CARMA in parallel with the VLBI observations. In Arizona, the 10-m Submillimeter Telescope (SMT) recorded dual polarizations. In Hawaii, seven 6-m dishes of the Submillimeter Array (SMA) were combined into a single-polarization phased array, while the nearby 15-m James Clerk Maxwell Telescope (JCMT) recorded the opposite polarization, forming a single effective dual-polarization station. Each station, except for the CARMA reference antenna, recorded two 512-MHz bands, centered on 229.089 and 229.601 GHz, and circular polarizations.

A linearly polarized signal manifests itself in the cross-hand correlations between stations, $\langle L_1 R_2^* \rangle$ and $\langle R_1 L_2^* \rangle$, where L_i denotes left circular polarization and R_i denotes right circular polarization at site i , and the asterisk denotes complex conjugation. These correlations are typically much weaker than their parallel-hand counterparts, $\langle R_1 R_2^* \rangle$ and $\langle L_1 L_2^* \rangle$, which measure the total flux. After calibrating for the spurious polarization introduced by instrumental cross-talk (20), quotients of the cross-hand to parallel-hand correlations on each baseline \mathbf{u} joining a pair of stations are sensitive to the fractional linear polarization in the visibility domain: $\tilde{m}(\mathbf{u}) = [\tilde{Q}(\mathbf{u}) + i\tilde{U}(\mathbf{u})]/\tilde{I}(\mathbf{u})$. Here, \tilde{I} , \tilde{Q} , and \tilde{U} are Stokes parameters, and the tilde denotes a spatial Fourier transform relating their sky brightness distributions to interferometric visibilities in accordance with the Van Cittert-Zernike Theorem. \tilde{m} provides robust phase information and is insensitive to station gain fluctuations and to scatter-broadening in the interstellar medium (20, 21). On baselines that are too short to resolve the source, \tilde{m} gives the fractional image-averaged polarization. On longer baselines, \tilde{m} mixes information about the spatial distribution of polarization with information about the strength and direction of polarization and must be interpreted with care. For instance, one difference from its image-domain analog $m = (Q + iU)/I$ is that $|\tilde{m}|$ can be arbitrarily large. Nevertheless, \tilde{m} readily provides secure inferences about the intrinsic polarization properties of Sgr A*.

Our measurements on long baselines robustly detect linearly polarized structures in Sgr A* on $\sim 6 R_{\text{Sch}}$ scales (Fig. 1). The high (up to $\sim 70\%$) and smoothly varying polarization fractions are an order of magnitude larger than those seen on shorter baselines (Fig. 2), suggesting that we are resolving highly polarized structure within the compact emission region. Measurements on shorter baselines show variations that are tightly correlated with those seen in simultaneous CARMA-only measurements (figs. S4 and S8). This agreement demonstrates that there is negligible contribution to either the polarized or total flux on scales exceeding $\sim 30 R_{\text{Sch}}$, conclusively eliminating dust or other diffuse emission as an important factor (20). Because CARMA does not resolve polarization structure in Sgr A*, these varia-

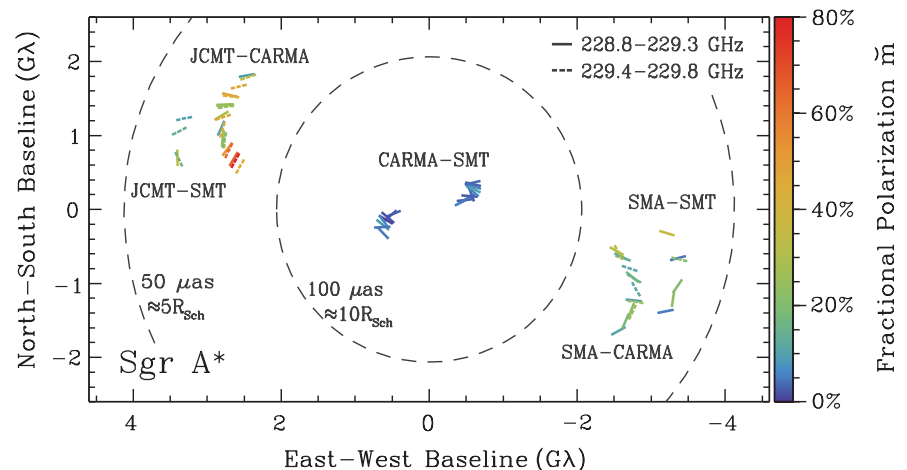
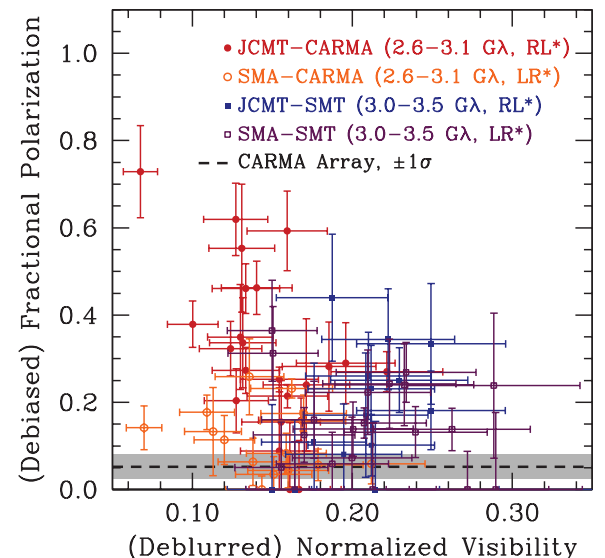


Fig. 1. Interferometric fractional polarization measurements for Sgr A*. Interferometric fractional polarization measurements, $\tilde{m}(\mathbf{u})$, for Sgr A* in our two observing bands during one day of EHT observations in 2013 (day 80). The color and direction of the ticks indicate the (noise-debiased) amplitude and direction of the measured polarization, respectively. For visual clarity, we omit CARMA-only measurements, show only long scans, show only low-band measurements for the SMT-CARMA baseline, and exclude points with a parallel-hand signal-to-noise below 6.5. The fractional polarization is expected to change smoothly as the baseline orientation changes with the rotation of the Earth, and the polarization of Sgr A* is also highly variable in time (fig. S8). The pronounced asymmetry in $\tilde{m}(\pm\mathbf{u})$ indicates variation in the polarization direction throughout the emission region.

Fig. 2. Signatures of spatially resolved fields from 1.3-mm VLBI. Long-baseline measurements of interferometric fractional polarization, \tilde{m} , are plotted against the “deblurred” and normalized total-flux visibilities (20, 35); errors are $\pm 1\sigma$ (details of the error analysis are provided in the supplementary materials). The black dashed line and gray shaded region show the average and SD of the CARMA measurements of fractional polarization, respectively. The sharp increase in the polarization fraction and variability on long baselines demonstrates that we are resolving the compact and polarized emission structure on scales of ~ 6 to $8 R_{\text{Sch}}$. The marked difference in the two polarization products, $\langle R_1 L_2^* \rangle$ and $\langle L_1 R_2^* \rangle$, on equal baselines indicates changes in the polarization direction on these scales (Fig. 1).



tions definitively reflect intrahour intrinsic variability associated with compact structures near the black hole.

We emphasize that $|\tilde{m}(\mathbf{u})| \sim 70\%$ does not imply correspondingly high image polarizations or that we are measuring polarization near a theoretical maximum. Because polarization can have small-scale structure via changes in its direction, disordered polarization throughout a comparatively smooth total emission region will result in long baselines resolving the total flux more heavily than the polarization (20). As a re-

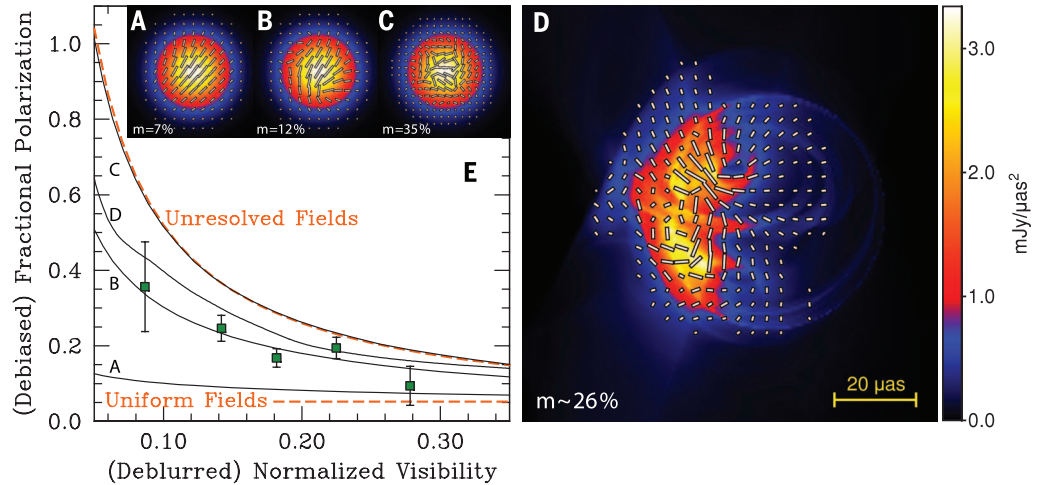
sult, $|\tilde{m}|$ can be arbitrarily large, especially in locations near a visibility “null,” where \tilde{I} is close to zero. Although our highest measured polarization fractions occur where \tilde{I} falls to only 5 to 10% of the zero-baseline flux (Fig. 2), the rise is slower than expected for completely unresolved polarization structure, showing that the long baselines are partially resolving coherent polarized structures on the scale of $\sim 6 R_{\text{Sch}}$ (Fig. 3). Because interferometric baselines only resolve structure along their direction and our long baselines are predominantly east-west, these conclusions

Fig. 3. Strength and order of the polarization field from 1.3-mm VLBI. (A, B, and C) Example

realizations from three models with Gaussian distributions of intensity. Color indicates total flux on a linear scale; ticks indicate polarization amplitude and direction. Each model has a constant polarization fraction but stochastically varying polarization direction with prescribed coherence lengths (0.64, 0.29, and 0.11 times the Gaussian full width at half maximum). The polarization fractions are determined by matching the ensemble-average zero-baseline polarization to the averaged CARMA measurements.

(D) A sample image from a general relativistic magnetohydrodynamic

simulation with polarimetric radiative transfer (9). The image-averaged polarization fraction, weighted by brightness, is 26%. (E) Points with errors ($\pm 1\sigma$) show the average of VLBI measurements from Fig. 2 after grouping in bins of width 0.05. Dashed orange lines indicate two limiting cases: a uniform polarization field and a highly disordered (unresolved) polarization field. Each is set equal to 5.2% when the normalized visibility is unity so that the zero-baseline polarization matches the average of all CARMA measurements. Our data differ from model (A) at a significance exceeding 4σ , differ from model (C) by 3.4σ , and are compatible with model (B) (20). The GRMHD simulation (E) also exhibits a balance between order and variation in the polarization field that is compatible with our observations.



describe the relative coherence of the polarization field in the east-west direction.

The current data, although too sparse for imaging, provide rich geometrical insights. For instance, if the fractional polarization is constant across the source image, then it will also be constant in the visibility domain. Furthermore, even if the polarization amplitude varies arbitrarily throughout the image, if its direction is constant then the amplitude of the interferometric polarization fraction will be equal for conjugate baselines (20). Our measurements (Fig. 1) eliminate both of these possibilities and thus detect variation in the polarization direction on event-horizon scales. These arguments also allow us to assess the spatial extent of the polarized emission because the detected polarization variation cannot arise from a region that is much smaller than the diffraction limit of our interferometer. The polarized emission must therefore span an extent comparable with that of the total flux (20).

The phase of $\vec{m}(\mathbf{u})$ likewise constrains the emission morphology. For example, on a short baseline, the leading-order geometrical contribution to the interferometric phase comes from the image centroid (21). Thus, just as a decrease in correlated flux with baseline length provides a characteristic angular extent of the emission, a linear change in the phase of $\vec{m}(\mathbf{u})$ with baseline length provides a characteristic angular separation of the polarized and total flux. The close agreement in phase between the two measurements on the short SMT-CARMA baseline establishes that the polarized and unpolarized flux are closely aligned—to within ~ 10 micro-arc sec when the polarization angle of Sgr A* is relatively steady (fig. S8). However, when variability is dominant, we measure much larger offsets, up to ~ 100 micro-arc sec, implicating dynamical activity near the black hole. For comparison, the apparent diameter of the innermost stable circular

orbit is $6\sqrt{3/2}R_{\text{Sch}} \approx 73$ micro-arc sec if the black hole of Sgr A* is not spinning. The tight spatial association of this linear polarization with the 1.3-mm emission region then cements low-accretion models for Sgr A* (11), which combined with the measured spectrum in the submillimeter bump and in the near-infrared imply a magnetic field of tens of gauss throughout the emitting plasma (3, 4, 7).

Even amid magnetically driven instabilities and a turbulent accretion environment, several effects can produce ordered fields near the event horizon. For example, as the orbits of the accreting material around the black hole become circular, magnetic fields will be azimuthally sheared by the differential rotation, resulting in a predominantly toroidal configuration (22). The high image-averaged polarization associated with the emission region necessitates that such a flow be viewed at high inclination because circular symmetry would cancel the polarization of a disk viewed face-on. The striking difference between the stability of compact structures in the total flux (17) relative to the rapid changes in the polarized structures on similar scales is then most naturally explained via dynamical magnetic field activity through coupled actions of disk rotation and turbulence driven by the magnetorotational instability (MRI) (23).

Alternatively, accumulation of sufficient magnetic flux near the event horizon may have led to a stable, magnetically dominated inner region, suppressing the disk rotation and the MRI (24–26). Emission from a magnetically dominant region provides an attractive explanation for the long-term stability of the circular polarization handedness and the linear polarization direction of Sgr A* (27, 28), and it has recently received observational support in describing the cores of active galaxies with prominent jets (29–31). However, the close alignment of the polarized and

total emission (20) severely constrains multi-component emission models for the quiescent flux, such as a bipolar jet (32) or a coupled jet-disk system (33). If a jet is present, then this constraint suggests substantial differences between the emitting electron populations in the jet and the accretion flow to ensure the dominance of a single component at 1.3 mm (26, 34).

With the advent of polarimetric VLBI at 1.3-mm wavelength, we are now resolving the magnetized core of our galaxy's central engine. Our measurements provide direct evidence of ordered magnetic fields in the immediate vicinity of Sgr A*, firmly grounding decades of theoretical work. Despite the extreme compactness of the emission region, we have unambiguously localized the linear polarization to the same region and identified spatial variations in the polarization direction. We also detected intrahour variability and spatially resolved its associated offsets. In the next few years, expansion of the EHT will enable imaging of these magnetic structures and variability studies on the 20-s gravitational time scale (GM/c^3) of Sgr A*.

REFERENCES AND NOTES

1. G. C. Bower *et al.*, *Astrophys. J.* **802**, 69 (2015).
2. F. Özel, D. Psaltis, R. Narayan, *Astrophys. J.* **541**, 234–249 (2000).
3. J. Dexter, E. Agol, P. C. Fragile, J. C. McKinney, *Astrophys. J.* **717**, 1092–1104 (2010).
4. F. Yuan, R. Narayan, *Annu. Rev. Astron. Astrophys.* **52**, 529–588 (2014).
5. T. W. Jones, P. E. Hardee, *Astrophys. J.* **228**, 268 (1979).
6. B. C. Bromley, F. Melia, S. Liu, *Astrophys. J.* **555**, L83–L86 (2001).
7. F. Yuan, E. Quataert, R. Narayan, *Astrophys. J.* **598**, 301–312 (2003).
8. A. E. Broderick, A. Loeb, *Mon. Not. R. Astron. Soc.* **367**, 905–916 (2006).
9. R. V. Shcherbakov, J. C. McKinney, *Astrophys. J.* **774**, L22 (2013).

10. G. C. Bower, H. Falcke, M. C. Wright, D. C. Backer, *Astrophys. J.* **618**, L29–L32 (2005).
11. D. P. Marrone, J. M. Moran, J.-H. Zhao, R. Rao, *Astrophys. J.* **654**, L57–L60 (2007).
12. S. G. Jorstad et al., *Astron. J.* **130**, 1418–1465 (2005).
13. G. C. Bower, M. C. H. Wright, D. C. Backer, H. Falcke, *Astrophys. J.* **527**, 851–855 (1999).
14. A. Eckart et al., *Astron. Astrophys.* **455**, 1–10 (2006).
15. M. Zamaninasab et al., *Astron. Astrophys.* **510**, A3 (2010).
16. S. S. Doeleman et al., *Nature* **455**, 78–80 (2008).
17. V. L. Fish et al., *Astrophys. J.* **727**, L36 (2011).
18. A. M. Ghez et al., *Astrophys. J.* **689**, 1044–1062 (2008).
19. S. Gillessen et al., *Astrophys. J.* **692**, 1075–1109 (2009).
20. Materials and methods are available as supplementary materials on Science Online.
21. M. D. Johnson et al., *Astrophys. J.* **794**, 150 (2014).
22. S. Hirose, J. H. Krolik, J.-P. De Villiers, J. F. Hawley, *Astrophys. J.* **606**, 1083–1097 (2004).
23. S. A. Balbus, J. F. Hawley, *Astrophys. J.* **376**, 214 (1991).
24. R. Narayan, I. V. Igumenshchev, M. A. Abramowicz, *Publ. Astron. Soc. Jpn.* **55**, L69–L72 (2003).
25. J. C. McKinney, A. Tchekhovskoy, R. D. Blandford, *Mon. Not. R. Astron. Soc.* **423**, 3083–3117 (2012).
26. C.-K. Chan, D. Psaltis, F. Özel, R. Narayan, A. Sądowski, *Astrophys. J.* **799**, 1 (2015).
27. G. C. Bower, H. Falcke, R. J. Sault, D. C. Backer, *Astrophys. J.* **571**, 843–855 (2002).
28. D. J. Muñoz, D. P. Marrone, J. M. Moran, R. Rao, *Astrophys. J.* **745**, 115 (2012).
29. M. Zamaninasab, E. Clausen-Brown, T. Savolainen, A. Tchekhovskoy, *Nature* **510**, 126–128 (2014).
30. P. Mocq, X. Guo, *Mon. Not. R. Astron. Soc.* **447**, 1498–1503 (2015).
31. I. Martí-Vidal, S. Müller, W. Vlemmings, C. Horellou, S. Aalto, *Science* **348**, 311–314 (2015).
32. S. Markoff, G. C. Bower, H. Falcke, *Mon. Not. R. Astron. Soc.* **379**, 1519–1532 (2007).
33. F. Yuan, S. Markoff, H. Falcke, *Astron. Astrophys.* **383**, 854–863 (2002).
34. M. Mościbrodzka, H. Falcke, *Astron. Astrophys.* **559**, L3 (2013).
35. V. L. Fish et al., *Astrophys. J.* **795**, 134 (2014).

ACKNOWLEDGMENTS

EHT research is funded by multiple grants from NSF, by NASA, and by the Gordon and Betty Moore Foundation through a grant to S.D. The SMA is a joint project between the Smithsonian Astrophysical Observatory and the Academia Sinica Institute of Astronomy and Astrophysics. The Arizona Radio Observatory is partially supported through the NSF University Radio Observatories program. The James Clerk Maxwell Telescope was operated by the Joint Astronomy Centre on behalf of the Science and Technology Facilities Council of the UK, the Netherlands Organisation for Scientific Research, and the National Research Council of Canada. Funding for CARMA development and operations was supported by NSF and the CARMA partner universities. We thank Xilinx for equipment donations. A.E.B. receives financial support from the Perimeter Institute for Theoretical Physics and the Natural Sciences and Engineering Research Council of Canada through a Discovery Grant. Research at Perimeter Institute is supported by the Government of Canada through Industry Canada and by the Province of Ontario through the Ministry of Research and Innovation. J.D. receives support from a Sofja Kovalevskaja award from the Alexander von Humboldt Foundation. M.H. was supported by a Japan Society for the Promotion of Science Grant-in-aid. R.P.J.T. receives support from Netherlands Organisation for Scientific Research. Data used in this paper are available in the supplementary materials.

SUPPLEMENTARY MATERIALS

www.sciencemag.org/content/350/6265/1242/suppl/DC1
Supplementary Text
Figs. S1 to S8
Tables S1 to S3
References (36–61)
Data Files S1 and S2

11 June 2015; accepted 13 October 2015
10.1126/science.aac7087

EDUCATION

Democratizing education? Examining access and usage patterns in massive open online courses

John D. Hansen^{1*} and Justin Reich²

Massive open online courses (MOOCs) are often characterized as remedies to educational disparities related to social class. Using data from 68 MOOCs offered by Harvard and MIT between 2012 and 2014, we found that course participants from the United States tended to live in more-affluent and better-educated neighborhoods than the average U.S. resident. Among those who did register for courses, students with greater socioeconomic resources were more likely to earn a certificate. Furthermore, these differences in MOOC access and completion were larger for adolescents and young adults, the traditional ages where people find on-ramps into science, technology, engineering, and mathematics (STEM) coursework and careers. Our findings raise concerns that MOOCs and similar approaches to online learning can exacerbate rather than reduce disparities in educational outcomes related to socioeconomic status.

For nearly a century, technologists have promised that new broadcast media will bridge resource gaps between students in more- and less-privileged environments. “With radio the underprivileged school becomes the privileged” was the promise in the 1930s (1); in the 1960s, boosters declared that television would “make available to these young people instruction of a higher order than they might otherwise receive” (2). In the first years of the 2010s, technologists have heralded the possibility that massive open online courses (MOOCs) can “democratize education” (3–5). Previous generations of broadcast and interactive technologies—film, radio, television, personal computers, Internet access, and Web 2.0 platforms—have yet to fulfill the promise of educational parity (6), and these new claims from MOOC advocates warrant empirical study. In this study, we took advantage of the data collected from MOOC students about their demographics and course performance—generally unavailable in studies of broadcast technologies—to present a portrait of registration and completion patterns in 68 courses offered by Harvard and MIT on the edX platform.

Our analytical framework was guided by Attewell’s argument that the “digital divide,” the gap in education technology opportunities between students from different backgrounds, is best understood as two divides: one of access and one of usage (7). More- and less-affluent students not only have different levels of basic access to emerging technologies; they have used them for different purposes with different levels of support from mentors. Historically, digital divides of usage have compounded digital divides of access. Surveys from the National Assessment of Educa-

tional Progress in 1996 and 2011 showed that students from schools serving mostly affluent students were more likely to use computers for simulations or modeling; by contrast, students from schools serving low-income students were more likely to use computers for drill and practice exercises (8, 9). Comparable patterns have been found across the sciences and other subject areas when comparing schools with similar computer-student ratios serving students from different backgrounds (10). Attewell found evidence of similar patterns of computer usage at home, where the academic benefits of home computers were greater for children from affluent families (11).

These patterns extend into the era of free Web tools as well. Reich and colleagues examined the use of freely available wikis—platforms for collaborative Web publishing—in U.S. kindergarten to high school (K–12) schools in the late ’00s (12). They found that free wikis were more likely to be created in affluent schools, and in these schools, wikis were more likely to be used to support collaborative problem-solving and new media literacy. In schools serving low-income students, wikis were more likely to be used for teacher-centered content delivery. This research suggests a potential paradoxical effect of free online-learning resources: They can disproportionately benefit the affluent—people who have the social, financial, and technological capital to take advantage of new innovations, including those that are free.

The earliest research on MOOCs hints at similar kinds of patterns. The majority of registrants in MOOC courses already had a college or graduate degree, and some studies have found a positive, substantively modest correlation between a student’s level of education and course completion (13–16). We built upon these studies with a much richer demographic portrait of students across a wider range of courses.

Socioeconomic status (SES) denotes one’s social and financial resources, and it is typically viewed through a combination of measures (17).

¹Harvard Graduate School of Education, Harvard University, Cambridge, MA 02138, USA. ²Office of Digital Learning, Massachusetts Institute of Technology, Cambridge, MA 02139, USA.

*Corresponding author. E-mail: john_hansen@mail.harvard.edu

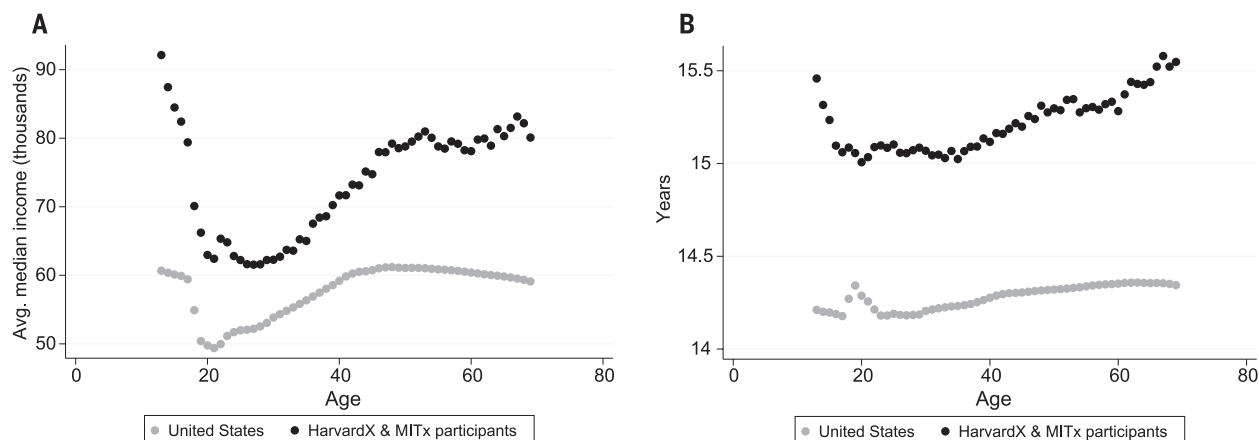


Fig. 1. Neighborhood income and educational attainment differences between MOOC participants and the U.S. population. (A) Average neighborhood median income. **(B)** Average neighborhood educational attainment.

In this study, we used three indicators for SES: (i) parental educational attainment, (ii) neighborhood median income, and (iii) neighborhood average educational attainment. When signing up for edX, students were asked to provide their mailing address, and for U.S. MOOC registrants, we used this address to identify each student's census block group, a "neighborhood" of ~1500 people for which we have census data about median income and educational attainment (18). Although more direct measures of family income or wealth are preferred, these neighborhood-level measures have proven useful in other studies (19). We are particularly interested in adolescents age 13 to 17, for several reasons. First, these are the years that have traditionally been critical for students finding an on-ramp into postsecondary science, technology, engineering, and mathematics (STEM) education and careers. Also, MOOC advocates have identified K-12 students as a promising target population for MOOCs (20, 21), and universities and MOOC platforms are increasingly targeting this population with their offerings (22). Pragmatically, these students likely live at home with their parents, and our three measures probably identified an individual's SES with greatest fidelity in this age range.

In the 2012–2014 academic years, Harvard and MIT offered 68 free courses and modules on the edX learning-management system, which attracted 1,028,269 unique participants (individuals who entered the courseware of one or more courses) (16). Our study examined 164,198 unique participants from the United States who reported an age between 13 and 69 and provided a mailing address that we could match to a census block group, which represented 57% of U.S. participants in this age range (table S1). Because many participants registered for multiple courses, these students accounted for more than 200,000 participant-course observations. We compared the demographic characteristics of U.S. MOOC participants to the U.S. population to better understand the digital divide of access. This comparison can be understood as a case-control study (23), with edX enrollees as cases and a synthetic set of one-to-one matched controls

Table 1. Differences in MOOC participation and certification likelihood attributable to a one-standard deviation increment in SES variables. Values are odds ratio plus or minus 1 SE. An odds-ratio of 1 means equivalent odds. For age 13 to 69 regressions, the sample sizes are ~232 million for participation and 201,225 for certification. For age 13 to 17 regressions, the sample sizes were ~20.5 million for participation, 8481 for neighborhood-SES certification models, and 2112 for parental education certification models. See supplementary materials for model specification details. Robust standard errors clustered at the course level are used for certification models. All coefficients are statistically significant ($P < 0.01$).

SES variable	Age	Participation	Certification
Neighborhood income	13–69	1.44 ± 0.003	1.06 ± 0.014
SD = \$30,536	13–17	1.59 ± 0.012	1.13 ± 0.026
Neighborhood education	13–69	1.95 ± 0.005	1.07 ± 0.022
SD = 1.27 years	13–17	2.09 ± 0.024	1.32 ± 0.049
Parental education	13–17	2.97 ± 0.086	1.28 ± 0.114
SD = 2.92 years			

by geographic area, with the assumption that controls were unlikely to be enrolled in edX, given the large population size. We then examined how measures of SES predicted course completion to understand the digital divide of usage.

We first described differences in neighborhood characteristics between HarvardX and MITx participants and the U.S. population as a whole. For individuals of all ages from 13 to 69, MOOC participants lived in neighborhoods that are more affluent and have higher average levels of educational attainment (Fig. 1). We found that, on average, MOOC participants resided in neighborhoods where median household income was \$69,641 dollars, which was \$11,998 dollars above the neighborhood national average of \$57,643 (table S2). When we restricted our comparison to individuals aged 13 to 17, the difference was \$23,181 (table S2). We found large differences in neighborhood educational attainment across all age groups as well.

We conduct a variety of sensitivity analyses (presented in the supplementary materials), which suggested that this finding was robust and per-

sisted at the individual level (fig. S4). Specifically, we found that the positive relationship between neighborhood SES and MOOC participation persisted across courses and within states, counties, and census tracts (table S6); survey respondents appeared similar to nonrespondents with respect to our measures of SES (tables S7 and S8); alternative demographic data sets and neighborhood identification approaches produced similar estimates; and participants also tended to live in more densely populated neighborhoods (tables S9 and S10), which suggested that MOOCs do not disproportionately serve the geographically isolated.

Predicting MOOC participation as a function of neighborhood SES allowed us to interpret these differences in terms of participation likelihood. The results of logistic regression models are shown in Table 1, where the odds of participation are estimated in terms of a one-standard deviation change in the predictor. Interpreting these results in dollars, we predicted that an additional \$20,000 in neighborhood median income increased the odds of participation by 27%. Each

Fig. 2. Odds ratio of certificate-earning for participants with a college-educated parent compared with participants without one. Diamonds

were estimated by means of a logistic regression model that includes sets of binary indicators for age, course, enrollment mode, and the interaction of each age indicator with a binary indicator for college-educated parent. Circles with error bars were estimated in an analogous specification where age group indicators (13 to 17 years, 18 to 22 years, etc.) replaced age indicators in the interaction. Error bars show ± 1 SE. Each point on the plot represents the multiplicative difference in the odds of certification among students of the same age whose parents had a bachelor's degree compared with those whose parents did not.

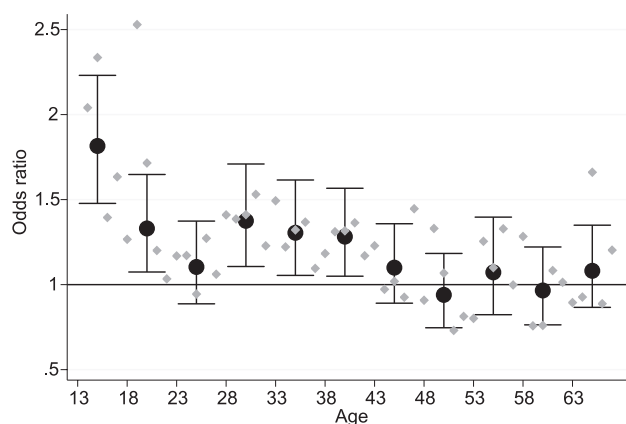
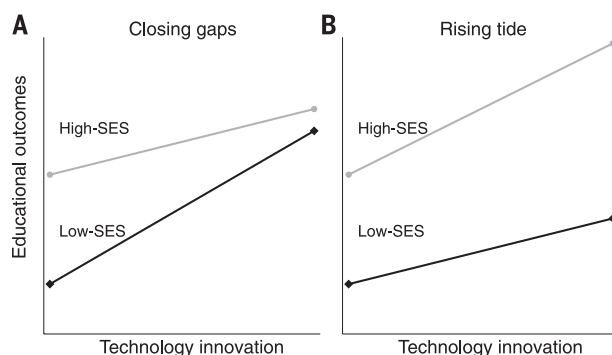


Fig. 3. Two stylized representations of the hypothesized effects of a technological innovation on educational outcomes for students from high-SES and low-SES backgrounds. We compare benefits from emerging technologies and gaps in educational outcomes.



additional year of neighborhood-average educational attainment increased the odds of participation by 69%. Among adolescents, the relationship between neighborhood SES and MOOC participation was even stronger (24).

Turning to the digital divide of usage, we found analogous patterns when we examined the relations between our measures and certificate attainment. Neighborhood- and individual-level SES measures were associated with higher rates of course completion, with larger magnitudes for younger participants. After examining the full age range of participants from 13 to 69, we interpreted the coefficients from Table 1 as modest in magnitude. Among the individuals who took the initiative to enroll and participate in a HarvardX course, neighborhood SES—like one's own educational attainment (17)—was a statistically significant but not substantively strong predictor of course completion on average (Fig. 2). These relatively modest overall differences, however, masked important differences in attainment by SES for young people. For an adolescent participant whose most educated parent has a bachelor's degree, the odds of certification were ~ 1.75 times those of an otherwise similar adolescent in the same course whose most educated parent has less than a bachelor's. Students from all backgrounds earned certificates in Harvard and MIT MOOCs, but especially among the young, high-SES students were more likely to earn a certificate.

Overall, individuals living in high-SES neighborhoods in the United States were substantially more likely to participate in Harvard's and MIT's MOOCs, and, conditional on participation, high-SES students earned certificates at higher rates. These patterns were particularly strong among adolescents, precisely the age at which we hope that students from low-income backgrounds can use education as a gateway to the middle class.

The rhetoric of democratizing education implies broad social benefits without precisely articulating how those benefits might be distributed. In Fig. 3, we present two stylized representations of the effects of a technological innovation, such as MOOCs, on educational outcomes from students from different backgrounds. In the scenario that we call "closing gaps" (Fig. 3A), expanding access simultaneously benefits all students and ameliorates inequality. In the "rising tide" scenario (Fig. 3B), all groups benefit from emerging technologies, but gaps in educational outcomes widen.

Whether particular gaps will widen or close, for whom, and under what circumstances, are all questions worthy of further study as MOOCs and other new learning opportunities expand. The findings from this observational study appeared more consistent with the rising tides than closing gaps scenario, but additional research will be necessary to identify causal effects on SES-education gaps. Despite early research that socially advantaged children watched more *Sesame*

Street and learned at least as much from watching (25), later research found that it narrowed an SES-related gap in school readiness (26).

MOOCs are one of many online learning opportunities, and our findings cannot be generalized to all open educational resources or education technologies. Nevertheless, our research on MOOCs—along with previous decades' research examining the access and usage patterns of emerging learning technologies—should provoke skepticism of lofty claims regarding democratization, level playing fields, and closing gaps that might accompany new genres of online learning, especially those targeted at younger learners. Freely available learning technologies can offer broad social benefits, but educators and policymakers should not assume that the underserved or disadvantaged will be the chief beneficiaries. Closing gaps with digital learning resources requires targeting innovation toward the students most in need of additional support and opportunity.

REFERENCES AND NOTES

1. L. Cuban, *Teachers and Machines: The Classroom Use of Technology Since 1920* (Teachers College Press, New York, 1986).
2. Ford Foundation, *Teaching by Television* (Ford Foundation and Fund for the Advancement of Education, New York, 1961).
3. R. Kanani, "EdX CEO Anant Agarwal on the future of online learning," *Forbes*, 21 June 2014.
4. D. Koller, "MOOCs can be a significant factor in opening doors to opportunity," *EdSurge*, 31 December 2013.
5. D. Faust, R. Reif, "The newest revolution in higher ed," *Boston Globe*, 3 March 2013.
6. S. Reardon, in *Whither Opportunity? Rising Inequality and the Uncertain Life Chances of Low-Income Children*, R. J. Murnane, G. Duncan, Eds. (Russell Sage Foundation Press, New York, 2011).
7. P. Attewell, *Sociol. Educ.* **74**, 252–259 (2001).
8. H. Wenglinsky, *Does It Compute? The Relationship Between Education Technology and Student Achievement in Mathematics* (Educational Testing Services, Princeton, NJ, 1998).
9. U. Boser, *Are Schools Getting a Big Enough Bang for Their Education Technology Buck?* (Center for American Progress, Washington, DC, 2013).
10. M. Warschauer, M. Knobel, L. Stone, *Educ. Policy* **18**, 562–588 (2004).
11. P. Attewell, J. Battle, *Inf. Soc.* **15**, 1–10 (1999).
12. J. Reich, R. J. Murnane, J. B. Willett, *Educ. Res.* **41**, 7–15 (2012).
13. E. J. Emanuel, *Nature* **503**, 342–342 (2013).
14. A. D. Ho et al., "HarvardX and MITx: The first year of open online courses, Fall 2012–Summer 2013" (Working paper no. 1, HarvardX and MITx, Cambridge, MA, 2014).
15. J. Reich, "MOOC completion and retention in the context of student intent," *EDUCAUSE Rev. Online* (2014); <http://er.educase.edu/articles/2014/12/mooc-completion-and-retention-in-the-context-of-student-intent>.
16. A. D. Ho et al., "HarvardX and MITx: Two years of open online courses" (Working paper no. 10, HarvardX, Cambridge, MA, 2015).
17. National Center for Education Statistics, *Improving the Measurement of Socioeconomic Status for the National Assessment of Educational Progress: A Theoretical Foundation* (National Center for Education Statistics, Washington, DC, 2012).
18. J. D. Hansen, J. Reich, *Socioeconomic Status and MOOC Enrollment: Enriching Demographic Information with External Datasets* (ACM, New York, 2015).
19. S. R. Sirin, *Rev. Educ. Res.* **75**, 417–453 (2005).
20. C. E. Finn, "MOOCs in size small please" [blog], *Educ. Next* (2012); <http://educationnext.org/moocs-in-size-small-please/>.
21. M. B. Horn, *Educ. Next* **14**, 82–83 (2014).
22. T. Lewin, "Promising full college credit, Arizona State offers online freshman program," *New York Times*, 22 April 2015, p. A14.
23. J. J. Schlesselman, P. D. Stolley, *Case Control Studies: Design, Conduct, Analysis* (Oxford Univ. Press, New York, 1982).

24. Regarding the SES of Harvard and MIT students compared with all MOOC participants, the most direct comparison we could make would be parental education. About 84% of Harvard and MIT undergrads have a parent with at least a bachelor's degree. In comparison, 80% of the 13- to 17-year-olds in Harvard or MIT MOOCs reported having a parent with at least a bachelor's, and 88% of 13- to 17-year-olds earning certificates reported a parent with at least a bachelor's. For 18- to 22-year-olds in MOOCs, the reports are 68% for participants and 75% for certificate-earners. Except perhaps for 13- to 17-year-olds who earn certificates, this suggests that SES among Harvard and MIT MOOC participants is lower than Harvard and MIT undergrads.
25. T. D. Cook, "Sesame Street" Revisited (Russell Sage Foundation, New York, 1975).

26. M. S. Kearney, P. B. Levine, "Early childhood education by MOOC: Lessons from Sesame Street" (NBER Working paper no. 104, National Bureau of Economic Research, Cambridge, MA, 2015).

ACKNOWLEDGMENTS

This work was funded in part by the Dean's Office of the Harvard Graduate School of Education. We are grateful to the HarvardX, MITx, and VPAL-Research research communities for comments and support and to three anonymous reviewers for helpful feedback. Data on HarvardX and MITx students are available from the Harvard Dataverse at <http://dx.doi.org/10.7910/DVN/29779>. These study files also include Stata code and log files for all analyses. Student-level data are restricted to qualified researchers approved by Harvard VPAL-Research. Esri data are available for a

fee from www.esri.com. The American Community Survey microdata are publicly available at www.ipums.org. The American Community survey ZIP Code-level data are available at http://factfinder2.census.gov/faces/nav/jsf/pages/download_center.xhtml.

SUPPLEMENTARY MATERIALS

www.sciencemag.org/content/350/6265/1245/suppl/DC1
Materials and Methods
Figs. S1 to S5
Tables S1 to S10
References (27–31)

19 April 2015; accepted 22 October 2015
10.1126/science.aab3782

WATER RESOURCES

Local flow regulation and irrigation raise global human water consumption and footprint

Fernando Jaramillo^{1,2*} and Georgia Destouni¹

Flow regulation and irrigation alter local freshwater conditions, but their global effects are highly uncertain. We investigated these global effects from 1901 to 2008, using hydroclimatic observations in 100 large hydrological basins. Globally, we find consistent and dominant effects of increasing relative evapotranspiration from both activities, and decreasing temporal runoff variability from flow regulation. The evapotranspiration effect increases the long-term average human consumption of fresh water by $3563 \pm 979 \text{ km}^3/\text{year}$ from 1901–1954 to 1955–2008. This increase raises a recent estimate of the current global water footprint of humanity by around 18%, to $10,688 \pm 979 \text{ km}^3/\text{year}$. The results highlight the global impact of local water-use activities and call for their relevant account in Earth system modeling.

Hydroclimatic changes on land determine the availability of freshwater resources required for human societies and ecosystems on Earth. However, the magnitude and key drivers of such changes historically (1, 2) and in the future (3) are highly uncertain, especially regarding the global role of human drivers and the magnitude of their related freshwater consumption. Both changes in the atmospheric climate and in the landscape may drive freshwater change (4, 5) (fig. S1). Among landscape changes, human-controlled flow regulation and irrigation (FRI) affect inter- and intra-annual freshwater conditions locally, but recent results indicate possible important effects on larger scales as well (6).

FRI developments over the past century have either moderately or strongly affected 59% of the world's largest river systems (7). They include around 45,000 large dams and many other smaller ones, spread over 140 countries around the world (8) and constructed mostly over the past century

to store water for irrigation, flood control, urban water supply, hydropower, or a combination of such purposes. These developments are linked with approximately 12 to 16% of the current global food production and 19% of the world's electricity supply (8), even though they only cover 0.3% (9) and 2% (10) of the global land area, respectively. Regarding the environmental impacts of FRI, attention so far has focused on ecosystem effects of river fragmentation and diversion (11) and water storage (12). More recently, studies at local to regional scales have found an FRI-related enhancement of the ratio of actual evapotranspiration (AET) to precipitation (P); i.e., of AET/P (6, 13, 14). For flow regulation, a concurrent decrease is also found in the short-term (daily and monthly) variability of runoff (R) (6, 14, 15). A combination of these effects on AET and R can be then used to distinguish the impacts of FRI developments from those of other drivers of freshwater change (6). At a global scale, some studies have addressed at least one of these FRI-related effects in global-scale modeling (16–21) but have not provided observation-based evidence of the global importance of FRI as a driver of freshwater change.

To fill this key observation gap, we analyzed global hydroclimatic data from 1901 to 2008 for

100 large hydrological basins (Fig. 1). For these basins, we computed hydroclimatic changes (supplementary materials) between the 54-year periods 1901–1954 and 1955–2008 and compared them with previously categorized impact levels (7, 11) and parameterized developments (9, 10) of FRI (table S1). From the results, we further quantified the magnitude of the FRI-driven hydroclimatic changes in each basin and assessed their implications for global human consumption of fresh water.

Globally, the quantified hydroclimatic changes reveal consistent characteristic signals of increased AET/P and decreased relative intra-annual variability of monthly runoff (CV_R) with higher FRI impact level (Fig. 2 and fig. S3). Further study of the distribution of AET/P changes among basins shows large variability (Fig. 3A and fig. S4), but still a significant AET/P increase with increasing basin measures of FRI development (Fig. 3, B and C). The latter measures are quantified from previous basin parameterization of total reservoir storage capacity (9) relative to basin area, specifically its change between 1901–1954 and 1955–2008 (ΔRES), and area equipped for irrigation (10) relative to basin area (I_A).

We also tested the possibility of the AET/P changes being explained by geographic basin location or atmospheric climate change. Specifically, we checked the relationship of AET/P change with relative potential evapotranspiration (PET/P, expressing water-relevant climate conditions in each basin) and change in PET/P (expressing water-relevant climate change occurring in the basin) (22). We did not find these explanatory patterns between AET/P change and PET/P or PET/P change (Fig. 3, D and E). Regarding PET/P, the water-limited basins ($PET/P > 1$) should have less water available for AET/P increase than the basins with mostly energy-limited conditions ($PET/P < 1$) (5, 22, 23). Rather, the relatively large AET/P increases in water-limited basins are consistent with irrigation developments occurring preferentially in their arid and semi-arid climates. Overall, changes in AET/P among the investigated basins are better explained by differences in the basin characteristics of reservoirs and irrigation than by differences in atmospheric climate conditions or their changes.

Changes in CV_R among the 100 basins are also variable (Fig. 4A), yet a dominant change pattern is seen as CV_R decreases with higher increase in

¹Department of Physical Geography and Bolin Centre for Climate Research, Stockholm University, SE-106 91, Stockholm, Sweden. ²Department of Biological and Environmental Sciences, University of Gothenburg, 40530 Göteborg, Sweden.

*Corresponding author. E-mail: fernando.jaramillo@natgeo.su.se

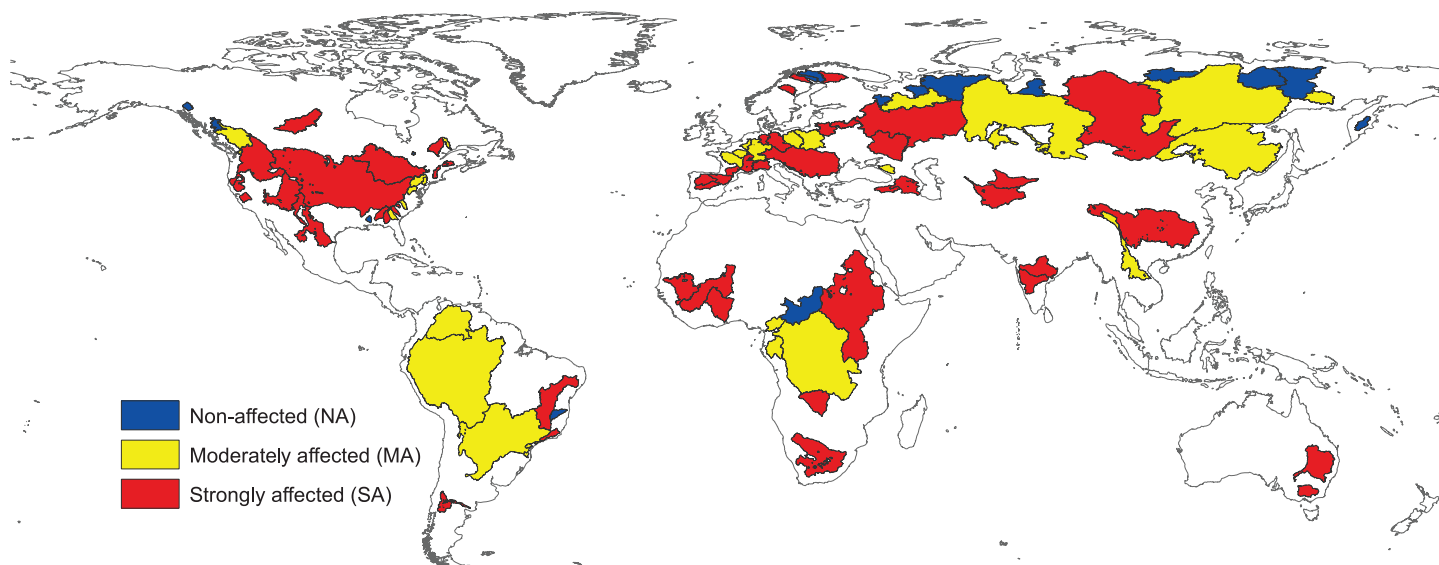


Fig. 1. Impact-level of (FRI) in 100 large hydrological basins. The global distribution of the 100 hydrological basins investigated in this study is shown. Colors differentiate the basins according to independent categorization of impacts of FRI (7, 11): non-affected (NA) in blue ($n = 17$ basins; 2,022,050 km² and 4% of total area); moderately affected (MA) in yellow ($n = 30$ basins; 20,695,803 km² and 46% of total area); and strongly affected (SA) in red ($n = 53$ basins; 22,578,466 km² and 50% of total area). The 100 basins cover a total area of 45,296,318 km² or 35% of the global land area, excluding Antarctica.

the relative storage capacity of reservoirs, ΔRES (Fig. 4B). Such a pattern should not be surprising as reservoir water management commonly aims at smoothing runoff variability. In general, CV_R changes are better explained by differences in the relative area equipped for irrigation among basins (Fig. 4C). This is understandable since irrigation does not per se imply the use of reservoir water storage that decreases CV_R ; the water used for irrigation can also be taken from groundwater and not all of the water reservoirs that decrease CV_R are used for irrigation. The CV_R changes are further not explained by atmospheric input conditions in terms of the relative intra-annual variability of monthly precipitation (CV_P) or the change in CV_P (Fig. 4, D and E). These results support previous regional findings of CV_R decrease as a flow regulation effect (6, 15) rather than an effect of irrigation per se, or of atmospheric input conditions or their changes.

Changes in AET/P and CV_R may also be driven by additional atmospheric climate conditions and changes to those we investigated [e.g., (24, 25)] and by other landscape drivers than FRI alone, such as deforestation, non-irrigated agricultural development, and/or other changes in landscape conditions for water storage and water phase [(5) and references therein]. The effects of such additional change drivers may explain more of the total variability of AET/P and CV_R changes among basins (Figs. 2 to 4 and figs. S4 and S5). Nevertheless, the FRI-related effects explain a large part of that variability. Overall, the FRI-related areas of surface water reservoirs and irrigation cover less than 3% (9) and 25% (10) of total basin area (maximum values for the Riviere aux Outardes and San Joaquin River basins), respectively. It is thus more as proxies for associated human water use, rather than as extensive land-use areas per

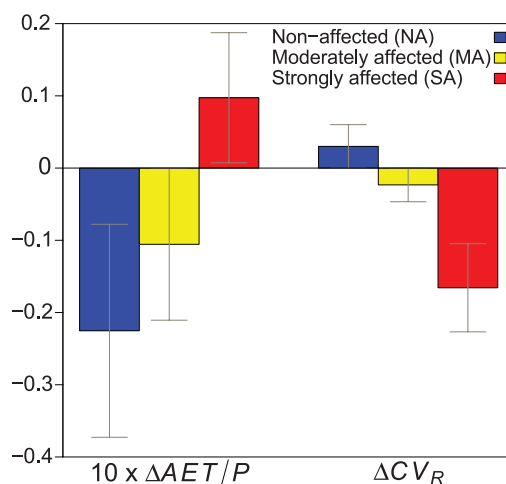


Fig. 2. Consistent FRI-related patterns of change in relative evapotranspiration and temporal runoff variability. Shown are the area-weighted mean (colored bars) and spatial standard deviation around the mean (whiskers) (supplementary materials) of changes in (left) the ratio of actual evapotranspiration to precipitation ($\Delta AET/P$) and (right) the relative intra-annual variability of monthly runoff (ΔCV_R), between the periods 1901–1954 and 1955–2008, in each FRI impact level.

se, that reservoir and irrigation extent measures can explain the FRI-related increase in AET/P and decrease in CV_R that were found on a global scale.

In order to estimate the absolute global FRI-related increase in AET, we assumed that, on average across the different world conditions and changes that are spanned by the basins of each FRI impact category, the change of area-normalized AET may be approximately similar among the three basin categories (Fig. 1), except for the FRI-related change component that distinguishes these categories. We applied this assumption in two different methods (see the supplementary materials) for estimating the FRI-related global AET change. Method 1 assumes similarity on average in all types of changes (except the FRI-related ones), whether they are driven by atmospheric climate change or by various (non-FRI) changes in the landscape. Method 2 assumes that only the landscape-driven changes

are, on average, similar among basin categories. In the estimation of global FRI-related AET increase, we also considered FRI-related changes in basin water storage that can be expected to be consumptive (7) because of the filling of constructed reservoirs and the use of groundwater for irrigation (26).

The combined estimates of methods 1 and 2 imply a global FRI-related increase in long-term average volumetric AET flow of 3563 ± 979 km³/year from 1901–1954 to 1955–2008. This implies an increased freshwater loss from the landscape to the atmosphere and thus a corresponding increase in the global human consumption of fresh water. Adding this FRI-related increase to previous estimates of global human freshwater consumption for various other sectors [in total, 807 km³/year (1) for non-irrigated agriculture, deforestation, industry, and municipalities] yields a total global human freshwater consumption of 4370 ± 979 km³/year. This long-term average

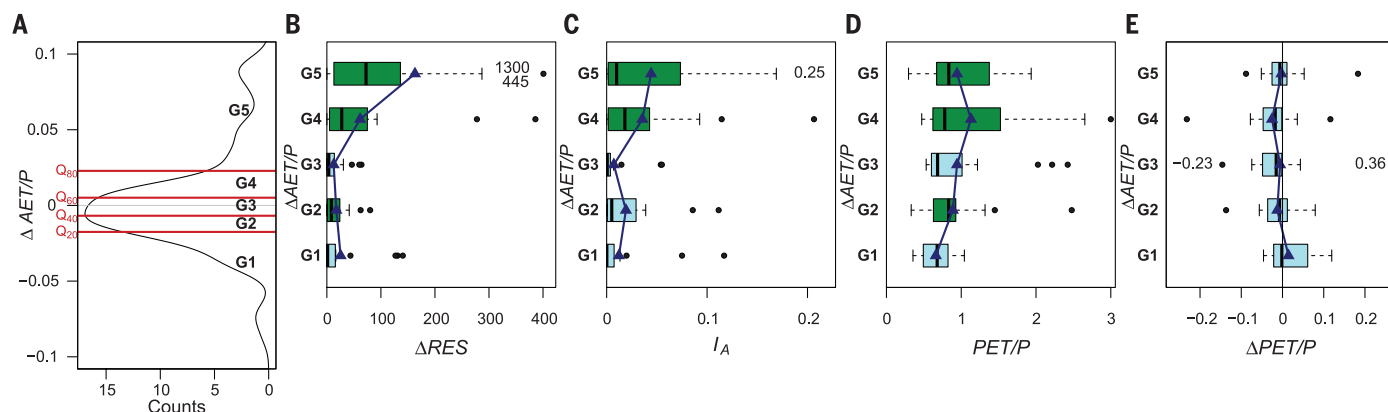


Fig. 3. Dominant human effects of FRI on relative evapotranspiration.

(A) Kernel density estimate curve of the distribution of changes in the ratio of actual evapotranspiration to precipitation ($\Delta AET/P$) between the periods 1901–1954 and 1955–2008 for 100 large basins in terms of (B) the change in total reservoir storage capacity relative to basin area between the two time periods (ΔRES ; in mm); (C) the area equipped for irrigation relative to basin area (I_A); (D) the ratio of potential evapotranspiration to precipitation (PET/P); and (E) the change in PET/P ; i.e., $\Delta PET/P$. The distribution of $\Delta AET/P$ is divided into five subgroups with 20 basins each: G1, the minimum value of $\Delta AET/P$ ($Q_{\min} = -0.09$) and the 20% quantile ($Q_{20} = -0.02$); G2, Q_{20} and the 40% quantile ($Q_{40} = -0.01$); G3, Q_{40} and the 60% quantile ($Q_{60} = 0.01$); G4, Q_{60} and the 80% quantile ($Q_{80} = 0.03$); and G5, between Q_{80} and the

maximum value of the distribution ($Q_{\max} = 0.10$). The box plots thus show the distribution of ΔRES , I_A , PET/P , and $\Delta PET/P$ values among the five subgroups. Box plot statistics include the arithmetic mean (blue triangles), median (thick vertical black lines), interquartile range (IQR) (boxes, colored blue or green depending on significance), whiskers (confidence interval of $\pm 1.58 \times IQR / \sqrt{20}$), and outliers (black circles). Values of outliers falling outside of the plot scale are also shown on the inner margin of each plot. The statistical significance ($P < 0.05$; by a one-sided unpaired Wilcoxon rank sum test) of the variable outcome distribution among the subgroups is shown by green box color when the variable values within a subgroup of the distribution are significantly greater than the variable values in at least one of the lower $\Delta AET/P$ subgroups (materials and methods of the supplementary materials). The P values of the statistical test are shown in table S4A.

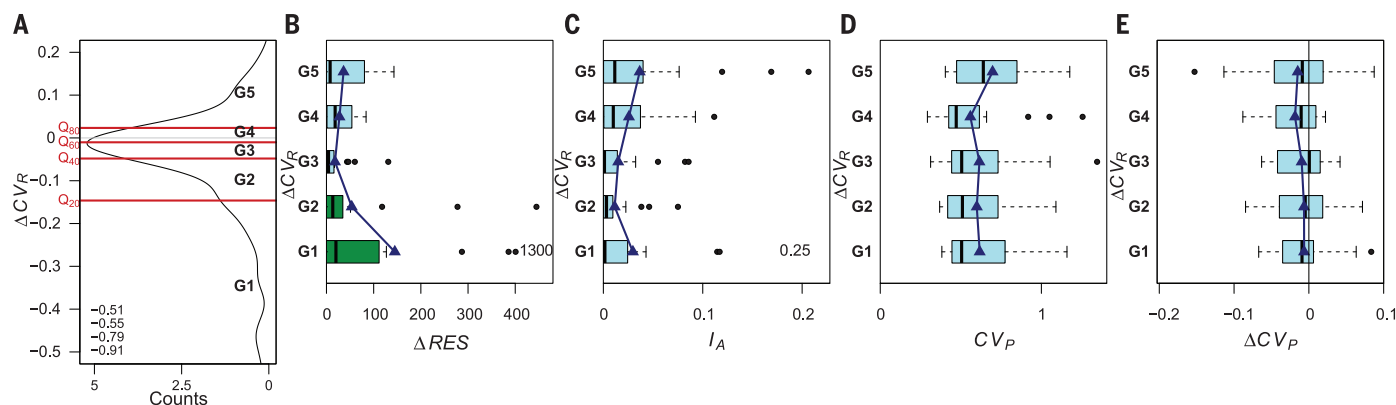


Fig. 4. Dominant human effect of flow regulation on temporal runoff variability.

(A) Kernel density estimate curve of the distribution of changes in relative intra-annual variability of monthly runoff (ΔCV_R) between the periods 1901–1954 and 1955–2008 for 100 large basins in terms of (B) the change in total reservoir storage capacity relative to basin area between the two time periods (ΔRES , in millimeters); (C) the area equipped for irrigation relative to basin area (I_A); (D) the relative intra-annual variability of monthly runoff (CV_P);

and (E) the change in CV_P ; i.e., ΔCV_P . The distribution of ΔCV_R is divided into five subgroups, and box plot statistics are shown similarly as in Fig. 3, where $Q_{\min} = -0.91$, $Q_{20} = -0.15$, $Q_{40} = -0.05$, $Q_{60} = -0.01$, $Q_{80} = 0.02$, and $Q_{\max} = 0.19$. Statistical significance is also tested and shown as in Fig. 3 but in this case regards whether the variable values within a subgroup of the distribution are significantly greater ($P < 0.05$) than the variable values in at least one of the higher ΔCV_R subgroups. The P values of the statistical test are shown in table S4B.

consumption over 1955–2008, including most of its uncertainty range, is above a proposed freshwater planetary boundary of 4000 km³/year (27) (fig. S6).

Furthermore, the FRI-related consumption increase from 1901–1954 to 1955–2008 corresponds to 39% of a recent estimate of 9087 km³/year for the current global water footprint of humanity (28). Updating the irrigation component of 1962 km³/year (with no flow regulation part) in the latter (29) by the present estimate of FRI-related water consumption raises the total global water

footprint of humanity by 18% to 10,688 \pm 979 km³/year; i.e., to a considerably more unsustainable level (30).

Even though coarse, the present estimates use a wide range of available long-term hydroclimatic observations for the quantification of FRI-related changes in global freshwater consumption. The results expand the uncertainty range of both the FRI-related and the total global human consumption of fresh water. They also show that worldwide observation data can and should be used to quantify global freshwater consumption effects of

FRI, in addition to only attempting to model such effects. Modeling alone may lead to considerable effect underestimation (9, 16, 21, 27, 31, 32) when compared with the present observation-based results. Finally, these results stress the importance of considering local water use as a key change driver in Earth system studies and in the modeling of global hydroclimatic change.

REFERENCES AND NOTES

1. F. Jaramillo, G. Destouni, *Science* **348**, 1217 (2015).
2. D. Gerten *et al.*, *Science* **348**, 1217 (2015).

3. A. Bring *et al.*, Implications of freshwater flux data from the CMIP5 multimodel output across a set of Northern Hemisphere drainage basins. *Earths Future* 2014EF000296 (2015).
4. P. C. D. Milly *et al.*, *Science* **319**, 573–574 (2008).
5. F. Jaramillo, G. Destouni, *Geophys. Res. Lett.* **41**, 8377–8386 (2014).
6. G. Destouni, F. Jaramillo, C. Prieto, *Nat. Clim. Change* **3**, 213–217 (2013).
7. C. Nilsson, C. A. Reidy, M. Dynesius, C. Revenga, *Science* **308**, 405–408 (2005).
8. World Commission on Dams, *Dams and Development: A New Framework for Decision-Making* (Dams and Development Project, United Nations Environment Programme, Nairobi Kenya; Earthscan, London, 2000).
9. B. Lehner *et al.*, *Front. Ecol. Environ* **9**, 494–502 (2011).
10. S. Siebert, V. Henrich, K. Frenken, J. Burke, *Global Map of Irrigation Areas*, version 5 (Rheinische Friedrich-Wilhelms-University, Bonn, Germany/Food and Agriculture Organization of the United Nations, Rome, Italy, 2013).
11. M. Dynesius, C. Nilsson, *Science* **266**, 753–762 (1994).
12. C. J. Vorösmarty *et al.*, *Ambio* **26**, 210–219 (1997).
13. Y. Shibuo, J. Jarsjö, G. Destouni, *Geophys. Res. Lett.* **34**, L21406 (2007).
14. L. Levi, F. Jaramillo, R. Andrićević, G. Destouni, *Ambio* **44**, 624–634 (2015).
15. N. L. Poff, J. D. Olden, D. M. Merritt, D. M. Pepin, *Proc. Natl. Acad. Sci. U.S.A.* **104**, 5732–5737 (2007).
16. P. Döll, K. Fiedler, J. Zhang, *Hydrol. Earth Syst. Sci.* **13**, 2413–2432 (2009).
17. O. Boucher, G. Myhre, A. Myhre, *Clim. Dyn.* **22**, 597–603 (2004).
18. S. Piao *et al.*, *Proc. Natl. Acad. Sci. U.S.A.* **104**, 15242–15247 (2007).
19. S. Rost, D. Gerten, U. Heyder, *Adv. Geosci.* **18**, 43–50 (2008).
20. I. Haddeland, T. Skaugen, D. P. Lettenmaier, *Geophys. Res. Lett.* **33**, L08406 (2006).
21. S. M. Sterling, A. Ducharme, J. Polcher, *Nat. Clim. Change* **3**, 385–390 (2013).
22. M. I. Budyko, *Climate and Life* (Academic Press, 1974).
23. V. K. Arora, *J. Hydrol. (Amst.)* **265**, 164–177 (2002).
24. P. C. D. Milly, *Water Resour. Res.* **30**, 2143–2156 (1994).
25. W. R. Berghuijs, R. A. Woods, M. Hrachowitz, *Nat. Clim. Change* **4**, 583–586 (2014).
26. S. Siebert *et al.*, *Hydrol. Earth Syst. Sci.* **14**, 1863–1880 (2010).
27. W. Steffen *et al.*, *Science* **347**, 1259855 (2015).
28. A. Y. Hoekstra, M. M. Mekonnen, *Proc. Natl. Acad. Sci. U.S.A.* **109**, 3232–3237 (2012).
29. M. M. Mekonnen, A. Y. Hoekstra, *Hydrol. Earth Syst. Sci.* **15**, 1577–1600 (2011).
30. A. Y. Hoekstra, T. O. Wiedmann, *Science* **344**, 1114–1117 (2014).
31. S. Rost *et al.*, *Water Resour. Res.* **44**, W09405 (2008).
32. M. M. Mekonnen, A. Y. Hoekstra, *Hydrol. Earth Syst. Sci.* **16**, 179–187 (2012).

ACKNOWLEDGMENTS

The Swedish Research Council (VR, project 2009-3221), the strategic environmental research project Ekoklim at Stockholm University, and the BECC strategic research area of Lund University and the University of Gothenburg have funded this study. All data used in our analysis are included in the supplementary materials available on Science Online. The authors thank the anonymous reviewers for their suggestions and recommendations, which have considerably improved this manuscript, as well as J.-O. Persson from the Department of Mathematics at Stockholm University for his statistical advice.

SUPPLEMENTARY MATERIALS

www.sciencemag.org/content/350/6265/1248/suppl/DC1
Materials and Methods
Figs. S1 to S7
Tables S1 to S4
References (33–62)

28 July 2015; accepted 3 November 2015
10.1126/science.12481010

NEURODEVELOPMENT

Single-cell transcriptomics reveals receptor transformations during olfactory neurogenesis

Naresh K. Hanchate,¹ Kunio Kondoh,¹ Zhonghua Lu,¹ Donghui Kuang,¹ Xiaolan Ye,¹ Xiaojie Qiu,^{2,3} Lior Pachter,⁴ Cole Trapnell,^{2*} Linda B. Buck^{1*}

The sense of smell allows chemicals to be perceived as diverse scents. We used single-neuron RNA sequencing to explore the developmental mechanisms that shape this ability as nasal olfactory neurons mature in mice. Most mature neurons expressed only one of the ~1000 odorant receptor genes (*Olfrs*) available, and at a high level. However, many immature neurons expressed low levels of multiple *Olfrs*. Coexpressed *Olfrs* localized to overlapping zones of the nasal epithelium, suggesting regional biases, but not to single genomic loci. A single immature neuron could express *Olfrs* from up to seven different chromosomes. The mature state in which expression of *Olf* genes is restricted to one per neuron emerges over a developmental progression that appears to be independent of neuronal activity involving sensory transduction molecules.

Odor detection in mammals is mediated by odorant receptors on olfactory sensory neurons (OSNs) in the nasal olfactory epithelium (1, 2). In mice, ~1000 odorant receptor genes (*Olfrs*) and 350 pseudogenes reside at dozens of distinct loci on 17 of 21 chromosomes (3–5). Each *Olf* is expressed by a small subset of OSNs scattered in one epithelial spatial zone (6–8). Previous studies suggest that each mature OSN expresses one intact *Olf* allele, but some coexpress an *Olf* pseudogene (9–11). In a prevailing model of “OR [*Olf*] gene choice,” the developing OSN selects a single *Olf* allele for expression, and the encoded receptor provides feedback that prevents expression of other *Olfrs* (12–17). OSNs are generated in a developmental progression from progenitors to precursors to immature OSNs to mature OSNs (18, 19). We investigated when and how the developing OSN selects one *Olf* for expression.

We used single-cell RNA sequencing (RNA-seq) (20) to analyze the transcriptomes of single epithelial neurons during development. We first prepared cDNA libraries from single isolated cells (10) and analyzed the libraries for markers of the four stages of OSN development, using polymerase chain reaction. We then conducted Illumina sequencing (21) of libraries from multiple cells in each stage, as well as duplicate libraries from some cells. We used TopHat (22) and Cufflinks (23) to identify genes expressed in each

cell and to estimate their relative mRNA abundances (see fig. S1 for technical quality metrics).

We compared 85 cell transcriptomes using Monocle, an unsupervised algorithm that determines each cell’s stage of differentiation in “pseudotime,” which represents progress through gene expression changes during development (24). Monocle showed a linear nonbranching trajectory of development (Fig. 1A). Based on cell stage markers in individual transcriptomes, the trajectory reflects the developmental progression from progenitors through mature OSNs. The following gene markers were used: for progenitors, *Ascl1* (achaete-scute complex homolog 1); for precursors, *Neurog1* (neurogenin 1) and/or *Neurod1* (neurogenic differentiation 1); for immature OSNs, *Gap43* (growth-associated protein 43) and/or *Gng8* (guanine nucleotide-binding protein gamma 8); and for mature OSNs, *Omp* (olfactory marker protein) and four olfactory sensory transduction molecules downstream of odorant receptors—*Gnal* (guanine nucleotide binding protein, alpha stimulating, olfactory type), *Adcy3* (adenylate cyclase 3), *Cnga2* (cyclic nucleotide gated channel alpha 2), and *Cnga4* (cyclic nucleotide gated channel alpha 4) (18, 19).

Immature OSNs were further divided into two subsets based on their expression of olfactory sensory transduction molecules. Early immature OSNs lacked one or more olfactory transduction molecules, whereas late immature OSNs expressed all four (Fig. 2).

A total of 3830 genes were differentially expressed over development. Clusters of genes changed in expression during specific developmental periods, suggesting sequential large and coordinated changes in gene expression during OSN development (Fig. 1B and table S1). By gene ontology, most clusters contained genes associated with transcriptional regulation and/or chromatin modification, suggesting potential regulators of development (table S1). In kinetic diagrams, markers of early and late

¹Howard Hughes Medical Institute, Basic Sciences Division, Fred Hutchinson Cancer Research Center, 1100 Fairview Avenue North, Seattle, WA 98109, USA. ²Department of Genome Sciences, University of Washington, Seattle, WA 98115, USA. ³Molecular and Cellular Biology Program, University of Washington, Seattle, WA 98115, USA. ⁴Departments of Mathematics, Molecular and Cell Biology, and Electrical Engineering and Computer Sciences, University of California–Berkeley, Berkeley, CA 94720, USA.
*Corresponding author. E-mail: coletrap@uw.edu (C.T.); lbuck@fhcr.org (L.B.B.)

developmental stages show peak expression early and late in the developmental progression, respectively (Fig. 1C and fig. S2).

Olfr expression first appeared at the late precursor to early immature OSN stages (Fig. 2). *Olfr* transcripts were found in one of nine precursors, 38 of 40 immature OSNs, and 25 of 25 mature OSNs (Fig. 2). None were seen in two non-neuronal epithelial supporting cells or in three cells of undetermined type. Overall, the number of *Olfr* transcripts per cell increased over OSN development (Fig. 2A). In early immature, late immature, and mature OSNs, *Olfrs* were detected at an average of 1998, 4146, and 8169 FPKM (fragments per kilobase of transcript per million mapped reads), respectively, with median values of 930, 2575, and 4026 FPKM. Transcripts of individual *Olfrs* were detected at an average of 657, 2156, and 6382 FPKM, with median values of 99, 807, and 2672 FPKM.

These studies indicate that the developing OSN can initially express multiple *Olfrs* (Fig. 2). Roughly half (48%, 12 of 25) of early immature OSNs with *Olfrs* expressed >1 *Olfr*. Coexpression of different *Olfrs* in single neurons declined as development progressed, with 46% (6 of 13) of late immature and 24% (6 of 25) of mature OSNs expressing >1 *Olfr*. Moreover, single early immature OSNs expressed up to 12 different *Olfrs*, whereas mature OSNs with >1 *Olfr* expressed two or at most three (Fig. 2B).

Early immature and mature OSNs with >1 *Olfr* also differed in the relative abundance of different *Olfr* transcripts (Fig. 2C). Most (10 of 12) of the early immature OSNs had similarly low levels of different *Olfrs*. The most abundant *Olfr* was detected at 55 to 396 FPKM in individual neurons and the next highest at, on average, 60.5% of this level (median, 60.1%). However, in three of six mature OSNs with >1 *Olfr*, the most abundant

was detected at 14,557 to 18,056 FPKM, with the next highest, on average, only 3.3% as abundant (median, 0.5%).

In mature OSNs, *Olfr* and *Omp* transcripts averaged 8169 and 10,167 FPKM per cell, respectively. However, 6 of 12 early immature OSNs that expressed >1 *Olfr* did not express *Omp* (Fig. 2D), arguing against the possibility that the *Olfr* transcripts detected were due to contamination from mature OSNs.

Data from eight duplicate cell samples (technical replicates) were analyzed (figs. S3 and S4). The duplicates confirmed the expression of >1 *Olfr* in specific OSNs (table S2). The data were consistent with reported stochastic losses of low-copy number transcripts in single-cell RNA-seq data. *Olfrs* present in both replicates tended to be expressed at higher levels, and those present in only one replicate tended to be expressed at lower levels.

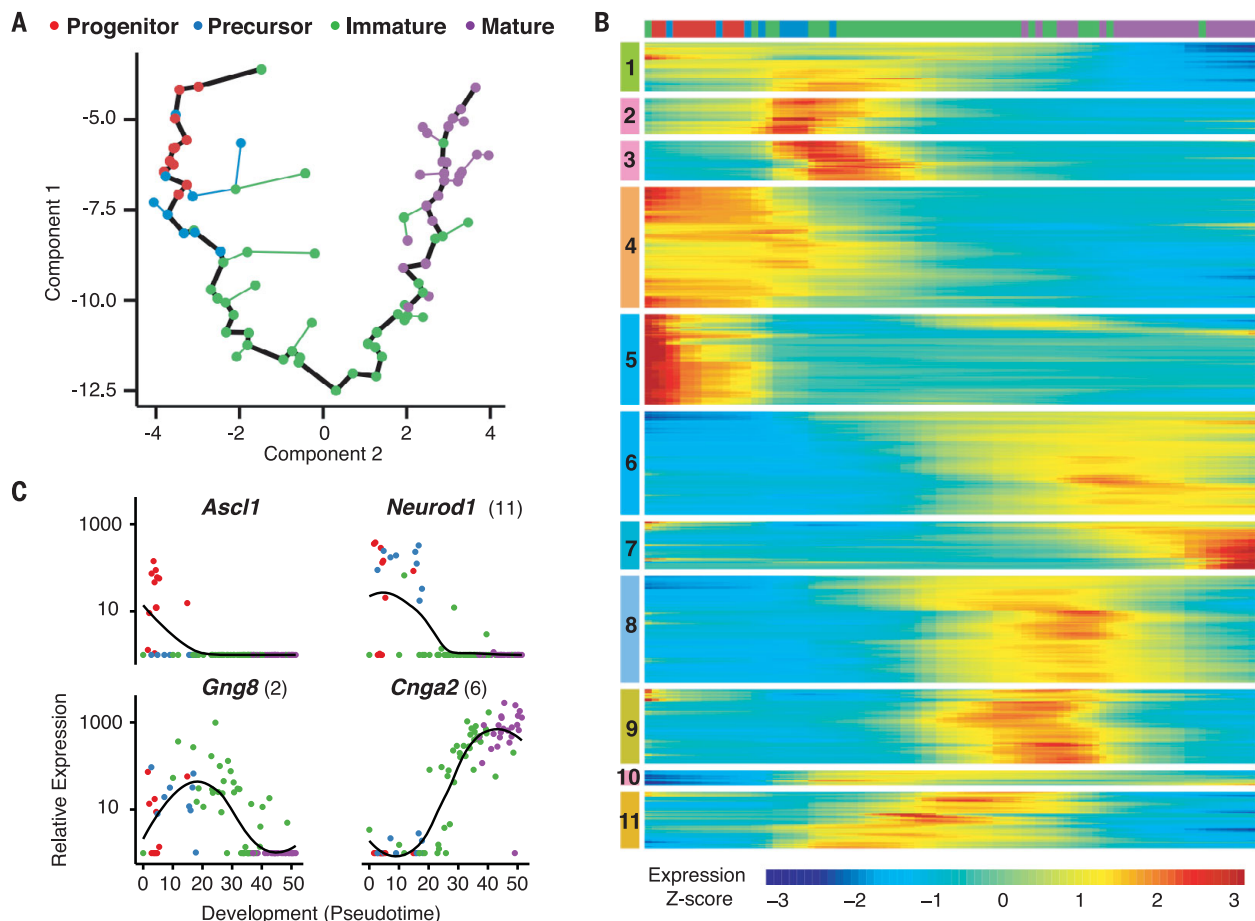


Fig. 1. Olfactory neurons exhibit large-scale shifts in gene expression during development. (A) Unsupervised analysis of single-cell gene expression profiles with Monocle revealed a linear trajectory (black line) along which cells develop in pseudotime. Coloring of cells based on the expression of developmental markers shows that the trajectory corresponds to a stepwise development from olfactory progenitors to precursors to immature OSNs to mature OSNs. (B) Global analysis of gene expression kinetics along the trajectory identified 3830 genes that vary significantly over developmental pseudotime (false discovery rate < 5%, determined by a Tobit-valued generalized linear model likelihood ratio test; supplementary materials). Hierarchical clustering of these genes via Ward's method recovered 11 nonredundant groups

that covary over the trajectory. Cluster analysis indicates that multiple large shifts in gene expression occur as neurons progress through development. The bar on top shows the locations of individual cells, colored by stage of development, along this developmental trajectory. The Expression Z score indicates changes in a gene relative to its dynamic range over pseudotime. (C) Kinetic diagrams show the expression of known markers of different developmental stages over the developmental progression. Numbers in parentheses indicate the groups in which genes are found in (B). Dots indicate individual cells and are colored according to developmental stage. Black lines indicate local polynomial regression smoothing (span, 0.75; degree, 2) of log-transformed FPKM values over developmental pseudotime.

The above results indicate that early immature OSNs can express low levels of multiple *Olfr*s, but, during subsequent development, two changes typically occur. Expression favors one *Olfr* by up to 100 times or more, and the expression of additional *Olfr*s declines or disappears.

To validate these findings, we used RNA–dual fluorescence in situ hybridization (dual RNA-FISH) with nasal tissue sections. At postnatal day 3 (P3), a peak time of OSN neurogenesis (19, 25), 0.22 ± 0.05 to $0.22 \pm 0.12\%$ of neurons labeled for a single *Olfr* were colabeled with a mix of probes for other *Olfr*s expressed in the same nasal zone (Fig. 3A and table S3). Neurogenesis decreases as mice mature, and no colabeled cells were seen in adults. Using a highly sensitive RNA-FISH method with branched DNA signal amplification (26), 0.41 ± 0.09 to $0.60 \pm 0.13\%$ of cells labeled for one *Olfr* were co-labeled for another *Olfr* at P3, and 0.10 ± 0.02 to $0.18 \pm 0.05\%$ were co-labeled for another at P21 (Fig. 3B and table S4). Among

neurons labeled for one *Olfr*, the percentage colabeled for the immature OSN markers *Gap43* and *Gng8* also changed, respectively, from $80.1 \pm 3.2\%$ and $62.8 \pm 0.9\%$ at P3 to $19.5 \pm 0.5\%$ and $14.3 \pm 1.1\%$ at P21 (table S5). These results confirm that single OSNs can express more than one *Olfr* and suggest that *Olfr* coexpression occurs predominantly, if not exclusively, in immature OSNs.

To examine whether odorant receptor-induced neuronal activity might be involved in the observed developmental shift in *Olfr* expression, we analyzed transcriptome data for the expression of olfactory sensory transduction molecules: *Gnal* (or *Gnas*, which may substitute for *Gnal*), *Adcy3*, *Cnga2*, and *Cnga4*. All four molecules were expressed in 6 of 18 immature OSNs and 6 of 6 mature OSNs with >1 *Olfr* (Fig. 2D). Furthermore, one or more were absent in data from 13 of 20 immature and 3 of 19 mature OSNs with only one *Olfr*. These results suggest

that odorant receptor-induced neuronal activity is neither necessary nor sufficient for the decline in coexpressed *Olfr*s during development.

We next tested whether the developing OSN is restricted to activating *Olfr*s expressed in a particular nasal zone. Using dual RNA-FISH, we compared the nasal expression patterns of 11 pairs of *Olfr*s coexpressed in six different OSNs. In every case, the paired *Olfr*s were expressed either in the same spatial zone or in partially overlapping zones (Fig. 3C and table S6). These results suggest that the developing neuron is restricted to the expression of a particular *Olfr* regional gene set, which can include *Olfr*s with only partially overlapping expression patterns in the adult.

To investigate whether early coexpression of multiple *Olfr*s could result from chromatin changes at a single genomic locus containing those *Olfr*s, we determined the chromosome locations of *Olfr*s coexpressed in individual OSNs. For OSNs expressing 4 to 12 *Olfr*s, coexpressed *Olfr*s mapped

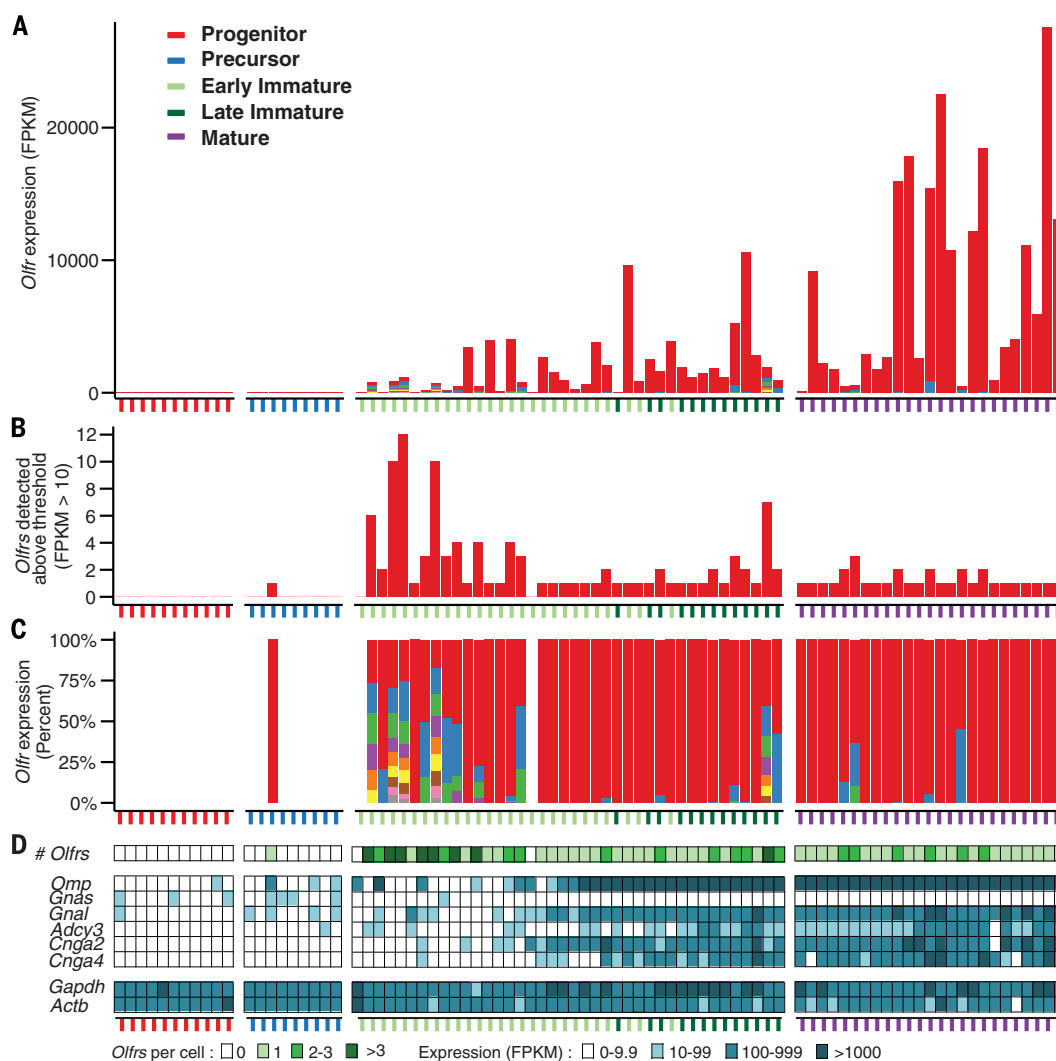


Fig. 2. Immature neurons can express multiple *Olfr*s. (A) Neurons assigned to different developmental stages were arranged by developmental progress, as measured in pseudotime. Different developmental stages are indicated by differently colored ticks.

Different *Olfr*s are represented by different colors in the bars. The total number of *Olfr* transcripts per cell shows a steady, though variable, increase during development. (B) Multiple different *Olfr* transcripts were detected in 12 of 25 early immature, 6 of 13 late immature, and 6 of 25 mature OSNs with *Olfr* transcripts. (C) The number of different *Olfr* transcripts per cell was highest in early immature OSNs and then declined over development. Early immature OSNs tended to express similar levels of different *Olfr*s. In contrast, the majority of mature OSNs expressed only one *Olfr* or high levels of one *Olfr* and low levels of one or two additional *Olfr*s. Each color in a bar represents a single *Olfr*, except gray, which represents >1 *Olfr*. (D) *Olfr*s stimulate neuronal activity via mechanisms involving sensory transduction molecules encoded by *Gnal* (or possible *Gnas* in immature OSNs), *Adcy3*, *Cnga2*, and *Cnga4*. Six immature and six mature neurons with >1 *Olfr* expressed all four genes, suggesting that neuronal activity downstream of odorant receptors

is not what reduces the number of *Olfr*s expressed per neuron. *Omp*, which is highly expressed in mature OSNs, was absent from six early immature OSNs with >1 *Olfr*, arguing against contamination from mature OSNs. *Gapdh* and *Actb* are housekeeping genes.

to three to seven different chromosomes and four to nine distinguishable *Olfr* gene loci (Fig. 4 and table S7). Thus, the immature OSN is not restricted to expressing *Olfr*s from a single chromosomal region.

Odor detection in the mouse nose is mediated by 1000 different odorant receptors, each expressed by a different subset of sensory neurons. We asked when and how a neuron comes to express a single *Olfr*. We found that the developing neuron can express low levels of multiple *Olfr*s. As development proceeds, this ability declines. The mature neuron typically expresses high levels of a single

Olfr. Coexpressed *Olfr*s tend to be expressed by other neurons in the same region of the olfactory epithelium, suggesting regional biases in *Olfr* gene choice, but they can reside at multiple chromosomal locations.

How does the developing OSN transition from expressing low levels of multiple *Olfr*s to expressing a high level of a single *Olfr*? One possibility is a “winner-take-all” mechanism. In this model, multiple *Olfr*s are initially expressed, but one becomes dominant—for example, by the capture of limiting factors required for high-level *Olfr* expression (fig. S5). In an alternative model, selection of a

single *Olfr* for high-level expression occurs independently of those initially expressed. In either model, early low-level expression of other *Olfr*s could subside, owing to the closing of a developmental time window or to feedback signals generated by the highly expressed *Olfr*. OSNs expressing multiple *Olfr*s are probably not pruned by apoptosis, as suggested for OSNs in the nasal septal organ (27), given genetic evidence that some OSNs expressing one *Olfr* previously expressed another (13). This *Olfr* “switching” may reflect the early expression of more than one *Olfr* per immature OSN, as observed in this study.

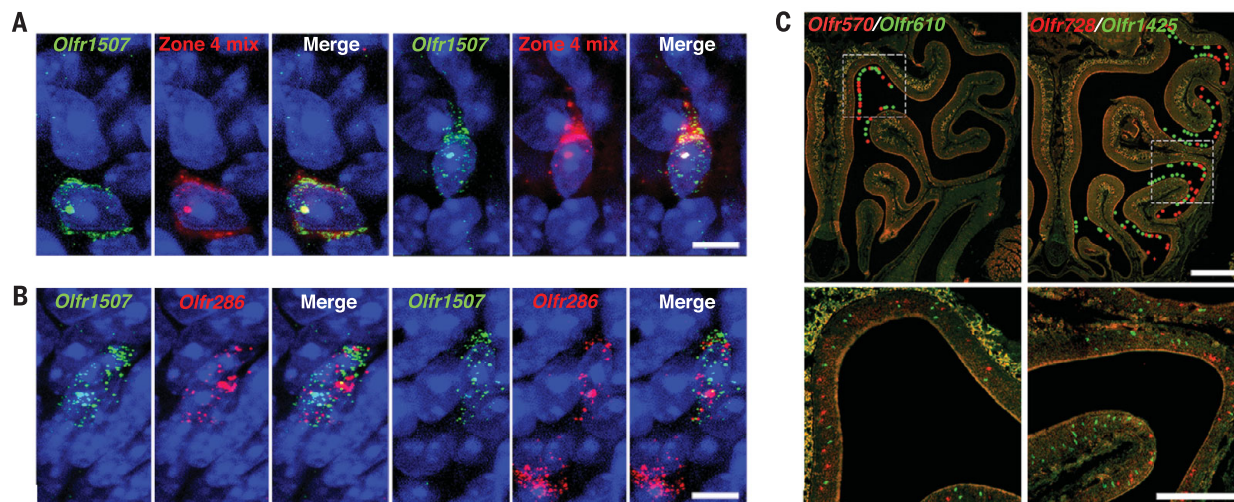


Fig. 3. *Olfr*s expressed in the same neuron belong to a regional gene set. (A) Dual RNA-FISH of P3 tissue sections using a conventional method showed a small percentage of OSNs co-labeled with an *Olfr1507* probe and a mix of probes for other *Olfr*s expressed in the same zone (zone 4). Cell nuclei were counterstained with 4',6-diamidino-2-phenylindole (blue). Two co-labeled cells are shown, one on the left half and the other on the right half of the panel. Scale bar, 5 μm. (B) Dual RNA-FISH of P3 tissue sections using a highly sensitive method showed a small percentage of OSNs coexpressing *Olfr1507* and *Olfr286*. Two co-labeled cells are shown [as in (A)], and a cell labeled with

only one probe (red only) is also shown on the right. Scale bar, 5 μm. (C) Dual RNA-FISH shows that *Olfr*s coexpressed in single immature OSNs (neurons D200 or D243) are singly expressed in neurons in the same or partially overlapping zones in adult olfactory epithelium sections. This correspondence suggests that *Olfr* expression in the immature OSN is restricted to a spatially determined set of *Olfr* genes. In the upper row, colored dots indicate the locations of labeled neurons. Boxed areas in the upper row are shown at higher magnification in the lower row. Scale bars, 500 μm (upper row) and 250 μm (lower row).

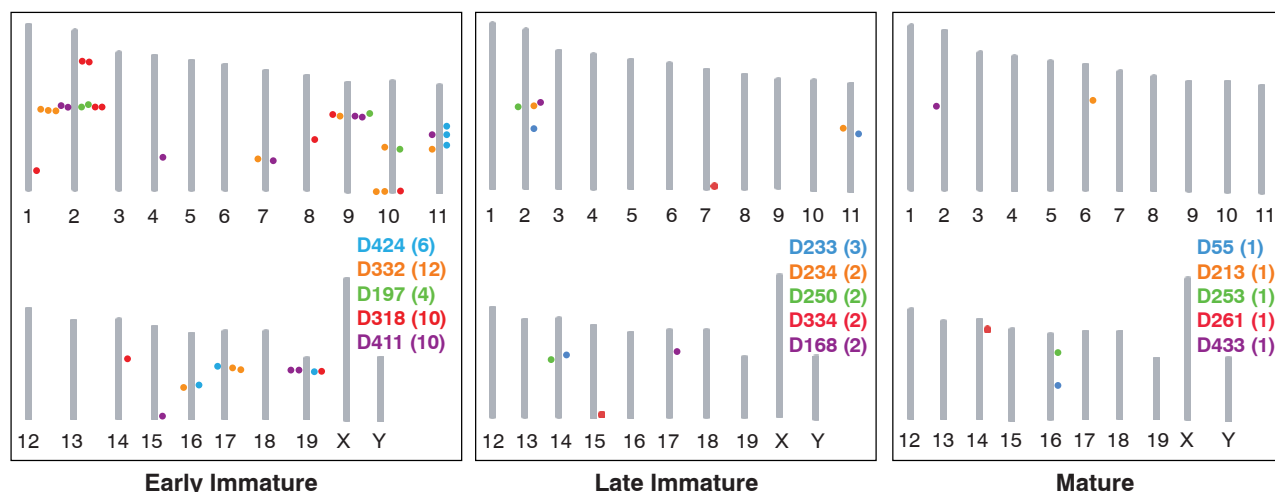


Fig. 4. Immature neurons coexpress *Olfr*s from multiple chromosomal loci. Diagrams show the chromosomal locations of *Olfr*s expressed in single OSNs of different stages. Each mouse chromosome is indicated by a vertical bar with its number below. The names of neurons, parenthesized number of *Olfr*s per neuron, and dots indicating the chromosomal locations of those *Olfr*s are shown in different colors for different neurons.

REFERENCES AND NOTES

1. L. Buck, R. Axel, *Cell* **65**, 175–187 (1991).
2. L. B. Buck, C. Bargmann, in *Principles of Neuroscience*, E. Kandel, J. Schwartz, T. Jessell, S. Siegelbaum, A. J. Hudspeth, Eds. (McGraw-Hill, New York, 2012), pp. 712–742.
3. X. Zhang, S. Firestein, *Nat. Neurosci.* **5**, 124–133 (2002).
4. P. A. Godfrey, B. Malnic, L. B. Buck, *Proc. Natl. Acad. Sci. U.S.A.* **101**, 2156–2161 (2004).
5. Y. Niimura, M. Nei, *Gene* **346**, 13–21 (2005).
6. K. J. Ressler, S. L. Sullivan, L. B. Buck, *Cell* **73**, 597–609 (1993).
7. R. Vassar, J. Ngai, R. Axel, *Cell* **74**, 309–318 (1993).
8. K. Miyamichi, S. Serizawa, H. M. Kimura, H. Sakano, *J. Neurosci.* **25**, 3586–3592 (2005).
9. A. Chess, I. Simon, H. Cedar, R. Axel, *Cell* **78**, 823–834 (1994).
10. B. Malnic, J. Hirono, T. Sato, L. B. Buck, *Cell* **96**, 713–723 (1999).
11. S. Serizawa *et al.*, *Science* **302**, 2088–2094 (2003).
12. S. Serizawa, K. Miyamichi, H. Sakano, *Trends Genet.* **20**, 648–653 (2004).
13. B. M. Shykind *et al.*, *Cell* **117**, 801–815 (2004).
14. J. W. Lewcock, R. R. Reed, *Proc. Natl. Acad. Sci. U.S.A.* **101**, 1069–1074 (2004).
15. R. P. Dalton, D. B. Lyons, S. Lomvardas, *Cell* **155**, 321–332 (2013).
16. M. Q. Nguyen, Z. Zhou, C. A. Marks, N. J. Ryba, L. Belluscio, *Cell* **131**, 1009–1017 (2007).
17. R. P. Dalton, S. Lomvardas, *Annu. Rev. Neurosci.* **38**, 331–349 (2015).
18. D. J. Nicolay, J. R. Doucette, A. J. Nazarali, *Cell. Mol. Neurobiol.* **26**, 801–819 (2006).
19. D. J. Rodriguez-Gil *et al.*, *Proc. Natl. Acad. Sci. U.S.A.* **112**, 5821–5826 (2015).
20. S. Islam *et al.*, *Genome Res.* **21**, 1160–1167 (2011).
21. D. R. Bentley *et al.*, *Nature* **456**, 53–59 (2008).
22. D. Kim *et al.*, *Genome Biol.* **14**, R36 (2013).
23. C. Trapnell *et al.*, *Nat. Biotechnol.* **28**, 511–515 (2010).
24. C. Trapnell *et al.*, *Nat. Biotechnol.* **32**, 381–386 (2014).
25. J. W. Hinds, P. L. Hinds, *J. Comp. Neurol.* **169**, 15–40 (1976).
26. M. L. Collins *et al.*, *Nucleic Acids Res.* **25**, 2979–2984 (1997).
27. H. Tian, M. Ma, *Mol. Cell. Neurosci.* **38**, 484–488 (2008).

ACKNOWLEDGMENTS

We thank J. Delrow, A. Marty, and A. Dawson at the Fred Hutchinson Cancer Research Center (FHCRC) Genomics Facility for assistance with RNA-seq; M. Fitzgibbon and J. Davidson at the FHCRC Bioinformatics Resource for early assistance with sequence analyses; and J. Vasquez and the FHCRC Scientific Imaging Facility for help with confocal microscopy. We also thank members of the Buck laboratory for helpful discussions. This work was supported by the Howard Hughes Medical Institute (L.B.B.), NIH grants R01 DC009324 (L.B.B.) and DP2 HD088158 (C.T.), an Alfred P. Sloan Fellowship (C.T.), and a Dale F. Frey Award for Breakthrough Scientists from the Damon Runyon Cancer Research Foundation (C.T.). L.B.B. is on the Board of Directors of International Flavors & Fragrances. The supplementary materials contain additional data. N.K.H., C.T., and L.B.B. designed the research; N.K.H. and C.T. performed the research; N.K.H., C.T., K.K., Z.L., D.K., X.Y., X.Q., and L.B.B. analyzed the data; L.P. provided guidance; and N.K.H., C.T., and L.B.B. wrote the paper. Raw sequencing data related to this study have been archived in the Gene Expression Omnibus (GEO) database under accession number GSE75413 (available at www.ncbi.nlm.nih.gov/geo/query/acc.cgi?acc=GSE75413).

SUPPLEMENTARY MATERIALS

www.sciencemag.org/content/350/6265/1251/suppl/DC1
Materials and Methods

Figs. S1 to S5
Tables S1 to S7
References (28–35)

13 August 2015; accepted 27 October 2015
Published online 5 November 2015
10.1126/science.12456

PROTECTED AREAS

Protected areas and global conservation of migratory birds

Claire A. Runge,^{1,2*} James E. M. Watson,^{1,3} Stuart H. M. Butchart,⁴ Jeffrey O. Hanson,⁵ Hugh P. Possingham,^{5,6} Richard A. Fuller⁵

Migratory species depend on a suite of interconnected sites. Threats to unprotected links in these chains of sites are driving rapid population declines of migrants around the world, yet the extent to which different parts of the annual cycle are protected remains unknown. We show that just 9% of 1451 migratory birds are adequately covered by protected areas across all stages of their annual cycle, in comparison with 45% of nonmigratory birds. This discrepancy is driven by protected area placement that does not cover the full annual cycle of migratory species, indicating that global efforts toward coordinated conservation planning for migrants are yet to bear fruit. Better-targeted investment and enhanced coordination among countries are needed to conserve migratory species throughout their migratory cycle.

From the writings of Aristotle (1) to the musings of Gilbert White in Georgian England (2), migratory birds have fascinated and inspired people for generations. Migrants undertake remarkable journeys, from endurance flights exceeding 10,000 km by bar-tailed godwits (*Limosa lapponica*) (3) to the annual relay of arctic terns (*Sterna paradisaea*), which fly the equivalent of the distance to the moon and back three times during their lives (4). Migratory species make major contributions to resource fluxes, biomass transfer, nutrient transport, predator-prey interactions, and food-web structure within and among ecosystems (5) and play an important role in human culture (6). Yet more than half of migratory birds across all major flyways have declined over the past 30 years (7).

Threats in any one part of a annual cycle can affect the entire population of a migratory species (8), and so environmental management actions for migrants need to be coordinated across habitat types, seasons, and jurisdictions (8). Protected area designation is a widely used approach for averting species loss (9) because it can reduce habitat loss, habitat degradation, hunting pressure, and disturbance (10). Yet the extent to which the distributions of migratory species are covered by protected areas globally is poorly understood. Many previous global and regional species conservation assessments and prioritization analyses either omit parts of the annual cycle or treat all species' distributions as static (9–12). Here, we explore how protected area coverage of migra-

tory birds varies across their annual cycle and among countries and compare their current levels of protected area coverage against standard conservation targets. Overlaying maps of protected areas (13) onto distribution maps of the world's birds, we assessed whether the proportion of each species' distribution covered by protected areas met a target threshold (9, 11). For migratory species, we set targets for each stage of the annual cycle separately for the 1451 migratory birds, with mapped distributions throughout their annual cycle.

We discovered that 91% of migratory bird species have inadequate protected area coverage for at least one part of their annual cycle, despite individual elements of the annual cycle being well protected for some species (Table 1). This is in stark contrast to 55% of nonmigratory species with inadequate protected area coverage across their global distribution. A typical migrant relies on two or three disjoint geographic locations, and the chance that they are all adequately conserved is probabilistically lower than for a single location (supplementary materials). We found that migratory species are less likely to meet protection targets as the number of seasonal areas increases and that the proportion of migratory species meeting targets is consistent with randomly allocated conservation effort (Fig. 1), indicating that despite widespread recognition of the need for an internationally coordinated approach to conservation of migratory species, protection is not yet systematically coordinated across the seasonal ranges of species. Twenty-eight migratory bird species have no coverage in at least one part of their annual cycle, and 18 of these have no protected area coverage of their breeding range. Two species lack any protected area coverage across their entire distribution (Table 1). Disturbingly, less than 3% of threatened migratory bird species have adequate protected area coverage across all parts of their annual cycle (table S1).

Widespread migrants may benefit more from broader-scale policy responses (such as targeting

¹School of Geography, Planning and Environmental Management, University of Queensland, Brisbane, QLD, 4072, Australia. ²National Center for Ecological Analysis and Synthesis (NCEAS), University of California, Santa Barbara, Santa Barbara, CA 93101, USA. ³Global Conservation Program, Wildlife Conservation Society, New York, NY, USA. ⁴BirdLife International, Wellbrook Court, Cambridge CB3 0NA, UK. ⁵School of Biological Sciences, University of Queensland, Brisbane, QLD 4072, Australia. ⁶Department of Life Sciences, Imperial College London, Silwood Park, Ascot, Berkshire SL5 7PY, England, UK.

*Corresponding author. E-mail: claire.runge@uqconnect.edu.au

Table 1. Protected area coverage of migratory and nonmigratory bird species. Representation targets are based on species' geographic range size, with a target of 100% of a distribution to be covered by protected areas where the geographic range is <1000 km, log-linearly decreasing to 10% where the range size is >250,000 km (10, 12).			
	Mean of range covered (%)	Number of gap species (defined as zero coverage)	Percentage of species meeting coverage targets
Nonmigrants	18.9	243	44.8
Full migrants	10.2	2	8.8
Part of annual cycle			
Resident	11.3	3	43.7
Breeding	14.1	18	34.4
Nonbreeding	10.9	8	39.8
Passage	13.4	2	26.2
Any part of cycle		28	
Total number of species			
Nonmigrants			7457
Full migrants			1451
Resident			898
Breeding			1260
Nonbreeding			1267
Passage			530
Any part of cycle			

forestry and agriculture planning and practices) than individual site-based interventions (14). However, for nearly all bird species worldwide for which site-based conservation is appropriate and needed, key sites—Important Bird and Biodiversity Areas (IBAs)—have been identified, so it is informative to assess protection levels for such sites (15). A total of 8283 IBAs has been identified for 885 migratory bird species, either because they congregate in sufficient numbers so that any individual site holds >1% of the global or flyway population of one or more migrant species (43% of sites) or because they support populations of one or more globally or regionally threatened migrant species (55% of sites; the remainder relate to other IBA criteria). The protected area coverage of IBAs for migrants provides a finer resolution metric of the degree to which protected areas adequately cover the key locations for the world's migrants and accounts for some of the variation in abundance of migratory species across their distribution; for example, some migratory species are widely dispersed when breeding but congregate in large numbers in a few particularly important sites when on migration or in their nonbreeding range. We discovered that for only 2.9% of migratory birds are their IBAs fully protected across each of their seasonal areas (table S2). On average, 22% of the IBAs identified for each migratory species are completely covered by protected areas, and an additional 41% are partially covered, which is consistent with nonmigrants (24 and 42%, respectively) (table S2). Most IBAs for migratory species are identified in their breeding distributions (77% of migratory species with an IBA), yet for the majority of those species, the breeding range is the least well-protected stage of the migratory cycle. IBAs along the migratory route from breeding to nonbreeding areas are most likely to be incompletely protected, with only 16% being completely covered.

Our results highlight an urgent need to coordinate the designation of protected areas across the annual cycle (Fig. 2). For example, habitat loss is one of the key threats to the Vulnerable red-spectacled amazon (*Amazona pretrei*), a mi-

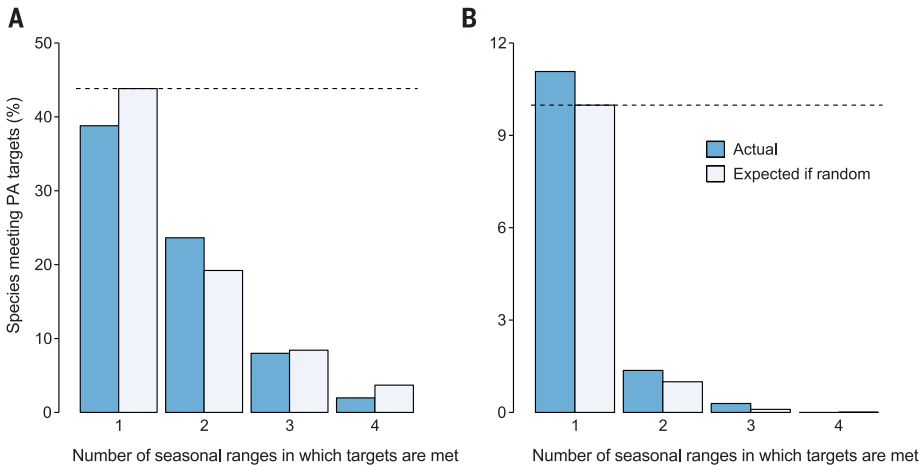


Fig. 1. The shortfall in protected area coverage for migratory species is related to their requirement for protection across each of their seasonal ranges—resident, breeding, nonbreeding, and passage ranges. (A and B) The proportion of migratory species meeting targets for (A) protected area coverage of their distribution and (B) complete coverage of all key sites (IBAs) identified for them decreases rapidly with the number of seasonal ranges, which is consistent with a random allocation of conservation effort. Dashed lines represent the proportion of species expected to meet targets where conservation is systematically coordinated across the seasonal ranges of species (so that an appropriate proportion of each part of the range is covered by protected areas).

gratory parrot of Brazil (16), yet less than 4% of its distribution occurs within protected areas, with negligible coverage of seasonal breeding and nonbreeding areas (17). Similarly, the great knot (*Calidris tenuirostris*), a once abundant migratory shorebird, is now classified as globally Vulnerable (18). Just 7% of its distribution is covered by protected areas during migration, where the species congregates in high numbers. Filling the protection gaps for such species throughout their annual cycle is necessary for their conservation.

Because migrants move across international borders, achieving their protection is a shared responsibility. Some countries (such as France and Venezuela) meet targets for protected area coverage for more than 80% of their migratory bird species, whereas others (such as China and India) meet targets for less than 10% (Fig. 2A and database S1). Countries across North Africa

and Central Asia stand out as having low protected area coverage of migratory bird distributions. We also discovered wide variation in the proportion of migratory bird species occurring in each country that meet their protection targets overseas—a consequence of the migratory connections linking jurisdictions and continents (Fig. 2B). For instance, Germany meets targets for protected area coverage for more than 98% of migratory bird species occurring within its borders, but less than 13% of Germany's migrants are adequately protected across their global range (Fig. 2). This is not simply a case of wealthy nations losing natural heritage to poor nations. Many Central American countries (with low gross domestic product) meet targets for more than 75% of their migratory species, but these species have lower levels of protected area coverage in Canada and the United States (Fig. 2).

Our analyses focus on coverage of species' distributions and key sites by protected areas and do not account for variation in management effectiveness of protected areas or consider broader-scale conservation actions beyond protected sites. Many protected areas are inadequately managed (10), and our results based on coverage thus overestimate true protection. Indeed, achieving effective management of existing protected areas may be just as beneficial as designating new sites. However, even when well managed so as to abate core threats to migratory species such as habitat loss and hunting, protected areas are just one tool for minimizing species loss (10), and broader-scale interventions will also be needed to address all threats to migratory species. Many migratory species are widespread and undertake broad-front movements, meaning that entire landscapes need to be managed to conserve them. For instance, intensification and mechanization of grassland management is a key threat to the migratory corn-crake (*Crex crex*), which breeds in agricultural meadows across Europe, and effective conservation outcomes for the species will involve both identifying key sites for strict protection during its annual cycle and developing incentives for farmers to implement agricultural practices that benefit the species in important areas outside reserves (16). Full knowledge of the spatial distribution of threats, how they can best be abated, and how they affect population dynamics across the annual cycle of each migratory species will allow conservation actions to be prioritized most efficiently (18). Alongside identifying key sites for protection, broader policy instruments need to be strengthened or developed in order to conserve migratory species.

Protected areas are usually designated at the national scale, but collaborative international partnerships and concerted intergovernmental coordination and action are crucial to safeguard migratory species (7). A number of international agreements [such as the Convention on the Conservation of Migratory Species of Wild Animals (CMS) and the Ramsar Convention on Wetlands] recognize the specific challenges associated with migratory species and attempt to deliver special protection to migrants. Migratory landbirds in particular lack coverage under flyway-based bird conservation instruments (19), although this is now being addressed through initiatives such as the African-Eurasian Migratory Landbird Action Plan being developed under the CMS (20). However, only 120 nations are parties to the CMS, and there is an urgent need to strengthen other agreements, including those between range states in specific migratory flyways. Internationally coordinated action (particularly within flyways) through these and other mechanisms will require substantially greater international leadership and resourcing.

Although there has been considerable focus through the Convention on Biological Diversity (CBD) Strategic Plan on increasing both the size and representation of the global protected area estate (21), with some success (12), our results highlight a failure to consider adequately the

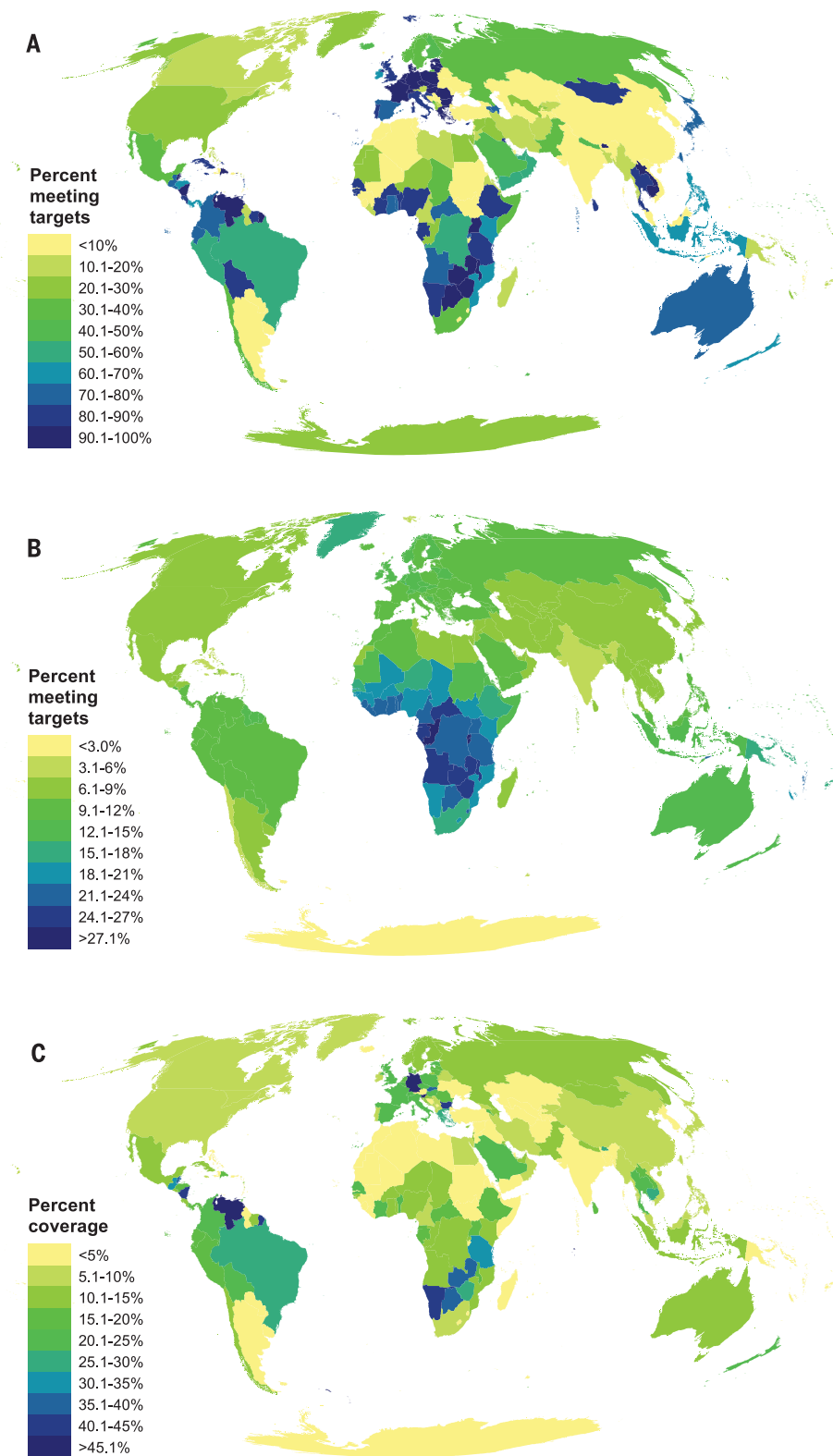


Fig. 2. Global inequity in protected area coverage of migratory birds. (A to C) The percentage of migratory bird species within each country meeting targets for protected area coverage (A) for each part of their migratory range within that country, (B) for each part of their migratory range globally, and (C) the percentage area covered by protected areas in that country. Targets are scaled by the size of each part of the seasonal distribution. There is a difference in the range of the color ramp between the three maps.

linkages between protected areas. Our data show that migratory species remain very poorly represented in the global protected area system. The CBD's Aichi Targets for 2020 (21) will likely drive the greatest expansion of protected areas in history and represent a key opportunity for conserving migrants (15). However, safeguarding the world's migratory birds will require better resourcing and use of existing international mechanisms to target new and expanded protected areas, enhance enforcement and management effectiveness, and greatly strengthen coordination between countries.

REFERENCES AND NOTES

1. Aristotle, *Historia Animalium*, J. A. Smith, W. D. Ross, Transl. (Clarendon Press, Oxford, 1910).
2. G. White, *The Natural History and Antiquities of Selborne* (B. White & Son, London, 1789).
3. P. F. Battley et al., *J. Avian Biol.* **43**, 1–12 (2012).
4. C. Egevang et al., *Proc. Natl. Acad. Sci. U.S.A.* **107**, 2078–2081 (2010).
5. S. Bauer, B. J. Hoyer, *Science* **344**, 1242552 (2014).
6. D. S. Wilcove, *No Way Home: The Decline of the World's Great Animal Migrations* (Island Press, Washington, DC, 2010).
7. J. S. Kirby et al., *Bird Conserv. Int.* **18** (suppl. 1), (2008).
8. C. A. Runge, T. G. Martin, H. P. Possingham, S. G. Willis, R. A. Fuller, *Front. Ecol. Environ.* **12**, 395–402 (2014).
9. O. Venter et al., *PLOS Biol.* **12**, e1001891 (2014).
10. J. E. M. Watson, N. Dudley, D. B. Segan, M. Hockings, *Nature* **515**, 67–73 (2014).
11. J. E. M. Watson et al., *Conserv. Biol.* **25**, 324–332 (2011).
12. S. H. M. Butchart et al., *Cons. Lett.* **8**, 329–337 (2015).
13. IUCN, UNEP-WCMC, *The World Database on Protected Areas (WDPA)*; accessed 1 February 2013 from www.protectedplanet.net.
14. C. Boyd et al., *Conserv. Lett.* **1**, 37–43 (2008).
15. BirdLife International, *Important Bird and Biodiversity Areas: A Global Network for Conserving Nature and Benefiting People* (BirdLife International, Cambridge, UK, 2014).
16. BirdLife International, *IUCN Red List for Birds*; accessed 8 May 2014 from www.birdlife.org.
17. M. A. Marini, M. Barbet-Massin, J. Martinez, N. P. Prestes, F. Jiguet, *Biol. Conserv.* **143**, 102–112 (2010).
18. V. J. D. Tulloch et al., *Front. Ecol. Environ.* **13**, 91–99 (2015).
19. T. Jones, T. Mundkur, "A review of CMS and non-CMS existing administrative/management instruments for migratory birds globally," prepared on behalf of the CMS Working Group on Flyways (UNEP, Bonn, Germany, 2010).
20. Convention on the Conservation of Migratory Species of Wild Animals, "Conservation of migratory landbirds in the African-Eurasian region," paper no. UNEP/CMS/COP11/Doc.23.1.4 (2014).
21. "Conference of the Parties 10 Decision X/2: Strategic plan for biodiversity 2011–2020," tenth meeting of the Conference of the Parties to the Convention on Biological Diversity, Nagoya, Japan (2010).

ACKNOWLEDGMENTS

This work was supported by the Australian Government's National Environmental Research Program, Australian Postgraduate Awards to C.A.R. and J.O.H., and an Australian Research Council Centre of Excellence for Environmental Decisions scholarship to C.A.R. The work was further supported by Australian Research Council Linkage Grant LP150101059 to R.A.F. and Discovery Grant DP140100733 to J.E.M.W. We thank V. Jones for comment and discussion and all contributors to BirdLife's International Union for Conservation of Nature Red List assessments. Data describing protected area coverage are available in the supplementary materials databases S1 to S3. C.A.R., R.A.F., and H.P.P. designed the study. C.A.R. analyzed data, created figures, and wrote the manuscript. J.O.H. prepared and analyzed data. All authors discussed the results and edited the manuscript.

SUPPLEMENTARY MATERIALS

www.sciencemag.org/content/350/6265/1255/suppl/DC1

Materials and Methods

Supplementary Text

Figure S1

Tables S1 to S5

References (22–28)

Databases S1 to S3

28 June 2015; accepted 5 November 2015

10.1126/science.aac9180

GENE REGULATION

Single-base pair differences in a shared motif determine differential *Rhodopsin* expression

Jens Rister, Ansa Razzaq, Pamela Boodram, Nisha Desai, Cleopatra Tsanis, Hongtao Chen,* David Jukam,† Claude Desplan‡

The final identity and functional properties of a neuron are specified by terminal differentiation genes, which are controlled by specific motifs in compact regulatory regions. To determine how these sequences integrate inputs from transcription factors that specify cell types, we compared the regulatory mechanism of *Drosophila Rhodopsin* genes that are expressed in subsets of photoreceptors to that of phototransduction genes that are expressed broadly, in all photoreceptors. Both sets of genes share an 11-base pair (bp) activator motif. Broadly expressed genes contain a palindromic version that mediates expression in all photoreceptors. In contrast, each *Rhodopsin* exhibits characteristic single-bp substitutions that break the symmetry of the palindrome and generate activator or repressor motifs critical for restricting expression to photoreceptor subsets. Sensory neuron subtypes can therefore evolve through single-bp changes in short regulatory motifs, allowing the discrimination of a wide spectrum of stimuli.

In the visual system, different photoreceptor neurons express specific light-sensing pigments (1); however, common downstream factors amplify and convert the response to the visual stimulus into a neuronal signal. For instance, each unit eye (ommatidium) of the *Drosophila* retina contains eight photoreceptors (R1 to R8) that express different light-sensing Rhodopsins (Rhs) that are restricted to specific photoreceptor subsets. Outer photoreceptors R1 to R6 express either Rh1. Inner photoreceptors R7 and R8 express either Rh3 in pR7s coupled with Rh5 in pR8s, or Rh4 in yR7s with Rh6 in yR8s (Fig. 1A) (2). R1 to R8 all share broadly expressed phototransduction factors (Fig. 1B and fig. S1A) that amplify and convert the response to the visual stimulus into a neuronal signal (2).

Here, we examine the cis-regulatory mechanisms that distinguish restricted from broad expression patterns for Rhodopsins and downstream phototransduction factors, respectively. All *Rhs* share the conserved *Rhodopsin* Core Sequence I (RCSI) (3, 4), which resembles the palindromic P3 motif (TAATYNRATTA), an optimal binding site for paired-class homeodomain proteins (5). Almost all known broadly expressed phototransduction genes contain a P3 motif in their proximal promoter (Fig. 1B, fig. S1A, and supplementary text). The presence of a conserved P3/RCSI motif within 100 base pairs (bps) of the *Rh* transcription start site (TSS) is significantly associated with enrichment in adult eyes (χ -square test, $P < 0.001$). P3/RCSI is required for activation in photoreceptors because its mutation caused either a loss or a strong reduction in expression of 16 broad or restricted reporters (figs. S1 to S3), with the exception of *Arr1* (fig. S2K). Moreover, expression of 10 out of 15 reporters was lost in mutants for the photoreceptor-specific transcription factor Pph13 (Fig. 1B and figs. S2 and S3), a paired-class homeodomain protein that binds P3 and the *Rh6* RCSI in vitro (6, 7).

Center for Developmental Genetics, Department of Biology, New York University, 100 Washington Square East, New York, NY 10003-6688, USA.

*Present address: Joseph Henry Laboratory of Physics, Lewis-Sigler Institute for Integrative Genomics, Princeton University, Princeton, NJ 08544, USA. †Present address: Department of Biology, Stanford University, Stanford, CA 94305, USA.

‡Corresponding author. E-mail: cd38@nyu.edu

Because each *Rh* promoter has a highly conserved RCSI variant (Fig. 1B) (4), we tested the sufficiency of P3 and RCSI to determine the significance of the specific differences between perfectly palindromic (P3) and imperfect motifs (RCSI) (Fig. 2). Four copies of the P3 motif (including four neighboring bps for spacing; the contribution of these additional bps was only tested for *Rh4*) from the broadly expressed *ninaC*, *rdgA*, or *trpl* drove broad expression in all photoreceptors (Fig. 2, A and A', and fig. S4, A and A'), consistent with our previous results (8). In sharp contrast, multimerized RCSI motifs drove expression in subsets of photoreceptors. The RCSI of *Rh3* and *Rh6* contains a K_{50} motif, a binding site for K_{50} homeodomain proteins such as the Dve repressor or the Otd activator (Fig. 1B). Expression of *[Rh3 RCSI]₄* and *[Rh6 RCSI]₄* was biased to inner photoreceptors: *[Rh3 RCSI]₄* mediated restricted expression in R8 and R7, with a strong bias toward the pR7 subset, where *Rh3* is normally expressed (Fig. 2, B and B'). This pattern is complementary to the expression of Dve (Fig. 1B) (9), which is indeed responsible for the restricted expression as *[Rh3 RCSI]₄* drove a broad, P3-like pattern in *dve* mutants (Fig. 2 B''). *[Rh6 RCSI]₄* drove restricted expression in R8s and R7s; expression in R1 to R6 was very weak in comparison to P3 motifs,

which was due to *dve*-dependent repression (fig. S4, D, D', and D'').

[*Rh1* RCSI]₄ drove variable expression in R1 to R6 (Fig. 2, C and C'), where *Rh1* is expressed. This outer photoreceptor-specific pattern is complementary to the inner photoreceptor expression of [*Rh3* RCSI]₄. *Rh4* has the same RCSI as *Rh1*. However, adding the synergistic 3' RCSI motif (fig. S1, F to I) (3) led to expression in yR7s, where *Rh4* is expressed (fig. S4, B and B', and fig. S4, C and C'). Although [*Rh5* RCSI]₄ was not sufficient for reporter expression (fig. S4, E and E'), adding three K₅₀ motifs to a single *Rh5* RCSI ([K₅₀]₃ + [*Rh5* RCSI]₁) led to expression in R8 and pR7 photoreceptors (fig. S4, F and F').

In summary, the RCSI motifs of specific *Rhs* differ from palindromic P3 motifs in broadly expressed genes: They drive expression that is biased toward the endogenous *Rh* expression patterns (Fig. 2D). We show below that full subtype specificity and activation often requires the repetition of motifs that are present in the RCSI.

As specific RCSI motifs directed restricted expression in different photoreceptor subsets (Fig. 2D), albeit with incomplete subtype specificity and with some variability in expression levels, we asked whether the single-bp differences are required for subtype specificity in a wild-type promoter context and which other motifs are required for full restriction. We mutated the K₅₀ (Otd/Dve) motifs (TAATCC) to Q₅₀ (Pph13) motifs (TAATTG/A) (Fig. 1B) to disrupt repression while preserving RCSI-mediated activation. Mutating the *Rh3* RCSI resulted in an expansion to yR7s, where Dve is present at low levels (Fig.

3, A and B). Mutating the *Rh6* RCSI caused derepression in R1 to R6 and the ocelli (fig. S5, A and B, and fig. S6A). *Rh3* and *Rh6* have K₅₀/Dve repressor motifs repeated upstream, and muta-

tion of individual motifs also caused derepression in yR7s (Fig. 3C) (10) and R1 to R6 and the ocelli (fig. S5D and fig. S6B), respectively. Taken together, single-bp changes create K₅₀ motifs in

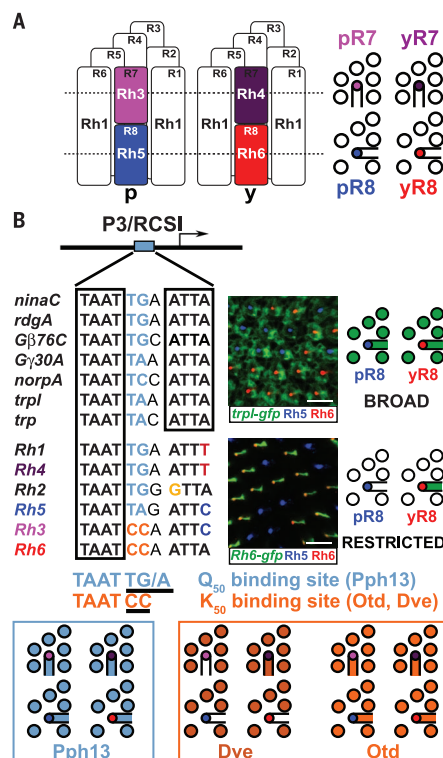


Fig. 1. Broadly expressed and restricted photoreceptor genes share a cis-regulatory motif.

(A) In "p" ommatidia, Rh3 in pR7 is coupled with Rh5 in pR8, whereas in "y" ommatidia, Rh4 in yR7 is coupled with Rh6 in yR8. Outer photoreceptors R1 to R6 express Rh1. (Right) Cross section at the level of R7 (top) or R8 (bottom). (B) Broadly expressed photoreceptor genes (seven upper genes) and restricted *Rhodopsins* *Rh1* to *Rh6* share the 11-bp P3/RCSI motif in their proximal promoters. (Left) All motifs contain a 5' TAAT homeodomain core binding site, which is repeated in reverse orientation (ATTA) in broadly expressed phototransduction genes. The 3' ATTA is modified in RCSI motifs of *Rh1* to *Rh5*. In *Rh6* and *Rh3*, central bp differences (orange) create K₅₀ sites (TAATCC) for the activator Otd and the repressor Dve (9). Q₅₀ sites (TAATTG/A) are bound by the photoreceptor-specific activator Pph13 (6). (Right) Reporter expression patterns of the broadly expressed phototransduction gene *trpl* and the restricted *Rh6* at the R8 level. Retinas were stained for green fluorescent protein (GFP) (green), Rh5 (blue) and Rh6 (red). Scale bars, 10 μm. (Bottom) Pph13 and Otd are expressed in all photoreceptors, whereas Dve is expressed at high levels in R1 to R6 and at low levels in yR7s.

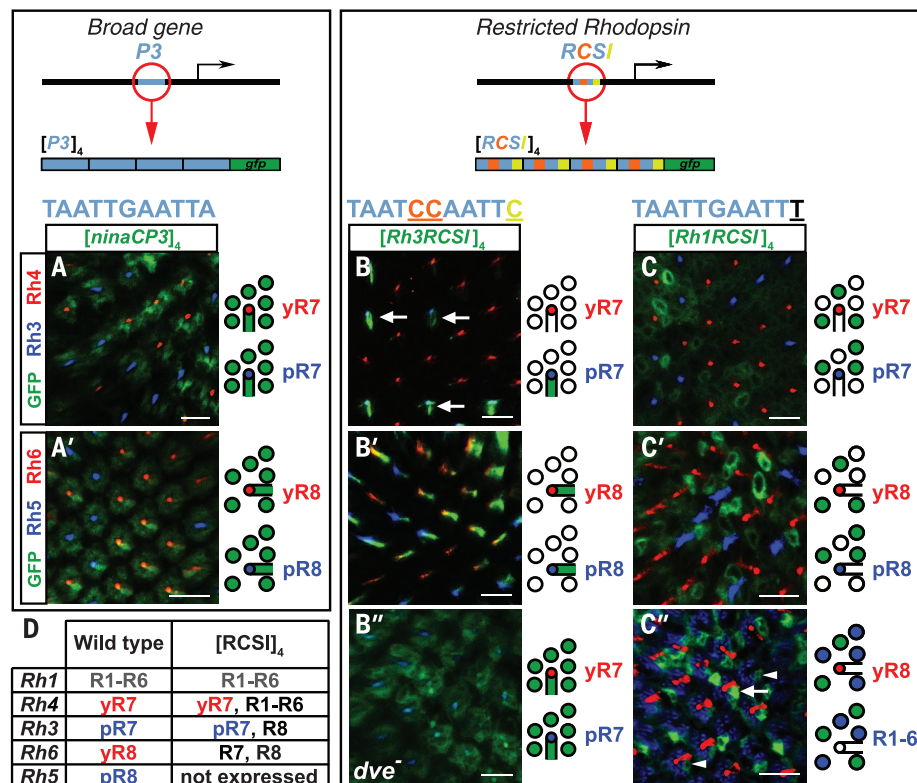


Fig. 2. The P3 motif is sufficient to drive expression in all photoreceptors, whereas RCSI motifs drive expression in subsets of photoreceptors. Multimerization of a P3 motif (left) found in broadly expressed phototransduction genes or of a specific RCSI motif (right) from a restricted *Rhodopsin*. (A and A') Tetramerization of a palindromic P3 motif from *ninaC* results in broad, pan-photoreceptor expression. (B, B', and B'') Four copies of the *Rh3* RCSI that contains a Dve repressor site (orange) drive expression in R7 and R8. (B) The reporter is strongly biased toward pR7s (arrows), where *Rh3* is expressed, and faint in yR7s. (B') GFP is expressed in all R8s, which lack Dve. (B'') Expression is expanded to all photoreceptors in a *dve*¹⁸⁶ mutant background. (C, C', and C'') Tetramerization of the *Rh1* RCSI drives variable reporter expression (arrows and arrowheads in C'') in individual R1 to R6 photoreceptors, where *Rh1* is expressed (blue in C''). Scale bars, 10 μm. (D) RCSI motifs are biased toward the respective endogenous *Rh* expression pattern (wild type).

the *Rh3* and *Rh6* RCSI, which are required for subtype-specific expression together with their upstream repeats.

We also examined the importance of the disrupted P3 palindrome—i.e., the imperfect 3' homeodomain binding motif in the RCSI of *Rh1* to *Rh5* (Fig. 1B). Creating a palindromic motif in the *Rh3* RCSI (TAATCCAATTC→TAATC-CAATTA) caused derepression in yR7s (Fig. 3D) that depended on *Pph13* (Fig. 3E). Therefore, derepression appears to be due to increased activation through the newly created Q₅₀/Pph13 site. The same ATTC→ATTA mutation in the *Rh5* RCSI led to partial derepression in yR8s (fig. S5, E and F). This single-bp change created a binding site for the activator Otd (AGATTA) (11), and indeed derepression in yR8s was

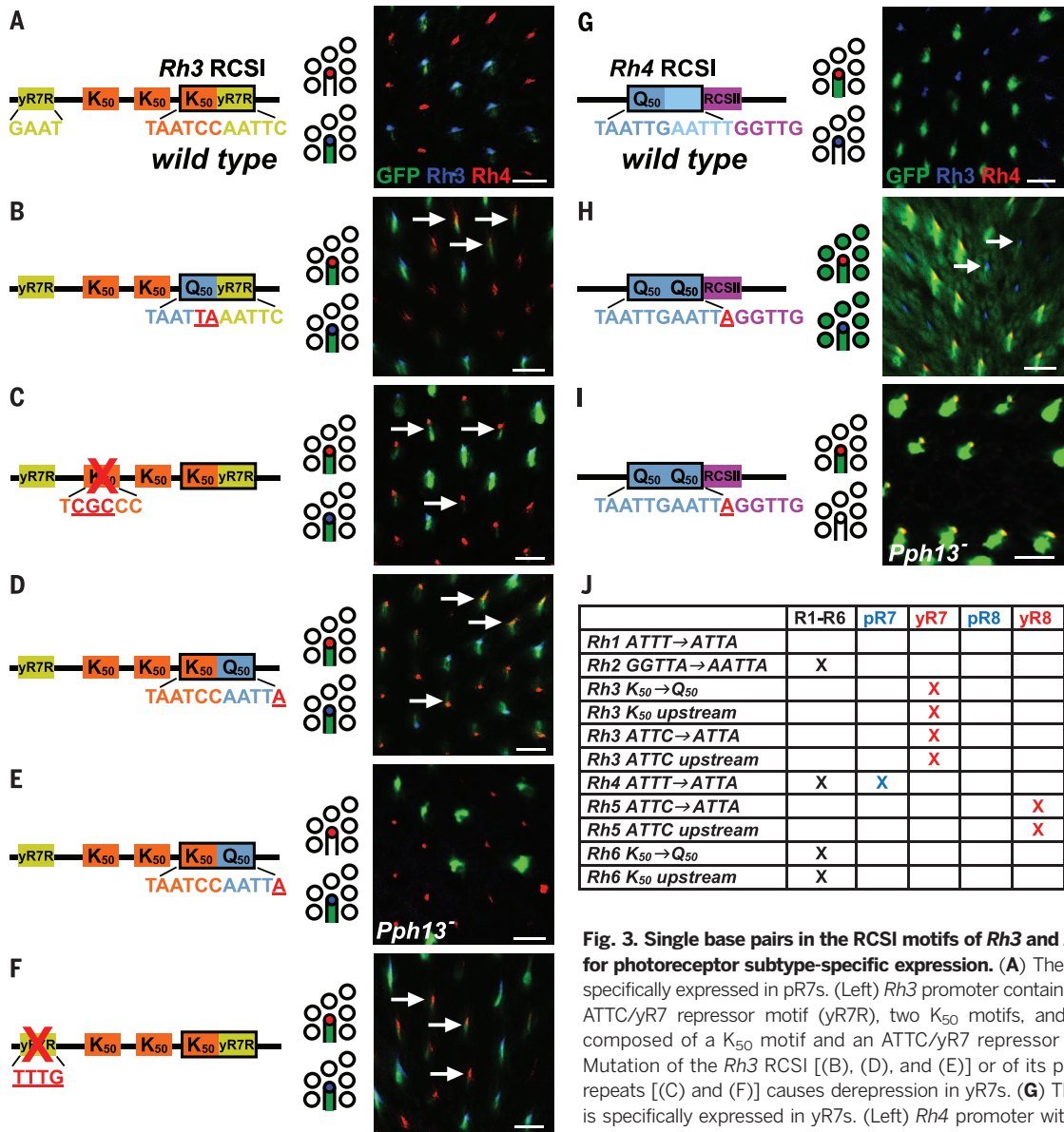
lost in *otd* mutants, as was activation in pR8s (fig. S5G).

The 3' ATTC motif in the RCSI of *Rh3* and *Rh5* is repeated upstream. Mutating the upstream repeat without creating a Q₅₀/Pph13 site (ATTC→CAAA) also caused derepression in yR7s (*Rh3*) or yR8s (*Rh5*) (Fig. 3F and fig. S5H). Mutating both ATTCs of *Rh5* enhanced derepression into almost all yR8s (fig. S5I). Therefore, we have identified repressor motifs in the RCSI of four *Rhs* (K₅₀/Dve motifs in *Rh3/Rh6* and ATTC motifs in *Rh3/Rh5*). These motifs are repeated upstream within less than 100 bps and are required for full subtype specificity.

A single-bp ATTT→ATTA mutation in the *Rh4* RCSI caused derepression in R1 to R6, pR7s, and the ocelli (Fig. 3, G and H, and fig. S6D). The

correct pattern was restored by crossing the mutant *Rh4* reporter in a *Pph13* mutant background (Fig. 3I), indicating that the A→T change prevents Pph13 from overcoming repression in the “wrong” photoreceptor subsets, as was the case for *Rh3* and *Rh6*. The same mutation in the *Rh1* RCSI caused no detectable derepression (fig. S5J). Replacing two bps in the RCSI of the ocelli-specific *Rh2* (fig. S6, E and F) to obtain a Q₅₀/Pph13 site led to derepression in R1 to R6 photoreceptors that depended on *Pph13* (fig. S6, G and H).

Our in vivo data revealed that a cell-fate decision requires single-bp differences in RCSI motifs (Fig. 3J). They complement previous findings in cell culture that subtle sequence differences in a glucocorticoid receptor or nuclear factor κB



causes derepression in pR7 and R1 to R6 that depends on *Pph13*. Scale bars, 10 μm. (J) Derepression in other photoreceptor subsets (indicated by X) caused by mutations of RCSI or upstream repeats.

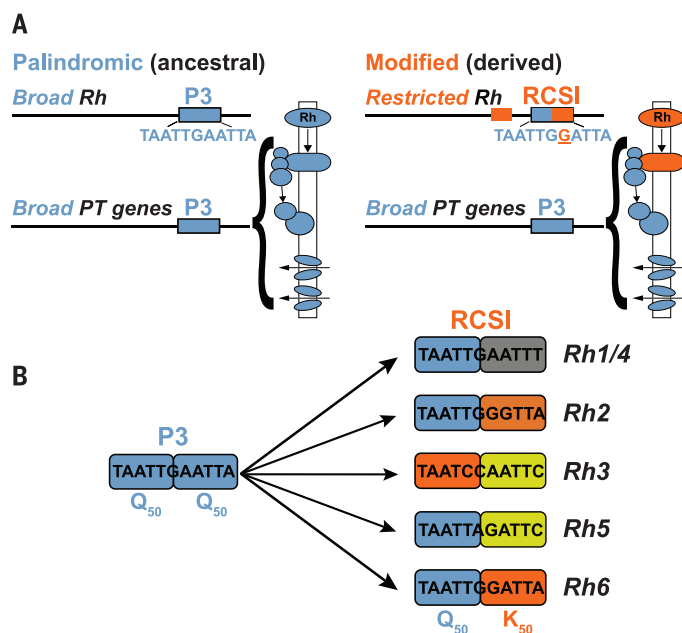


Fig. 4. Modification of a shared cis-regulatory motif for color vision. (A) A palindromic P3 motif (TAATNNNATTA) provides broad activation of an ancestral *Rh* and a set of phototransduction (PT) genes in all photoreceptors (left). Modification of single bps yields an RCSI motif (orange) that is essential for restricting *Rh* expression to subsets of photoreceptors (right). The upstream repetition of parts of the RCSI (orange box) is required for full subtype specificity. (Right schematic) Phototransduction cascade. The downstream-acting factors (broad PT genes) remain expressed in all photoreceptors. (B) Palindromic P3 motifs bound by a photoreceptor-specific Q₅₀ activator like Pph13 provide broad activation, whereas single-bp changes in RCSI motifs specific to each *Rh* create new activator or repressor motifs (right).

(NF-κB) binding site can specify the mode of transcriptional regulation (12, 13) and that small differences in binding-site sequences can lead to distinct Hox specificities in vivo and in vitro (14–16). (i) Single bps in RCSI prevent binding of dimers of broadly expressed activators such as Pph13 (5) (fig. S8B), tipping the balance of activator/repressor binding. This weakened activation allows repressors to prevent activation in other photoreceptor subtypes (17). (ii) They generate specific combinations of overlapping activator and repressor motifs, often repeated upstream to provide robust expression and full subtype specificity. Creating overlap of activator and repressor motifs is an efficient way of blocking a key activator site in the “wrong” cell types that express a repressor (18), especially because the RCSI motifs are very close to the transcription start site and repression there could block other activators (19). The precise tuning of RCSI motifs within their respective promoter context leads to incompatibility in other *Rh* promoters, as revealed by RCSI swap experiments: Replacing a given RCSI with another one resulted in two main outcomes: loss of expression or derepression in specific subsets of photoreceptors (fig. S7 and supplementary text).

The RCSI/P3 motif resembles “terminal selector” motifs that allow the coordinated expression of effector genes that define a particular neuron type (20, 21). Yet, RCSI motifs exhibit additional layers of regulation that are integrated in a single regulatory element, as their sequence is modified for subtype specificity. Mutating a cis-regulatory motif in many cases appears to be the shortest evolutionary path toward a novel phenotype (22). Although we found that it is possible in some cases to eliminate ectopic expression by removing the broadly expressed activator Pph13 (Fig. 3, E and I), this simultaneously causes a loss of expression of several broad phototransduction

genes, defects in photoreceptor morphology, and a severe loss of light sensitivity (23).

We propose that the modification of a P3-type motif into different RCSI-type motifs allowed partitioning *Rh* expression to different subtypes of photoreceptors (Fig. 4 and fig. S8). This opened the possibility to discriminate wavelengths and likely conveyed a selective advantage. In this model, P3 motifs represent a positive regulatory element shared by ancestral genes that were expressed in all photoreceptors. This regulation is conserved, as the promoter of the long-wavelength *Rh*, as well as *Gβ76C* that are both expressed in all photoreceptors in the beetle *Tribolium*, contain a palindromic P3-type motif and depend on Pph13 (24, 25).

Our study revealed a high level of precision at every base pair in a short cis-regulatory element that is critical for proper spatial (broad or restricted) expression. It will be interesting to see whether similar modifications of shared cis-regulatory motifs are used to diversify neuronal cell types in other developmental contexts, for instance in human photoreceptor and olfactory genes (fig. S9 and supplementary materials).

REFERENCES AND NOTES

- J. Rister, C. Desplan, D. Vasilaukas, *Development* **140**, 493–503 (2013).
- K. W. Yau, R. C. Hardie, *Cell* **139**, 246–264 (2009).
- M. E. Fortini, G. M. Rubin, *Genes Dev.* **4**, 444–463 (1990).
- D. Papatsenko, A. Nazina, C. Desplan, *Mech. Dev.* **101**, 143–153 (2001).
- D. S. Wilson, B. Guenther, C. Desplan, J. Kuriyan, *Cell* **82**, 709–719 (1995).
- M. Mishra et al., *Development* **137**, 2895–2904 (2010).
- D. Jukam et al., *Science* **342**, 1238016 (2013).
- G. Sheng, E. Thouvenot, D. Schmucker, D. S. Wilson, C. Desplan, *Genes Dev.* **11**, 1122–1131 (1997).
- R. J. Johnston Jr. et al., *Cell* **145**, 956–968 (2011).
- S. U. Thanawala et al., *Dev. Cell* **25**, 93–105 (2013).

- L. J. Zhu et al., *Nucleic Acids Res.* **39** (Database), D111–D117 (2011).
- S. H. Meijnsing et al., *Science* **324**, 407–410 (2009).
- T. H. Leung, A. Hoffmann, D. Baltimore, *Cell* **118**, 453–464 (2004).
- J. Crocker et al., *Cell* **160**, 191–203 (2015).
- M. Slattery et al., *Cell* **147**, 1270–1282 (2011).
- R. S. Mann, K. M. Lelli, R. Joshi, *Curr. Top. Dev. Biol.* **88**, 63–101 (2009).
- J. F. Etchberger, E. B. Flowers, R. J. Poole, E. Bashllari, O. Hobert, *Development* **136**, 147–160 (2009).
- D. Stanojevic, S. Small, M. Levine, *Science* **254**, 1385–1387 (1991).
- M. Levine, J. L. Manley, *Cell* **59**, 405–408 (1989).
- E. S. Deneris, O. Hobert, *Nat. Neurosci.* **17**, 899–907 (2014).
- E. H. Davidson, *The Regulatory Genome: Gene Regulatory Networks in Development and Evolution* (Elsevier Science, San Diego, 2006).
- G. A. Wray, *Nat. Rev. Genet.* **8**, 206–216 (2007).
- A. C. Zellhof, E. Koundakjian, A. L. Scully, R. W. Hardy, L. Pounds, *Development* **130**, 4383–4392 (2003).
- M. Jackowska et al., *Front. Zool.* **4**, 24 (2007).
- S. Mahato et al., *PLOS Genet.* **10**, e1004484 (2014).

ACKNOWLEDGMENTS

We thank K. Basler, J. Bischof, S. Britt, C. Zuker, the Bloomington Stock Center, and the Vienna *Drosophila* Resource Center for reagents. We thank T. Blackman for injections and J. Corbo, R. Datta, M. Friedrich, O. Hobert, R. Mann, F. Payre, S. Small, D. Taatjes, and past and present members of the Desplan laboratory for comments on the manuscript. C.D. was supported by National Institutes of Health/National Eye Institute grant R01 EY13010, J.R. by National Institutes of Health/National Eye Institute award K99EY023995 and European Molecular Biology Organization long-term fellowship ALTF 462-2008, and D.J. by a New York University Dean's Dissertation Award. The content is solely the responsibility of the authors and does not necessarily represent the official views of the NIH.

SUPPLEMENTARY MATERIALS

www.sciencemag.org/content/350/6265/1258/suppl/DC1
 Supplementary Text
 Materials and Methods
 Figs. S1 to S9
 References (26–60)

13 April 2015; accepted 23 October 2015
 10.1126/science.aab3417

HUMAN GENETICS

De novo mutations in congenital heart disease with neurodevelopmental and other congenital anomalies

Jason Homsy,^{1,2*} Samir Zaidi,^{3*} Yufeng Shen,^{4*} James S. Ware,^{1,5,6*} Kaitlin E. Samocha,^{1,7} Konrad J. Karczewski,^{1,7} Steven R. DePalma,^{1,8} David McKean,¹ Hiroko Wakimoto,¹ Josh Gorham,¹ Sheng Chih Jin,³ John Deanfield,⁹ Alessandro Giardini,⁹ George A. Porter Jr.,¹⁰ Richard Kim,¹¹ Kaya Bilguvar,^{3,12} Francesc López-Giráldez,¹² Irina Tikhonova,¹² Shrikant Mane,¹² Angela Romano-Adesman,¹³ Hongjian Qi,^{4,14} Badri Vardarajan,¹⁵ Lijiang Ma,¹⁶ Mark Daly,^{1,7} Amy E. Roberts,¹⁷ Mark W. Russell,¹⁸ Seema Mital,¹⁹ Jane W. Newburger,²⁰ J. William Gaynor,²¹ Roger E. Breitbart,²⁰ Ivan Iossifov,²² Michael Ronemus,²² Stephan J. Sanders,²³ Jonathan R. Kaltman,²⁴ Jonathan G. Seidman,¹ Martina Brueckner,^{3,†} Bruce D. Gelb,^{25,†} Elizabeth Goldmuntz,^{26,27,†} Richard P. Lifton,^{3,28,††} Christine E. Seidman,^{1,8,29,††} Wendy K. Chung^{30,††}

Congenital heart disease (CHD) patients have an increased prevalence of extracardiac congenital anomalies (CAs) and risk of neurodevelopmental disabilities (NDDs). Exome sequencing of 1213 CHD parent-offspring trios identified an excess of protein-damaging de novo mutations, especially in genes highly expressed in the developing heart and brain. These mutations accounted for 20% of patients with CHD, NDD, and CA but only 2% of patients with isolated CHD. Mutations altered genes involved in morphogenesis, chromatin modification, and transcriptional regulation, including multiple mutations in *RBFOX2*, a regulator of mRNA splicing. Genes mutated in other cohorts examined for NDD were enriched in CHD cases, particularly those with coexisting NDD. These findings reveal shared genetic contributions to CHD, NDD, and CA and provide opportunities for improved prognostic assessment and early therapeutic intervention in CHD patients.

Extracardiac congenital anomalies (CAs, structural or functional anomalies that arise in utero) occur in approximately 13% of newborns with congenital heart disease (CHD), including 2% with a genetic syndrome, which is almost twice the prevalence observed in infants without CHD (1). Newborns with CHD are also at risk for the emergence of neurodevelopmental disorders (NDDs), including cognitive, motor, social, and language impairments. NDDs occur in 10% of all children with CHD and in 50% with severe CHD (2). Explanations to account for the high frequency of CA and NDD in CHD patients include embryonic circulatory deficits and stresses associated with postnatal therapeutic interventions (3), but these hypotheses remain unproven.

We sequenced exomes in 1213 CHD trios (proband and their unaffected parents) enrolled in the Pediatric Cardiac Genetics Consortium (PCGC) (4) or the Pediatric Heart Network (5), after excluding CHD cases with clinically recognized genetic syndromes. Analyses included 353 previously reported CHD trios (6). We compared de novo mutations identified in CHD that occurred in isolation, or accompanied by CA, NDD, or both (phenotypes in table S1 and database S1). Previously sequenced trios ($n = 900$) from the Simons Foundation Autism Research Initiative Simplex Collection, each consisting of the unaffected parents and sibling of a child with autism spectrum disorder, served as control trios (7–9).

CHD and control probands were analyzed for de novo mutations (databases S2 and S3). To evaluate the significance of mutation frequencies, we adapted a recently reported de novo expectation model (10) to assess mutation rates by variant class [synonymous, loss of function (LoF; such as nonsense, frameshift, or canonical splice disruptions), or missense]. We derived gene-based rates of de novo mutation from local sequence context and adjusted by per-base coverage separately in case and control cohorts (databases S4 and S5). We extended the model by merging all possible transcripts to obtain transcript-independent probabilities and by adding rates for deleterious missense variants predicted by the Meta-SVM score (D-Mis) (11). This yielded an overall mean expected mutation rate of 1.1 de novo variant per proband.

The expected and observed numbers of de novo mutations in each variant class in all CHD and control study participants (Table 1) were compared using a Poisson distribution. De novo mutation rates per variant class were accurately predicted in controls, replicating previous model validations (10). However, among all CHD trios, we detected significant enrichment (i.e., observed divided by expected frequencies) of LoF and D-Mis variants of 1.3 ($P = 0.0016$) and 1.6 ($P = 1.8 \times 10^{-10}$), respectively, across all genes. The combination of LoF+D-Mis variants (hereafter denoted as “damaging”) was 1.4-fold enriched in CHD cases as compared to expectation, similar to

the observed case versus control comparison (table S2). This burden persisted after excluding 353 previously studied CHD trios (table S3) and was found in each CHD category (conotruncal defects, left ventricular outflow tract obstruction, and “other”), except for heterotaxy, which showed no excess (table S4).

Damaging de novo mutations were markedly increased in CHD cases (enrichment = 2.4, $P = 5.1 \times 10^{-24}$) among 4420 genes in the top quartile of expression during heart development [high heart expression, HHE (6)] (Table 1). Conversely, controls had no significant enrichment in de novo mutations in HHE genes. Neither cases nor controls were enriched in de novo mutations among genes within the lower three quartiles of developing heart expression (LHE) (Table 1). From the observed and expected values, we estimated that 58% of these damaging de novo mutations contributed to CHD.

Twenty-one genes had multiple damaging de novo mutations only in cases, an unlikely chance

¹Department of Genetics, Harvard Medical School, Boston, MA, USA. ²Cardiovascular Research Center, Massachusetts General Hospital, Boston, MA, USA. ³Department of Genetics, Yale University School of Medicine, New Haven, CT, USA.

⁴Departments of Systems Biology and Biomedical Informatics, Columbia University Medical Center, New York, NY, USA. ⁵NIHR Cardiovascular Biomedical Research Unit at Royal Brompton & Harefield NHS Foundation and Trust and Imperial College London, London, UK. ⁶National Heart & Lung Institute, Imperial College London, London, UK. ⁷Analytical and Translational Genetics Unit, Massachusetts General Hospital and Harvard Medical School, Boston, MA, USA. ⁸Howard Hughes Medical Institute, Harvard University, Boston, MA, USA. ⁹Department of Cardiology, University College London and Great Ormond Street Hospital, London, UK. ¹⁰Department of Pediatrics, University of Rochester Medical Center, The School of Medicine and Dentistry, Rochester, NY, USA. ¹¹Section of Cardiothoracic Surgery, University of Southern California Keck School of Medicine, Los Angeles, CA, USA. ¹²Yale Center for Genome Analysis, Yale University, New Haven, CT, USA. ¹³Steven and Alexandra Cohen Children's Medical Center of New York, New Hyde Park, NY, USA. ¹⁴Department of Applied Physics and Applied Mathematics, Columbia University, New York, NY, USA. ¹⁵Department of Neurology, Columbia University Medical Center, New York, NY, USA. ¹⁶Department of Pediatrics, Columbia University Medical Center, New York, NY, USA. ¹⁷Department of Cardiology, Children's Hospital Boston, Boston, MA, USA. ¹⁸Division of Pediatric Cardiology, University of Michigan, Ann Arbor, MI, USA. ¹⁹Department of Pediatrics, The Hospital for Sick Children, University of Toronto, Toronto, Ontario, Canada. ²⁰Department of Cardiology, Boston Children's Hospital, Boston, MA, USA. ²¹Department of Pediatric Cardiac Surgery, The Children's Hospital of Philadelphia, Philadelphia, PA, USA. ²²Cold Spring Harbor Laboratory, Cold Spring Harbor, NY, USA. ²³Department of Psychiatry, University of California San Francisco, San Francisco, CA, USA. ²⁴Heart Development and Structural Diseases Branch, Division of Cardiovascular Sciences, NHLBI/NIH, Bethesda, MD, USA. ²⁵Mindich Child Health and Development Institute and Department of Pediatrics, Icahn School of Medicine at Mount Sinai, New York, NY, USA. ²⁶Department of Pediatrics, The Perelman School of Medicine, University of Pennsylvania, Philadelphia, PA, USA. ²⁷Division of Cardiology, The Children's Hospital of Philadelphia, Philadelphia, PA, USA. ²⁸Howard Hughes Medical Institute, Yale University, New Haven, CT, USA. ²⁹Cardiovascular Division, Brigham & Women's Hospital, Harvard University, Boston, MA, USA. ³⁰Departments of Pediatrics and Medicine, Columbia University Medical Center, New York, NY, USA.

*These authors contributed equally to this work. †These authors contributed equally to this work. ††Corresponding author. E-mail: bruce.gelb@mssm.edu (B.D.G.); goldmuntz@mail.chop.edu (E.G.); martina.brueckner@yale.edu (M.B.); richard.lifton@yale.edu (R.P.L.); cseidman@genetics.med.harvard.edu (C.E.S.); wkc15@cumc.columbia.edu (W.K.C.)

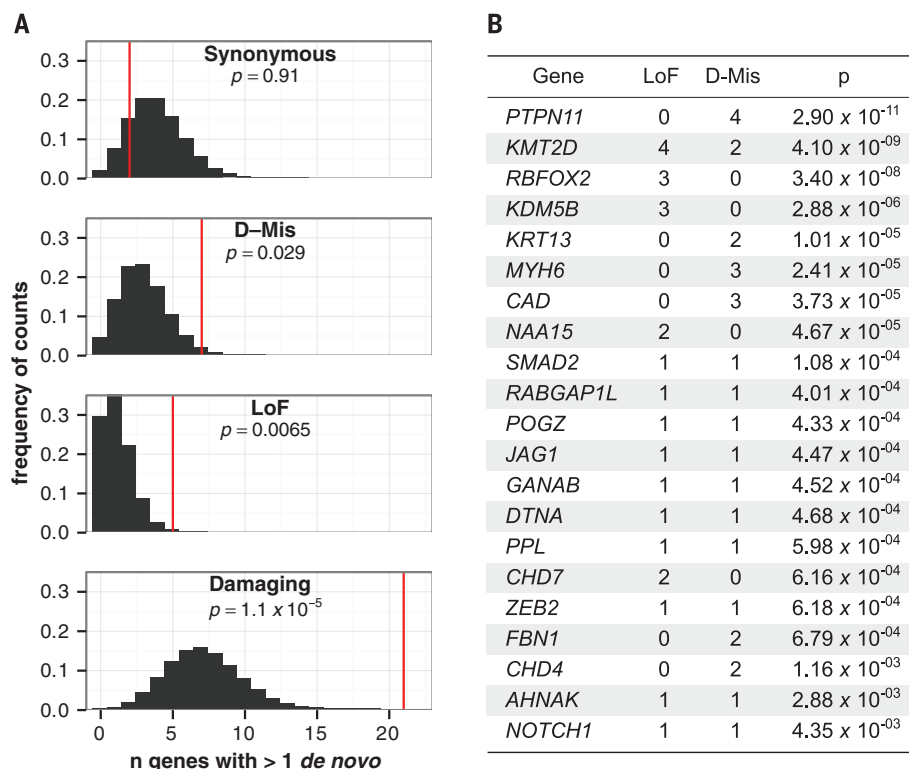


Fig. 1. Genes with multiple de novo mutations are candidate CHD risk genes. (A) Histograms show the expected distribution of the number of genes containing multiple de novo mutations (empirically derived using 1M permutations, black) and the observed number of genes with multiple mutations in cases (red line) for each class. *P* values were calculated by permutation. **(B)** Twenty-one genes with multiple damaging de novo mutations in cases. *P* values are from Poisson test against expectation, with significance threshold $<9 \times 10^{-7}$. Further details are shown in table S6.

Table 1. De novo enrichment in cases versus controls by expectation analysis. *n*, number of de novo mutations; rate, number of de novo mutations divided by the number of individuals in the cohort (*N*); enrichment, ratio of observed to expected numbers of mutations; HHE, high heart-expressed genes (top quartile of expression); LHE, lower heart-expressed genes (bottom three quartiles of expression); D-Mis, damaging missense predicted by Meta-SVM; Damaging, D-Mis+LoF. Bold numbers indicate enrichment >2 or $P < 0.005$.

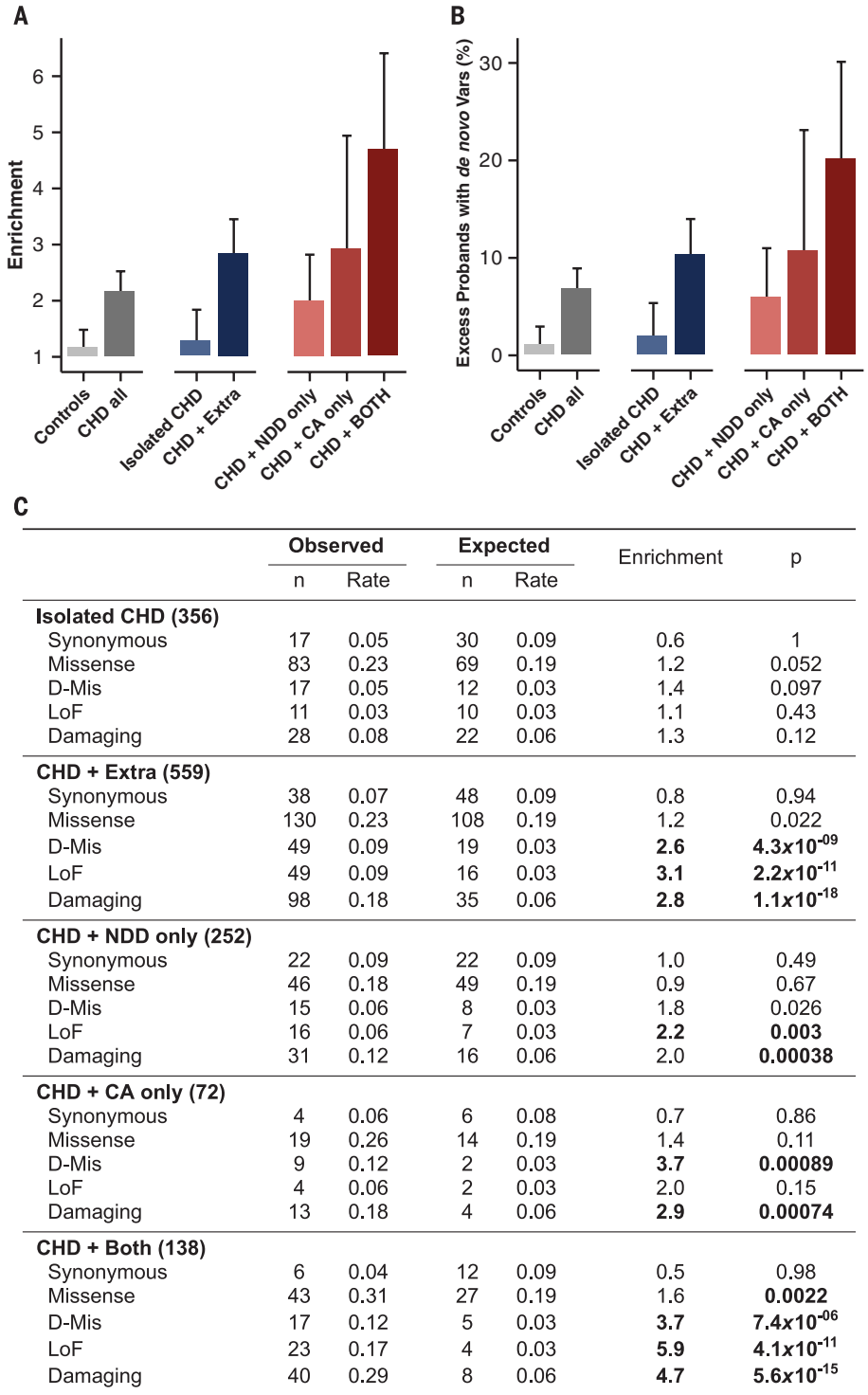
	Cases, <i>N</i> = 1213						Controls, <i>N</i> = 900					
	Observed		Expected		Enrichment	<i>P</i>	Observed		Expected		Enrichment	<i>P</i>
	<i>n</i>	Rate	<i>n</i>	Rate			<i>n</i>	Rate	<i>n</i>	Rate		
All genes												
Total	1273	1.05	1312.7	1.08	1.0	0.87	925	1.03	979.7	1.09	0.9	0.96
Synonymous	277	0.23	371.4	0.31	0.7	1	229	0.25	277.4	0.31	0.8	1
Missense	846	0.70	824.9	0.68	1.0	0.24	614	0.68	615.6	0.68	1.0	0.53
D-Mis	212	0.17	133.1	0.11	1.6	1.8 × 10⁻¹⁰	119	0.13	99.3	0.11	1.2	0.03
LoF	150	0.12	116.5	0.10	1.3	0.0016	82	0.09	86.7	0.10	0.9	0.71
Damaging	362	0.30	249.5	0.21	1.4	1.5 × 10⁻¹¹	201	0.22	186.0	0.21	1.1	0.14
HHE genes												
Total	448	0.37	372.4	0.31	1.2	7.8 × 10⁻⁰⁵	271	0.30	277.7	0.31	1.0	0.66
Synonymous	81	0.07	103.5	0.09	0.8	0.99	80	0.09	77.3	0.09	1.0	0.39
Missense	288	0.24	234.3	0.19	1.2	0.00038	163	0.18	174.7	0.19	0.9	0.82
D-Mis	99	0.08	40.6	0.03	2.4	7.7 × 10⁻¹⁵	37	0.04	30.3	0.03	1.2	0.13
LoF	79	0.07	34.5	0.03	2.3	6.2 × 10⁻¹¹	28	0.03	25.7	0.03	1.1	0.35
Damaging	178	0.15	75.1	0.06	2.4	5.1 × 10⁻²⁴	65	0.07	55.9	0.06	1.2	0.13
LHE genes												
Total	825	0.68	940.3	0.78	0.9	1	654	0.73	702.1	0.78	0.9	0.97
Synonymous	196	0.16	267.8	0.22	0.7	1	149	0.17	200.1	0.22	0.7	1
Missense	558	0.46	590.5	0.49	0.9	0.91	451	0.50	440.9	0.49	1.0	0.32
D-Mis	113	0.09	92.4	0.08	1.2	0.021	82	0.09	69.0	0.08	1.2	0.069
LoF	71	0.06	82.0	0.07	0.9	0.9	54	0.06	61.1	0.07	0.9	0.83
Damaging	184	0.15	174.4	0.14	1.1	0.24	136	0.15	130.1	0.14	1.1	0.31

occurrence (Fig. 1A; median expected = 7; $P = 1.1 \times 10^{-5}$ by permutation), suggesting that these genes are likely to be pathogenic for CHD (Fig. 1B). Indeed, this list includes seven genes previously implicated in CHD (*PTPN11*, *KMT2D*, *CHD7*, *MYH6*, *JAG1*, *NOTCH1*, and *ZEB2*). Enrichments were not observed among genes with multiple de novo synonymous variants in CHD cases or across any variant class among controls (Fig. 1A and table S5). A variety of cardiac mal-

formations were associated with mutations in each of these 21 genes (Fig. 1B and table S6). From simulations based on these data (12), we estimate that de novo mutations in ~392 HHE genes contribute to CHD pathogenesis (fig. S1). Within this 21-gene set, *PTPN11*, *KMT2D* (*MLL2*), and *RBFOX2* each had significantly more damaging de novo mutations than expected (Bonferroni corrected threshold for genome-wide significance = $P < 9 \times 10^{-7}$; Fig. 1B). *RBFOX2*,

an RNA-binding protein that regulates alternative splicing, has not been previously implicated in CHD. *RBFOX2* harbored three distinct de novo LoF mutations, a highly significant finding (Fig. 1B; $P = 3.4 \times 10^{-8}$). Additionally, we previously identified a de novo copy number loss that encompasses *RBFOX2* in another CHD proband (13). These four probands all had hypoplastic left heart syndrome (HLHS). *RBFOX2* is critical for zebrafish heart development (14) and regulates

Fig. 2. Burden of damaging de novo mutations in HHE genes among CHD cases with extra-cardiac phenotypes. (A) The enrichment (ratio of observed to expected) of damaging de novo mutations in HHE genes is shown for each phenotype ($\pm 95\%$ confidence interval). Case probands were excluded if they carried de novo mutations in known CHD syndrome genes ($n = 19$), had unknown extracardiac phenotype for both NDD and CA ($n = 6$), or had one unknown phenotype and were negative for the other ($n = 273$). Cases with either CA or NDD and unknown status for the other phenotype ($n = 97$) were included in the “Extra” category but excluded from the “only” categories. (B) Percent excess of individuals carrying damaging de novo mutations in HHE genes by indicated phenotype ($\pm 95\%$ confidence interval). An explanation of the calculation is provided in (12). (C) Table of observed and expected de novo rates for the indicated variant classes by phenotype.



epithelial-mesenchymal transitions (EMTs) (15). Disruption of EMTs is felt to underlie HLHS pathogenesis (16). We observed significant enrichment of damaging mutations in *RFX2* target genes (17) in CHD cases (1.9-fold, $P = 6.6 \times 10^{-8}$) but not controls (table S7).

Analyses of gene (GO) and human phenotype (HP) ontologies revealed enrichment of damaging de novo mutations in genes involved in anatomic structure morphogenesis (GO:0009653; 2.4-fold; Bonferroni $P = 3.4 \times 10^{-14}$), cardiovascular system development (GO:0072358; 3.2-fold; Bonferroni $P = 7.5 \times 10^{-9}$), neurodevelopmental abnormality (HP:0012759; 2.6-fold; Bonferroni $P = 1.8 \times 10^{-6}$), and others (database S6). We replicated the reported excess of de novo LoF mutations affecting genes involved in chromatin modification (6), even after including only newly studied cases (GO:0016568, 5.1-fold enrichment, P value = 7.2×10^{-10} ; database S7). In the full CHD cohort, there were 25 de novo LoF mutations in chromatin-modifying genes, a 5.3-fold enrichment over expectation ($P = 5.7 \times 10^{-11}$, table S8; fig. S2), strongly supporting the conclusion that these damaging de novo mutations have large effects on CHD risk.

We examined the prevalence of damaging de novo mutations in CHD with or without NDD and/or CA (Fig. 2) after excluding 19 participants found to have de novo mutations in known syndromic CHD genes and 279 participants with uncertain NDD/CA status. Damaging de novo mutations in HHE genes were not significantly enriched in 356 participants with isolated CHD or in controls but were ~3-fold

enriched in 559 CHD cases with CA and/or NDD (CHD + Extra, $P = 1.1 \times 10^{-15}$), including 97 probands diagnosed with either NDD or CA but unknown for the other phenotype. Excluding these 97 probands, we observed a 4.7-fold enrichment of damaging de novo mutations in HHE genes among 138 CHD cases with both NDD and CA ($P = 5.6 \times 10^{-15}$), a 2-fold enrichment in CHD cases with only NDD (252 probands, $P = 3.8 \times 10^{-4}$), and a 2.9-fold enrichment in CHD cases with only CA (72 probands, $P = 7.4 \times 10^{-4}$). By comparing de novo rates in cases against expectation, we estimate that damaging de novo mutations in HHE genes contributed to 20% of CHD with both NDD and CA (95% confidence interval 12 to 30%), 10% (7 to 14%) of CHD with CA and/or NDD, 10% (2.5 to 23%) and 6% (2 to 11%) of CHD with CA only or NDD only, respectively, and 2% (0.5 to 5%) of isolated CHD (Fig. 2B). These results implied frequent pleiotropic effects of de novo mutations in CHD and raise the possibility that mutations in these same genes might also contribute to nonsyndromic NDD and/or other CA. We find that genes mutated in CHD are not only enriched for high expression in the developing heart, they are also enriched for high expression in the developing brain (table S9).

To further explore these pleiotropic effects, we considered whether genes with damaging de novo mutations in CHD with NDD overlapped with 1161 genes (database S8) found to contain damaging de novo mutations in seven cohorts ascertained for NDD phenotypes ex-

cluding CHD (published NDD, P-NDD gene set) (7, 18–23). Sixty-nine genes (table S10) with damaging de novo mutations ($n = 85$ mutations) were shared in CHD and P-NDD cohorts, far more than expected by chance (expected = 32 mutations; 2.6-fold enrichment; $P = 8.9 \times 10^{-15}$, Fig. 3A and table S11). HHE genes were particularly enriched among P-NDD genes that were mutated in CHD (4.4-fold for all CHD cases, $P = 1.2 \times 10^{-23}$, Fig. 3A and table S11). Moreover, genes mutated both in P-NDD and CHD cohorts are in the top quartile of both developmental heart and brain expression far more than expected by chance (observed = 38, expected = 11, $P = 6.1 \times 10^{-11}$, binomial test, Fig. 3B). The input of these 69 overlapping genes into GO ontology analysis revealed significant terms that were broadly involved in the regulation of developmental transcription programs. These included 19 chromatin modifiers (GO:0016568 9.3-fold, $P = 8.5 \times 10^{-10}$; database S9 and fig. S2), including genes responsible for altering the methylation, acetylation, or ubiquitination status of numerous regulatory lysine residues on the nucleosome. Additionally, there were 32 transcriptional regulators (GO:0006355 2.8-fold $P = 1.5 \times 10^{-4}$; database S9), including genes involved in Wnt (*CTNNT1*, *DVL3*, and *LRP5*) and Notch (*NOTCH1* and *EP300*) signaling, important pathways in cardiac development. These findings demonstrate shared genetic etiologies for CHD and NDD patients and confirm the pleiotropic effects of mutations in these genes. Because it is unlikely that many NDD-ascertained patients with these

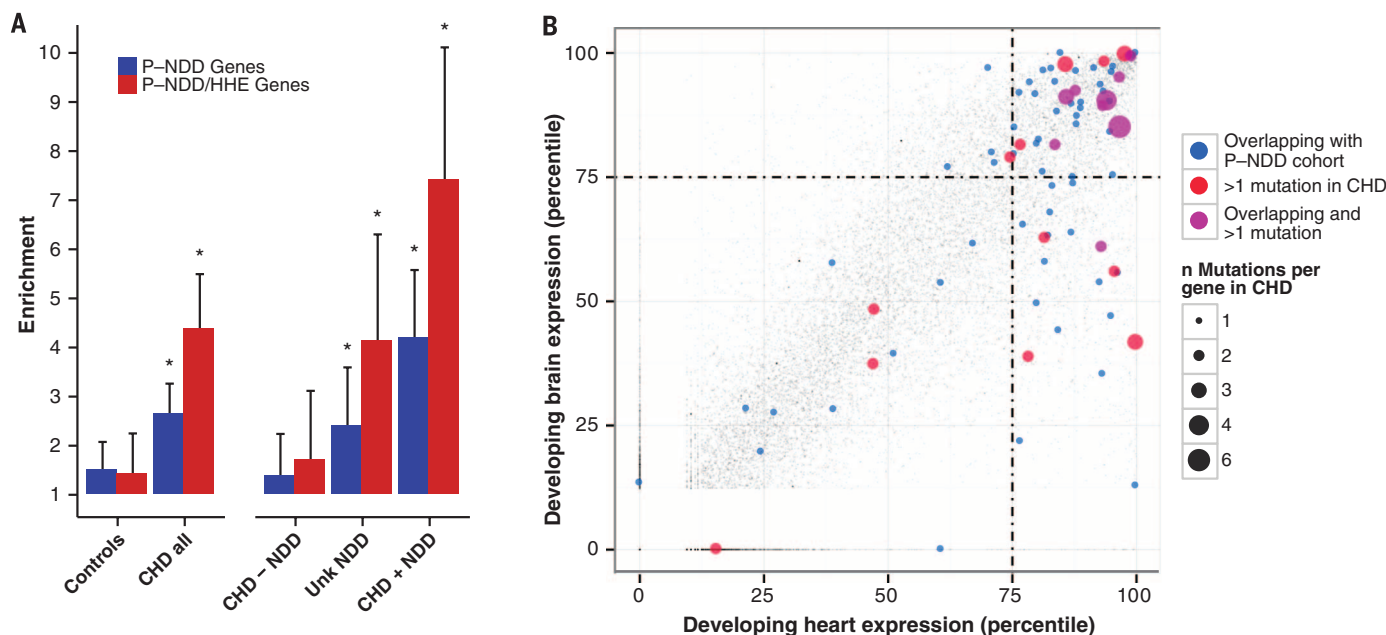


Fig. 3. Genes containing de novo mutations in CHD cases show pleiotropic developmental effects. (A) Individuals with CHD carry an excess of damaging de novo mutations among 1161 genes identified by containing damaging de novo mutations in seven published studies of NDD (P-NDD cohort) (7, 18–23). All CHD cases were subdivided by NDD status (CHD + NDD: $n = 417$ patients; CHD – NDD: $n = 440$; unknown NDD: $n = 363$). P values ≤ 0.005 as indicated (stars) were calculated from a Poisson test against a model-derived distribution

(values in table S11). The P-NDD gene set (blue) was further filtered for HHE genes (P-NDD/HHE, red, 564 genes). Enrichments are shown $\pm 95\%$ confidence intervals. (B) Percentile gene expression ranks (100 = high) are shown for all genes (gray) in the developing brain and heart, highlighting 69 genes with damaging de novo mutations in both CHD cases and the P-NDD cohort (blue or purple). Genes with multiple de novo mutations in CHD (red or purple) are shown. The point size represents the numbers of de novo events.

mutations had clinically important CHD, and not all CHD patients with these mutations have NDD (table S10), our findings also indicate that these mutations have variable expressivity, including isolated CHD, isolated NDD, or both.

Consistent with these observations, CHD participants with damaging de novo mutations in these 69 overlapping genes (Fig. 3A) had a significantly increased risk of NDD (absolute risk of 73%, odds ratio 3.1, $P = 7.9 \times 10^{-5}$, Fisher exact test). Damaging mutations (28 mutations in 27 participants) in chromatin modifiers showed the highest risk of NDD (19 participants with NDD, 8 with unknown NDD status due to age <1 year at evaluation). Moreover, the marked enrichments in damaging de novo mutations among P-NDD genes with HHE (Fig. 3A and table S11), 7.4-fold in 413 CHD cases with NDD ($P = 3.9 \times 10^{-22}$), 4.1-fold in 362 CHD infants with unknown NDD status ($P = 2.2 \times 10^{-7}$), and no significant enrichment in 438 CHD cases without NDD ($P = 0.075$), strongly imply a future risk of NDD among CHD infants with these variants. These observations suggest that genotype is a strong predictor for future development of NDD in CHD infants. Despite these highly significant findings, our estimates are based purely on statistical grounds and limited to in silico predictions of damaging variants, a caveat that should be considered when extrapolating these results to identify causative or predictive mutations in individual patients.

Contemporary therapeutic interventions have substantially improved survival among newborns with serious CHD. Despite these advances, many lifelong medical issues remain. The demonstration that damaging de novo gene mutations cause CHD, particularly when associated with NDD and other congenital anomalies, has both clinical and research implications. First, clinical genotyping may help stratify CHD patients and identify those

at high risk for NDD, enabling surveillance and early interventions to improve school performance, employability, and quality of life. Second, the pleiotropic consequence of these mutations implies that further study of these genes may uncover critical regulation of broad developmental programs. Finally, the high frequency of mutation in transcriptional regulators suggests that mutations in regulatory elements (promoters and enhancers) may be additional causes of CHD, particularly isolated CHD.

REFERENCES AND NOTES

1. A. Egbe, S. Lee, D. Ho, S. Uppu, S. Srivastava, *Ann. Pediatr. Cardiol.* **7**, 86–91 (2014).
2. B. S. Marino *et al.*, *Circulation* **126**, 1143–1172 (2012).
3. J. W. Gaynor *et al.*, *Pediatrics* **135**, 816–825 (2015).
4. B. Gelb *et al.*, *Circ. Res.* **112**, 698–706 (2013).
5. R. G. Ohye *et al.*, *N. Engl. J. Med.* **362**, 1980–1992 (2010).
6. S. Zaidi *et al.*, *Nature* **498**, 220–223 (2013).
7. I. Iossifov *et al.*, *Nature* **515**, 216–221 (2014).
8. S. J. Sanders *et al.*, *Nature* **485**, 237–241 (2012).
9. B. J. O’Roak *et al.*, *Nat. Genet.* **43**, 585–589 (2011).
10. K. E. Samocha *et al.*, *Nat. Genet.* **46**, 944–950 (2014).
11. C. Dong *et al.*, *Hum. Mol. Genet.* **24**, 2125–2137 (2015).
12. Materials and methods are available as supplementary materials on Science Online.
13. J. T. Glessner *et al.*, *Circ. Res.* **115**, 884–896 (2014).
14. T. L. Gallagher *et al.*, *Dev. Biol.* **359**, 251–261 (2011).
15. C. Braeutigam *et al.*, *Oncogene* **33**, 1082–1092 (2014).
16. E. J. Hickey, C. A. Caldarone, B. W. McCrindle, *J. Am. Coll. Cardiol.* **59** (suppl.), S43–S54 (2012).
17. G. W. Yeo *et al.*, *Nat. Struct. Mol. Biol.* **16**, 130–137 (2009).
18. EuroEPINOMICS-RES Consortium, Epilepsy Phenome/Genome Project, Epi4K Consortium, *Am. J. Hum. Genet.* **95**, 360–370 (2014).
19. J. de Ligt *et al.*, *N. Engl. J. Med.* **367**, 1921–1929 (2012).
20. A. Rauch *et al.*, *Lancet* **380**, 1674–1682 (2012).
21. S. De Rubeis *et al.*, *Nature* **515**, 209–215 (2014).
22. B. Xu *et al.*, *Nat. Genet.* **43**, 864–868 (2011).
23. Deciphering Developmental Disorders Study, *Nature* **519**, 223–228 (2015).

ACKNOWLEDGMENTS

The authors are grateful to the patients and families who participated in this research and team members who supported subject recruitment and sequencing: D. Awad, C. Breton, K. Celia, C. Duarte, D. Etwaru, N. Fishman, M. Kaspakova, J. Kline, R. Korsin, A. Lanz, E. Marquez, D. Queen, A. Rodriguez, J. Rose, J. K. Sond, D. Warburton, A. Wilpers, and R. Yee (Columbia Medical School); B. McDonough, A. Monaf, J. Stryker (Harvard Medical School); N. Cross (Yale School of Medicine); S. M. Edman, J. L. Garbarini, J. E. Tusi, S. H. Woyciechowski (Children’s Hospital of Philadelphia); J. Ellashek and N. Tran (Children’s Hospital of Los Angeles); K. Flack L. Panesar, N. Taylor (University College London); D. Gruber and N. Stellato (Steve and Alexandra Cohen Children’s Medical Center of New York); D. Guevara, A. Julian, M. Mac Neal, C. Mintz (Icahn School of Medicine at Mount Sinai); and E. Taillie (University of Rochester School of Medicine and Dentistry). We thank P. Candrea, E. Mazaika, K. Pavlik, V. Spoltow, and M. Sotiropoulos for production exome sequences and variant confirmation. This work was supported by grants from the National Heart, Lung, and Blood Institute (PCGC, Pediatric Heart Network, and Cardiovascular Development Consortium) and the National Human Genome Research Institute of the National Institutes of Health (NIH), Howard Hughes Medical Institute, Simons Foundation for Autism Research, John S. LaDue Fellowship at Harvard Medical School, Medical Scientist Training Program and National Research Science Award, Academy of Medical Sciences, British Heart Foundation, Wellcome Trust, Arthritis Research UK and the NIHR Cardiovascular Biomedical Research Unit at Royal Brompton and Harefield NHS Foundation Trust and Imperial College London, Leducq Foundation, Heart and Stroke Foundation of Ontario, Ted Roger Centre for Heart Research, Kostin Family Innovation Fund, Aaron Stern Professorship at the University of Michigan, and Braylon’s Gift of Hope Fund. The views expressed are those of the authors and do not necessarily reflect those of the National Heart, Lung, and Blood Institute or NIH. R.P.L. is on the Board of Directors of Roche. J.G.S. and C.E.S. are founders of and own shares in Myocardia, a biotechnology company developing small molecules for the treatment of inherited cardiomyopathy.

SUPPLEMENTARY MATERIALS

www.sciencemag.org/content/350/6265/1262/suppl/DC1
Materials and Methods
Tables S1 to S12
Figs. S1 to S3
Databases S1 to S10
References (24–29)
Additional Acknowledgments

1 July 2015; accepted 16 October 2015
10.1126/science.aac9396

BOYALIFE
& Science
Science Translational Medicine
Award in
Stem Cell
and Regenerative
Medicine

Call for entries: a global award in stem cell and regenerative medicine

Stem cell and regenerative medicine is the new frontier in life sciences.

Boyalife, Science and Science Translational Medicine jointly establish a global award to recognize significant contributions in advancing basic science to clinical applications in this field.

The award is to recognize and reward scientists in the fields of stem cell and/or regenerative medicine with a focus on developing cell-based treatments for cancer, degenerative disorders, immunotherapy and stem cell transplantation.

You could be next to win this prize and to receive

- ★ A Grand Prize of **\$25,000** and a Runner-Up Prize of **\$5,000** will be awarded.
- ★ The Grand Prize Winning Essay will be published in Science; a brief abstract of the Runner-Up Essay will be published in Science.

The 2016 Award is now open. The deadline for submissions is March 1, 2016
For more information, please visit: <http://bitly.com/BoyalifeSciencePrize>



300



BIO-RAD'S DROPLET DIGITAL™ PCR SYSTEMS

Over 300 Peer-Reviewed Droplet Digital PCR (ddPCR™) Publications*

From detection of rare mutations and cancer biomarkers to quantification of gene editing events and miniscule viral loads, the QX100™ and QX200™ Droplet Digital PCR Systems have been used to redefine the limits of absolute nucleic acid quantification. With over 300 peer-reviewed publications, ddPCR platforms have outperformed other digital PCR systems by several orders of magnitude. The third-generation QX200™ AutoDG™ System now brings automation and scalability to digital PCR.

Visit bio-rad.com/info/ASCB300 for the publication list and to learn more.

BIO-RAD

* Based on PubMed data, October 2015.

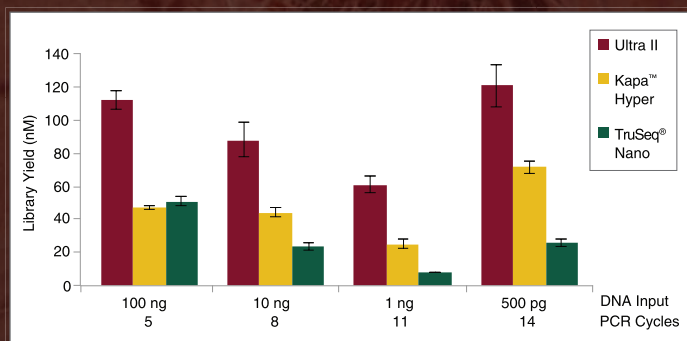
Even more *from less.*

NEBNext[®] Ultra[™] II DNA Library Prep Kit for NGS

Are you challenged with trying to get higher library yields using ever-decreasing input amounts? Each component in the NEBNext Ultra II DNA Library Prep Kit from NEB[®] has been reformulated, resulting in a several-fold increase in library yield with as little as 500 picograms of input DNA. These advances deliver unprecedented performance, while enabling lower inputs and fewer PCR cycles. Get even more from less with NEBNext Ultra II.

Visit **NEBNextUltraII.com** to learn more and request a sample.

The NEBNext Ultra II DNA Library Prep Kit for Illumina[®] produces the highest yield libraries from a broad range of input amounts.



Libraries were prepared from Human NA19240 genomic DNA using the input amounts and numbers of PCR cycles shown. Manufacturers' recommended protocols were followed, with the exception that size selection was omitted.

Finding cures starts with research tools that actually work...

- Proteomic products and services
- Focused product portfolio
- Products tested for specificity and sensitivity
- Antibodies rigorously tested across a wide range of research applications
- Custom formulations
- GMP-grade recombinant rabbit monoclonal antibodies*
- Bulk orders and lot reservations

* Custom formulations of certain monoclonal antibodies can be produced by CST in compliance with FDA regulations governing ASRs. Such products would be classified as Analyte Specific Reagents. Analytical and performance characteristics are not established. All other products are for Research Use Only. Not For Use In Diagnostic Procedures.

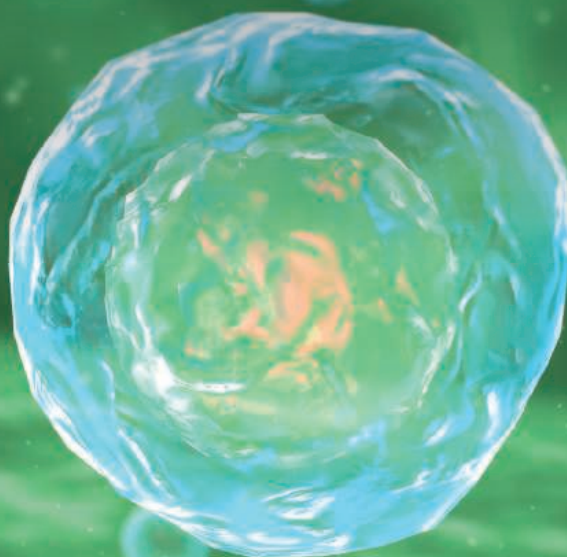


Learn more at: www.cellsignal.com/drugdiscovery



Visualize Cellular Responses

CELLESTIAL® Fluorescent Probes

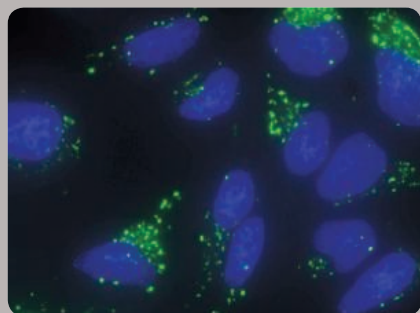


High-Specificity Next Generation Fluorescent Probes

Our CELLESTIAL® portfolio of fluorescent probes and assay kits for cellular analysis provides a complete set of tools for monitoring cell viability, proliferation, death, oxidative stress and toxicology on flow cytometry, microscopy and microplate platforms. Our assays and probes are optimized for the most demanding imaging applications, where consistency and reproducibility are essential.

CYTO-ID® Autophagy Detection Kit

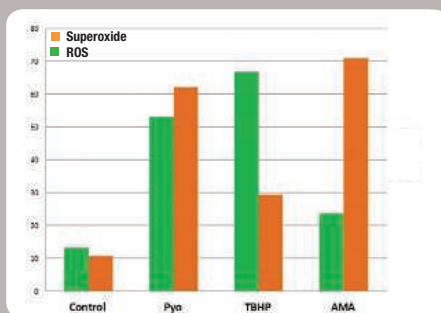
A no-transfection assay for monitoring autophagy



Fluorescent Microscope

ROS-ID™ Total ROS/Superoxide Detection Kit

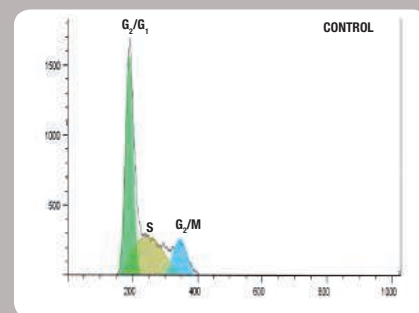
Accurately profile Total ROS and Superoxide with dual-readout assay



Fluorescent Microplate Reader

NUCLEAR-ID® Red DNA Stain

Brighter cell permeable DNA stain






Flow Cytometer



X2 for CRISPR

***TransIT-X2®* Dynamic Delivery System**

Cas9:	-	pDNA protein	
gRNA:	-	+	+
uncut			
cut			
Cleavage Efficiency (%)		44	42

-  **DNA**—deliver plasmid DNA expressing Cas9 or guide RNA
-  **RNA**—deliver sgRNA or crRNA:tracrRNA
-  **Protein**—deliver Cas9:gRNA RNP complexes

mirusbio.com

Providing gene delivery expertise since 1995

©2015 All rights reserved Mirus Bio LLC. *TransIT-X2* is a registered trademark of Mirus Bio LLC.



**AAAS 2016
ANNUAL MEETING**

WASHINGTON, DC
FEBRUARY 11–15

Global Science Engagement

Register and book your housing now to use funds from fiscal year 2015. Reduced rates are available until January 19, 2016. AAAS members are eligible for further discounts

aaas.org/meetings

AAAS, publisher of *Science*, thanks the sponsors and supporters of the 2016 Annual Meeting



for its generous support of
the Science Journalism Awards



As of November 16, 2015

"What I do with my Octet HTX time? Climb."

Shave weeks off your lead selection programs.

Broader antibody cross-competition ups your odds of finding the best candidates, but larger epitope binning studies take time. The Octet HTX system lets you use any binning assay format, any size matrix, start a run and get analyzed results the same day or the next day for larger studies. You can also combine multiple experiments into one dataset to easily visualize and cluster antibodies in similar bins or binding groups.

Lucy gets out of the lab more often now to climb.
What will you do with your extra time?



fortéBIO
A Division of **Pall Life Sciences**

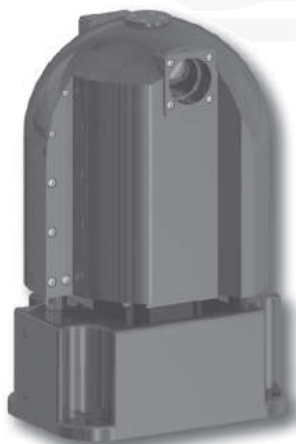
PALL Life Sciences

fortebio.com | 888-OCTET-75

Fast. Accurate. EASY.

LAMBDA VF-5 Tunable filter changer

NEW!



Introducing the world's first filter changer to use tunable thin-film optical filters. The Sutter **LAMBDA VF-5** allows you to quickly access any center bandpass from 330 to 800nm in nanometer increments. Building on the VersaChrome® filters from Semrock®, the **LAMBDA VF-5** maintains transmission over the tuning range of each filter.

Easy Wavelength Selection

Wavelength range as wide as 330-800nm
Keypad or computer interface (USB or serial)

Flexible

Suitable for excitation or emission
Easily switch between fluorophore combinations
Optional liquid light guide offers absolute vibration isolation
Images pass through filters

Thin filter advantage

High transmission
Steep spectral edges
High out-of-band blocking
Polarization independence
(s and p nearly identical)

SUTTER INSTRUMENT

PHONE: 415.883.0128 | FAX: 415.883.0572
EMAIL: INFO@SUTTER.COM | WWW.SUTTER.COM

AAAS Travels



Discover KAMCHATKA & Lake Baikal!

Including the Trans-Siberian Express
July 22–August 6, 2016

Explore the two finest natural areas in Russia—Kamchatka Peninsula and Lake Baikal! Take the Trans Siberian Express from the Russian Far East across the vast taiga of Russia to Irkutsk and Lake Baikal. Baikal is the richest single location in Russia for endemism, a fabulous reservoir of unique flora and fauna. It is the oldest and deepest lake in the world. We invite you to join Dr. Victor Kuzevanov for a fascinating adventure! \$5,995 pp + air.

For a detailed brochure, call (800) 252-4910

All prices are per person twin share + air



BETCHART EXPEDITIONS Inc.
17050 Montebello Rd, Cupertino, CA 95014
Email: AAASInfo@betchartexpeditions.com
www.betchartexpeditions.com

myIDP:
A career plan customized
for you, by you.



For your career in science, there's only one **Science**



Recommended by
leading professional
societies and the NIH

Features in myIDP include:

- Exercises to help you examine your skills, interests, and values
- A list of 20 scientific career paths with a prediction of which ones best fit your skills and interests
- A tool for setting strategic goals for the coming year, with optional reminders to keep you on track
- Articles and resources to guide you through the process
- Options to save materials online and print them for further review and discussion
- Ability to select which portion of your IDP you wish to share with advisors, mentors, or others
- A certificate of completion for users that finish myIDP.

Visit the website and start planning today!
myIDP.sciencecareers.org

ScienceCareers In partnership with:





Organelle recitals

To isolate and study organelles from cells, scientists use methods that range from primitive to modern. **By Alan Dove**

Over 50 years ago, Albert Claude and George Palade of Rockefeller University found a way to separate the individual organelles of cells for analysis. Their method, differential centrifugation, relied on breaking the cells' outer membranes and then sedimenting the lysate through fluids of different viscosities. This work helped start the era of modern cell biology.

The field has since blossomed and expanded in ways its founders never anticipated, but as a new generation of researchers brings modern proteomic and genomic tools to bear on organelle biology, they often find that the first few steps in their protocols have hardly changed. Dounce homogenizers, centrifuges, and sucrose gradients still feature prominently in cellular laboratories everywhere. "I don't think we have seen any revolution in the field since Claude and Palade's differential centrifugation," says Luca Scorrano, scientific director of the **Venetian Institute of Molecular Medicine** in Venice, Italy.

Old school

Cell biology's reliance on classical techniques can be both reassuring and annoying. The standard approaches use equipment and reagents most researchers probably already have in their labs, but figuring out exactly how to purify a particular organelle can be surprisingly difficult. Scorrano explains that newcomers to the field quickly find that methods sections in modern papers often reference work from decades earlier. "It takes quite a while to dig into the original literature to find how they really isolate [organelles]," he says.

Even with a published protocol in hand, the process

may not work as expected. "There are a number of tricks which are usually passed from researcher to researcher by word of mouth," says Scorrano. Several years ago, he and his colleagues crystallized one such artisanal protocol for mitochondrial isolation by publishing it in a peer-reviewed journal. Unfortunately, Scorrano says that few others have followed suit, because so much of the field's technical knowledge continues to reside in oral traditions. "If you have [access to] somebody who is knowledgeable about [organelle] preparation, use them," he adds.

When researching an organelle isolation method, investigators should also consider what they intend to do with the final product. For example, studying the physiological state of mitochondria in a rat liver at a particular time may call for a rapid but crude extraction of the organelles before they begin to degrade. Proteomic analysis of the same mitochondria would require more careful purification, with less concern about maintaining the organelles' physiology.

Scorrano points out that the mitochondrial field also has a historical division between researchers working on protein import, who often study yeast, and those studying bioenergetics using rat liver cells. Yeast mitochondrial isolation generally involves hyperosmotic buffers that could derail the physiology of rat mitochondria.

Despite the challenges of starting from scratch, Scorrano takes a dim view of prepackaged organelle purification kits, preferring that those in his lab learn the entire process. "You might need some time to get to a level in which you can easily isolate organelles with decent purity and with decent function, but [kits] are banned in my lab," he says.

Kitting up

Researchers with less experience in organelle isolation tend to be more open to off-the-shelf solutions, and several companies cater to that market. "These are definitely well-established protocols; there's nothing new under the sun," says George Yeh, product manager for protein biology at **Sigma-Aldrich** in St. Louis, Missouri. However, Yeh adds that "one concern is uniformity of technique from lab to lab." Using a prepared reagent kit and protocol from an established company can improve reliability. "I think what we bring to it is consistency—that you know that every lot of the kit is going to look the same—and the ease of use," says Yeh.

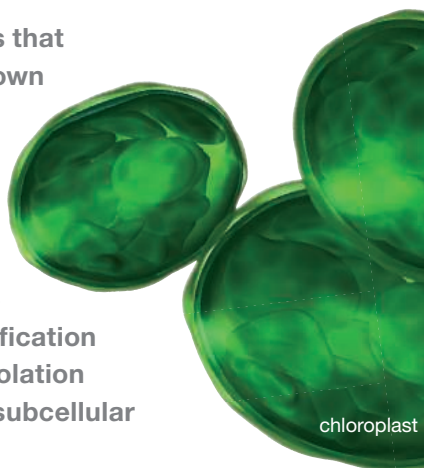
Sigma-Aldrich currently offers over a dozen different organelle isolation kits, each optimized for a specific organelle or type of analysis. "We have kits for isolation of peroxisomes or Golgi or endoplasmic reticulum, [or] chloroplasts for those working on plants," says Yeh. For organelles that contain their own DNA, such as mitochondria and chloroplasts, researchers can follow the organelle purification with a DNA-isolation step to track subcellular genetics.

Scientists studying organelle-associated proteins increasingly use mass spectrometry after purifying the target organelle, which has added a new **continued**

Upcoming Features

Automated Sample Preparation—January 15 ■ **Genomics—February 12** ■ **Tissue Analysis—March 4**

For organelles that contain their own DNA, such as mitochondria and chloroplasts, researchers can follow the organelle purification step to track subcellular genetics.



challenge: Reagents used in some older protocols may interfere with mass spectrometers. In response, Sigma-Aldrich has launched a series of reagents and kits designed to be mass spectrometry-compatible.

Besides kits, the chemical supply giant also sells individual reagents, and Yeh concedes that ready-made kits may not always be the most cost-effective choice. "If you're going to do it a hundred times over, I would bet you're better off making your own kit," he says, adding that "the market we serve [with kits] are people who do it once or twice."

Regardless of which approach they choose, Yeh echoes Scorrano's assessment that any lab should be able to execute competent organelle isolations once they've taken the time to learn and practice the procedures. "There's always that first hurdle to jump over, but once they do that they're on their way," says Yeh.

Smart shopping

Over the years, some researchers and lab suppliers have also developed their own special tricks to improve organelle isolation procedures. Although most of the modifications are minor, they add up for certain types of analyses. "Traditional methods will provide purified proteins to the extent of doing Western blots, where even a degraded protein might work . . . but when you go for any activity analysis, you will need the protein to be in its functional state," says Payal Khandelwal, product manager for assay kits at **Biovision** in Milpitas, California. "That is where the more enhanced techniques come into the picture," adds Khandelwal.

Besides protein degradation, older techniques may be less effective at separating different organelles from cytoplasmic components. That may not matter for physiological experiments, but in highly sensitive genomic or proteomic studies, the contaminants could mask the phenomena the researcher is trying to track.

Biovision is one of several companies working to solve those problems with carefully optimized organelle purification

kits. "It's not involving any extra machinery or instrumentation; it just involves some very specific and very advanced reagents which are provided along with the kit," says Khandelwal. Other than the kit, researchers need only ordinary centrifuges and related equipment they probably have on hand.

Perhaps the most challenging part of using such kits is deciding which one will work best. Comparing the protocols to see which is the most straightforward is one approach, but companies don't disclose the proprietary ingredients in their buffers, so it can be hard to predict which will work best for a particular lab's needs. Khandelwal suggests asking about the expected yield of a kit and the assays required to determine whether the isolation worked. "If the client is looking at, say, mitochondrial DNA, of course DNA is going to be isolated, but how do you know whether it is pure mitochondrial DNA, or [if there is] contamination from nuclear DNA?" asks Khandelwal.

Another advantage of using kits optimized for a particular type of experiment is support. If the experiment doesn't work, researchers who've used kits can call the manufacturer for troubleshooting help, whereas those who've mixed their own reagents will have to figure out the problem on their own.

More than the sum of its parts

Although biochemists may be anxious to separate organelles from their cellular contexts, it often pays to take a close look at the intact system first. That's particularly true for mitochondria, which can adopt different configurations depending on the cell's physiological state. "We once described the mitochondrion as a small football-shaped organelle," says James Murray, general manager of **Abcam** in Cambridge, United Kingdom. He adds, "We've come to realize that that's actually not the case; they're not discrete organelles necessarily."

Indeed, depending on the cell type and its current state, mitochondria can be individual ellipsoids or may form reticulated networks that connect to other structures such as the endoplasmic reticulum and plasma membrane. "It's a very dynamic and fluid situation," says Murray.

That raises problems for researchers who want to study isolated mitochondria. Pulling a spaghetti-like network of membranes out of a cell is considerably harder than separating discrete organelles. Murray suggests that researchers begin by using techniques such as immunofluorescence to visualize a cell's organization before deciding whether to break it open. If the question is whether a particular protein localizes to a particular organelle, microscopy could provide all the necessary data without requiring researchers to resort to any isolation techniques.

For those who do need to fractionate cells, Murray reiterates other experts' advice to pick the right protocol for the ultimate analysis. Experiments that require intact, physiologically active mitochondria are among the most finicky organelle isolations. Starting with healthy, fresh cells, experimenters need to complete the entire protocol



Featured Participants

Abcam
www.abcam.com

Biovision
www.biovision.com

New England Biolabs
www.neb.com

Sigma-Aldrich
www.sigmaaldrich.com

Simon Fraser University
www.sfu.ca

**Venetian Institute of
Molecular Medicine**
fondbiomed.it/vimm

and analysis as quickly as possible. Efforts to revive mitochondria after storage in a freezer generally fail.

Getting active mitochondria also requires one step that kit makers haven't been able to simplify: sucrose gradient centrifugation. Researchers must mix two different concentrations of sucrose together while slowly transferring the mixture into a centrifuge tube, generating a smoothly increasing density gradient from the bottom to the top of the tube. The gradient has to be mixed immediately before use, and getting consistent results takes practice.

Abcam and other companies are working on antibody-based organelle purifications that would omit the tedium of sucrose gradients, but those products are still in development. "I think maybe we're on the cusp of taking a step forward and having affinity-based methods to isolate organelles," says Murray.

The methyl lab

For investigators who just want to isolate mitochondrial or chloroplast DNA and don't care about the organelles' physiological states, that future has already arrived. Scientists at **New England Biolabs** (NEB) in Ipswich, Massachusetts have developed an antibody-based protocol for separating organelle and nuclear DNA. The technique exploits differences in methylation between the two pools of genetic material.

"In nature, organellar DNA is not methylated, or is methylated at a very low level," explains Erbay Yigit, applications and product development scientist at NEB. Yigit and his colleagues created a methyl-binding protein fused to an antibody constant region, which binds DNA only if it's relatively well-methylated. By allowing the engineered protein to bind total isolated cellular DNA, the team can precipitate the nuclear DNA from the mitochondrial or chloroplast DNA.

The researchers originally developed the protocol to separate microbial from human genomic DNA for microbiomics research, but quickly found that it works well for organelle DNA separation as well. NEB now sells the reagents in kit form, including magnetic beads covered in Protein A, which bind the antibody constant region to precipitate the methylated nuclear DNA without a centrifugation step. "This protocol is really straightforward, so you can start with extracted DNA [and] there's nothing

to be scared of," says Yigit. After a standard DNA purification protocol, researchers need to perform only a few additional steps to separate the organelle and nuclear DNA fractions.

Plant biologists may still have to deal with a tricky separation problem, however. Yigit explains that the NEB kit leaves mitochondrial and chloroplast DNA in the same fraction. "DNA from these organelles is very similar," he says.

Download the app

Although the growing collection of kits certainly speeds many types of experiments, some scientists may be able to get a head start on their subcellular studies without even getting their hands dirty. "If you know the protein sequence, you can deduce, in some cases very accurately, where that protein is located," says Fiona Brinkman, professor in the School of Computing Science at **Simon Fraser University** in Burnaby, British Columbia, Canada.

Brinkman and her colleagues have developed a software application called "PSORT" to make such predictions. The team initially focused on bacterial and archaeal proteins, but a branch of the program also works for eukaryotic cells. "We're [increasingly] appreciating [that bacteria] have organellar-like structures," says Brinkman.

PSORT uses a machine learning algorithm, which takes examples of well-proven protein localizations and then extrapolates to predict which other proteins will localize similarly in cells. Brinkman explains that "there's a lot of power in getting more lab data" to train the algorithm further, but the search for those data has revealed some of the pitfalls of fractionating cells. Brinkman emphasizes that researchers need to analyze all of the fractions they isolate, rather than just the one that interests them most. "You can have contamination from other fractions, so you want to see that [a protein] is actually located predominantly in one fraction," she says.

After being fed carefully vetted data, however, PSORT has matured into a powerful tool. "It's impressively accurate now for the organisms that have been traditionally well-studied," says Brinkman, adding that her team is now extending the program to make predictions for a broader range of organisms. Since its development, PSORT has been downloaded thousands of times and cited in numerous publications.

PSORT's popularity suggests that many investigators with little bioinformatics training are using it. Brinkman encourages that, but cautions users to read the associated publications. "For any computational method . . . make sure you're aware of the accuracy and how that's been investigated for a particular method," she says.

That advice echoes what Scorrano says about traditional differential centrifugation: "It's easy. [But] it's much more complicated to interpret [the results]."

Alan Dove is a science writer and editor based in Massachusetts.

DOI: 10.1126/science.opms.p1500100

Mass Cytometry System

The CyTOF platform enables system-level biology at single-cell resolution, on an accessible, expandable system designed for breakthrough discovery. Mass cytometry has driven the revolution of single-cell proteomics, enabling the most comprehensive understanding of cell phenotypes, signaling pathways, and function. Helios is the most advanced tool for cellular exploration, with streamlined workflows and multimodal capabilities that can transform single-cell biology. The Helios platform delivers an extensive list of features and advances to the core CyTOF technology, enhancing performance and convenience of operation. These include a more intuitive and easy-to-use software interface with real-time data display, normalization, and control. Helios also provides improved sensitivity to detect and resolve lower-abundance targets and an expanded mass range of 135 discrete channels with virtually no signal overlap or background noise as compared to conventional techniques. This enables more comprehensive and straightforward panel designs and higher-quality data sets.

Fluidigm

For info: 866-358-4354
www.fluidigm.com

Broadband Filter Sets

Three exciting new broadband filter sets that support Brilliant Violet and Ultraviolet dyes are now available. When used in conjunction with these 10× brighter dyes, the new filter sets allow microscopists to visualize molecules of small quantities or low expression within the cell. For laser applications, including flow cytometry, these new emission filters are designed to block common laser lines of 355 nm and 405 nm. The BUV395-3018A, BV421-3824A, and BV510-3825A sets are all available for purchase online and immediate shipment. All Semrock products carry their industry-leading 10-year warranty. All of the new BD Bioscience Brilliant dyes and Semrock filter products are available to test and model in SearchLight, the online toolbox that allows you to easily see all of the elements of your fluorescence system. SearchLight allows engineers and biologists alike to quickly calculate relative signal brightness, signal-to-noise ratio, and autofluorescence levels for best filter compatibility.

Semrock

For info: 866-736-7625
www.semrock.com



Cell Counter

The Cell Counter model R1 offers user-friendly and cost-effective cell counting for routine cell culturing. The R1 uses innovative liquid-lens autofocus technology, which mimics the way the human eye focuses. It features software with a unique algorithm for accurate, automated cell counts in as little as 15 seconds. The R1 is designed to be user friendly and includes a 7-inch touchscreen display with an intuitive interface. The software is easily optimized and features cell-size and roundness-based sorting capabilities, the ability to identify live and dead cells, clumped cell declustering, and an automatic dilution calculator. Users can easily adjust the minimum and maximum cell size so that only desired cells are detected. Counts can then be displayed as a histogram for analyzing certain cells based on size distribution. The R1 can store up to 1,000 counts and 300 different cell protocols, facilitating quick setup and counting for routine culturing procedures.

Olympus

For info: +49-(0)-40-23773-5913
www.olympus-lifescience.com

Fluorescence Illumination System

The new Lumen 1600-LED fluorescence illumination system is designed for the most advanced fluorescent techniques; however, it has intuitive controls making it easy to use. The light-emitting diodes (LEDs) in the Lumen 1600 last at least 25,000 hours and deliver evenly distributed, high-intensity light for optimal excitation of fluorophores. Incorporating 16 LEDs and covering the spectrum from 365 nm to 770 nm, the Lumen 1600 is an ideal illumination tool for work involving multiple fluorophores. Using an innovative four-channel system, the Lumen 1600 allows up to four distinct fluorophores to be excited simultaneously. These LED groupings allow the use of almost all stains used in multiband combinations, allowing great flexibility in experimental work. Multiple preset modes are possible, from simple white light illumination to more advanced options with different intensities of individual LED emissions. This flexibility makes the Lumen 1600 ideal for use by imaging facilities where multiple users with different requirements use the same equipment.

Prior Scientific

For info: +44-1223-881711
www.prior.com

Cell Disruption Device

The Spiral Mill from Cellcrusher is a cooled-bead homogenizer for disrupting tough microorganisms. It is designed specifically for protein-scale work, accommodating 1–6 g samples. These samples are disrupted in reusable grinding chambers made of stainless steel to facilitate cooling. The unique cell-disruption process involves a rotating spiral inside the grinding chamber. In the narrow space between the spiral and the chamber wall, violent collisions occur between glass beads and cells, resulting in fast, effective cell lysis. The frictional

heat generated by these collisions is conducted away through the steel chamber walls. Unlike those found in other bead homogenizers, the Spiral Mill's sample chamber does not move, because agitation is induced by the rotating spiral. This design facilitates an uncomplicated, reliable cooling system involving pumped ice water. The temperature remains around 2°C during processing. The novel chamber design and simple cooling system make the Spiral Mill the ideal device for disrupting mid-size samples of the toughest microorganisms.

Cellcrusher

For info: +353-879905282
www.cellcrusher.com

Electronically submit your new product description or product literature information! Go to www.sciencemag.org/products/newproducts.dtl for more information.

Newly offered instrumentation, apparatus, and laboratory materials of interest to researchers in all disciplines in academic, industrial, and governmental organizations are featured in this space. Emphasis is given to purpose, chief characteristics, and availability of products and materials. Endorsement by Science or AAAS of any products or materials mentioned is not implied. Additional information may be obtained from the manufacturer or supplier.

Discover the future

4 leading positions at SciLifeLab



To further **strengthen** our **unique** research environment, we are looking to **recruit** four **outstanding** young group leaders



- Assistant Professor in Systems Biology



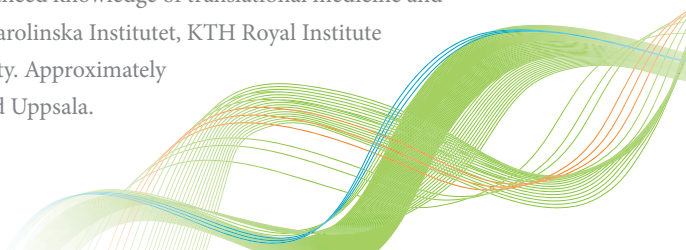
- Assistant Professor in Medical Infection Biology
- Assistant Professor in Computational Biology or Environmental Toxicology



- Assistant Professor in Bioinformatics

For more information, please visit: www.scilifelab.se/fellows

SciLifeLab is a Swedish national center for molecular biosciences with focus on health and environmental research. The center combines frontline technical expertise with advanced knowledge of translational medicine and molecular bioscience. SciLifeLab is a joint effort between Karolinska Institutet, KTH Royal Institute of Technology, Stockholm University and Uppsala University. Approximately 1 200 people work at the center's two sites in Stockholm and Uppsala.



WHY WORRY ABOUT CROSS-REACTIVITY?

Introducing Superclonal secondary antibodies,
a breakthrough technology designed to
eliminate cross-reactivity

The results are in, and the images are stunning. Our completely new category of secondary antibodies uses recombinant technology to offer accurate and precise detection of primary antibodies for bright, clear images. Thermo Scientific™ Superclonal™ Secondary Antibodies — a precisely better antibody.

See the difference at thermofisher.com/superclonal

ThermoFisher
SCIENTIFIC



There's only one **Science**

Science Careers Advertising

For full advertising details, go to ScienceCareers.org and click For Employers, or call one of our representatives.

Tracy Holmes

Worldwide Associate Director
Science Careers
Phone: +44 (0) 1223 326525

THE AMERICAS

E-mail: advertise@sciencecareers.org

Fax: +1 (202) 289 6742

Tina Burks

Phone: +1 (202) 326 6577

Nancy Toema

Phone: +1 (202) 326 6578

Online Job Posting Questions

Phone: +1 (202) 312 6375

EUROPE / INDIA / AUSTRALIA / NEW ZEALAND / REST OF WORLD

E-mail: ads@science-int.co.uk

Fax: +44 (0) 1223 326532

Sarah Lelarge

Phone: +44 (0) 1223 326527

Kelly Grace

Phone: +44 (0) 1223 326528

Online Job Posting Questions

Phone: +44 (0) 1223 326528

JAPAN

Katsuyoshi Fukamizu (Tokyo)

E-mail: kfukamizu@aaas.org

Phone: +81 3 3219 5777

Hiroyuki Mashiki (Kyoto)

E-mail: hmashiki@aaas.org

Phone: +81 75 823 1109

CHINA / KOREA / SINGAPORE / TAIWAN / THAILAND

Ruolei Wu

Phone: +86 186 0082 9345

E-mail: rwu@aaas.org

All ads submitted for publication must comply with applicable U.S. and non-U.S. laws. *Science* reserves the right to refuse any advertisement at its sole discretion for any reason, including without limitation for offensive language or inappropriate content, and all advertising is subject to publisher approval. *Science* encourages our readers to alert us to any ads that they feel may be discriminatory or offensive.

Science Careers

FROM THE JOURNAL SCIENCE AAAS

ScienceCareers.org

Advance your career
with expert advice from
Science Careers.



Download Free Career
Advice Booklets!

ScienceCareers.org/booklets

Featured Topics:

- Networking
- Industry or Academia
- Job Searching
- Non-Bench Careers
- And More



Science Careers

FROM THE JOURNAL SCIENCE AAAS

POSITIONS OPEN

Vice Chair for Research Pennsylvania State University

An opportunity exists for a Vice Chair for Research and Director of the Division of Musculoskeletal Sciences within the Department of Orthopaedics and Rehabilitation at The Pennsylvania State University College of Medicine. This is a tenure or tenure track faculty position at the rank of Associate or Full Professor. This position will provide administrative oversight of the Department's research programs and includes a highly competitive salary and start-up funds. This is a unique opportunity to join and direct a well-established, highly interactive research group consisting of engineers, material, clinical and basic scientists focusing on musculoskeletal research. A joint academic appointment will include a primary appointment in the College of Medicine at the Hershey, PA campus and a secondary appointment in an appropriate department at Penn State University main campus at State College, PA.

The professional qualifications for this position include: The ideal candidate will have an advanced degree of Ph.D., M.D., or M.D./Ph.D. Will have established an independent and extramurally funded research program in the area of musculoskeletal sciences or engineering. Demonstrated strong leadership skills; have experience in teaching and mentoring junior investigators, post-doctoral fellows, graduate and medical students; and have a record of strong publications in peer-reviewed journals. Will be an individual who can apply modern biomedical science and engineering concepts to the study of musculoskeletal tissues and lead others in developing their own research programs.

As part of one of the country's pre-eminent universities, our 551-bed tertiary medical center is the central Pennsylvania's region's only level I adult and pediatric trauma center and academic medical center. Also home to Penn State Children's Hospital, we are considered a resource for the most complex adult and pediatric cases. Hershey, PA, and the surrounding area offer a pleasant alternative to the pressures of urban living with a mix of well-maintained communities with quiet tree-lined streets, safe shopping districts, beautiful farmland, and state parks and game lands. It's the best of both worlds, with cultural events and nightlife both within Hershey and driving distance to Harrisburg; Philadelphia; the Pocono Mountains; Baltimore; Washington, D.C.; and New York City. The area is home to two professional sports teams, an amusement park, golf courses, professional and amateur theater, symphonies, and opportunities for hunting, fishing, and mountain biking.

Apply to job 58934 at website: <http://apptkr.com/690803>

CAMPUS SECURITY CRIME STATISTICS: For more about safety at Penn State, and to review the Annual Security Report which contains information about crime statistics and other safety and security matters, please go to website: <http://www.police.psu.edu/clery/>, which will also provide you with detail on how to request a hard copy of the Annual Security Report.

Penn State is an Equal Opportunity, Affirmative Action Employer, and is committed to providing employment opportunities to all qualified applicants without regard to race, color, religion, age, sex, sexual orientation, gender identity, national origin, disability or protected veteran status.

Download the
Science Careers
Job App

SEARCH JOBS
ON THE GO!

apps.sciencemag.org





**Deputy Director, Office of Extramural Research
National Institutes of Health
Department of Health and Human Services**



The National Institutes of Health (NIH) in Bethesda, Maryland, the world's largest medical research facility and an operating division of the U.S. Department of Health and Human Services (HHS), seeks applications from exceptional candidates for the position of Deputy Director, Office of Extramural Research (OER), Office of the Director (OD). This position reports to the NIH Deputy Director for Extramural Research/Director (DDER), OER and will coordinate activities across NIH, among other federal agencies and external organizations.

Leadership Responsibilities: On behalf of the DDER, the Deputy Director for the OER (DDOER) is responsible for the oversight and management of highly complex, cross-cutting, and sensitive assignments that include:

- leading and serving on trans-NIH activities to formulate, implement, and evaluate relevant extramural programs, policies, procedures, and priorities;
- representing the NIH on government-wide committees, task forces, and working groups;
- developing plans for future initiatives and preparing and/or presenting position papers on extramural issues of broad impact;
- directly engaging in legislative issues including actual testimony and preparing legislative testimony for use by the NIH;
- collaborating with other OD offices to address scientific and policy issues that affect extramural grantees; and
- serving as the Agency Extramural Research Integrity Officer.

Additional Responsibilities: The DDOER serves as the second authority for the OER and directs the OER Office of Communications Analysis and Planning. In this role, the DDOER allocates budgets and provides supervisory oversight for 28 staff.

Position Requirements: Candidates must have an M.D., Ph.D., or equivalent degree in a field relevant to the position. This position will be filled under a Title 42(f) excepted service appointment. An integral function of this position is bringing the appropriate individuals from across the NIH to coalesce around critical matters requiring immediate response, with the flexibility to move quickly from one issue to another with independence and authority. As such, the position requires professional interaction with the extramural scientific community. In addition, the DDOER must possess the ability to gain support of constituents that often may have competing interests, both internal and external to the NIH, on key public health policy issues. This is a highly visible position with significant impact on the NIH extramural community.

Salary/Benefits: Salary is competitive and will be commensurate with the experience of the candidate. A recruitment or relocation bonus may be available, and relocation expenses may be paid. A full package of Federal Civil Service benefits is available, including: retirement, health and life insurance, long-term care insurance, leave, and a Thrift Savings Plan (401K equivalent). The successful candidate is subject to a background investigation and public financial disclosure requirements.

How to Apply: Applicants must submit a current curriculum vitae, bibliography, and full contact details for three references. In addition, applicants are asked to prepare two statements: a vision statement and a statement that addresses the specific qualification requirements (please limit both statements to two pages each). Send application package by email to T42OER@od.nih.gov **OR** via mail to:

**Tamla Ransford
National Institutes of Health
Office of Extramural Research
6705 Rockledge Drive, MSC 7986, Suite 5016, Room 5110
Bethesda, MD 20892 (or 20817 for overnight delivery services)**

For additional information about this vacancy, contact Tamla Ransford at 301-451-7784. All applications must be postmarked by the closing date. OER will begin accepting applications on **December 4, 2015** and plans to have the position open for 30 days. To learn more information about the OER, please visit <http://grants.nih.gov>.

HHS and NIH are Equal Opportunity Employers



Basic Scientist – Oncology and Blood Disorders

The Department of Pediatrics, Northwestern University Medical School, Ann & Robert H. Lurie Children's Hospital of Chicago, and Robert H. Lurie Comprehensive Cancer Center are seeking a full-time physician scientist, M.D. or M.D./Ph.D., board certified in pediatric hematology/oncology to join a growing program of patient care, education and academic research. The individual must have a commitment to research in an area relevant to one of the following areas: pediatric oncology, neuro-oncology and/or blood disorders, molecular diagnostics/genetics, experimental hematopoiesis, stem cell biology, cancer bioinformatics, etc.



Protected time and space/support for research are available with an expectation for generating peer-reviewed publications and external funding. Participation in the inpatient/outpatient clinical oncology program is an expectation. A commitment to teaching and providing training opportunities for students and fellows is a requirement. Appointment will be made at the Associate or Professor level, commensurate with experience.

Please send CV and letter of interest by **December 15, 2015:**

Stewart Goldman, MD

**Division Head, Hematology, Oncology, Neuro-Oncology & Stem Cell Transplantation
Ann & Robert H. Lurie Children's Hospital of Chicago**

225 E. Chicago Box 30

Chicago, IL 60611

Tel: 312-227-4090

Fax: 312-227-9756

Email: sgoldman@luriechildrens.org

Northwestern University is an Equal Opportunity, Affirmative Action Employer of all protected classes, including veterans and individuals with disabilities. Women and minorities are encouraged to apply. Hiring is contingent upon eligibility to work in the United States.



**HARVARD
MEDICAL SCHOOL**

MASTER OF MEDICAL SCIENCES DEGREE in IMMUNOLOGY

A comprehensive program in Basic and Clinical Immunology taught by renowned Harvard faculty and intended for biology graduates interested in immunology research and medicine, as well as for research-oriented clinical fellows (MD, MBBS, and equivalent degrees) from all disciplines.

Visit <http://mmscimmunology.hms.harvard.edu/> for information on our comprehensive two-year program, including extensive coursework and laboratory-based research, at Harvard Medical School.

Email: mmsc_imm@hms.harvard.edu



Postdoctoral Program

Novartis Institutes for
BioMedical Research

Do you have a passion for innovative
fundamental research in drug discovery?

We are seeking creative postdoctoral
scholars to conduct exciting research in
biology, chemistry, and computational
sciences at the frontier of drug discovery.

Postdocs at NIBR who will subsequently
pursue faculty positions in academia are
eligible for start-up funds through our new
and highly competitive Young Investigator
Awards.

Visit <http://postdoc.nibr.com> to view our
mentors' research profiles and to apply.



Translational cell biology careers turn on technological savvy

Translational cell biologists pursue research questions that have a direct impact on treating human diseases. But to build a successful career, young cell biologists must also be well versed in technologies, such as those for advanced imaging, data mining, and biophysics, to push their research ahead. These cell biologists must embrace skills usually found in other departments—such as programming, performing heavy-duty statistical analysis, and even building devices from scratch in the machine shop. Turning laboratory findings into the foundations for potential new therapies also takes strong communication skills and a willingness to collaborate in team science or even across academia-industry borders. **By Kendall Powell**

Bernd Bodenmiller has never been quite satisfied with the state of current technology. As a graduate student in one of the founding laboratories of systems biology, he was fascinated with the power of new proteomics tools to survey all the proteins of a cell type. But he eventually grew frustrated by the fact that these measurements had to be averaged across millions of cells.

As a postdoc, he joined Garry Nolan's laboratory at Stanford University, in large part because it was the first lab to try out a new device called a "mass cytometer," or CyTOF, which married time-of-flight mass spectrometry with single-cell analysis of cells in solution. However, he soon realized that to answer his burning questions about what influences a stationary cancer cell to strike out and invade the rest of the body, he needed the technology to be able to analyze cells sitting in native tissues.

Bodenmiller's wanderlust to find and improve technolo-

gies for analyzing cell signaling led him to develop a laser-assisted mass cytometer that could analyze up to 50 different protein signals found in a single cell within a slice of tissue. It also drove his success as an assistant professor of quantitative biology at the University of Zurich, earning him highly competitive grants.

Now, Bodenmiller encourages young scientists in his group at the University of Zurich's Institute of Molecular Life Sciences to follow in his own footsteps for shaping a career on the frontiers of cell biology: to become established at the intersection of biology and new methods development.

"Developing a novel method and then applying this bleeding-edge technology to biological questions will yield novel views in biology and important findings with little competition," he notes. Focusing only on technologies or only on biology does not push either one forward with as much momentum or potential for breakthroughs, he explains.

Successful scientists working at the intersection of cell biology and human health are following this recipe for success, too, in slightly different variations. Many of them are both developing and applying new tools to build an increasingly complex view of the cell and its signaling networks during disease. Others are sifting through massive data sets to find new ways to target diseases. And still others are using advanced imaging and computing to find the subtle patterns that govern cell behaviors.

Young researchers who want to pursue a career in translational cell biology, whether in academic research or in industry, must be comfortable with data analysis, programming, and computational biology. They must also be collaborative and be able to work well in teams, which often include physicists, bioinformaticists, and software engineers.



Anne Carpenter

Problem-solving PIs

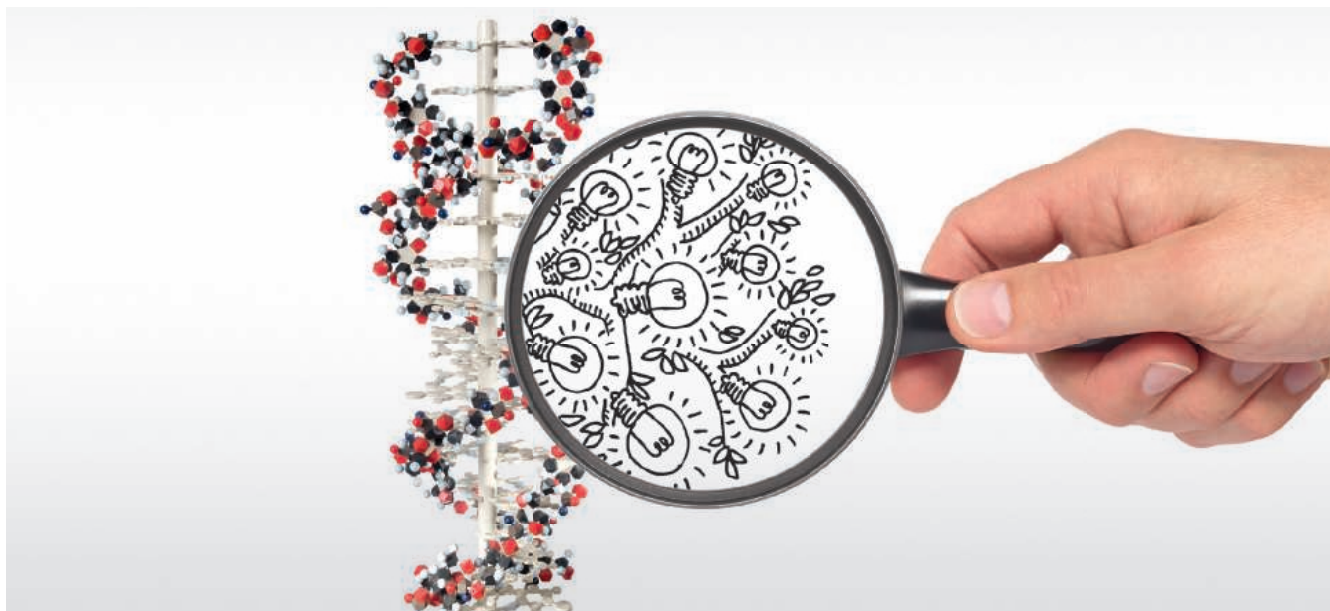
Several cell biology principal investigators (PIs) have made their mark as Bodenmiller did, by pushing technologies forward to help them answer their own research questions. As a postdoctoral fellow at the Whitehead Institute, **Anne Carpenter** found her lab's imaging software was not up to the task she needed to tackle—identifying phenotypic

changes in cell size and growth across thousands of cells in response to a genome-wide RNA interference (RNAi) screen. So she rolled up her sleeves, taught herself to program, and found a computer science graduate student from nearby MIT willing to lend a hand.

That collaboration eventually yielded CellProfiler, a software application used to do high-throughput imaging screens and to quantify phenomena observed **continued>**

Upcoming Features

Regional Focus: Asia—December 11 ■ Faculty Careers—January 29 ■ Postdoc Careers—March 25



Think beyond. Make a difference.

8.9 billion Swiss francs in core research and development expenditure in 2014 makes Roche one of the most research focused companies worldwide.

Our 120 year heritage and a stable shareholder structure ensure a long-term view and a strong and stable commitment to researching and developing novel treatments in the areas of oncology, immunology, infectious diseases, ophthalmology and neuroscience in order to improve the lives of patients all over the world.

Because it's not just a job.
It's a responsibility.
A big one.

The next step is yours.
careers.roche.ch/research





“The most important part is figuring out what cool, exciting data sets are out there and what are the unanswered questions you can ask using them.”

— Marina Sirota



by eye in the microscope. The program allows researchers to screen hundreds of thousands of drug compounds or genetic perturbations to find the conditions that give researchers the complex cellular readout they would like to see—such as a change in cell shape, organelle number, or cytoskeleton structure.

“A lot of our collaborators are trying to make in vitro systems more reflective of real biology,” which often requires using more complex cell-culture systems, says Carpenter, who is now leading a computational biology group at the Broad Institute of MIT and Harvard in Cambridge, Massachusetts. Through machine learning, a biologist trains the software to recognize subtle cellular differences.

Marina Sirota knew as early as college that she wanted to take “interesting biological experiments and map computer science onto them,” to perform sophisticated data analyses in order to query the explosion of genomic data. Sirota saw that researchers would need computational methods to wrangle data and to make real progress against human diseases.

As part of her Ph.D. work at Stanford University, Sirota launched a study to find potential new uses for drugs already on the market. The idea was based on matching human disease gene expression patterns with opposite or inverse drug gene expression patterns. In other words, if a disease caused a group of genes to be upregulated, was it possible to identify a drug that caused those same genes to be downregulated?

She ran an analysis of 164 drug compounds against gene profiles of about 100 diseases. One very promising hit was the antiseizure drug topiramate, which scored better against Crohn’s disease in the analysis than a known treatment for Crohn’s symptoms. The lab went on to show that topiramate worked better in an animal model of Crohn’s disease, too.

“It taught me how to ask questions in big data science,” says Sirota, now an assistant professor at the University of California, San Francisco’s Institute for Computational Health Sciences. “The most important part is figuring out what cool, exciting data sets are out there and what are the unanswered questions you can ask using them”

Finding creative new ways to manipulate big genetic or imaging data sets is a key skill for translational researchers looking to make an impact on disease. Likewise, working in collaborative, interdisciplinary teams is also a must. Bodenmiller’s project to adapt the CyTOF technique to image single cells in tissue exemplifies both skill sets.

“In the beginning it was a somewhat crazy idea,” says Bodenmiller of his moving a laser system into his lab to add to the CyTOF equipment. By adding the high-resolution laser to the microscope, his team developed a way to peel off tiny, 1-square micron tissue areas with surgical precision.

The CyTOF mass spectrometer can read information from up to 50 different heavy metal isotope markers tagging cellular proteins and protein modifications in each tiny spot. Using the laser’s coordinates, “we computationally generate an image by putting the marker information back in the right spots,” says Bodenmiller. His group uses the technique to define cellular signals that initiate metastasis in breast cancer. For such projects, he needs researchers with backgrounds in analytical sciences, cancer biology, and computational biology.

“My primary advice is to become very good at one of those areas,” he says. “But also to learn to interact with other people who have another expertise that you do not have.” Big data science absolutely requires collaboration, whether in academia or industry. “No single person can achieve every aspect of these projects,” says Bodenmiller. Successful young researchers learn to speak the different languages of a technology.

Skill building

Adam E. Cohen started his scientific life as a theoretical physicist, but became a biophysicist by immersing himself in biology’s language and all of its messy details. His group’s website at Harvard University has a tagline that sums up its mission: “Physical tools to study molecules, cells, and organisms.”

“The number one piece of advice I would give [young cell biologists] is to learn to program,” says Cohen. “If you can’t program, you are dead in the water when it comes to extracting meaning from digital data and analyzing it numerically.”

Researchers can take a boot camp or introductory class or simply learn by doing as Carpenter did in her work. Biology graduate students should all be learning to code as part of their training, Cohen insists.

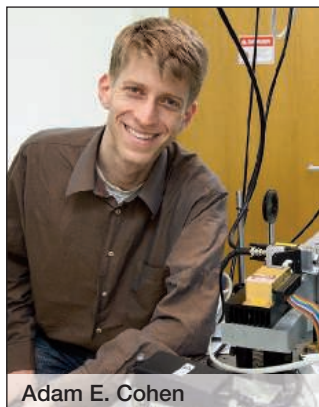
Strong quantitative skills will also help cell biologists distinguish themselves as researchers capable of extracting meaningful information from patient genomes, disease phenotypes, or cellular image-based screening. “If someone comes to me and asks, ‘What can I do to make myself more marketable?’ I tell them to become an expert in statistics or data mining,” says Carpenter.

Along those same lines, **Jennifer Gerton**, a geneticist at the Stowers Institute for Medical Research in Kansas City, Missouri encourages every trainee in her lab to take a class in bioinformatics. “Everyone is going to have to interact with bioinformatics experts in their career—they should at least learn the language so they can communicate,” she notes. She also advises trainees to think deeply about their research problem and how they might apply the latest explosion of imaging technologies toward solving it.

And sometimes it’s not a specific technical skill that’s required for success in these technology-based projects, but rather a fearless personality to handle whatever needs doing. Cohen’s lab experiments can run the gamut, from cell

culture to building lasers and doing hefty numerical analysis. So he looks for trainees with a “can do” attitude—including researchers who aren’t afraid to build things in the machine shop with the lathe and milling machine when needed.

Gerton adds another personality trait that all translational cell biologists should possess: a love of learning new things. Gerton studies cohesinopathies, a group of rare human developmental disorders. “I love sitting down with a big pile of papers. I did a lot of reading to try to understand the human diseases and the available models,” Gerton says.



Adam E. Cohen

Strategic career planning

Another key characteristic of successful investigators in this realm is the ability to think strategically about handling the high-risk nature of projects. Cohen says that because many of these projects do not ultimately succeed, he tries to steer his group to “fail as quickly as possible” by finding the weakest, most challenging nodes of an effort.

For academic job searches, Cohen advises candidates to build a nice balance between being visionary and realistic in their research proposals. “Propose things that are straightforward that you know you can do and things that are more exploratory or speculative. And be clear about those differences,” he says.

Both strategic thinking and deliberately acquired skills helped **Sam Hasson** achieve his desired career path in drug discovery in the pharmaceutical industry. Exceptional mentoring also secured his success.

Several experiences during graduate school, including a three-month internship immersed in drug discovery at Schering-Plough, showed Hasson that he belonged in the team-based and technology-driven research found in the pharma industry. So when looking for a postdoctoral fellowship, he asked himself, “How can I build up a skill set to make me attractive to industry?”

He found that opportunity at Richard Youle’s laboratory at the National Institute of Neurological Disorders and Stroke in Bethesda, Maryland. Youle’s lab had found that the protein Parkin normally translocates to the outer mitochondrial membrane when there is mitochondrial stress or damage. However, certain mutations in Parkin block this movement and are associated with an early-onset, inherited form of Parkinson’s disease.

Hasson took on a project to run a high-throughput imaging screen to find other genes that, when inhibited, either boosted or blocked Parkin’s normal activity. With Youle’s encouragement, Hasson designed and ran the screen with co-mentors at the National Center for Advancing Translational Science (NCATS), a National Institutes of Health (NIH)

Featured Participants

Broad Institute of MIT
and Harvard
www.broadinstitute.org

Harvard University
www.harvard.edu

Institute of Molecular Life
Sciences, University of Zurich
www.imls.uzh.ch

National Institute of Neurological
Disorders and Stroke
www.ninds.nih.gov

Pfizer
www.pfizer.com

Stowers Institute for
Medical Research
www.stowers.org

University of California,
San Francisco
www.ucsf.edu

center located just 10 miles north in Rockville. Youle knew that learning all the ins and outs of the entire functional genomics screening process would give Hasson experience that is highly valued by industry.

In addition, when Youle was invited to give a talk at a Pfizer forum on mitochondrial health, he sent Hasson to give the presentation instead. “Because of his act of advocacy, I had an opportunity to be seen in front of a large crowd of people at Pfizer,” says a grateful Hasson. “Getting exposure from an industry audience is one of the hardest things to do as a [young scientist].”

Sure enough, when a position opened up within Pfizer’s neuroscience team at the end of 2013, Hasson was invited to apply. Now, as a principal investigator at Pfizer in Cambridge, Massachusetts, he applies emerging technologies to find new drug targets for neurodegenerative diseases.

Translational scientists can also gain that crucial exposure by attending the same scientific conferences as industry researchers, says Carpenter. These include meetings such as those held by the American Society for Clinical Oncology and the Society for Laboratory Automation and Screening. Casual conversations over posters or meals can give scientists a glimpse into the day-to-day operations at specific companies.

Sirota says no matter which environment a translational researcher might be aspiring toward, “Figure out who you will be working with and how to make a good team with them.”

“The lines between academia and industry are blurring more and more and in many different ways,” notes Sirota, whose career has included successful stints in both arenas. As someone who has hired researchers in both spaces, too, Sirota says it’s extremely difficult to find the gems among the piles of résumés that come with each open position. So how to shine in a tough market?

Sirota advises: “Quantitative skills that are unique, personal connections, and very targeted applications that show me your research interests are a good match for the position will all make an application stand out if I have to go through a hundred of them.”

Kendall Powell is a freelance science writer based in Lafayette, Colorado.

DOI: 10.1126/science.opms.r1500161

FOCUS ON CELL BIOLOGY

UConn | SCHOOL OF MEDICINE

Faculty Positions

Assistant Professor Positions, Department of Cell Biology

The Department of Cell Biology (<http://cell.uchc.edu/>) invites applications for two tenure-track Assistant Professor positions (search code 2016-379), over the next two years. Outstanding individuals working in any area of cell biology are encouraged to apply. Candidates' research should be aimed at addressing fundamental questions related to cellular, molecular, or physiological mechanisms of biological or biomedical relevance. Questions regarding this search should be addressed to cellsearch@uchc.edu.

Senior Faculty Position, Center for Cell Analysis and Modeling

The Berlin Center for Cell Analysis and Modeling (<http://www.ccam.uchc.edu>) is a multidisciplinary research center focused on development of new photonic, microscopic, and computational approaches for the study of cellular systems. We invite applications at the Associate or Full Professor (search code 2012-1038) level for an established funded Investigator whose research program elucidates processes that control cell function. A research program that integrates laboratory experiments with computational modeling would be especially appropriate. The successful candidate will be expected to assume a leadership role in the continued growth of CCAM. Questions regarding this search should be addressed to cellsystems@uchc.edu.

The University of Connecticut School of Medicine has a highly interactive research environment with interdisciplinary graduate and medical science training programs. The environment is enhanced by generous support from the State's BioScience Connecticut initiative and by the newly established Jackson Laboratory for Genomic Medicine on our campus.

ALL APPLICATIONS SHOULD BE SUBMITTED VIA THE UCONN HEALTH EMPLOYMENT SERVICES WEBSITE, <http://jobs.uchc.edu>. Applications should include a cover letter, curriculum vitae, research plan, statement of teaching interests, and names and addresses of at least 3 references.

The University of Connecticut is an Equal Opportunity Employer M/F/V/PWD/PV.

POSITIONS OPEN

Northeastern University College of Engineering

With **151** tenured/tenure-track faculty (**36** hired since 2013), and **12** federally-funded research centers, Northeastern's College of Engineering is in a period of dynamic growth. Our emphasis on interdisciplinary, use-inspired research—tied to Northeastern's unique history of industry collaboration via the university's signature cooperative education program—enables partnerships with academic institutions, medical research centers, and companies near our centrally located Boston campus and around the globe.

The college seeks outstanding faculty candidates in all five departments.

Particular consideration will be given to candidates at the associate or full professor level; successful applicants will lead internationally recognized research programs aligned with one or more of the college's strategic research initiatives. Exceptional candidates at the assistant professor level will also be considered.

**Learn more and apply at
coe.neu.edu/faculty/positions**

Northeastern University is an Equal Opportunity, Affirmative Action Educational Institution and Employer, Title IX University, committed to excellence through diversity.

FOCUS ON CELL BIOLOGY

The University of Georgia CELL BIOLOGY – TENURE TRACK

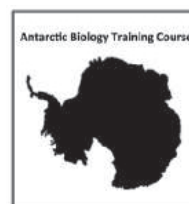
The Department of Cellular Biology at the University of Georgia invites applications for a tenure track Assistant Professor of Cell Biology. The candidate's research must address important questions in cell biology. Individuals whose work bridges cell biology with other disciplines (e.g. biophysics, chemical biology, proteomics, or systems biology) are also encouraged to apply. Successful applicants will be expected to develop an extramurally-funded research program, and teach cell biology at undergraduate and graduate levels. A competitive package of start-up funds and salary will be offered.

Candidates must have a Ph.D. degree in cell or molecular biology. They should submit a CV, teaching philosophy (1 page limit) and concise statement of proposed research (2 page limit) electronically at <http://facultyjobs.uga.edu/postings/494>. Three confidential letters of recommendation are required, and applicants should list the contact information for their references when applying through <https://facultyjobs.uga.edu/>. Application materials submitted in other ways will not be accepted. Questions about the search should be sent to: cbsearch@uga.edu. Applications received by **December 31, 2015** will be reviewed. Evaluation of applications will continue until the position has been filled.

The Franklin College of Arts and Sciences and the University of Georgia is committed to increasing the diversity of its faculty and students, and sustaining a work and learning environment that is inclusive. Women, minorities, and people with disabilities are encouraged to apply. Georgia is well known for its quality of life both outdoor and urban (www.georgia.gov). UGA (www.uga.edu) is a land grant/sea grant institution located 75 miles northeast of Atlanta.

The University of Georgia is an Equal Opportunity/Affirmative Action Employer. All qualified applicants will receive consideration for employment without regard to race, color, religion, sex, national origin, disability, gender identity, sexual orientation or protected veteran status.

COURSE



NSF Advanced Training Program in Antarctica for Early Career Scientists: Biological Adaptations to Environmental Change

This US National Science Foundation sponsored course will be held in Antarctica at Palmer Station (Antarctic Peninsula) in July 2016. The course is designed to train scientists who are interested in the study of extreme environments and the biology of Antarctic organisms. Applications are invited from graduate students currently enrolled in a PhD program and researchers who have an earned Ph.D. within the past five years. This is an international course, open to all nationalities. Partial scholarships are available to cover the cost of travel from home institution and full support is provided for room/board and science activities while in Antarctica. The emphasis of the Antarctic Biology Course is on integrative biology, with laboratory- and field-based projects focused on adaptations in an extreme polar environment. This program will also provide opportunities to understand and appreciate the complexities and logistical challenges of undertaking successful science in Antarctica. A diverse teaching faculty will offer students the opportunity to study a wide range of Antarctic organisms (bacteria, algae, invertebrates, and fish), using several different levels of biological analysis (molecular biology, physiological ecology, species diversity, and evolution).

Deadline for receipt of completed applications is **January 25, 2016**. For more information and the on-line application see <https://www.usfca.edu/arts-sciences/antarctic-biology-training-program> and <http://goo.gl/forms/aoNP63pRhF>.

FUNDING OPPORTUNITIES

ENABLING TODAY'S SCIENTIFIC LEADERS

Novo Nordisk Foundation Laureate Research Grants

Call for applications – biomedicine & biotechnology

For outstanding established scientists to come to Denmark to strengthen their leading research programs

Applicants have directed their own independent groups for 7 or more years in total

GRANT FUNDING

- Individual grants up to **DKK 40 million** over 7 years
- Grant holders can apply for continued L.R.G. funding, up to DKK 35 million over 7 additional years

APPLICATIONS

December 4, 2015 - January 14, 2016

SUPPORTING TOMORROW'S LEADING SCIENTISTS

Novo Nordisk Foundation Young Investigator Awards

Call for applications – biomedicine & biotechnology

For outstanding younger scientists to come to Denmark to expand their leading research programs

Applicants have directed their own independent groups for less than 7 years in total

GRANT FUNDING

- Individual grants up to **DKK 20 million** over 7 years
- Award holders can apply for further funding from other eligible Novo Nordisk Foundation programs

APPLICATIONS

December 4, 2015 - January 14, 2016

CONNECTING FRONTIER SCIENTISTS

Copenhagen Bioscience Conferences

World-leading researchers and young talents discuss the latest scientific results and hottest topics within biomedicine and biotechnology.

- Top-level debate and knowledge sharing in a unique setting
- Speakers and participants of all career levels selected for their scientific accomplishments and motivation
- Registration fee and accommodation covered by the Novo Nordisk Foundation

APPLY FOR

- **The Stem Cell Niche.** May 22-26, 2016
Application deadline: January 2016
- **Protein Signaling.** October 2-6, 2016
Application deadline: June 2016

EDUCATING THE NEXT GENERATION OF SCIENTISTS

Copenhagen Bioscience PhD Programme

The programme offers talented students from outside of Denmark an opportunity to launch their careers in the vibrant research environment of the Novo Nordisk Foundation Research Centre Cluster.

The Novo Nordisk Foundation will fund up to **16 students** to be enrolled in the 4-year PhD programme after the summer of 2016.

- Selection will be based on academic achievements, research experience, references and interviews
- Interviews will take place in Copenhagen, April 18-19, 2016

APPLICATIONS

January 4 – February 29, 2016

FURTHER INFORMATION

To learn more about these opportunities and the Novo Nordisk Foundation, please visit
www.novonordiskfoundation.com



**NOW HIRING
300
LADDER FACULTY**

**Join us in defining the
new American research
university**

clusterhiring.ucr.edu

WHERE SOLUTIONS GROW.

Want to help meet the agronomic challenges of the 21st century? Then Iowa State University wants you for our NSF Research Traineeship (NRT) in Predictive Plant Phenomics (P3). P3 fellows will be trained in engineering, plant science and data sciences. Learn more and get application information at predictivephenomicsinplants.iastate.edu.

This program is part of Iowa State University's Plant Sciences Institute's new research focus on P3.



**IOWA STATE
UNIVERSITY**

This material is based upon work supported by the National Science Foundation under grant number 1545453.



CSIR-Central Drug Research Institute

Council of Scientific and Industrial Research
Sector 10, Jankipuram Extension, Sitapur Road
Lucknow – 226 031, Uttar Pradesh, India



SCIENTIST RECRUITMENT - 2015

Advertisement No 04/2015, Date 23 November 2015

Last Date for Registration for Online Application: Friday, 22 January 2016; 23.59 Hrs IST
Last Date for Submission of Online Application: Friday, 05 February 2016; 23.59 Hrs IST

**A unique opportunity for research career in Science & Technology in
the area of Drugs, Pharmaceuticals and Biomedical Research**

CSIR-Central Drug Research Institute, Lucknow, a premier institute under the Council of Scientific and Industrial Research (CSIR), is involved in the multidisciplinary R&D programs of both basic and applied nature. In the year 2012, Institute shifted to its state of the art new campus, which has been set up with a vision to serve as a nodal center of the CSIR in new drug discovery and development. With an aim to expand and strengthen the areas of Parasite biology, Life style diseases, Medicinal and Natural Product Chemistry, and Safety & Clinical Development, the Institute is looking for enthusiastic, talented young researchers / professionals with brilliant academic record, proven scientific achievements and zeal to conduct biomedical research as per the mandate of the Institute. For further details about the Institute, please visit our website <http://www.cdriindia.org>.

Applications are invited from the Indian nationals for the following Scientific Positions.

Designation	No. of Posts	Pay Band	Grade Pay	*Total Emoluments
Scientist	14 (UR-6, SC-1, ST-1, OBC-3, & PWD-3 including 2 backlog)	Rs.15600-39100 (PB-3)	Rs.6600/-	Rs. 69,274/-
Senior Scientist	07	Rs.15600-39100 (PB-3)	Rs.7600/-	Rs. 79,433/-

For detailed advertisement, terms & conditions and further instructions, please visit <https://recruit.cdri.res.in> or access the link 'SCIENTIST RECRUITMENT-2015' on <http://www.cdriindia.org>.

(Controller of Administration)



National Heart, Lung,
and Blood Institute

Director, Division of Cardiovascular Sciences
National Heart, Lung, and Blood Institute
National Institutes of Health
Department of Health and Human Services

The National Heart, Lung, and Blood Institute (NHLBI), a component of the National Institutes of Health (NIH) and the Department of Health and Human Services (HHS), is seeking exceptional candidates for the position of Director, Division of Cardiovascular Sciences (DCVS). The incumbent will be a dynamic scientific leader widely recognized for his/her scientific vision and research credentials related to cardiovascular sciences. In addition to providing scientific vision, leadership, and management for the NHLBI DCVS, he/she will serve as a member of the NHLBI senior leadership team and advise the Director, NHLBI, on issues related to cardiovascular research and relevant Institute research directions.

This individual will report to the Director, NHLBI, and may also coordinate activities with NIH, other institutes and Federal agencies. He/she will provide scientific leadership in managing a portfolio budget of approximately \$1.7 billion and a staff of approximately 135 employees. The ideal candidate will have professional experience in organizational management, training and development of research scientists, and development of a diverse biomedical and behavioral research workforce.

The incumbent will provide strategic leadership at the NHLBI. The Director will assume responsibility for nurturing internationally renowned research programs in cardiovascular science across the spectrum of basic research, clinical science, and population sciences/epidemiology, including translational research and the conduct of a wide variety of clinical trials. The Director will recruit scientists and scientific administrators, develop and nurture a strong workforce, and build depth in a variety of scientific disciplines and in cardiovascular disease-specific programs and branches. Key challenges include establishment of program priorities, integration of basic and clinical science, building teams, and interaction with scientific colleagues in a wide variety of settings. Functioning as a key member of the senior leadership team of the Institute, the incumbent will collaborate with peers and others within the Institute on closely aligned programs. The DCVS Director will have a profound impact upon the nation's investment in research and the service and support of the broader cardiovascular research community. The Director, DCVS, will have the opportunity to advocate for areas of critical importance to the national and global populace, to establish and implement programs congruent with the NHLBI's strategic plan, and to improve the health of the public. Applicants must possess an M.D., Ph.D., or equivalent degree, as well as senior-level research experience, management experience, interpersonal skills, and the ability to engage stakeholders. The successful candidate will be a respected, accomplished researcher with maturity, integrity, and outstanding communication skills.

Information about the Division is available at www.nhlbi.nih.gov/about/org/dcvs.

Position Requirements: Candidates must have an M.D., Ph.D., or equivalent degree in a field relevant to the position. This position will be filled under a Title 42(f) excepted service appointment.

Salary/Benefits: Salary is competitive and will be commensurate with the experience of the candidate. A recruitment or relocation bonus may be available, and relocation expenses may be paid. A full package of federal Civil Service benefits is available, including retirement, health and life insurance, long-term care insurance, leave, and a Thrift Savings Plan (401K equivalent). The successful candidate is subject to a background investigation and public financial disclosure requirements.

How to Apply: Applicants must submit a current curriculum vitae, bibliography, and full contact details for three references. In addition, applicants are asked to prepare two statements: a vision statement and a statement that addresses the specific qualification requirements (please limit both statements to two pages each). Applications can be sent to nhlbi_careers@mail.nih.gov.

Information about the NHLBI can be found at www.nhlbi.nih.gov.

Applications will be accepted beginning on November 16, 2015. The closing date for accepting applications is January 18, 2016.

You may contact Barry Rubinstein with questions and for more information about this vacancy at rubinstb@nhlbi.nih.gov or 301-594-9923.

HHS and NIH are Equal Opportunity Employers.

Tufts

UNIVERSITY

www.tufts.edu

GERALD J. AND DOROTHY R. FRIEDMAN SCHOOL OF NUTRITION SCIENCE AND POLICY

Tufts University is recognized as a premier university dedicated to educating new leaders for a changing world. With campuses in Boston, Medford, Grafton, and in Talloires, France, Tufts is internationally renowned in the academic community (<http://www.tufts.edu/>). The University is a perfect blend of research and liberal arts - a special combination that attracts students, faculty and staff who thrive in our environment of curiosity, creativity and engagement.

The Gerald J. and Dorothy R. Friedman School of Nutrition Science and Policy is a leader in nutrition research (<http://www.nutrition.tufts.edu>). This vigorously growing graduate school has a world-wide reach, an interdisciplinary faculty, and a cutting-edge research agenda. The Friedman School is actively growing and recruiting faculty in many multidisciplinary areas. The candidates will join the School during an exciting period of growth combined with increasing national and international awareness of the crucial importance of nutrition for health, equity, and the environment.

We bring together biomedical, social, behavioral, public health, economics, and food systems scientists to conduct work that improves the nutrition and well-being of populations throughout the world. Our interdisciplinary vision, our focus on public impact and service, and the integrative nature of our nutrition science and policy education and research complement the intellectually-rich environment across Tufts, a "Research Class I" university.

We are currently accepting applications for the following positions:

- **Director of the Feinstein International Center**
- **Associate or Full Professor in Water, Health and Security**
- **Associate or Full Professor in Behavioral Health Science**
- **Associate or Full Professor in Food Industry Management and Marketing**
- **Associate or Full Professor in Food Policy Implementation and Evaluation**
- **Associate or Full Professor in Food Systems, Sustainability and Climate Change**
- **Associate or Full Professor in Global Nutrition and Chronic Disease**
- **Assistant, Associate or Full Professor in Data Analytics**
- **Assistant, Associate or Full Professor in Biostatistics**

Interested candidates should submit the following through the online submission system at (<http://www.nutrition.tufts.edu/about/jobs-at-friedman>):

- A cover letter summarizing qualifications with a statement of research and teaching objectives and contact information for three (3) professional references combined in one document
- Curriculum vitae (CV)

Applications will be reviewed until the position is filled or the search is closed.

Tufts University is an Affirmative Action/Equal Opportunity Employer. We are committed to increasing the diversity of our faculty, and thus, women and members of underrepresented groups are strongly encouraged to apply.

Be the force
behind the cures.

EXPLORE AN EXCITING **FACULTY POSITION**
IN CHEMICAL BIOLOGY.

The Department of Chemical Biology and Therapeutics at St. Jude Children's Research Hospital invites applications for a faculty position at the level of Assistant Member (Professor) in Chemical Biology. We are specifically seeking applicants who will develop an independent research program focused on the application of chemical biology approaches towards a greater understanding of cancer and tumor cell biology. The successful applicant will have an outstanding training record in chemical biology and a clearly articulated research plan in the area of cancer.

The Department of Chemical Biology and Therapeutics is a multidisciplinary, thematically integrated and well-resourced department focused on the discovery and development of small molecules for perturbing cellular functions. St. Jude offers a competitive package for these positions, including a generous start-up allowance with newly remodeled space and equipment; state of the art facilities for chemical biology; complete faculty salary support; and operational support positions.

Those interested in joining this department and making a difference in the fight against pediatric cancer should arrange to have their CV and a concise future research plan sent by email to: CBTfacultyrecruiting@stjude.org

EOE/Minorities/Females/Vet/Disability/Sexual Orientation/Gender Identity
©2015 St. Jude Children's Research Hospital-Biomedical Communications.



AAAS is here –
helping scientists achieve career success.

Every month, over 400,000 students and scientists visit ScienceCareers.org in search of the information, advice, and opportunities they need to take the next step in their careers.

A complete career resource, free to the public, *Science Careers* offers hundreds of career development articles, webinars and downloadable booklets filled with practical advice, a community forum providing answers to career questions, and thousands of job listings in academia, government, and industry. As a AAAS member, your dues help AAAS make this service freely available to the scientific community. If you're not a member, join us. Together we can make a difference.

To learn more, visit aaas.org/plusyou/sciencecareers





Sainsbury Wellcome Centre



Director of Sainsbury Wellcome Centre for Neural Circuits and Behaviour

University College London (UCL), the Gatsby Charitable Foundation, and the Wellcome Trust invite applications for the post of Director of a major neuroscience centre based at UCL: the Sainsbury Wellcome Centre for Neural Circuits and Behaviour. The Centre addresses a fundamental challenge in modern biology, determining how neural circuits process information and direct behaviour. Advances in this field will transform understanding of brain function, and ultimately lead to new ways of monitoring and regulating brain activity in health and disease.

The Sainsbury Wellcome Centre, completed in 2015, is housed in a new state-of-the-art building embedded at the heart of UCL. It seeks to develop and exploit new approaches for determining anatomical and functional connectivity in neural circuits and for recording, imaging and manipulating activity in genetically defined ensembles of neurons. This experimental work is tightly integrated with the theoretical and computational neuroscience carried out by the Gatsby Computational Neuroscience Unit which has relocated to the new building.

The Centre will ultimately comprise 12 research groups (including the Director's) and will conduct a vibrant interdisciplinary research effort, investigating information processing in neural circuits across a range of model systems and behaviours. UCL provides the ideal environment for a Centre undertaking such a major interdisciplinary effort in neuroscience. The Centre draws on and catalyses the rich, wide-ranging neuroscience community at UCL, currently ranked 2nd in the world for ISI citations in neuroscience and behaviour. It also benefits from important strengths in allied fields such as physics, chemistry, engineering, nanotechnology and biomedicine.

The post of Director carries with it a professorial title and the post holder will play a significant role in the strategic development of Neuroscience at UCL. The Director will be responsible for recruiting and nurturing outstanding research groups; and for promoting links between the Centre, UCL, and the wider scientific community. Substantial and long-term resources are and will be available to support the scientific work of the Director and other researchers in the Centre.

The appointment will be full time on the UCL Professorial Grade. The salary will be negotiable on the professorial scale. A generous relocation package will be available.

The successful applicant will be of international standing and have a world-leading track record in neuroscience research. Experience in running a comparable research centre or significant research programme(s), scientific management and/or strategic planning is highly desired and will receive preferential review.

The appointment is available from September 2016.

For further information about the vacancy and how to apply online, please go to <http://www.ucl.ac.uk/hr/jobs/> and search on Reference Number 1525895.

If you have any queries regarding the application process, please contact Nick McGhee, email: n.mcghee@ucl.ac.uk, tel: +44 (0)20 3108 8217. If you wish to discuss the post informally, please contact Professor David Lomas, email: d.lomas@ucl.ac.uk, tel: +44 (0)20 7679 0878.

Closing Date: 16th January 2016

We particularly welcome female applicants and those from an ethnic minority, as they are under-represented within UCL at this level.



wellcometrust

中国·北京高校招聘

Recruitment for Universities in Beijing, China

www.edu.cn/zhaopin



北京理工大学
www.bit.edu.cn



华北电力大学
www.ncepu.edu.cn



北京邮电大学
www.bupt.edu.cn



北京工业大学
www.bjut.edu.cn



北京工商大学
www.btbu.edu.cn



首都师范大学
www.cnu.edu.cn

Looking for more positions? Please send your CV to
acabridge@163.com or call the direct line: 86-10-62603334



中国东北高校招聘

Recruitment for Universities in Northeast China



东北大学
www.neu.edu.cn



哈尔滨工程大学
www.hrbeu.edu.cn



东北林业大学
www.nefu.edu.cn



东北师范大学
www.nenu.edu.cn

Looking for more positions? Please send your CV to
acabridge@163.com or call the direct line: 86-10-62603334

www.edu.cn/dbzp

Science made me a better parent

Chefs can cook delightful meals for their families. Musicians can enliven social gatherings with friends. And having medical doctors, mechanics, or lawyers on call can be a great help if you get into trouble. As a biochemist with a Ph.D. in molecular biology, however, I always felt that my professional skills were of little value outside the lab. Let's face it: As fun as they can be, cutting and pasting DNA and growing cells are not things that you do very often when you're home or out with friends. Until recently, I didn't think anything I had learned in the lab could be used in the rest of my life. Since I became a father, though, my view has been steadily changing.

I have found that parenthood is, in many ways, an extension of research: overcoming unknowns, learning constantly, and holding both a big responsibility and a great privilege. And neither science nor parenting is an individual endeavor. Whether you are giving a baby a bath or isolating mitochondria, teamwork is essential, and the list of collaborators can be quite long—including, in the case of parenting, partners, parents, siblings, uncles, aunts, and friends. As with the author list for a scientific paper, each of these players makes their own important contribution.

Advice from colleagues and mentors is also very important, although instead of conferences, parents have barbecues and get-togethers. These are usually not in distant and exotic places, but other than that, they are strikingly similar to scientific conferences: You get a chance to show your peers how your project—or baby—is progressing, exchange tips and experiences, and pave the way for future collaborations. And although learning about how others have handled similar situations or how they interpret certain signs is helpful, in the end, it is up to you to figure out how to solve each particular dilemma.

A slew of skills that I acquired while conducting my research—including being patient, learning how to do new things, and handling setbacks—are helping me more than I could have imagined in raising my baby. At a practical level, my experience learning new methodologies in the lab helped me unveil the secrets of diapering and bottle-feeding. The protocols are fairly simple and straightforward. The sterilization procedures are much more flexible than those used in the lab, and most of the items can be obtained over the counter. And I already knew how to open doors and work around



"I have found that parenthood is, in many ways, an extension of research."

the house with my hands full, because I often have to do it in the lab.

Of course, every time you start in a different field there is new vocabulary to learn (percentile, colostrum, meconium) and unfamiliar equipment to master—securing a car seat or folding a stroller can be more complicated than it seems. But that's also part of the fun. As for the vast literature devoted to parenting, discriminating reliable sources from misinformation can be daunting. Luckily, having spent a good number of hours with the scientific literature, I have learned to read everything with a healthy dose of skepticism.

But, without any doubt, the most useful thing that I've learned in the lab is the ability to cope with failure. When the baby is finally asleep in my arms and I put her in the crib

and, holding my breath, leave the room on tiptoes, it feels almost natural to hear, a second later, a growing moan that turns into desperate sobbing. Knowing how to tame my frustration, make the best out of difficult situations, and get back on my feet are the things that I've found most helpful. That, and the conviction that the sum of what I've learned from all those small defeats is a valuable asset.

There is a Spanish proverb that says, "Patience is the mother of science," and I think that I now understand how those three concepts—patience, parenting, and science—became so intertwined in the first place. Whether you are starting a Ph.D. or becoming a parent, patience and perseverance will serve you well. The rest will come, after a few sleepless nights. ■

Ignacio Amigo is a postdoctoral researcher in the biochemistry department of the Chemistry Institute at the University of São Paulo in Brazil. Send your story to SciCareerEditor@aaas.org.